ELECTROCATALYTIC HYDROGENATION OF MONOMERIC, DIMERIC, AND POLYMERIC LIGNIN MODEL COMPOUNDS WITH RANEY NICKEL: CHEMISTRY, MECHANISTIC, AND PRODUCT TOXICITY STUDIES

By

Pengchao Hao

A DISSERTATION

Submitted to
Michigan State University
in partial fulfillment of the requirements
for the degree of

Chemistry - Environmental Toxicology - Doctor of Philosophy

2018

ABSTRACT

ELECTROCATALYTIC HYDROGENATION OF MONOMERIC, DIMERIC, AND POLYMERIC LIGNIN MODEL COMPOUNDS WITH RANEY NICKEL: CHEMISTRY, MECHANISTIC, AND PRODUCT TOXICITY STUDIES

By

Pengchao Hao

If lignocellulosic biomass is to serve as the carbon feedstock for future energy and chemical manufacture, it will be necessary to develop chemistry tools to disassemble it into fragments for further upgrading. Of particular interest is the lignin fraction of the biomass, as it is the most carbon- and energy-rich component and currently underutilized. This complex polymer consists of highly oxygenated and methoxy-substituted phenylpropane building blocks, mainly guaiacyl and syringyl moieties, held together by C-O or C-C linkages. This dissertation examines the use of Electrocatalytic Hydrogenation (ECH) at a Raney® nickel cathode to depolymerize, hydrogenate, and deoxygenate lignin to biofuel and meanwhile investigates the reaction mechanisms of the ECH surface reactions of lignin monomer and dimer models.

Along with new technology development, the safety of personnel should always be considered. Due to the expected major changes of chemical structures of the components of lignin biofuels, their potential impact on the human health is unexplored. Thus, this project seeks to analyze the risk associated with the newly emerging cyclic compounds in biofuel by comparing the toxicities for two of the representative compounds: cyclohexanol and cyclohexane.

TABLE OF CONTENTS

LIST OF TABLES

LIST OF FIGURES

Chapter 1

Literature Review on Electrocatalytic Hydrogenation Reactions and the Applications to Lignocellulosic Biomass

The knowledge of chemical to thermal energy conversion perhaps has existed at the beginning of human civilization history since people used fire for heat and cooking. Thermal to electric energy conversion was discovered as early as 1821 when Thomas Johann Seebeck found that a thermal gradient between two conductors can produce electricity.[31] Chemical to electrical energy conversion is perhaps the most popular and convenient energy transform process nowadays such as batteries. The first true battery was invented as early as 1800 by Alessandro Volta, who made it from pairs of copper and zinc discs piled on top of each other separated by cardboard soaked with brine solution.[32] Just a few weeks after the voltaic pile invention, the opposite process, conversion of electricity to chemical energy, had been developed when William Nicholson and Anthony Carlisle used the battery for water electrolysis.[33] Now at the beginning of the 21st century, humans have planned to inhabit Mars where CO_2 is abundant in the atmosphere and solid water has been detected at the

north polar ice cap.[34] Solar-electricity to chemical (fuel) energy conversion has become one of the essential technologies to accelerate the great dream of human Mars inhabitation. Electrocatalytic hydrogenation (ECH) is one part of the solar-electricity to chemical energy conversion processes.

Electrocatalytic Hydrogenation (ECH) has been suggested to be an electroreduction process in which substrates are adsorbed onto the surface of a catalytic cathode, along with surface hydrogen atoms derived from reduction of protons. Further reactions then occur between surface hydrogen atoms and surface adsorbed substrates.[35] Classical ECH cathode metals are Ni, Ru, Pd, Pt etc. The early studies were mainly simple Electrochemical Reduction (ECR), where a noncatalytic mercury cathode was widely used and electron transfer reactions usually occurred along with radical rearrangement or coupling of the resulting radical ions. Common ECR type cathode metals are Hg, Pb, C etc.

Tafel and Naumann found that in sulfuric acid solution, caffeine was reduced more readily than succinimide at a mercury cathode, while the reverse was the case at a lead cathode.[36] This finding inspired the establishment of adsorption involved in catalysis as another factor.

Catalytic effect of cathode was realized as important; summarizing observations reaching back as early as the 1800s, Frank Popp noted that some reactions are ECH instead of ECR:

It has been ascertained that certain cathodes appear to have a definite catalytic effect upon certain reactions which is unexplained in terms of cathode potential or over-voltage.

Essentially, ECH is a special type of ECR reaction where the cathode also plays a role as catalyst. ECR reduces substrates via single electron transfer and lead and mercury are the commonly used cathode material; while ECH is a catalytic process making use of metals,

such as nickel, platinum, palladium etc, as catalysts. In this review, some ECR reactions resulting in the hydrogenation of substrates, although technically not ECH reactions, are also included since that these reactions are important reference points for our on-going research.

The focus of this thesis is on ECH of lignin for the production of biofuels and chemicals. Two reaction types are of particular interest for increasing the gross heat values of chemicals: hydrogenation and deoxygenation. Hence, both hydrogenation and deoxygenation strategies through ECH or ECR are reviewed. On the basis of these academic works, applications of ECH to biomass model compounds are summarized to connect with real life practical problems.

1.1 Historical review: electrochemical reduction and electrocatalytic hydrogenation of organic substrates since the late 19th century

During the 19th and early 20th centuries, Electrochemical Reduction (ECR) and Electrocatalytic Hydrogenation(ECH) were usually conducted in single-compartment cells unless otherwise specified.

1.1.1 Carboxylic acid

1.1.1.1 ECR of carboxylic acids

The ECR of unsaturated organic compounds have been investigated since the beginning of the 20th century, and early research focused on the reductions of olefin functional groups in natural unsaturated carboxylic acids.[35] As far as we know, Professor Marie was the

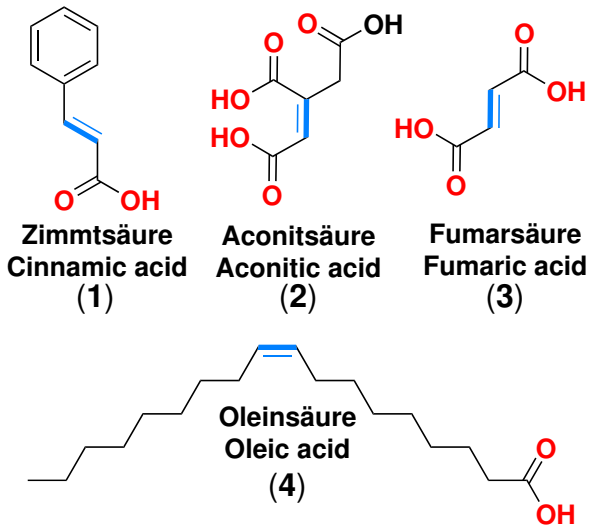

Figure 1.1: Early ECR of organic substrates studied in 1902 by Jedoch, C. H. Marie and Julius Petersen. In the figure, the German chemical names from the original papers are included.

first one conducting electroreduction on unsaturated organic acid in 1903. A yield of 60% propane-1,2,3-tricarboxylic acid was produced by electroreduction of aconitic acid with mercury cathode and platinum anode; he also explored oleic acid (**4**) to stearic acid and cinnamic acid (**1**) to phenylpropanoic acid reduction,[37] with multiple cathode materials including Pt, Cu, Pb, Sn, Al giving similar results (reaction conditions were not found).[38,39] In 1905, Peterson reduced oleic acid over 4 days with 64.4% yield.[6] He also explored Ni, Pb, Pt, Zn and Hg cathode and concluded that character of the cathode had no appreciable influence on the yield and speed of the reaction in alcohol/water solution (no reaction condition details were found).[39] K. Elbs found cinnamic acid was so easily reduced in an electrolysis that no diaphragm was needed and no anodic oxidation reaction products were observed (no reaction conditions were reported).[6,37]

The ECR of carboxylic acid functional group to aldehyde and alcohol were reported by Ellis in 1906. He wrote that lead, spongy nickel, iron, cobalt were advantageous for reducing formic acid or fatty acid and platinized platinum cathode might be also employed.[40]

However, it should be mentioned that subsequent researchers were unable to duplicate Ellis' result.[41] Generally, in acidic media at low overpotential electrodes such as platinum, nickel, or iron, no reaction occurs.[41]

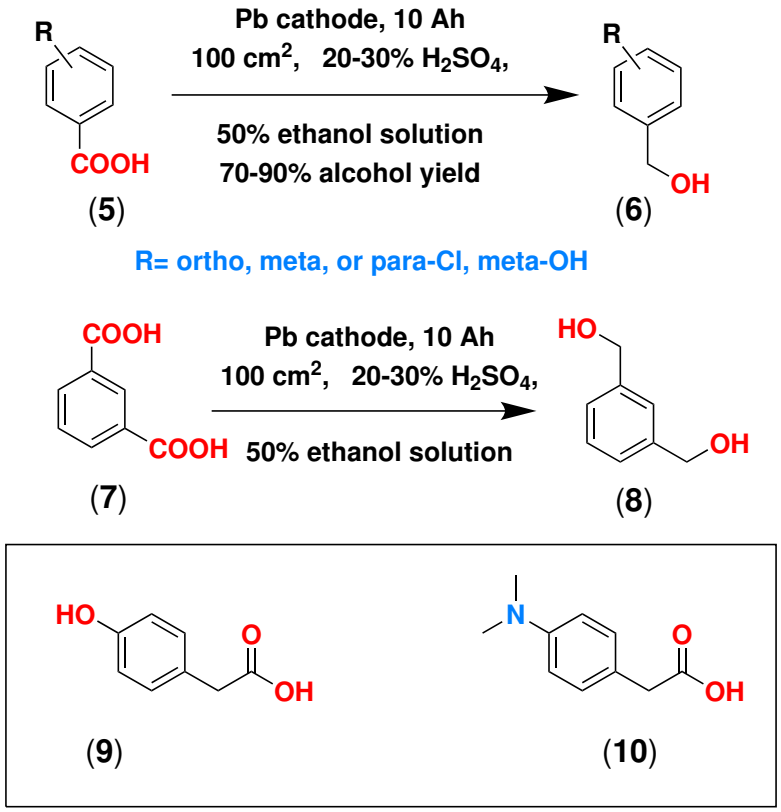

Figure 1.2: ECR of aryl carboxylic acids.

Aromatic carboxylic acids are readily reduced to benzyl alcohols with high overvoltage lead or mercury cathodes in high concentration sulfuric acid solution. Usually, water-ethanol mixture are used to increase the solubility of carboxylic acids.[41] Room temperature or cooling bath conditions are required to preclude ethyl ester formation. Haloaryl carboxylic acid (**5**) was successfully reduced to the haloaryl methanol (**6**) without the removal of halogen in good to excellent yields.[42] 1,3-Benzenedicarboxylic acid (**7**) was successfully reduced to the diol (**8**).[43]

Aryl substituents also have influences on the reduction of carboxylic acid. 4-Hydroxyphe-

nylacetic acid (**9**) cannot be reduced by mercury cathode under acid condition, while 4-dimethylaminophenylacetic acid (**10**) does get reduced to the desired carbinol.[41] Presumably, the latter case works because of the more basic amino group of (**10**) getting protonated, making it positively charged and thus, easier to reduce.

1.1.1.2 ECH of carboxylic acids

Compared with ECR, ECH reaction does not lead to radicals and the reaction conditions are much milder (0.01 M dilute acid). The reduction of simple alkanoic acids is very difficult and in assembling this review, no ECH examples were found. However, when there are electron-withdrawing groups at the α-position of the carboxylic acid, reduction via ECH was reported.

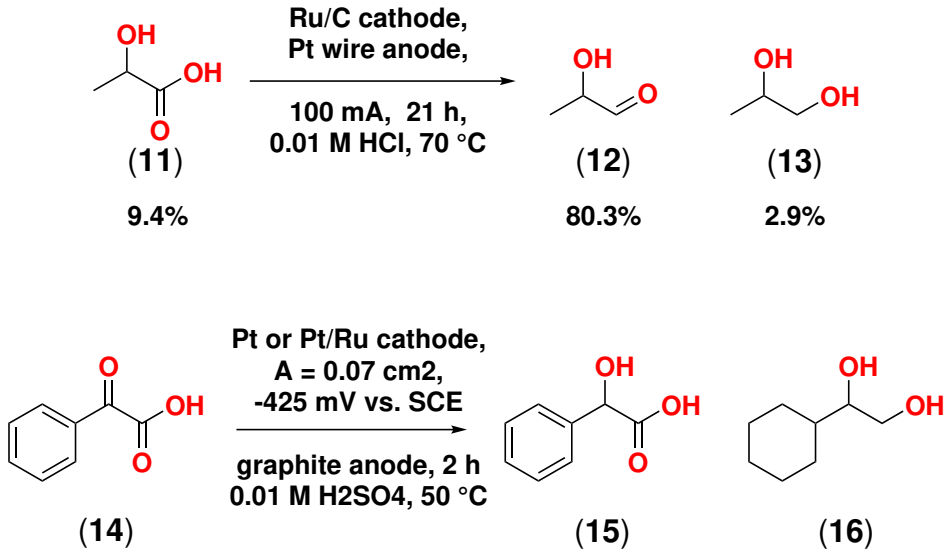

Figure 1.3: ECH of lactic acid and phenylglyoxylic acid under mild conditions.

When an electron-withdrawing hydroxyl group is at α-position of carboxyl group, as shown in the figure above, lactic acid (**11**) was reduced via ECH on a Ru cathode at only 70 °C in the presence of dilute acid.[44]

α-keto-carboxylic acid (**14**) can also be reduced efficiently to its corresponding alcohol (**16**) with a 74% mole percentage in the product, and 26% (**15**) with intact carboxylic group. It was also shown that no alcohol (**16**) appeared in product under neutral and basic conditions.[45]

1.1.2 Ketones and aldehydes

1.1.2.1 ECR of ketones

The ECR of dialkyl ketones (**17**) and alkyl-aryl ketones (**18**) were investigated under both acid and base conditions with lead cathodes, and the products are similar in both cases as shown in Table 1.1. In addition to the direct hydrogenation of (**19**) and (**20**) and pinacol coupling products (**20**) and (**21**) with better selectivities for the mono-alcohol products under base condition.[46,47]

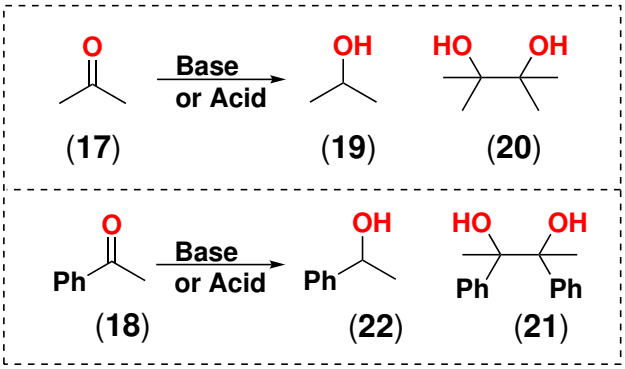

Figure 1.4: ECR of alkyl-substituted ketones under both acid and base conditions with lead cathode

The ECR of diaryl ketones (**23**) and (**25**) shows different reactivities under base or acid conditions. Only alcohol (**24**) was observed under base condition; while the pinacol coupling products (**27**) were also produced either as intermediates or final products for all acid condition reactions with no (**26**) were isolated. When R=*p*-Tolyl and 2,4-dimethylphenyl, the

Table 1.1: ECR of ketones with lead cathodes.

Substrates	**Conditions**	**Yields %**		
		Pdt1	**Pdt2**	**Pdt3**
		(**19**)	(**20**)	
(**17**)	10% NaOH in acetone, 16 °C, 0.3 A, 100 cm^2, 310 Ah	massive	small	-
(**17**)	10% H_2SO_4, 16 °C, 0.5 A, 100 cm^2, 320 Ah	40	17	-
		(**22**)	(**21**)	
(**18**)	ethanol/water (4:1), NaOAc, 16 °C, 0.5 A, 100 cm^2, 9 Ah	60-65	35-40	-
(**18**)	ethanol/water (9:1), 10% H_2SO_4, 16 °C, 0.5-0.8 A, 100 cm^2, 10.5 Ah	38	38	-
(**23**)		(**24**)		
R=*p*-tolyl	ethanol/water (5:1), NaOAc, 16 °C, 0.6-0.8 A, 100 cm^2, 8.46 Ah	80-90	-	-
R=2,4-dimethylphenyl	ethanol/water (5:1), NaOAc, 16 °C, 0.6 A, 100 cm^2, 10 Ah	pure	-	-
R=Ph	ethanol/water (5:1), NaOAc, 16 °C, 0.6 A, 100 cm^2, 10 Ah	90	-	-
R=α-naphthyl	ethanol/water (11:1), NaOAc, 16 °C, 0.6-1.0 A, 100 cm^2, 7.2-8.1 Ah	pure	-	-
R=*p*-hydroxyphenyl	ethanol/water, NaOAc, 16 °C, 0.6 A, 100 cm^2	0	-	-
R=*p*-benzoylphenyl	ethanol/water, NaOAc, 16 °C, 0.6 A, 100 cm^2	pure	-	-
(**29**)	ethanol/water, 10% NaOH, 16 °C, 0.75 A, 100 cm^2, 4.2 Ah	60	-	-
(**25**)		(**26**)	(**27**)	(**28**)
R=*p*-tolyl	ethanol, 10% H_2SO_4, 16 °C, 2 A, 100 cm^2, 1.5 Ah	-	87	-
R=2,4-dimethyphenyl	acetone, NaOAc, 16 °C, 0.6-0.8 A, 100 cm^2, 8.46 Ah	-	40-50	-
R=Ph	10% H_2SO_4, 0-2 °C, 0.5 A, 100 cm^2	-	-	25
R=α-naphthyl	ethanol, 10% H_2SO_4, 16 °C, 100 cm^2	-	-	pure
R=*p*-ethoxylphenyl	ethanol, 10% H_2SO_4, 16 °C, 0.6 A, 100 cm^2	-	-	some

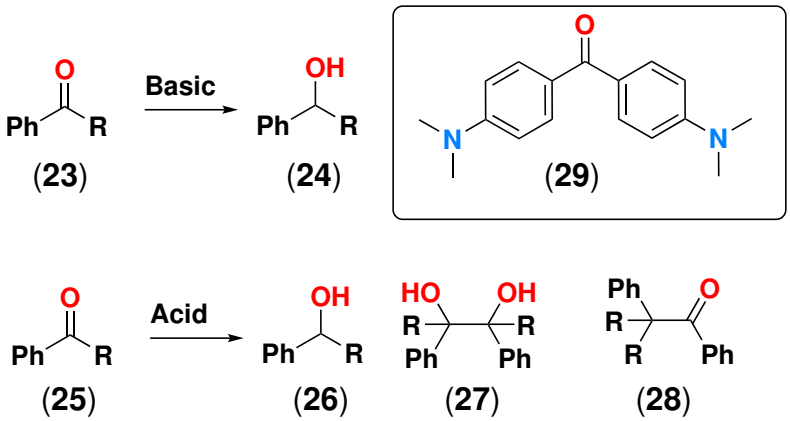

Figure 1.5: ECR of diaryl ketones under both acidic and basic conditions with lead cathode.

pinacol products are stable in acid solution and they were isolated as final product (**27**). In the case where (**27**) was unstable in acid solutions, migrations of R-groups of (**27**) form pinacolone rearrangement products (**28**); these compounds include R=Ph, α-naphthyl, and *p*-ethoxyphenyl substituted benzophenones (**25**).[46,47]

1.1.2.2 ECH of simple ketones, aldehydes, and selective reduction of enones

The ECH of ketones, enones and aldehydes had been studied extensively as shown in Figure 1.6 and Table 1.2. There are two main types of cathodes: polymer film cathodes (entries **1, 2, 9, 10, 20, 24-27, 30**) and metal cathodes.

There was no apparent universal advantage in terms of current efficiency (CE) to the use of a polymer film cathodes compared with metal cathodes. As shown from Table 1.2, when (**55**) was used as substrate, entry **10** Table 1.2 the polymer cathode has a CE much smaller than all other metal cathodes (entries **11**–**16**); meanwhile, when isophorone (**41**) as substrate, all polymer cathodes (entries **20, 24, and 25**) had a much smaller CE than all metal cathode reactions (entries **21-23**).

We can safely draw the conclusion that enones can be selectively reduced to ketones by

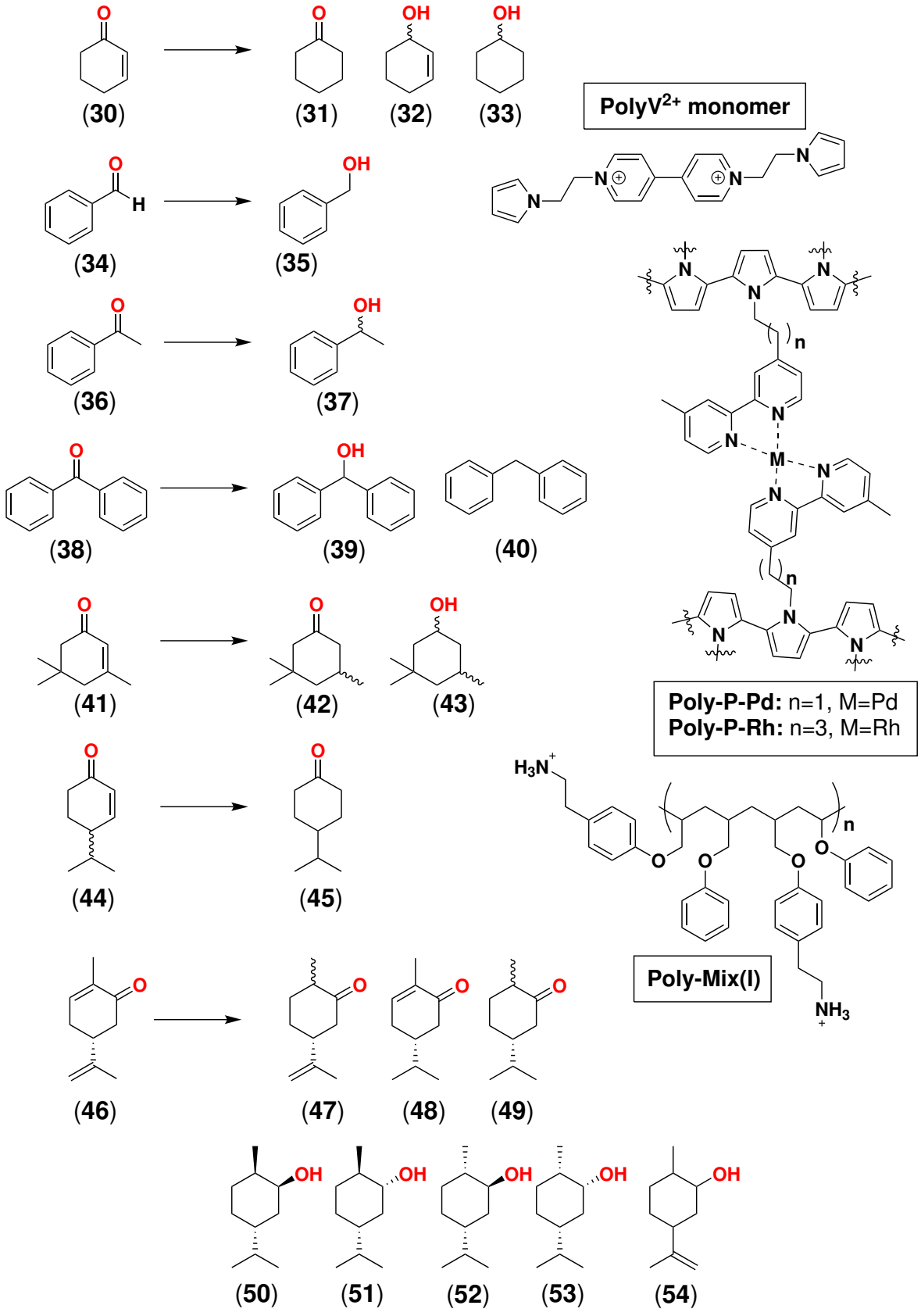

Figure 1.6: ECH of ketones.

comparing the ECH of (**30**), (**41**), (**44**), and (**46**). Under ECH conditions, alkenes undergo preferential reduction, regardless of conjugation to carbonyl moieties. However, exceptions do exist in the cases of entries **1** and **2**; when polymer film cathodes on platinum were used, significant or even selective reductions of carbonyl prior alkene were observed.

Table 1.2: ECH of ketones and aldehyde compounds.

								Yield%		
	S	**Cat.**	**T**	**Solvent**	**Q**	**CD**	**CE%**	**P1**	**P2**	**P3**	**Ref**
	(**30**)							(**31**)	(**32**)	(**33**)	
1		PL[a]/Pt	r.t.	H_2SO_4	832	12.7	0.18[j]	54	23	-	[48]
2		PLM[b]/Pt	r.t.	H_2SO_4	208	13.9	1.0[j]	-	92.6	4.2	[48]
3		Fe	r.t.	M/H_2O	2.1	-	88.5	89	-	2	[49]
4		Fe/Ni	r.t.	M/H_2O	2.1	-	92	87	-	5	[49]
5		Cu	r.t.	M/H_2O	2.1	-	88.5	87	-	3	[49]
6		Ni	r.t.	M/H_2O	2.0	-	95	95	-	0	[49]
7		Ni	r.t.	M/H_2O	2.0	1.5	110	62	-	38	[50]
8		RaNi	r.t.	$NaClO_4$	2.0	0.5	85	69	-	31	[50]
9		PLP[c]/Pd	r.t.	EE/H_2O[c]	4	-	50	98	-	0	[51]
	(**34**)							(**35**)			
10		PLM[b]/Pt	r.t.	H_2SO_4	104	13.9	1.9[j]	95	-	-	[48]
11		Ni/Fe	r.t.	M/H_2O	5.6	1.8	32	89	-	-	[52]
12		Ni/Fe	r.t.	M/H_2O	1.2	2.6	93	56	-	-	[52]
13		Fe	r.t.	M/H_2O	4	-	47	95	-	-	[49]
14		Fe/Ni	r.t.	M/H_2O	4	-	48	96 -		-	[49]
15		Ni	r.t.	M/H_2O	4	-	45	90 -	-	-	[49]
16		Cu	r.t.	M/H_2O	4	-	48	96 -	-	-	[49]
	(**36**)							(**37**)			
17		Ni/Fe	r.t.	M/H_2O	1.2	2.6	23	14	-	-	[52]
18		Ni/Fe	r.t.	M/H_2O	7.1	1.8	25	90	-	-	[52]
	(**38**)							(**39**)	(**40**)		
19		Pd/Al_2O_3	r.t.	HOAc[g]	3.8	-	68	70	30	-	[53]
	(**41**)							(**42**)	(**43**)		
20		PLM*b*/Pt	r.t.	H_2SO_4	832	21	0.06[j]	25.3	-	-	[48]
21		Fe	r.t.	M/H_2O	6	-	30	90	-	-	[49]
22		Fe/Ni	r.t.	M/H_2O	6	-	32	97	-	-	[49]

Continued on the next page

Table 1.2 (cont'd)

								Yield%			
	S	**Cat.**	**T**	**Solvent**	**Q**	**CD**	**CE%**	**P1**	**P2**	**P3**	**Ref**
23		Ni[d]	r.t.	M/H_2O	4	-	60	52	34	-	49
24		PLV[e]/Pd	r.t.	E/H_2O	9.6	-	10	48	-	-	54
25		PLP/Pd[c]	r.t.	EE/H_2O[h]	4.5	-	2	5.3	-	-	51
	(**44**)							(**45**)			
26		PLV*e*/Pd	r.t.	M/H_2O	2	-	100	100	-	-	54,55
27		PLP/Pd[c]	r.t.	EE/H_2O[h]	2	-	63	63	-	-	51
	(**46**)							(**47**)-(**49**)	(**50**)-(**53**)		
28		RaNi	30	M/H_2O[i]	4.6	-	93	15	66[k]	-	56
29		RaNi	30	M/H_2O	4.6	-	74	21	42[l]	-	56
30		PLP/Ru[f]	r.t.	E/H_2O	-	-	52	0	0	99(**54**)	57

S: substrate. **Cat.**:cathode. **T**: temperature in °C. **Q**: moles of electrons applied per mole of substrates, in F/mol. **CD**: current density in mA/cm^2. **CE**: current efficiency. **M/H_2O**: methanol/water mixture. **E/H_2O**:ethanol water mixture with 0.1 M KCl. **EE/H_2O**: 2-ethoxylethanol water mixture with 0.1 M KCl. **Fe/Ni**: 64:36 alloy.

[a] **PL**: The structure of Poly-(I) is shown in Figure 1.6.

[b] **PLM**: The structure of Poly-Mix(I) is also shown in Figure 1.6.

[c] **PLP/Pd** is a cathode made from coating Poly-P-Pd polymer-Pd complex on a carbon matrix.

[d] micro-particles of Ni dispersed on matrix.

[e] **PLV** is the Poly V^{2+} polymer from the pyran polymerizationwith Poly V^{2+} monomer shown in Figure 1.6 in a fasion similar to that of Poly-P-Pd polymers, at the 2 and 5 position.

[f] **PLP/Ru** is a cathode made from coating Poly-P-Ru polymer-Ru complex on a carbon matrix.

[g] Acetic acid is 0.5 M in ethanol water mixture.

[h] pH = 2 and contains 0.1 M $LiClO_4$.

[i] It contains 5.5 x 10^{-2} M CTAB (cetyltrimethylammonium bromide) with a pH = 5-9.

[j] The CE is not given and is calculated based on the assumption that the whole carbon vitreous plate (45 mm × 26 mm × 15 mm) is plated with polymer and submerged in solution, and the assumption that the resistant of cathode stays constant when the voltage is changed from 1 V to 0.6 a 0.9 V, which lead to a current of 621 mA at 0.6 V and 929 mA at 0.9 V; the substrate was 0.001 mol; reaction times varied from 4.5 h (0.6 V, Q=104 F/mol), 6 h (0.6 V, Q=208 F/mol) to 24 h (0.9 V, Q=832 F/mol).

[k] The ratio of (**50**):(**51**):(**52**):(**53**) = 59:23:9:9.

[l] The ratio of (**50**):(**51**):(**52**):(**53**) = 47:10:17:26.

Although there is not enough data to draw firm conclusions about the ECH reactivity of enones, based on the data available, simple enones ((**30**), (**44**), and (**46**)) are more easily reduced than enones such as (**41**) with sterically demanding groups, and alkyl enones are faster to be reduced than more electron rich aryl ketones and aldehydes ((**34**), (**36**), and

(**38**)).

Different metal catalysts had very similar ECH activity on these substrates. However, when a cathode made from nickel microparticles dispersed in polymer films was used (entry **23**), the current efficiency of ECH on a high sterically hindered (**41**) improved significantly over others (entries **20-22, 24-25**).

1.1.3 Esters

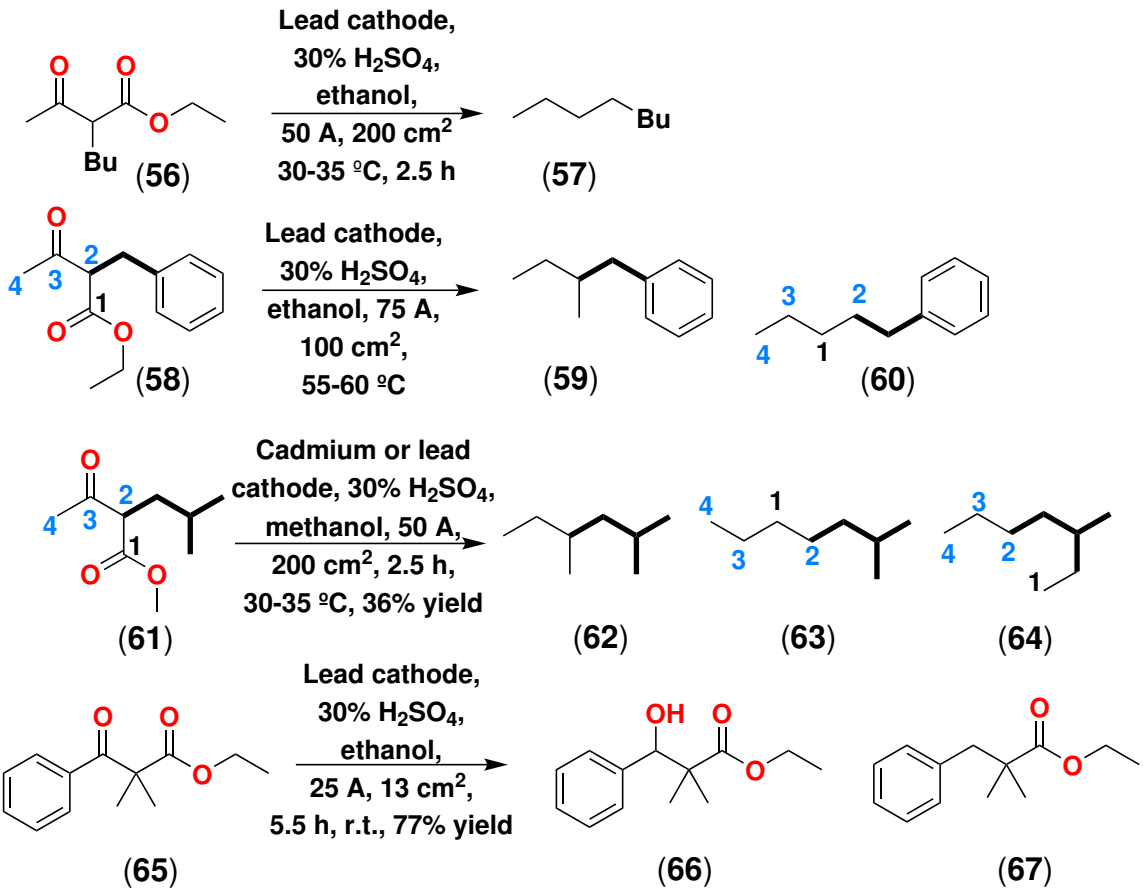

Figure 1.7: ECR of esters under strong acid conditions.

Unlike ketones, the β-keto esters undergoing ECR do not undergo dimerizations presumably because the radicals generated are less reactive due to the stabilization of the intermediate radicals in the enol-carbonyl conjugated system. The ECR of acetoacetate esters was fully investigated by Tafel and the famous Tafel rearrangement was discovered based on these series of experiments.[41,58–62] The production of (**57**) via reduction of (**56**) was suggested by Tafel to follow the same mechanism as from (**58**) to (**60**), and from (**61**) to (**63**): carbonyl carbon 1 was reduced and migrated into between carbon 2 and carbon 3. However, no Tafel rearrangement happened when a aryl β-ketoester (**65**) was treated with

a similar condition, and only the direct reduction products (**66**) and (**67**) were observed.[62]

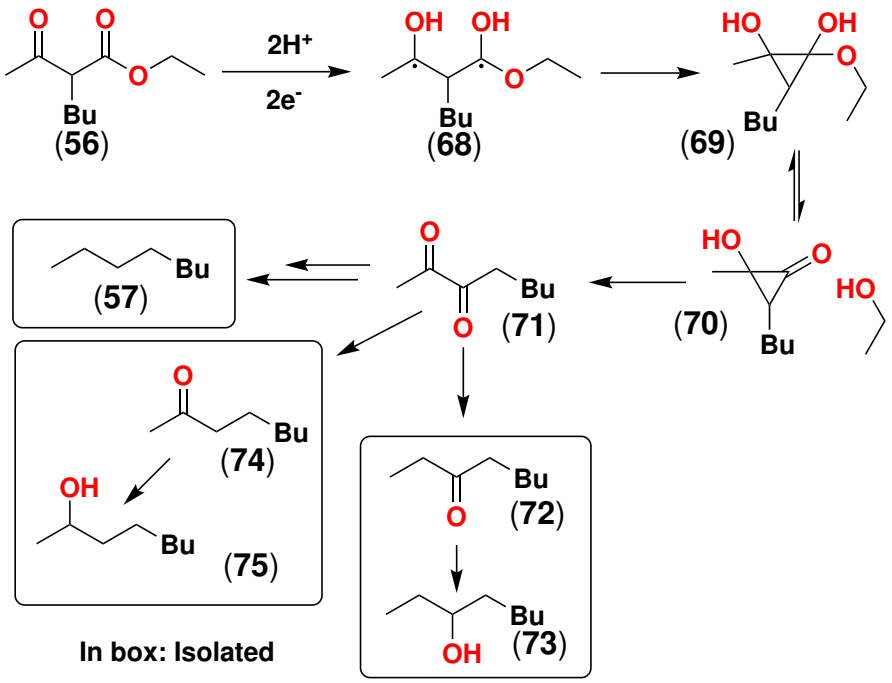

Figure 1.8: The mechanism of Tafel rearrangement reaction.

The mechanism of the Tafel rearrangement was proved to be through a cyclopropane intermediate (**69**) shown in Figure 1.8.[63] Since under non-acid condition no rearrangement products were observed, protonation of carbonyls in (**56**) was the initial step followed by the ECR of activated carbonyls to 1,3-diradical compound (**68**); cyclopropane (**69**) was generated by coupling the two radicals and the hemiacetal (**69**) interconverted with ketone (**70**) and ethanol, which went through a irreversible α-hydroxyketone to 1,2-diketone product (**71**) conversion, and all other products were generated via the reduction of diketone (**71**).[62] Aryl α-ketoester (**65**) does not generate Tafel rearrangment products probably due to the difficulty to form the cyclopropane intermediate considering the benzylic radical is relatively unreactive. This mechanism does not explain the formation of (**64**) from (**61**).

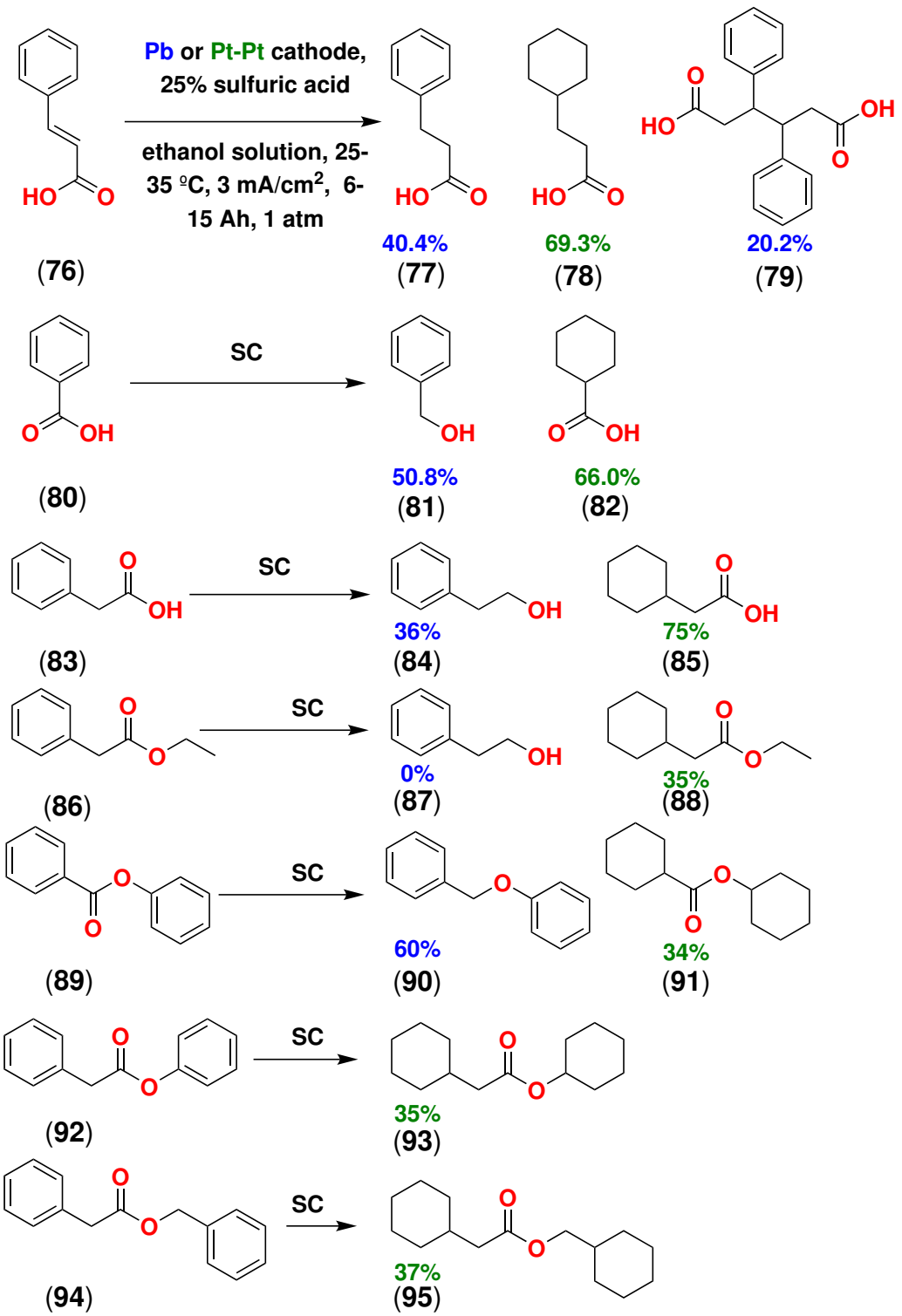

Figure 1.9: ECR and ECH of aromatic ester and carboxylic acid derivatives with lead and platinized platinum cathodes and their yields. The yields for Pb cathode are colored blue and those for Pt-Pt are colored green. **SC** stands for standard conditions: Pb or Pt-Pt cathode, 100 cm^2, 20 °C or 50 °C, H_2SO_4 ethanol solution.

1.1.4 Benzene and benzene derivatives

The ECH and ECR of benzene derivatives that leads to saturation of the benzene ring were observed by Ono with low overpotential platinized-platinum (Pt-Pt) cathode, while the sole reductions of carboxylic acid or ester groups were observed with lead cathodes under similar conditions.[64]

With the Pt-Pt cathode, all substrates (**76**), (**80**), (**83**), (**86**), (**89**), (**92**) and (**94**) follow the same pattern of benzene and olefin saturation. On the other hand, with the Pb cathode, olefin (**76**) undergoes radical dimerization to form (**79**). Regardless of whether the carboxylic acid is conjugated with benzene or not, it can be reduced to alcohol, except in the case of (**89**) and (**90**), the ester formed from phenol and benzyl alcohol, was formed in good yield.

1.1.5 Nitro compounds

ECH or ECR of the nitro-aryl compounds are different from those of alkylbenzene and acylbenzene substrates in that the aniline products are rarely reduced to saturated cyclohexyl amine. As shown in Figure 1.10, the reduction of (**96**) gives the corresponding amino compounds; while (**114**) gives not only aniline, but also azobenzene (**115**) along with reduction products (**103**) and (**116**).[65]

Compound (**97**)'s reduction mechanism was a mechanistic puzzle in organic chemistry. The reduction of nitrobenzene forms (**98**), (**99**) and (**100**); the electrophilic nitrosobenzene (**98**) and the nucleophilic (**99**) react with each other to form (**101**), which is reduced to azobenzene (**102**), the corresponding hydrazobenzene (**103**), and (**104**); for (**104**), the para-position to the amine is unsubstituted and it proceeds further through [5,5] sigmatropic rearrangement to produce (**105**). This step was proved to be concerted by kinetic isotope

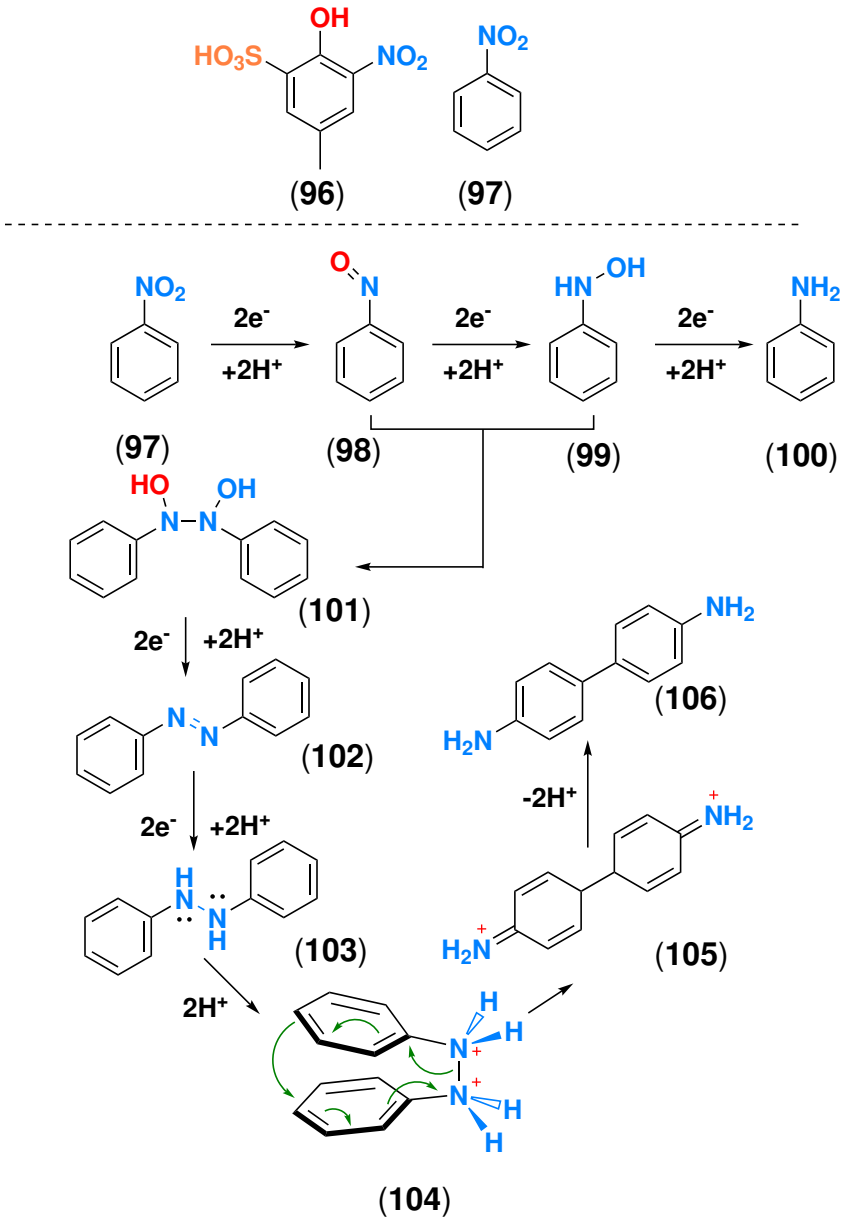

Figure 1.10: The electroreduction reactions patented by Lucius & Brüning in 1940. Original compound names[6] in German are (English translations are in parenthesis): Nitro-*p*-Kresol-*o*-Sulfonat (nitro-*p*-cresol-*o*-sulfonate; the metal ion is not specified, therefore the acid form is drawn)), Nitrobenzol (nitrobenzene), and Azobenzol (azobenzene). The mechanism of azobenzene reduction and rearrangment to benzidine was also investigated in detail in the late 1960s.

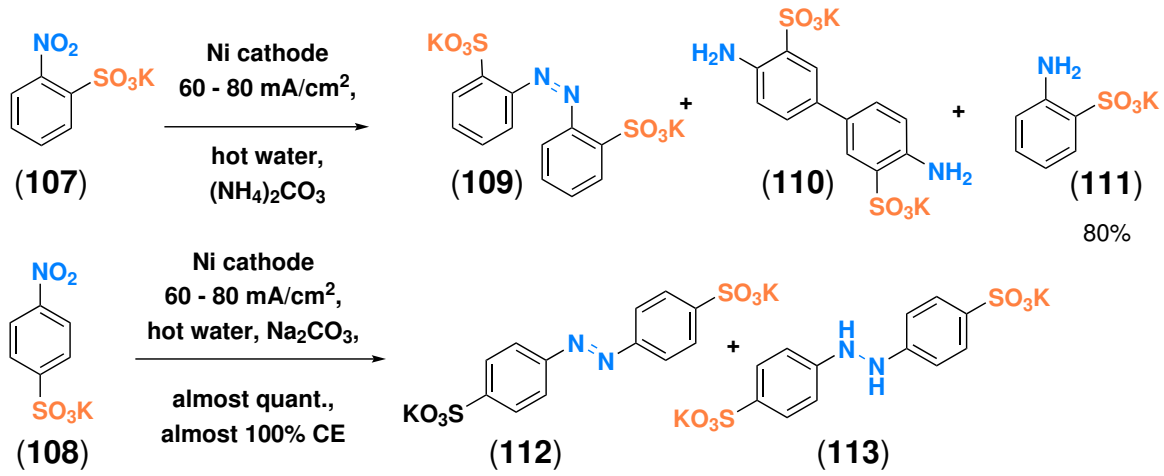

Figure 1.11: ECH of potassium *o*-nitrobenzene sulfonate and *m*-nitrobenzene sulfonate.

effects from deuterium and ^{15}N labeling.[66,67]

In 1902, Elbs conducted ECH on a pair of nitrobenzene sulfonate compounds (**107**) and (**108**), with results indicating that they followed the same mechanism as nitrobenzene reduction via azobenzene intermediates and formed the corresponding hydrazobenzene; the [5,5] sigmatropic rearrangment reaction took place only for (**117**) to form (**110**) since the para-position to the amine is unsubstituted. For ortho compound (**107**), the reduction of (**99**)-type intermediate to the amino-product (**111**) was fast, and a 80% yield of (**111**) was observed with a small amount of dimer product(**110**). For para compound (**108**), pure azo(**112**) was obtained when the solution was hot (no temperature reported); when the temperature was raised to boil the water solution, pure (**113**) was obtained.[46]

1.1.6 Nitriles

ECR of Acetonitrile under both acidic and basic condition with platinum cathode was studied by Ahrens who found that acidic conditions are much more efficient than basic for the reduction of acetonitrile. But among the acidic conditions, more concentrate sulfuric acid

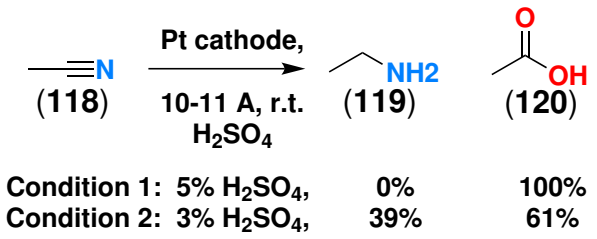

Figure 1.12: ECR of acetonitrile.

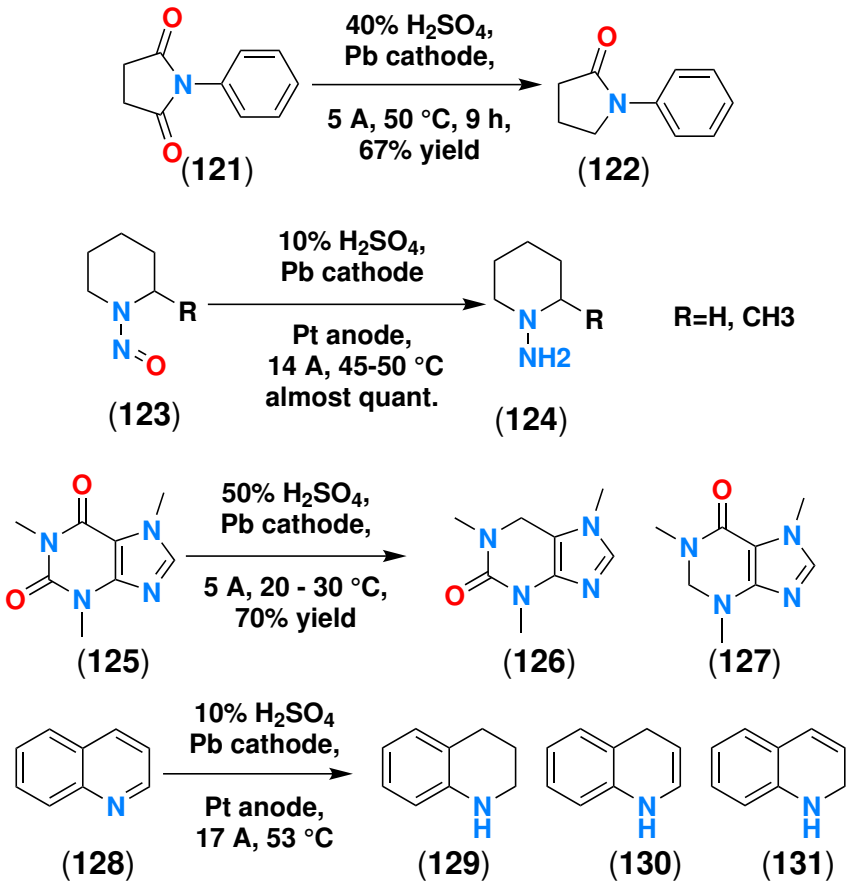

Figure 1.13: ECR of heterocycles: phenylpyrrolidone, nitrosopiperidine, caffeine, and quinoline with lead cathode and platinum anode.

solution led to the full hydrolysis of acetonitrile to ammonia and acetic acid, and under less concentrate solutions, some ethyl amine was generated. No other products were reported.[68]

1.1.7 Heterocycles

Heterocyclic compounds were also studied by lead cathode and platinum anode under strong acid conditions. Amide (**121**) and (**125**) can be hydrogenated to the deoxygenated amine presumably through the reduction of α-amino alcohol and iminium intermediates.[69] The benzene ring remains intact during the hydrogenation. Nitrosoamine (**123**) can go through a similar pathway to get to hydrazine (**124**).[70] Non-cyclic amide compounds follow similar reduction pathways as these cyclic heterocycles, for instance, benzamide was reduced to benzyl amine.[69]

The more polarized pyridine ring of protonated quinoline (**128**) was hydrogenated through non-selectively at either carbon 4 to get (**130**) or carbon 2 to get (**131**), and fully reduced product (**129**).[70]

1.1.8 Sulfur compounds

It is well known that sulfide compounds can poison many catalysts including Pt, Rh, Pd, Raney nickel etc by forming surface metal-sulfide.[71,72] The reduction of disulfide compounds to thiols can be realized by using a low over-potential cathode such as platinum in acid medium, and it is also possible with a high over-potential cathode like mercury in basic medium. Homocystine (**132**) can be reduced to homocysteine (**133**) successfully with quantitative conversion under the condition shown in Figure 1.14; the homocysteine HCl salt was isolated with 52.5% yield.[73] The aryl-aryl disulfide (**134**) was easily reduced to the

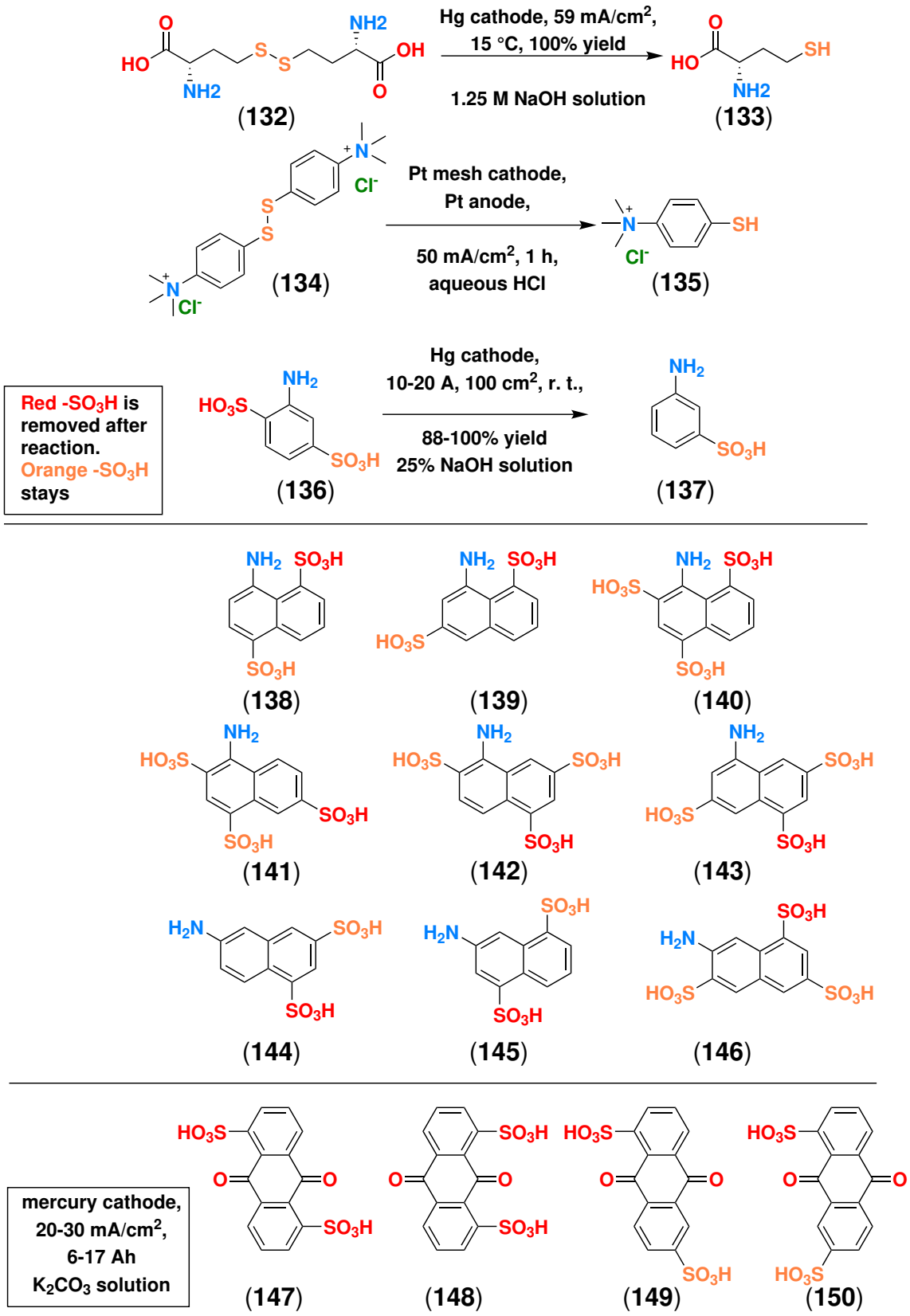

Figure 1.14: ECR of sulfur compounds: disulfides and aryl-sulfonic acids.

(**135**).[74]

Traditionally, sulfonyl groups can be removed for arene rings by acidic hydrolysis under heating, and the sulfonyl groups ortho or para to the amino group can be removed in this way. Via ECR, a similar desulfonylation was observed to convert (**136**) to (**137**) on a high over-potential mercury cathode under room temperature; for polysulfonyl naphthylamine, the sulfonyls on the non-activated benzene ring, in most cases, were preferably removed.[75] In contrast, as in Figure 1.11, with a low over-potential cathode nickel, no desulfonylation of (**111**) was observed under basic condition.

The desulfonylation of anthraquinone sulfonates showed that the α-position (C1, 4, 5, 8 positions of anthraquinone) sulfonyls were selectively removed with little removal of the β-sulfonyl under slightly basic conditions at mercury cathodes. One of the two carbonyls of anthraquinone can be reduced to alcohol, while it was quickly oxidized back to a carbonyl in the presence of oxygen under basic conditions.[76] However, it is unclear about the fate of sulfonyl groups after reduction.

1.2 Application of ECH or ECR to sugar and sugar derivatives

1.2.1 Sugar monomers, and cellulose and hemicellulose depolymerized products

Nowadays reduced sugars are important industrial products stemming from the growing need for food with diminished calorie values, and for sweeteners that are well tolerated by healthy people and diabetics.[77] The production of reduced sugars have been patented in early 20 century.

Hexoses were successfully converted to reduced products on a commercial scale with an electrochemical process by the Atlas Power company located at Delaware in 1934. The cathode material was mercury or amalgamated lead; it was found that glucose and fructose were reduced to sorbitol and mannose was reduced to mannitol.[78,79] Different metal cations in the catholyte were found to differentially affect the reduced glucose yields; for example, even ppm levels of magnesium ion inhibited strongly[80] while sodium sulfate did not inhibit the reduction of glucose,[79] and zinc sulfate was shown to markedly increase the reduction efficiency at an amalgamated lead cathode, presumably Hg/Pb amalgam.[81]

It is important to realize that the reducible forms of sugar are neither the hemiacetal (sugar closed chain ring structure), nor the ketose formed by Lobry de Bruyn transformation (keto-enol tautomerization), but either the free aldehyde, for instance, open chain structure of glucose, or its equivalent hydrate. The concentration of reducible form can be influenced by pH, temperature, the concentration of sugar, etc. A comprehensive study on this subject can be found by Sidney M. Cantor and Quintin P. Peniston.[82]

1.2.1.1 Glucose

Table 1.3: The yields of different glucose reduction products under various conditions.

Cathode	**Solution**	**Time**	**Yields**		**C.E.%**
	g(NaOH)/L	**hour**	**D-sorbitol**	**D-mannitol**	
Zn(Hg)	0.5-1.5	93	99%	0%	50.2
Zn(Hg)	10-20	164	83.1%	15.9%	43.4
Pb(Hg)	0.5-1.5	182	99%	0%	24.3
Pb(Hg)	0.5-1.5 + 2 g/L $ZnSO_4$	113	99%	0%	39.9
Pb(Hg)	10-20	154	85%	14%	47.0
	g(H_2SO_4)/L				
Zn(Hg)	0.5-1.5	104	99%	0%	41.9
Pb(Hg)	0.5-1.5	200	87%	0%	26.8

Reactions were conducted at 68-70 °C, current density 1.0 A/cm^2 with 325 g/L concentration glucose. 10-20 g(NaOH)/L entries have solution volume of about 1.7 time that of 0.5-1.5 concentration cases.

As shown in Table 1.3, glucose was mainly reduced to D-sorbitol by a simple hydrogenation of the C-1 aldehyde, but can also be reduced to mixtures of sorbitol and mannitol in strong basic condition. Presumably, the keto-enol tautomerization was enhanced by strong basic condition, leading to the epimerization at C-2. Zinc amalgam is better than lead amalgam as cathodes for glucose ECR reactions proved by the higher C.E. (current efficiency) of Zn(Hg) entries at both acid and base conditions and indicated by the phenomenon that, in entry **4**, 2 g/L $ZnSO_4$ enhanced the C.E. of Pb(Hg) cathode ECR reaction. The current efficiencies are normally less than 50% except in 0.5-1.5 g(NaOH)/L solution with Zn(Hg) cathode. Generally speaking, basic condition is more efficient than acidic conditions.[79]

Wolfrom studied the electro-reduction products of glucose under mild alkaline condition (pH=7-10) at below 30 °C, and this study standardized the commercial process for the Atlas Power company. He found that the products consisted of sorbitol together with 1% of D-mannitol (2-epi sorbitol) (**154**), 5% of 2-deoxy-sorbitol (**153**), very small amount of

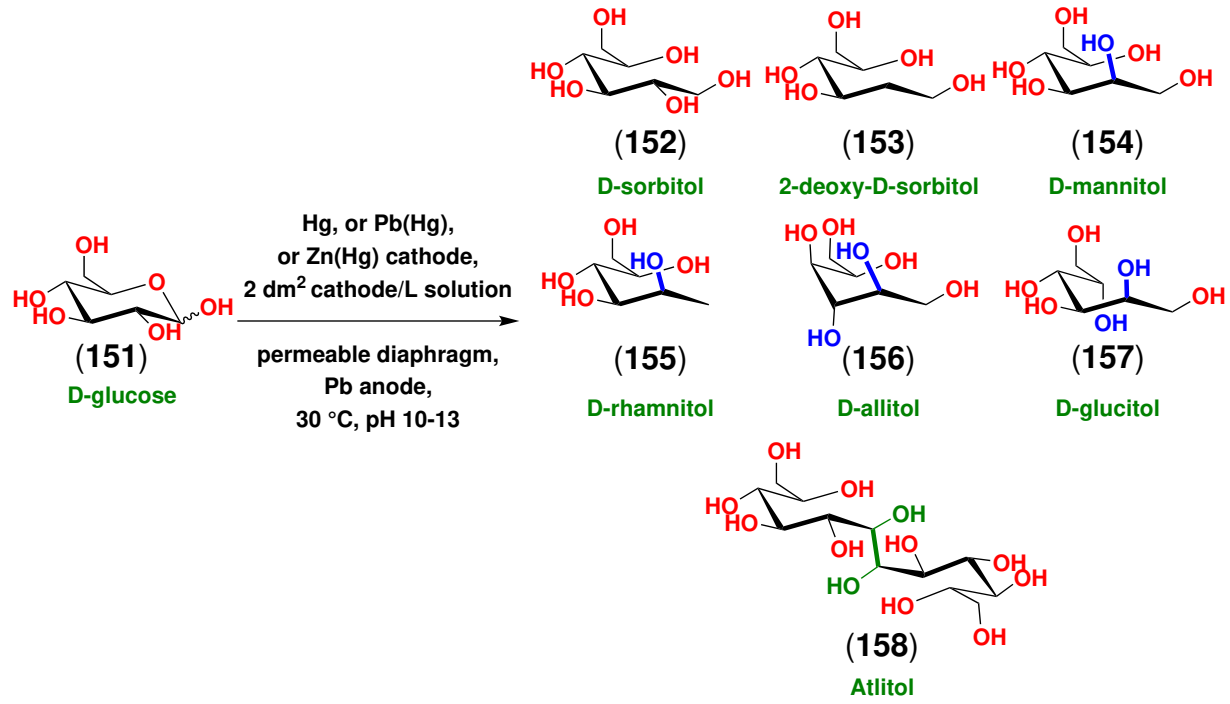

Proposed mechanisms for the formation of main products from alkaline electroreduction of D-glucose

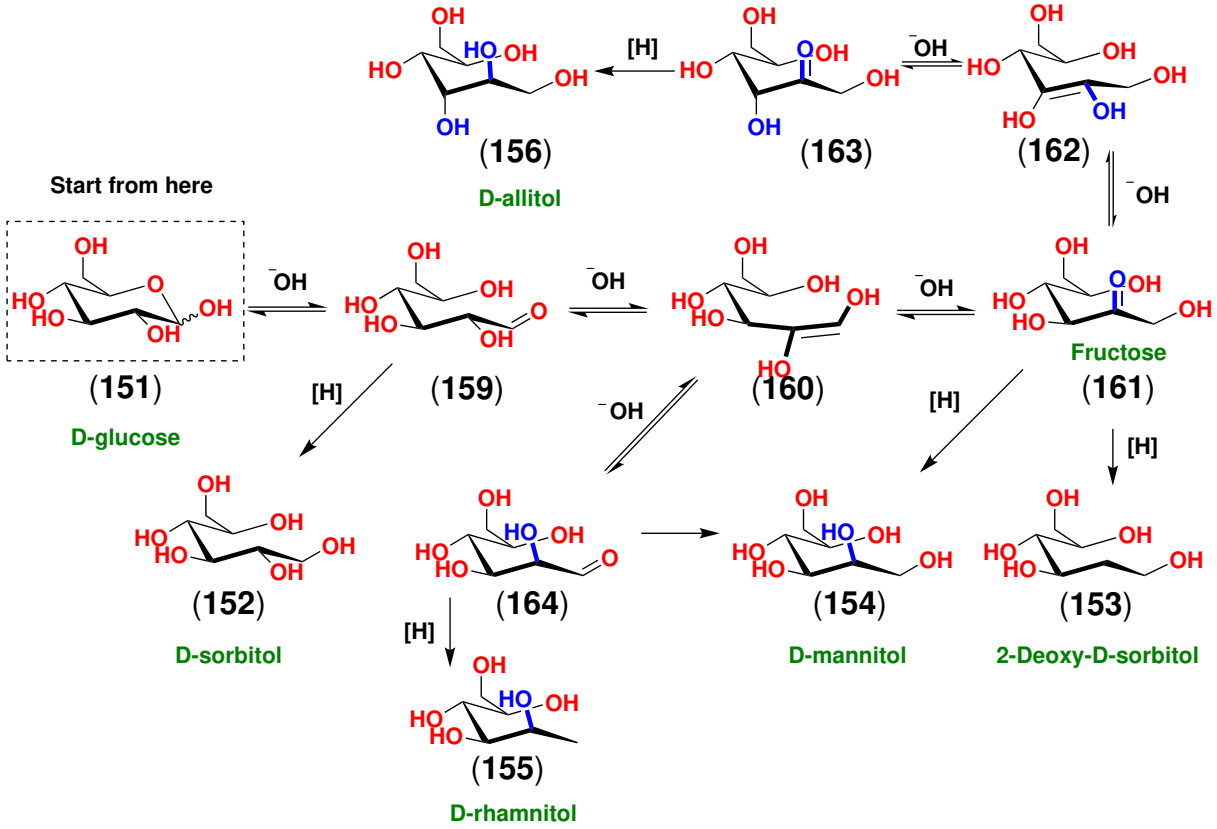

Figure 1.15: The products of ECR of glucose and proposed mechanisms by Wolfrom. Blue bonds means reversed chirality relative to D-glucose and green bonds means undetermined chirality.[7–11]

D-rhamnitol (1-deoxy-mannitol)(**155**), D-allitol (2,3-epi sorbitol) (**156**), D-glucitol (2,5-epi sorbitol) (**157**) and dimerization product atlitol (**158**). The formation of (**155**) can be attributed to the tautomerization of C-1 aldehyde of glucose lead to the reverse of C-2 chirality as shown by the conversion of (**160**) to (**164**) followed by the reduction of aldehyde to alkane. The formation of D-allitol (**156**) follows a similar ketone to endiol tautomerization mechanism through intermediates of (**161**) (**162**), and (**163**). Glucitol (**157**) is possibly formed by C-5 carbonyl formation on the surface of cathode following a reduction reversing the stereochemistry of C-5. Atlitol was believed to be formed by radical coupling reactions through ECR of two C-1 aldehyde sites in the open chain structure of glucose.[7–11]

Table 1.4: ECH or ECR of glucose to sorbitol at various metal cathodes.

Cathode	**Current Efficiency**
Hg + NaHg	69.0%
Amalgamated Pb	60.0-68.0%
Pb sheet	62%
Tl	59-47%
Cd	53-47%
Zn	55%
Bi	43%
Ag 1st run	38.5%
Ag 2nd run	6-12%
Au	34.5%
Cu, Fe[a]	11-13%
Ni, W, Mo, Co, Sn, Pt, Cr, Mg[a]	<10%

The reaction was conducted in a divided cell with 2 A/dm^2 current density at 30-31 °C in 100 mL of 0.5M NaOH, 7.5% Na_2SO_4, 20% sugar solution.

[a] these cathodes were made separately with only one type metal each time, and the current efficiency represents that of each single metal cathode reaction.

The ECH or ECR of glucose was also investigated with various metal cathodes as shown in Table 1.4.[78] The most active groups of metals were those which have a close relationship with mercury in the periodical table and the further removed it is from mercury, the less

active it is. The most active cathode was sodium amalgamated with mercury. The author mentioned that the use of alkaline solution (NaOH and Na_2SO_4) instead of acidic solutions greatly improved the rate of reduction. The second most active group of metals was composed of elements to the left of mercury in the periodic table. However, in the cases of both Au and Ag cathodes, after the first run, the cathodes were heavily etched and the subsequent experiments gave poor results. Current efficiency less than 13% took place at the other metals.[78]

Table 1.5: ECH of glucose to sorbitol with Raney Nickel (RaNi) cathode study: concentration, current density, and pulsed current of a flow system.

	Conc. M.	Current mA	C.D. mA/cm^2	t_h s	t_l s	Freq. s^{-1}	C.E. %
1	0.4	125	5.3	-	-	-	100
2	1.6	250	10.5	-	-	-	100
3	1.6	500	21.0	-	-	-	79
4	0.8	200	8.4	-	-	-	90
5	0.8	250	10.5	-	-	-	74
			Pulse Current Studies				
6	-	-	35.2	1.50	3.50	0.2	75
7	-	-	35.2	0.60	1.40	0.5	82
8	-	-	35.2	0.30	0.70	1.0	93
9	-	-	35.2	0.15	0.35	2.0	94
10	-	-	35.2	0.03	0.07	10.0	95

t_h: Time intervals of high-current
t_l: Time intervals of low-current
Freq.: Pulsing frequency = $1/(t_h+t_l)$
Reaction conditions: 333 K, 23.7 cm^2 cathode area, RaNi catalyst loading 10 g, pH=7 solution, electrolyte velocity is 0.064 cm/s.
C.E.: Current efficiency

Raney Nickel catalyst behaves differently than plain nickel catalyst. In contrast to the less than 10% current efficiency from nickel catalyst as in Table 1.4., the much more porous Raney Nickel catalyst reduces glucose with current efficiencies upto 100% as shown in Table 1.5. Perfect current efficiency can be achieved with adjusted amount of glucose and an appropriate

current density; in general, a lower current density at the same glucose concentration leads to higher current efficiency.

For a flow system, the current efficiency can be improved by using pulsed currents. As shown in Table 1.4, at a relatively high current density, the higher the pulse frequency is, the better the current efficiency.

Although Table 1.6 does not show a ECH study, we can still learn how other metals affect RaNi catalyst hydrogenation of glucose, and presumably, this phenomenon can be extrapolate to the ECH of glucose. Cr, Mo, Fe, and Sn improved the activities of catalyst by acting as a Lewis-acid adsorption sites for the oxygen of carbonyl group polarizing the carbonyl so that it is more electrophilic and therefore easier to reduce. High homogeneity of promoter in the catalyst is required for the best catalytic activities (see entries **3&5, 7&8**). On the other hand, the addition of Fe and Sn destabilized the RaNi catalyst proved by the rapid decreased rates after several recyclings in successive hydrogenation experiments; while Mo and Cr destabilized the catalyst slightly and the catalysts were still more active than RaNi after 5 recycles.[1]

Table 1.6: Hydrogenation of glucose at Raney Nickel (RaNi) cathode and metal-promoted RaNi cathodes.[1]

				Initial Rates of Repeated Batches						
		Ni:Al:M	**Metal Area**	1		2	3	4	5	
	Catalysts	**ratio**	m^2/g	a	b	a	a	a	a	b
1	RaNi	91:9	106	68	0.88	68	68	56	50	0.78
2	RaNi-Cr1	82:10:1	-	350	-	300	293	287	250	-
3	RaNi-Cr2	83:14:2	146	375	3.75	350	318	293	275	3.90
4	RaNi-Cr3	70:17:7	-	84	-	58	36	-	-	-
5	RaNi-Cr2[c]	82:11:2	-	350	-	331	318	293	-	-
6	RaNi-Mo1	83:11:0.6	-	243	-	206	187	175	156	-
7	RaNi-Mo2	84:12:1.2	113	262	3.15	237	231	187	175	2.97
8	RaNi-Mo2[c]	88:9:1.3	-	431	-	281	225	218	212	-
9	RInd[d]	-	-	231	-	181	156	137	125	-
10	RaNi-Fe1	82:13:5	-	106	1.23	93	68	62	60	0.92
11	RaNi-Fe2	74:13:8	-	287	3.19	187	125	106	88	-
12	RaNi-Fe3	70:15:12	-	575	5.92	312	181	143	113	1.51
13	RaNi-Fe4	63:15:16	-	406	5.07	262	150	131	119	-
14	RaNi-Sn1	83:9:3	91	213	3.38	112	51	-	-	-
15	RaNi-Sn2	81:8:5	41	289	4.13	144	48	-	-	-
16	RaNi-Sn3	78:8:9	29	349	6.58	121	22	-	-	-

[a] mmol/h/g

[b] $mmol/h/m^2$

[c] Derived from precursor alloys annealed at 1223 K for 3 weeks to improve further the homogeneity of the solid solution of metal M in the Ni_2Al_3 lattice.

[d] Commercial catalyst containing molybdenum.

1.2.1.2 Furans

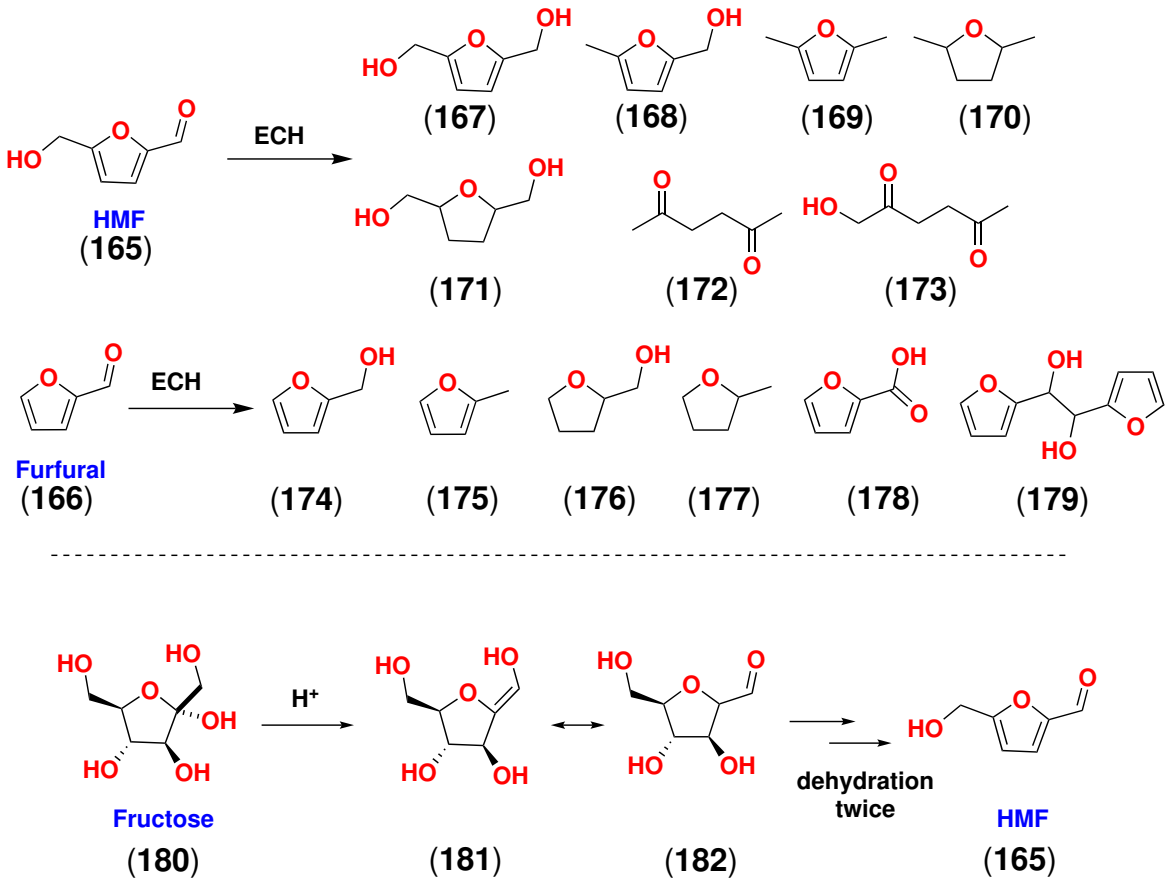

Figure 1.16: ECH of furanic compounds and the mechanism of HMF formation from fructose.

Hydroxymethylfurfural (HMF) (**165**) is the double dehydration product of fructose (**180**) as shown in Figure 1.16, which can be generated from glucose, the hydrolysis product of cellulose. Furfural is a C5 platform chemical which can be obtained from hydrolysis and dehydration of hemicellulose.[83] The ECH of these two substrates have been studied with different catalyst recently.[83–88]

For the ECH of HMF, the Zn cathode was found to be the most active one to reduce HMF to diketone (**172**) with a high current efficiency of 72.4% (entry **1** of Table 1.7). Cu produced higher yields of 2,5-Bis(hydroxymethyl)furan (**167**), and Ag was the best catalyst for production of (**167**). However, these studies (entry **1-5**) only explored the short time

Table 1.7: ECH of HMF and furfural.

								Yield%				
	S	**Cat.**	**T**	**Solvent**	**Q**	**CD**	**CE%**	**Pdt1**	**Pdt2**	**Pdt3**	**Other**	**Ref**
								(**172**)	(**167**)	(**173**)		
1	(**165**)	Zn	r.t.	sulfate	0.74	14.4	72.4	8.9	0.3	1	-	[86]
2	(**165**)	Cu	r.t.	sulfate	0.74	39.6	13.6	0.5	2.3	0.7	-	[86]
3	(**165**)	Au	r.t.	sulfate	0.74	50.1	8.9	0.3	1.8	0.3	-	[86]
4	(**165**)	Pt	r.t.	sulfate	0.74	57.4	4.8	0	1.8	0	-	[86]
5	(**165**)	Ag	r.t.	borate	0.74	6.9	99	-	36	-	-	[87]
								(**174**)	(**175**)	(**178**)	(**179**)	
6	(**166**)	Ni	r.t.	pH 5[a]	-	6	56	63	3.3	-	-	[88]
7	(**166**)	Ni	r.t.	pH 1[a]	-	6	39	39	6.4	-	-	[88]
8	(**166**)	Cu	r.t.	NH_4Cl[b]	4	10	12.5	23	1	-	-	[83]
9	(**166**)	Cu	r.t.	H_2SO_4[b]	4	10	34	8	30	-	-	[83]
10	(**166**)	Cu	8	H_2SO_4[b]	-	10	-	10	80	-	-	[84]
11	(**166**)	Ni	8.	H_2SO_4[b]	-	10	-	31	30	25	13	[84]
12	(**166**)	Pt	8	H_2SO_4[b]	-	10	-	58	20	-	-	[84]
13	(**166**)	C	8	H_2SO_4[b]	-	10	-	8	7	15	70	[84]
									(**175**)	(**176**)	(**177**)	
14	(**166**)	Pd/C	30	H_2SO_4[b]	-	10	25	-	17	13	3	[85]

S is substrate, the starting material. **Cat.** is catalyst. **T** is temperature in °C. **Q** is the moles of electrons applied per mole of substrates, in units of F/mol. **CD** is current density in units of mA/cm^2. **CE** is current efficiency. **Sulfate buffer** had pH = 2, **borate** had pH = 9. All of the **H_2SO_4** solutions listed were 0.5 M.

[b] Contents of acetonitrile 20% for entries **8** and **9**, and 30% for entry **10**.

[a] 0.2 M NH_4Cl in 50 mL water + methanol (4:1, V/V).

reactivities of these cathodes; no attempts for reports of the current efficiency under higher conversions for synthetic purposes.

ECH of furfural was studied with various cathodes (entries **6-14**) and in a flow system (entry **14**). Cu was found to be the catalyst most favorable for the formation of (**175**) without any ECR radical reactions to produce (**179**). It was quite surprising that Ni (entry **11**), similar to C (entry **13**), produced a significant amount of (**179**) and even some oxidation product (**178**), which was explained by the author as resulting from furfural migration to the anode side and where it got oxidized.

Pd/C was found to be the best aromatic ring hydrogenation catalyst, and it was the only one to produce fully hydrogenated furans (**176**) and (**177**). Although not studied in detail to improve the synthetic efficacies of the catalysts, these initial studies showed that the order of activity for the aqueous phase hydrogenation of furfuryl alcohol followed: Pd > Ni > Ru > Rh = Pt (at 80 °C, 800 psi for 3 hours with 4.8 wt% furfuryl alcohol solution).[85]

In summary, for the purpose of fuel production, Zn must be considered the best cathode for the reduction of HMF since the main product (**172**) can be easily reduced to hexane by Pd/C hydrogenation[89] or other ECH processes for ketones. For ECH of furfural, Ni had the best current efficiency of the metals reviewed, however, Pd/C cathode showed excellent aromatic ring reduction capability in the flow system. For full deoxygenation, one concern would be that THF derivative products are very difficult to hydrogenate to alkanes.[89] If a catalyst can induce the ring opening of furfural reduction intermediates to form the 1,4-diketone from furfural, synthesis of alkanes from furfural by mild ECH would be much closer to reality.

1.3 Prior ECH or ECR studies of lignin and lignin model compounds

1.3.1 Phenol

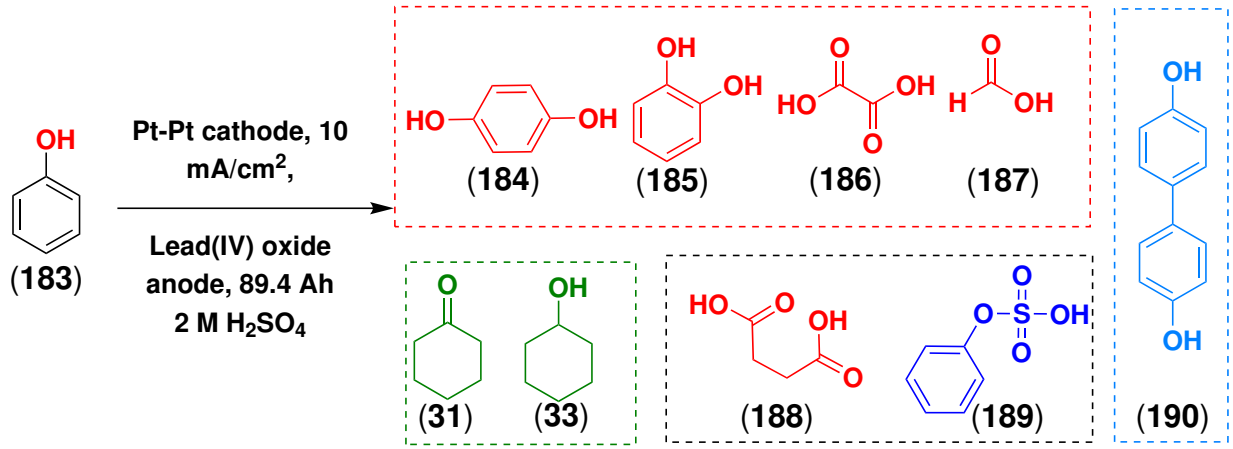

Figure 1.17: ECH of phenol showing both oxidation and reduction products from cathodic and anodic processes.

Phenol is the smallest model of lignin reflecting its water solubility under a basic condition. It has been studied extensively since the early 20th century. Bancroft and George reported that phenol is not at all practically electro-reduced by either a lead or mercury cathodes, but well reduced to cyclohexanol at a platinized platinum cathode. They pointed out that the catalytic effect of platinum is evidently more important than the reducing power of hydrogen.[36,90]

In early studies, one of the problems for ECH of phenol with Pt-Pt (Platinized Platinum) is that anodic oxidation products coexist with the reduction products due to the limitation of one compartment cell setup. As shown in Figure 1.17, the ECH of phenol to cyclohexanone (**31**) and cyclohexanol (**33**), was accompanied by the anodic oxidation of phenol to several oxidized products (**184**), (**185**), (**186**) and (**187**), including the ring opened succinic acid

(**188**), the sulfate ester product (**189**) and the radical coupling product (**190**) making the ECH of phenol in an open cell impractical.[91,92] Therefore, learning from history, all of our ECH reaction of phenolic compounds are conducted in a two compartment cell to avoid the formation of complicated oxidation and coupling products.

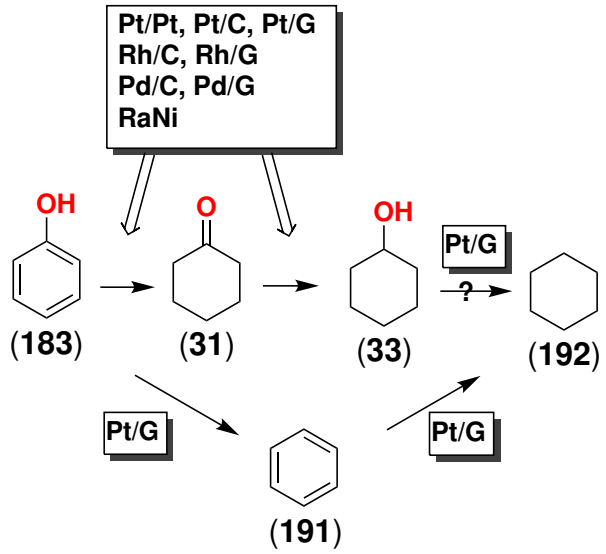

Figure 1.18: ECH of phenol. G in the figure stands for graphite.

ECH of phenol had been extensively studied with different hydrogenating metal catalyst on different supports. As shown in Figure 1.18 and Table 1.8, phenol can be reduced to cyclohexanol by ECH quite efficiently but not at all by ECR with mercury or spongy lead cathodes (Table 1.8 entries **2** and **3**).

It was reported that a Pt cathode is not able to reduce phenol (entry **11**), however, platinized platinum (Pt-Pt) cathodes do successfully reduce phenol to cyclohexanol and small amount of cyclohexane in 22 - 79% current efficiency (entries **1, 5, 20, 21, 22**).

Compared with Pt-Pt, Rh is even more efficient (entries **4, 7, 9, 13, 24**); when Rh/C was used with sulfuric acid at room temperature, the reaction had the highest current efficiency of all reviewed reactions (entry **7**).

Table 1.8: ECH of phenol with various catalysts and different conditions.

	Catalyst	Solvent	T (°C)	CD	Q	CE%	CH-ol%	Other%	Ref
1	Pt-Pt	2 M H_2SO_4	37	3.6	-	30	near pure	-	[36]
2	Spongy Pb	2 M H_2SO_4	37	3.6	-	0	0	-	[36]
3	Hg	2 M H_2SO_4	-	-	-	0	0	-	[36]
4	Rh/C	H_2O/NaOAc	23	-	-	-	near 100	-	[93]
5	Pt-Pt	0.2 M H_2SO_4	r.t.	1.5	6	22	17	7[a]	[94]
6	Pt/C	0.2 M H_2SO_4	r.t.	11.8	6	47	43	6[a]	[94]
7	Rh/C	0.2 M H_2SO_4	r.t.	11.8	6	84	74	15[a]	[94]
8	Pd/C	0.2 M H_2SO_4	65	2.9	6	15	5	15[a]	[94]
9	Rh/C	AcOH pH 5	25	-	11	55	100	0[a]	[95]
10	Pt/C	AcOH pH 5	25	-	28	19[e]	70	30[a]	[95]
11	Pt	0.1 M H_2SO_4	25	3.2	12	0	0	0[a]	[96]
12	Ni/G	0.1 M H_2SO_4	25	3.2	12	0	0	0[a]	[96]
13	Rh/G	0.1 M H_2SO_4	25	3.2	12	41	65.7	24.3 [a]	[96]
14	Pd/G	0.1 M H_2SO_4	25	3.2	12	8	12.6	5.4 [a]	[96]
15	1.5% Pt/G	0.1 M H_2SO_4	25	3.2	12	52	58.9	5.7[a] 30.4[b]	[96]
16	2% Pt/G	0.1 M H_2SO_4	25	3.2	12	43	60.3	9[a], 13.4[b], 7.2[c]	[96]
17	RaNi	0.04 M HCl 9 mM DDAB	30	1.5-2	6	20	42	0	[97]
18	RaNi	0.04 M HCl 0.2 mM DDAB	30	1.5-2	6	77	79	0	[97]
19	RaNi	0.04 M HCl 0 mM DDAB	30	1.5-2	6	27	30	0	[97]
20	Pt-Pt	2 M $HClO_4$ 5 mM TEAB	r.t.	12.7	-	68	-	-	[98]
21	Pt-Pt	2 M $HClO_4$ 0.1 mM TEAB	r.t.	12.7	-	77	-	-	[98]
22	Pt-Pt	2 M $HClO_4$ 0 mM TEAB	r.t.	12.7	-	79	-	-	[98]
23[d]	Pt	AcOH	20	with H_2	-	-	some	40[b]	[99]
24	Rh/C	NaOAc pH 5	18	0.11	-	68	100	0 [a]	[100]
25	RaNi	1 M NaOH	50	-	18	11	33	-	[101]

CD is current density in mA/cm^2. **Q** is in units of F/mol. **CE** is current efficiency. **CH-ol** is cyclohexanol. **NaOAc** is sodium acetate. **AcOH** is acetic acid. **Pt/G** is Platinum on Graphite.

[a] is for the yield of cyclohexanone.

[b] is for the yield of cyclohexane

[c] is the yield of benzene.

[d] is the reduction of phenol at 1 atm H_2 gas in acetic acid with Pt at 20 °.

[e] Adjusted number based on Fig. 9 in the original paper since the CE contradicted between values in Table 4 and what had been shown in Fig. 9.

Graphite was also used as a support instead of the commonly used carbon black (entries **12 - 16**). The resulting Pt/G catalysts (entries **15, 16**), remarkably, deoxygenated phenol directly to benzene, and cyclohexane was observed from ECH of phenol for the first time.[96] It was not known if the cyclohexane was formed via cyclohexanol or benzene, but benzene was known to be reduced to cyclohexane under ECH on Pt cathode.[102,103] It is noteworthy that in early 1912, 40% of phenol was reduced to cyclohexane with platinum in acetic acid with hydrogen gas (entry **23**).

Tetraalkylammonium halide salts were studied to probe their influence on ECH reactions with phenol (entries **17 - 22**). However, it is still not clear whether tetraalkylammonium halides benefit current efficiency. One thing clear is that at high concentration, it inhibit ECH reactions, while at low concentration, it may benefit ECH reactions. In one study,[97] DDAB (Didodecyldimethylammonium bromide) was used along with the ECH of phenol on a RaNi cathode, and low concentrations of DDAB were found to increase the current efficiency from 27% to 77% (entries **17-19**). On the other hand, another group reported that both lower and higher concentrations of TEAB (Tetraethylammonium bromide) decreased the current efficiency of phenol ECH reactions with the Pt-Pt cathode (entries **20-22**) and the reaction current efficiencies varied greatly among replicates in these reactions.[98]

In summary, Rh/C gave the best current efficiency for the hydrogenation of phenol, while RaNi, Pt-Pt were also good catalysts with over 77% current efficiencies. Pd/C or Pd/G were not effective catalysts and Pb, Hg, Pt, and Ni/C did not reduce the aromatic ring of phenol at all. Rh/C and Pd/C produced significant amounts of cyclohexanone, but only Pt/G cathode experiments observed cyclohexane production, and RaNi did not produce cyclohexanone product. Tetraalkylammonum surfactants did not perform consistently on assisting ECH reactions at lower concentrations, while they inhibited ECH on high concentrations.

1.3.2 Cresol

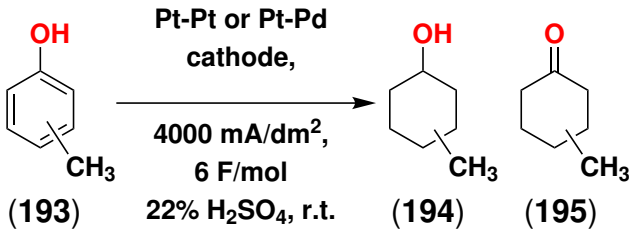

Figure 1.19: ECH of ortho-, meta-, and para-cresol.

Table 1.9: ECH of cresols with various catalysts and different conditions.

						Yield%		
	Compound	**Cathode**	**CD**	**Q**	**CE%**	**(194)**	**(195)**	**Ref**
1	o-cresol	Pt-Pt	40	6	30	22.5	11.0	104
2		Pt-Pd	40	6	21	11.3	13.8	104
3		Rh/C	14.7	6	62	42	30	94
4		Rh/C	11.8	10.8	46	83[a]	0	94
5	m-cresol	Pt-Pt	40	6	34	20.5	20.5	104
6		Pt-Pd	40	6	24	6.5	26.4	104
7	p-cresol	Pt-Pt	40	6	21	15.6	8.7	104
8		Pt-Pd	40	6	34	16.0	27.0	104
9		Rh/C	0.05	-	31	38	58	100

[a] cis:trans=7:3. **CD**: current density in mA/cm^2. **Q** is in unit of F/mol. Entry **3, 4** was conducted in 0.2 M H_2SO_4 solution.

Three cresol isomers, ortho-cresol (o-cresol), meta-cresol (m-cresol), and para-cresol (p-cresol) were electrocatalytically hydrogenated with Pt-Pt cathodes under the exact same conditions.[104] Table 1.9 (entries **1, 2, 5, 6, 7, 8**) shows that m-cresol is the most reactive of these substrates, implying that the methyl group positions influence the oriented adsorption of cresol molecule on the electrode surface. With a Pt-Pd cathode (a mixed deposit of platinum and palladium in equal proportions), para-cresol becomes the most reactive subtract and an increase of ketone product (**195**) was observed in all three cases.

Rh/C cathodes (entries **3, 4, and 9**) reduced cresols to higher yields of methyl cyclohexanols (**194**) and methyl cyclohexanone (**195**), with higher current efficiencies in most cases according to Table 1.9. This is another case that shows the powerful aromatic ring saturation ability of Rh catalysts. With extra currents, o-cresol can be reduced up to 83% yield. Overall, by comparing entries **3, 4,** and **9**, it is clear that a higher CD led to a higher CE of the hydrogenation on Rh/C.[94]

1.3.3 Anisole

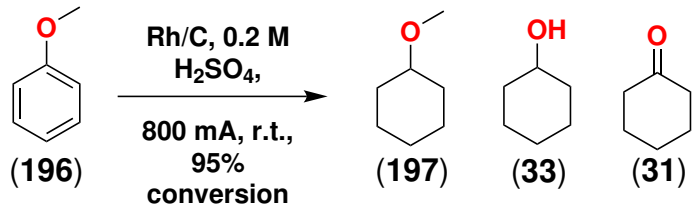

Figure 1.20: ECH of anisole.

Anisole, also called methoxybenzene, has very limited solubility in water, so not much aqueous ECH has been conducted on it. One study showed that with Rh/C catalyst, anisole can be reduced by ECH in 0.2 M H_2SO_4 aqueous solution, producing 54% methoxycyclohexane (**197**) with 6 F/mol amount of electricity; cyclohexanone and cyclohexanol were also observed but were not quantified. No further reaction was observed with extended amounts of electricity passed, up to 12 F/mol.

1.3.4 Guaiacol

Guaiacol (**198**) was less studied by ECH than phenol. Compared with phenol, it required much higher temperatures to get a reasonable ECH conversion. Saffron et al. reported that with a ruthenium on ACC (Activated Carbon Cloth) cathode, guaiacol can be hydrogenated

more efficiently under 50 °C (entry **2**) than at 80 °C (entries **3, 4**). The argument is that the desorption of substrates increased as temperature was raised up.[105] Jackson et al. reported that a RaNi cathode can deoxygenate guaiacol as well to cyclohexanol, while only trace amounts of 2-methoxycyclohexanol (**199**) was observed under basic condition with the majority product being cyclohexanol (**33**).

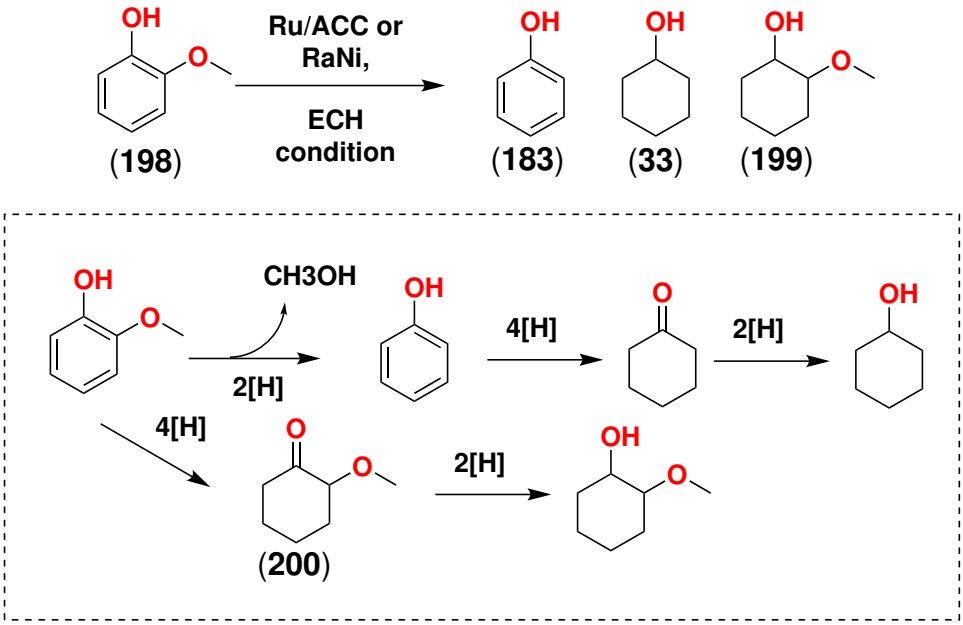

Figure 1.21: ECH of guaiacol.

Table 1.10: ECH of guaiacol with various catalysts and different conditions.

					Yield%			
	Cathode	**Temp.**	**Solvent**	**CE%**	**(183)**	**(33)**	**(199)***	**Ref**
1	Ru/ACC	25	HCl	19	0	13	38	105
2	Ru/ACC	50	HCl	31	0	23	37	105
3	Ru/ACC	80	HCl	30	0	40	35	105
4	Ru/ACC	80	NaOH	28	0	30	32	105
5	RaNi	75	pH 8 Borate	26	0	79	trace	19
6	RaNi	50	NaOH	3.4	19	3	0	101

ACC: Activated Carbon Cloth; **RaNi**: Raney Nickel; **Temp.** is temperature; **CE**: Current Efficiency. *Both cis- and trans-isomers were observed and the *cis*:*trans* ratio decreased from 5:1 to 3:1 from 25 to 80 °C.

One observation from the Ru/ACC cathode reactions is that the *cis*-(**199**):*trans*–(**199**) ratio decreased from 5:1 to 3:1 when temperature was increased from 25 to 80 °C. The *trans* compound is more stable than the *cis*-(**199**), the preferable production of *cis*-(**199**) can be envisioned from the hydrogenation of the benzene aromatic ring bound flat on the surface of the catalyst; the H atoms would then be delivered to the same face, leaving the hydroxy and methoxy groups in a cis relationship. As temperature increases, more *trans*-(**199**) may indicate that the energy is enough to overcome the unfavorable steric interactions in (**201**), with methoxy pointed to the surface, enabling the hydrogenation of (**201**) produced the more thermodynamically favorable *trans*-product.

On the RaNi cathode, higher temperature (entry **5**) led to greater CE than lower temperature (entry **6**). Phenol was captured as an intermediate at 50 °C and only 3% of cyclohexanol was produced, while 79% of cyclohexanol was captured under 75 °C.

These results suggested that deoxygenation occurs at higher rates at higher temperature for both Ru and RaNi catalysts. RaNi at higher temperature had advantages on deoxygenation of phenol without generating alkyl-alkyl ether (**199**). Since after saturating the aromatic ring, the aryl-methyl ether becomes a very inert alkyl-methyl ether, the subsequent deoxygenation of (**199**) is limited in the case of Ru/ACC.

1.3.5 Vanillin

The ECR of vanillin was conducted with a lead cathode on a large scale (100 g of vanillin) and similar to the ECR of ketones, the homo-coupling of two reduced vanillin radicals generated hydrovanilloin (**203**) in excellent yield. The dehydration and reduction stilbene product (**204**) was also isolated. No vanillyl alcohol was reported. No ECH of vanillin was found in literature.[106]

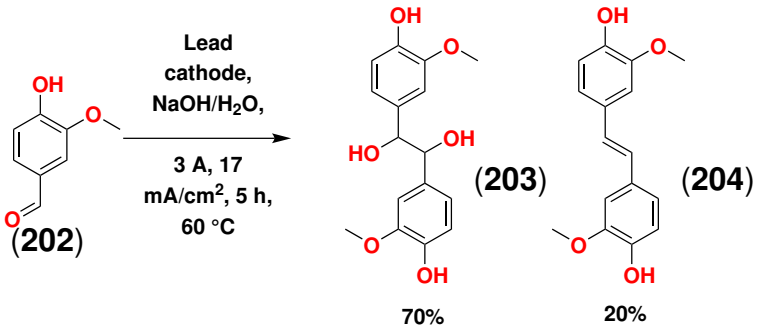

Figure 1.22: ECR of vanillin.

1.3.6 Other phenol monomers

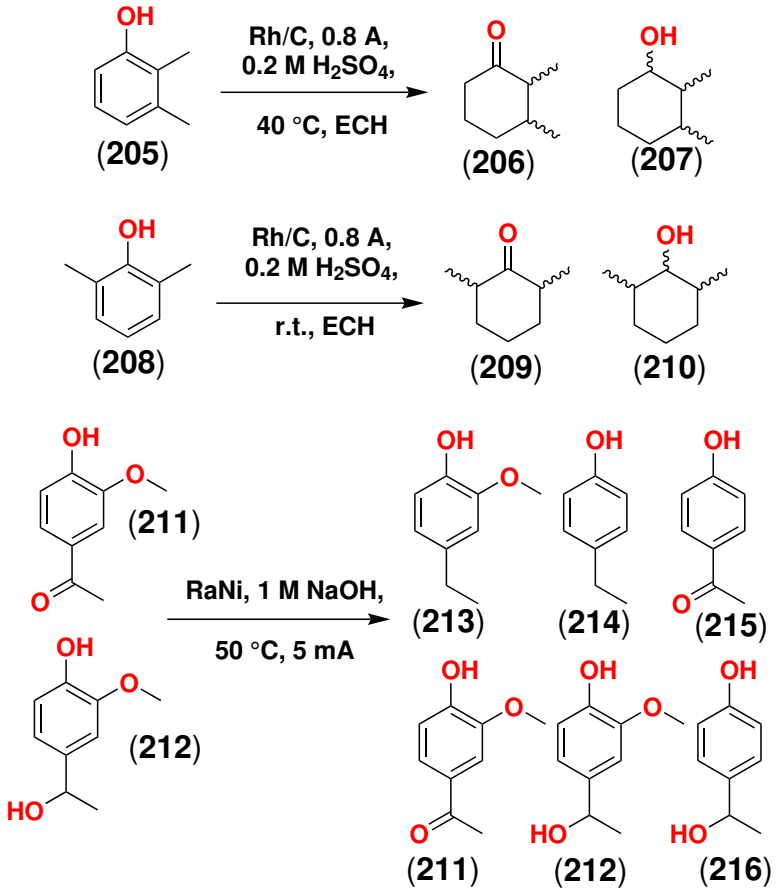

Figure 1.23: ECH of phenolic monomer models.

The ECH of phenolic compounds were studied with Rh/C and RaNi catalyst. The results shown in Table 1.11 may indicate that Rh/C was more effective on the hydrogenation of ben-

Table 1.11: ECH of lignin monomers with various catalysts and different conditions.

								Yield%				
	S	**Cataly.**	**T**	**Solvent**	**Q**	**CD**	**CE%**	**Pdt1**	**Pdt2**	**Pdt3**	**Other**	**Ref**
1	(**205**)	Rh/C	40	H_2SO_4	12	11.8	39	7 (**206**)	73 (**207**)	-	-	94
2	(**208**)	Rh/C	r.t.	H_2SO_4	12	11.8	41	1 (**209**)	82 (**210**)	-	-	94
3	(**211**)	RaNi	50	NaOH	18	-	12	53 (**212**)	11 (**214**)	9 (**216**)	other<2	101
4	(**212**)	RaNi	50	NaOH	18	-	3	21 (**211**)	13 (**214**)	9 (**216**)	6 (**213**) 3.5(**215**)	101

S is substrate. **Q** is in unit of F/mol. **T** is temperature in °C. **CD** is current density in mA/cm^2. **CE** is current efficiency. H_2SO_4 was 0.2 M. NaOH was 1 M.

zene rings of phenols than RaNi, in which case no cyclohexanol or cyclohexanone derivatives were observed, while one has to notice that alkyl 2-methoxyphenol rings were more electron rich than alkylphenol, making (**211**) and (**212**) more challenging to reduce than (**205**) and (**208**).

It was important to realize that benzylic alcohol as in (**212**) can be dehydrogenated very effectively to ketone (**211**) on the surface of a RaNi cathode, which was confirmed by the reduction of a secondary benzylic alcohol (**212**) as shown in entry **4** of Table 1.11, 21% of (**212**) was dehydrated to (**211**).[101] Meanwhile, via deoxygenation by the removal of benzylic hydroxyl from (**213**) and demethoxylation to (**214**), (**215**), and (**216**), these important reactions can improve the energy density of these chemicals, although further optimizations were still needed to increase the yields and make aromatic ring hydrogenation possible.

1.3.7 Lignin dimer models

The ECH of lignin dimer models entailing α-O-4 (entries 1-5 of Figure 1.24), β-O-4 (entries **6-10**), and 4-O-5 (entries **11-21**) linkages have been explored by both Lessard, et al. and Lercher, et al.

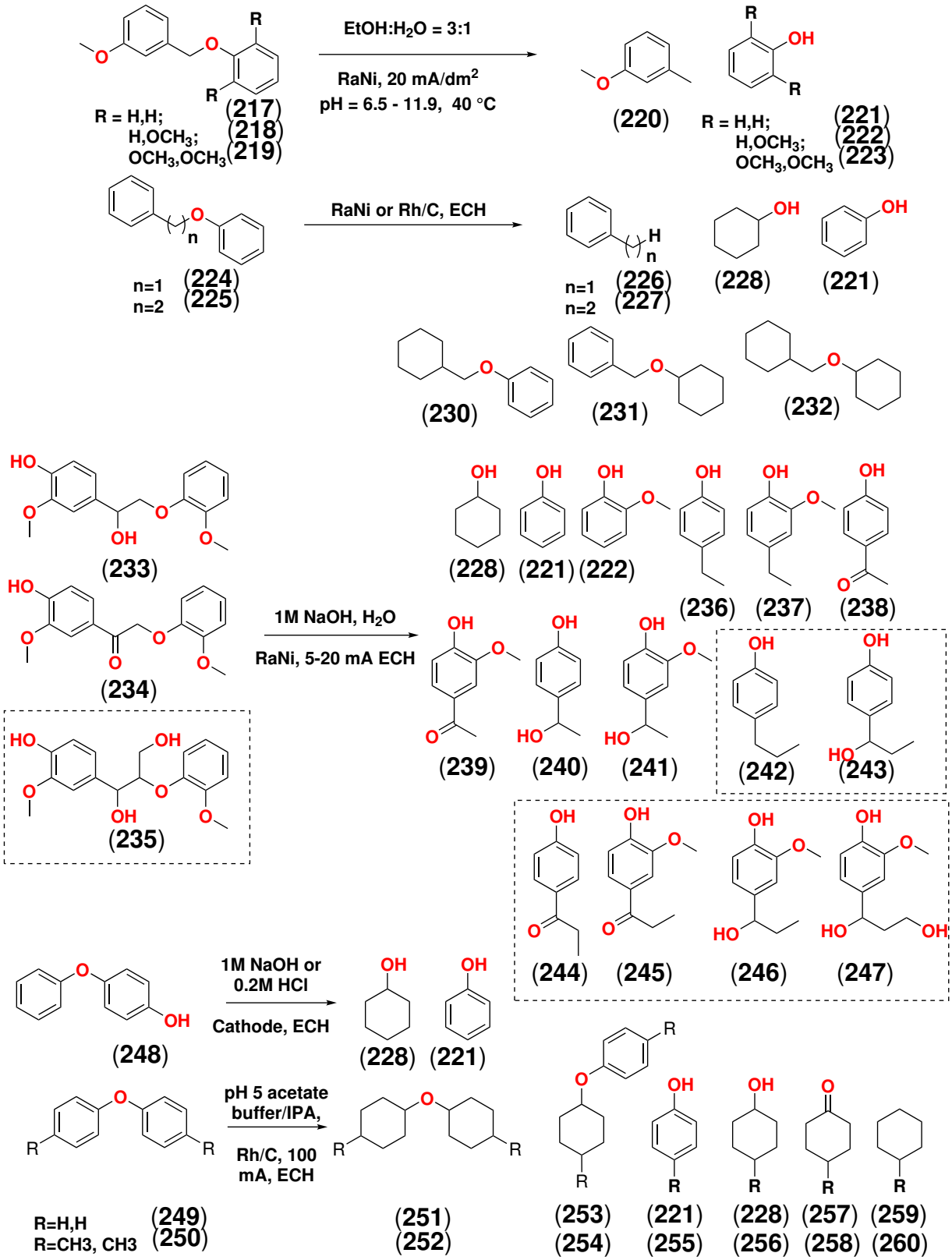

Figure 1.24: ECH of lignin dimer models.

Table 1.12: ECH of with various catalysts and different conditions.

								Yield%				
	S	**Cataly.**	**T**	**Solvent**	**Q**	**CD**	**CE%**	(**221**)	(**228**)	(**222**)	**Other**	**Ref**
1	(**217**)	RaNi	40	EtOH/H_2O	-	0.2	111	-	93	-	93 (**220**)	[107]
2	(**218**)	RaNi	40	EtOH/H_2O	-	0.2	103	-	-	94	94 (**220**)	[107]
3	(**219**)	RaNi	40	EtOH/H_2O	-	0.2	71	-	-	-	71 (**220**) 71 (**261**)	[107]
4	(**224**)	RaNi	40	EtOH/H_2O	-	0.2	124	100	0	-	100(**226**)	[107]
5	(**224**)	Rh/C	18	IPA/H_2O*	-	0.11	36		5	-	40(**232**) 15(**260**) 10(**231**)	[100]
6	(**225**)	RaNi	40	EtOH/H_2O	-	0.2	64	100	-	-	100(**227**)	[107]
7	(**233**)	RaNi	50	1 M NaOH	18	0.12	8.5	7	2.5	37	21 (**241**) 8 (**236**) 7 (**239**) 6 (**240**)	[101]
8	(**233**)	Pd/Al2O3	50	1 M NaOH	1	0.12	100	0	0	51	51 (**239**)	[101]
9	(**234**)	RaNi	50	1 M NaOH	8	0.12	16	0	0	48	27 (**239**) 15 (**241**) 1.5(**240**)	[101]
10	(**235**)	RaNi	75	1 M NaOH	18	0.48	8.1	5	1	29	3.5(**239**) 3 (**245**) 2.5(**246**) 2.5(**236**) others<2	[101]
11	(**248**)	RaNi	50	1 M NaOH	6	-	42	90	5	-	-	[108]
12	(**248**)	Rh/C	50	1 M NaOH	6	-	0	0	0	-	-	[108]
13	(**248**)	Rh/Al_2O_3	50	1 M NaOH	6	-	3	8	0	-	-	[108]
14	(**248**)	Pt/C	50	1 M NaOH	6	-	2	7	0	-	-	[108]
15	(**248**)	Ru/C	50	1 M NaOH	6	-	1	4	0	-	-	[108]
16	(**248**)	Pd/Ni	50	1 M NaOH	6	-	1	3	0	-	-	[108]
17	(**248**)	Pd/C	50	1 M NaOH	6	-	13	38	0	-	-	[108]
18	(**248**)	Pd/Al_2O_3	50	1 M NaOH	6	-	21	62	0	-	-	[108]
19	(**248**)	RaNi	50	1 M NaOH	6	0.12	28	84	0	-	-	[101]
20	(**249**)	Rh/C	18	IPA/H_2O**	-	0.11	25	5	6	-	38 (**251**) 20 (**253**) 10 (**262**)	[100]
								(**254**)	(**252**)	(**260**)	(**258**)	
21	(**250**)	Rh/C	18	IPA/H_2O**	-	0.11	18	22	20	12	10	[100]

S is substrate. **Q** is in unit of F/mol. **T** is temperature in °C. **CD** is current density in mA/cm^2. **CE** is current efficiency. **NaAc** is acetate pH5 buffer solution with 30 vol.% IPA. * It also contained acetic acid. ** It also contained acetate.

Although not widely distributed in lignin structures, α-O-4 bonds do occur.[17] The essence of an α-O-4 linkage is as a benzylic ether bond, a weaker bond that can be easily cleaved by reduction with the evidence that the benzyl group is a widely used alcohol protecting group that can be easily deprotected by reduction without affecting of normal aliphatic ether bonds.[109] The ECH result of (**217**), (**218**), (**219**), and (**224**) were not surprisingly very efficiently cleaved on RaNi and moderately on Rh/C at a lower temperature.

Compared with Rh/C (entry **5**), RaNi was more efficient on cleaving the benzylic ether bonds, showing close to 100% yields and CE (current efficiencies) for substrates (**217**), (**218**), and (**224**). An apparent decrease of both yield and CE was seen when the phenol unit was switched to the doubly methoxylated syringol in (**219**), which indicated that methoxy, by increasing the electron density of the benzene ring, tended to decrease ECH efficiency.

Rh/C (entry **5**) was found to hydrogenate benzene rings prior cleavage of benzylic ether bonds, generating large amount of (**231**), and (**232**). One interesting observation was the very little amount of (**230**) produced compared with a relatively large amount of (**231**), indicating that the more electron-rich phenol ring is less probable to be hydrogenated than benzene ring.

The ECH cleavage of β-O-4 lignin dimers into monomers was very successfully conducted on RaNi catalyst with both demethoxylation and aromatic ring reduction (entries **7, 9, 10**) although with low current efficiencies. Pd/Al_2O_3 and Pd/C gave clean cleavage of the β-ether bond of (**233**) with a perfect current efficiency with 2 F/mol current, while further extended reaction time led to no demethoxylation and no hydrogenation of aromatic rings.[101] Essentially, Pd catalysts have much lower reductive activity than RaNi catalyst on methoxylphenol derivatives.

The α-keto dimer (**234**) (entry **9** of Table 1.12) was much more effectively reduced

compared with (**233**) since the ether bond next to the keto-group in (**234**) was more labile than a normal ether bond in (**233**). Importantly, it was observed that the benzylic-α-hydroxyl can form (**234**) via in situ dehydrogenation to a keto group on the surface of RaNi during ECH, thereby forming (**239**) and (**238**); similar phenomena were observed in the ECH of (**235**).[101]

The 4-O-5 diaryl ether linkage represents a non-cleavable linkage that resists cleavage via traditional oxidation, acid and base hydrolysis reactions. This happens to be one type of bond that is easily hydrogenated with ECH at RaNi, Pd/C, and Pd/Al_2O_3 cathodes (entries **11, 14-19**), but is hardly cleaved on Rh, Pt and Ru catalysts (entries **12, 13, 20, 21**). Similar to the observation in (**224**) (entry **5**), Rh was exceptional in the hydrogenation of aromatic rings but performed poorly on cleavages of benzyl-aryl and aryl-aryl ether bonds. A large amount of aromatic ring hydrogenation products were observed in all cases with Rh cathodes (entries **5, 12, 13, 20, 21**).

1.3.8 The mechanism of ECH of phenol derivatives on surfaces of heterogeneous catalysts

Electrocatalytic hydrogenation of unsaturated compounds on metal surfaces in an aqueous media generally involves four type of reactions: (1) the generation of chemisorbed hydrogen $M(H_{ads})$ from reduction of water (Eq 1.1 and 1.2), (2) adsorption of organic substrates: alkenes/arenes or ethers/alcohols (Eq 1.3 and 1.6), (3) hydrogenations of organic substrates by surface hydride $2\,M(H)_{ads}$ (Eq 1.4, 1.5, and 1.7), and (4) side reactions, mainly hydrogen evolution, that decrease current efficiency (Eq 1.9, 1.8, and 1.10).

Chemisorbed hydrogen formation:

$$H_2O + e^- + M \rightleftharpoons M(H)_{ads} + HO^- \tag{1.1}$$

$$H_3O^+ + e^- + M \rightleftharpoons M(H)_{ads} + H_2O \tag{1.2}$$

Alkene/Arene hydrogenation:

$$CR_2{=}CR_2 + M \rightleftharpoons M(CR_2{=}CR_2)_{ads} \tag{1.3}$$

$$M(CR_2{=}CR_2)_{ads} + 2\,M(H)_{ads} \rightleftharpoons M(CHR_2{-}CHR_2)_{ads} + 2\,M \tag{1.4}$$

$$M(CHR_2{-}CHR_2)_{ads} \rightleftharpoons CHR_2{-}CHR_2 + M \tag{1.5}$$

Ether/Alcohol hydrogenation:

$$CR_3{-}OR + M \rightleftharpoons M(CR_3{-}OR)_{ads} \tag{1.6}$$

$$M(CR_3{-}OR)_{ads} + 2\,M(H)_{ads} \rightleftharpoons CHR_3 + ROH + 3\,M \tag{1.7}$$

Hydrogen evolution:

$$M(H)_{ads} + e^- + H_3O^+ \rightleftharpoons H_2 + H_2O + M \tag{1.8}$$

Heyrovsky:

$$M(H)_{ads} + e^- + H_2O \rightleftharpoons H_2 + HO^- + M \tag{1.9}$$

Tafel:

$$2\,M(H)_{ads} \rightleftharpoons H_2 + 2\,M \tag{1.10}$$

1.3.8.1 Phenol

Phenol has at least 9 possible orientations in which it can adsorb on Ni (111) surface with the benzene ring horizontally attached to the surface[2] as shown in Figure 1.25; meanwhile, it is also possible to imagine that the long-pairs of oxygen from phenol hydroxyl group can form bond with the empty d-orbitals of Ni atoms.[12] As shown in Table 1.13, the theoretical calculation results for phenol-Ni (111) complex show that the BridgeA2 geometry is energetically the most favorable one, while AtopA, AtopB from the horizontal ring geometry group and Atop-a, Atop-b from the vertical ring geometry group are much less favorable. Therefore, the center of the aromatic ring prefers to avoid landing on a nickel atom; meanwhile,

orientations with the aromatic ring lying horizontally on the Ni surface is more preferably than vertical ring geometries with oxygen bonding to the Ni surface.[2,12]

Table 1.13: Adsorption energies of phenol and benzene on Ni (111) surface as reported by Delle Site based on calculations with DFT method.[2]

Position	**Ni (111) E_{ads} (kcal/mol)**		**Ref**
	Phenol	**Benzene**	
a) Horizontal ring geometry			
HollowA1	-12.79	-17.94	2
HollowA2	-18.17	-17.94	2
HollowB	-15.41	-21.62	2
AtopA	-0.46	-	2
AtopB	-0.46	-9.66	2
BridgeA1	-19.78	-23.00	2
BridgeA2	-20.93	-23.00	2
BridgeB1	-17.02	-17.02	2
BridgeB2	-14.72	-17.02	2
b) Vertical ring geometry			
Atop-a	-3.22	-	12
Atop-b	-0.23	-	12

[a] it is calculated with explicit water solvation corrections and most likely the adsorption energy is from a bridge orientation.

Although there is no theoretical work directly addressing ECH of phenol, the mechanism insights from simulations of phenol reduction on heterogeneous metal surfaces with H_2 presumably should be transferable to ECH reactions, which happens on the metal surfaces populated with hydrogen from proton reduction under electrical fields.

The H_2 reduction of phenol on Ni or Pt surfaces at 500 K and 4 MPa pressure in aqueous media has been studied with first-principles density functional theory (DFT).[13] As shown in Figure 1.26, the three double bonds of phenol were reduced stepwise. In the first step, the newly formed CH_2 after addition of a hydrogen was energetically more favorable when located ortho to the phenol hydroxyl group than in the meta or para positions.

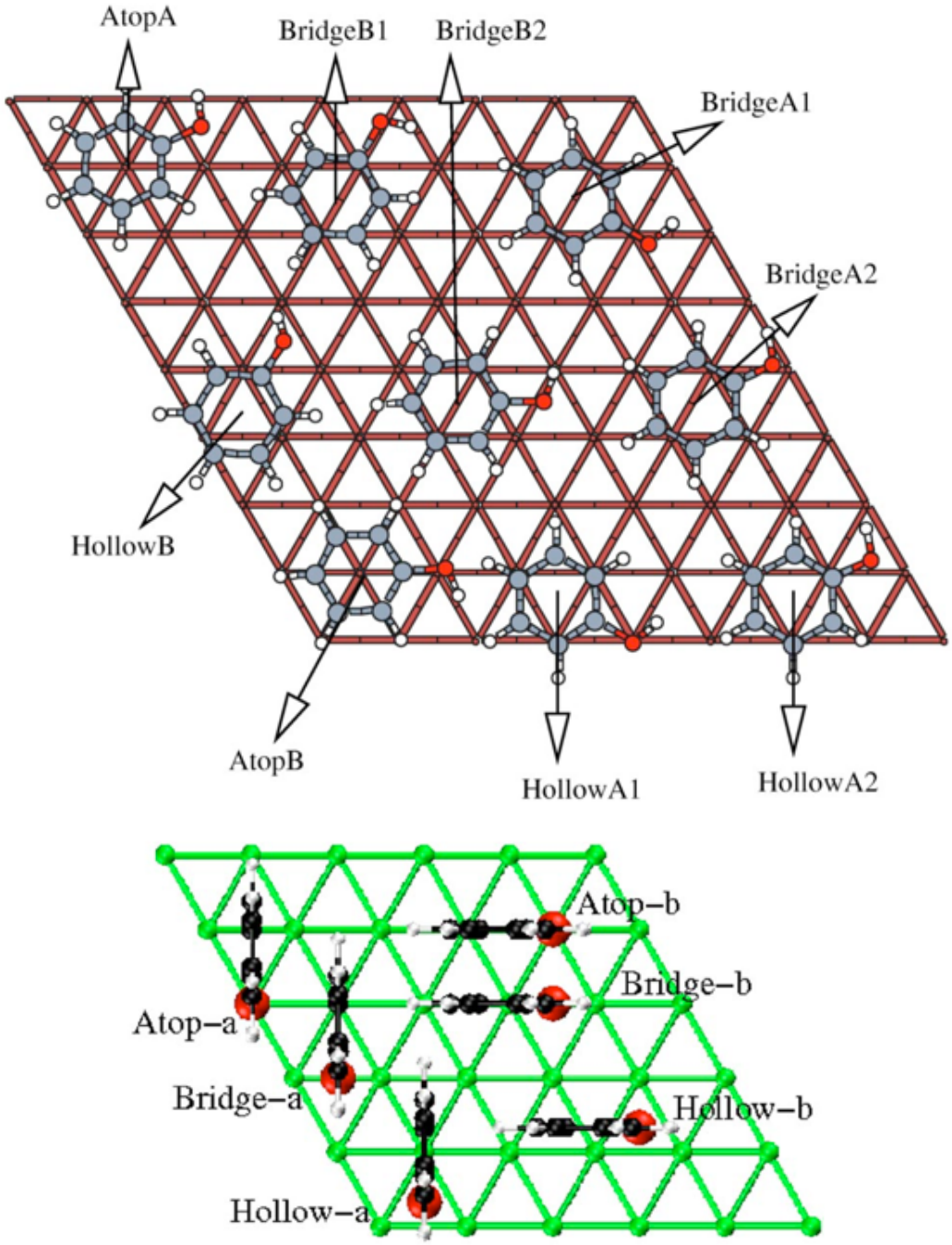

Figure 1.25: Theoretical mechanism studies of phenol hydrogenation from the work of Delle Site, C. F. Abrams et al.[2,12] A, B specify the carbon ring orientation while numbers 1, 2 specify the O-H position; a, b specify vertical or horizontal orientations of benzene rings. Picture above: phenols at the nickel (111) surface with benzene rings attaching to nickel atoms. Picture below: phenols at the Ni (111) surface with oxygen atoms attaching with nickel atoms. Reprinted with permission from Delle Site, L. et al. *Physical Review B* **2003**, *67* (19), 193406; and Ghiringhelli, L. M. et al. *Physical Review B* **2007**, *75* (11), 113403. Copyright {2018} American Physical Society.

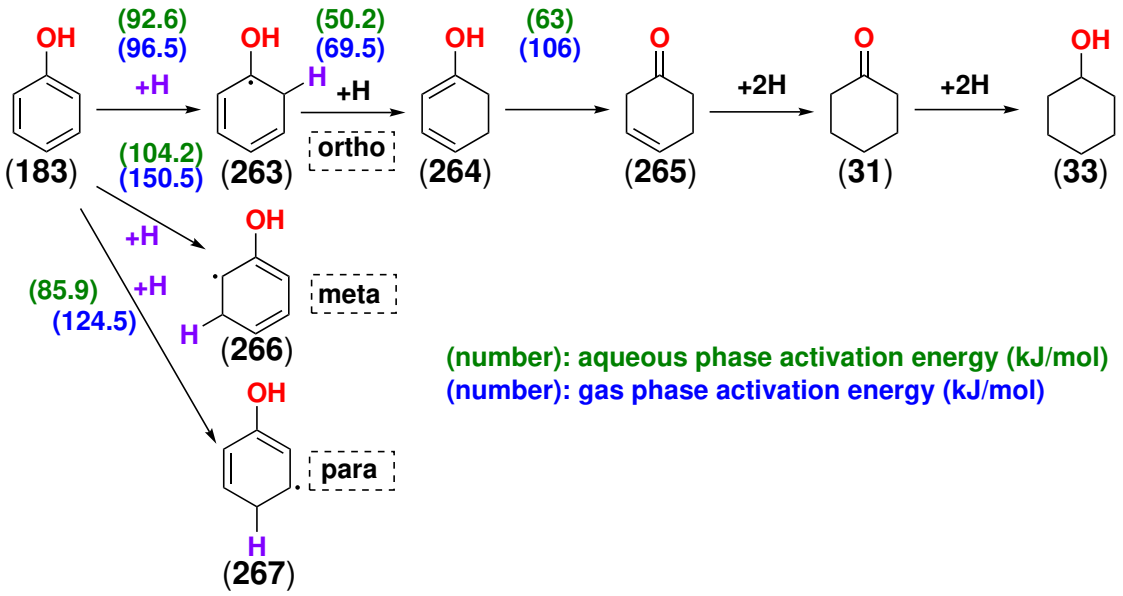

Figure 1.26: The reaction pathway and energetic profiles of phenol reduction on Ni (111) under a gas and an aqueous phases. Data was extracted from the work of Johannes A. Lercher et al.[13]

The aqueous environment has little effect on the ortho-selectivity of the first hydrogen addition to phenol on Ni surfaces, and the energy barrier for the first hydrogen atom ortho-addition only decreased by 3.9 kJ/mol from 96.5 kJ/mol in the gas phase to 92.6 kJ/mol in the aqueous phase, while it pronouncedly decreased by 46.3 kJ/mol from 150.5 kJ/mol (gas) to 104.2 kJ/mol (aqueous) for the meta hydrogen atom addition, and by 38.6 kJ/mol from 124.5 kJ/mol (gas) to 85.9 kJ/mol (aqueous) for para additions. Moreover, keto compound 3-cyclohexenone (**265**) was so dramatically stabilized by the appearance of water molecules that it was 80.1 kJ/mol more stable than the enol form (1,3-cyclohexadienol). In addition, it was suggested that 1,3-cyclohexadienol might desorb from Ni surface before further hydrogenation at 500 K since its adsorption energy was only -12 kcal/mol.[13] Afterwards 1,3-cyclohexadienol (**264**) rapidly underwent keto/enol tautomerization in the bulk water solution but establish an equilibrium more favorable towards enol (**264**) since it was 1.9 kcal/mol more stable than the keto (**265**).[13]

1.3.8.2 Guaiacol

No explicit theoretical analyses of on ECH of guaiacol (2-methoxyphenol) were found, but a DFT study of guaiacol hydrogenation over a heterogeneous Pt catalyst at high temperature has been reported. We reviewed this study since it may offer a guide to understand the mechanisms of ECH reactions on guaiacol and its derivatives.

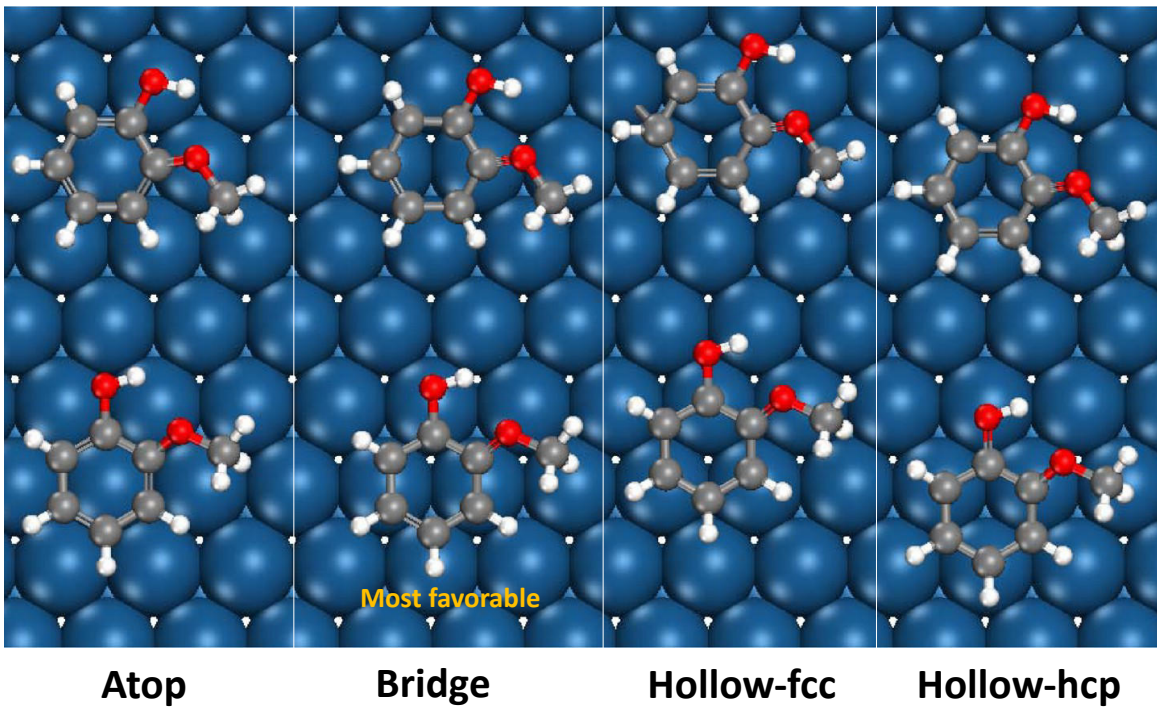

Figure 1.27: Possible adsorption sites for guaiacol on Pt (111) surface. From left to right they are Atop, Bridge, Hollow-fcc and Hollow-hcp with two orientations at each sites. The most favorable adsorption geometry is marked. Reprinted with permission from Heyden, A. et al. *ACS Catalysis* **2015**, *5*, 2423-2435.. Copyright {2018} American Chemical Society.

Like phenol, guaiacol has four types of adsorption sites on a Pt (111) surface: Atop, Bridge, Hollow-fcc, and Hollow-hcp as shown in Figure 1.27.[14] Meanwhile, surface-adsorbed guaiacol has no planes or centers of symmetry, and each type of adsorption has two orientations with 0° and 30° between the C(OH)-C(OMe) bond of guaiacol and the nearest neighboring Pt-Pt bond. The bridge site with 30° angle adsorption orientation is the most

stable one among the eight adsorption orientations. Importantly, for all eight, the hydroxyl and methoxy groups of guaiacol are repelled by the surface compared to the carbons of the aromatic ring which is essentially parallel to the Pt (111) surface[14]

The gas phase DFT simulation showed possible reaction pathways for the hydrogenation of guaiacol to phenol, anisole, catechol, and possibly benzene on Pt (111) at above 573 K with low H_2 partial pressures. In Figure 1.28, the greener (lower than 20 kcal/mol) activation energies, the more likely that pathway happens.

Similar to the hydrogenation of phenol as shown in Figure 1.26, the addition of hydrogen atoms to the carbon C(OH) (23.69 kcal/mol) or C(OMe) (28.29 kcal/mol) sites of a guaiacol followed by the direct eliminations of OH (14.23 kcal/mol) or OMe (23.00 kcal/mol) radicals to form an anisole or phenol seem to be the most feasible pathways.

Meanwhile, anisole can be converted to phenol with only three low-activation energy (AE) steps (18.17, 21.39, 6.67 kcal/mol). Moreover, catechol can be formed through four low-AE steps (16.33, 22.77, 13.57, 7.59 kcal/mol) from guaiacol by the hydrogen abstraction from the guaiacol methoxyl group (OCH_3) to an oxymethylene (OCH_2) radical,then to an aryloxy carbene (OCH), elimination of methylidynyl and hydrogen abstraction from Pt surface to form the α-hydroxyl ketone radical intermediate, and finally produce the catechol by the addition of a surface bonded hydrogen atom to the keto-oxygen.

In summary, RaNi was found to be the best cathode for the hydrogenation and cleavage of lignin α-O-4, β-O-4, and 4-O-5 dimer models, whereas Pd/Al_2O_3 could cleave β-O-4 ether completely but did not achieve much hydrogenation of the produced monomers. In contrast, Rh/C was a good catalyst for the hydrogenation of aromatic rings while the cleavage of β-O-4 ether linkage was less effective. It would be interesting to see if cathodes with both Pd and Rh could be effective as a dual hydrogenation and ether-cleavage catalyst. The effectiveness

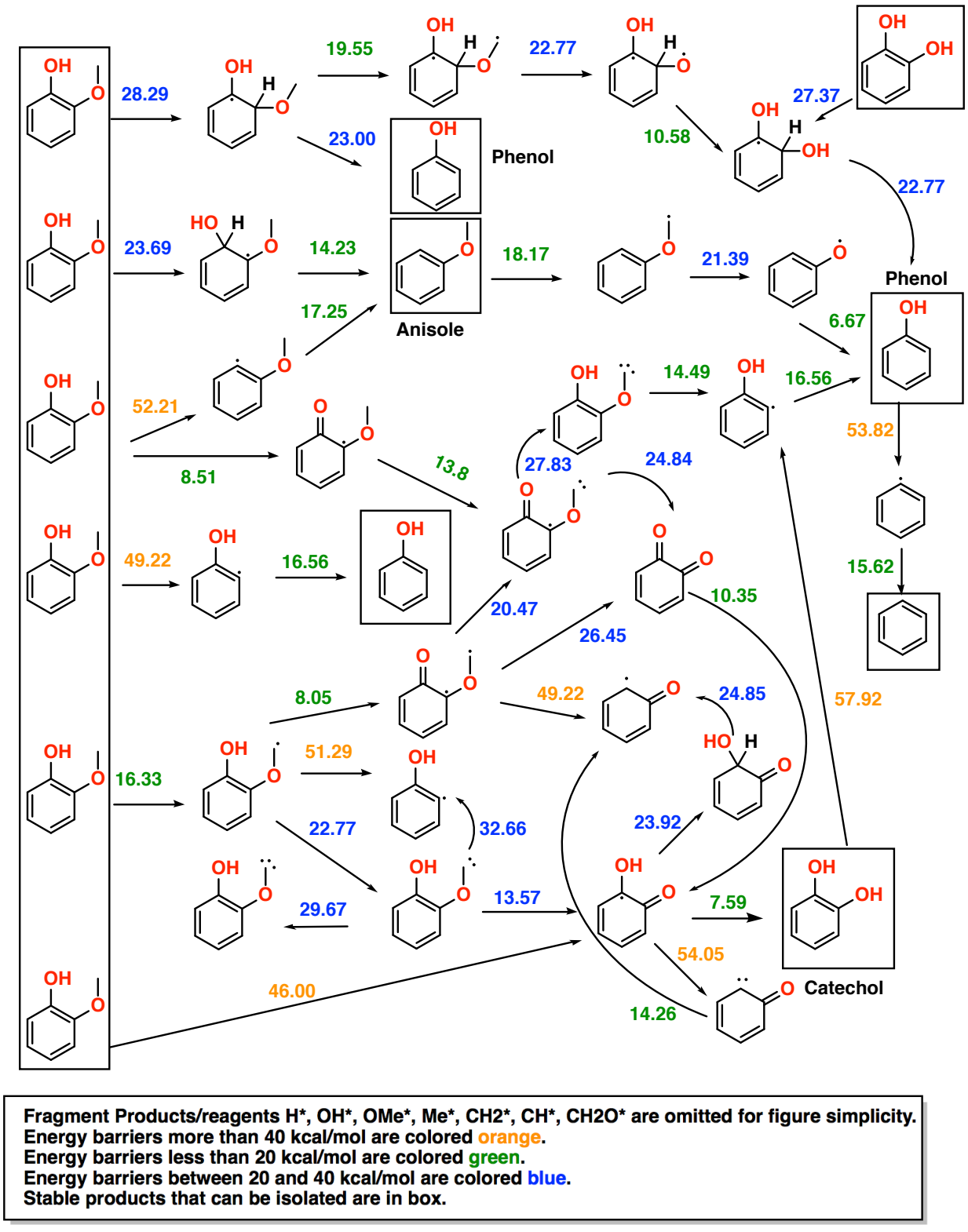

Figure 1.28: Work from Heyden, A. et al. *ACS Catalysis* **2015**, *5*, 2423-2435.[14] DFT calculation of the energy barriers (kcal/mol, numbers in blue) of guaiacol hydrogenation on Pt (111) at 573 K with low hydrogen pressure.

order of catalysts for aryl-aryl ether bond (4-O-5) cleavage catalyst is RaNi > Pd/Al_2O_3 > Pd/C > Rh/Al_2O_3 > Pt/C > Ru/C = Pt/Ni > Rh/C. Meanwhile, mechanisms of guaiacol to phenol conversion were suggested to follow hydrogen atom addition and the elimination of methoxy radical on the Pt metal surface. There are no studies found to investigate the reaction pathways starting from the meta- or para-addition of a hydrogen atom to the C(OMe) carbon of guaiacol. The hydrogenation of phenol to cyclohexanol was judged most likely to follow the reaction pathway:

Phenol $\longrightarrow$ 1,3-cyclohexadien-1-ol $\longrightarrow$ 3-cyclohexenone $\longrightarrow$ cyclohexanone $\longrightarrow$ cyclohexanol.

Chapter 2

The Activation, Recycle and Reactivation of RANEY® Nickel Cathodes in Electrocatalytic Hydrogenation (ECH) of Lignin Monomers

2.1 Introduction

The finite nature of fossil fuels and environmental climate changes caused by the excessive emission of CO_2 are driving society to seek alternative fossil-free renewable energy and fuel sources. Conversion of biomass, the sole source of the renewable carbon needed to produce liquid fuels, begins with fast pyrolysis, an oxygen-free rapid heating method that "melts" biomass to produce a complex liquid mixture termed "bio-oil".

Compared with other bio-fuel production strategies (fermentation, gasification/water-shift reaction/Fischer-Tropsch diesel synthesis,[110]) pyrolysis is the most carbon-efficient scheme. For instance, upon fermentation of glucose to ethanol (eqn. (2.1)), 1/3 of the

carbon is lost as CO_2. For gasification (eqn. (2.2)), similarly, at least 1/3 of the carbon input is discarded as CO_2 in the process of the water-gas shift reaction (eqn. (2.3)), which adjusts the CO:H_2 ratio from 1:1 to the 1:2 needed for Fischer-Tropsch hydrocarbon synthesis (eqn. (2.4)). Fast pyrolysis ($400 - 600$ °C, residence time 1 s) thermally decomposes biomass to form up to 75 wt.% of liquid (bio-oil) along with gases (CO, H_2, small amounts of CH_4 and CO_2) and char.[111,112]

$$\text{Fermentation: } C_6H_{12}O_6 \longrightarrow 2\,CH_3CH_2OH + 2\,CO_2 \tag{2.1}$$

$$\text{Gasification: } C_6H_{12}O_6 \longrightarrow 6\,CO + 6\,H_2 \tag{2.2}$$

$$\text{Water-Gas Shift: } 2\,CO + 2\,H_2O \longrightarrow 2\,CO_2 + 2\,H_2 \tag{2.3}$$

$$\text{Fischer-Tropsch: } 4\,CO + 8\,H_2 \longrightarrow 4\text{“}CH_2\text{”(alkane)} + 4\,H_2O \tag{2.4}$$

Though pyrolysis is an effective method for lignin deconstruction, pyrolytic bio-oil is an acidic (pH < 4), highly reactive organic mixture that undergoes self-catalyzed polymerization under ambient conditions. Its reactivity is due to the presence of acetic acid, aldehydes, furans, phenolic compounds and carboxylic acid derivatives.[113] Our biomass to biofuel conversion strategy is to upgrade via Py-ECH, the combination of Pyrolysis-pretreatment (Py) and Electrocatalytic Hydrogenation (ECH) of the resulting bio-oil. As shown in our prior study,[114] the Py-ECH strategy appears to be advantaged in terms of energy, mass and carbon balances. As a first step toward bio-oil valorization, ECH can stabilize pyrolytic bio-oil by reducing reactive carbonyl,[88,115] furanic,[115] phenolic and olefinic compounds,[19,105] as well as carboxylic acids.[116]

Lignin comprises 10-33 wt.% of the pyrolysis feedstock biomass and is the component

of highest energy content; its higher heating value is 26.7 MJ/kg, more than 50% greater than that of cellulose (17.5 MJ/kg).[117] A major source of lignin today is from wood pulping for paper production, and a further supply, lignin from the byproduct of biomass-to-ethanol conversion, may be expected as projected cellulosic ethanol plants come on line.[118] Currently, lignin is simply burned to supply heat and power;[119] as an amorphous crosslinked macropolymer (as in Figure 2.1), it resists more selective depolymerization. Hence its carbon content can not be easily extracted and utilized. Our Py-ECH strategy offers one possible way of making use of the carbon from lignin as biofuel.

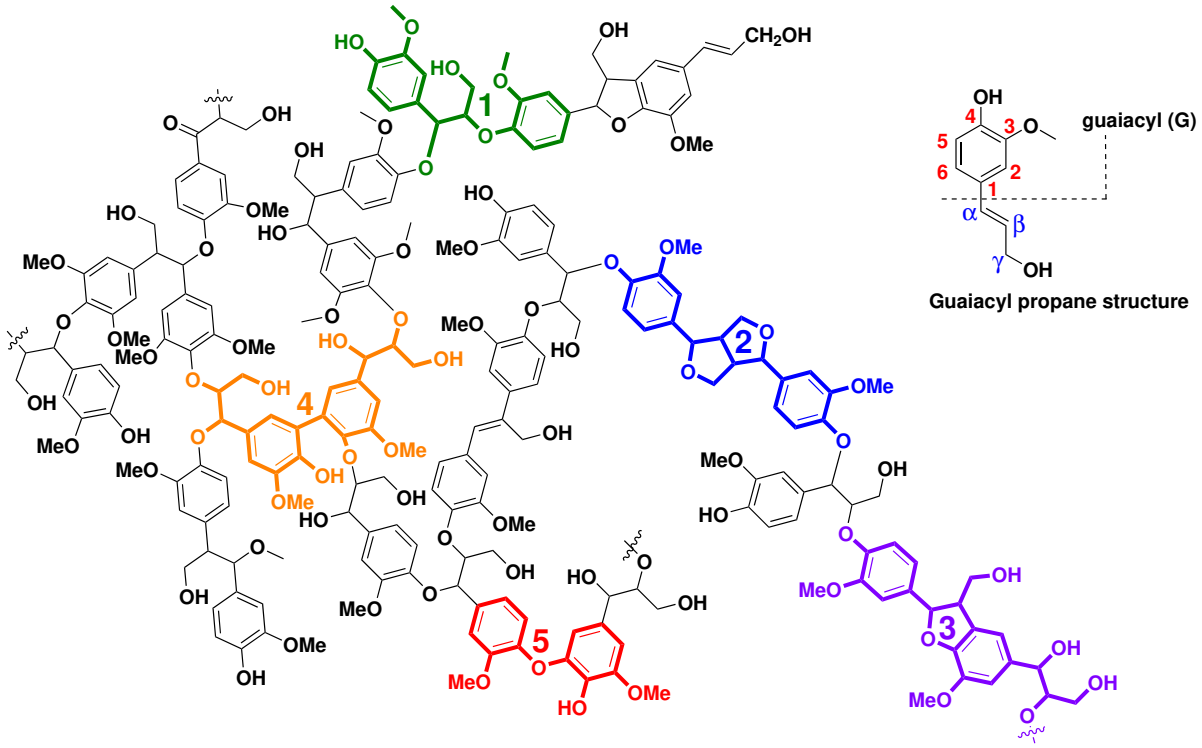

Figure 2.1: Structure of beech lignin proposed by Nimz, H.[15] The figure includes different major linkages of lignin. (1): β-O-4 linkage. (2): β-5 linkage. (3): β-β linkage. (4): 5-5 linkage. (5): 4-O-5 linkage. It is important to note that the lignin nomenclature numbering system is different from the conventional IUPAC system, where the phenolic OH carbon should be carbon 1.

ECH of lignin-type model compounds has been studied[36,90,92,99,120,121] since the early 20th century. As early as 1912, Willstätter and Hatt reported that phenol could be electro-

catalytically reduced to cyclohexanol over platinum cathodes.[99] Fisher and Bancroft later summarized that phenol was not at all practically electroreduced by either lead or mercury cathodes, but was well reduced to cyclohexanol at a platinized platinum cathode; the catalytic effect of platinum was evidently more important than the reducing power of hydrogen.[36] More recently, Martel, Lessard, and co-workers found that a nickel alloy cathode with 3.5% of Ru catalyzed the ECH of phenol to almost pure cyclohexanol,[122] similar to the result at a Raney® nickel (RaNi) cathode reported by Thomalla and Cyr,[123,124] meanwhile nickel with 3.5% of Rh cathodes and platinized platinum cathodes reduced phenol to a mixture of cyclohexanone and cyclohexanol.[122] Lercher et al., using a carbon-supported Rh cathode, reported a complete conversion of phenol to cyclohexanol with 68% Faradaic-efficiency; cyclohexanone was not observed.[100] Guaiacol (2-phenoxyphenol), representing the G-type aromatic moiety of lignin, was easily demethoxylated, hydrogenated and isolated as almost pure cyclohexanol at a RaNi (Raney® nickel) cathode, as reported by Lam, Jackson et al.; meanwhile guaiacol was also converted to a mixture of cyclohexanol, *trans*-, and *cis*-2-methoxycyclohexanols at a ruthenium-activated carbon cloth cathode.[105] Cyr et al. had also studied other lignin monomer models related to the guaiacylpropane structures (see Figure 2.1) of lignin such as acetovanillone (guaiacyl methyl ketone)[124] and α-methyl vanillyl alcohol[124] at RaNi cathodes. In that work, however, only phenol derivatives were observed; no further reduction to cyclohexanol derivatives was seen.

Building on the work of Cyr et al.[124] and our own prior studies,[19] we have found that guaiacol and syringaldehyde can be upgraded effectively to fuel-level compounds, such as cyclohexanol.[19] However, there are two main limitations to this strategy: 1) the cathode has low reactivity towards more substituted methoxyphenols such as eugenol and 4-propylguaiacol; 2) the Raney® nickel cathode loses its reactivity over hours to days of running.

The present account detail efforts to increase the lifetime and reactivity of the RaNi electrocatalysts, while extending the ECH treatments to more challenging lignin-relevant substrates, specifically, the high steric hindrance 4-alkylguaiacols. The focus is to explore the efficiency of ECH in reducing and deoxygenating such substrates to cyclohexanol products. Alcohol activation makes active MA-RaNi and IPA-RaNi cathodes (methyl- and isopropyl alcohol treated Raney® nickel cathodes) enhancing catalytic reactivity, lifespan, and recyclability.

2.2 Experimental

Nickel-ammonia plating solution preparation procedure: To a 1 L volumetric flask was added 213.02 g nickel(II) chloride hexahydrate powder and 30.00 g of ammonium chloride. 250 mL of DI water was then added and the flask was swirled to dissolve the solids. Next, 200 mL of 30% ammonium hydroxide solution was added slowly to the flask over 5 mins. The solution was then diluted with deionized (DI) water up to a total volume of 1 L.

Cathodic 0.1 M pH 8 borate buffer solution preparation procedure: To a 500 mL volumetric flask was added 3 g of boric acid, 1 g potassium tetraborate tetrahydrate, and DI water to dilute the solution up to 500 mL.

Anodic 0.1 M pH 7 phosphate buffer solution preparation procedure: To a 1 L volumetric flask was added 10.81 g of potassium phosphate dibasic and 5.3 g of potassium phosphate monobasic.

RaNi cathode preparation standard procedure: Preparation of the RaNi cathode used a slightly modified version of the method reported by Lessard[19,125] that traps nickel-aluminum alloy particles in an electro-deposited nickel matrix. The nickel(II) chlo-

ride hexahydrate and nickel-aluminum alloy were purchased from Sigma-Aldrich. On the cathodic side, a square of stainless steel 314 screen (50 mesh, 2.5×2.5 cm^2) was submerged in 50 mL of nickel-ammonia plating solution with nickel aluminum alloy powder stirred in suspension; and a nickel bar facing parallel to the stainless mesh was used as the sacrificial anode. The plating current density was maintained at 60 mA cm^{-2} (calculated based on the area of the mesh side facing the anode) for 6 h. Every 0.5 h, the electrode was turned 180° to get even deposition on both sides. Afterward, the plated electrodes were activated in NaOH solution (30 wt.%) for 6 h at 70 °C.

IPA-RaNi cathode preparation: a RaNi cathode was put into a container with 50 mL of isopropyl alcohol, the container was capped, and stored at room temperature for at least 12 h. The cathode was then removed and rinsed with deionized water before use or reuse.

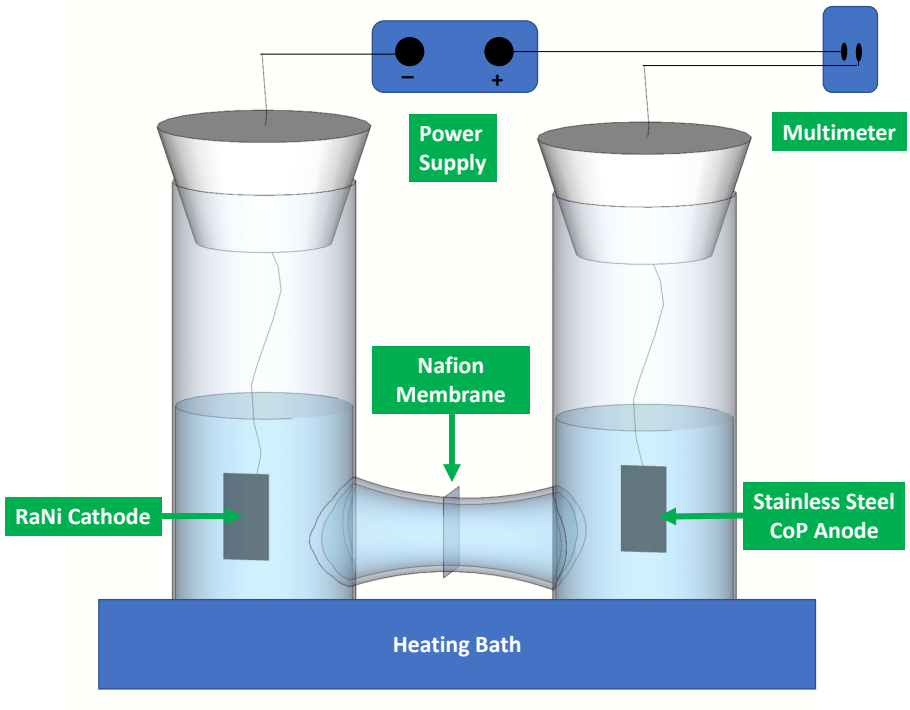

Figure 2.2: The conventional divided ECH cell setup.

ECH standard procedure: ECH was conducted with a conventional divided cell separated by a Nafion 117 membrane with RaNi cathode (see preparation above) and **CoP** anode (stainless steel from a 12 × 4 cm^2 stainless steel 314 screen rolled up tightly into a cylinder of about 3 cm diameter and coated with cobalt phosphate). In the cathodic half cell, 30 mL of 0.1 M pH 8 potassium borate buffer was added and on the anodic side was 30 mL of 0.1 M pH 7 potassium phosphate buffer. 10 mg of $Co(NO_3) \cdot 6\,H_2O$ was added to enable galvanic *in situ* deposition of a black film of cobalt phosphate (CoP) water splitting catalyst on the anode surface. The current was set to 50 mA (8 mA cm^{-2}, calculated based on the electrode single side facing the membrane and anode compartment) and the temperature to 90 °C unless otherwise specified. Before adding organic substrate, the electrode was equilibrated via electrolysis at 50 mA and 90 °C for 30 min depositing the black CoP film on the anode, which serves as a protection layer against the corrosion of the stainless steel. Afterward, a solution of the substrate was added to achieve 20 mM concentration in the cathode compartment, and the assembled experiment was subjected to ECH for 6 h unless otherwise specified. In the course of the reaction, a 0.5 mL aliquot of the sample was withdrawn from the ECH cathodic cell into a 2.0 mL conical vial every 1 h. The sample was acidified by adding 2 drops of concentrated HCl and extracted with 1.0 mL of DCM; 0.5 mL was then withdrawn from the DCM layer carefully without the transfer of water. The drying step was omitted here since we found that Mg_2SO_4 drying reduced significant amounts of products observed. The DCM solution in the GC-MS vial was double checked by watching through against a light source to make sure no visible water and then was sent for GC-MS analysis.

ECH procedure for reactivation experiments: the cathode reusability experiments were conducted according to the procedures above with minor changes. Since the cathodes

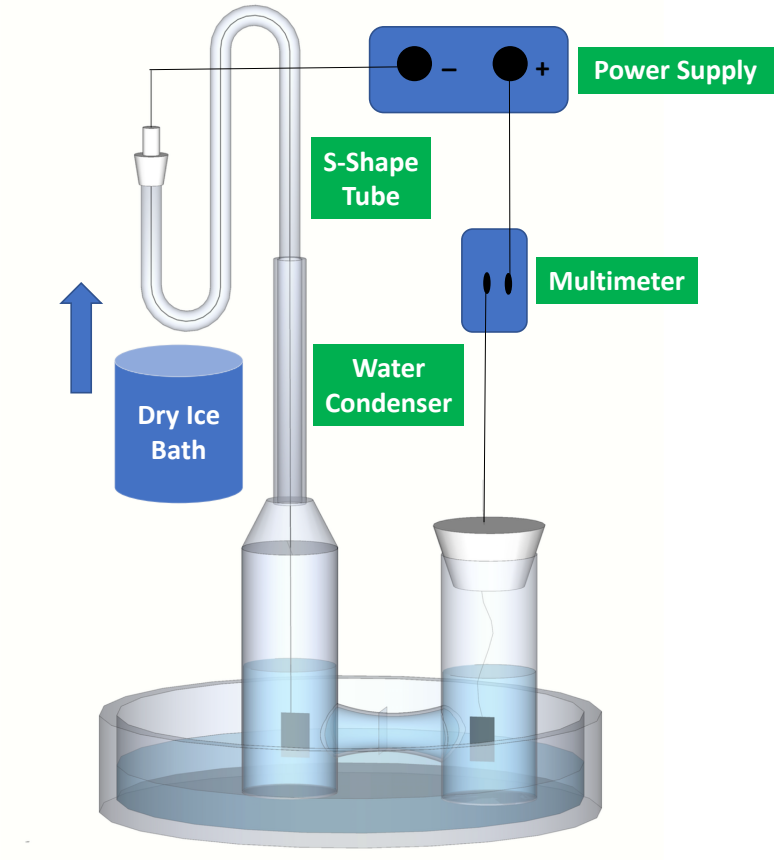

Figure 2.3: The ECH setup for improving mass balance.

were not fresh catalyst after the first use, a 1 h pre-run in pH 8 borate buffer was conducted and the cathode half-cell was emptied and replaced with a new 30 mL volume of pH 8 borate buffer solution before substrate eugenol was added into the cathode side.

ECH setup to maximize product recovery and quantify mass balance: Due to the volatile nature of some ECH products, specifically 4-propylcyclohexanol (**PrC**, structure see Figure 2.4), 4-propylcyclohexane and 4-propylbenzene (**PrB**), to calculate the mass balance of the reaction, the quantitative analysis was conducted with a modified ECH setup (see Figure 2.3) and analysis procedures. The cathode half-cell was connected with a double U-shape condenser containing 1 mL of isopropyl alcohol (IPA) with the bottom part submerged in a -78 °C dry ice-acetone trap to capture possible volatile products. The end

of water condenser was capped with a rubber stopper with a needle inserted on the rubber to vent H_2 gas. At the end of ECH, another 2 mL of isopropyl alcohol (IPA) was added to the double U-shape condenser to capture products trapped, and the IPA solution was injected into GC-MS directly for quantification analysis. 3 mL of octane was used to wash possible aliphatic products on the walls of the cathode half-cell and the condenser connected directly to the cathode-side. The octane-water bilayer solution was allowed to sit for 30 min to reach an equilibrium. Then a 0.5 mL of the water layer was acidified with 2 drops of HCl and extracted with 1 mL of DCM, and the water-DCM bilayer solution was allowed to equilibrate for 30 min. Then 0.5 mL of DCM and 0.5 mL of octane layer were diluted to the concentration range of a linear GC-MS response for the standard calibration curve and were analyzed by GC-MS. The drying step was avoided here since introduced additional mass balance losses. All GC-MS calibration standards were run along with the isopropyl alcohol, octane, and DCM samples to allow most accurate quantification results.

2.3 Results and discussion

Guaiacol (2-methoxyphenol) and syringol (2,6-dimethoxyphenol) were subjected to ECH under aqueous conditions in our previous work,[19] showing effective aryl ether (C-O) bond cleavage followed by reduction of the aromatic ring at 1 atm and 75 °C to produce mainly cyclohexanol and methanol.

ECH of eugenol, a more sterically hindered molecule than guaiacol, under the same conditions gives a low demethoxylation product yield of 38% (RaNi entry in Figure 2.6), in contrast with the almost 100% completion for guaiacol. The general products of ECH of eugenol (abbreviated here as **Eug**) include the olefin hydrogenation product 4-propylguaiacol (**PrG**), the

demethoxylation product 4-propylphenol (**PrP**), the arene hydrogenation product both cis- and trans-4-propylcyclohexanol (**PrC**) (typically formed in roughly equal amounts), and the phenol dehydroxylation product propylbenzene (**PrB**); trace amounts of propylcyclohexane and 2-methoxy-4-propyl cyclohexanol were also observed in some cases.

To develop an effective and general method for the ECH of lignin model compounds, eugenol was chosen as the main model for the studies of cathode material, solvent, temperature effects, and cathode-reactivation mechanism studies.

2.3.1 The advantage of water as solvent — solvent effects

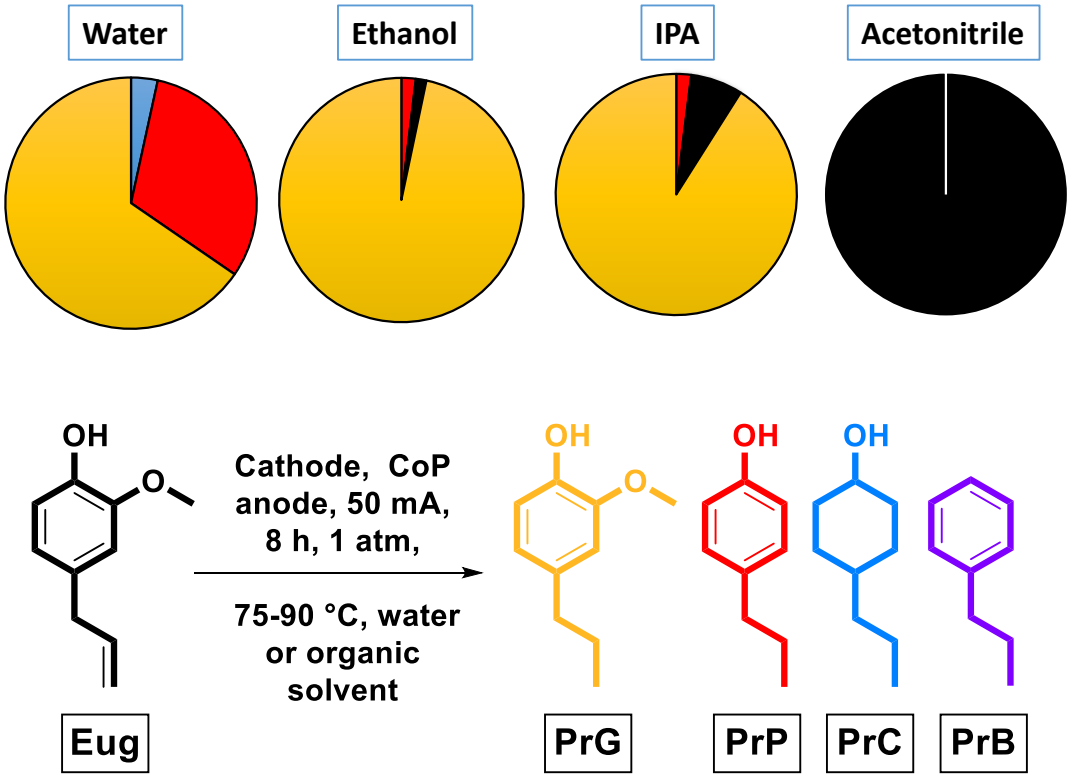

Figure 2.4: **Solvent effect** Solvent effects on ECH of eugenol with a RaNi cathode at 75 °C. As indicated by the color in the reaction scheme, in the pie diagrams, black stands for eugenol; yellow is PrG (4-propylguaiacol), red is PrP (4-propylphenol), blue is PrC (*cis and trans*-4-propylcyclohexanol) and purple is PrB.

The ECH of eugenol in water, ethanol, IPA (isopropyl alcohol), and acetonitrile were studied at 50 mA and 75 °C for 8 h. For ethanol and IPA experiments, NH_4Cl was the electrolyte and 3 mL of water was added in 30 mL ethanol or IPA to provide a proton source; for the acetonitrile study, tetrabutylammonium chloride was used due to solubility considerations, and 3 mL of water was added as a proton source. Isopropyl alcohol and ethanol are well known to undergo hydrogen transfer reactions with nickel as a catalyst.[126–136] However, as shown in Figure 2.4, ECH reactions in alcohols only hydrogenated olefin and achieved little demethoxylation and no aromatic ring hydrogenation reactions.

Acetonitrile is a high boiling organic solvent whose wide redox window suits it well as a medium for electroreduction or oxidation. In theory, 3 mL of water could provide excess protons for the electrocatalytic hydrogenation. However, during the reaction, acetonitrile hydrogenation and hydrogen evolution were apparently more favorable than hydrogenation of the organic substrate, giving no yield of hydrogenation or demethoxylation reaction products. That acetonitrile as a poor ECH solvent was also confirmed by attempts at ECH of guaiacol (one of the most reactive substrates) in acetonitrile/water solution, which also gave no substrate reduction products.

Compared with organic solvents, ECH in water gave the best yields of both hydrogenation and demethoxylation reactions. The 3 mL of water added to all organic solvents should supply sufficient protons for the ECH of eugenol. Presumably because of their hydrophobicity, phenol or cyclohexanol derivatives favor adsorptions at the metal surface more in water than in organic solvents where they are better solvated.

2.3.2 Cathode electrode material studies — identifying the key elements for high cathode reactivity

Multiple cathodes were prepared to further explored and optimize reactivity beyond the RaNi catalysts used in the previous study.[19] The RaNi cathodes were prepared according to the standard procedure, which includes three key steps: (1) electro-deposition of nickel along with Ni/Al alloy powder, (2) NaOH etching, and (3) storage of cathode in NaOH solution. The resulting Raney® nickel has a macroscopically rough, porous structure and at micro-scale, spiky crystalline-appearing surface features as shown in Figure 2.5 (A & a). By varying the preparation steps, we created several different cathodes as described in Table 2.1 to identify the factors that maximize cathode electrocatalytic reactivity.

Table 2.1: Preparation procedures of various cathodes studied in this paper

Cathodes	**Preparation procedures**			**SEM**
	Step 1, co-stirred powder[e]	**Step 2, NaOH digestion**	**Step 3, storage of cathode in**	**Image**
RaNi	Ni/Al alloy	✓	4 wt% NaOH solution	**A** & **a**
IPA-RaNi	Ni/Al alloy	✓	IPA[a]	**B** & **b**
IPA-NiAl	Ni/Al alloy	No	IPA[a]	**C** & **c**
IPA-Al	Al powder	✓	IPA[a]	**D** & **d**
IPA-Ni	Ni powder	✓	IPA[a]	**E** & **e**
Ni-ACC	Wet-impregnated method[b]	No	IPA[a]	**F** & **f**
IPA-RaNi-Oct	Ni/Al alloy	✓	IPA and then octane[c]	
MA-RaNi	Ni/Al alloy	✓	IPA and then MeOH[d]	

[a] IPA is isopropyl alcohol. The cathode was soaked in each alcohol for more than 12 h. [b] Soaked activated carbon cloths in $Ni(NO_2)_2$ solution, dry, and then hydrogen gas reduction with a similar method as reported by Menendez.[137] [c] Soaked the cathode in isopropyl alcohol for more than 12 h and then octane for 1 h. [d] Soaked the cathode in both alcohols for more than 12 h. [e] This was the powder that was stirred and captured onto the cathode along with the deposition of nickel from the plating bath solution. **RaNi**: Raney nickel; **IPA**: isopropyl alcohol; **ACC**: activated carbon cloth; **Oct**: octane; **MA**: methanol.

The porous and heterogeneous structural features of a RaNi cathode is essential to its demethoxylation reactivity. An activated carbon cloth (ACC) cathode doped with nickel nanoparticles failed to give any demethoxylation product PrP, PrC, or PrB, though it was still effective for olefin hydrogenation, yielding 92\{}% PrG in the final ECH product mixture, along with 3\{}% of eugenol and 5\{}% isoeugenol.

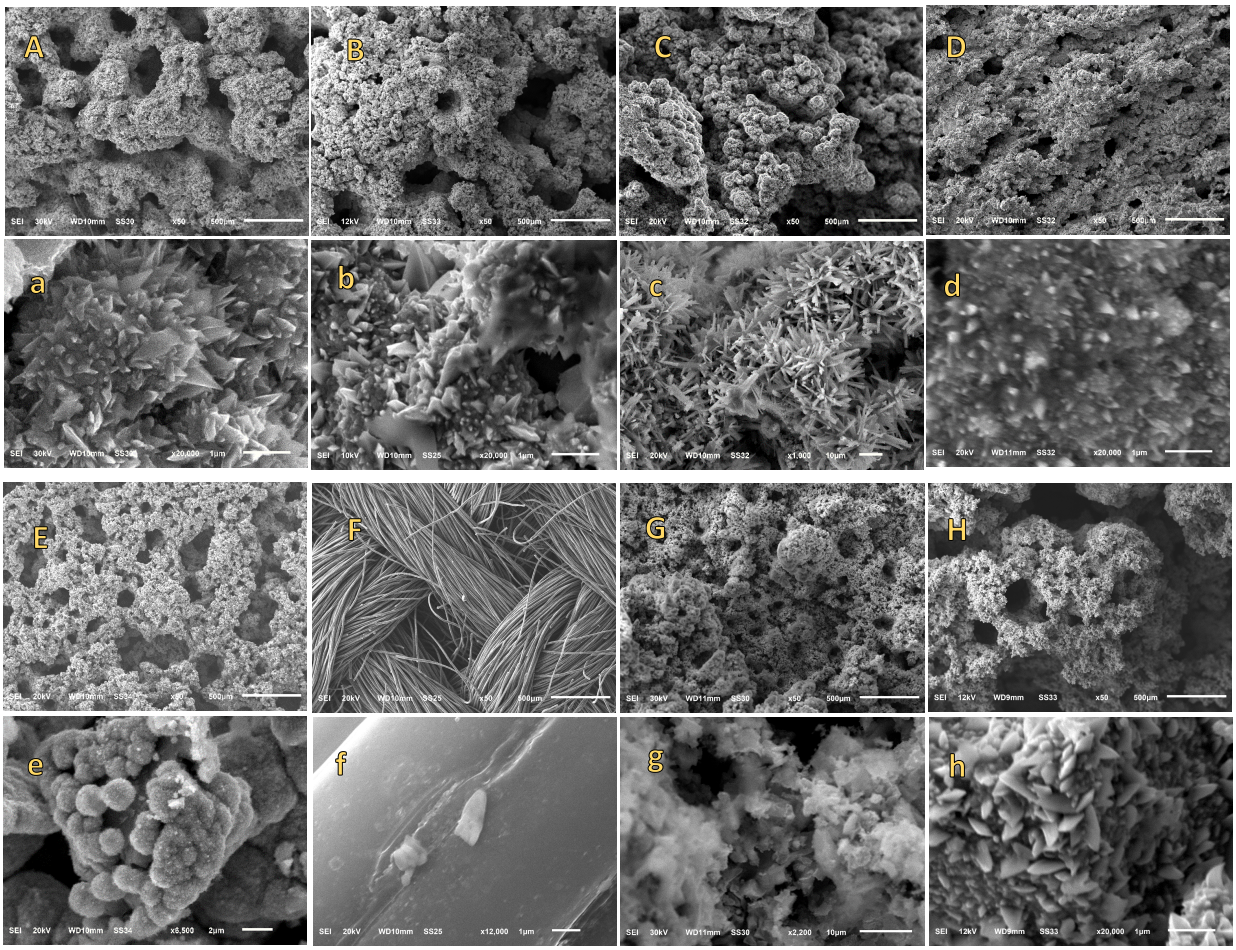

Figure 2.5: **SEM images of modified nickel cathodes**: Capital letter images are x50 magnification with 500 μm ruler bars. Lower-case letter images **a, b, d,** and **h** are at x20,000 magnification with 1 μm ruler bars, and **c** (X1,000, 10 μm), **e** (X6,500, 2 μm), **f** (X12,000, 1 μm), and **g** (X2,200, 10 μm) are at different magnifications to show the best micro-structure features that can be obtained. All images are the cathode after the 2nd time usage, except **A, a, B** and **b** are from fresh cathodes, and **G, g, H,** and **h** are from 10 time used spent cathodes.

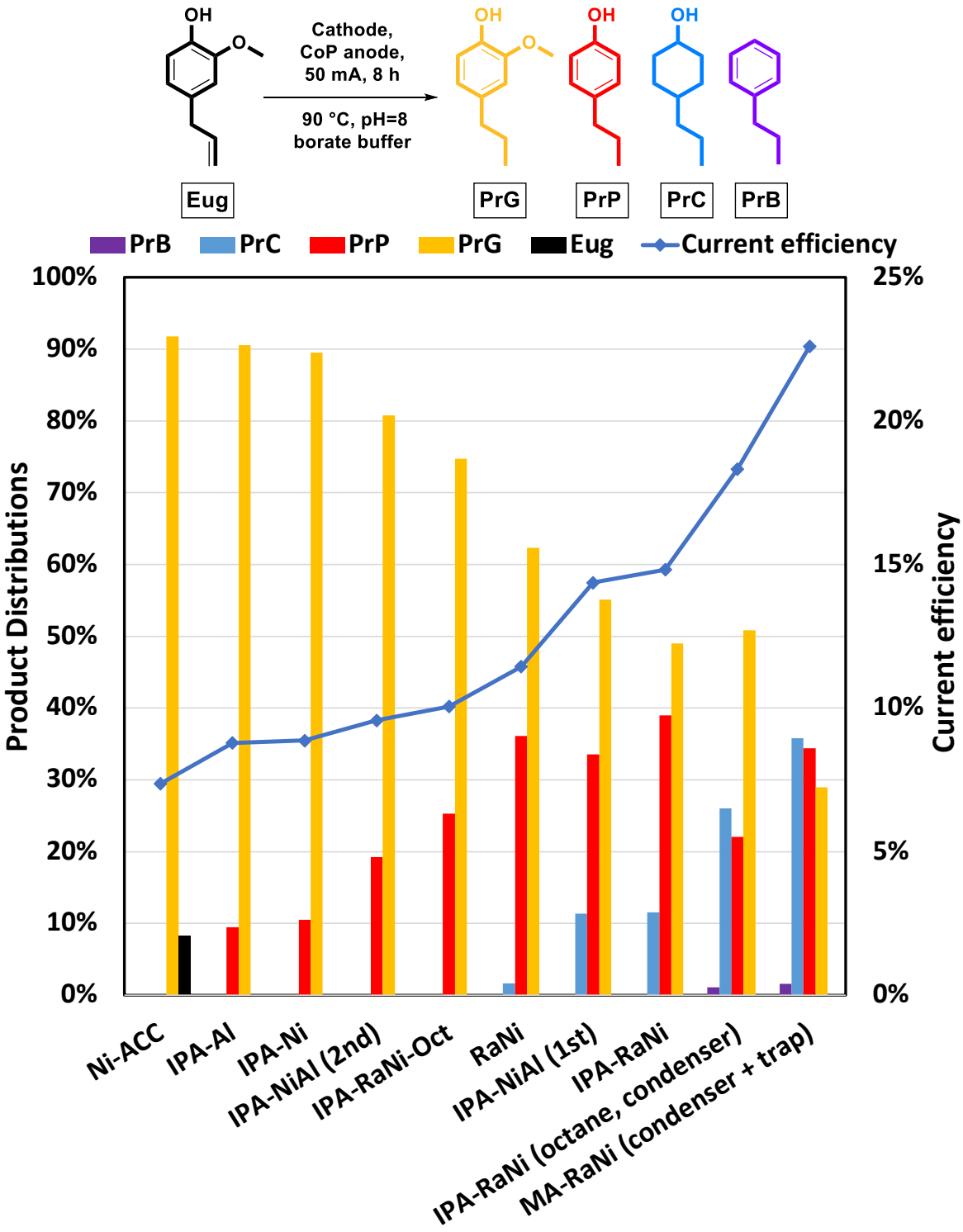

Figure 2.6: ECH of eugenol with different cathodes. Conditions: at 90 °C, pH 8 borate buffer, 50 mA current, 8 h reaction time, 0.1 g NaOH. The Eug in the Ni-ACC case stands for a mixture of 3% of eugenol and 5% of iso-eugenol. Octane in parenthesis means octane was added on top of the aqueous solution without directly contacting the cathode; while the IPA-RaNi-Oct cathode was immersed in octane). All experiments have an end pH above 12 after ECH. All numbers shown are the percentage of total products.

The Raney® Ni/Al alloy was unique in delivering catalytically effective cathodes; replacing it with either Al or Ni powders, the current efficiencies dropped from 14.8% for IPA-RaNi to only 8.8% (IPA-Al) and 8.9% (IPA-Ni) as shown in Figure 2.6. Presumably, Ni/Al alloy is most effective in creating the catalytically required porous, highly reduced structures upon NaOH treatment to remove Al. Although Al powder can also react with NaOH, SEM images (Figure 2.5 D & d) showed that the IPA-Al cathode was not porous even after NaOH treatment; presumably either the Ni deposition encapsulated most of the Al powder blocking NaOH access, or the Al powder was not well captured onto the surface. Some spiky micro surface features were observed in the IPA-Al cathode (see SEM image d), but the size (less than 0.2 μm) of the nickel spikes on the almost 2-dimensional IPA-Al surface was much smaller than that of RaNi or IPA-RaNi cathodes (up to 1 μm). Meanwhile, the IPA-Ni cathode was porous but had globular surface microstructures and low catalytic efficiency.

Step 2, the NaOH treatment was also a necessary step for optimal reusability. The current efficiency of IPA-NiAl (1st) (the cathode without of NaOH treatment, the first use), as shown in Figure 2.6 was 14.4%, which is only slightly lower than that of IPA-RaNi (14.3%). During the second use, however, its current efficiency dropped to only 9.6%, and it turned a white color, suggesting the formation of Al_2O_3; this interpretation was confirmed by the SEM analysis (see Figure 2.5 c) which showed the surface covered with Al_2O_3 star-shape crystals. The traditional NaOH treatment digests out surface Al metal from the NiAl alloy, and thus creats the more stable IPA-RaNi electrode; without NaOH etching, surface Al reacts with aqueous hydroxide to form Al_2O_3, insoluble at mild pH. As time goes on, Al_2O_3 covers the surface and decreases the accessible area for hydrogenation on the active metal Ni.

2.3.3 Cathode activation and reactivation

With the above knowledge, we further explored methods to make RaNi more active for ECH of eugenol. We tested two categories of alcohol: reducing alcohols with alpha hydrogen to the hydroxyl (MeOH and IPA), and a non-reducing alcohol with no alpha hydrogens (t-butyl alcohol).

Table 2.2: Activation, reactivation and deactivation of RaNi cathodes with alcohol and octane.

Cathode Treatment			**Product Distribution%**		
Step1	**Step2**	**Step3**	**PrG**	**PrP**	**PrC**
1M NaOH	-	-	68±6	29±5	3±3
IPA	-	-	49±3	39±3	12±1
IPA	MeOH	-	24±1	28±5	49±7
IPA	t-BuOH	-	64±2	24±3	12±1
IPA	Oct.	-	74	26	0
IPA	Oct.	IPA	67	25	8

All numbers shown are the percentage of total products. These ECH studies were run in the pH 8 borate buffer at 90 °C for 8 h with 50 mA current. All cathodes were used once after step1 to ensure the consistency of yields, and then were immersed in methanol (MeOH), t-butyl alcohol (t-BuOH), or octane (Oct.).

The RaNi cathode treated with IPA was found to consistently have a high demethoxylation product (PrC and PrP) yield 51% (see Table 2.2), compared with 32% when a RaNi cathode was used without alcohol treatment. MeOH can further modify the IPA-RaNi cathode to an even more active form with 72% demethoxylation yield and 49% of PrC, the best that we have observed so far at these reaction conditions. When t-butyl alcohol was used to treat an IPA-RaNi cathode, no activation was observed, instead, a slight inhibiting effect indicated by a slight yield drop in demethoxylation products. Octane, on the other hand, deactivated IPA-RaNi cathode strongly leading to a low demethoxylation of 26% and no aromatic hydrogenation to PrC product. Ethanol was also tried once with no effect found

on an IPA-RaNi cathode.

The activation mechanism of Raney® nickel cathode may occur via one or both of the following modes: (1) alcohols activating the cathode via reduction. This notion is supported by the activation effect of reductive alcohols MeOH and IPA, and the absence of an activating effect with the non-reductive alcohol t-BuOH; (2) alcohols activate the cathode by removal of hydrophobic surface poisons. When a cathode that had been treated with a non-oxidizable hydrophobic surface poisons octane was briefly rinsed with IPA and then immersed in IPA for 24 h, the IPA-RaNi-Oct cathode recovered much though not all ECH activity as shown in Table 2.2. We speculate that octane on and in the surface was not completely removed by IPA since the post-octane treatment catalyst was not as effective as the IPA-RaNi cathode.

One interesting, seemingly contradictory result to a previous observation[135] was that IPA-RaNi cathode activated by MeOH performs better than IPA-RaNi. In the previous report by Rinaldi, IPA was observed to be an active H-transfer solvent for Raney® nickel catalysts, whereas methanol preforms not as good as IPA and was suggested as surface poisoning solvent because of the blockage of reaction sites by the surface methoxyl groups generated from the adsorption and cleavage of the O-H bond. This could be true in Rinaldi's case where methanol was used as a reaction solvent, however, in our system, no significant amount of methanol was present in the actual reaction solution since the MA-IPA-RaNi cathode was washed with DI water before it was used.

2.3.4 Extending the cathode active life-span

Raney® nickel catalysts were known for their high reactivity and short life-span, and there are several methods that have been proposed to reactivate the spent catalyst.[138] However, attempts using the reported KOH and NaOH aqueous solution reactivation methods

produced cathodes with low demethoxylation reactivity cathode, similar to the catalytic efficiency of the RaNi cathode prior to IPA activation.

There are several factors that could decrease the catalytic efficiency of the Raney® nickel cathodes:

1) Mechanical damage. This is usually caused by the physical impact of cathodes with stir bars or other objects during handling of the cathode. We found that simply depositing more Raney® nickel on top of the damaged cathode with the RaNi cathode preparation standard procedure can solve this problem.

2) Oxidative damage. Oxygen is recognized as one of the most important factors contributing to the aging of Raney® nickel.[139] Water, especially basic solution, is also known to oxide Raney® nickel slowly to nickel hydroxide.[139] When a RaNi cathode was stored in an open container filled with DI water for one month, it only produced 3% of PrP and mostly (97%) PrG after 8 h ECH of eugenol at 90°C and 50 mA, compared with 29% of PrP production for a fresh RaNi cathode. The olefin hydrogenation activity still remained high, as no eugenol starting material remained in the product.

3) Surface poisons. There are many types of poisons for Raney® nickel, such as hydrogen chloride and organic halides poising styrene hydrogenation by H_2 at neat condition,[140] thiophene poising p-nitrotolutene hydrogenation in methanol,[141] heavy metal compounds ($HgCl_2$ and $Zn(OAc)_2$) poising p-nitrotoluene hydrogenation in methanol,[141] and sulfur such as CS_2 poising organic substrate reductions in aqueous solution[72] etc.

In our system, hydroxide anion itself may be a surface poison. When 0.5 g of NaOH was added into a pH 8 borate buffer to adjust its pH to more than 12, IPA-RaNi cathode only produced 30% demethoxylation products at the otherwise standard ECH of eugenol at 90 °C and 50 mA current, this value may be compared with the 51% demethoxylation products

found using the same cathode but starting from pH 9 at otherwise the same conditions.

Another surface poison may be the final hydrophobic products, specifically PrC from the ECH of eugenol, which is discussed in a later section of this work.

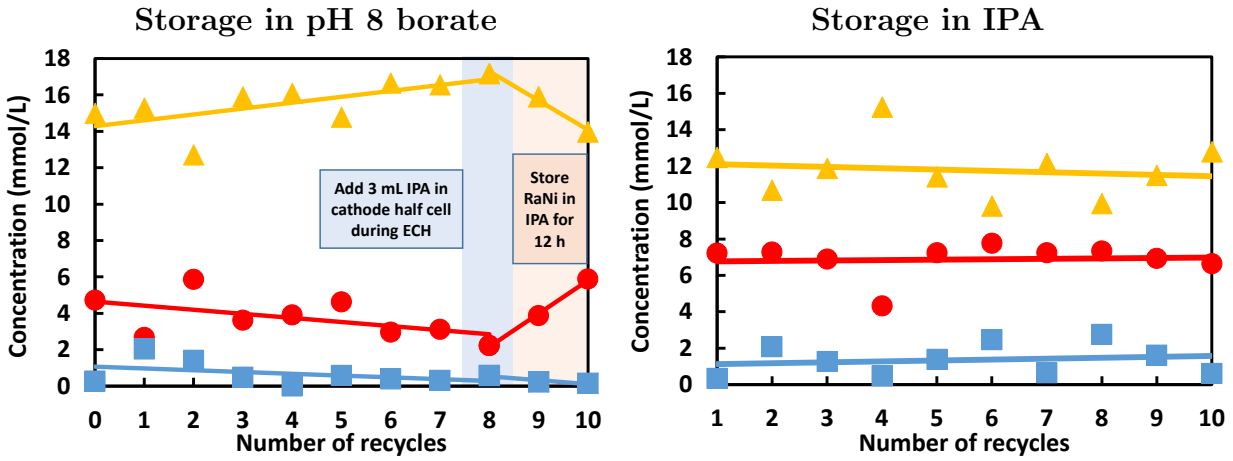

Figure 2.7: Two parallel recycle studies of two RaNi cathodes. (Left) Results with the cathode stored in pH 8 borate buffer. (Right) Results with the cathode stored in IPA. Yellow triangle = PrG, red circle = PrP, blue square = PrC. The conditions were 80 °C, 20 mM eugenol in pH 8 borate buffer with cathode, and CoP anode in pH 7 potassium phosphate buffer.

IPA was found to extend the cathode active life-span. As shown in Figure 2.7, when the catalyst was immersed in IPA for 12 h between two consecutive ECH runs with eugenol as a substrate, the cathode retained its reactivity for at least 10 reuse cycles; in contrast, the RaNi cathode slowly lost its reactivity when it was stored in fresh pH 8 borate buffers.

3 mL of IPA was added to the cathodic solution at the 8th recycle for the RaNi cathode storing in pH 8 borate buffer, no effect was observed and the cathode continued the trend losing the catalytic ability. However, when the deactivated cathode was stored in IPA for 12 h, for at least the next two recycles, it regained its demethoxylation catalytic activity. This ability to reactivate the deactivated catalyst represents a significant saving in effort and material, obviating the need to prepare fresh electrodes for each new experiment.

Although this 10-time spent RaNi cathode was reactivated when treated with IPA, it still

had a lower efficiency compared with an IPA-RaNi cathode, since the yield of PrC remained low. Due to the cumulative oxidation over a month, the catalyst surface was clearly deformed as shown in Figure 2.5 G and g. In contrast, on the cathode stored in IPA, even after 10 usage cycles, the surface retained its original characteristic spiky crystals (see Figure 2.5 H and h). The cathode stored in pH 8 borate buffer appears to be less porous than its IPA treated counterpart, which could be the result of continuous oxidation erosion from oxygen and hydroxide over a month.

2.3.5 Temperature effects — an unexpected kinetic finding

At room temperature, ECH selectively reduced the olefin functional groups of eugenol.

ECH reactions of eugenol with RaNi cathodes at 60, 80, 90, and 100 °C were examined under otherwise similar conditions. To avoid water boiling at 100 °C, 10 times more concentrated borate buffer solution (1.0 M instead of 0.1 M) and phosphate buffer solution (1.0 M) were used.

As reaction temperatures were raised up, the demethoxylation of eugenol speeded up. As shown in Figure 2.8, the hydrogenation of eugenol produced PrG and it was further demethoxylated to PrP much faster at 100 °C than 60 °C.

An unexpected "equilibrium" state was observed for both 90 and 100 °C after 6 hours of ECH, where both reactions reached a similar endpoint. The current was still supplied while no further organic reaction proceeds. Noteworthy, a similar phenomenon was observed by Lercher's group on ECH of phenol at a Rh/C cathode, and their conclusion was that surface poisons generated from the thermal but not electrochemical process, such as dehydrogenation of phenol, deactivated the catalyst.[93]

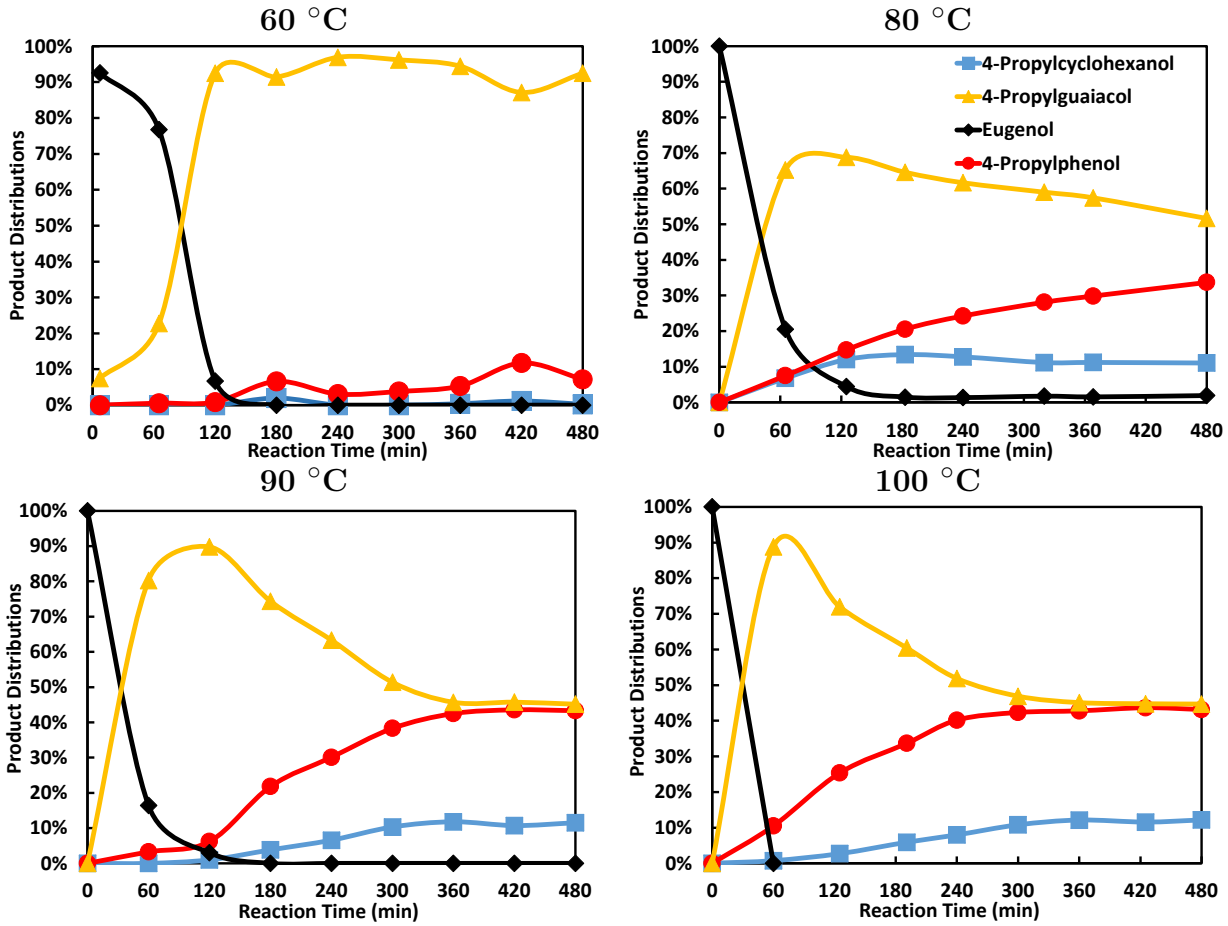

Figure 2.8: ECH of eugenol at 60 °C, 80 °C, 90 °C and 100 °C at IPA-RaNi cathodes with 50 mA currents. The pH of solutions were all above 12 except 11.5 for 100 °C at the end of ECH (8 h). All numbers in the figures shown are percentage of total products.

2.3.6 Explaining the unexpected temperature effect

Several factors could be invoked possible to account for the above-unexpected endpoint: (1) The catalyst was decomposed and loss all catalytic ability. (2) The hydrophobic product PrC cover the surface and stopped the reaction. (3) The catalyst was deactivated by the raising up of pH and hydroxide was the surface poison.

The catalyst did not decompose after the ECH. As shown in the recycling experiment, the cathode can still reduce Eug to PrG and PrC after 12 h of storage in both borate buffer and IPA, and usually, during the second time, the catalyst was even more active than the

first run as seen in both borate and IPA storage case. We measured the adsorption capacity of our RaNi catalysts and the total adsorption amounts of PrG, PrP, and PrC amounted to no more than 5% of the initial concentration. Thus, the significant yields of PrP and PrC observed in the second runs were mainly due to the reduction capacity of the cathode, not carry over from the prior experiment.

High concentrations of hydrophobic PrC does have some degree of deactivating effect but does not totally stop the reaction. A pH 8 borate buffer solution containing 6.7 mM of PrG, 6.7 mM of PrP and 6.7mM of PrC was subjected to ECH with an IPA-RaNi cathode at 90 °C. This experiment was subjected to rapid loss of substrates (a loss of 58% mass balance after 6 h) similarly to the evaporation conducted in the later section of this chapter. The product distribution of three substrates started from 33% equally for PrG, PrP, and PrC, and after 6 h of ECH with an IPA-RaNi cathode at 90 °C and 50 mA current, the product distribution becomes 32% PrC, 39% PrP, and 29% PrG. Essentially, nearly no reaction was observed.

One important observation is that when the ECH was conducted for 6 h where the reaction reached the endpoint, the solution was highly basic (pH 12.5), which means the protons produced in the water oxidation reaction from the anode chamber were not effectively being transported to the cathode half-cell through the Nafion membrane. Recently, we found that in one case where the solution ended with pH 10 after 8 h of ECH did not show the unexpected temperature effect was absent. The factor that led to this stabilized pH of the solution is still under investigation.

Based on all the data available, the most likely factor that led to this unexpected endpoint of reaction is the rise in pH. PrC may possibly play a role in the deactivation process.

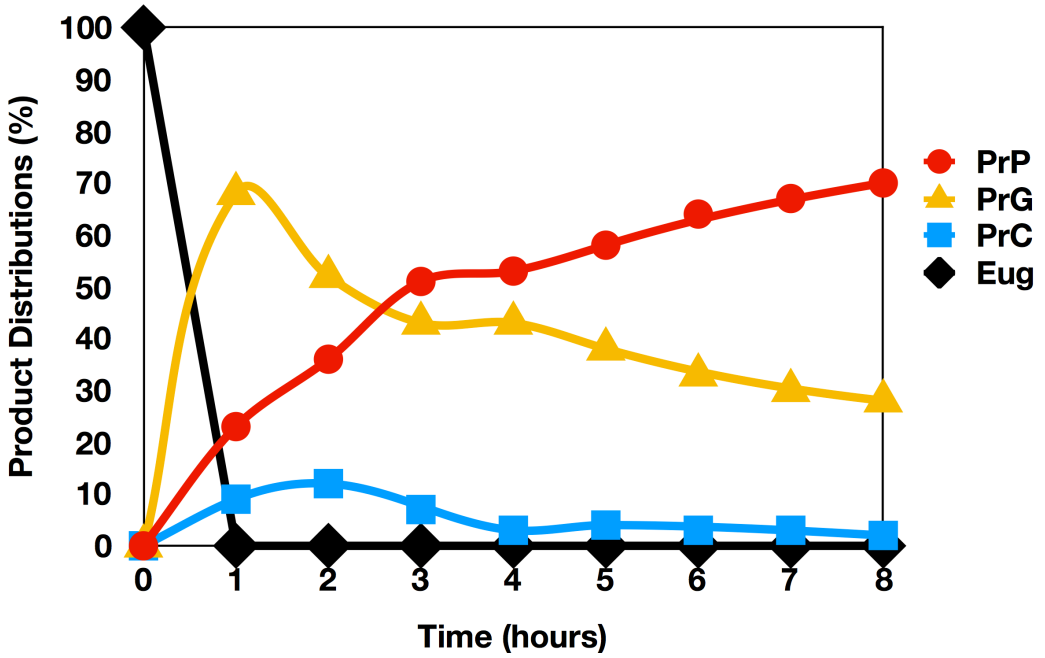

Figure 2.9: The ECH of eugenol with a RaNi cathode at 90 °C with 50 mA in pH 8 buffer solution, end pH 10 (8 h).

2.3.7 Mass balance

The ECH of eugenol at 90 °C had better conversion than lower temperatures, however, this strategy had a drawback of low mass balance (around 35%) as shown in Table 2.3).

The low mass balance was not due to the migration of substrates through the membrane to the anode side since only 1.2% of substrates could be detected on the anode side, mainly PrC (0.9%). It appeared that the reason was also not irreversible adsorption retaining on the cathode surface; only 0.13% of the substrates or products could be extracted from the cathode by using IPA to soak the cathode for 24 h.

Evaporation accounts for most of the mass balance losses. To an ECH cathodic cell was added 30 mL of pH 8 borate buffer made of D_2O and the pH was adjusted to 11 by adding 0.2 g NaOH. PrG (6.7 mM), PrP (6.7 mM), and PrC (3.2 mM) were then transferred to the preheated solution (90 °C). No cathode was added. The concentrations of PrG, PrP, and

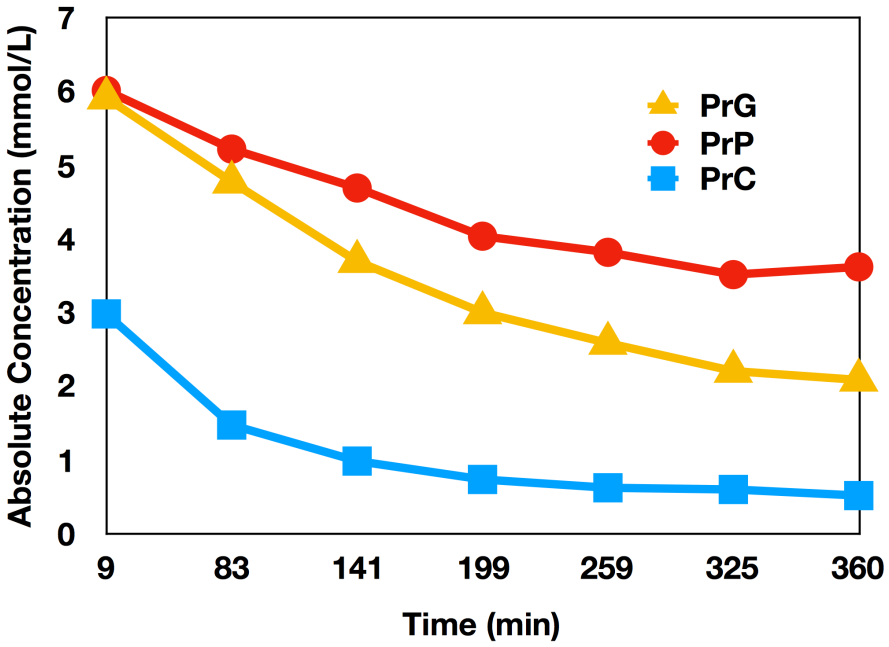

Figure 2.10: The evaporation of PrG, PrP, and PrC at 90 °C.

PrC were monitored by proton NMR with dimethylformamide as the internal standard. As shown in Figure 2.10, the evaporation, the absolute concentration of PrG, PrP, and PrC kept decreasing. Within 6 h, 59% of the total amounts of substrates were evaporated away. This explained the low mass balance observed in the ECH conducted in a conventional divided ECH cell as shown in Figure 2.2.

Initially, octane (3 mL) was explored as a strategy for preventing loss of material. However, it was very difficult to adjust the stirring so that the octane layer did not get disturbed. As discussed earlier, a surface coating of octane inhibited ECH with a Raney® nickel catalyst.

To address the mass balance issue, octane was not used and the setup shown in Figure 2.3 was employed when conducting ECH. The cathodic cell was connected to a condenser with an S-shape tube on the top. 1 mL of IPA was added to the bottom of the S-shaped tube and the tube was immersed in a −78 °C acetone/dry ice bath to prevent the evaporation of

Table 2.3: The mass balance (M.B.) of different cathodes and methods for the ECH of eugenol at 90 °C for 8 h.

Cathodes	**ECH Setup**		**PrC%**	**M.B.**
	Cond.[a]	**Trap**[b]		
IPA-RaNi	-	-	12±3%	35±3%
MA-RaNi	-	-	49±7%	37±3%
MA-RaNi	✓	✓	36±6%	86±9%

All PrC% numbers shown in this table are percentage of total products, not absolute value. [a] Cond. is condenser. The water condenser used is 20 cm long. [b] The Trap setup is a S shape tube immersed in a −78 °C dry-ice/acetone trap.

organic substrates. This method further improved the mass balance to 86% with a MA-RaNi cathode.

2.3.8 The first observation of deoxygenation of phenol under mild ECH conditions

One bonus of the above low-temperature condensation effort emerged to our delight. A fully deoxygenated product, propylbenzene (PrB, about 1%), and occasionally its hydrogenation product propylcyclohexane (trace amount) were observed in the dry-ice trap of the MA-RaNi experiments and the octane/water bisolvent experiments. The appearance of propylbenzene is not due to the alcohol activation process, as confirmed by its appearance when a RaNi cathode was used with the dry-ice trapping system. To the best of our knowledge, this is the first observation of a phenol deoxygenation product with nickel catalyst under mild ECH conditions. Further efforts are underway in the lab to discover methods to maximize such complete deoxygenation paths.

2.4 Conclusions and outlook

In this work, we identified the key factors for an active and long-lasting Raney® nickel electrocatalyst. These are: (1) the use of Ni/Al alloy powder, (2) convention Raney® nickel preparation via NaOH digestion to remove Al, (3) storage in alcohol (isopropyl or methyl alcohol), (4) avoid highly basic ECH conditions, (5) avoid cathode in contact with strongly hydrophobic compounds such as octane. To maximize yield and reaction rate, higher temperatures, and simple vapor condensation strategies are needed.

IPA and methanol were found to activate the RaNi cathode, t-BuOH was found to have a slight inhibitory effect, while Oct inhibited the ECH reaction almost completely. IPA was able to remove the octane inhibition effect only partially by the method employed. The activation mechanism was taken to derive from the reductive ability of the alcohol that can reduce surface oxidation from hydroxide.

IPA was found to extend the cathode active lifespan through at least ten reuse cycles. With IPA, the RaNi cathode lost its catalytic ability slowly. IPA was even able to bring back some degree of the catalytic effect of the nearly spent RaNi cathode.

Temperature plays a role in accelerating the demethoxylation and hydrogenation reactions of eugenol. An unexpected plateau was observed, attributed to the rising up of the solution pH, with inhibition by PrC possibly also playing a role. This observation is especially important in the search for strategies to improve the current efficiency of the Raney® nickel electrocatalyst.

The low mass balance of the "standard" reactions was a drawback in the study of ECH at higher temperatures. We found that the loss of mass balance was neither due to substrates migrating across the membrane to the anode nor because of cathode adsorptions; evaporation

accounts for most of the mass loss; only less than 2% of the mass loss were due to the adsorption to the cathode and the migration to the anode half-cell. By employing a condenser equipped with a dry ice cold trap, the mass balance was increased to 86%. Moreover, a fully deoxygenated product, PrB was found in the cold trap. As far as we know, this was the first observation of deoxygenation of phenol under ECH conditions over a Raney® nickel cathode.

Since basicity of the cathodic solution plays one of the most important roles in determining the current efficiency of ECH, further development of strategies to stabilize pH of the solution is important. One key factor here is the proton selectivity of the membrane. Choice of electrolyte on the anode side may also offer new options to address this point.

Chapter 3

Synthesis of Lignin Dimer and Several Monomer Models — A Practical and Economically Feasible Approach

3.1 Introduction

Having improved the Raney Nickel electro-catalyst to conduct ECH with high steric hindrance monomer models effectively, the next goal was to synthesize lignin dimer models and test how ECH can disconnect the linkages between monomers. These lignin dimer models not only enable us to develop methods to depolymerize lignin but also are tools to reveal the mechanisms of lignin depolymerization via ECH.

3.1.1 Lignin structures

Lignin is crucial to vascular plants (softwood, hardwood, grass) as a key component of their second cell walls. It is the fiber that allows plants to live on land by contributing to the stiffness and strength of the stem. It also protects cellulose and hemicellulose from attack by insects and pathogens.[17,142] Based on these functions, it is understandable that the polymer structure of lignin is tough and difficult to depolymerize.

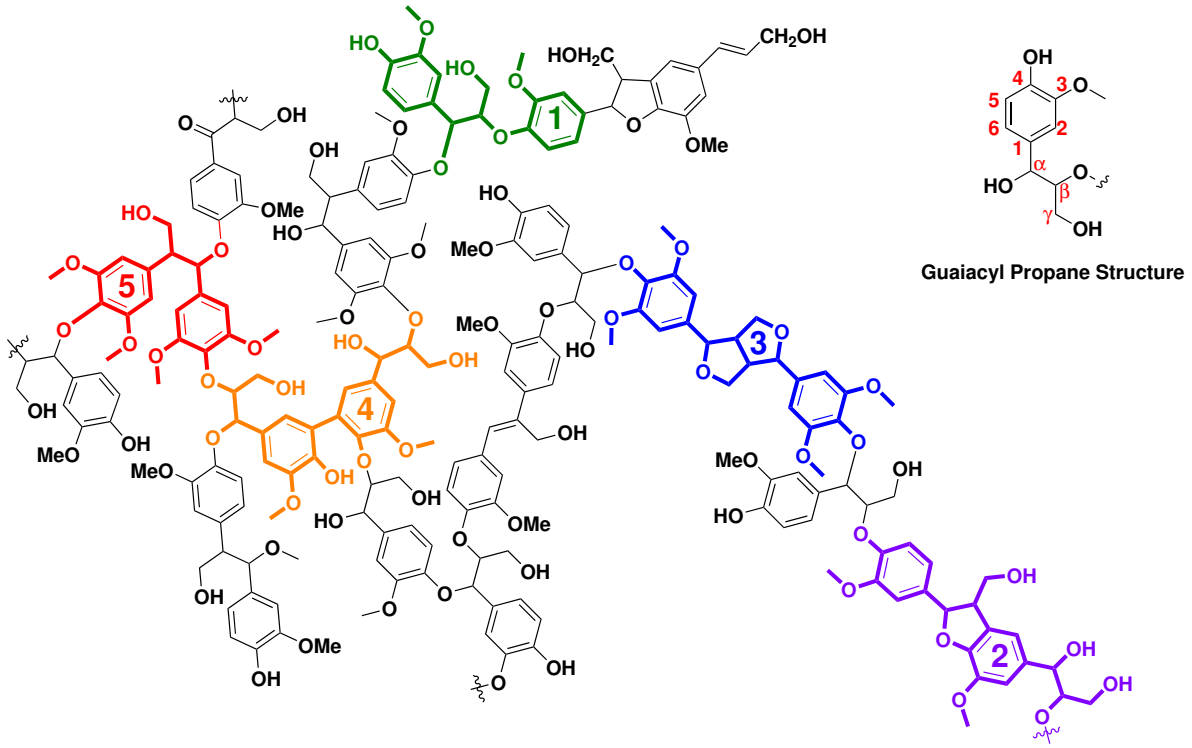

Figure 3.1: Structure of beech lignin proposed by Nimz, H.[15] linkage **1**: β-O-4; **2**: β-β; **3**: β-5; **4**: 5-5; **5**: 4-O-5. The lignin nomenclature is different from the conventional IUPAC system and is shown in the guaiacyl propane structure.

3.1.2 Three monomer precursors to lignin

Lignin is believed to be a heterogenous cross-linked polyphenolic complex (as illustrated in Figure 3.1) consisting mainly of three phenolic alcohol monomers: coniferyl alcohol, sinapyl alcohol, and p-coumaryl alcohol. Coniferyl alcohol, as shown in Figure 3.2 is the one most widely distributed in all three types of plants: softwood, hardwood, and grass. Sinapyl alcohol is a major monomer in hardwood. p-Coumaryl alcohol only appears in relatively large amounts in grasses, while only trace amounts of it can be detected in both softwood and hardwood.[16]

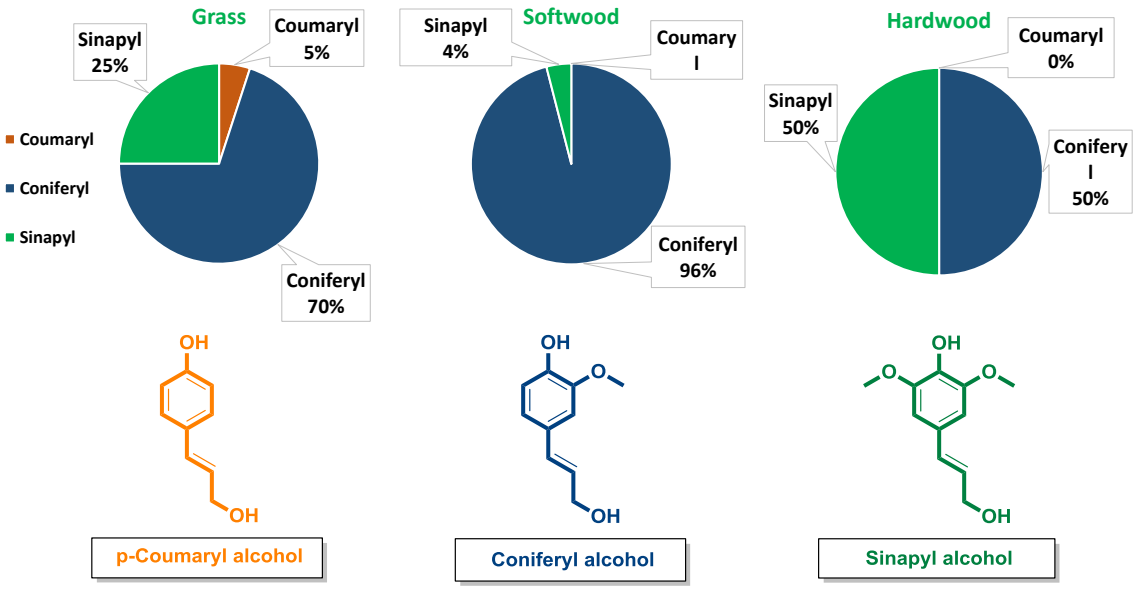

Figure 3.2: Three monomers of lignin and their distribution in different plants.[16]

3.1.3 Common linkages between monomers of lignin

The nomenclature of lignin is different from that of IUPAC. For the aromatic ring, as shown in Figure 3.1 the carbon connecting with the propanyl side chain is designated carbon 1; the one with the methoxyl group is carbon 3; the one with the hydroxyl group is carbon 4. For

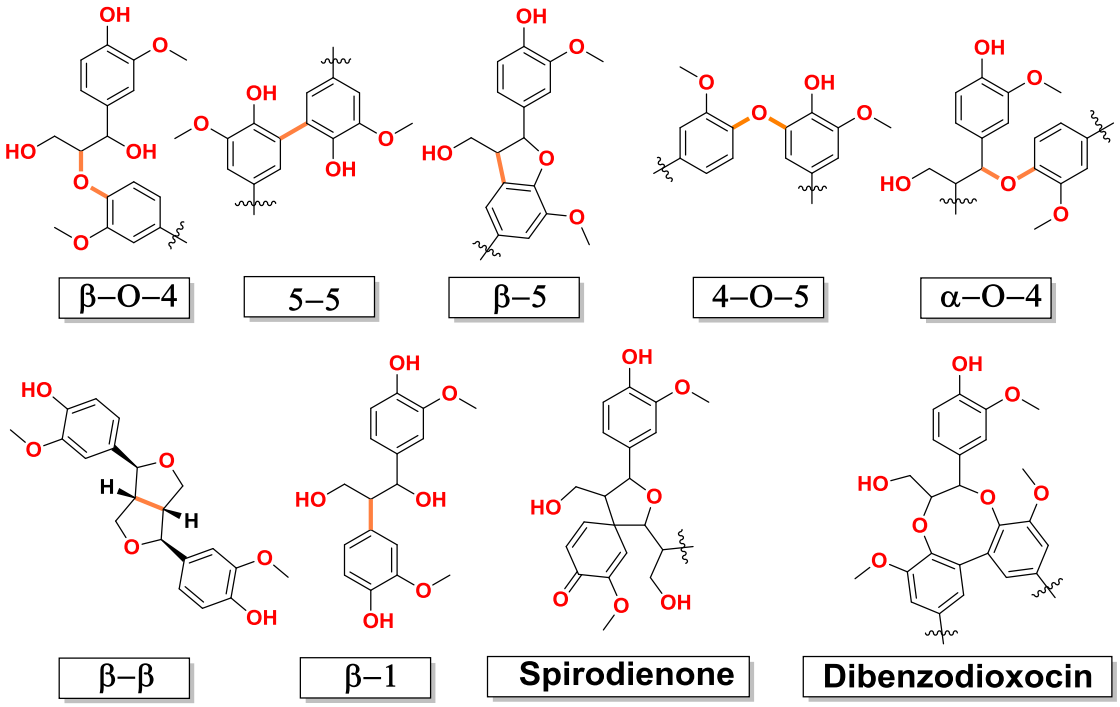

Linkage type	Percentage of total linkages	
	Softwood	Hardwood
β-O-4	45%-50%	60%-62%
5-5	19%-27%	3%-9%
β-5	9%-12%	3%-11%
β-β	2%-6%	3%-12%
4-O-5	4%-7%	7%-9%
α-O-4	2%-8%	7%
β-1	1%-9%	1%-2%
Spirodienone	2%	3%-5%
Dibenzodioxocin	5%-7%	0%-2%

Figure 3.3: The common linkages and the percentage of total linkages in lignins.[17,18]

the C3 side chain, the carbon connected to the aromatic ring is the α-carbon; the next one is the β-carbon, and then is the γ-carbon.

The nine common linkages appeared in lignin are shown in Figure 3.3, of which β-O-4 is the most widely distributed: this linkage occurs in both softwood and hardwood (45-50% in softwood, 60-62% in hardwood). Other linkages include the 5-5 (19-27% in softwood, 3-9% in hardwood), β-5 (9-12% in softwood, 3-11% in hardwood) as the second and third most common linkages. Notably, β-β appears in hardwood a lot (2-6% in softwood, 3-12% in hardwood), owing to the fact that, sinapyl alcohol which is a greater fraction of hardwood lignin favors the β-β linkage as its 5-position is occupied by a methoxyl group.[143–147] β-1 is attributed a larger percentage in some reports (7-9% in softwood, 7% in hardwood),[144] while only 1-2% in other literatures.[145,146] Spirodienone and dibenzodioxocin were found later and only appears in small percentages of the lignin structures.

The structure proposed by Nimz, Figure 3.1, roughly illustrates the above proportions; it shows all of these common crosslinks and their frequency appearing in lignin as mentioned above.

3.1.4 Biosynthesis of lignin from monomers

Lignin monomers are believed to go through a dehydrogenation following an oxidation process to generate radicals, which leads to the polymerization of lignin monomers. Although lignin has been studied for more than a century, the biochemical process for the dehydrogenation of monomers and polymerization process of dehydrogenated monomers are still in active discussion.[142]

Sarkanen and Ludwig[17] suggested that lignin polymer formation occurs through formation of free monomer radicals by oxidative enzymes (laccases or peroxidases) which is

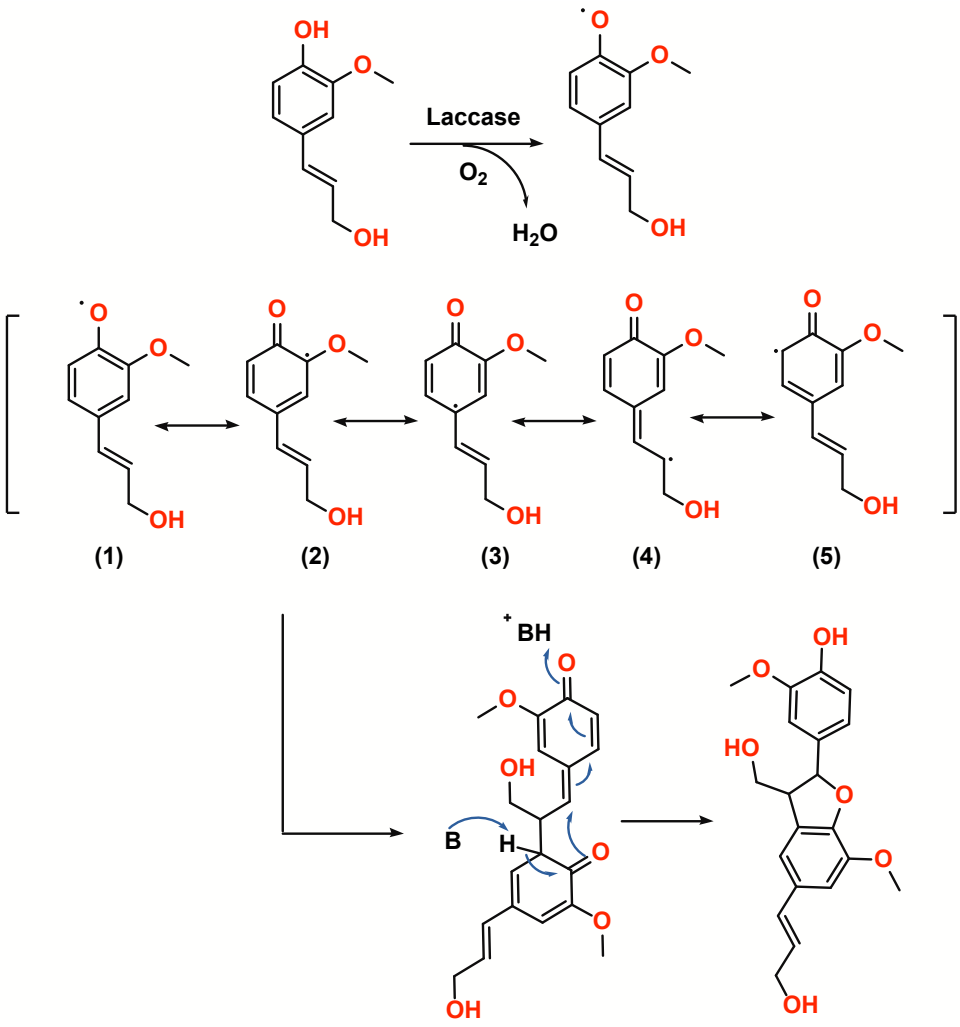

Figure 3.4: Mechanism for the formation of lignin dimer linkage β-5.[17]

followed by random coupling. However, this random coupling mechanism does not explain many aspects of lignin; for instance, in nature β-O-4 occurs at 45-50%, while for synthetic lignin prepared in vitro from monomers oxidized by peroxidase-H_2O_2, a much higher β-O-4 content (70%) is found.[147] In 1997, Lewis suggested that the lignin free radicals could be controlled by dirigent proteins.[148] However, no strong evidence has been reported for a role for dirigents in lignification.[142] The following polymerization process is from the commonly accepted model based on lignification occurring without the direction of biochemical controls.

The dimerization of monolignol does happen, but it is less significant in the lignification

process which mostly couples a monolignol with an oligomer (growing polymer).[142] Herein, the proposed mechanism for the formation of β-5 is shown as an example in Figure 3.4.

The enzyme, horseradish peroxidase or Laccase, makes use of oxygen and dehydrogenates the phenolic hydroxyl of coniferyl alcohol. The generated radical has five resonance structures (1) to (5), but only (1), (4) and (5) are likely sites for coupling reactions. The β-5 bond is produced by radical coupling followed by an intramolecular cyclization reaction.[149] However, 5-5 and 4-O-5 are rarely generated by dimerization reactions. Instead, they are generated from the lignification process where one pre-formed lignin oligomer couples with one coniferyl alcohol with the aid of dehydrogenation oxidation by the enzyme to generate 5-5 and 4-O-5.[142]

3.1.5 Functional groups, minor structures and the suggestions to our lignin dimer modeling

To design the lignin dimer models, it is important to understand the functional groups and structures in lignin.

1) 20% of the α-position is hydroxyl group, 9% of which exists as double bond.[17] Therefore, lignin models with α-β double bond were studied as in coniferyl alcohol, methylferulate, ethyl ferulate, dimer II (see Figure 3.15), dimer III, and dimer V.

2) 84% of the γ-OH is free alcohol; 13% of the γ-alcohol exists as ether in β-β linkage;[17] and 3% exists as γ-aldehyde. γ-OH model dimers I and II, β-β linkage dimer IV, and aldehyde models vanillin and coniferyl aldehyde were selected to study γ-OH and γ-ether effects.

3) Coniferyl alcohol exists in lignin as an end-group (6 %),[17] as shown in Figure 3.1

colored with purple. Thus the coniferyl alcohol and β-5 dimer II are considered as a good model to represent this characteristic of lignin.

4) Coumaryl esters exist in lignin as the linkers with polysaccharide; the ester ethyl ferulate and methyl ferulate are synthesized to study as a model for such system.

5) Lignin is polyphenolic compounds with about 32% of phenolic units having free phenolic hydroxyls.[17] The free phenolic hydroxyl systems can go through quinone methide mechanism of degradation while phenolic ethers cannot. Thus both models with free phenolic and no free phenolic OH models should be considered. However, the present work focuses on a green methodology to depolymerize lignin, with water as the ideal solvent. Due to the limited solubility of non-phenolic models in water, for this stage of study, the ether forms were omitted. It should be noted that the methyl ether version of dimer models can be synthesized readily via methylation of free phenolic OH models with methyl iodide when necessary.

3.2 Results and discussion

3.2.1 The preparation of lignin monomer building blocks

Many lignin monomers are commercially available, but some of them are too expensive as starting points for large-scale synthesis. This work aimed to design economically affordable synthesis pathways. We synthesized lignin monomers which are both good ECH models and key precursors for dimer synthesis such as compound (**1**), (**2**), (**3**), (**4**) and (**5**). Compound (**5**), (**6**), and (**7**) used as ECH models for the test of steric hindrance influence were also synthesized.

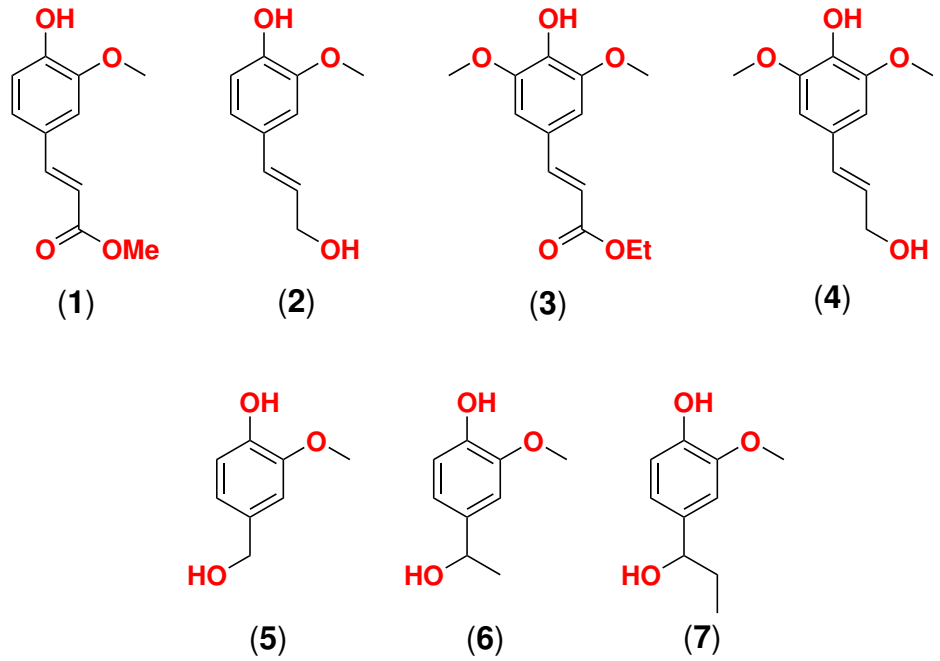

Figure 3.5: Lignin monomer models and key precursors to dimers. Top from left to right: methyl ferulate, coniferyl alcohol, ethyl sinapate, and sinapyl alcohol; bottom from left to right: vanillyl alcohol, apocynol, and 1-guaiacylpropan-1-ol.

3.2.1.1 Synthesis of methyl ferulate

Methyl ferulate (**1**) represents the ester functional group in lignin, where it is an arabinofuranoside instead of the methyl ester of ferulate.[150] Methyl ferulate can also be used as a precursor of β-β, β-5, and β-O-4 dimer models (coniferyl alcohol version), which are three of the most important linkages in lignin. Therefore, identifying an efficient, cheap, and robust pathway of synthesis is important, considering the large quantity of it needed.

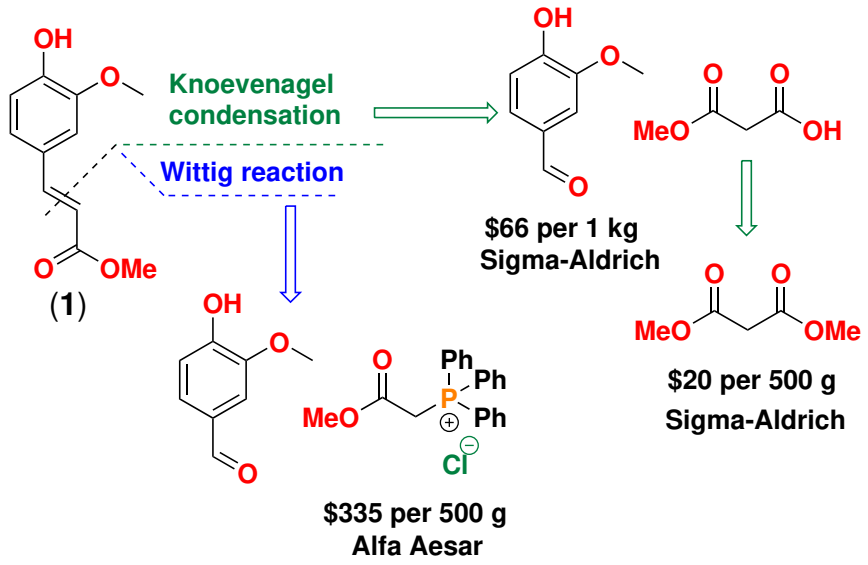

Figure 3.6: The retro-synthesis of methyl ferulate.

There are two common approaches to the synthesis of the methyl ferulate: 1) Two steps through Knoevenagel condensation of mono-methyl malonate with vanillin. 2) One step from triphenylphosphonium salt condensate with vanillin. Realizing the Knoevenagel condensation can be conducted in the same solvent as the hydrolysis of diethyl malonate, we chose the one-pot synthesis of methyl ferulate by Knoevenagel condensation since the starting material is much cheaper than that of the Wittig reaction as shown in Figure 3.6.

However, after several trials, we realized that the final ester product (**1**) does not form crystals easily, and the purification requires expensive column chromatography. Therefore,

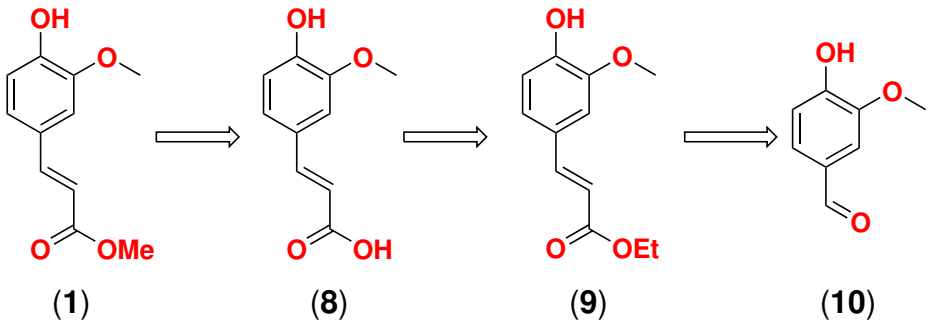

Figure 3.7: Revised retro-synthesis for methyl ferulate.

we designed another longer, but an easily purified pathway to (**1**) as shown in Figure 3.7.

The new synthesis of methyl ferulate (**1**) started from the preparation of mono-ethyl malonate (**11**) from the hydrolysis of diethyl malonate (**12**). This selective mono-hydrolysis reaction was very successful since the ethyl potassium malonate produced is insoluble in ethanol and crashed out as a solid. Once it was neutralized with acetic acid, the mono-ethyl malonate (**11**) re-dissolve into ethanol solution, and the potassium acetate generated can still act as a base for the following Knoevenagel condensation.

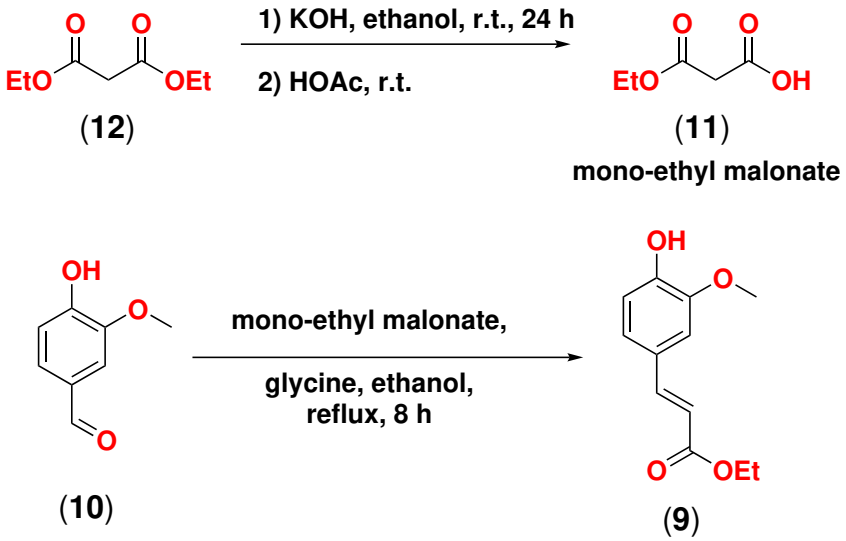

Figure 3.8: Synthesis of ferulic acid.

Adding vanillin (**10**) into the resulted mono-ethyl malonate (**11**) solution did not result

in very fast reaction even under reflux condition. Piperidine was reported to enable this condensation to proceed smoothly,[151] but in our experiences, the final product is difficult to purify because of the quantitative amount of piperidine used, the high-boiling point of the co-solvent toluene, and a small number of unidentified compounds generated along with (**9**). On the other hand, a method reported by Zeng,[152] which used a trace amount of glycine as a catalyst to accelerate the condensation, was investigated and the pure target compound (**9**) was readily produced within 8 h.

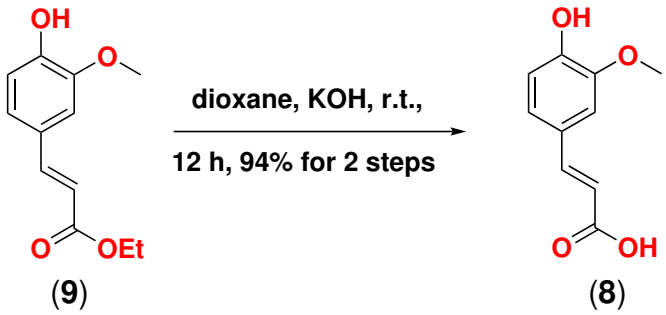

(**9**) (**8**)

Figure 3.9: The hydrolysis of ethyl ferulate to ferulic acid.

The resulted relatively pure (**9**) cannot be recrystallized from any combinations of the solvent pair studied: alcohol (methanol, ethanol, isopropyl alcohol) with water, ethyl acetate with hexane, toluene with hexane, and sodium hydroxide aqueous solution (1 eq NaOH) with ethanol. The crude product (**9**) was hydrolyzed without purification in a NaOH-water-1,4-dioxane solution. A large amount of ferulic acid (**8**) was produced and yellow needle-shaped crystals were obtained from methanol/water recrystallization. Moreover, an excellent 94% yield from (**10**) to (**8**) was achieved.

The methylation of ferulic acid proceeds smoothly with a catalytic amount of sulfuric acid in methanol under reflux conditions.[153] Care needs to be taken, as a side product, generated from the Michael-addition of methanol to the enoate, will be produced if reaction time is not well monitored or if the amount of sulfuric acid is too much. The side product

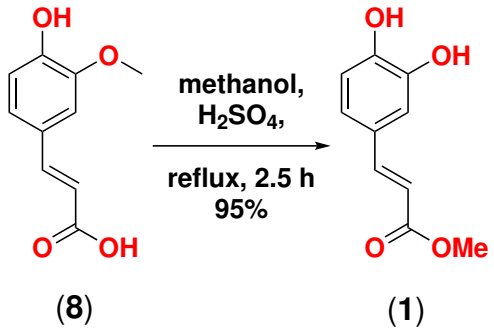

Figure 3.10: The methylation of ferulic acid to methyl ferulate.

can, however, be controlled to less than 5%.

3.2.1.2 Synthesis of coniferyl alcohol

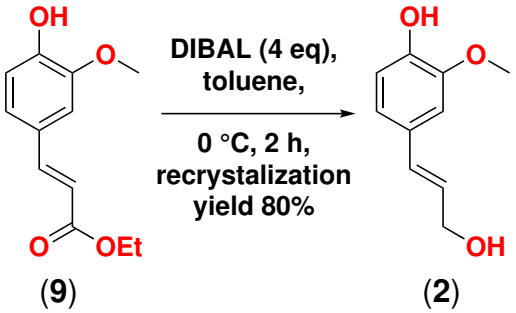

Figure 3.11: The reduction of ethyl ferulate to coniferyl alcohol.

Coniferyl alcohol (**2**) can be easily recrystallized as a whitish yellow powder, therefore, the synthesis can start from the crude product (**9**). No olefin reduction was observed even after the temperature was raised to r.t. at the end. However, a consistently low isolation yield was obtained with the literature procedure.[154] We found that the aluminum hydroxide generated from the addition of water absorbed most of the product. Once it was treated with HCl, the majority of the product was released. Nonetheless, the final product is sensitive to acid treatment and temperatures higher than 80 °C, and a black polymeric oil is generated if the product is not handled correctly. Consequently, we choose to use Rochelle salt (potassium

sodium tartrate) as a chelating agent for aluminum and successfully released most of the product as a colorless oil. After recrystallization from dichloromethane and hexane, a decent yield of 80% of light yellow powder (**2**) was obtained with excellent yield.

3.2.1.3 Synthesis of ethyl sinapate and sinapyl alcohol

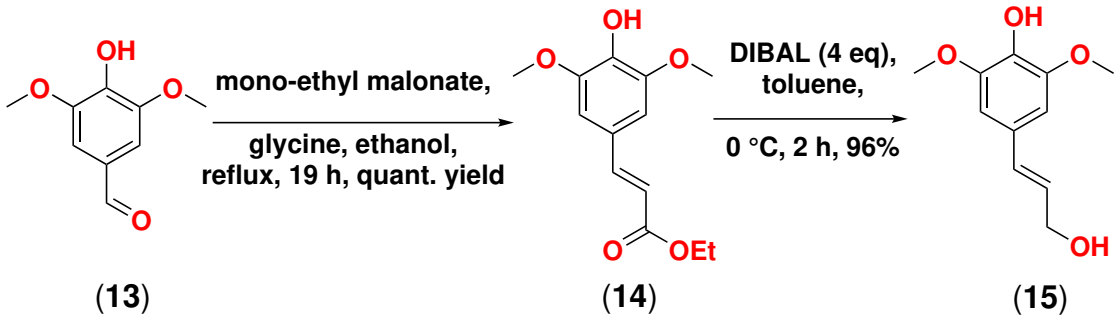

Figure 3.12: The synthesis of ethyl sinapate and sinapyl alcohol.

The synthesis of ethyl sinapate (**14**) and sinapyl alcohol (**15**) are very similar to those of ethyl ferulate (**9**) and coniferyl alcohol (**2**), but require longer reaction times. The purification of (**14**) is very simple since its solubility in diethyl ether is very low, an excess amount of malonate impurities can be rinsed away by using diethyl ether, yielding pure (**14**). Using the same reduction and isolation process as in the DIBAL reaction of ethyl ferulate (**16**), a yield of 96% pure sinapyl alcohol (**15**) is obtained.

The DIBAL reaction has to be conducted with a much excessive amount (2-5 equivalent). Moreover, DIBAL is expensive ($159 per 114 g in hexane from Sigma-Aldrich) compared to cheap sodium borohydride ($NaBH_4$) ($78 per 100 g from Sigma-Aldrich) and more expensive than lithium aluminum hydride ($LiAlH_4$) ($141 per 100 g from Sigma-Aldrich) if considering the 1-4 equivalent excess amount of DIBAL usage and 0-0.5 equivalent excess for $LiAlH_4$.

The ester (**14**) is very inert to $NaBH_4$ hydrogenation, no reaction was observed within 24 h with methanol as solvent. However, $LiAlH_4$ is well known for its high reactivity but

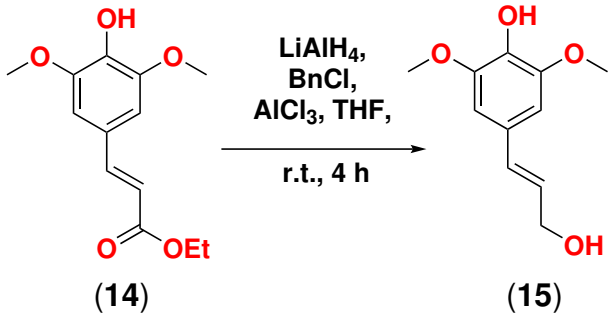

Figure 3.13: Synthesis of sinapyl alcohol with $LiAlH_4$.

lower selectivity between 1,2-addition and 1,4-addition of enoate; in this case 1,4-addition byproduct was likewise observed in preliminary reduction attempts. Reported by Wang,[155] $LiAlH_4$ reacts with alkyl halide and generate AlH_3, which is a more effective 1,2-addition reductant. However, this reaction is not a clean reaction and always produces unknown byproducts.

All in all, DIBAL is recommended to reduce enoate (**14**) the allyl alcohol (**15**) since it generates no byproduct. Reduction of the amount of DIBAL from 10 down to 4 equivalents led to no yield reduction.

3.2.1.4 Synthesis of benzyl alcohol monomer models

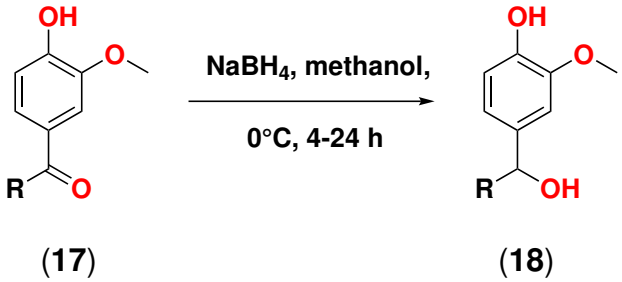

Figure 3.14: The reduction of guaiacyl carbonyls to guaiacyl alcohols. R = H: vanillin and vanillyl alcohol; R = Me: acetovanillone and apocynol; R = Et: guaiacylethylketone and guaiacylpropan-1-ol.

The reduction of carbonyl (**17**) to alcohol (**18**) by sodium borohydride can be applied to

the synthesis of vanillyl alcohol (R = H) (**5**), apocynol (R = Me) (**6**), and guaiacylpropan-1-ol (R = Et) (**7**). No protection of phenol hydroxyl is required for the successful quantitative conversion.

The final products (**18**) are prone to be polymerized in the presence of acid and heat during the isolation step. The reduction at room temperature gives pure products sometimes, but the reaction process is not robust and can lead to black oil polymer products. Therefore, ice cold temperature control is crucial for the consistently successful isolation of the pure product. Moreover, DCM is recommended as the extraction solvent since ethyl acetate has a higher boiling point and rotovap at above 60 °C can encourage the polymerization of products.

3.2.2 The synthesis of major lignin dimer models

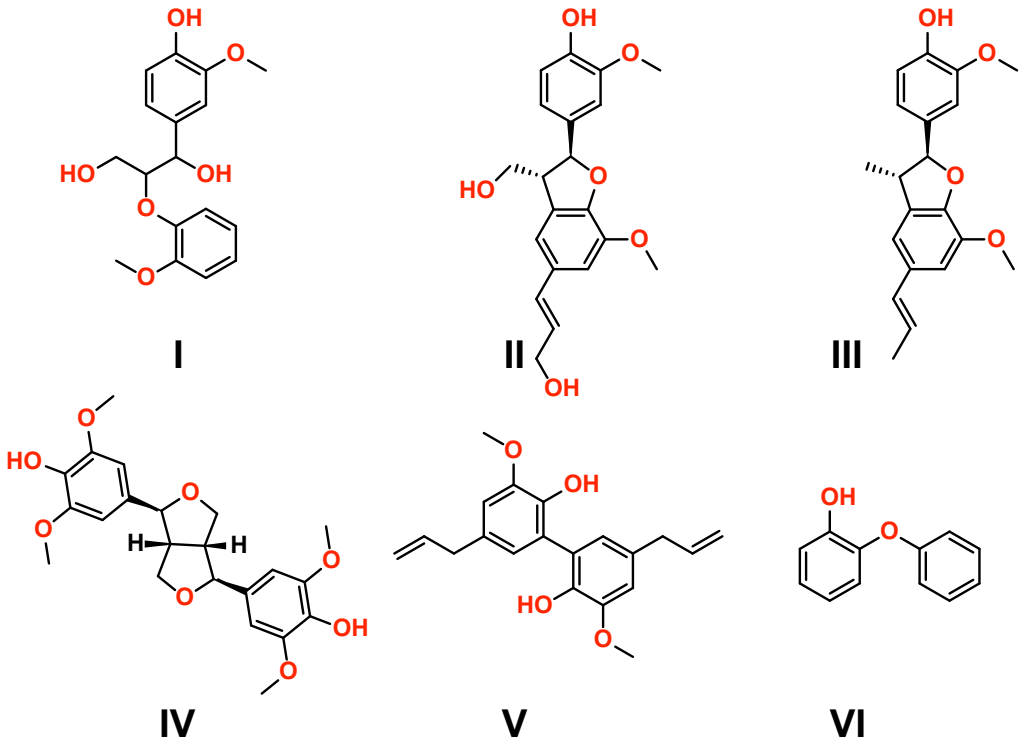

Figure 3.15: The synthesis of major dimer models of lignin.

Considering that the β-O-4, β-5, β-β, 5-5, and 4-O-5 linkages are the majority of linkages existing in the lignin structure, and that no comprehensive ECH research is available on all of these linkage dimers, we synthesized (I) to represent the most abundant linkage in lignin; (II) and (III) are both β-5 linkage models, except that the latter is much cheaper to make but still has the same type of linkage. (IV) represents the β-β linkage and (V) is a 5-5 linkage dimer; (VI) is a model for 4-O-5 aryl-aryl ether linkage.

3.2.2.1 β-O-4 linkage dimer synthesis

There are two approaches building the β-O-4 linkage lignin dimer; Approach I makes use of aldehyde alkylation reaction initiated by lithium diisopropylamide (LDA), while Approach II take advantages of a S_N2 displacement at a carbonyl α-C to couple (**32**) and (**30**) followed

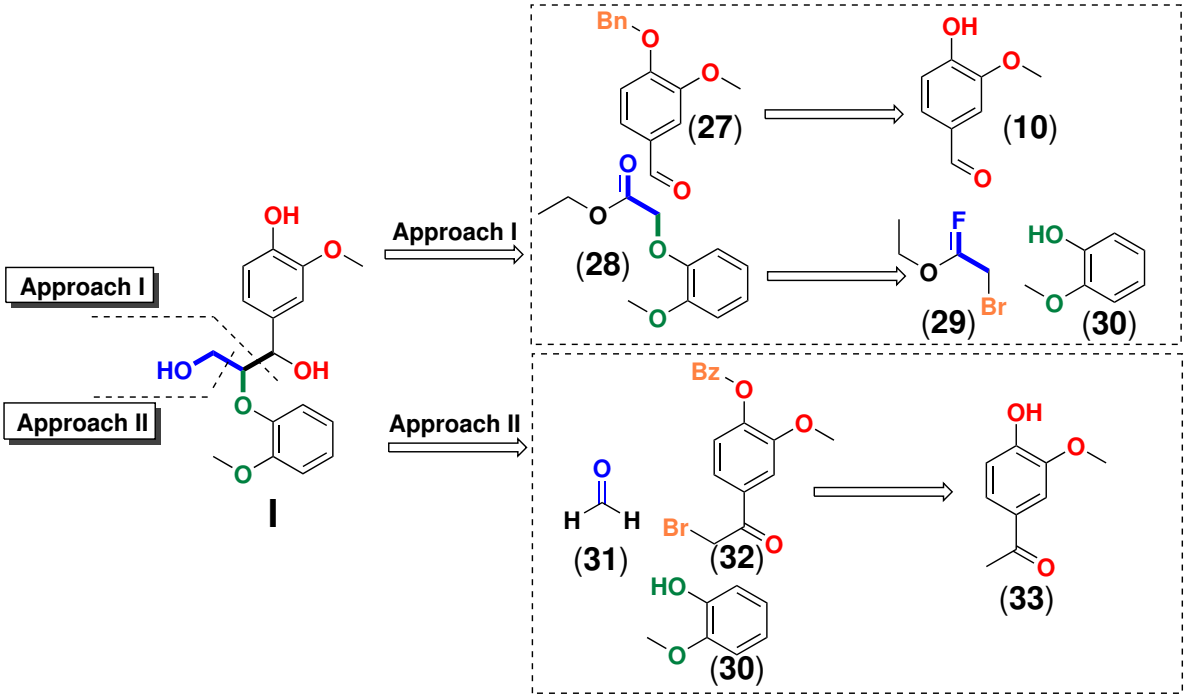

Figure 3.16: The retro-synthesis analysis of β-O-4 **I**.

by $NaBH_4$ reduction of α-carbonyl to α-OH. We tested both approaches and found that Approach I is easier to synthesize dimer I because the formaldehyde tends to polymerize with phenols in Approach II.

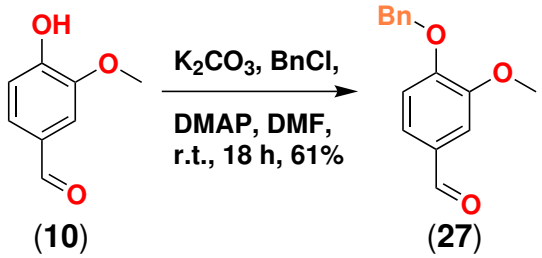

Figure 3.17: The protection of vanillin with benzyl group.

The synthesis of dimer I started from the protection of vanillin (**10**) and carbonyl-alkylation of guaiacol (**30**). We tested several protecting groups including trimethylsilyl (TMS), tert-butyldimethylsilyl (TBS) groups, and benzyl (Bn) groups, and found that TMS protected phenol tended to be protected under a neat condition, while TBS protected phenol

was much more stable than the TMS aryl ether. However, even this compound decomposed after several weeks of storage. Benzyl vanillin (**27**) is easily crystallized and after one recrystallization, very pure (**27**) is obtained; this material can be stored exposed to the air for months without decomposing or oxidation by oxygen.

We employed the mild synthesis of benzyl vanillin (**27**) reported by Njiojob[156] as in Figure 3.17. Compared with other strategies,[157] this method uses cheap benzyl chloride instead of more expensive benzyl bromide and needs only room temperature as opposed to with reflux condition. Without DMAP, the reaction did not proceed to completion within 24 h. The 61% was isolated yield from recrystallization

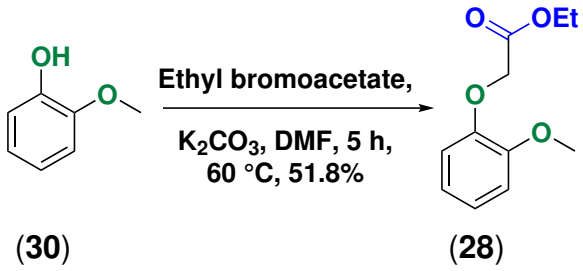

Figure 3.18: The alkylation of guaiacol hydroxyl.

To build the other half of the intended dimer targets, the guaiacol hydroxyl site was alkylated via a simple S_N2 reaction by deprotonation of guaiacol with a weak base (K_2CO_3) followed by the addition of ethyl bromoacetate. A clean crude product (**28**) was obtained quantitatively. After recrystallization, pure (**28**) was obtained with a yield of 51.8%.

The coupling of moieties (**27**) and (**28**) makes use of a simple aldol reaction initiated by enolate formation for α-carbonyl of (**28**) with LDA (lithium diisopropylamine), generated in situ from *n*-BuLi and diisopropylamine (DIPA). The enolate nucleophilically attacks the electrophilic aldehyde carbonyl of (**27**), which produces β-O-4 linked ester (**34**) in two diastereomeric forms.

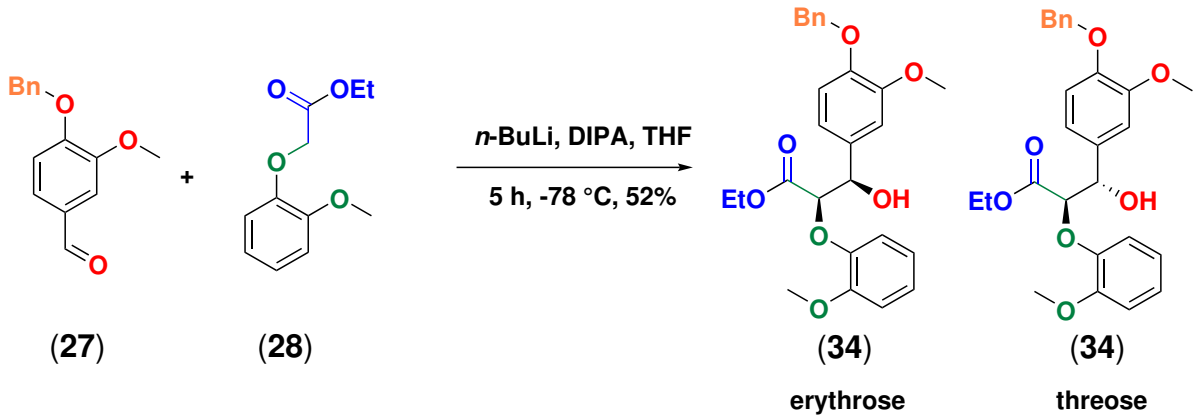

Figure 3.19: The coupling of benzyl protected vanillin and ethyl guaiacylacetate.

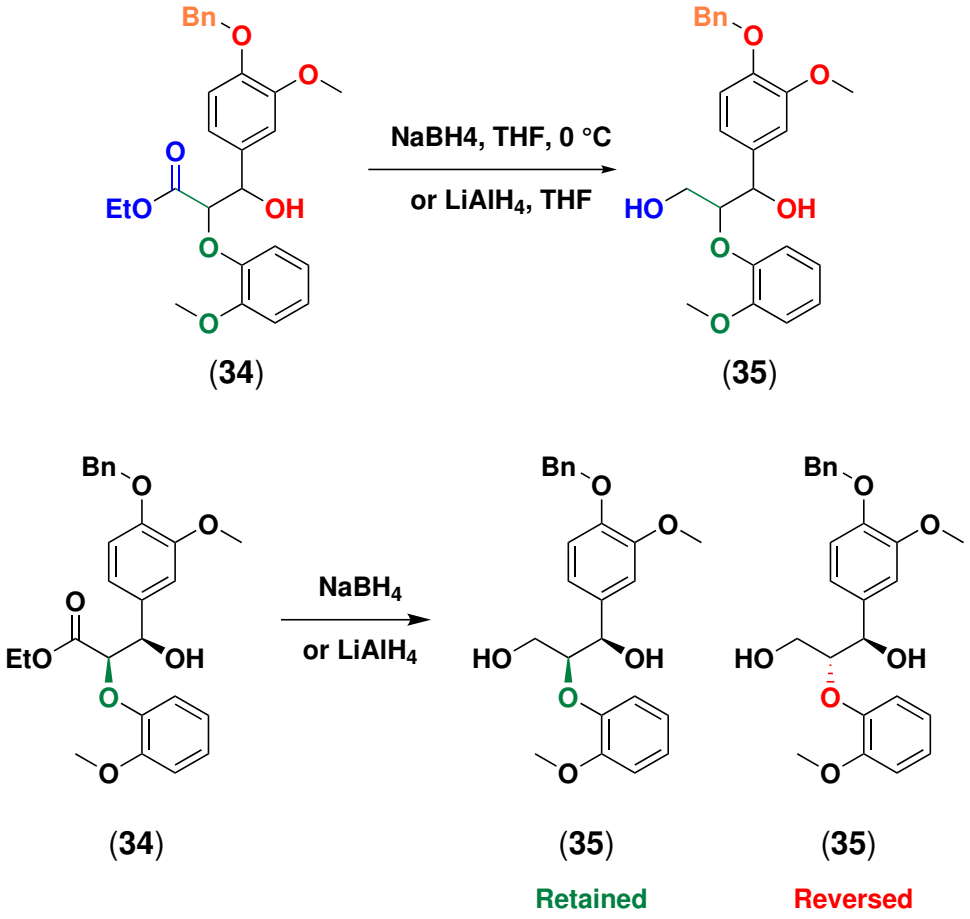

Figure 3.20: The reduction of ester to alcohol.

This method is effective but sensitive to moisture. If all solvent, glassware, and reagents are not dried properly, low conversions result.

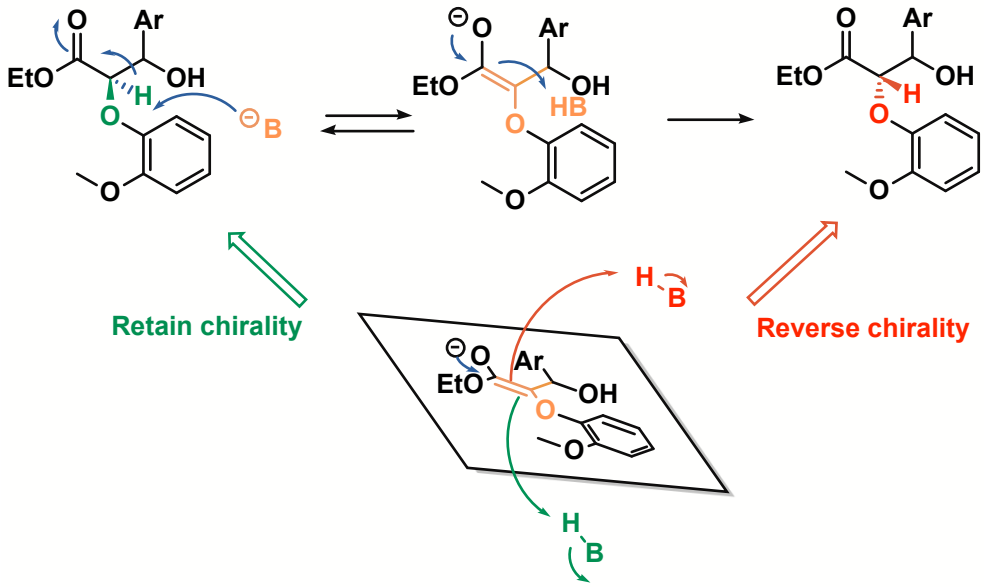

Figure 3.21: The reduction of ester to alcohol.

The reduction of ester (**34**) to primary alcohol (**36**) can be achieved with either $NaBH_4$ or $LiAlH_4$. However, after the reaction, the pure isomer (**37**) not only undergoes the reduction of an ester to alcohol but is also isomerized to its diastereomers. One possible explanation is shown in Figure 3.21. The α-carbonyl proton can be deprotonated by the base generated from either $NaBH_4$ or $LiAlH_4$, after which the flat enolate generated can pick up a proton from either face. If it picks up a proton from the same face where it lost the proton originally, the chirality is retained, otherwise, the chirality is reversed.

To overcome this drawback, the protocol reported by Bolm[158] makes use of a bulkier tert-butyl ester of (**34**) instead of ethyl ester; this modification greatly improved the erythro/threo selectivity. Thus the tert-butyl ester is recommended for future synthesis of β-O-4 dimer models.

With pure (**35**) in hand, a simple deprotection by removal of the benzyl group with

hydrogen gas and a Pd on carbon catalyst completed the synthesis of dimer I.

3.2.2.2 β-5 dimer II and dimer III synthesis

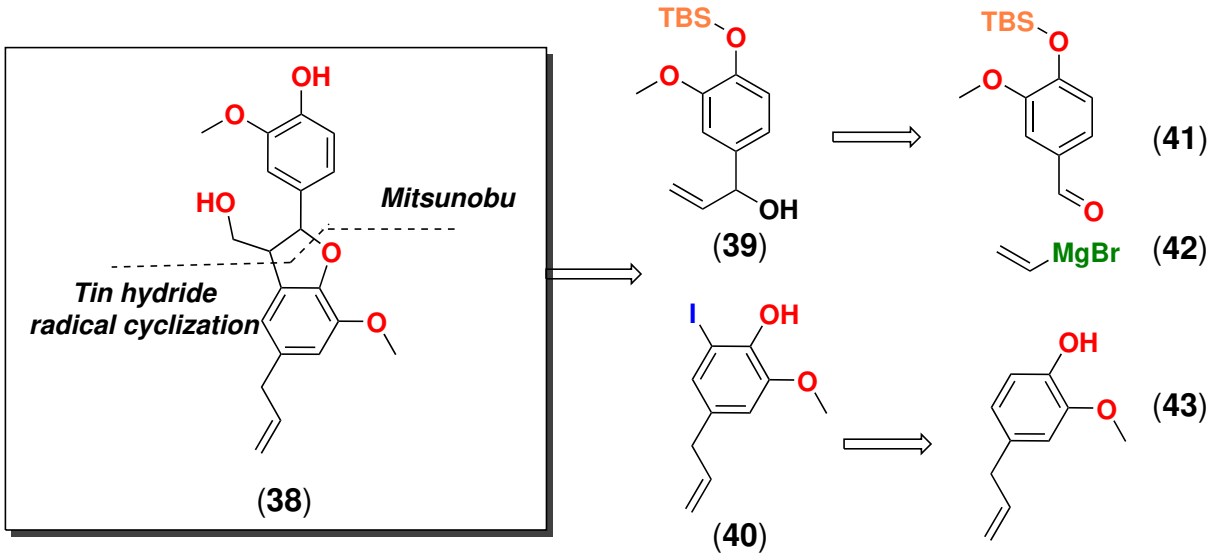

Figure 3.22: The retro-synthesis of a β-5 dimer model.

The β-5 dimer has two linkages between the two monomer moieties, the α-O-4 linkage, and β-5 linkage. The former linkage can be connected by Mitsunobu reactions between (**39**) and (**40**) proposed in the retro-synthesis shown in Figure 3.22, while the β-linkage can be formed from a radical cyclization reaction between an aryl iodide (**40**) and an olefin (**39**). Therefore, it was proposed that the complicated dimer (**38**) can be disconnected into simple molecules (**41**), (**42**), and (**43**).

The protection of vanillin with TBS forms a much more stable product than TMS; the TMS ether decomposed within several days possibly due to water hydrolysis. After protection, (**41**) reacted with vinyl Grignard reagent completely.

The selective aryl iodination of eugenol was realized by adding iodine in a basic solution of eugenol under cold conditions to form (**40**); remarkably, no olefin addition side reaction

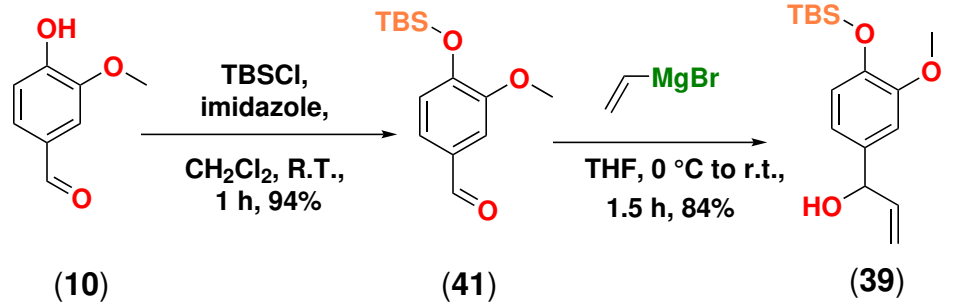

Figure 3.23: The synthesis of olifen moiety of dimer.

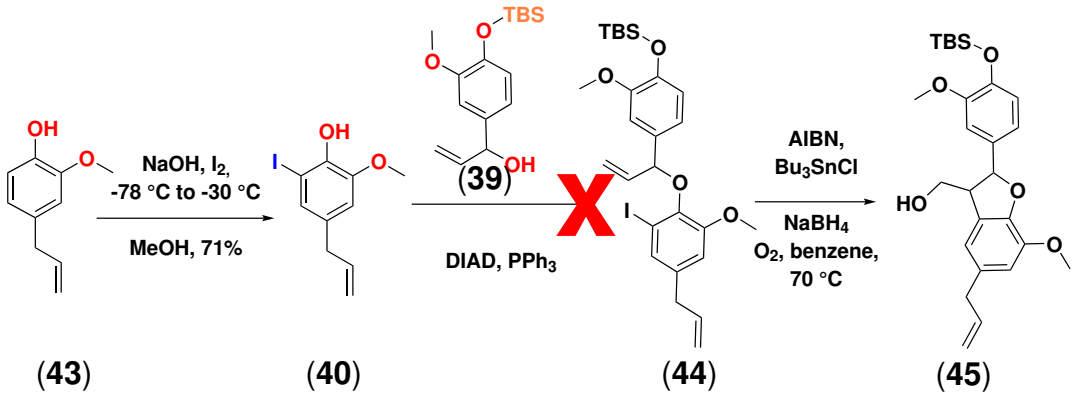

Figure 3.24: The unsuccessful synthesis of a β-5 dimer.

was observed. However, the Mitsunobu reaction between allyl alcohol (**39**) and phenol (**40**) was unsuccessful, forms a complicated product mixture. One possible explanation could be that once the benzylic hydroxyl of (**39**) was activated by the adduct of DIAD (diisopropyl azodicarboxylate) and PPh_3, the secondary benzylic carbocation could be formed and encourages other side reactions such as desilylation and phenol aromatic substitution reactions to produce oligomeric or even polymer products.

A new approach to build β-5 lignin dimer was then designed, as shown in Figure 3.25. This new approach was inspired by the radical mechanism of the horseradish peroxidase enzymatic dimerization of coniferyl alcohol to form all types of lignin dimers and eventually lignin.[17] We anticipated that if the terminal hydroxymethyl group of coniferyl alcohol (**2**) was replaced by a methyl ester group as in (**1**), the possibility to form the β-β dimer would

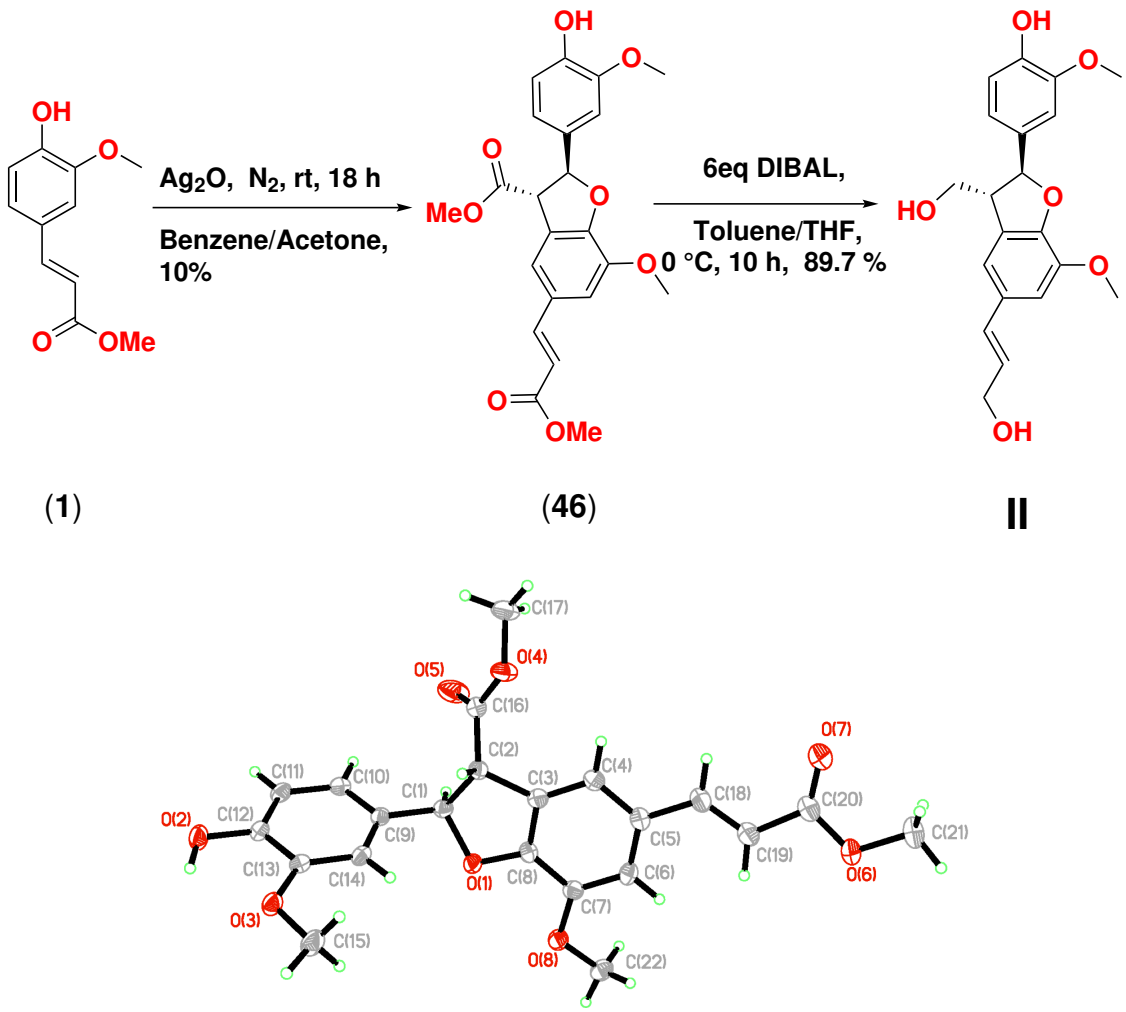

Figure 3.25: The new synthesis of β-5 lignin dimer II and the crystal structure of the ester intermediate.

be eliminated, therefore given a greater yield of the β-5-type dimer.

Ag_2O was found to encourage β-5 dimer (**46**) formation as reported by Tokoroyama.[159] Although the reaction failed a couple of times with purchased Ag_2O, it eventually worked very well with fresh prepared[160] Ag_2O to form easily separated (**46**). The Ag_2O in this reaction should be an oxidant since, after the dimerization reaction, there is a thin layer of silver formed on the wall of the flask indicating that silver(I) is reduced to silver(0). The low yield, only 10%, of this reaction is not due to the formations of major byproducts but a result of extensive purifications by the column chromatography and several times of recrystallizations

from methanol. The needle-shaped crystals of ester dimer can be obtained by slowly evaporation of a toluene/hexane solution. As confirmed both by the NOSEY NMR and the crystal structure of (**46**), the relative-stereochemistry of the guaiacyl group and the ester group is anti-geometry. Excess diisobutylaluminum hydride (DIBAL) reduced the methyl ester (**46**) to alcohol (II) smoothly with excellent yield. Efforts have been made to obtain the crystals of the final product (II), however, it only forms very tiny crystals if at all from all of the recrystallization methods that we tried in methanol, ethanol, ethanol/water, DCM, ethyl acetate/hexane, toluene/hexane. The final product structure and relative stereochemistry were confirmed by mass spectroscopy, proton, carbon, COSY, HSQC, HMBC NMR.

Although we finished the synthesis of β-5 dimer II, the mode II took a lot of effort to obtain started from vanillin (**10**). With the success of dimer II, we saw the opportunity to synthesize a β-5 dimer III in only one single step.

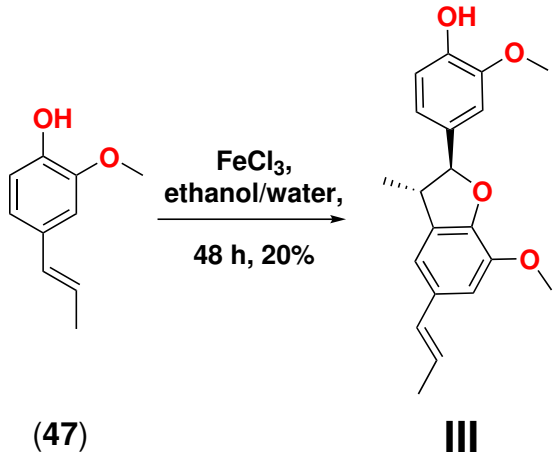

Figure 3.26: The synthesis of β-5 lignin dimer III.

Isoeugenol (**47**) has the same reactive sites as (**1**) towards radical dimerization reaction, and it can be purchased for only $150/kg from Sigma-Aldrich. The dimerization of isoeugenol was initiated by iron(III) chloride. The product dimer III is insoluble in the EtOH/H_2O mixture and slowly precipitated out as white needle-shaped crystals if the reaction was kept

unstirred.

3.2.2.3 The synthesis of lignin β-β dimer IV

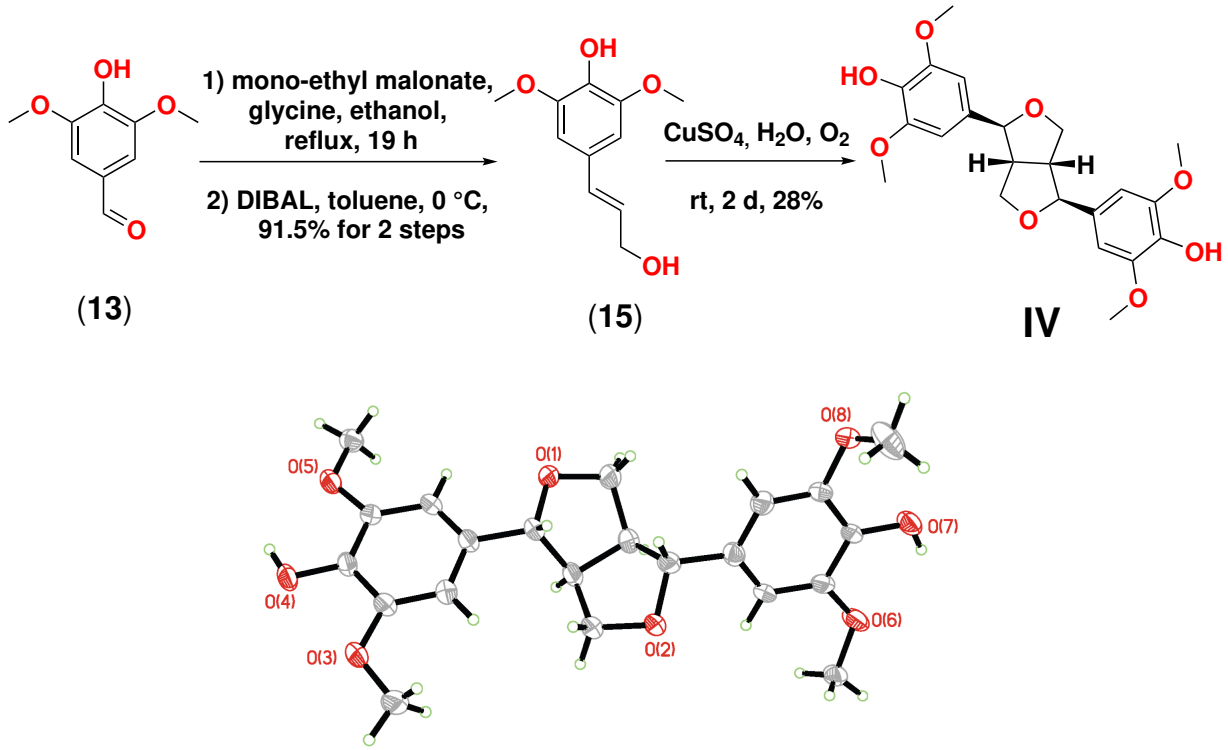

Figure 3.27: The synthesis of β-β dimer IV and its crystal structure.

Based on the failure and success of dimer II synthesis, we thought that the β-β dimer synthesis should also be planned to mimic the way nature makes this dimer. By using two methoxyl on the phenol aryl ring to block the possibility to form the β-5 dimer, sinapyl alcohol (**15**) can be used to synthesize dimer IV with much higher selectivity. After (**15**) is oxidized by copper(II) sulfate to its radical form, IV can be formed after a cascade of radical and nucleophilic reactions.

The crystal structure shows that the two β-protons and the two arene groups are all cis-isomeric relationships with each other. The methoxy groups are all almost in-plane (dihedral angle are between 6-16°C between the C-O bond and C=C double bond of the arene) with

the arene groups except one methoxyl group (O8-Me) almost perpendicular (dihedral angle 95°) to the aryl plane. However, since there is only one peak for the methoxyl groups in proton NMR, it is reasonable to conclude that this interesting geometry is related with the crystal packing and the methoxyl group can rotate in the solution at room temperature.

3.2.2.4 The synthesis of 5-5 lignin dimer model V

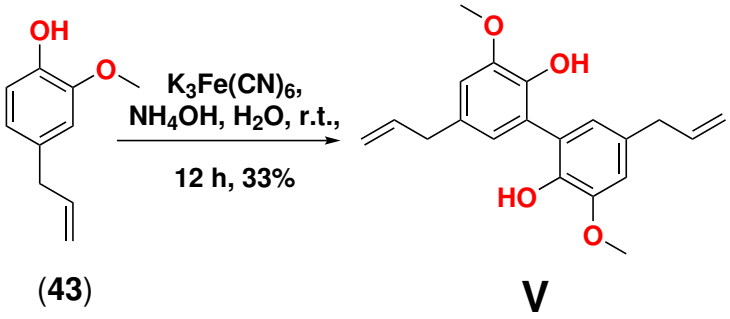

Figure 3.28: The synthesis of lignin 5-5 dimer V.

By using the same strategy, the 5-5 dimer can be easily synthesized by choosing a phenol such that after it is oxidized, the radical can only be formed on the phenol ring 5-position or on the phenol oxygen. Eugenol has one isolated double bond, therefore, the radical initiated by iron(III) is isolated to be on the aromatic ring or oxygen. The 5-5 dimer V can be obtained with good selectivity in this way.

3.2.2.5 The synthesis of 4-O-5 lignin dimer model VI

The synthesis routes of dimer VI starts from an aryl-hydroxyl aryl-halide coupling catalyzed by copper oxide catalyst with potassium hydroxide. The ortho-phenoxyanisole (**48**) can be recrystallized from ethanol and isolated purely as cubic crystals. The demethoxylation reactions are done by using BBr_3. The demethoxylation is initiated by the methoxyl nucleophilic attack of the electrophilic boron atom. Since the positive charge on the oxygen, bromide

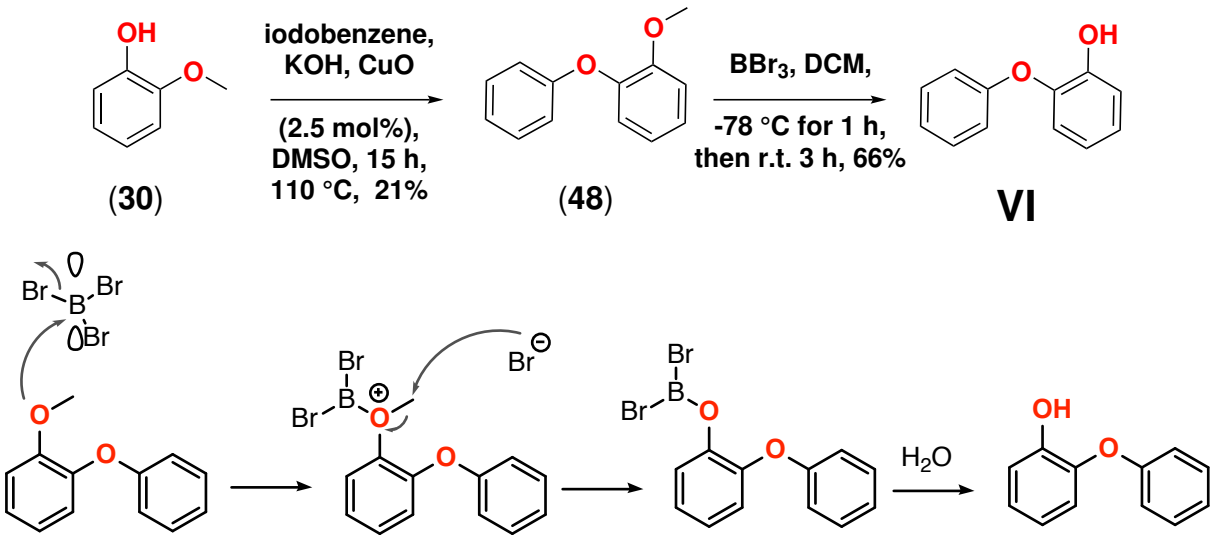

Figure 3.29: The synthesis of 4-O-5 dimer VI.

anion attacks the methyl group and kicked out phenoxyl group. Water quenching breaks the dibromophenoxyborane complex and releases the 2-phenoxyphenol VI.

3.3 Experimental

3.3.1 The synthesis of monomers

(9) Ethyl ferulate

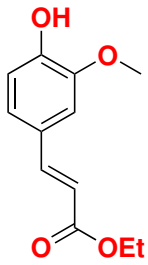

Figure 3.30: Ethyl ferulate.

The synthesis for ethyl ferulate[161] (**9**) started from the mono-hydrolysis of diethyl malonate (**12**). 30 g (0.54 mol) of potassium hydroxide was dissolved in 300 mL ethanol in a 1 L three-neck flask. A large magnetic stirring bar was added into the flask, and keeping a high stirring rate, then 75 g (0.47 mol) of diethyl malonate (**12**) dissolved in 200 mL ethanol, was added to the same flask over 20 minutes. The solution was stirred vigorously overnight, and quenched by adding 26.3 g (0.44 mol) of acetic acid and stirring for 1 h to get the mono-ethyl malonate (**11**).

Then, 40.7 g (0.27 mol) of vanillin (**10**) and glycine 4 g (0.054mol) were added to the mono-ethyl malonate solution; refluxed for 8h, the while solid turn to yellow liquid. 200 mL of DI water was added to the solution. After cooling down to room temperature, the mixture was extracted with 3 aliquots of dichloromethane 3 × 200 mL. Drying with sodium sulfate and evaporated the solvent to give 58.8 g (99%) of viscous yellow oil ethyl ferulate (**9**). Yellow solid can be formed slowly when the ethyl ferulate oil was stored in a container over a week. Recrystallization of the ethyl ferulate in methanol/water, ethanol/water, toluene,

dichloromethane/hexane were all failed.

MS (ES^-): 221.0841 ($M-H^+$). Calculated MS for $C_{12}H_{13}O_4$ is 221.0814.

^{1}H NMR (500 MHz, Chloroform-*d*) δ 7.62 (d, J = 15.9 Hz, 1H), 7.06 (dd, J = 8.2, 2.0 Hz, 1H), 7.02 (d, J = 2.0 Hz, 1H), 6.91 (d, J = 8.1 Hz, 1H), 6.28 (d, J = 15.9 Hz, 1H), 5.97 (s, OH), 4.25 (q, J = 7.1 Hz, 2H), 3.91 (s, 3H), 1.33 (t, J = 7.1 Hz, 3H).

^{13}C NMR (126 MHz, Chloroform-*d*) δ 167.34, 147.89, 146.75, 144.70, 126.98, 123.01, 115.57, 114.71, 109.28, 60.39, 55.90, 14.34.

This reaction was conducted according to literature procedure.[152] Our NMR values agree with literature values.[162]

(**8**) **Ferulic acid**

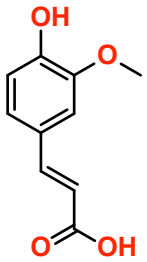

Figure 3.31: Ferulic acid.

In a 500 mL flask, 45 g of the ethyl ferulate (**9**) crude product was dissolved in 135 mL of 1,4-dioxane, then 350 mL of NaOH (2 M) aqueous solution was added. The flask was capped and sit for overnight. 80 mL 1 M HCl solution was used to acidify the solution until pH below 3, and the solution slowly turned to cloudy yellow and solid precipitated out. The flask was cooled with an ice bath for a half hour, suction filtration gave 37 g of crude ferulic acid (**8**) light yellow powder with 94% yield. The ferulic acid (**8**) was recrystallized from methanol/water to get 20 g of yellow needle crystals.

MS (ES^-): 193.0534 ($M-H^+$). Calculated MS for $C_{10}H_9O_4$ is 193.0501.

^{1}H NMR (500 MHz, DMSO-d_6) δ 12.14 (s, 1H), 9.57 (s, 1H), 7.48 (d, J = 15.9 Hz, 1H), 7.27 (d, J = 1.9 Hz, 1H), 7.07 (dd, J = 8.2, 1.9 Hz, 1H), 6.78 (d, J = 8.1 Hz, 1H), 6.36 (d, J = 15.9 Hz, 1H), 3.80 (s, 3H).

^{13}C NMR (126 MHz, DMSO-d_6) δ 168.46 , 149.50 , 148.32 , 144.97 , 126.15 , 123.23 , 115.99 , 115.94 , 111.50 , 56.07.

This reaction was not conducted according to literature procedure.[163] Our NMR values agree with literature values.

(**1**) **Methyl ferulate**

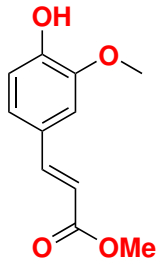

Figure 3.32: Methyl ferulate.

The obtained ferulic acid (**8**) 20 g (0.11 mol) was dissolved in 210 mL of methanol in a 500 mL flask. With ice bath cooling, 5.1 g (0.053 mol) of concentrated H_2SO_4 was added dropwise into the solution, and the system was heated up to reflux and the reaction was monitored by TLC until starting material disappeared (2.5 h). It was cooled down and poured into100 g ice water. The aqueous solution was extracted with 5 aliquots of dichloromethane (DCM) 5 $\times$ 200 mL. The combined DCM was extracted with brine solution 100 mL and it was dried over Na_2SO_4. After the removal of the solvent at room temperature over a vacuum, 24.2 g of crude light yellow oil was obtained. The oil was further dried by blowing under nitrogen gas for one week, and the extra solvents (DCM and methanol) was removed and 19.8 g (95%) yellow solid was obtained. Too much sulfuric acid and too long reaction time (for instance,

overnight) produce a byproduct, most likely from the Michael-addition of methanol to the enoate.

Yellow oil turns to yellow solid slowly.

MS (EI): 208.1

^{1}H NMR (500 MHz, Chloroform-*d*) δ 7.61 (d, J = 15.9 Hz, 1H), 7.05 (ddd, J = 8.2, 2.0, 0.5 Hz, 1H), 7.00 (d, J = 1.9 Hz, 1H), 6.90 (d, J = 8.2 Hz, 1H), 6.28 (d, J = 15.9 Hz, 1H), 3.89 (s, 3H), 3.78 (s, 3H).

^{13}C NMR (126 MHz, Chloroform-*d*) δ 167.78, 148.00, 146.78, 145.00, 126.89, 123.03, 115.08, 114.75, 109.36, 55.92, 51.64.

This reaction was conducted according to literature procedure.[153] Our NMR values agree with literature values.[164]

General procedures for DIBAL reduction of Guaiacyl or Sinapyl esters to make allylic alcohols (2) and (4): The numbers in the parenthesis are for the reduction of sinapyl ester, and the numbers before parenthesis are for guaiacyl ester. 0.1 M of ester was fully dissolved in dry toluene 700 mL (400 mL) at room temperature with a magnetic stir bar in a 2 L round bottom flask. The toluene solution was cooled in an ice bath and protected with nitrogen gas. A 196 mL (168 mL) of 1.5 M diisobutylaluminum hydride (DIBAL) in hexane solution was injected into the toluene solution slowly via a syringe over 1 h. After the addition was complete, stirring was continued for another 2 h (4 h). The solution was carefully quenched with methanol 150 mL (90 mL), and a 140 mL (80 mL) saturated potassium sodium tartrate water solution was added to prevent the precipitation of $Al(OH)_3$, followed by the addition of 200 mL (100 mL) ethyl acetate. The solution was vigorously stirred until the aqueous layer becomes clear. The aqueous layer was further extracted with 200 mL (100 mL) ethyl acetate for another 5 times. The combined ethyl

acetate layer was dried over sodium sulfate. After filtration, the solvents were removed over vacuum at room temperature and blowing with nitrogen gas for overnight. Light yellow (sinapyl alcohol) or light orange (coniferyl alcohol) color solids 12.3 g (8.6 g) were obtained. Do not heat the solution during the removal of the solvent since dark red color polymer oil may form during the heat. The coniferyl alcohol product can be recrystallized from methanol to generate a white powder 10.1 g. The light yellow sinapyl alcohol was used for the next step of synthesis without further purification.

(**2**) **Coniferyl alcohol**

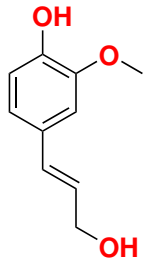

Figure 3.33: Coniferyl alcohol.

MS (EI): 180.1

^{1}H NMR (500 MHz, Chloroform-*d*) δ 6.93 – 6.83 (m, 3H), 6.52 (dt, J = 15.8, 1.5 Hz, 1H), 6.21 (dt, J = 15.8, 6.0 Hz, 1H), 5.77 (s, 1H), 4.29 (dd, J = 6.0, 1.5 Hz, 2H), 3.89 (s, 3H).

^{13}C NMR (126 MHz, Chloroform-*d*) δ 146.62, 145.54, 131.36, 129.20, 126.09, 120.28, 114.46, 108.30, 63.84, 55.85.

This reaction was conducted according to literature procedure[154] with important modifications (extraction method). Our NMR values agree with literature values.

(**4**) **Sinapyl alcohol**

MS (EI): 210.1

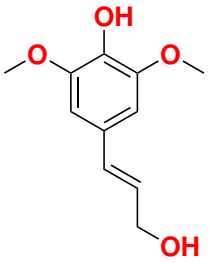

Figure 3.34: Sinapyl alcohol

^{1}H NMR (500 MHz, Chloroform-*d*) δ 6.59 (s, 2H), 6.48 (d, J = 15.8 Hz, 1H), 6.20 (dt, J = 15.8, 5.9 Hz, 1H), 4.27 (dd, J = 5.9, 1.5 Hz, 2H), 3.85 (s, 6H).

^{13}C NMR (126 MHz, Chloroform-*d*) δ 147.09, 134.68, 131.31, 128.20, 126.58, 103.26, 63.65, 56.22.

This reaction was conducted according to literature procedure[154] with important modifications. Our NMR values agree with literature values.[165]

General procedures for $NaBH_4$ reduction of guaiacyl aldehyde and ketones to corresponding alcohols (5), (6), and (7): 0.5 M of guaiacyl aldehyde or ketones was dissolved in methanol 100 mL and then the solution was cooled down with an ice bath. 3 equivalent (for vanillin reaction) or 5 equivalent (for guaiacyl ketone reactions) of $NaBH_4$ was added to the cold solution slowly, pellet by pellet over 1 h. The solution was stirred in an ice bath until all the $NaBH_4$ pellets were dissolved. Stirring continued for 3 h (vanillin) or 4 h (guaiacyl ketones) at room temperature. The solution was added NH_4Cl solution 50 mL and diluted with 150 mL DI water and extracted with dichloromethane 3 $\times$ 200 mL. The combined dichloromethane solution was dried over sodium sulfate and the solvent was removed with rotavap at 40 °C. The vanillyl alcohol white powder can be recrystallized from ethanol and water (1:10) solution.

(**5**) **Vanillyl alcohol**

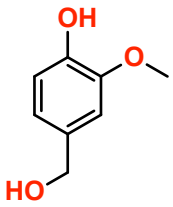

Figure 3.35: Vanillyl alcohol.

White solid can become colorless crystals.

MS (EI): 154.0

^{1}H NMR (500 MHz, Chloroform-*d*) δ 8.79 (s, 1H), 6.86 (d, J = 1.5 Hz, 1H), 6.68 (d, J = 2.3 Hz, 2H), 5.01 (td, J = 5.8, 1.5 Hz, 1H), 4.36 (d, J = 5.5 Hz, 2H), 3.73 (s, 3H).

^{13}C NMR (126 MHz, DMSO-d_6) δ 147.75, 145.66, 133.87, 119.49, 115.42, 111.40, 63.40, 55.89.

This reaction was conducted according to literature procedure[166] with important modifications (ice bath). Our NMR values agree with literature values.[167]

(**6**) **Apocynol**

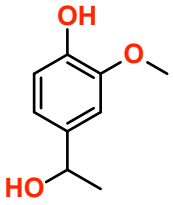

Figure 3.36: Apocynol.

White solid.

MS (EI): 168.0

^{1}H NMR (500 MHz, Chloroform-*d*) δ 6.93 (d, J = 1.9 Hz, 1H), 6.89 – 6.79 (m, 2H), 5.69 (s, 1H), 4.83 (q, J = 6.4 Hz, 1H), 3.89 (s, 3H), 1.47 (d, J = 6.5 Hz, 3H).

^{13}C NMR (126 MHz, Chloroform-*d*) δ 146.58, 144.94, 137.90, 118.30, 114.14, 107.97, 70.32, 55.88, 25.08.

This reaction was conducted according to literature procedure[166] with important modifications. Our NMR values agree with literature values.[168]

(**7**) **1-Guaiacyl-1-propanol**

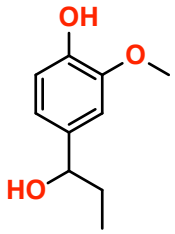

Figure 3.37: 1-Guaiacyl-1-propanol.

White solid.

MS (EI): 182.1

^{1}H NMR (500 MHz, Chloroform-*d*) δ 6.90 – 6.84 (m, 2H), 6.79 (dd, J = 8.1, 1.9 Hz, 1H), 5.72 (s, 1H), 4.50 (t, J = 6.7 Hz, 1H), 3.87 (s, 3H), 1.88 – 1.62 (m, 2H), 0.89 (t, J = 7.4 Hz, 3H).

^{13}C NMR (126 MHz, Chloroform-*d*) δ 146.59, 144.96, 136.65, 119.01, 114.05, 108.36, 76.02, 55.87, 31.81, 10.27.

This reaction was conducted according to literature procedure[166] with important modifications. Our NMR values agree with literature values.

3.3.2 The syntheses of lignin dimers

3.3.2.1 The synthesis of β-O-4 dimer model I

In a 1 L round-bottom flask, guaiacol (**30**) (24.86 g) was dissolved in 250 mL of DMF. K_2CO_3 (50.94 g) and ethyl bromoacetate (36.94 g) were added to the solution and most of the K_2CO_3 was present at the bottom of the flask during the whole reaction time. A magnetic

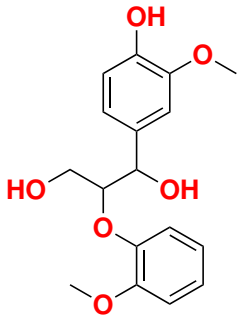

Figure 3.38: Dimer I

stir bar was added and an air condenser was attached to the flask, and the flask was placed in a 60 °C oil bath. The solution was stirred vigorously for 5 hours, after which the heat was removed. The product was added 250 mL of water and DCM (3 × 200 mL) to extract. The organic layers were combined and extracted with brine solution 100 mL and then DI water (2 × 100 mL) to remove any DMF residue. The organic layer was then dried with $MgSO_4$ before being rotovapped at 70 °C. The crude product ethyl guaiacylacetate (**28**) was recrystallized from methanol/water (3:7) solution and obtained 21.7 g (51.8% yield) white crystals.

In a 1 L round bottom flask, vanillin (**10**) (27 g) was dissolved in 250 mL of DMF. K_2CO_3 (34.25 g) and 3 g of 4-dimethylaminopyridine (DMAP) were added to the flask and then was added benzyl chloride (22.7 mL). The round bottom flask was added a magnetic stir bar and the solution was stirred for overnight (18 h) at room temperature, after which 250 mL of 0.1 M NaOH water solution was added to the flask. The aqueous solution was then extracted with ethyl acetate (3x 250 mL). The organic layers were combined and extracted with 100 mL brine solution. The ethyl acetate layer was then dried with $MgSO_4$ before being rotovaped at 70 °C. The crude product was purified by recrystallization in hexane/ethanol (1:4) to provide benzyl vanillin (**27**) 26.65 g (61% yield).

The next step required strict dry conditions. All glassware and stir bar were dried in the

oven overnight and cooled down in the desiccator. THF and diisopropylamine were freshly distilled. Starting materials ethyl guaiacylacetate (**28**) and benzyl vanillin (**27**) were dried in a desiccator for at least one day. Diisopropylamine (10.5 mL) in 30 mL THF was added to a dry, nitrogen-flushed 500 mL Schlenk flask equipped with a magnetic stir bar, an addition funnel, and nitrogen line. After being flushed with nitrogen, the flask was then placed in an acetone/dry ice bath and cooled to -78 °C. before 0.075 mol *n*-BuLi in hexanes (29.7 mL, 2.5 M solution) was added in dropwise using a syringe. After stirring for 30 min, guaiacol ethyl acetate (**28**) (10.44 g) in 80 mL THF was added in dropwise, and the solution was stirred for 1 hour. Then benzyl vanillin (**27**) (11.99 g) in 80 mL THF was added in dropwise, and the solution was left to stir for 1.5 h at -78°C. The solution was then allowed to warm up to room temperature and was quenched with 30 mL saturated NH_4Cl solution and extracted with ethyl acetate (3 × 150 mL). The combined ethyl acetate was extracted with 100 mL brine. The organic layer was dried with $MgSO_4$ and the solvent was removed under vacuum. Yellow solid was purified with column chromatography with petroleum ether/ethyl acetate (7:3) as the eluent and two separable diastereomer β-O-4 products (**34**) were obtained with a yield of 52% (11.1 g).

Light yellow solid.

MS (ES^-): found 497.1805 ($M+HCOO^-$), calculated MS for $C_{27}H_{29}O_9$ 497.1812.

Diastereomer one (Erythro): ^{1}H NMR (500 MHz, Chloroform-*d*) δ 7.49 – 7.39 (m, 2H), 7.40 – 7.33 (m, 2H), 7.32 – 7.26 (m, 1H), 7.09 (d, J = 1.9 Hz, 1H), 7.01 (ddd, J = 8.1, 7.3, 1.7 Hz, 1H), 6.96 – 6.81 (m, 5H), 5.14 (s, 2H), 5.13 (d, J = 5.4 Hz, 1H) 4.72 (d, J = 5.1 Hz, 1H), 4.12 (qd, J = 7.1, 1.3 Hz, 2H), 3.88 (s, 3H), 3.82 (s, 3H), 1.12 (t, J = 7.1 Hz, 3H).

^{13}C NMR (126 MHz, Chloroform-*d*) δ 169.36, 150.48, 149.37, 147.83, 147.20, 137.16, 132.35, 128.52, 127.79, 127.24, 123.83, 121.08, 119.22, 118.59, 113.51, 112.30, 110.66, 83.79,

73.81, 70.93 , 61.23, 55.92, 55.83, 14.08.

Diastereomer two (Threo): ^{1}H NMR (500 MHz, Chloroform-*d*) δ 7.45 – 7.39 (m, 2H), 7.35 (ddd, J = 8.0, 7.0, 0.8 Hz, 2H), 7.31 – 7.27 (m, 1H), 7.07 – 6.99 (m, 2H), 6.95 – 6.79 (m, 5H), 5.14 (s, 2H), 5.05 (d, J = 7.1 Hz, 1H), 4.49 (d, J = 7.1 Hz, 1H), 4.08 – 3.96 (m, 2H), 3.88 (s, 3H), 3.85 (s, 3H) 1.02 (t, J = 7.1 Hz, 3H).

^{13}C NMR (126 MHz, Chloroform-*d*) δ 169.42, 150.31, 149.61, 148.12, 147.27, 137.04, 131.14, 128.51, 127.81, 127.21, 123.86, 121.04, 119.53, 118.10, 113.56, 112.24, 110.52, 85.39, 74.88, 70.90 , 61.21, 55.98, 55.80, 13.94.

The above step was conducted according to literature procedure.[169] Our NMR values agree with literature values.

To a nitrogen-flushed Schlenk flask equipped with a water condenser and a magnetic stir bar was added 7.5 mL THF and 0.3 g of $LiAlH_4$. The flask was placed into an ice bath. A solution of 0.3 g of the ester (**34**) in 11.5 mL of THF was added to the flask dropwise over 20 mins. The solution with powder of $LiAlH_4$ at the bottom was stirred at 60 °C for 3 h and was cooled down in an ice bath. The reaction was carefully quenched with 3 mL water dropwise. The solution was allowed to stir for another 30 min at room temperature before the aluminum salts were filtered. The aluminum salts were washed with DCM (5 × 10 mL). The filtrate solution was dried with $MgSO_4$, rotovaped at 40 °C under vacuum, and was further dried over nitrogen gas for 12 h. 0.27 g of white solid was obtained. The solid was dissolved in 5 mL of methanol and transferred into a 25 mL Schlenk flask equipped with nitrogen line, a magnetic stir bar, and a rubber septum. 42 mg of 10% Pd/C catalyst was added to the flask in a liquid nitrogen bath. After the methanol solution was frozen, the vacuum was applied for 3 min. Then the vacuum was removed and the flask was allowed to warm up to room temperature. Repeat the nitrogen bath and warming up processes

for another two times and a needle connecting with a H_2 balloon was inserted through the rubber septum. The solution was stirred for 4 h and was filtered. The Pd/C catalyst was washed with DCM (3 × 5 mL) and combined with the methanol solution. The solvent was removed by blowing nitrogen gas. A mixture of two pairs of diastereomers was obtained. One threo diastereomer of dimer I was separated purely as a white solid (0.023 g) and a mixture of the two diastereomers (0.167 g) as yellow solid by column chromatography with DCM/MeOH (99:1 to 90:10) and the pure threo diastereomer NMR is shown as follows:

White powder.

MS (ES^-): found 319.1209 ($M-H^+$), calculated MS for $C_{17}H_{19}O_6$ 319.1182.

^{1}H NMR (500 MHz, Chloroform-*d*) δ 7.13 (dd, J = 7.9, 1.6 Hz, 1H), 7.06 (ddd, J = 8.1, 7.4, 1.6 Hz, 1H), 6.99 – 6.83 (m, 5H), 5.79 (s, OH), 4.96 (dd, J = 8.0, 1.2 Hz, 1H), 4.09 – 3.96 (m, 1H), 3.90 (s, 3H), 3.86 (s, 3H), 3.75 (d, J = 1.9 Hz, OH), 3.62 (dt, J = 12.5, 3.7 Hz, 1H), 3.48 (ddd, J = 12.2, 7.8, 3.9 Hz, 1H), 2.84 (dd, J = 8.3, 5.0 Hz, OH).

^{13}C NMR (126 MHz, Chloroform-*d*) δ 151.25, 147.58, 146.68, 145.56, 131.45, 124.24, 121.69, 121.02, 120.24, 114.35, 112.12, 109.40, 89.52, 73.98, 61.02, 55.95, 55.89.

The above two steps are conducted according to the literature procedures from Bolm[170] and Lancefield.[169] Our NMR values agree with literature values.

3.3.2.2 The synthesis of β-5 dimer model - II

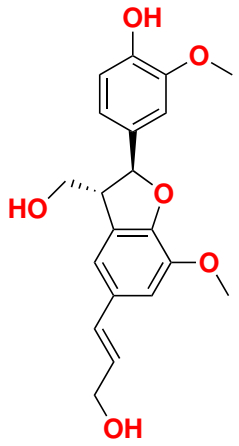

Figure 3.39: Dimer II.

Methyl ferulate (**1**) 12.5 g (0.060 mol) was dissolved in 100 mL acetone in a 500 mL round bottom flask, capped with a rubber stopper and equipped with a magnetic stir bar. 200 mL benzene was injected into the flask. The solution was bubbled with nitrogen gas for 10 min, and 8.3 g (0.036 mol) freshly prepared Ag_2O^{160} was added into the flask, capped and stirred for 19 h. The suspension was filtered and the solvent was removed. The product was purified by chromatography with silica gel, hexane : ethyl acetate (7:3). 1.2 g of the white needle crystal dimer (**46**) was obtained from recrystallization from methanol. The yield is 10%.

The methyl ferulate dehydrogenated dimer (**46**), 1.45 g (0.0035 mol), was dissolved in 55 mL of toluene and 30 mL of THF. Chilled with an ice bath, under nitrogen gas, 21 mL (0.021 mol, 1 M in hexane) DIBAL was slowly injected into the flask and stirring for 10 h. The solution was carefully quenched with 10 mL methanol, and then 100 mL of ethyl acetate and 50 mL of potassium sodium tartrate saturated aqueous solution was added to the flask. The solution was vigorously stirred until the aqueous layer became clear. The aqueous layer

was extracted with 50 mL of ethyl acetate for two times, and the solvent was removed and 1.02 g of crude product dimer **II** was isolated. It was recrystallized from ethyl acetate and 0.70 g (0.002 mol)of white fine powder was obtained with a yield of 89.7%. The melting point of the product is 153.1 - 154.8 °C.

White solid.

MS (ES^-): found 357.1343 ($M-H^+$), calculated MS for $C_{20}H_{21}O_6$ 357.1338.

^{1}H NMR (500 MHz, DMSO-d_6) δ 9.04 (s, 1H), 6.97 – 6.89 (m, 3H), 6.75 (d, J = 1.5 Hz, 2H), 6.46 (dt, J = 15.7, 1.6 Hz, 1H), 6.21 (dt, J = 15.9, 5.3 Hz, 1H), 5.46 (d, J = 6.6 Hz, 1H), 5.04 (t, J = 5.3 Hz, 1H), 4.80 (t, J = 5.5 Hz, 1H), 4.08 (td, J = 5.4, 1.6 Hz, 2H), 3.79 (s, 3H), 3.74 (s, 3H), 3.78 – 3.67 (m, 1H), 3.62 (ddd, J = 10.7, 6.8, 5.4 Hz, 1H), 3.44 (q, J = 6.3 Hz, 1H).

^{13}C NMR (126 MHz, DMSO-d_6) δ 147.55, 147.08, 146.38, 143.69, 132.33, 130.51, 129.47, 128.97, 128.01, 118.55, 115.31, 114.95, 110.29, 110.25, 87.25, 62.94, 61.68, 55.66, 55.63, 53.02.

The first step was conducted according to literature procedures[171] with minor modifications. The second step adopted a methodology[154] making coniferyl alcohol from ethyl ferulate. There is only one literature[172] reported a picture of the l ^{1}H-NMR with very low resolution. Our NMR is similar to that in the literature.

3.3.2.3 The synthesis of β-5 model III

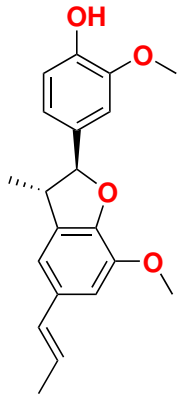

Figure 3.40: Dimer III.

Isoeugenol, 25 g (0.15 mol) was dissolved in 285 mL of ethanol and 125 mL of water. 100 mL of water containing 35 g (0.22 mol) ferric chloride was added and shaken for 1 min, then left to stand for 48 h. White crystals precipitated and the mixture was filtered and washed with water and ice cold ethanol. The crystals were dissolved in dichloromethane and passed through a 10 cm silica plug. The solvent was removed and the solid was recrystallized from ethanol. 10 g (0.031 mol) pure dimer **III** was obtained with 20% yield. Melting point: 115.0-117.0 °C.

White needle crystals.

MS (ES^-): found 325.1440 ($M-H^+$), calculated MS for $C_{20}H_{21}O_4$ 325.1440.

^{1}H NMR (500 MHz, Chloroform-*d*) δ 6.99 (d, J = 1.5 Hz, 1H), 6.96 – 6.86 (m, 2H), 6.80 (dd, J = 10.6, 1.5 Hz, 2H), 6.38 (dq, J = 15.7, 1.7 Hz, 1H), 6.13 (dq, J = 15.7, 6.6 Hz, 1H), 5.66 (s, 1H), 5.12 (d, J = 9.5 Hz, 1H), 3.90 (d, J = 8.8 Hz, 6H), 3.47 (dtd, J = 9.5, 7.4, 6.3 Hz, 1H), 1.89 (dd, J = 6.6, 1.7 Hz, 3H), 1.39 (d, J = 6.8 Hz, 3H).

^{13}C NMR (126 MHz, Chloroform-*d*) δ 146.65, 146.54, 145.76, 144.14, 133.26, 132.19, 132.06, 130.91, 123.51, 119.99, 114.06, 113.29, 109.15, 108.91, 93.82, 55.98, 55.92, 45.63,

18.42, 17.55.

This reaction was conducted according to literature procedure.[173] Our NMR values agree with literature values.

3.3.2.4 The synthesis of β-β dimer model - IV

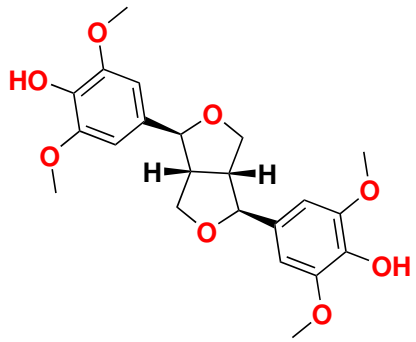

Figure 3.41: Dimer IV.

Mono-ethyl malonate was made as described previously as in model III, starting with 75.8 g (0.47 mol) of the diethyl malonate with KOH 30.1 g (0.54 mol) in 500 ml of ethanol. The mixture was neutralized with 26.3 g (0.44 mol) acetic acid. Then 19.5 g (0.11 mol) of syringaldehyde (**13**), glycine 4.0 g (0.054 mol) was added to the mono-ethyl malonate solution; after 8 h of reflux, the white solid had turned to yellow liquid. The solution was cooled down to room temperature. 100 mL of DI water was added and the mixture was extracted with DCM (3 × 250 mL). Drying over sodium sulfate and evaporation of the solvent gave 72.2 g (theoretical yield 71.2 g). The yellow solid was a mixture of ethyl sinapate (**14**) and water. The water could not be easily removed by a flow of nitrogen gas blowing.

In a 1 L flask, 10.6 g (0.040 mol)of the (**14**) crude product from the last step was dissolved in 400 mL of toluene. Chilled with an ice bath, under nitrogen gas, 168 mL (0.168 mol, 1.5

M in hexane) DIBAL was slowly injected into the flask for 1 h and the mixture was stirred for 10 h. The solution was carefully quenched with methanol 50 mL, 400 mL of ethyl acetate and 50 g of potassium sodium tartrate in 100 mL water was added to the flask. The solution was vigorously stirred until the aqueous layer became clear. The aqueous layer was extracted with 100 mL of ethyl acetate for two times, the solvent was removed, and 8.63 g of sinapyl alcohol (**15**) was isolated. The sinapyl alcohol was used for next step without purification.

A solution of sinapyl alcohol (**15**) 8.63 g in 30 mL of methanol was added $CuSO_4$ 10.47 g in 1.65 L water. The whole mixture was stirred for 48 h at room temperature. It was extracted with 250 mL of dichloromethane for three times. The combined organic solution was evaporated and the resulting crude solid syringaresinol, the dimer **IV**, was purified by recrystallization from methanol. White fine powder 2.5 g (0.0057 mol) was obtained with a yield of 28%. Melting point: 163.2-164.9 °C.

White powder. Crystal is colorless needle-shape.

MS (ES^-): found 417.1546 ($M-H^+$), calculated MS for $C_{22}H_{25}O_8$ 417.1549.

^{1}H NMR (500 MHz, Chloroform-*d*) δ 6.58 (s, 4H), 5.53 (s, OH), 4.73 (d, J = 4.2 Hz, 2H), 4.32 – 4.24 (m, 2H), 3.91 (d, J = 3.4 Hz, 2H), 3.89 (s, 12H), 3.12 – 3.06 (m, 2H).

^{13}C NMR (126 MHz, Chloroform-*d*) δ 147.12, 134.22, 132.05, 102.62, 86.06, 71.79, 56.35, 54.33.

This reaction was conducted according to literature procedure.[174] Our NMR values agree with literature values.

3.3.2.5 The synthesis of cheap 5-5 model V

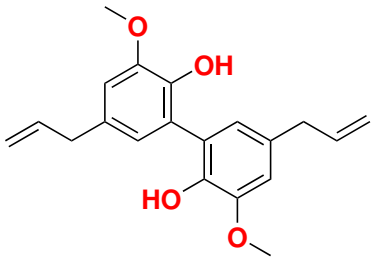

Figure 3.42: Dimer V.

Eugenol 15.4 g (0.094 mol) was dissolved in 300 mL acetone and water 150 mL. 200 mL of 25% NH_4OH was added and the solution becomes green-yellow color. $K_3Fe(CN)_6$ 31.0 g (0.094 mol) was dissolved in 100 mL water and added to the mixture dropwise for 1 h. 200 mL of NH_4OH was added to the mixture and it was stirred for 12 h. The reaction was neutralized by adding 250 g HCl aqueous solution (35% HCl 150 g mixed with 100 mL water). After cooling in an ice bath, a large amount of white solid precipitated out, which was dissolved in ethanol and mixed with NaOH solution (8 g NaOH with 200 mL water). This mixture was filtered to remove the solid and the procedure repeated 2 times. The resulting red liquid was combined in a 2 L beaker placing in an ice bath and concentrated HCl was added until white crystals precipitated out. The crystals, dehydrodieugenol **V** 5 g (0.0156 mol) as isolated gave a yield of 33%. The melting point is 104.0-105.7 °C.

White to light yellow powder.

MS (ES^-): found 325.1458 ($M-H^+$), calculated MS for $C_{20}H_{21}O_4$ 325.1440.

^{1}H NMR (500 MHz, Chloroform-*d*) δ 6.77 – 6.70 (m, 2H), 6.03 (s, 1H), 5.98 (ddt, J = 16.9, 10.0, 6.7 Hz, 1H), 5.11 (dq, J = 17.0, 1.7 Hz, 1H), 5.10 – 5.03 (m, 1H), 3.92 (s, 3H), 3.37 (d, J = 6.7 Hz, 2H).

^{13}C NMR (126 MHz, Chloroform-*d*) δ 147.34, 141.00, 137.78, 132.07, 124.51, 123.22,

115.87, 110.80, 56.23, 40.13.

This reaction was conducted according to literature procedures.[175] Our NMR values agree with literature values.

3.3.2.6 The synthesis of 4-O-5 model VI

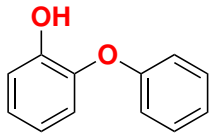

Figure 3.43: Dimer VI.

To a nitrogen flushed round bottom flask, iodobenzene (1.33 g, 12 mmol) and Cu(II)O (0.0203g, 2.5 mol%) was added to a solution of KOH (0.8516 g, 15 mmol) and guaiacol, (1.2486 g, 10 mmol) in 10 mL DMSO. The reaction was run at 110 °C for 15 hours. Upon completion, the reaction was quenched with NH_4Cl (5 mL) and H_2O (100 mL) and extracted with DCM (200 mL). The DCM layer was then dried with $MgSO_4$ and concentrated under vacuum. The tanish crystals were recrystallized from EtOH and vacuum filtered to give a final mass of 0.1964 g, a 10% yield.

The next step involved a demethylation. To a nitrogen flushed flask, 1.8 mmol, 0.17 mL of BBr_3 was added to a solution consisting of 0.2807 g, 1.4 mmol of the first 4-O-5 dimer in 3 mL of DCM. An additional 2 mL of DCM was added to the reaction. The reaction was stirred at -70 °C for one hour and an addition 3 hours at room temperature and monitored with TLC. After completion, the reaction was quenched with 3 mL of H_2O and 6 mL of a 1 M NaOH solution was added. The water layer was extracted and 12 M HCl was added until all precipitate formed. The precipitate was dissolved in ethyl acetate and dried over $MgSO_4$. The dried organic layer was concentrated in vacuum to give a final mass of 0.0775

g of tanish, light crystals for a 30% yield. The reaction was also run on a scale 5.3 x the original and gave a final mass of 0.9112 g, 66% yield. Melting point is 102.1 – 102.8 °C.

Colorless crystal, flake shape.

MS (ES^-): found 185.0600 ($M-H^+$), calculated MS for $C_{12}H_9O_2$ 185.0603.

^{1}H NMR (500 MHz, Chloroform-*d*) δ 7.39 – 7.31 (m, 2H), 7.13 (tt, J = 7.2, 1.1 Hz, 1H), 7.09 – 6.99 (m, 4H), 6.92 – 6.80 (m, 2H), 5.78 (s, OH).

^{13}C NMR (126 MHz, Chloroform-*d*) δ 156.87, 147.61, 143.58, 130.02, 124.91, 123.75, 120.76, 119.00, 118.13, 116.30.

3.4 Conclusions and outlook

Major lignin dimers with β-O-4, β-β, β-5, 5-5, and 4-O-5 linkages were synthesized. Enzyme-mimicking radical coupling and cyclization strategies were shown to be very effective to construct key linkages for lignin dimers by employing models blocking byproduct formation pathways.

Lignin dimer VI has the important 4-O-5 linkage, but it is far from the real structure. Our previous extensive attempts had all failed to make a real 4-O-5 models by applying radical dimerization of vanillyl alcohol strategy,[176] but this synthesis is still worthy of a trial since recently another group synthesized the dimer with the same method.[177]

All of the monomer and dimers in this work have been reported by literature. The proton and carbon NMR values of the synthesized compounds in this work agree with the literature values. All dimer structures have been assigned according to the mass spectrum, proton, carbon, COSY, HSQC, and HMBC NMR.

3.5 Supplementary material

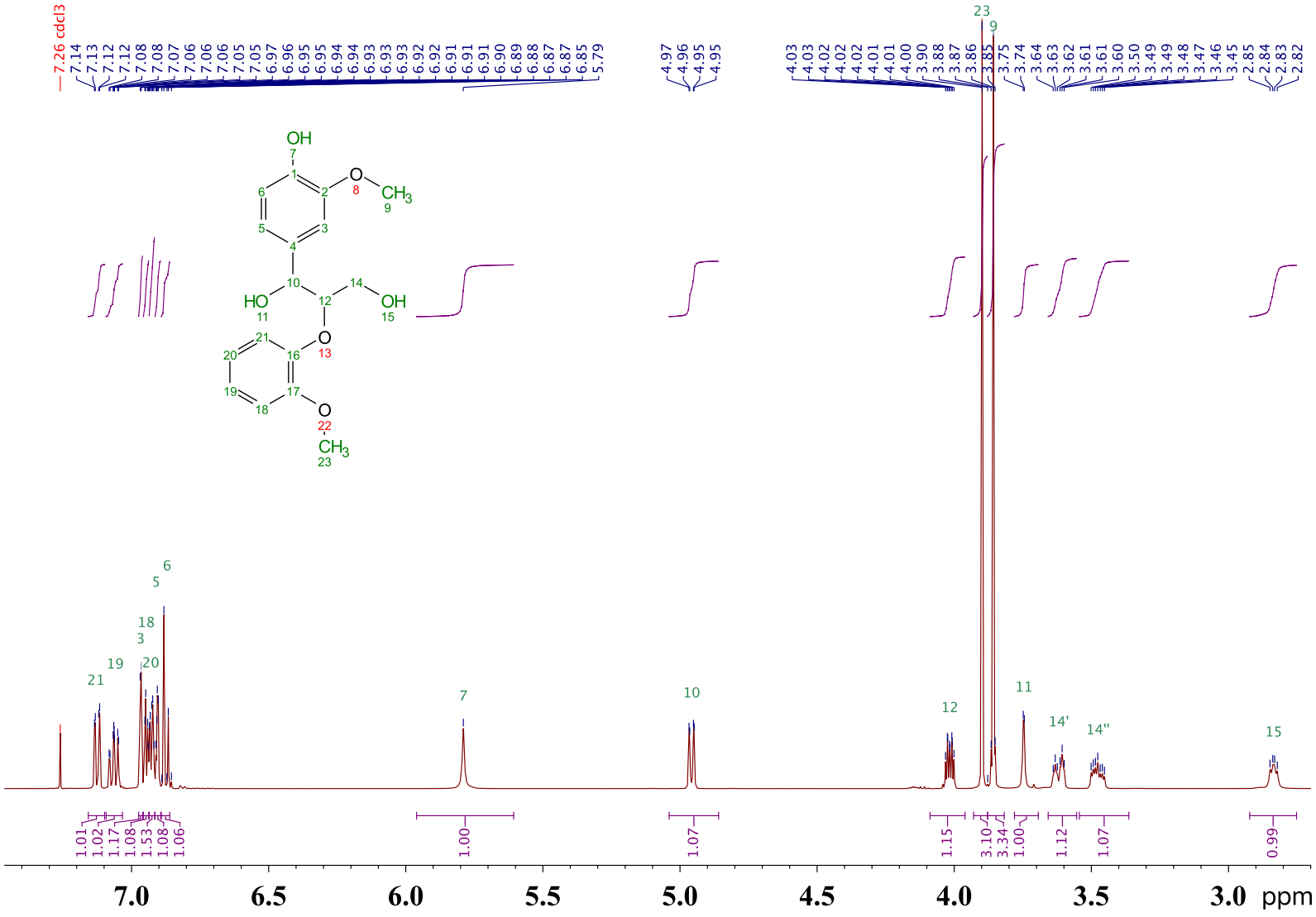

Figure 3.44: Proton NMR of dimer I

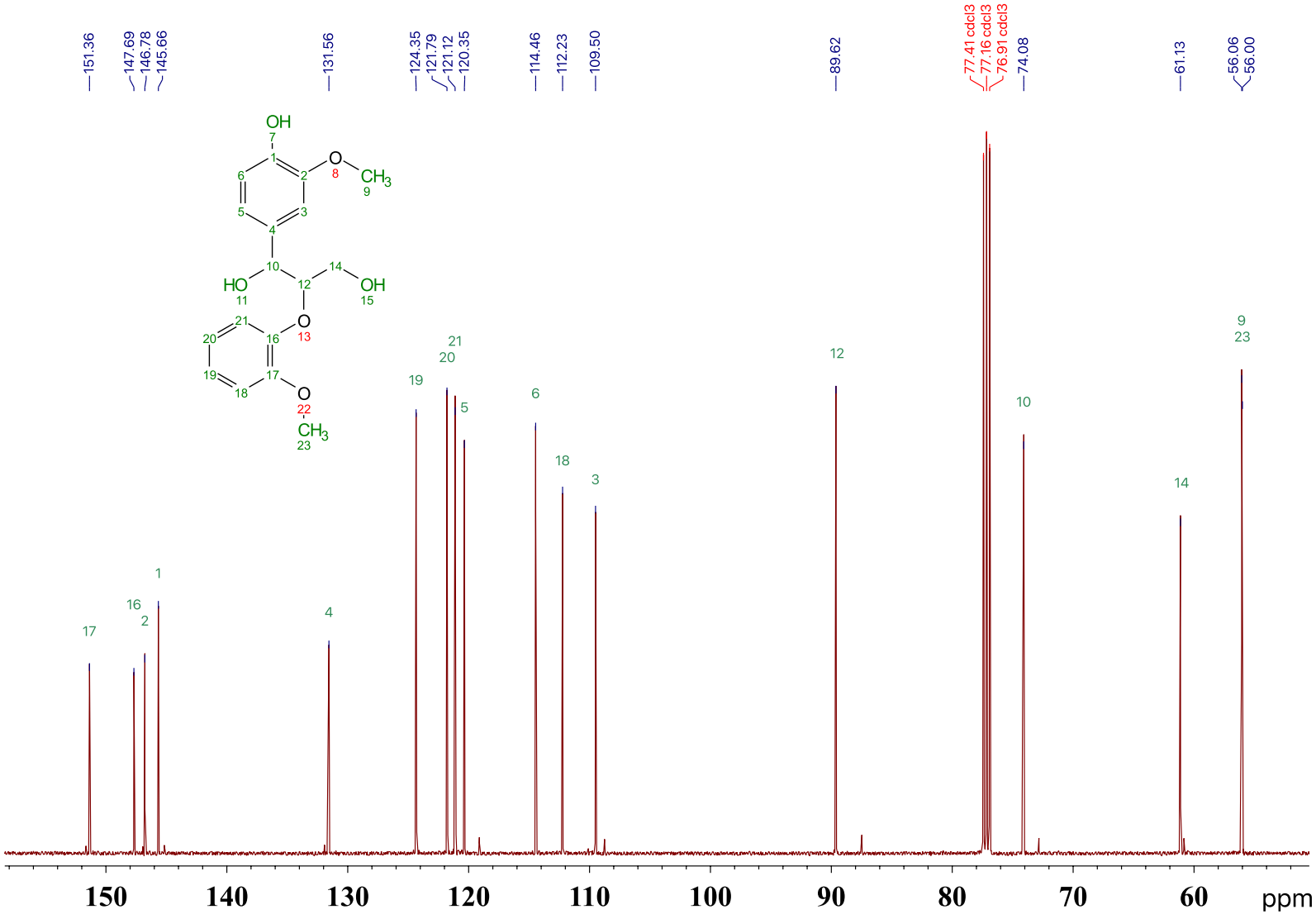

Figure 3.45: Carbon NMR of dimer I

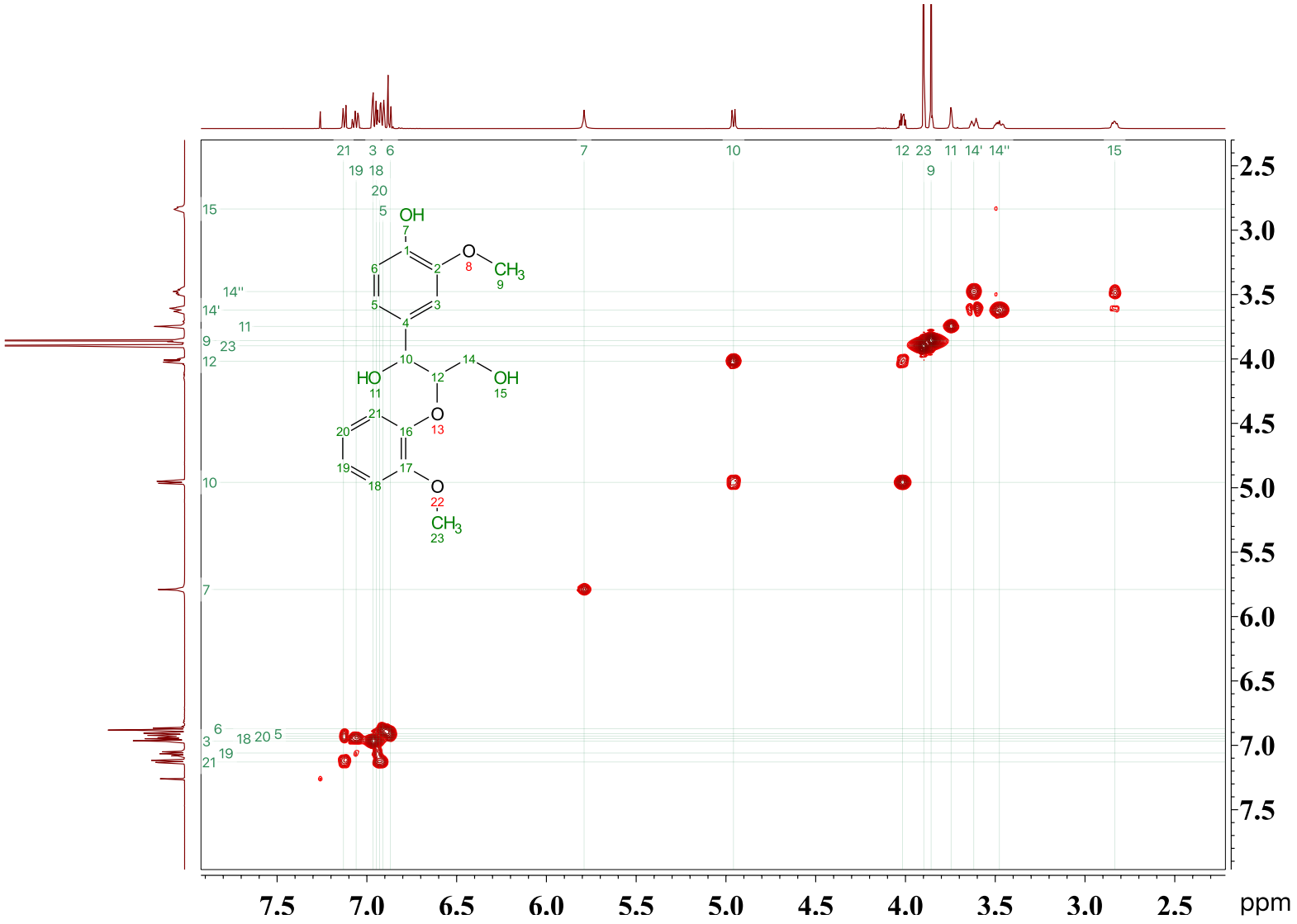

Figure 3.46: gCOSY NMR of dimer I

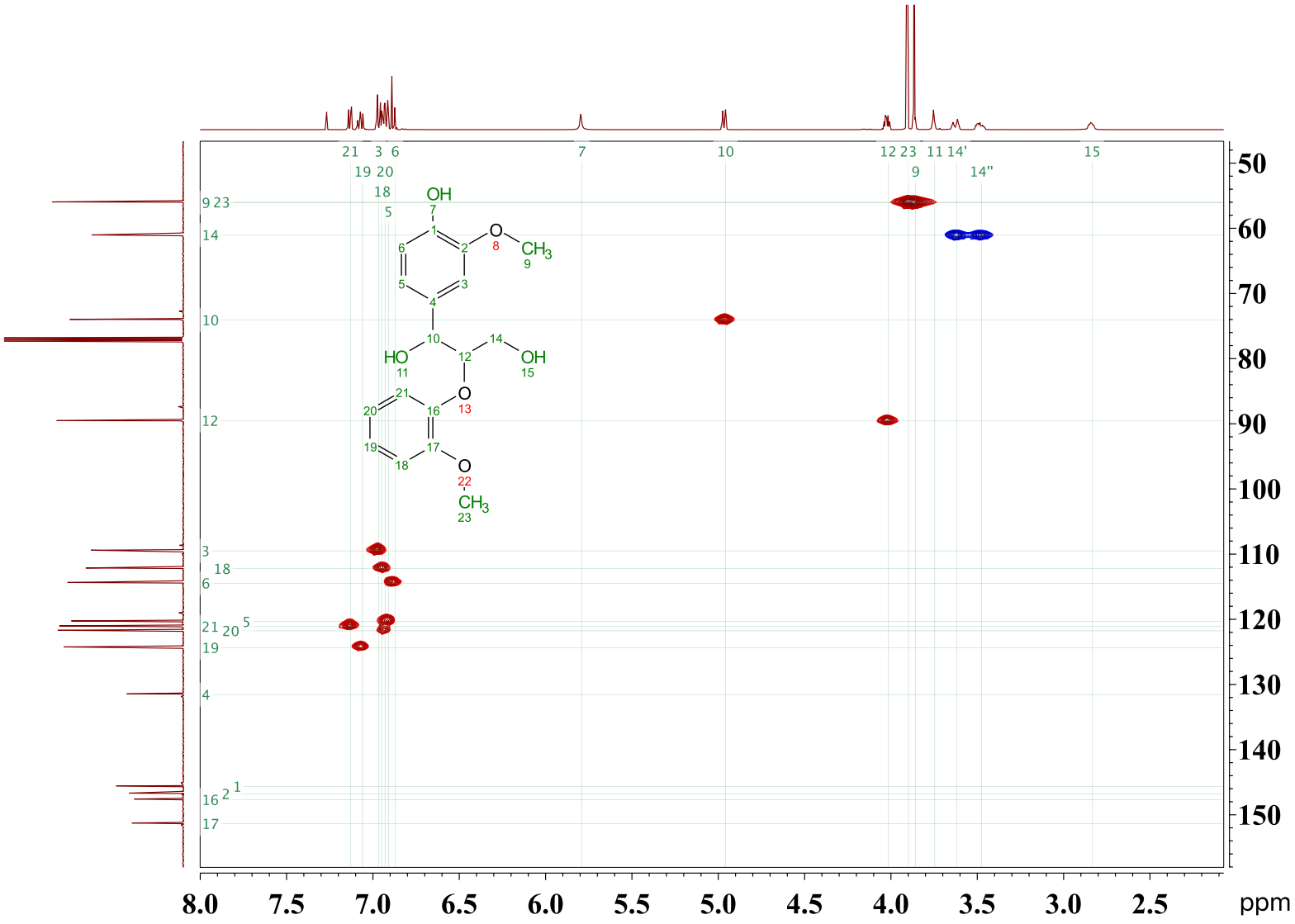

Figure 3.47: gHSQCAD NMR of dimer I

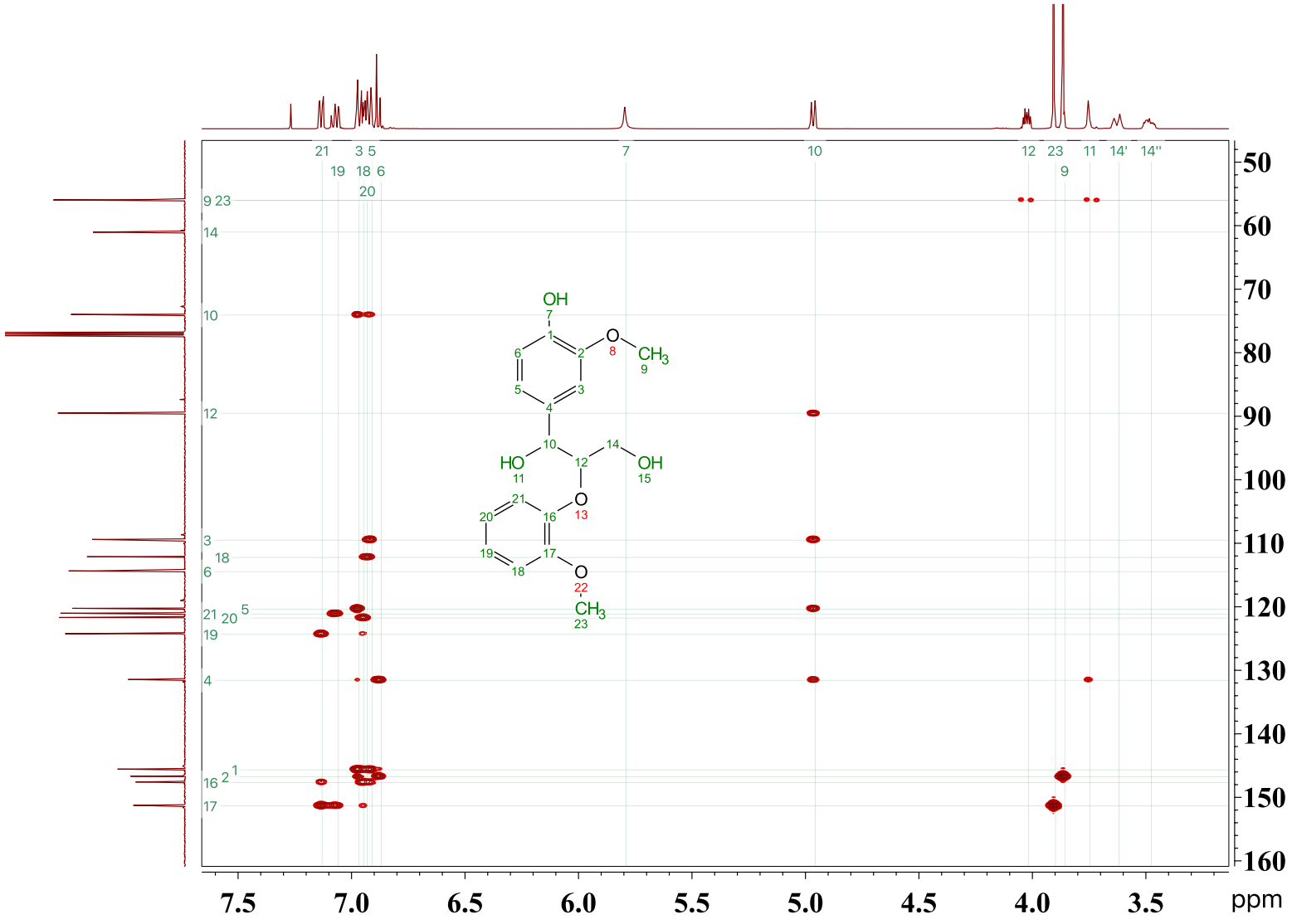

Figure 3.48: gHMBCAD NMR of dimer I

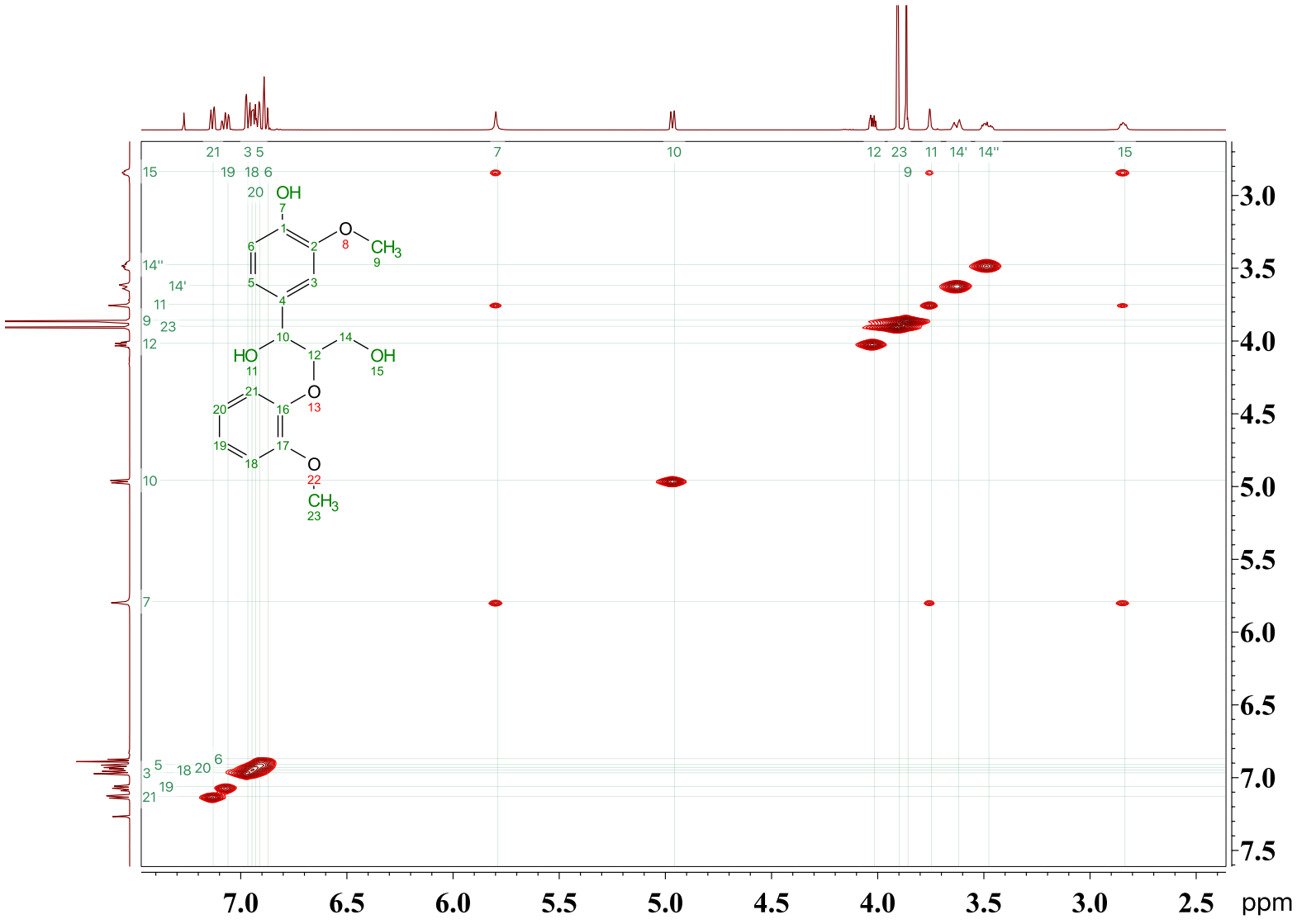

Figure 3.49: NOSEY NMR of dimer I

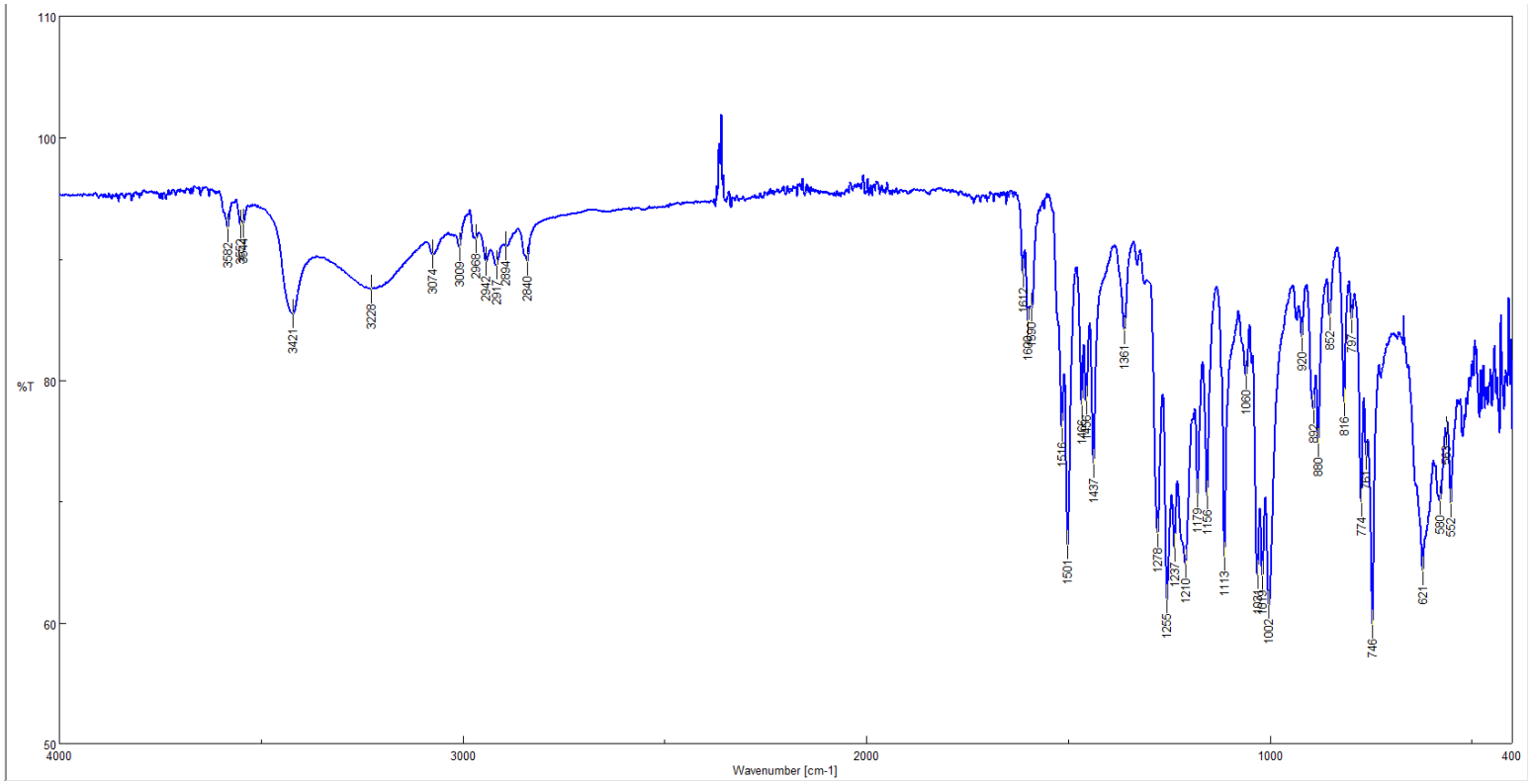

Figure 3.50: IR (neat) of dimer I

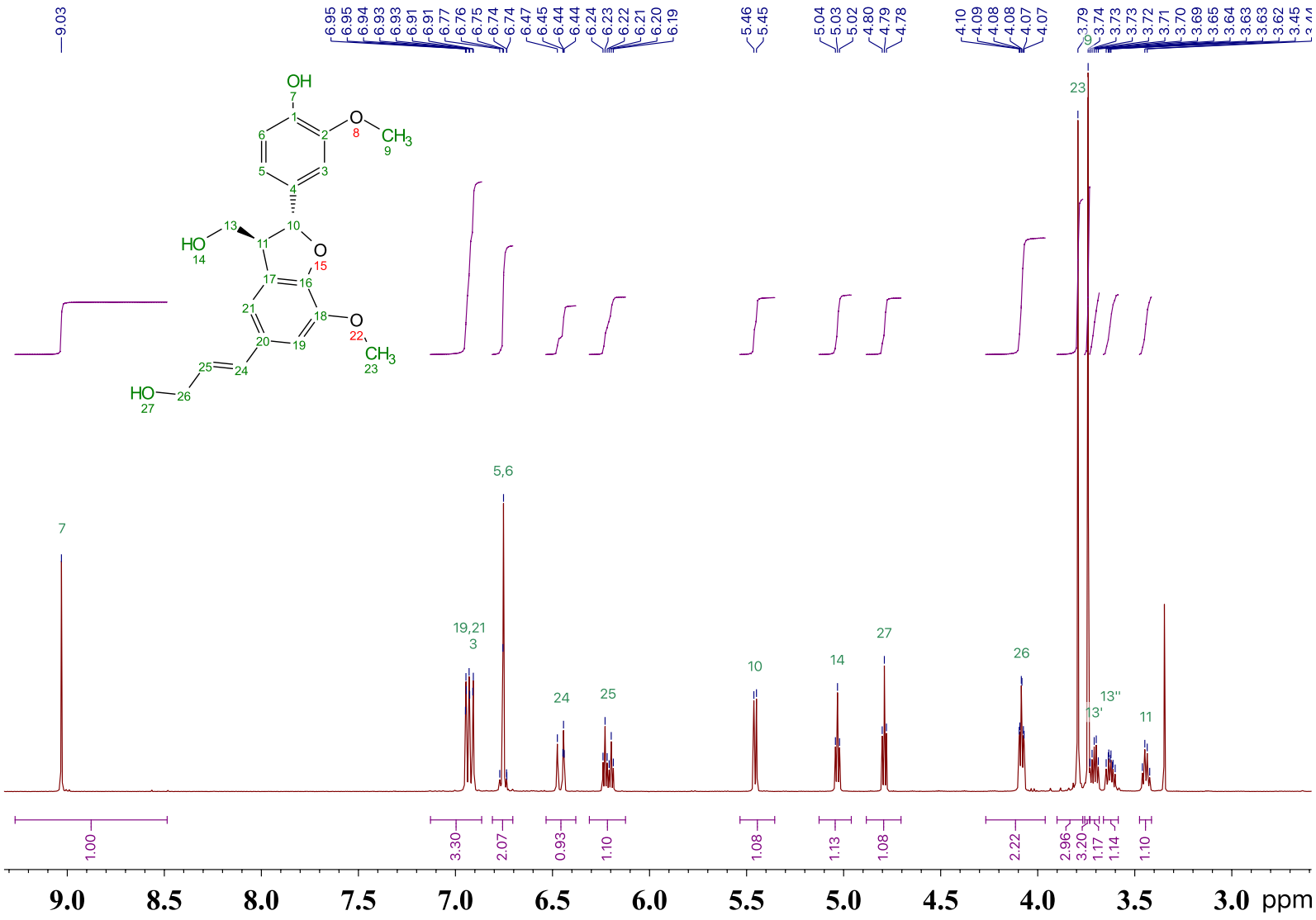

Figure 3.51: Proton NMR of dimer II

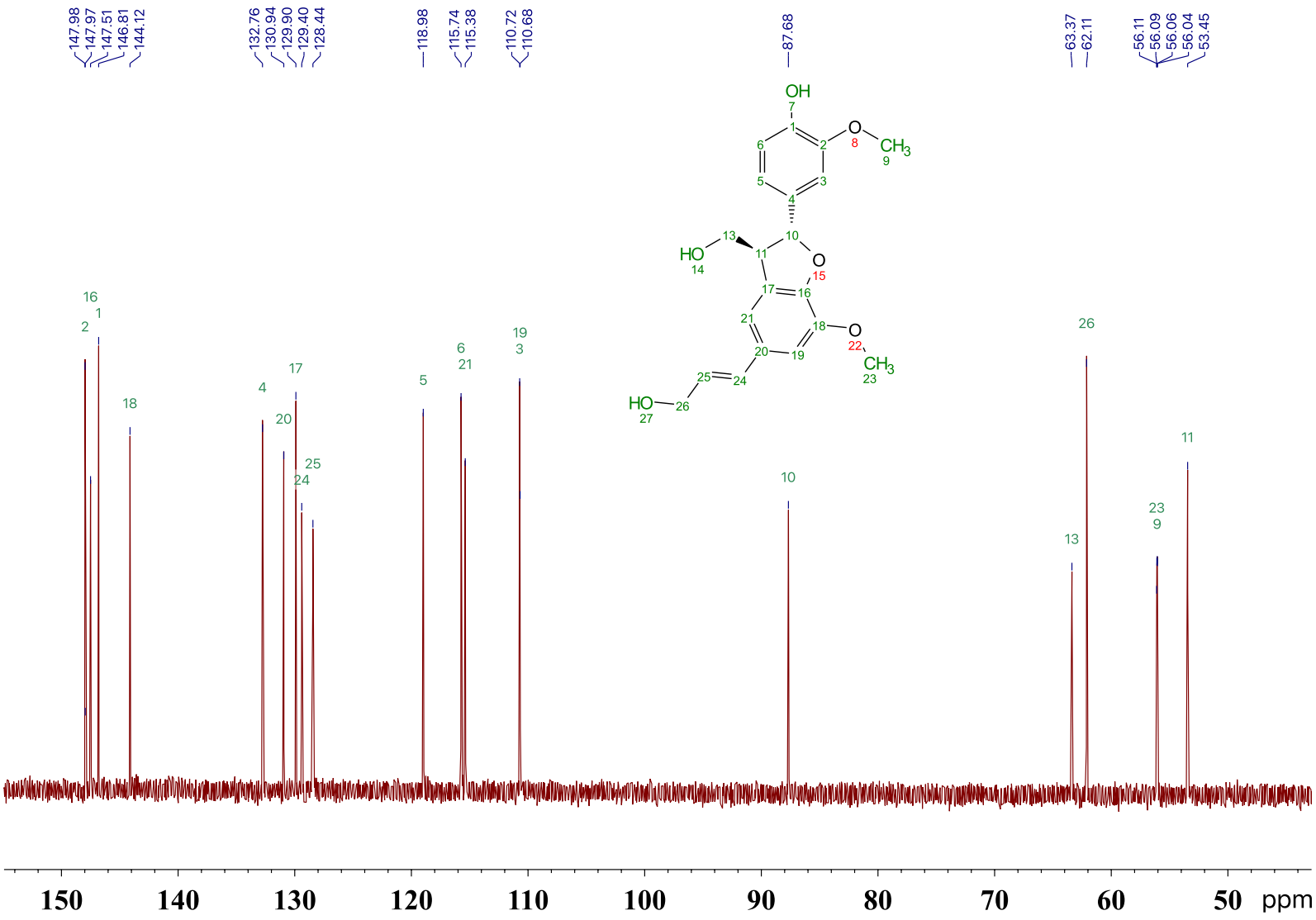

Figure 3.52: Carbon NMR of dimer II

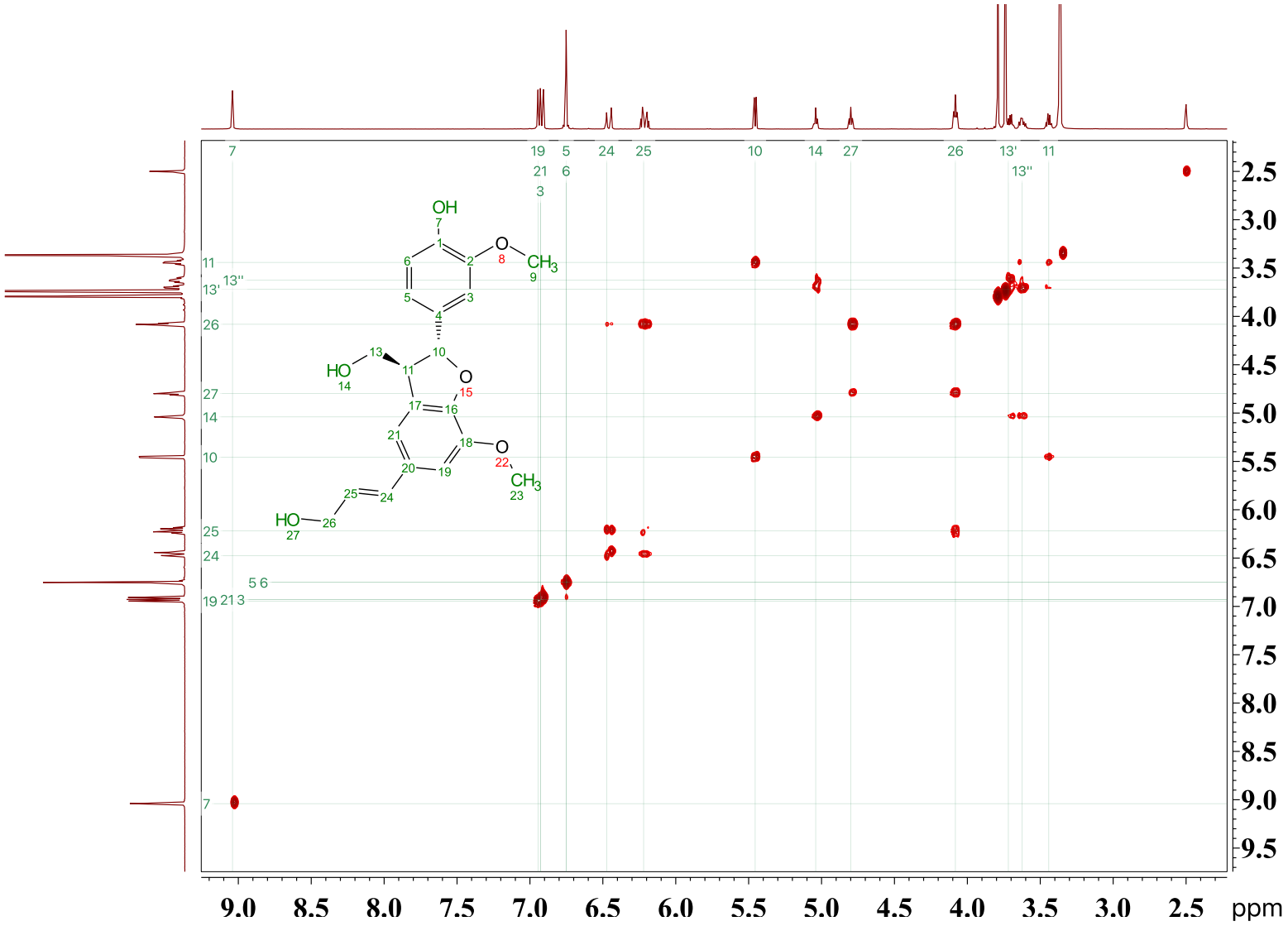

Figure 3.53: gCOSY NMR of dimer II

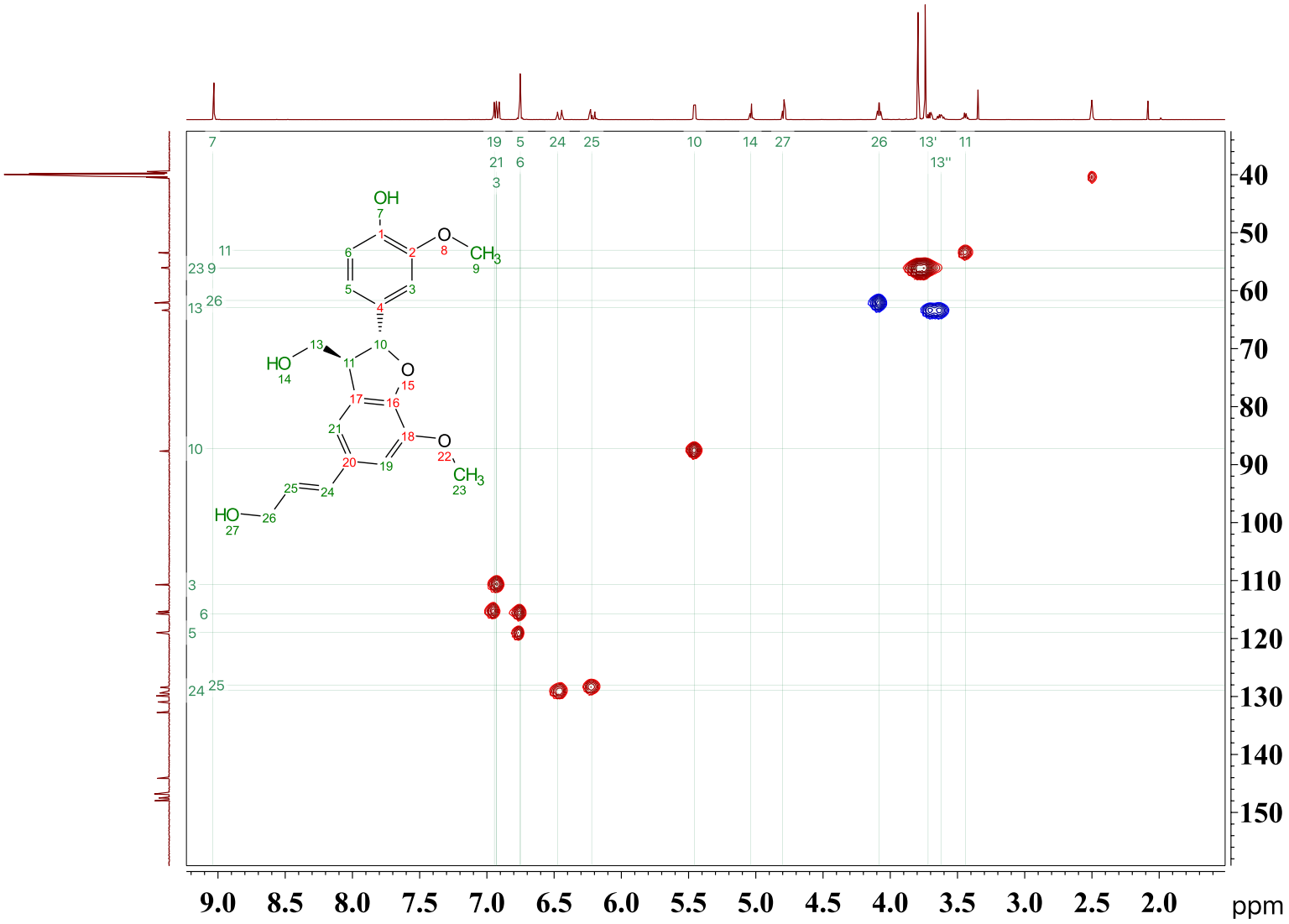

Figure 3.54: gHSQCAD NMR of dimer II

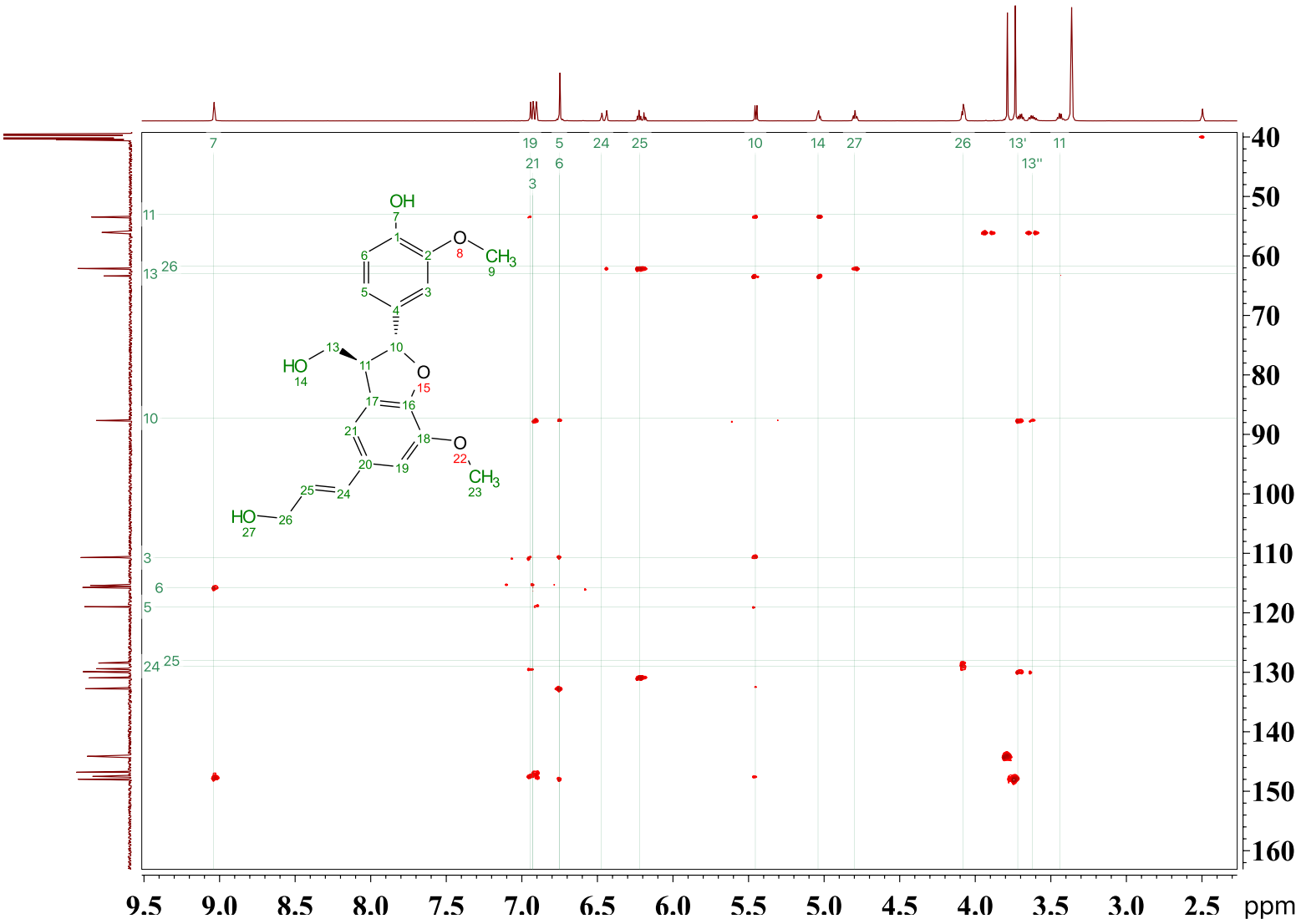

Figure 3.55: gHMBCAD NMR of dimer II

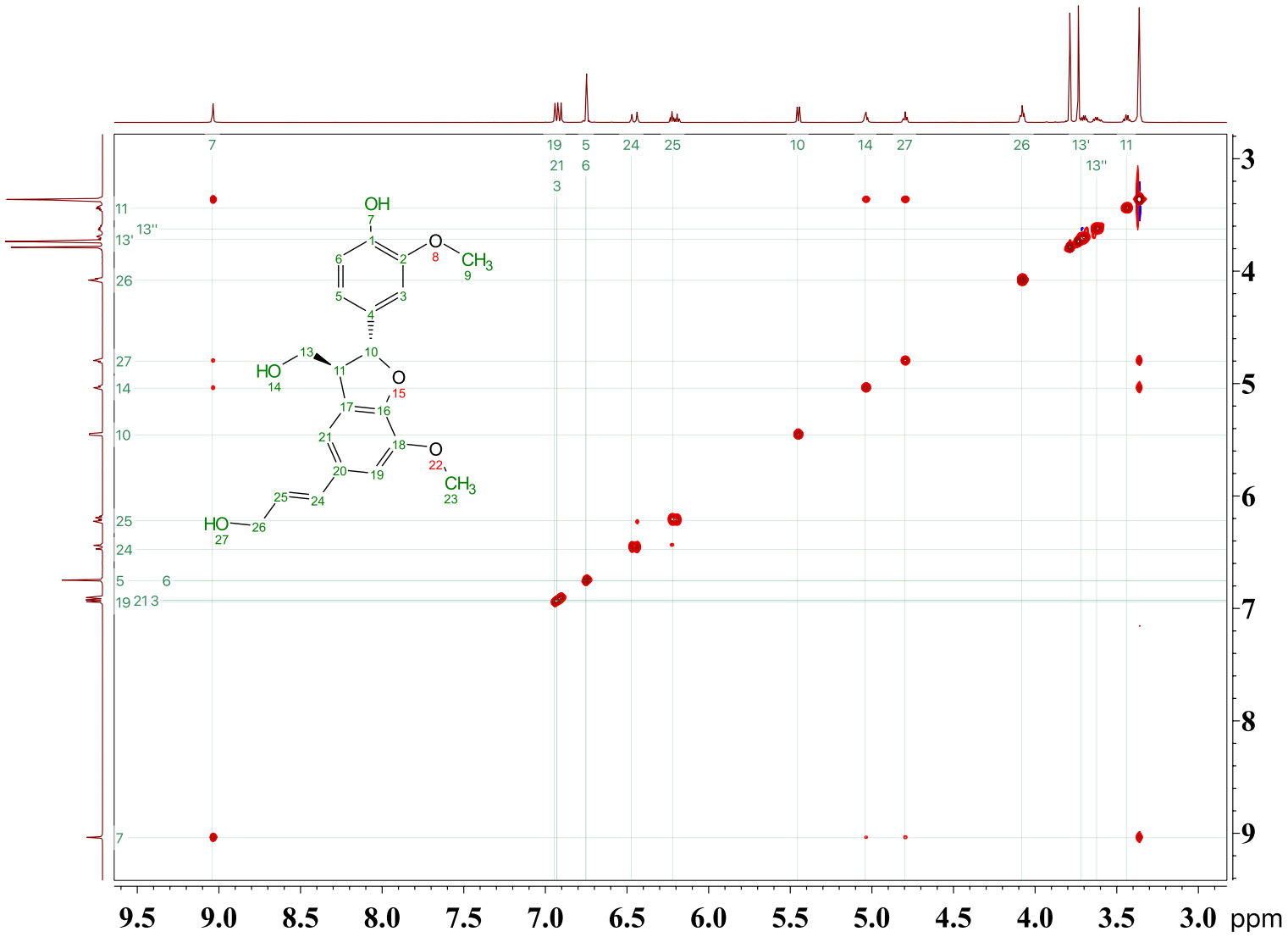

Figure 3.56: NOSEY NMR of dimer II

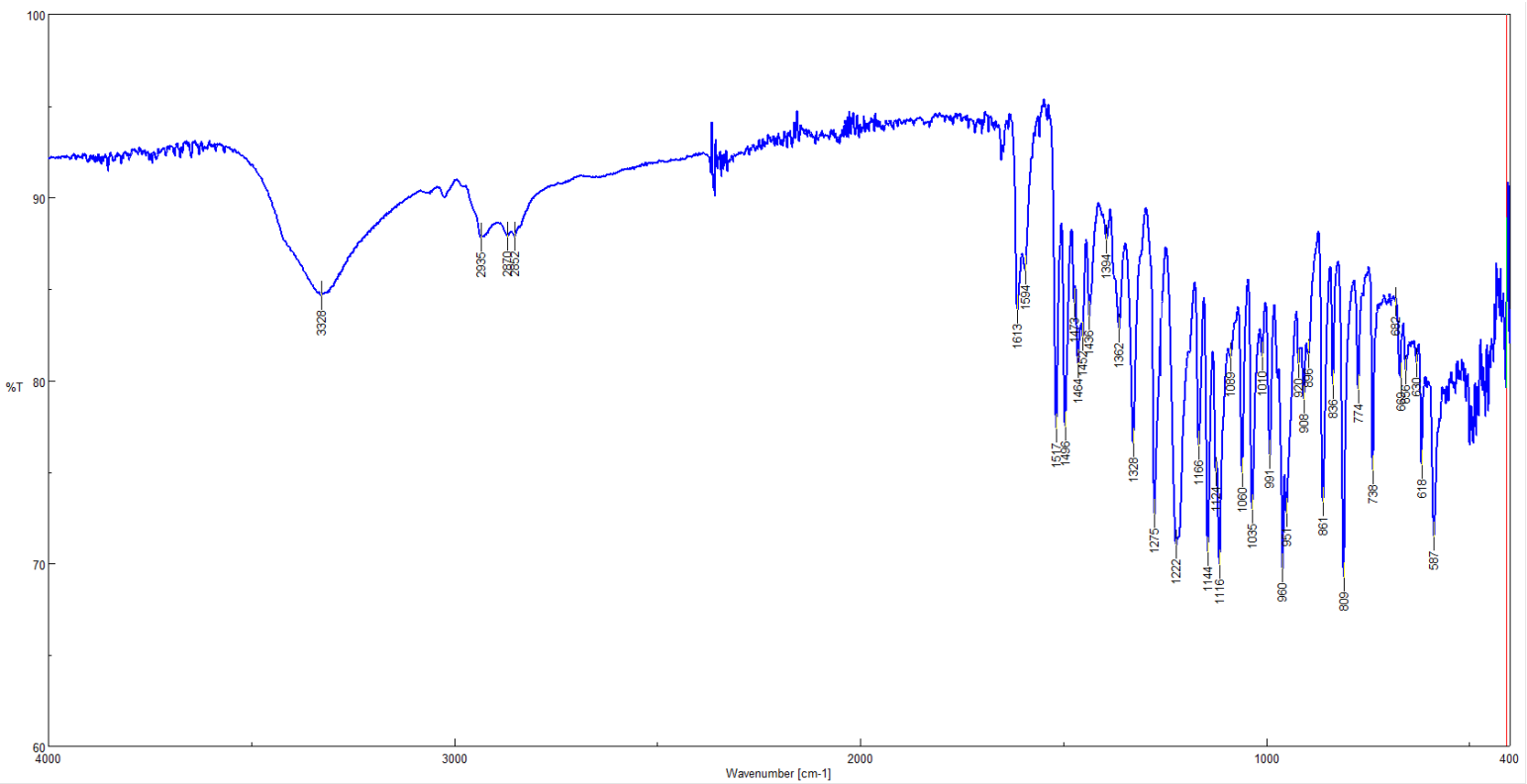

Figure 3.57: IR (neat) of dimer II

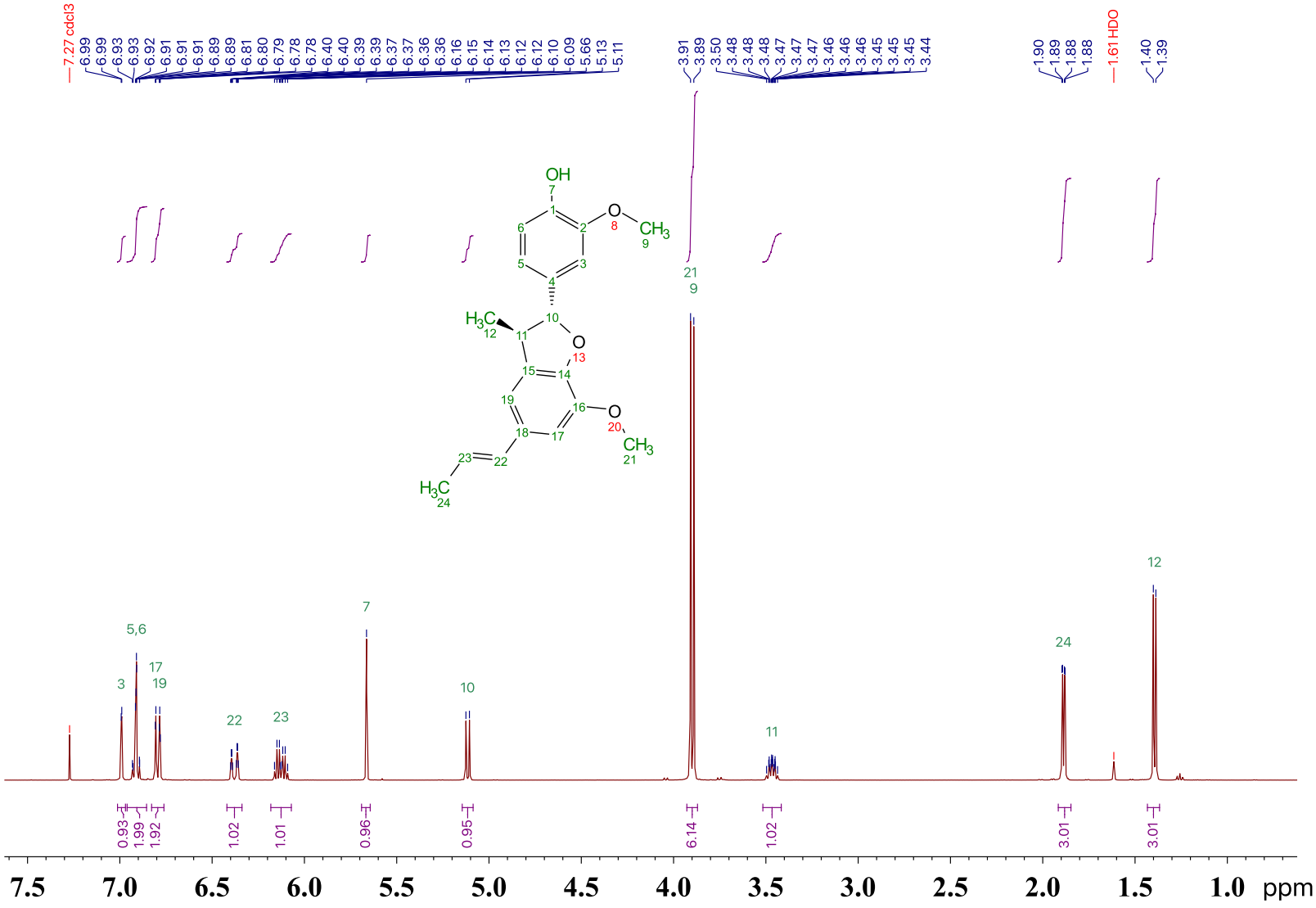

Figure 3.58: Proton NMR of dimer III

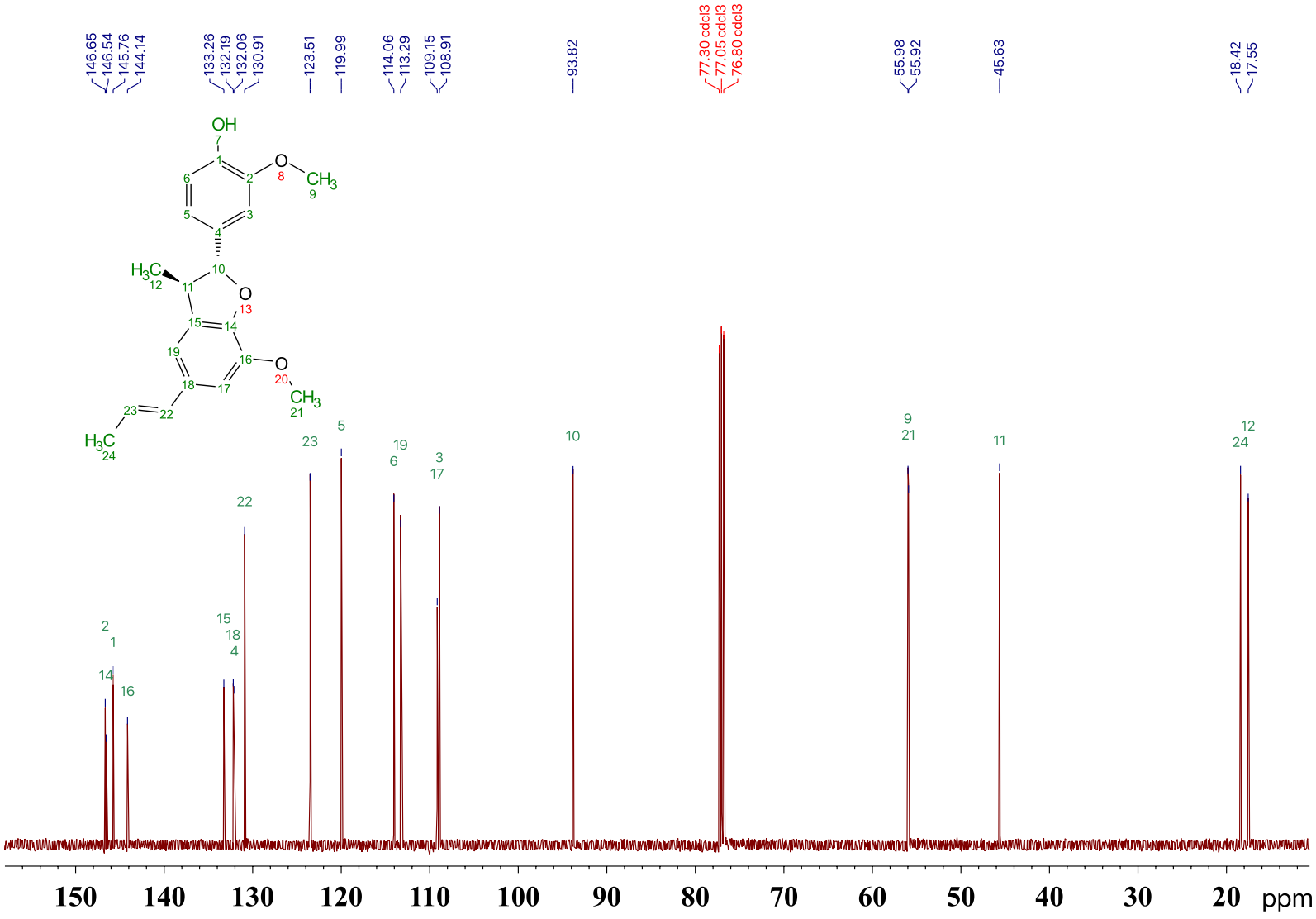

Figure 3.59: Carbon NMR of dimer III

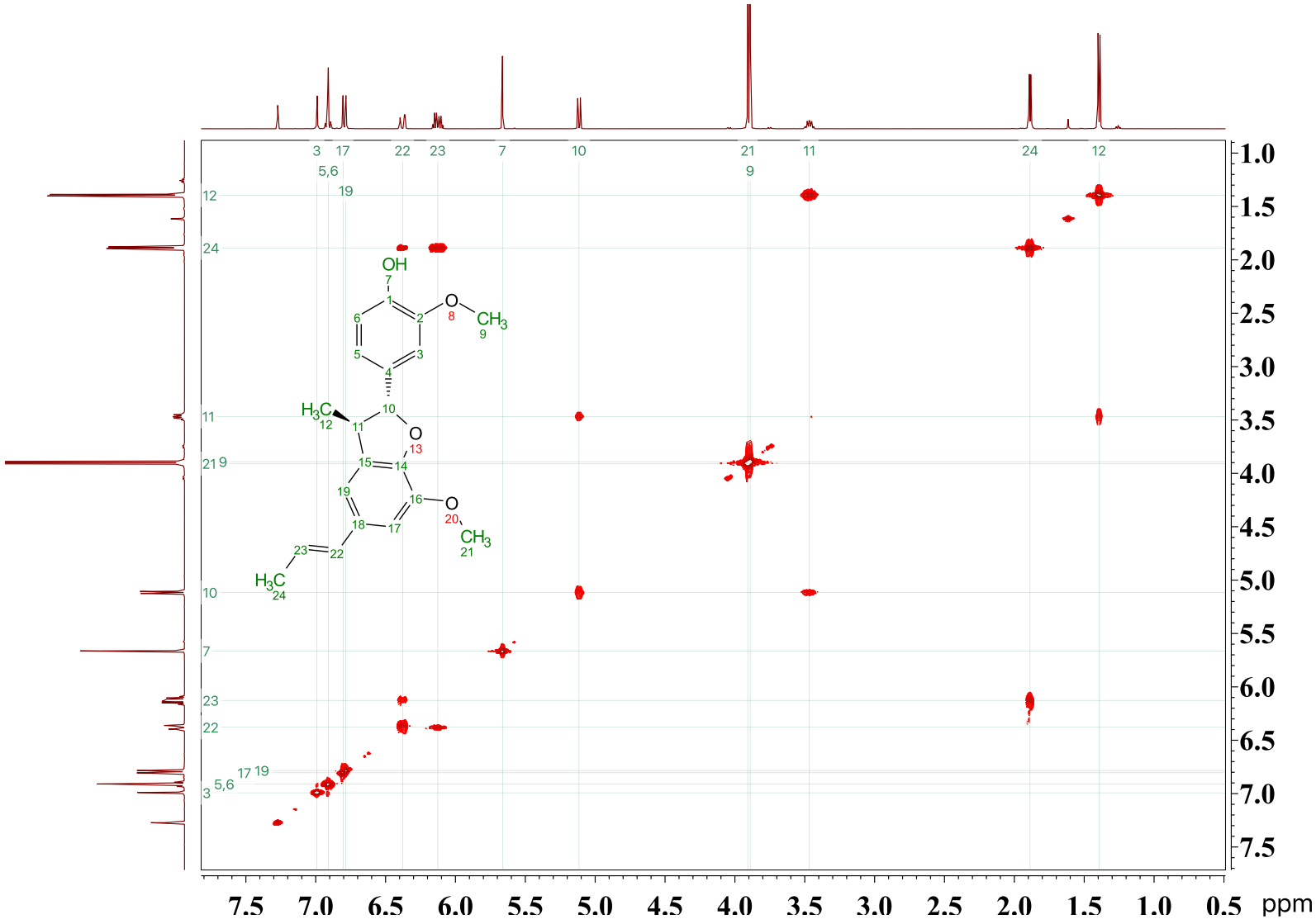

Figure 3.60: gCOSY NMR of dimer III

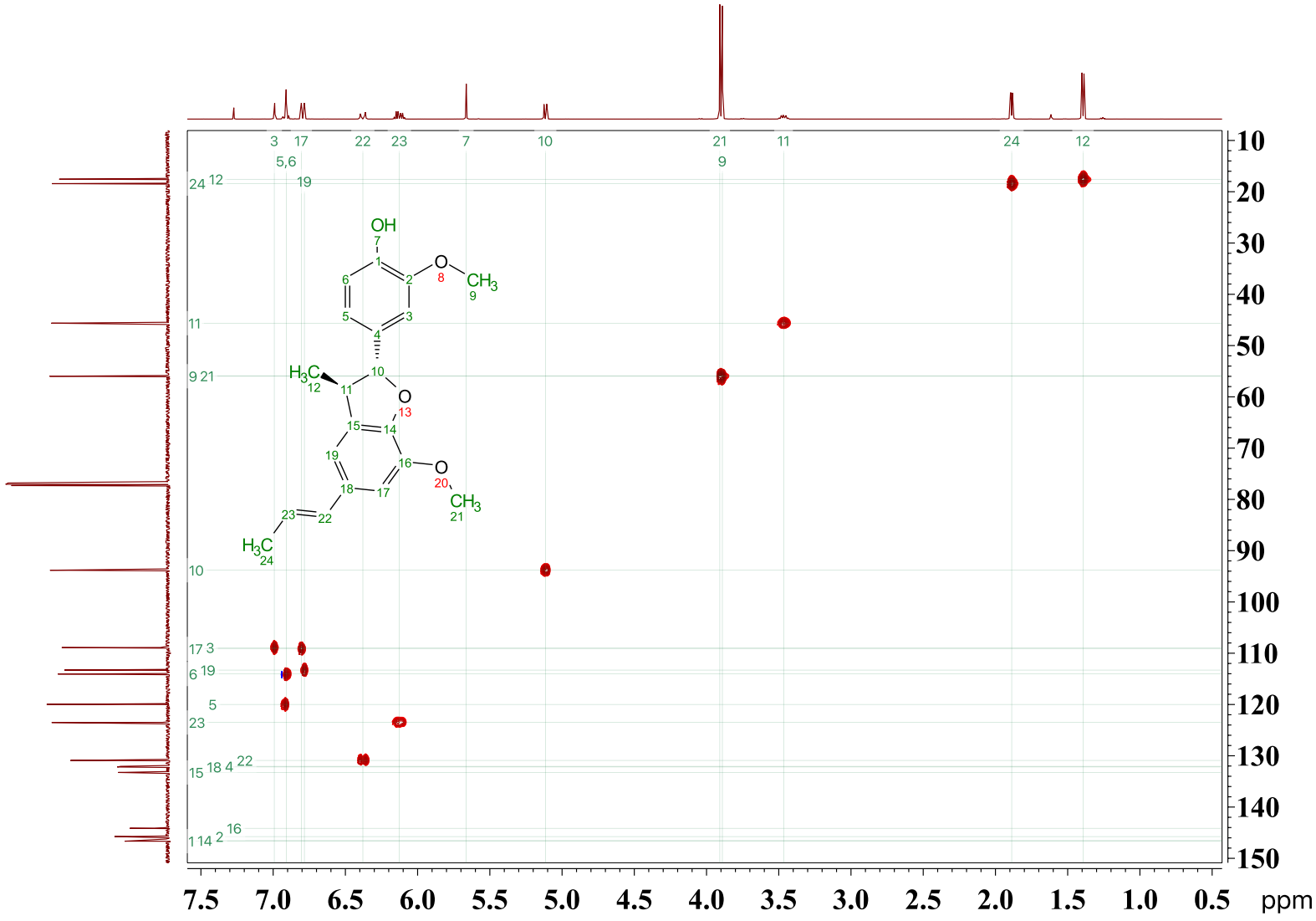

Figure 3.61: gHSQCAD NMR of dimer III

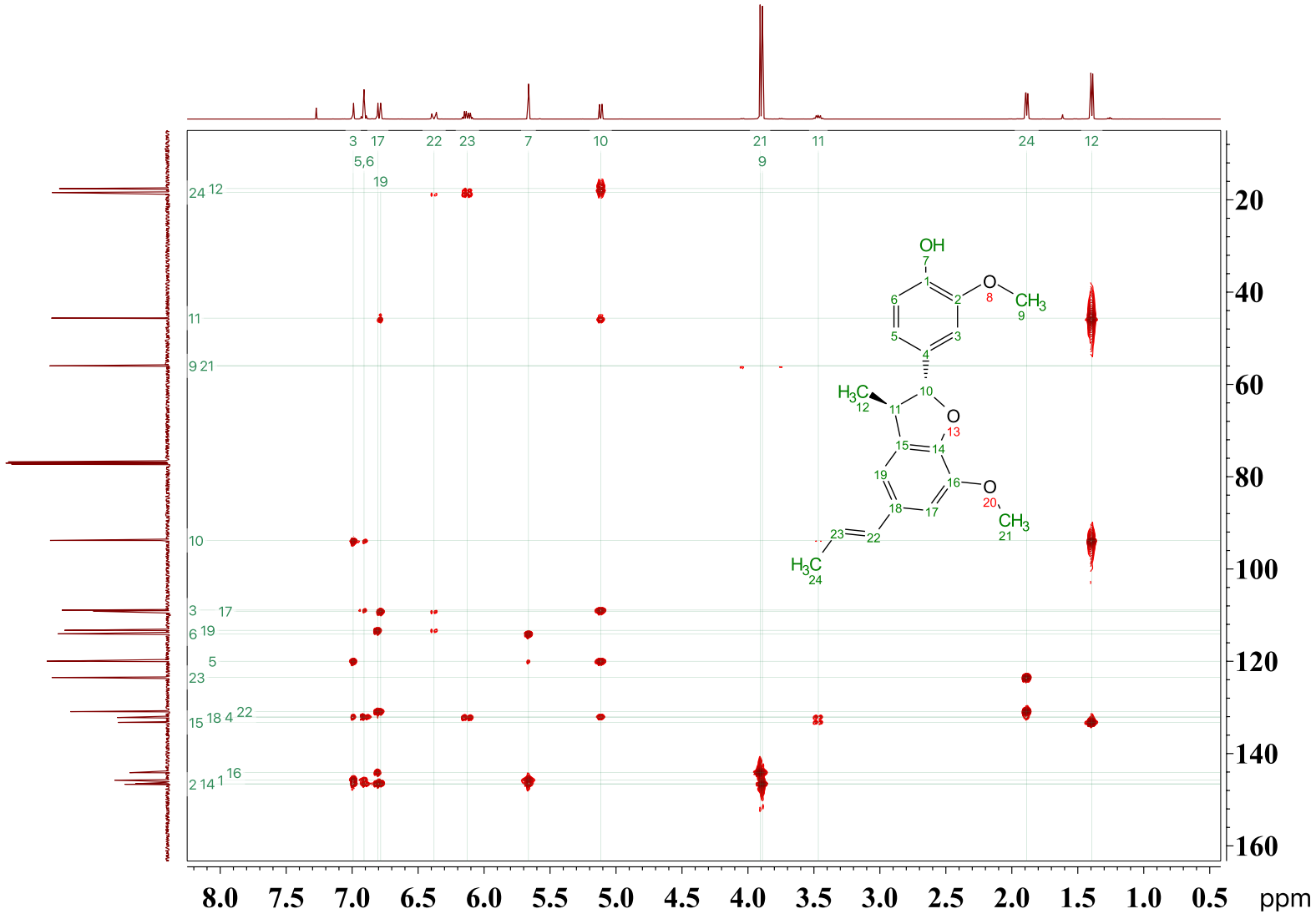

Figure 3.62: gHMBCAD NMR of dimer IV

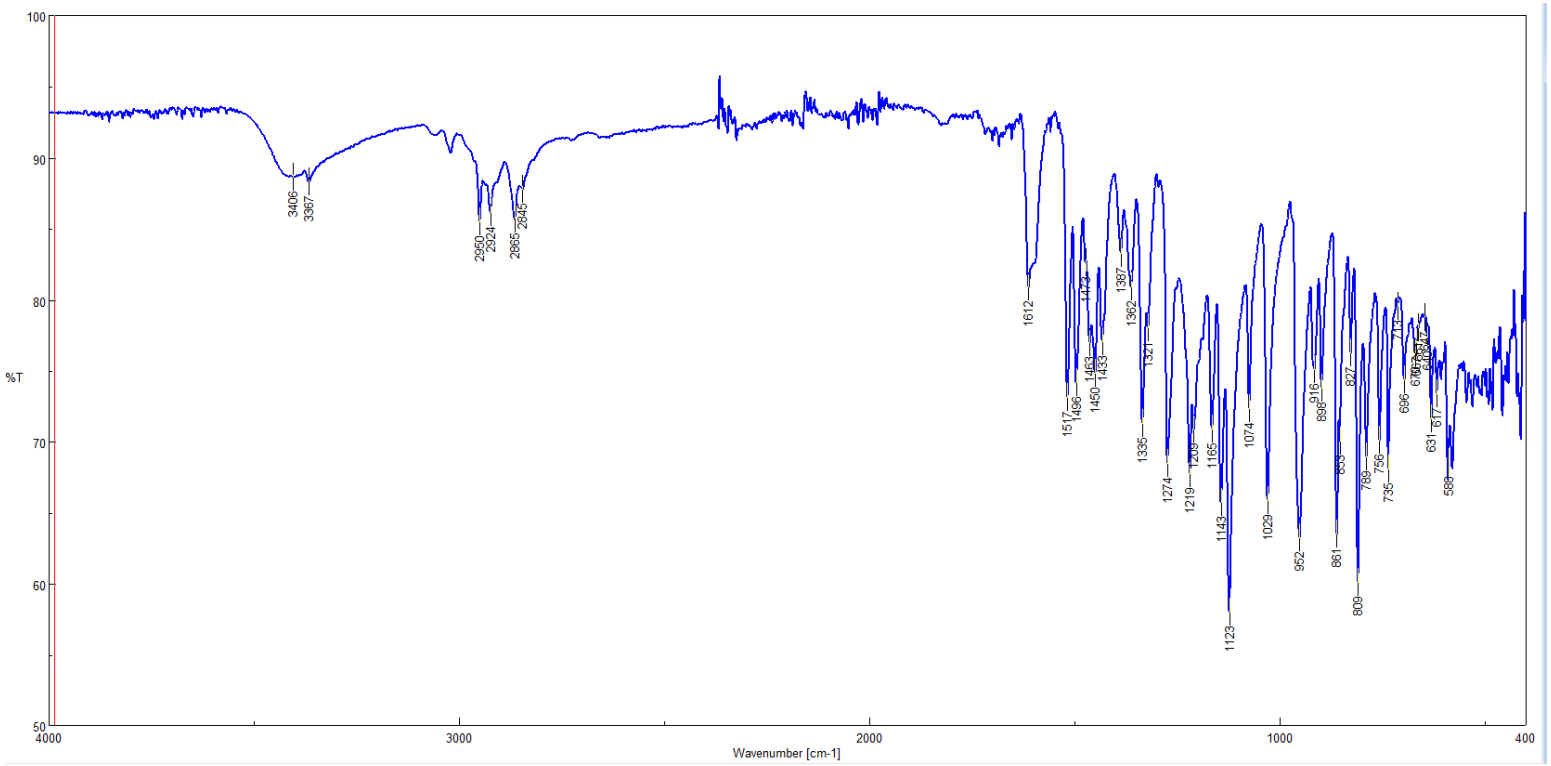

Figure 3.63: IR (neat) of dimer III

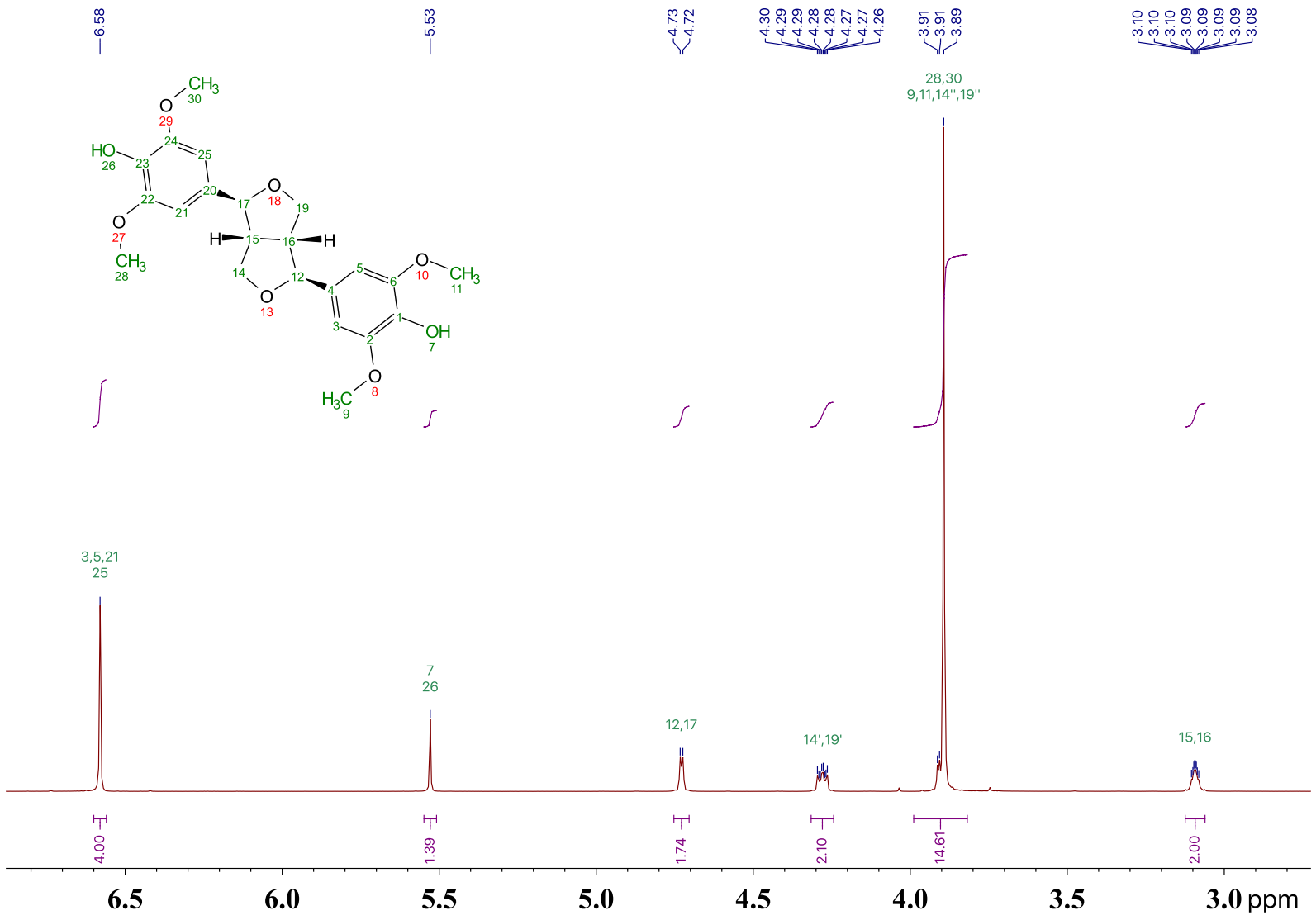

Figure 3.64: Proton NMR of dimer IV

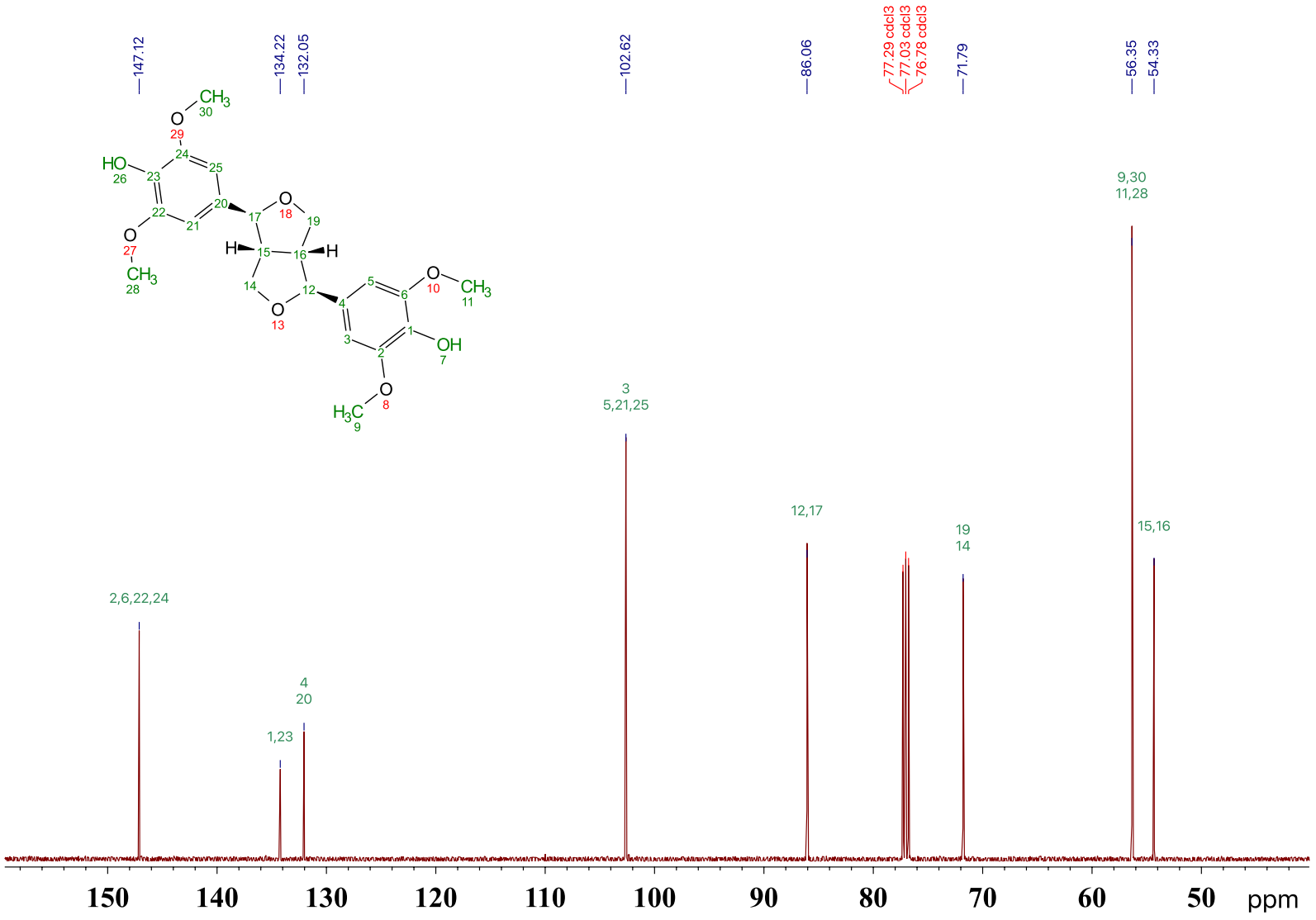

Figure 3.65: Carbon NMR of dimer IV

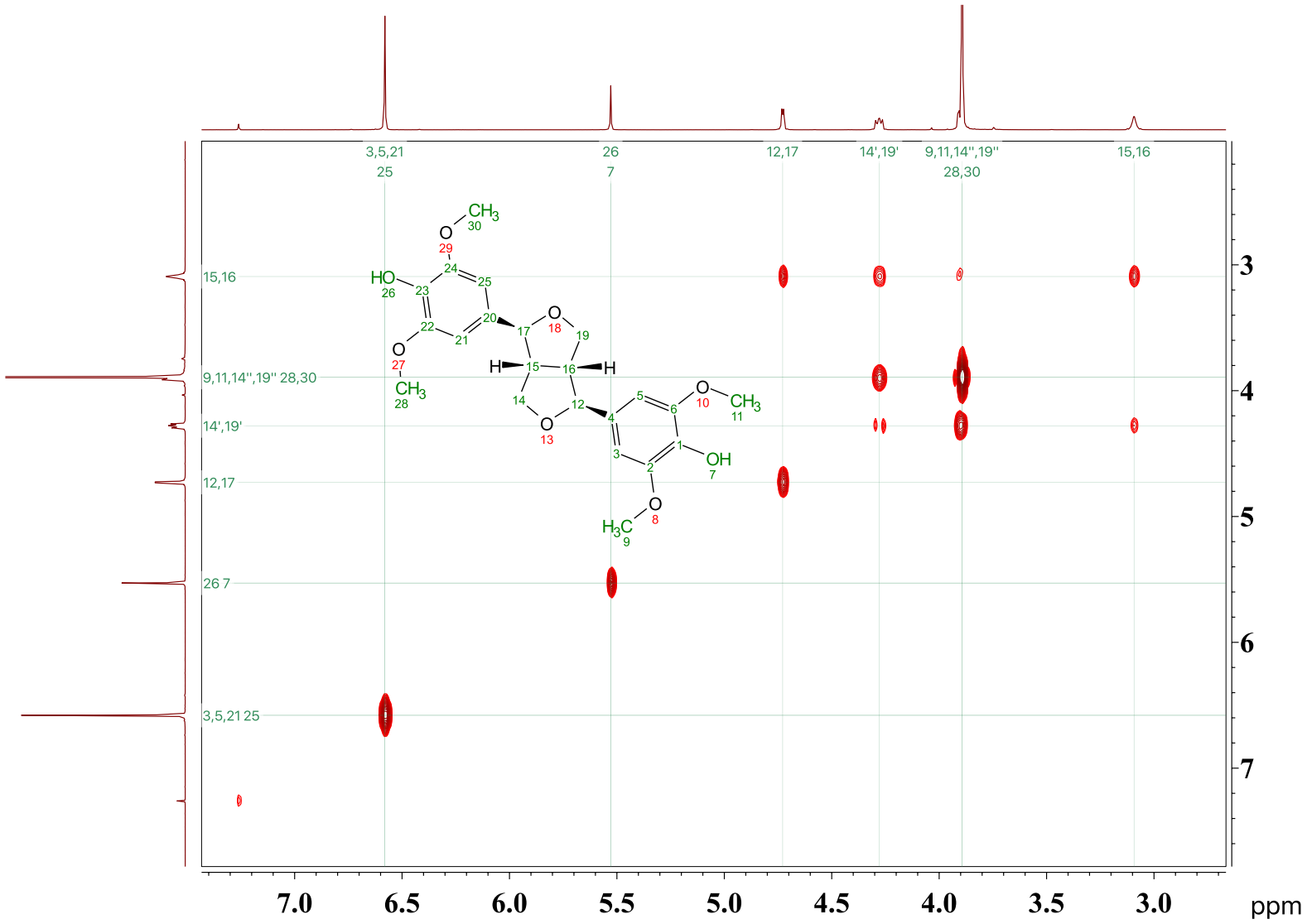

Figure 3.66: gCOSY NMR of dimer IV

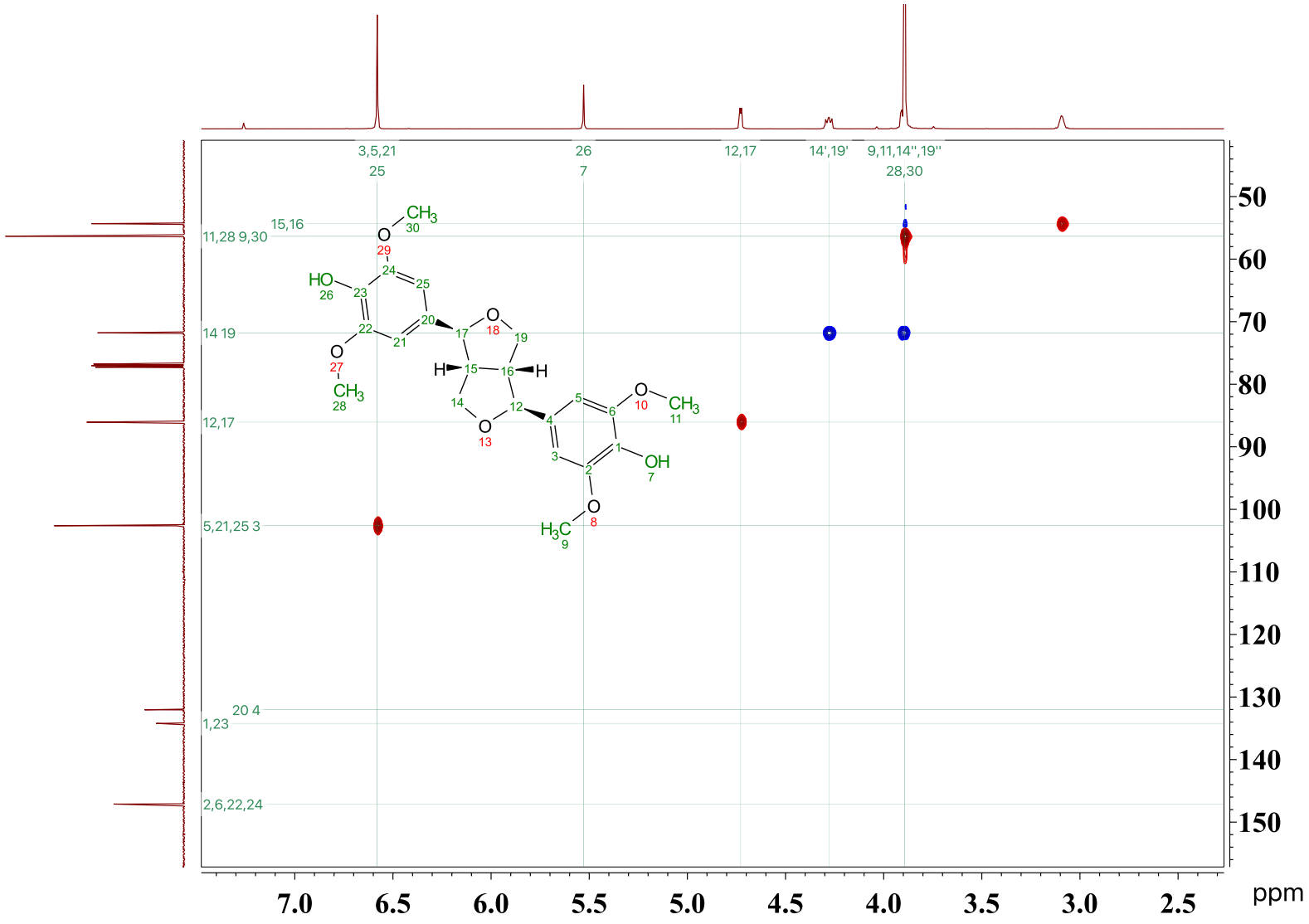

Figure 3.67: gHSQCAD NMR of dimer IV

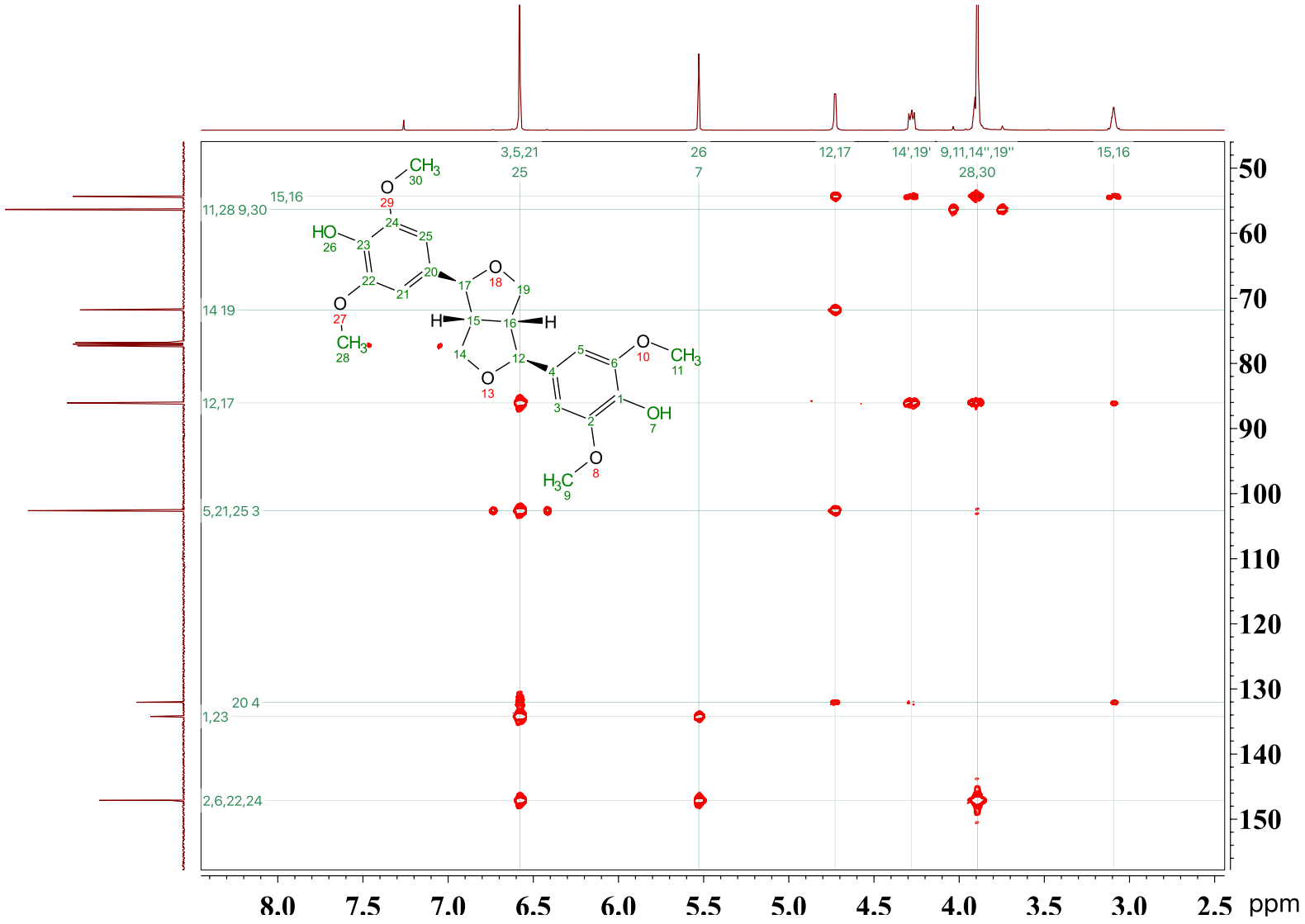

Figure 3.68: gHMBCAD NMR of dimer IV

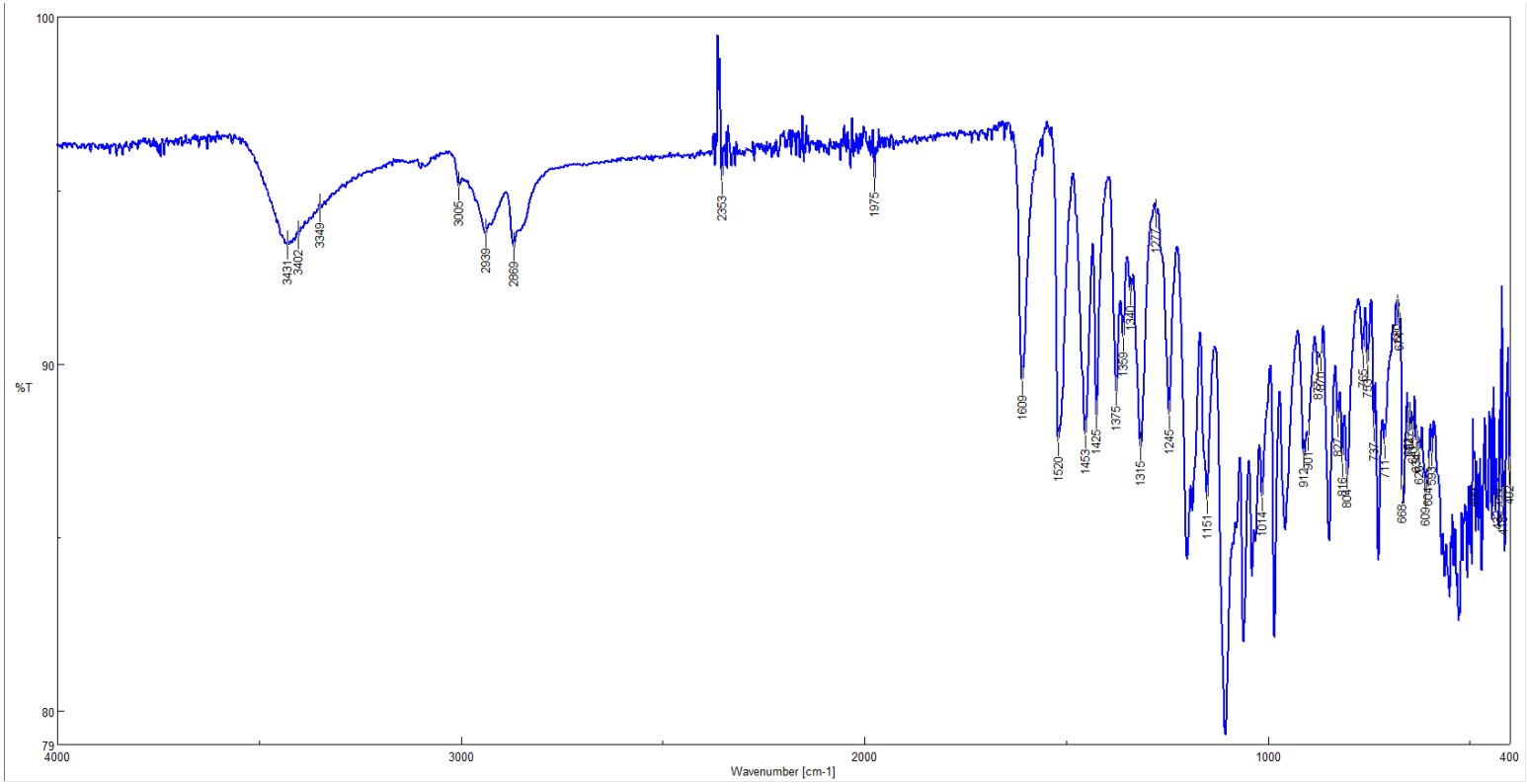

Figure 3.69: IR (neat) of dimer IV

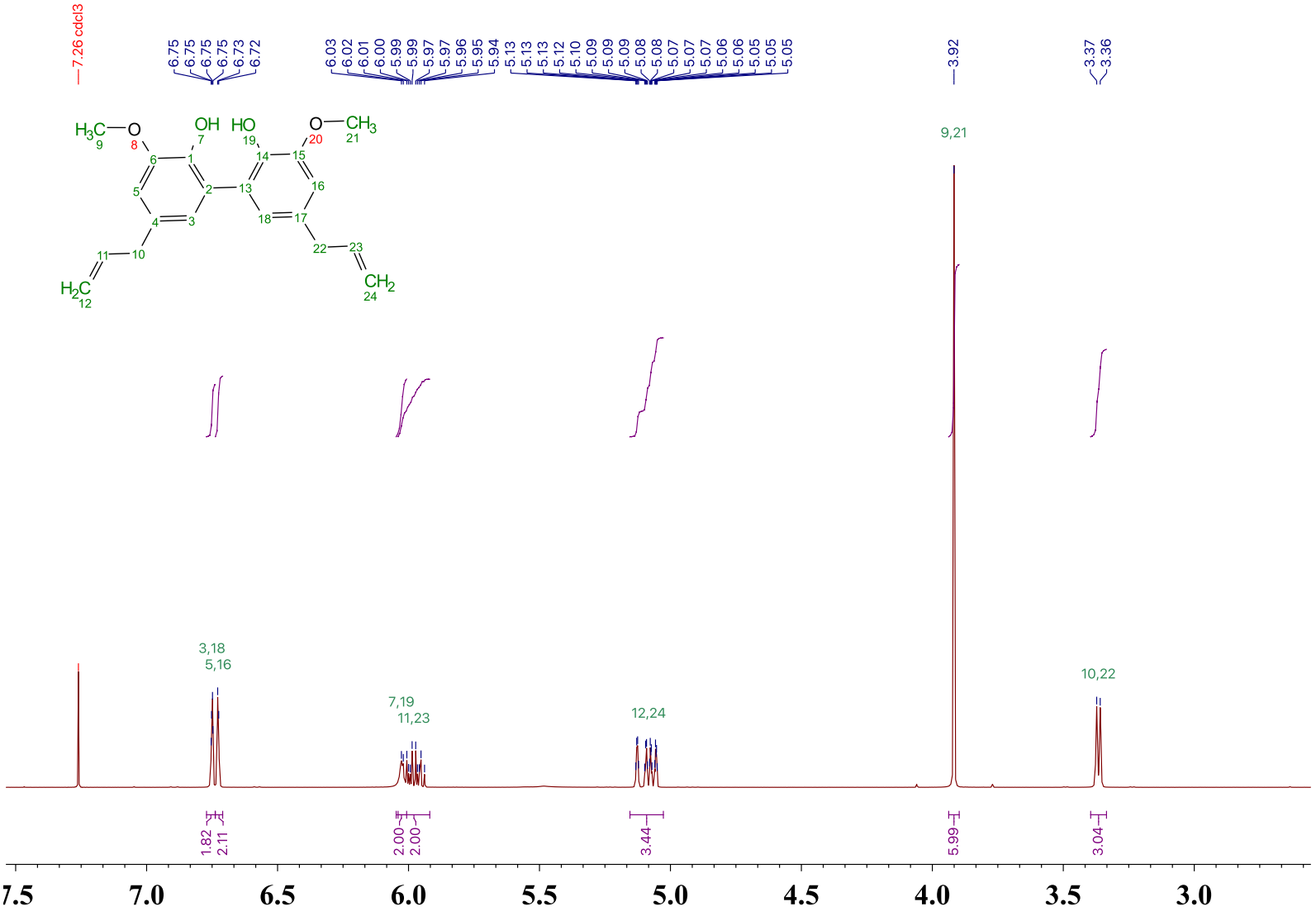

Figure 3.70: Proton NMR of dimer V

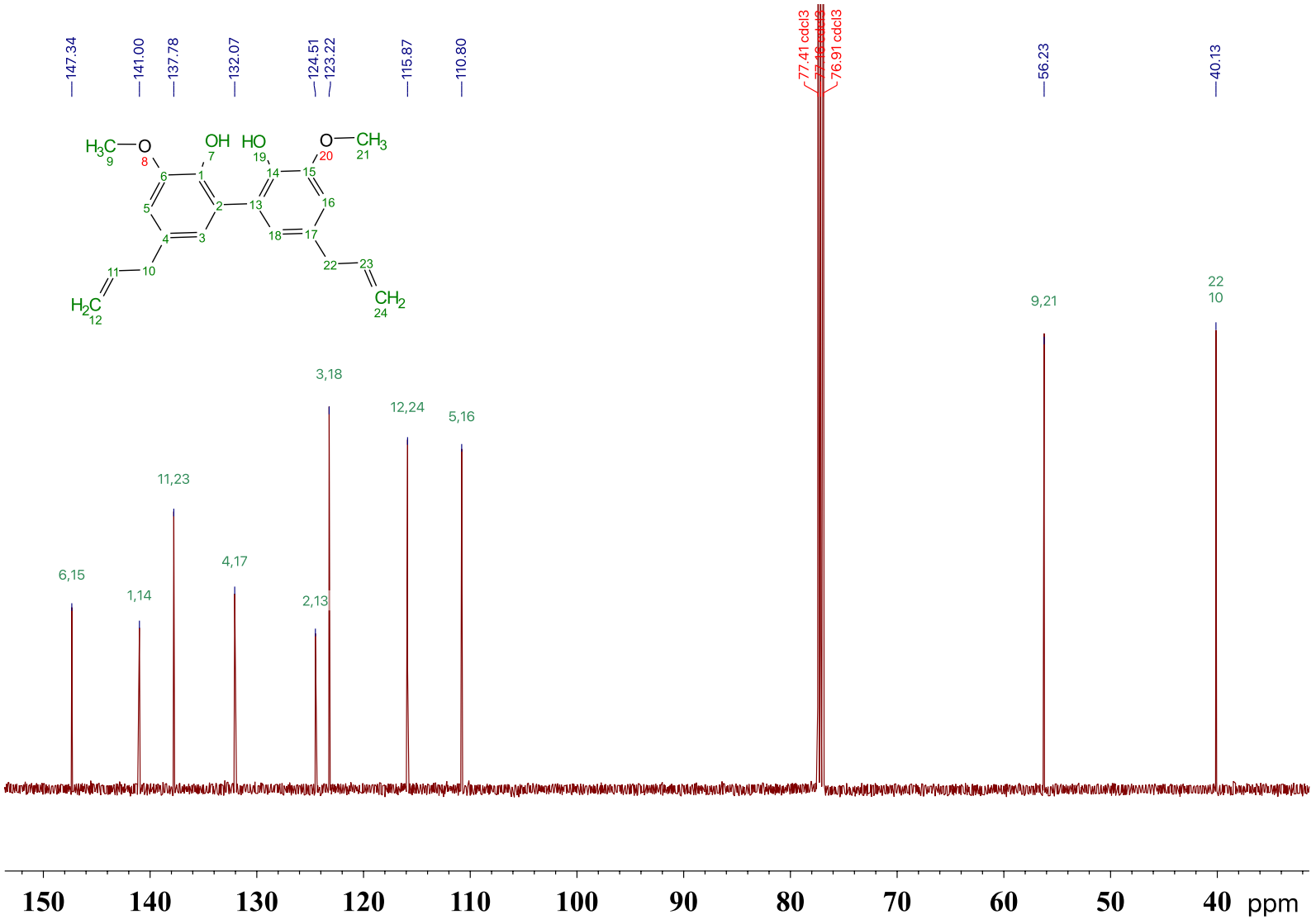

Figure 3.71: Carbon NMR of dimer V

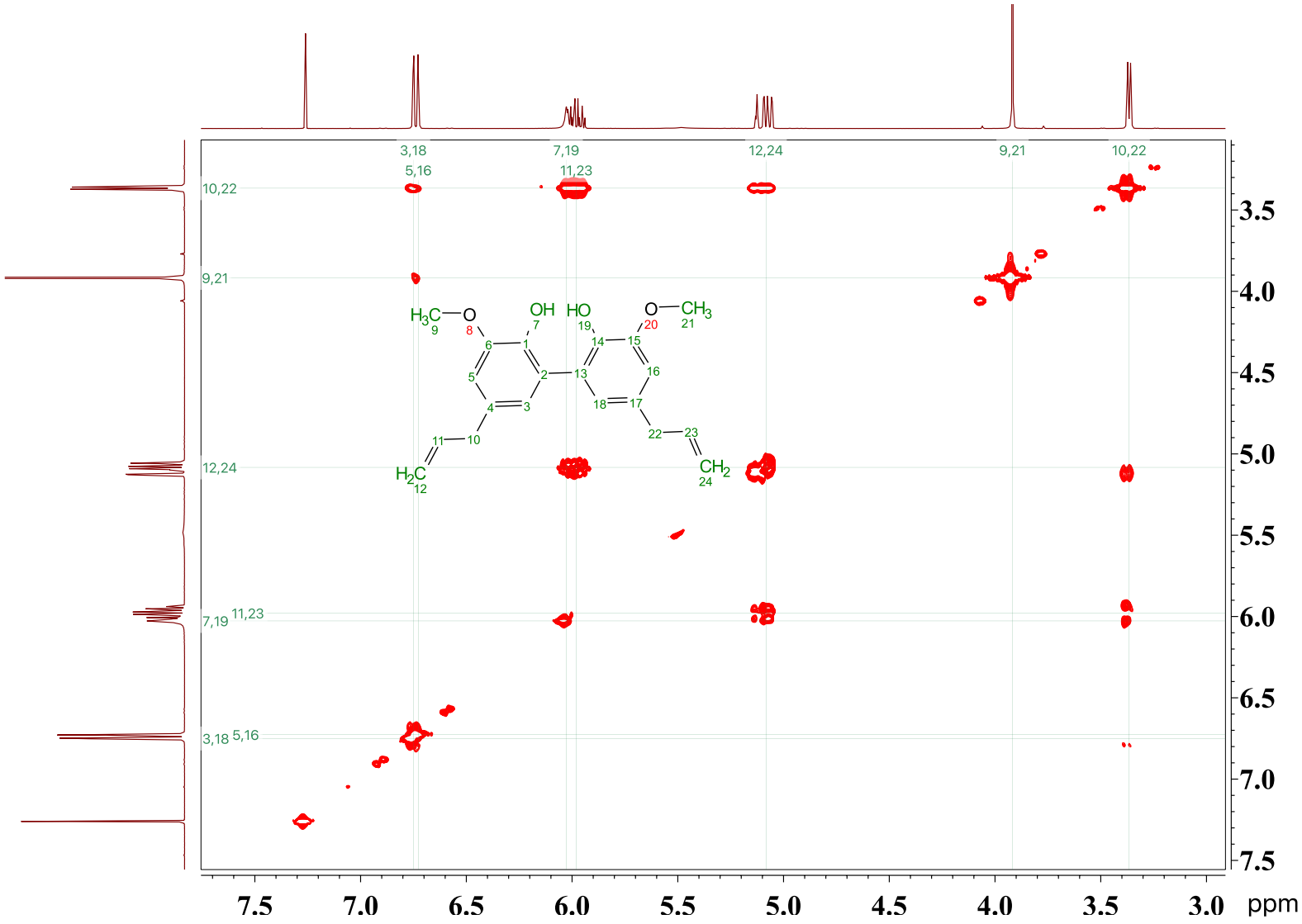

Figure 3.72: gCOSY NMR of dimer V

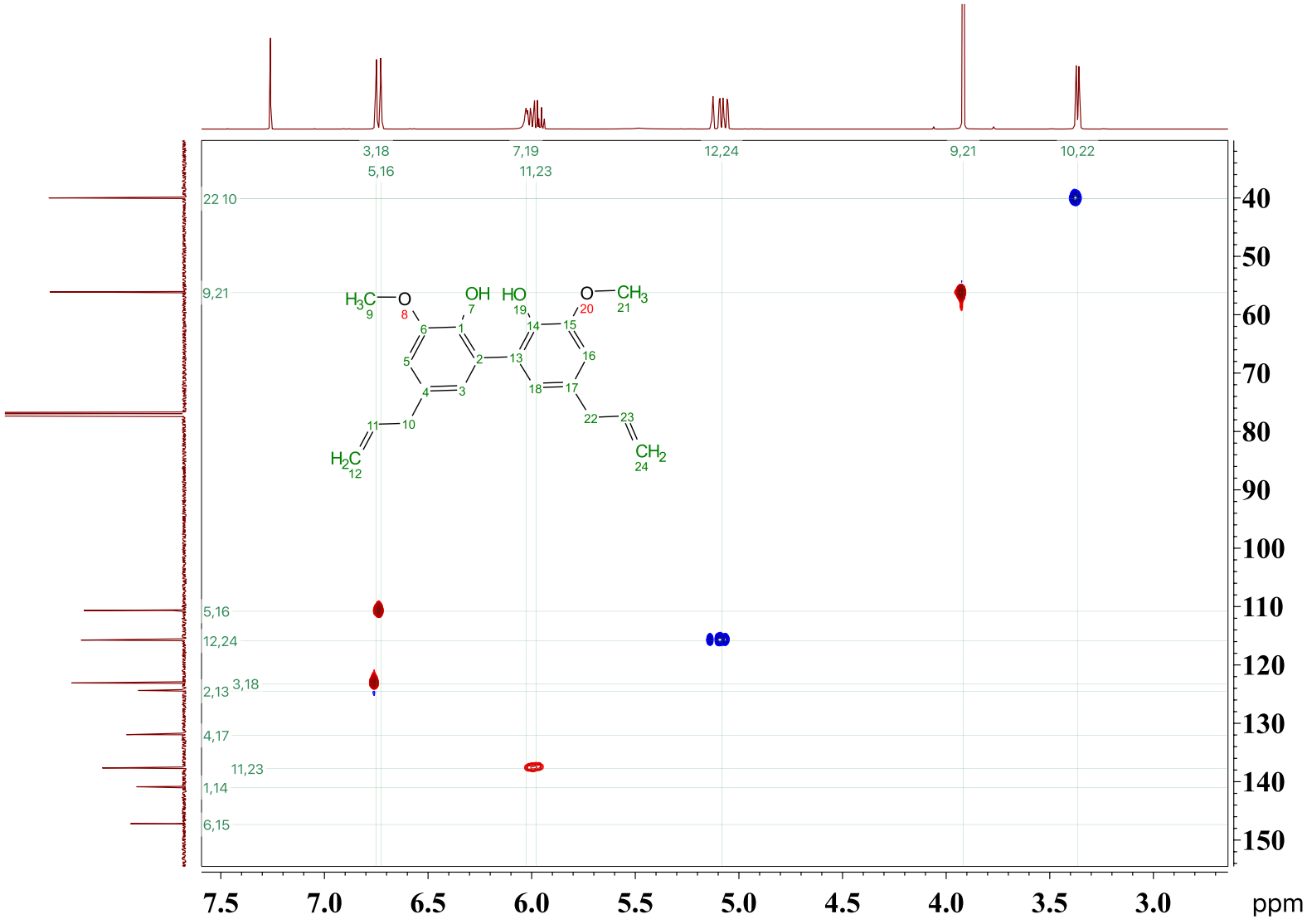

Figure 3.73: gHSQCAD NMR of dimer V

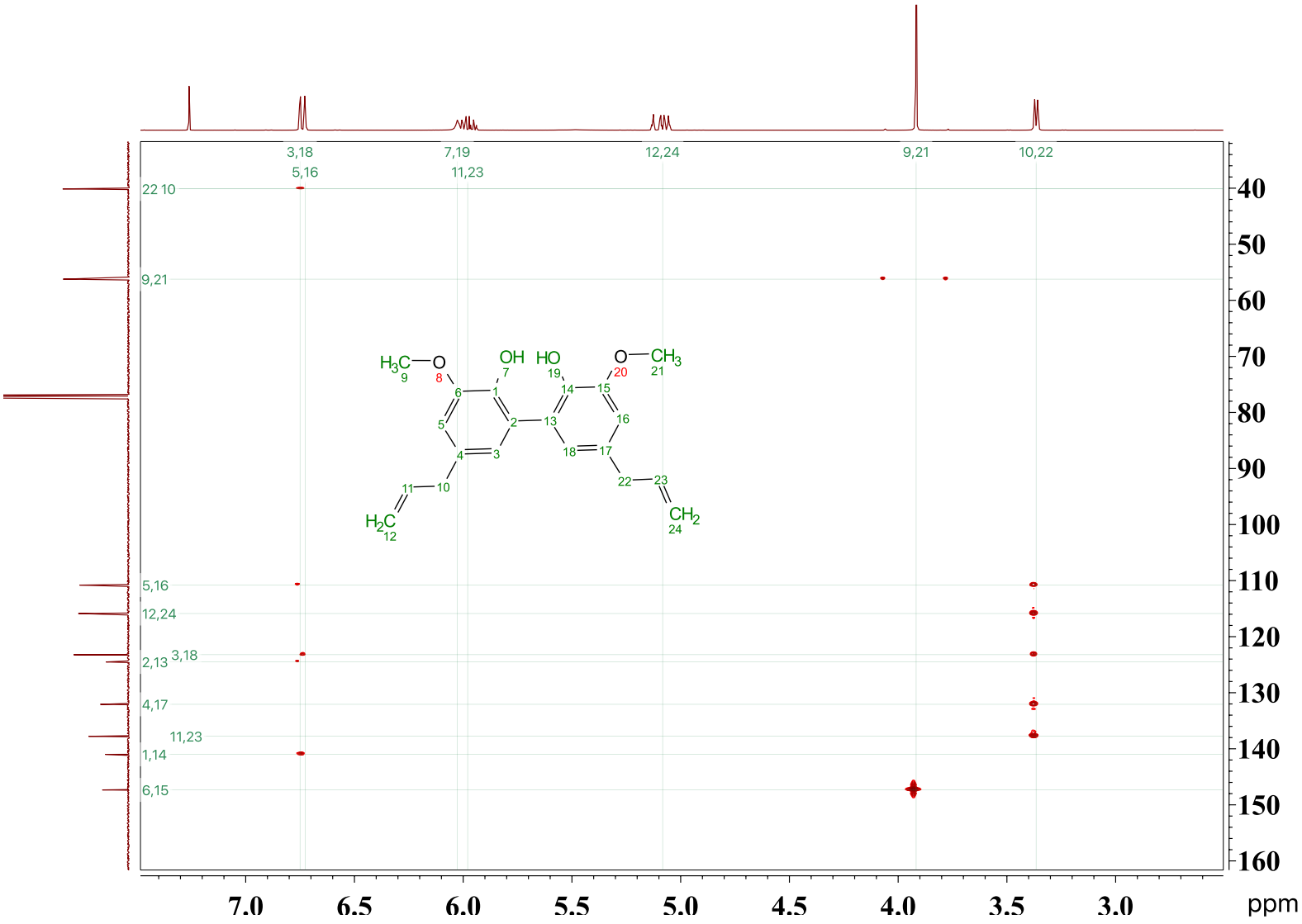

Figure 3.74: gHMBCAD NMR of dimer V

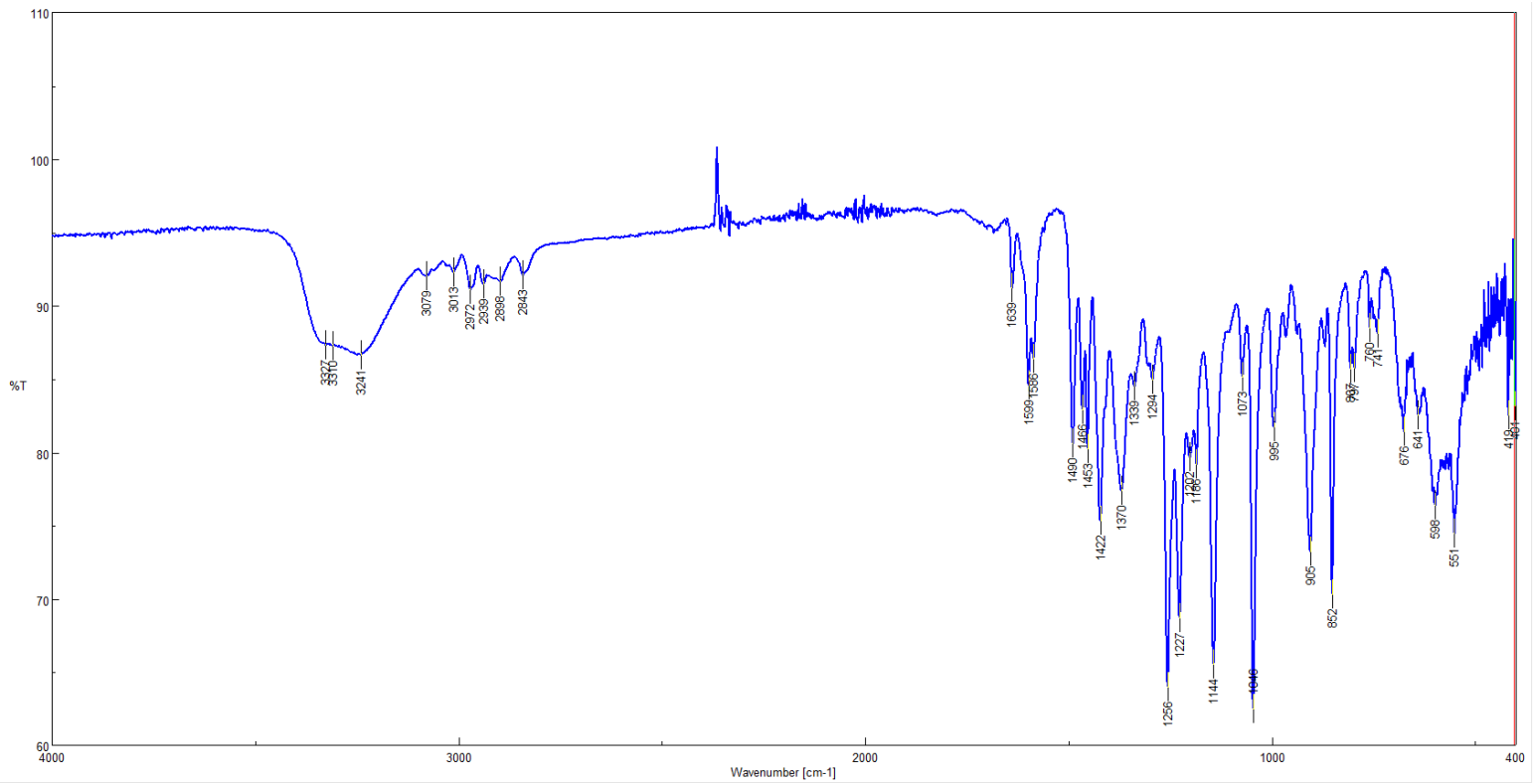

Figure 3.75: IR (neat) of dimer V

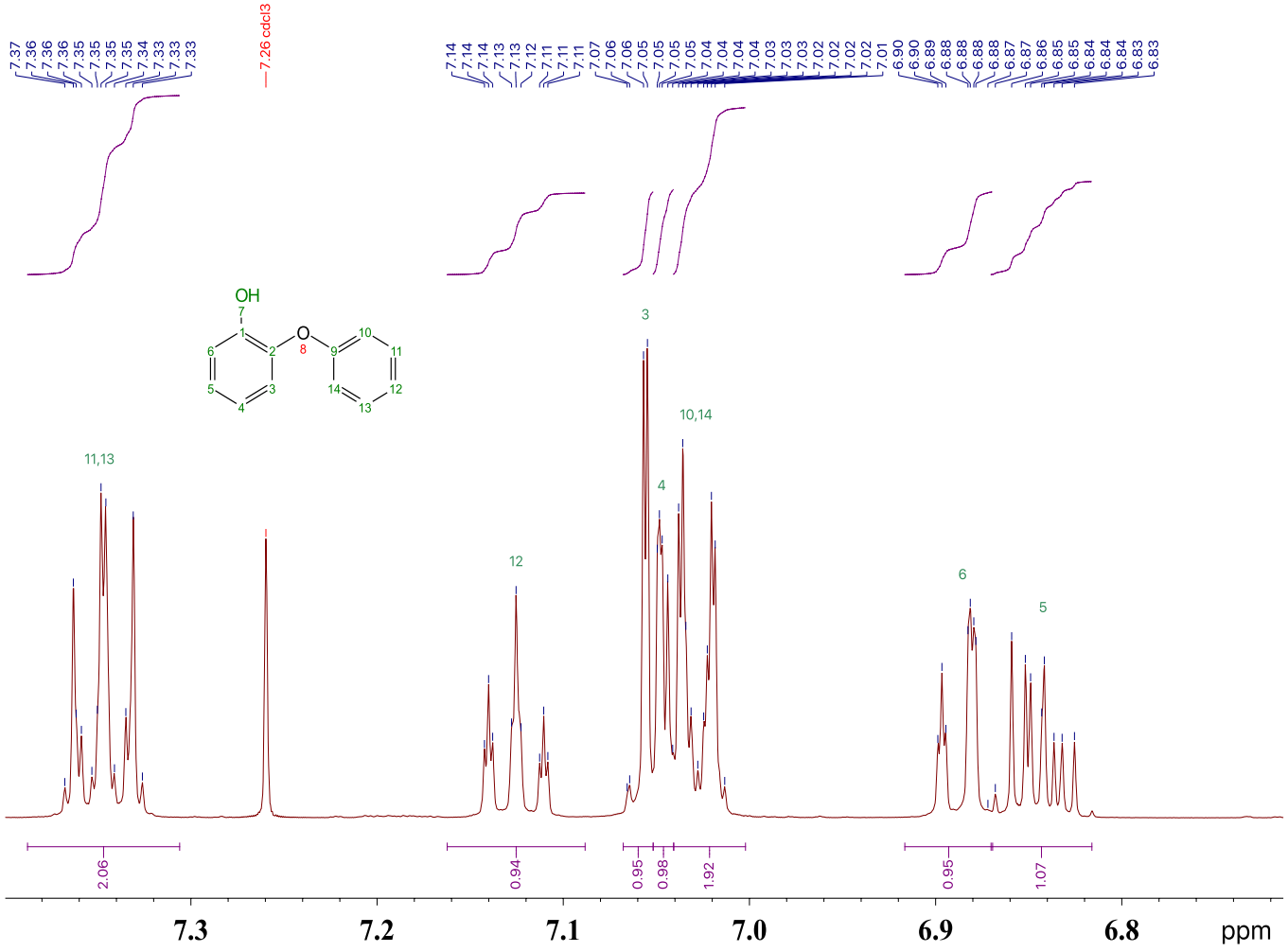

Figure 3.76: Proton NMR of dimer VI

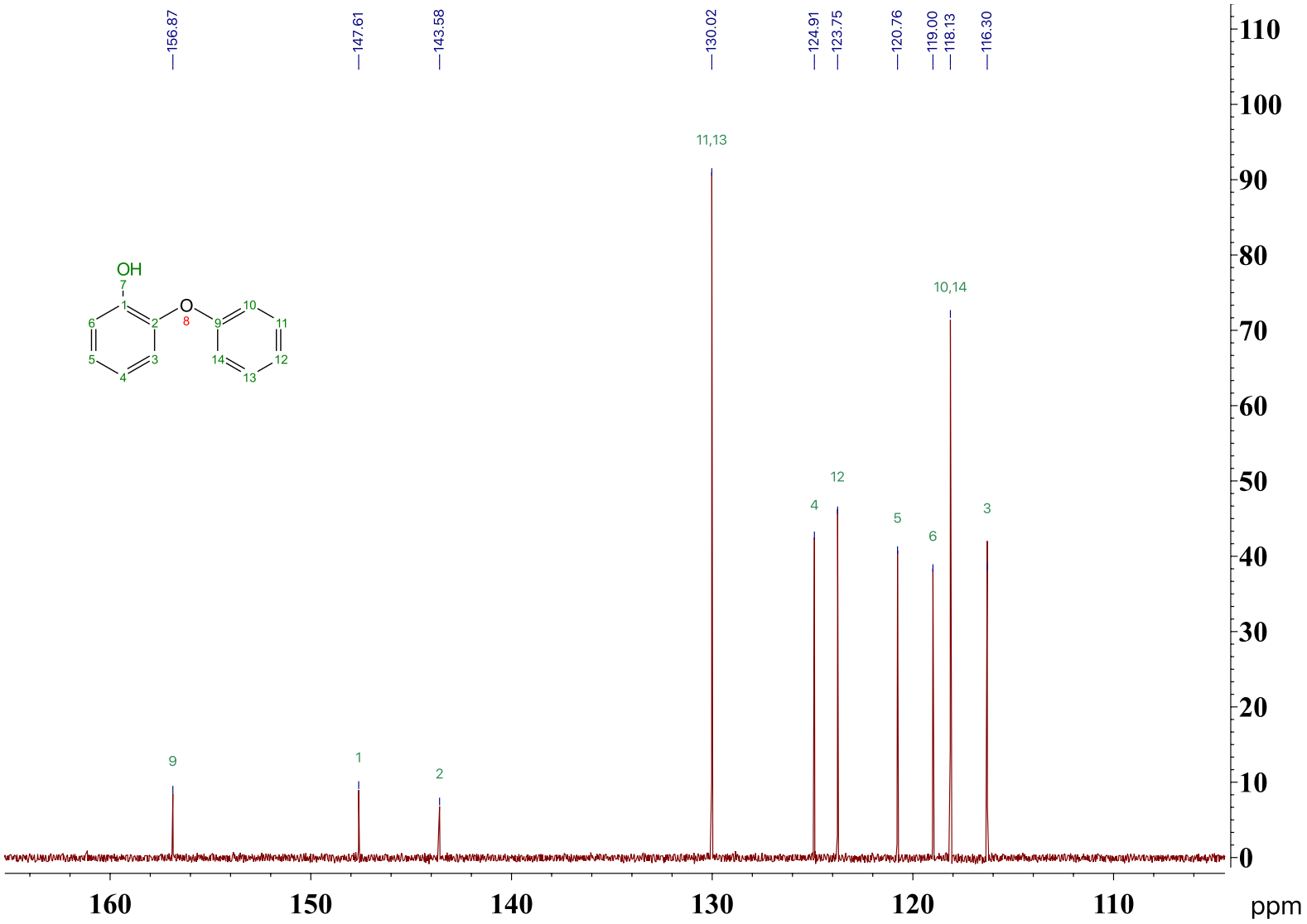

Figure 3.77: Carbon NMR of dimer VI

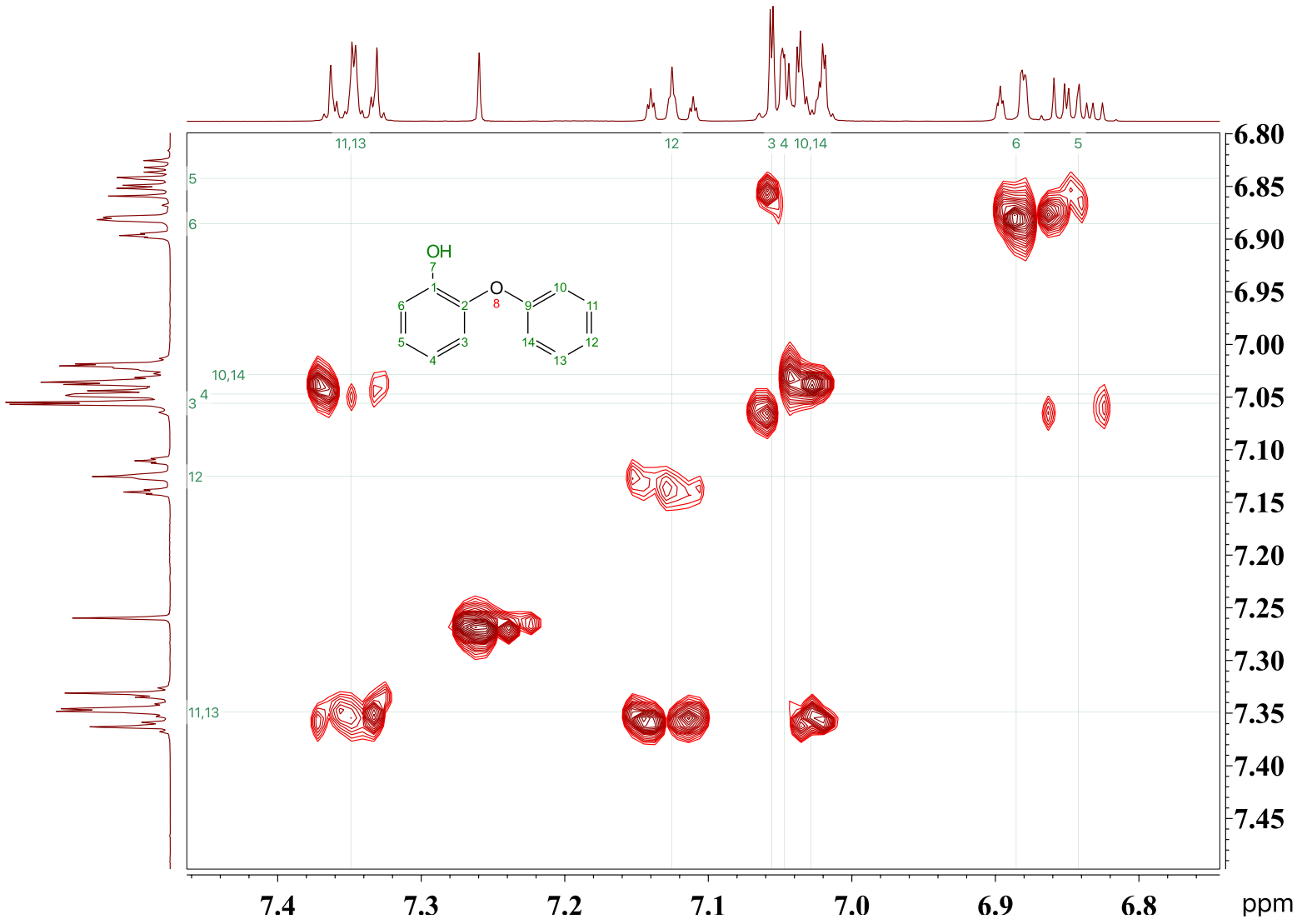

Figure 3.78: gCOSY NMR of dimer VI

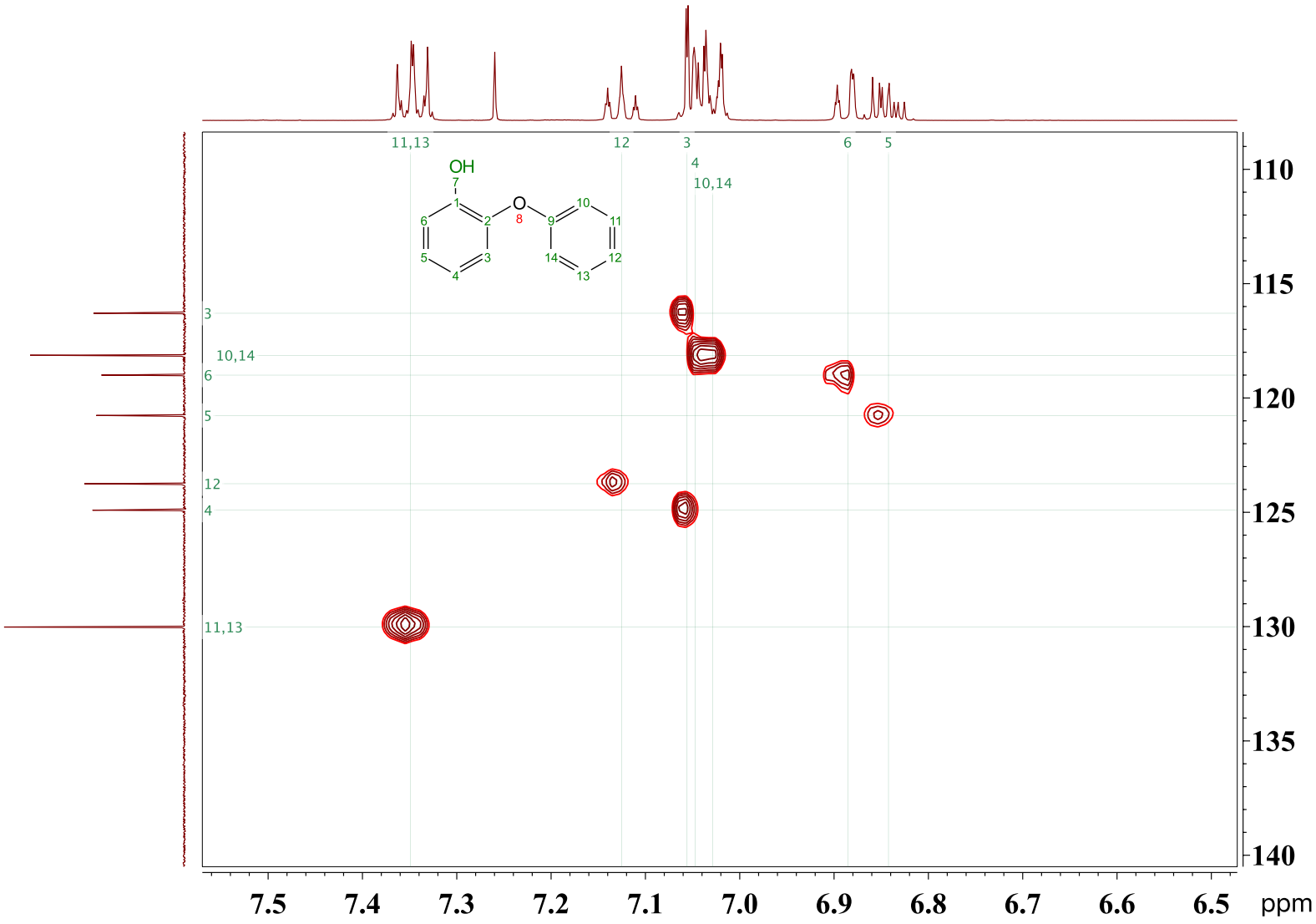

Figure 3.79: gHSQCAD NMR of dimer VI

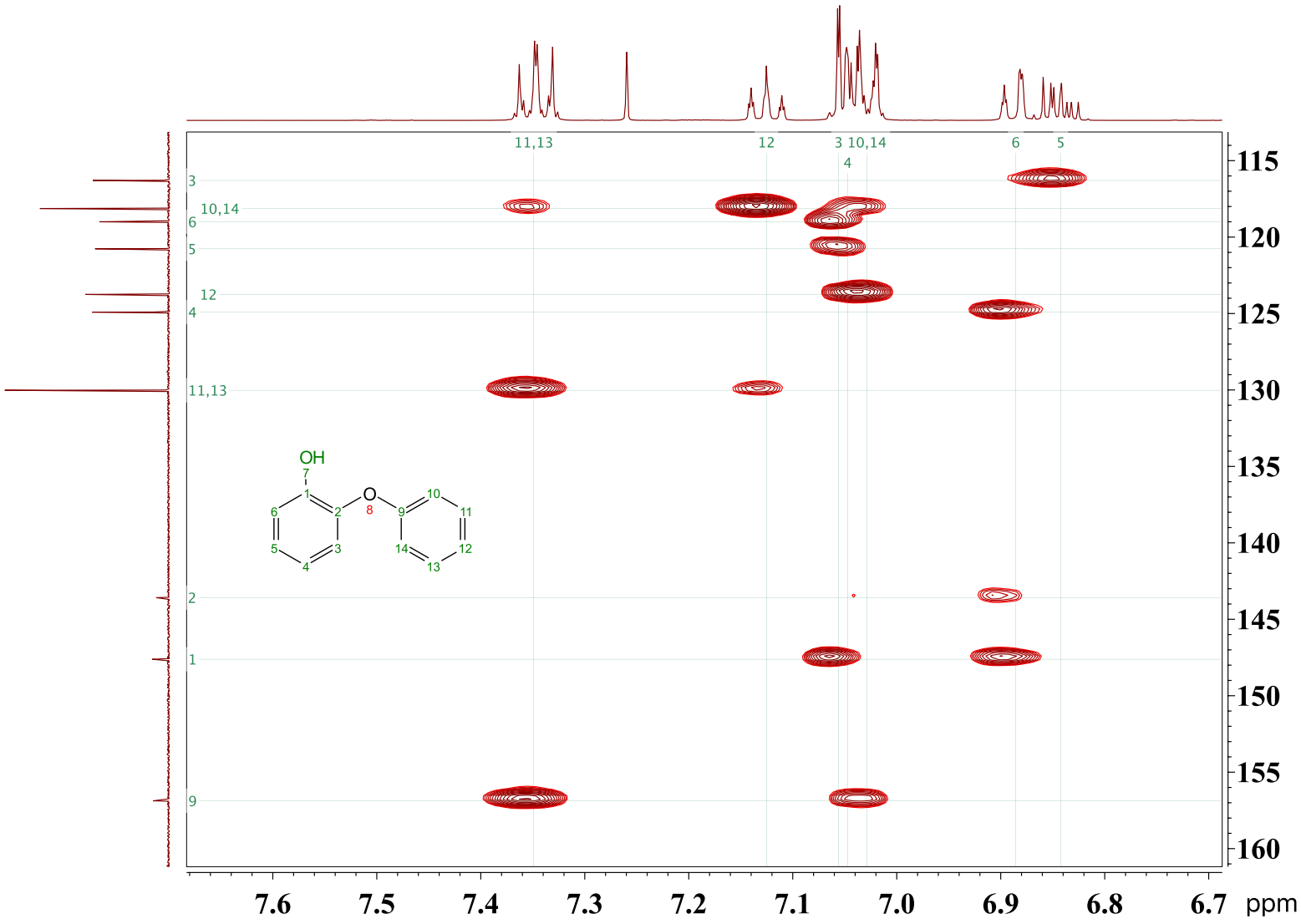

Figure 3.80: gHMBCAD NMR of dimer VI

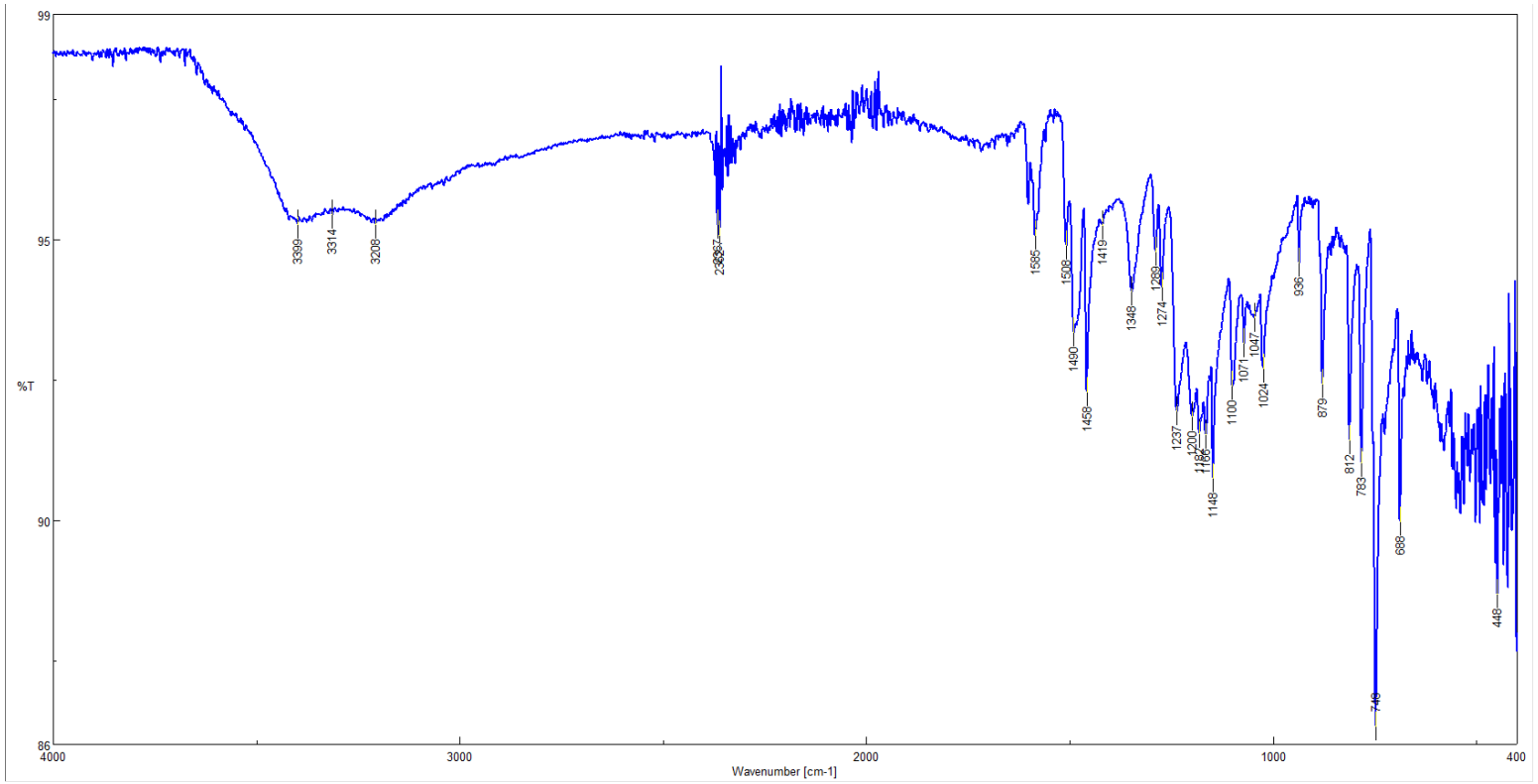

Figure 3.81: IR (neat) of dimer VI

Chapter 4

Electrocatalytic Hydrogenation of Lignin Monomers with Raney® Nickel: Product and Mechanistic Studies

4.1 Introduction

With ongoing consumption of finite fossil petroleum stores and increasing address climate change due to the rising carbon dioxide content in the atmosphere, a shift to biofuel is a strategy offering solutions to both energy security and carbon dioxide reduction issues. The most familiar biofuel, ethanol produced from corn starch or sugar cane, faces the double challenge of the world food security and low greenhouse gas emission (GHG) reduction (20%).[178] Ethanol derived from cellulosic biomass could in principle achieve GHG emission reductions greater than 60% relative to gasoline; its production has been demonstrated and is predicted to make up the majority of the biofuel market by 2022, beyond the market share of conventional ethanol biofuel.[178] Cellulosic ethanol biorefineries produce massive amounts of lignin byproduct since biomass contains 25-35 wt% lignin. Meanwhile, the paper and

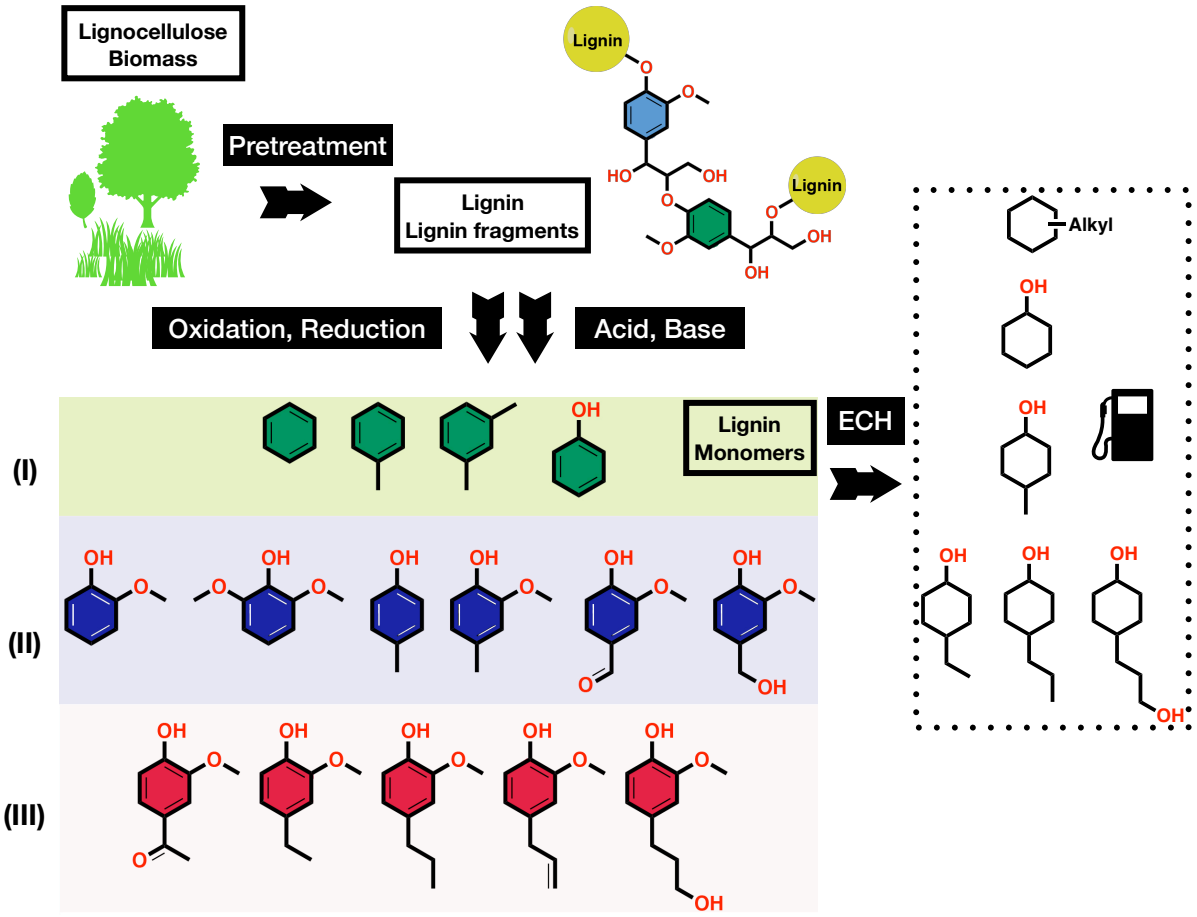

Figure 4.1: Utilization of lignocellulosic biomass to produce fuels.

pulping industry extracts cellulose from biomass for paper making and produces lignin in the order of 130 million tonnes annually.[179] However, less than 2% of the lignin byproducts are commercially used for products other than simply being burned in a recovery boiler for heat.[179]

Considering lignin is the highest energy and carbon content polymer in biomass with a higher heating value of 26.7 MJ/kg, around 50% more than that of cellulose (17.5 MJ/kg),[117] chemical conversions of lignin to more energy-dense fuels are more appealing than converting lower energy content cellulose to fuels. However, the U.S. Department of Energy estimates that the over one billion tons of biomass resources from agricultural and forestland in the

U.S. could only displace 30% of U.S. petroleum consumption.[180] Therefore, an addition of other renewable energy streams such as solar and wind electricity into biofuel are needed to further meet U.S. energy need. One solution is to use Electrocatalytic Hydrogenation (ECH) to upgrade lignin into higher energy content fuels by conducting hydrogenation and deoxygenation reactions on the surfaces of heterogeneous catalysts in aqueous solutions.

Due to difficulties with the massive molecule size and complicated structure of lignin, our preliminary study has suggested that ECH of lignin to produce biofuel is not economically practical at this point. However, it is encouraging that recent advances in various strategies to depolymerize lignin to monomers with high yields offer new opportunities for application of ECH to lignin monomers. These lignin monomers, as summarized in Figure 4.1, can be classified into three categories: (I) monomers that can be directly used as fuels or can be reduced into fuels by ECH at room temperature effectively; (II) monomers that can be or in principle can be converted into category I chemicals via ECH deoxygenation and hydrogenation reactions; (III) monomers that cannot be directly converted to category I chemicals and for which it is unclear if ECH can convert them into fuel level molecules effectively.

The ECH of benzene, toluene, and xylene have been studied with Au,[181] Pd,[182] Pt,[181–184] Ru[182] and Raney Nickel (RaNi)[103] cathode, and the ECH went through smoothly with current efficiency ranging from 73% to 100% at room temperature in alcohol solutions or neat condition.

ECH of phenol had been extensively studied with different hydrogenating metal catalysts on different supports, and the aromatic ring reduction current efficiencies, the moles of electrons that ending up in the target product over the moles of electrons supplied, of these metals roughly follow this order: Rh, Pt (activated), RaNi >> Pd >> Ni, Pt (plain), Pb, Hg.

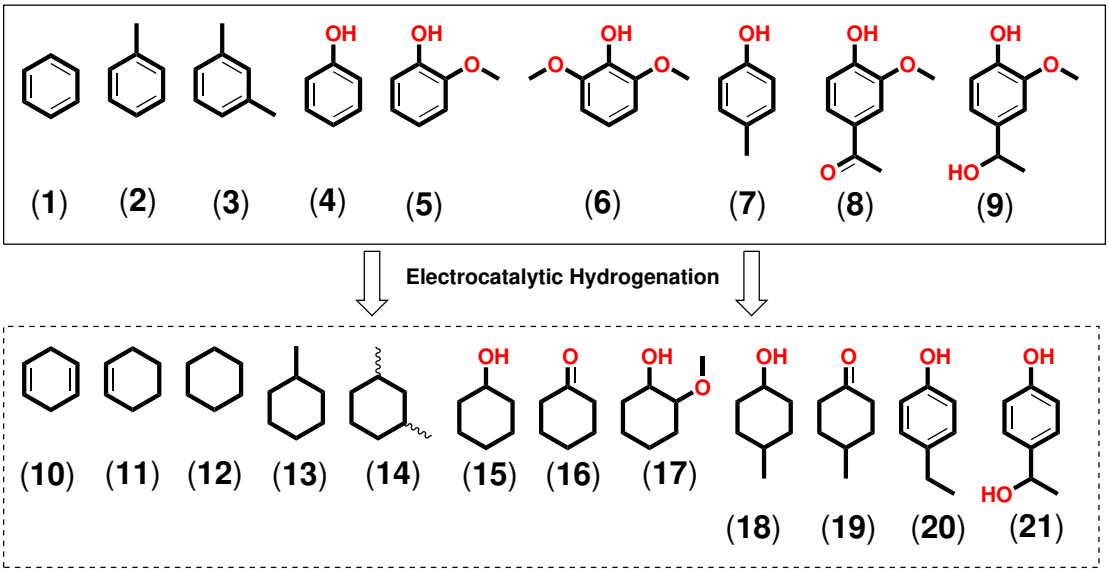

Figure 4.2: Lignin monomer models and their ECH products.

Table 4.1: Historical ECH of lignin monomers and the products.

	Cat.	Electrol.	T	CD	Q	CE%	Yield% Pdt1	Yield% Pdt2	Yield% Pdt3	Ref
Category (I) Compounds										
Benzene (1)							**(10)**	**(11)**	**(12)**	
1	Pt	LiCl[a]	r.t.	7.5	1.8	87	44.3	10.8	4.9	181
2	Pt	TBATS[b]	50	4	0.4	73	-	-	4.7	103
Toluene (2)									**(13)**	
3	Pt/C	H^+/H_2O	r.t.	25	-	95	-	-	-	184
4	Rh/C	H^+/H_2O	r.t.	50	-	>99	-	-	-	184
5	Ru/C	H^+/H_2O	r.t.	50	-	98	-	-	-	184
6	Pd/C	H^+/H_2O	r.t.	50	-	trace	-	-	-	184
7	PtRu/C	H^+/H_2O	r.t.	50	-	99	-	-	-	184
Xylene (3)									**(14)**	
8	Pt/Pt	H_2SO_4	r.t.	-	5.9	100	-	-	-	183
Phenol (4)							**(15)**	**(16)**	**(12)**	
9	Pt-Pt	H_2SO_4	37	3.6	-	30	pure	-	-	36
10	Pb	H_2SO_4	37	3.6	-	0	0	-	-	36
11	Hg	H_2SO_4	-	-	-	0	0	-	-	36

Continued on the next page

Table 4.1 (cont'd)

							Yield%			
	Cat.	**Electrol.**	**T**	**CD**	**Q**	**CE%**	**Pdt1**	**Pdt2**	**Pdt3**	**Ref**
12	Rh/C	NaOAc	23	-	-	-	100	-	-	[93]
13	Pt-Pt	H_2SO_4	r.t.	1.5	6	22	17	7	-	[94]
14	Pt/C	H_2SO_4	r.t.	11.8	6	47	43	6	-	[94]
15	Rh/C	H_2SO_4	r.t.	11.8	6	84	74	15	-	[94]
16	Pd/C	H_2SO_4	65	2.9	6	15	5	15	-	[94]
17	Rh/C	AcOH	25	-	11	55	100	-	-	[95]
18	Pt/C	AcOH	25	-	28	19[g]	70	30	-	[95]
19	Pt	H_2SO_4	25	3.2	12	0	0	0	-	[96]
20	Ni/G	H_2SO_4	25	3.2	12	0	0	0	-	[96]
21	Rh/G	H_2SO_4	25	3.2	12	41	66	24	-	[96]
22	Pd/G	H_2SO_4	25	3.2	12	8	13	-	-	[96]
23	Pt/G	H_2SO_4	25	3.2	12	52	59	6	30	[96]
24	RaNi	HCl[c]	30	1.5-2	6	20	42	0	-	[97]
25	RaNi	HCl[d]	30	1.5-2	6	77	79	0	-	[97]
26	RaNi	HCl	30	1.5-2	6	27	30	0	-	[97]
27	Pt-Pt	$HClO_4$[e]	r.t.	12.7	-	68	-	-	-	[98]
28	Pt-Pt	$HClO_4$ [f]	r.t.	12.7	-	77	-	-	-	[98]
Phenol (4)							**(15)**	**(16)**	**(12)**	
29	Pt-Pt	$HClO_4$	r.t.	12.7	-	79	-	-	-	[98]
30	Rh/C	AcOH	18	0.11	-	68	100	-	-	[100]
31	RaNi	NaOH	50	-	18	11	33	-	-	[101]
Category (II) Compounds										
Guaiacol (5)							**(4)**	**(15)**	**(17)**	
32	Ru/ACC	HCl	25	13	12	19	0	13	38	[105]
33	Ru/ACC	HCl	50	13	12	31	0	23	37	[105]
34	Ru/ACC	HCl	80	13	12	30	0	40	35	[105]
35	Ru/ACC	NaOH	80	13	12	28	0	30	32	[105]
36	RaNi	Borate	75	4	19	26	0	79	trace	[19]
37	RaNi	NaOH	50	4	19	3.4	19	3	0	[101]
Syringol (6)							**(5)**	**(15)**	**(17)**	
38	Ru	HCl	80	13	12	29	16	35	36	[105]
4-Methylphenol (7)							**(18)**	**(19)**		
39	Pt-Pt	H_2SO_4	r.t.	40	6	21	15.6	8.7	-	[104]
40	Pt-Pd	H_2SO_4	r.t.	40	6	34	16.0	27.0	-	[104]

Continued on the next page

Table 4.1 (cont'd)

	Cat.	Electrol.	T	CD	Q	CE%	Yield% Pdt1	Yield% Pdt2	Yield% Pdt3	Ref
41	Rh/C	AcOH	r.t.	0.05	-	31	38	58	-	[100]
Acetovanillone (8)							**(20)**	**(21)**	**(9)**	
42	RaNi	NaOH	50	-	18	12	11	9	53	[101]
1-Guaiacyl-1-ethanol (9)							**(20)**	**(21)**	**(8)**	
43	RaNi	NaOH	50	-	18	3	13	9	31	[101]

Water is the default solvent to dissolve the cathodic electrolyte unless otherwise specified. **Cat.**: cathode. **Electrol.**: electrolyte. **T**: temperature in °C. **CD** is current density in mA/cm^2. **Q** is the amount of electricity applied and is in units of F/mol starting material. **CE** is current efficiency. **NaOAc** is sodium acetate. **AcOH** is acetic acid. **Pt/G** is Platinum on Graphite.

[a] in ethanol-HMPA solution.

[b] tetrabutylammonium p-toluenesulfonate in t-butanol/water solution.

[c] with 9 mM DDAB

[d] with 0.2 mM DDAB

[e] with 5 mM TEAB

[f] with 0.1 mM TEAB

[g] Adjusted number based on Fig. 9 in the original paper since the CE contradicted between values in Table 4 and what had been shown in Fig. 9.

As shown in Table 4.1, phenol can be reduced to cyclohexanol by ECH at room temperature on RaNi, Pd, Pt and Rh cathode with current efficiencies varying between 8 to 84%, but not at all by a Hg, spongy Pb, plain Pt, or Ni/C cathode (Table 4.1 entries **10**, **11**, **19**, **20**).[36] It was reported that a Pt cathode was not able to reduce phenol (entry **19**), however, platinized platinum (Pt-Pt) cathodes did successfully reduce phenol to cyclohexanol and a small amount of cyclohexane in 22 - 79% current efficiency (entries **9, 13, 27–29**). Meanwhile, compared with Pt-Pt, Rh is even more efficient (entries **12, 15, 17, 21, 31**); when Rh/C was used with sulfuric acid at room temperature, the reaction had the highest current efficiency of all reviewed reactions (entry **15**). In addition, Graphite (G) was also used as a support (entries **20 - 23**). The resulting Pt/G catalyst (entry **23**), remarkably, deoxygenated phenol directly to benzene, and cyclohexane was observed from ECH of phenol for the first time.[96] It was

not known if the cyclohexane was formed via cyclohexanol or benzene, but benzene was known to be reduced to cyclohexane under ECH on Pt cathode.[102,103] Rh/C (entry **15**) gave the best current efficiency for the hydrogenation of phenol, while RaNi and Pt-Pt were also good catalysts with over 77% current efficiencies. Pd/C or Pd/G were not effective catalysts. In terms of product selectivity, Rh/C and Pd/C produced significant amounts of cyclohexanone, and only Pt/G cathode yields cyclohexane, while RaNi did not produce products other than cyclohexanol.

4-Methylphenol (cresol) (**7**) in Table 4.1 is a category (II) compound that cannot be as efficiently hydrogenated by ECH as all category (I) compounds. As shown in Table 4.1, category (I) compounds can achieve very high current efficiencies up to 80-100%, while 4-methylphenol (**7**) can only achieve around 30%. It is likely that the steric effect by methyl group stagnates the reaction rate.

Relative to 4-methylphenol (**7**), all other categories (II) compounds are much more difficult to reduce at room temperature via ECH, usually, they require even higher temperatures than the ECH of phenol (**4**). Guaiacol (**5**) can be demethoxylated and hydrogenated into cyclohexanol (**15**) by both Ru and RaNi cathodes but the demethoxylation is more completely on RaNi; Ru cathodes produce a significant amount of 2-methoxycyclohexanol (**17**). Although no guaiacol (**5**) ECH at a Rh cathode has been reported, Lercher et al. found that Rh could demethoxylate 10% 4-methoxyphenol to cyclohexanol (**15**) while the other 90% was non-demethoxylated product 4-methoxycyclohexanol.[100] In addition, as far as we know, no ECH of guaiacol (**5**) at a Pt-Pt or Pt/C cathode has been reported. Therefore, from all information available, RaNi seems the best catalyst for both demethoxylation and phenol aromatic ring reduction. It is noteworthy that Ni is also the least expensive of the metals that do achieve reductions.

Category (III) compounds are rarely studied and the only ECH study of a category (III) compound, acetovanillone (**8**), shows very little demethoxylation and no aromatic ring reduction reaction at a RaNi cathode; the reduction of the carbonyl group and the deoxygenation of the resulting benzylic alcohol are the main reactions. Conditions for these more ECH-resistant compounds should be further optimized to yield more demethoxylation and aromatic ring hydrogenation products with a RaNi cathode.

Building on the work of Cyr et al.,[124] we have explored the use of an earth-abundant RaNi cathode, finding that guaiacol and syringaldehyde can be upgraded to fuel-level compounds such as cyclohexanol effectively.[19] Meanwhile, we used eugenol as a model compound to optimize the ECH conditions on reducing lignin monomers and improved the yields of cyclohexanol derivative products by using higher temperatures (80-90 °C), much more active IPA-RaNi cathodes (the RaNi cathodes that are further activated by storage in isopropyl alcohol) compared with our traditional RaNi cathode, along with understanding the solvent, temperature effects and deactivation factors of RaNi cathodes. Building on the previous paper, we further investigated the ECH reactions of lignin monomers shown in Figure 4.3 to explore how lignin monomer structures affect ECH effectiveness, to reveal reaction kinetics, steric effects, and functional group effects, and to acquire deeper understanding of ECH mechanisms of lignin monomers.

4.2 Results and discussion

In this work, although IPA-RaNi cathodes are more active, RaNi cathode was chosen to reveal steric factors or other functional group effects unless otherwise specified. The RaNi cathode does not produce large amounts of 4-alkylcyclohexanols, which are surface inhibitors

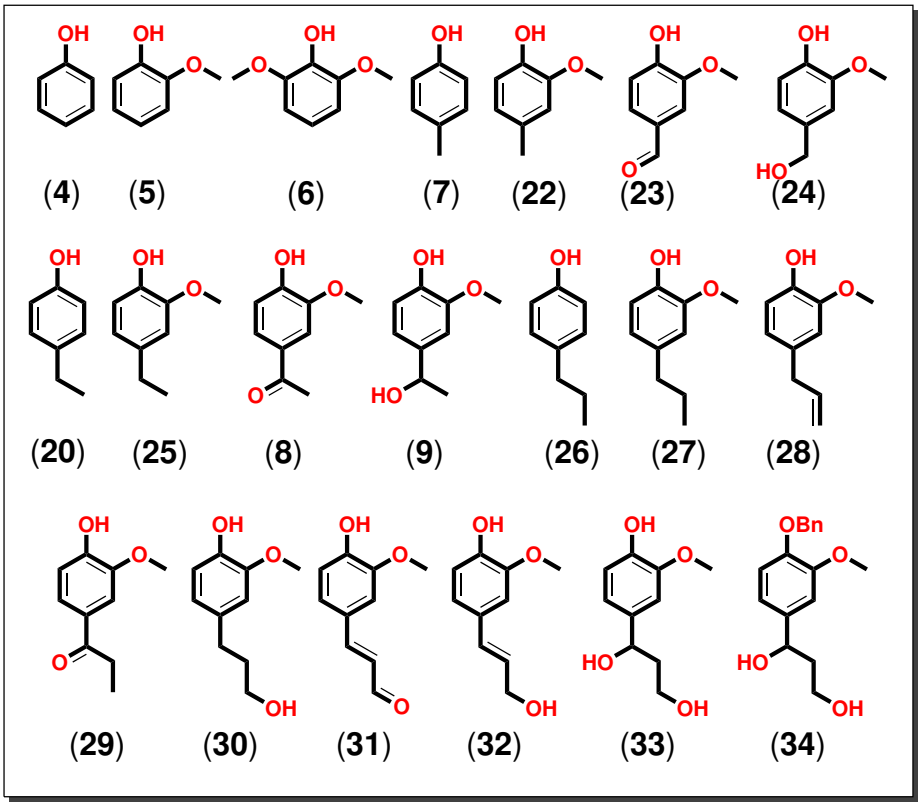

Figure 4.3: Lignin monomers studied in this work.

and may complicate or even dominate the reactions so much that steric or functional group effects are not easy to observe.

4.2.1 Functional group-adsorption energy relationships of lignin monomers

ECH reactions are initiated by the adsorption of substrates, so a study on functional group effects on the adsorption energy is important to understand the ECH of lignin monomers. The electronic effects of different functional groups at the 4-position of lignin monomers on the adsorption energy on different Ni crystal faces were investigated via Density Function Theory (DFT) using the Vienna Ab Initio Simulation Package (VASP) with parameters described in the Experimental section. The simulations use periodic boundary conditions to

approximate a large infinite system by calculating a small unit cell which is repeated along three (or two) vectors. Two different surfaces were calculated: Ni (111) surface that has the smallest repeated unit of a rhombus with a 60° angle, and Ni (100) that has the smallest repeated unit of a square.

Table 4.2: The adsorption energy of lignin monomers from DFT simulations of lignin monomers on Ni(111) and Ni(100).

			Adsorption Energy (E0, kcal/mol)	
Entry	**Mol.**	**Name**	**Ni (111)**	**Ni (100)**
1	(**5**)	Guaiacol	-6.4	-32.1
2	(**4**)	Phenol	-12.1	-35.0
3	(**1**)	Benzene	-14.6	-37.0
4	(**22**)	4-Methylguaiacol	-5.9	-30.7
5	(**25**)	4-Ethylguaiacol	-6.1	-30.2
6	(**27**)	4-Propylguaiacol	-6.7	-31.4
7	(**7**)	4-Methylphenol	-10.7	-36.6
8	(**20**)	4-Ethylphenol	-11.1	-36.9
9	(**26**)	4-Propylphenol	-11.8	-37.2
10	(**35**)	4-Vinylguaiacol	-24.0	-55.5
11	(**28**)	Eugenol	-21.1	-56.7
12	(**23**)	Vanillin	-10.3	-48.2
13	(**24**)	Vanillyl alcohol	-5.9	-32.9
14	(**8**)	Acetovanillone	-7.2	-43.7
15	(**9**)	1-Guaiacyl-1-ethanol	-4.9	-31.3
16	(**29**)	Propiovanillone	-8.1	-43.2
17	(**36**)	1-Guaiacyl-1-propanol	-4.0	-32.3
18	(**31**)	Coniferyl aldehyde	-31.5	-61.5
19	(**32**)	Coniferyl alcohol	-16.7	-49.7
20	(**30**)	Dihydroconiferyl alcohol	-4.1	-26.1
21	(**33**)	1-Guaiacyl-1,3-propanediol	-10.0	-36.6

Several structure changes lead to the change of adsorption energies of the substrates:

1) Numbers of aryl hydroxyl and methoxyl groups. The more oxygens on an aryl ring, the fewer the adsorption energy of the substrate is, which can be found by comparing Table 4.2

entries **1** & **2** & **3**, entries **4** & **7**, **5** & **8**, and **6** & **9** .

2) Olefin increases the adsorption energy. This is because the olefin contributes two extra anchoring sites on the surface from the interactions between the π-bond of olefin and the d-orbital of nickel. The increases of adsorption energies from 4-ethylguaiacol (entry **5**) to 4-vinyl guaiacol (entry **10**), and from 4-propylguaiacol (entry **6**) to eugenol (entry **11**) demonstrate this trend.

3) Carbonyls increase the adsorption energies of substrates; and more specifically, an aldehyde increases the adsorption energy of a substrate much more than the amount that a ketone does, as shown by the fact that vanillin (**23**) has more adsorption energy than that of 4-methylguaiacol (**22**) by 17.5 kcal/mol on the Ni (100) and 4.4 kcal/mol on the Ni (111) surface, while acetovanillone (**8**) and propiovanillone (**29**) have more adsorption energies than of 4-ethylguaiacol (**25**) and 4-propylguaiacol (**27**) by only 13.5 kcal/mol and 11.8 kcal/mol on a Ni (100), respectively, and 1.1 kcal/mol and 1.4 kcal/mol, respectively, on a Ni (111) surface. The same trend is true for propiovanillone (**29**). It is not hard to believe this since aldehydes usually are much more electrophilic than ketones.

4) Hydroxyl groups on the 4-alkyl chain do coordinate to nickel atoms but the influences on adsorption energies of substrates are only minimal. Vanillyl alcohol (**24**), 1-guaiacylethanol (**9**), and 1-guaiacylpropanol (**36**) have adsorption energies less than 3 kcal/-mol stronger than the corresponding 4-alkylguaiacols (**22**), (**25**), and (**27**).

5) The length of the alkyl chain on the 4-position does not contribute to the adsorption energy change to any significant degree considering almost no adsorption energy changes among the 4-alkylguaiacols (**22**), (**25**), and (**27**).

4.2.2 Methoxyl group positions on the phenol ring change demethoxylation efficiencies

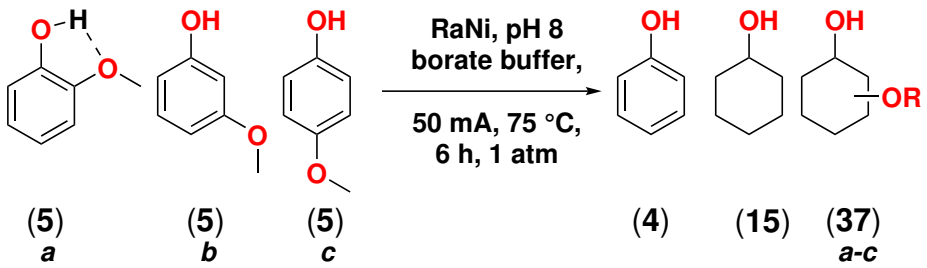

(5) *a* (5) *b* (5) *c* (4) (15) (37) *a-c*

Demethoxylation is more favorable at the ortho- than meta- and para-positions

	Product Distribution%			
S.	**(4)**	**(15)**	**(37)**	**Conv.%**
(5)*a*	-	99	-	99
(5)*b*	1	49	39	88
(5)*c*	-	48	52	100

Figure 4.4: Methoxyl position changes affect the demethoxylation efficiencies. The data was extracted from the previous study by Lam et al.,[19] and the product distribution was calculated by using the moles of a given compound divided by the sum of moles of all compounds observed in the final products.

As reported earlier by Lam et al.,[19] changing the methoxyl group from ortho **(5)*a***, to meta **(5)*b*** and para-positions **(5)*c*** decreased the demethoxylation yields by about half; the implication is that the existence of intramolecular hydrogen bonding between the phenol hydroxyl group and the methoxyl oxygen in the case of **(5)*a*** assists demethoxylation, but is not essential since demethoxylation happens in both **(5)*b*** and **(5)*c*** where intramolecular hydrogen bonding is absent. The reason that the presence of hydrogen bonding accelerates the demethoxylation is still not fully understood and further investigations are undergoing in our research group to reveal it.

4.2.3 Steric bulk at the 2-position do not affect ECH reactions significantly

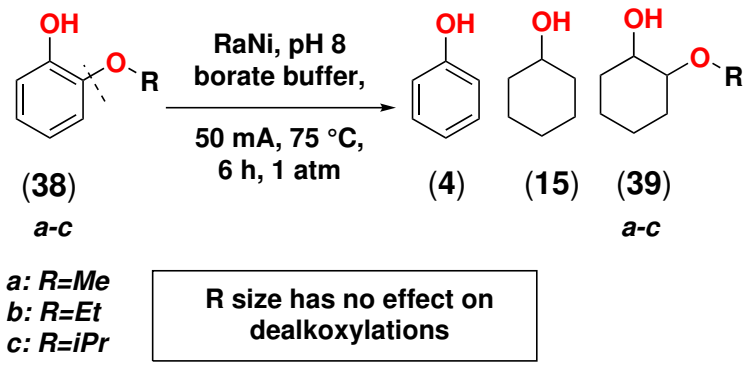

		Product Distribution%			
Sub.	**R**	**(4)**	**(15)**	**(39)**	**Conv.%**
(40)*a*	Me	-	99	trace	99
(40)*b*	Et	-	98	-	98
(40)*c*	iPr	2	93	-	95

Sub. is substrate.

Figure 4.5: Steric effects on ECH at the 2-position and methoxyl group position. Data was extracted from the previous study by Lam et. al,[19] and the product distribution was calculated by using the moles of a compound divided by the sum of moles of all compounds observed in the final products.

ECH is not as sensitive to steric hindrance at the 2-position as at the 4-position relative to the phenol OH. As shown in Figure 4.5, there is almost no change in reactivity from substrates (**38**)***a-c***, as the methoxyl group is replaced by ethoxy and isopropoxy groups.[19]

4.2.4 Steric bulk at the 4-position slows down ECH reactions

From the historical data, we realize that 4-methylphenol is much less readily reduced over RaNi than phenol. Since the ECH of guaiacol on a RaNi surface is hypothesize to involve adsorption of the aromatic ring in a flat fashion with hydroxyl and methoxy groups repelled

from the surface according to both literature[14] and the DFT optimized geometry, the steric-hindrance from substituents in the para-position relative to the phenolic OH may inhibit adsorption in this flat fashion. Several natural questions then arise: 1) is the reaction rate correlated with the length of the alkyl group as it increased from methyl to ethyl and propyl groups in the 4-position? 2) does the steric effect more strongly affect demethoxylation or phenol ring hydrogenation reaction, or is it similar for both?

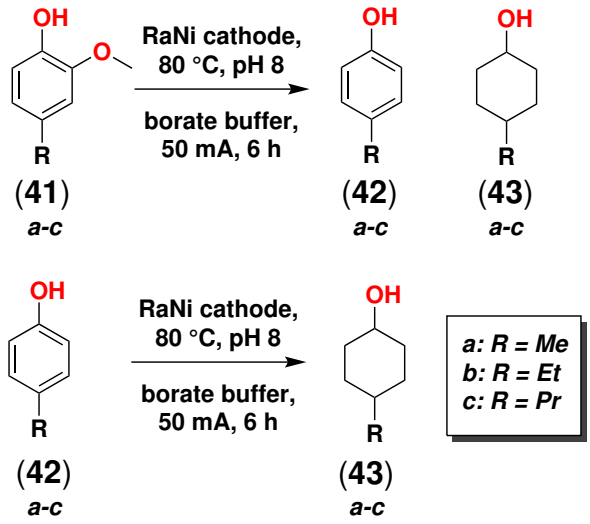

		Product Distribution%		
	R	**(42) *a-c***	**(43) *a-c***	**Conv.%**
(41) *a*	Me	35	35	70
(41) *b*	Et	43	19	62
(41) *c*	Pr	50	7	57
(42) *a*	Me	11	89	89
(42) *b*	Et	22	78	78
(42) *c*	Pr	73	27	27

Figure 4.6: ECH of individual 4-alkyl guaiacol models with a RaNi cathode. Me is methyl, Et is ethyl and Pr stands for n-propyl.

Although bigger alkyl groups at the 4-position do not significantly change the adsorption energies of substrates (**44**) since the limited electronic differences among methyl, ethyl and propyl groups, they do decrease the probabilities that alkyl guaiacols adsorbing on the surface

since the longer the alkyl chain is, the more freedoms of rotation there are, which would be lost as the phenol ring adsorbs to the nickel surface in a parallel fashion. With alkyl guaiacol **(41)*a-c*** as starting materials, a clear steric inhibition effect seen was found since the demethoxylation yields decrease accordingly as the alkyl chain gets longer from Me to Pr. The influence of the steric factor on alkyl phenol models **(41)*a-c*** was also clear.

Another clear example of a steric effect is seen in the ECH of α-carbonyl compounds as shown in Figure 4.7 (see section 1.2.7), where increasing amounts of starting materials remain in the final product mixture as the 4-position substitutes get longer.

4.2.5 The ECH of carbonyl lignin monomers

The hydrogenation of carbonyl is not as fast as olefin and the starting materials (**23**), (**8**), and (**29**) remain in the solution after 8 h of ECH while the ECH of double completes within the first hour. The reduction of carbonyl seems to be largely affected by steric effect indicated by the increasing remaining amount of (**23**) (7%), (**8**) (15%), and (**29**) (36%) in the products as the 4-alkyl chains getting longer.

The carbonyl compound vanillin (**23**) was deoxygenated much more completely than its corresponding alcohol compound (**24**). At the end of the reaction, there was 59% of deoxygenation products of vanillin (**23**) compared with only 42% for vanilly alcohol (**24**). Deoxygenation of the benzylic alcohol also happens for all three carbonyl substrates (**23**), (**49**), and (**29**) to produce alkyl guaiacols (**22**), (**25**), and (**27**). The resulted alkyl guaiacols were further demethoxylated to alkyl phenols (**7**), (**20**), and (**26**).

The major reactivity difference except for lower steric-hindrance between the aryl-aldehyde vanillin (**23**) and the other two aryl-ketone compounds is that significant amount (25%) of C-C bond cleavage product guaiacol (**5**) was produced from the ECH of vanillin (**23**) but

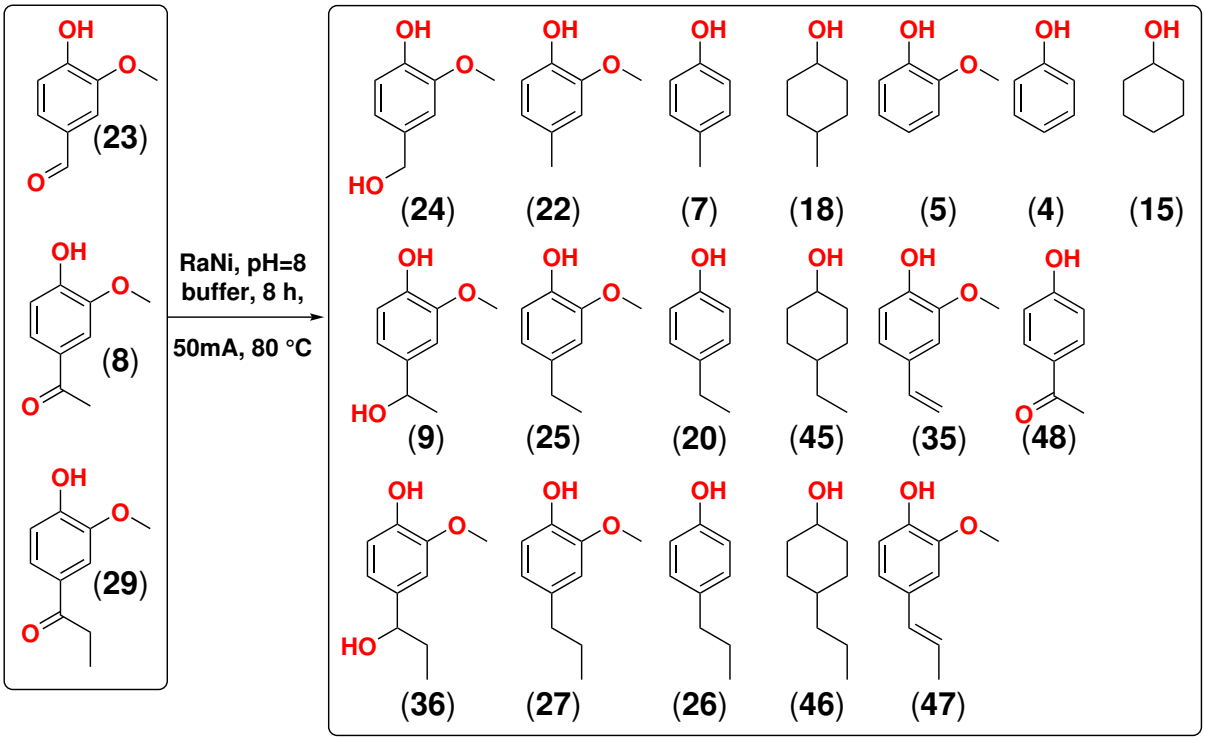

Sub.	Product distribution%								Conv.%
	(23)	**(24)**	**(22)**	**(7)**	**(18)**	**(5)**	**(4)**	**(15)**	
(23)[a]	7	34	8	15	2	21	5	8	93
(24)[a]	3	55	13	13	5	9	0	2	45
	(8)	**(9)**	**(25)**	**(20)**	**(45)**	**(35)**	**(48)**		
(8)	15	17	3	55	7	1	1		85
	(29)	**(36)**	**(27)**	**(26)**	**(46)**	**(47)**			
(29)[b]	36	12	12	29	0.4	3			64

Sub. is substrates, the starting materials of each individual ECH. **Conv.**: conversion.
[a] The ECH of vanillin and vanillyl alcohol produced two dimers (around 10% of the total peak areas) which was excluded from the product distribution calculations; the major dimer has MW = 260, which indicated two guaiacol dehydration-dimerization with a formaldehyde ($124 \times 2 + 30 - 18$) or guaiacol condensed with a vanillyl alcohol via aromatic nucleophilic substitution reaction, the attack from guaiacol to the benzylic alcohol of vanillyl alcohol ($124 + 154 - 18$).
[b] There was one broad peak (accounts for 7% of total peak areas) right after isoeugenol which had the same mass and fragmentation patterns as isoeugenol but the elution time was not the same with either (E)-isoeugenol or eugenol; it was also assigned as isoeugenol by the GC-MS NIST database. Product distributions in this line were calculated based on the assumption that this broad peak was the (Z)-isomer of isoeugenol and it was assumed to have the same response factor as (E)-isoeugenol. If it was truly isoeugenol, the corrected number for (**47**) should be 9.1%.

Figure 4.7: ECH results of lignin monomers with carbonyl moieties and their corresponding reduction products, alcohol, and alkyl analogues.

none from the other compounds. The mechanism for this C-C bond cleavage reaction is discussed in following sections 1.2.6 and 1.2.7.

4.2.6 γ-hydroxyl and γ-carbonyl effects: carbon-carbon bond cleavage

Unlike the ECH products of α-carbonyl monomer (**29**) where 36% of the carbonyl was conserved in the product, ECH reduced the more reactive carbonyl of (**31**) completely. The unsaturated γ-carbonyl monomer (**31**) and γ-hydroxyl lignin monomers (**32**), (**30**), and (**34**) all however produce small fragments of ethyl compounds (**25**), (**20**), (**45**), and even (**22**). Formation of these products requires cleavage of C-C bonds, which is usually not considered a reaction pathway for mild temperature hydrogenation reactions. Careful checking verifies that starting materials are all free of any 4-ethylguaiacol or its derivatives.

Observation of this unexpected C-C reaction first in compounds (**30**) and (**44**) encouraged us to investigate the kinetics of ECH of coniferyl aldehyde (**31**). As shown in Figure 4.9, a hydrated form of the starting material, presumably (**52**), was identified by GC-MS as an intermediate, which can be formed from the Micheal addition of water to the double bond of the α, β-unsaturated aldehyde (**31**). The intermediate can be hydrogenated to a primary alcohol (**53**) and under the basic conditions in the ECH reaction can form an unstable quinone methide intermediate, followed by a retro-aldol to produce a vinyl guaiacol (**35**), which is quickly hydrogenated to form the final product 4-ethylguaiacol (**25**). However, the vinyl guaiacol was not captured in the kinetic study.

Another more straightforward pathway (solid arrows in Figure 4.9) was discovered when we further studied the ECH kinetics of alcohol (**30**), (**32**), and α,γ-diol (**34**).

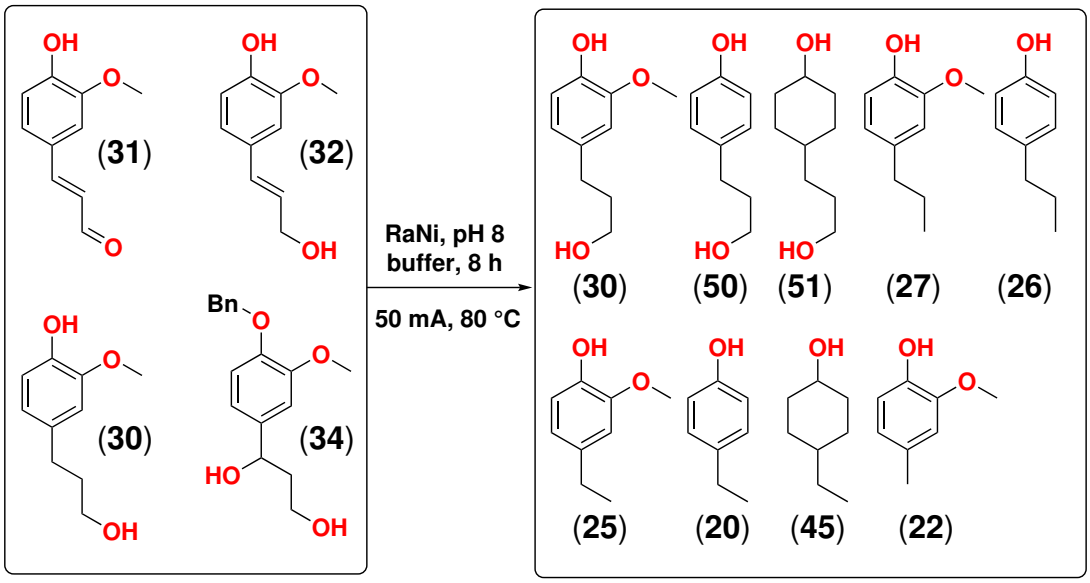

Sub.	Product distribution %									
	(30)	(50)	(51)	(27)	(26)	(46)	(25)	(20)	(45)	(22)
RaNi Cathode at 80 °C										
(31)	74	3	8	0.8	0.4	-	3	7	3	0.4
(32)	79	2	13	1	0.4	-	0.6	3	-	0.7
IPA-RaNi Cathode, a more active cathode, at 90 °C										
(30)	33	14	33	0.4	7	1	0.8	8	3	-
(34)	33	5	24	13	9	4	10	-	2	-

Figure 4.8: ECH results of lignin monomers with γ-carbonyl or hydroxyl groups.

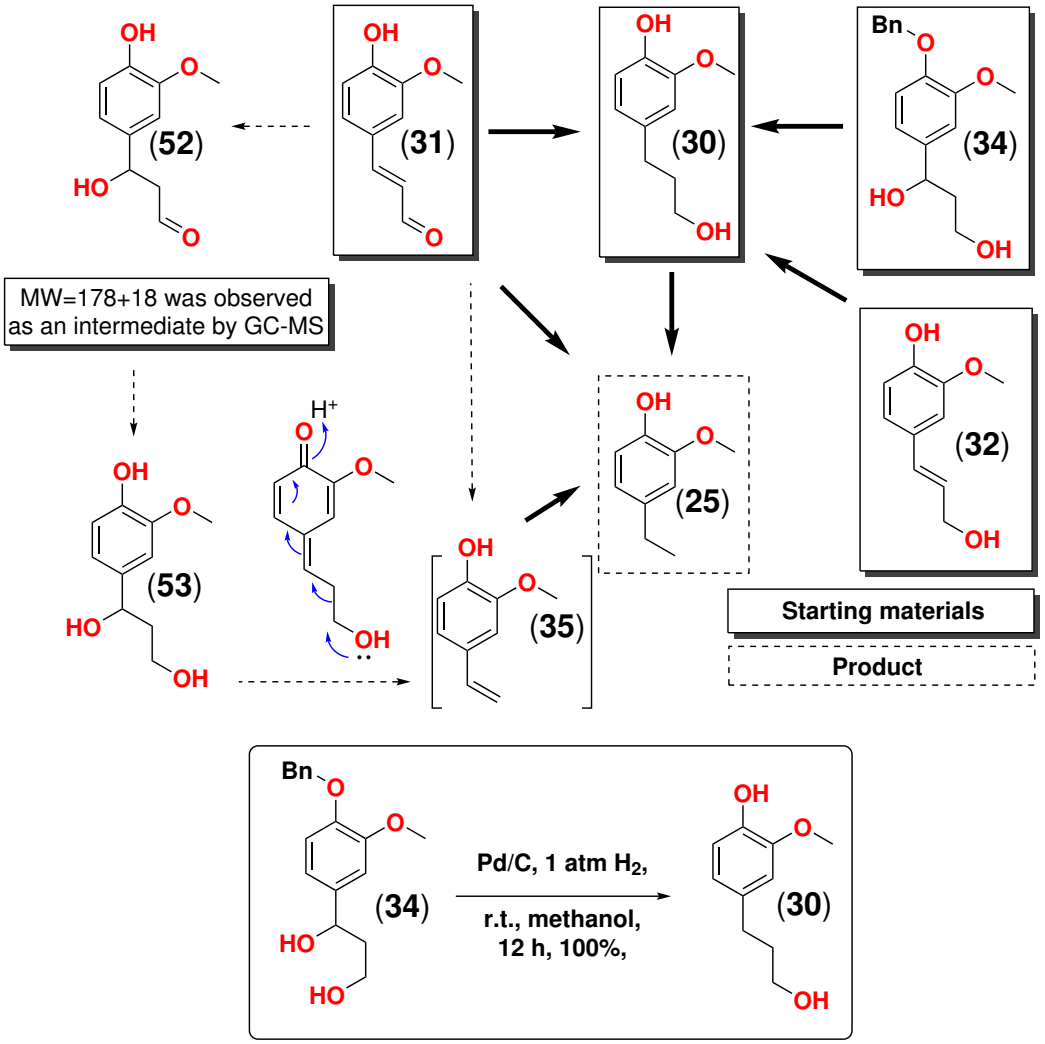

Figure 4.9: Proposed mechanisms for the transformation of ethylated products from 4-γ-hydroxyl guaiacol compounds. Solid arrows are proven pathways, and dashed arrows are, if any, minor pathways. Structures shown in brackets means that that intermediate was inferred but not observed.

Aliphatic alcohol (**30**) cannot follow the above mechanism since the absence of a α,β-unsaturated aldehyde system, but the ECH of pure (**30**) produces a total of 10% C-C cleavage products (**25**), (**20**), and (**45**) as shown in Figure 4.8. Thus 4-ethylguaiacol (**25**) can be produced directly from (**30**). It should be noted that an IPA-RaNi cathode, a more active cathode than RaNi cathode, was used for the ECH of both (**30**) and (**34**) attempted to see if the C-C cleavage products become more with a more active cathode. The result appears that the C-C cleavage products were not increased but

The ECH of coniferyl alcohol (**32**) in the first hour produced 97% of olefin reduction product (**30**) with almost no C-C cleavage products. Although only around 4% of C-C cleavage products were produced after 8 h ECH, it is clear that the (**25**) was produced from (**32**) via (**30**) as well.

The ECH of coniferyl aldehyde (**31**), in contrast to the ECH of coniferyl alcohol (**32**), produced 89% of its total C-C cleavage products within the first 1 hour of ECH. Remarkable, just 3 mins after the addition of coniferyl aldehyde into the ECH cells, a small amount of 4-ethylguaiacol (**25**) was observed in the solution. This suggests that unlike coniferyl alcohol (**32**) where most of the C-C cleavage products are produced via its olefin hydrogenation intermediate (**30**), coniferyl aldehyde (**31**) produced its C-C cleavage product (**25**) directly from the deformylation of coniferyl aldehyde (**31**). However, we do not know if the hydrogenation of olefin happens before, after, or at the same time of the deformylation. No matter which path was followed, the olefin intermediate (**35**), if it was formed at all, was rapidly hydrogenated likely before the desorption from the electrocatalyst, since no (**35**) intermediate was observed during the kinetic study. In addition, a very small amount of 4-methylguaiacol was produced from the ECH of both coniferyl aldehyde (**31**) and coniferyl alcohol (**32**). We do not fully understand the mechanism. It is possible that the 4-methylguaiacol was produced

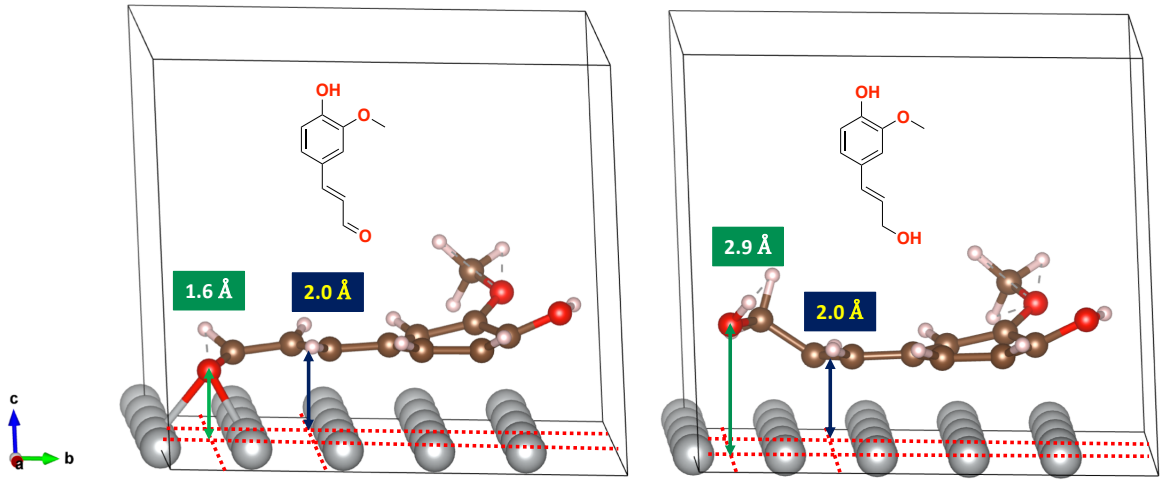

Figure 4.10: The optimized structure of coniferyl aldehyde (left) and coniferyl alcohol (right) on Ni (111) surfaces. The green double arrows represent the distances between the center of an oxygen atom and the Ni (111) planes; the blue double arrow represent the distances between the horizontal centers of double bonds and the Ni (111) planes.

from the deformylation of 2-guaiacyl-1-ethanol (also called homovanillyl alcohol).

This explanation is further supported by the computational result as shown in Figure 4.10. When coniferyl aldehyde (**31**) adsorbs on a Ni (111) surface, both the aldehyde and olefin groups appear to strongly coordinate with nickel atoms. Thus deformylation has a chance to happen once that the substrate is adsorbed. In contrast, for coniferyl alcohol, the olefin interacts with the surface, but the hydroxyl group does not.

When it comes to the 1,3-diol monomer (**34**), one important fact is that the benzyl group and the α-hydroxyl of (**34**) can both be easily removed by a mild hydrogenation with Pd/C and 1 atm H_2 at room temperature. The benzyl protecting group can be selectively removed by Pd/C and 1 atm H_2 in the presence of the benzylic alcohol in the case of β-O-4 dimer model synthesis (see chapter 3 dimer I synthesis), but the ECH of (**34**) cleaves the α-C-OH ether bond as well, possibly due to the weakening effect by hydrogen bonding of the γ-hydroxyl group. The kinetic study of the ECH of (**34**) show that both the benzyl group and

the α-OH are removed within the first hour of ECH. Thus the formation of 4-ethylguaiacol (**25**) from (**34**) is also likely achieved via (**30**) if not entirely.

4.2.7 Possible mechanisms for C-C bond cleavage reactions from terminal alcohol or carbonyl lignin monomers

Since a majority of real lignin subunits bear both α- and β-hydroxyl or ether groups, the C-C bond cleavage reactions described above offer an opportunity to reduce the steric hindrances of lignin monomers via ECH, enabling ECH reduction and deoxygenation of the less hindered molecules to proceed with higher efficiency. Therefore, understanding the mechanisms of C-C bond cleavage reactions is essential to improve our deoxygenation and hydrogenation methodology.

There are two types of C-C bond cleavage reactions observed in this work: the cleavage of a terminal γ-hydroxyl or γ-carbonyl monomers, and the cleavage of α-hydroxyl or α-carbonyl monomers. When the hydroxyl and carbonyl are not at the terminal position, for instance in the case of Figure 4.7 acetovanillone (**8**) or its hydroxyl derivative (**9**) (see Figure 4.7), no C-C cleavage products were observed.

The simple compound 3-phenylpropan-1-ol (**54**) was studied under ECH conditions to further examine C-C cleavage reactions. Due to the volatile nature of this substrate and its product, a liquid nitrogen cold trap was installed to capture them. Similar to the ECH results of other γ-OH lignin monomers, ECH of (**54**) deoxygenates the alcohol, forming propyl benzene (**56**), C-C cleavage product ethylbenzene, and even toluene. However, all products combined are less than 5% including 3.3% of ethylbenzene and 0.8% propylbenzene, and the majority (95.2%) of the product mixture was the starting material.

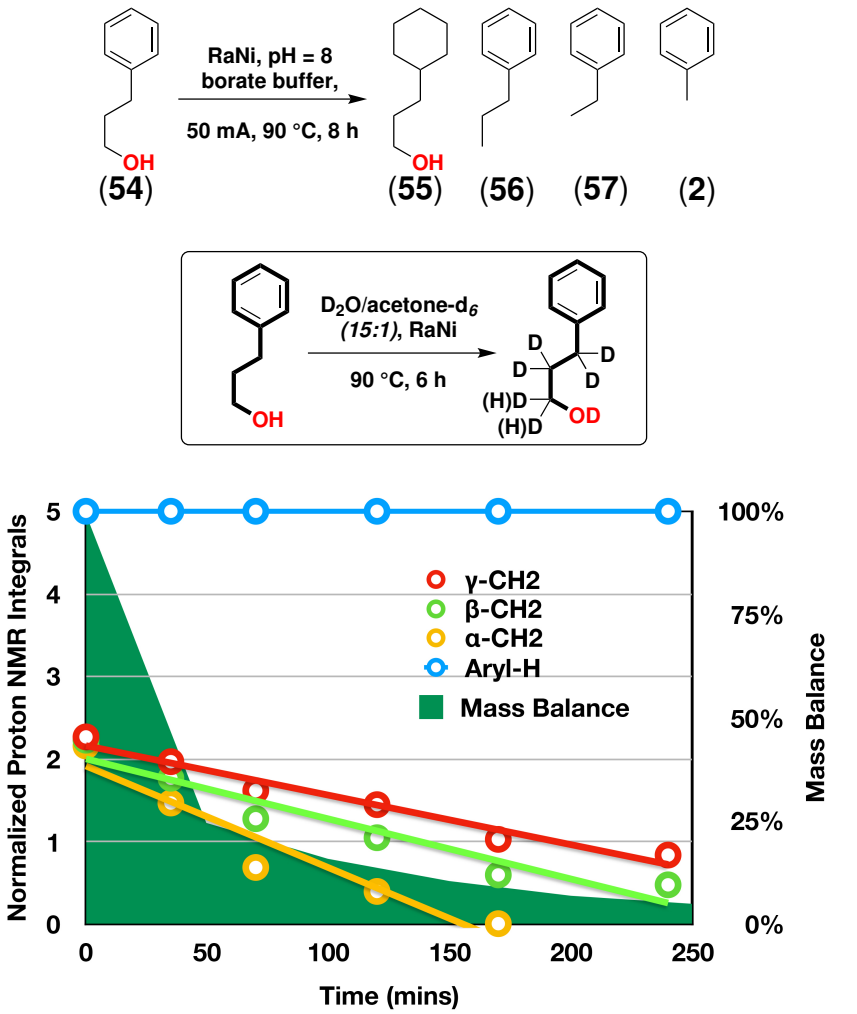

Figure 4.11: The kinetic study of H/D exchange reaction of phenylpropan-3-ol on IPA-RaNi cathode. The reaction condition was 90 °C, 30 mL D_2O with 2 mL acetone-d*6*. α-CH_2 refers to the benzylic methylene and the γ-CH_2 is from the CH_2OH. The mass balance was determined by additions of internal standard DMF to the 1 mL hourly withdrawn samples to achieve a final concentration of 1 mM.

H-D (hydrogen-deuterium) exchange experiment was conducted with 3-phenylpropan-1-ol (**54**) with IPA-RaNi catalyst without electric currents. As shown in Figure 4.11 The H-D exchange rates follow this order: α-CH_2 > β-CH_2 > γ-CH_2. Their H-D exchange rate equations are as follow where x is the reaction time in mins and y is the proton integral of each methylene normalized relative to the total aryl proton integral value of 5:

α-CH_2 (Yellow Line):

$$y = -0.013x + 1.95,\ R^2 = 0.91$$

β-CH_2 (Green Line):

$$y = -0.0075x + 2.03,\ R^2 = 0.93$$

γ-CH_2 (Red Line):

$$y = -0.0061x + 2.18,\ R^2 = 0.96$$

These H/D exchange phenomena and the decreasing rate of exchange as a function of distance from the benzene ring suggest that the nickel coordinates to the aromatic ring and gradually activates α, β, and γ-C to exchange the H with D via presumably oxidative addition and reductive elimination processes. It is most likely that several different nickel atoms participate in the H/D exchange at the three carbons considering that the length of three C-C bonds (about 1.54 Å for each C-C bond) is far beyond a Ni-Ni bond (about 2.49 Å) and the molecule can lie flat on the nickel surface. A nickel atom mostly likely first inserts in between the weakest C-H bond of the benzylic methylene; then, if there is a surface deuterium atom in the vicinity, reductive elimination of the α-C and deuterium installed the deuterium on the molecule. During the whole reaction time, the ^{1}H NMR splitting pattern of aryl-protons did not change suggesting there was no visible H/D exchange on the benzene

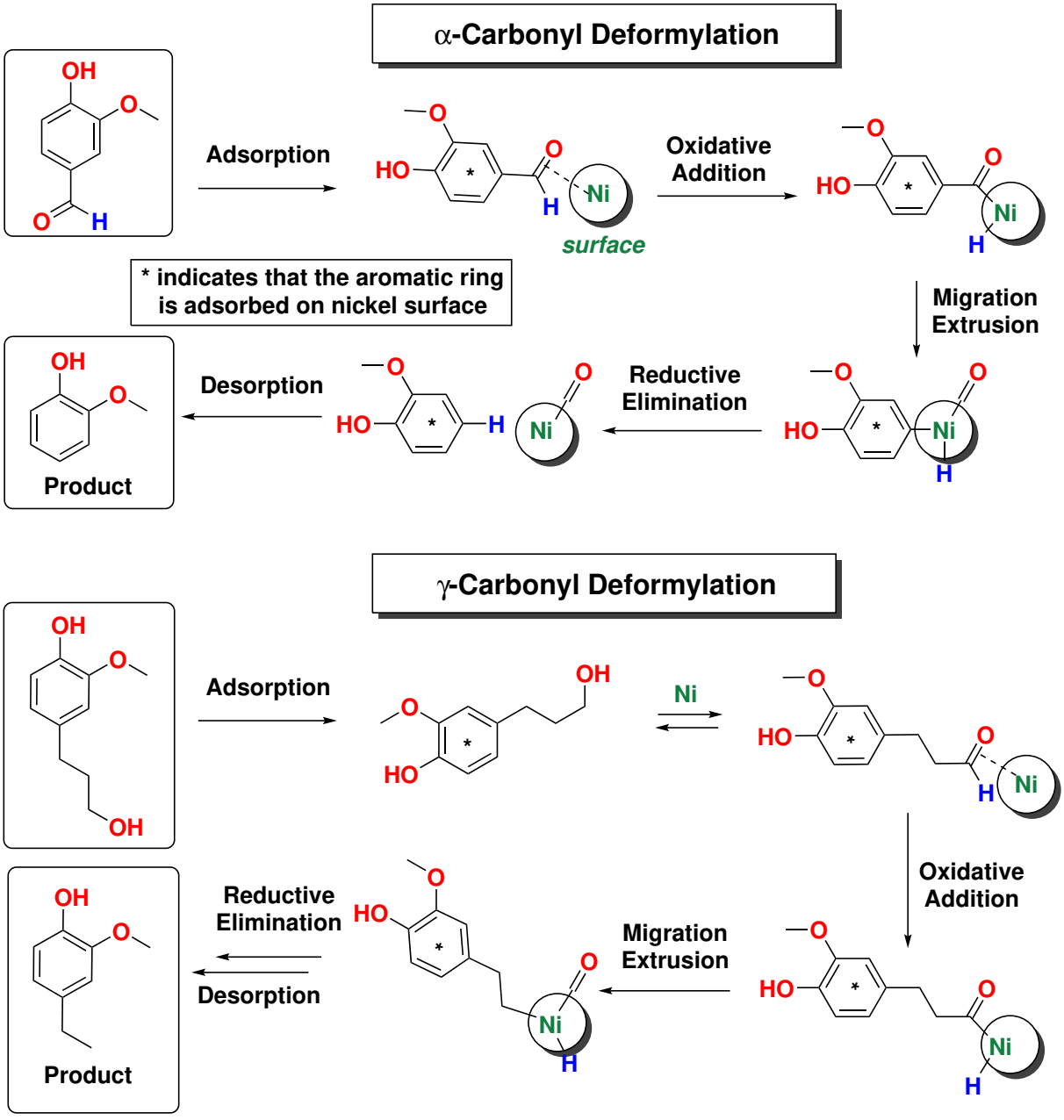

Figure 4.12: The proposed mechanism for the C-C cleavage reactions. The Ni ball represents one nickel atom on the nickel surface, not an isolated nickel atom.

ring.

It is well known that both benzylic and aliphatic alcohols can be dehydrogenated into carbonyl on the surface of nickel.[101,132,133] The ECH results for vanillyl alcohol (**24**) also show that 3% of dehydrogenation product vanillin (**23**) was found in the final solution of products. If the hydroxyl group is at a terminal site, the dehydrogenation reaction can generate an aldehyde. Decarbonylations of aldehydes were known to proceed with Rh, Ir, Ru, and Pd catalyst under somewhat harsh conditions (above 180 °C).[185] Recently, Ding et al. reported a synthetic allyl useful decarbonylation of an aromatic aldehyde with 15 mol% of a Ni catalyst $Ni(COD)_2$ and 30 mol% ligand tricyclohexylphosphine in cyclohexane at 140 °C for 24 h.[185]

Based on the above our H/D exchange data and calculations, it appears the terminal γ-OH methylene can adsorb on the nickel surface and undergo dehydrogenation to form an aldehyde, from which further decarbonylation proceeds. Although no research on decarbonylation on heterogeneous nickel surface has been reported, inspired by the well known Rh decarbonylation mechanism,[186] we propose in Figure 4.12 that both types of C-C cleavage reactions are occurring in the decarbonylations of aldehydes explicitly added or formed in situ on the surface of RaNi from terminal alcohols. The decarbonylation reaction was initiated by the adsorption of the lignin monomer with both the aromatic ring and carbonyl bonding to the nickel surface. The nickel atom in the vicinity of the aldehyde can insert in between the C-H bond of the aldehyde group via an oxidative addition; after the CO migration, extrusion, and reductive elimination reactions, the carbonyl was removed and the stable aromatic product can desorb into the bulk solution. Though the figure appears to suggest that the hydrogen (blue color) ending in the product is the same as the hydrogen of the aldehyde, it is possible that hydrogen from the water reduction process exchanges

with the nickel-bound hydrogen atom removed from the aldehyde and ends up in the final product considering the cathode is attached to the negative side of a power supply.

This proposed mechanism is also consistent with the fact that the ECH of aldehyde compounds, in general, leads to more deformylation products than the corresponding alcohol compounds. Vanillin (**23**) produces 21% deformylation product in contrast to the 9% from vanillyl alcohol (**24**), and coniferyl aldehyde (**31**) produces a total of 13% deformylation products vs less than 4% from coniferyl alcohol (**32**).

Meanwhile, the H/D exchange experiment also shows that the γ-methylene site's rate of H/D exchange is much slower than that of the α-methylene, which is consistent with the data in this work showing that α-carbonyl and alcohol substrates (**23**) and (**24**) produce more decarbonylation products, 21%, and 9%, respectively, than γ-carbonyl and alcohol substrates (**31**) and (**32**)(13% and 3.6%, respectively).

4.2.8 Mapping the intermediates and products of the ECH of α- and γ-carbonyl and hydroxyl lignin monomers

Till this point, we have interpreted the C-C cleavage products as coming from decarbonylation reactions. Figure 4.13 summarizes the major ECH reaction pathways for all terminal alcohol or aldehyde lignin monomers considered here.

Hydrogenations of olefin sites are fast, usually completely reduced within 2 hours, whereas those of aldehydes and ketones are relatively slower. Demethoxylation is much slower than hydrogenation of olefin and carbonyls, and the hydrogenations of aromatic rings are mostly following the demethoxylation steps. All transformations between species drawn as thinner line structures in Figure 4.13 are straightforward and no other intermediates are expected

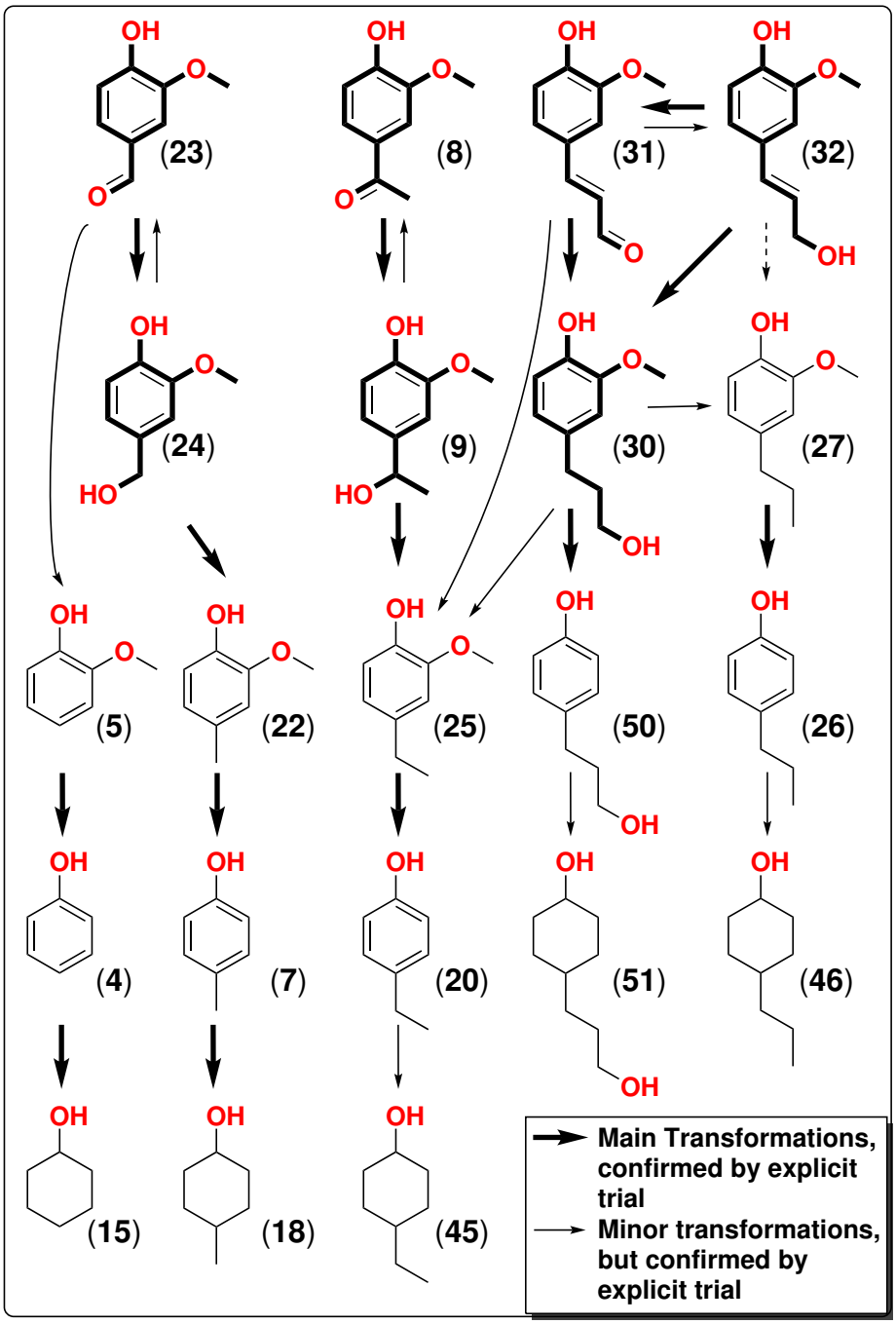

Figure 4.13: ECH reaction network of transformations of substrates studied. Molecules in bold are starting points of each reaction path. The dashed arrow between coniferyl alcohol and 4-propylguaiacol represents a possible transformation, where we observed the 4-propylguaiacol from the ECH of coniferyl alcohol and possible to be a single-step transformation instead of a two-step transformation.

in those transformations.

The transformations involved bold-line structures are more complicated. Surface intermediates that are either not stable in solution or are transformed to other products before desorption from the surface are expected to play roles in these cases. For instance, the transformation between (**30**) and (**25**) likely includes a surface bonded aldehyde intermediate to allow the deformylation to happen, although this species was not directly detected in the solution. For transformation between (**32**) and (**27**), if the C-O hydrogenolysis of the allyl alcohol pathway does exist, an intermediate isoeugenol (**47**) would have been expected as an intermediate, but it is never detected in solution, probably due to the fast hydrogenation before desorption. Moreover, as discussed above, a vinyl intermediate was expected for the transformation of coniferyl aldehyde (**31**) and 4-ethyl guaiacol (**25**) if deformylation happens before hydrogenation of the olefin.

4.3 Experimental

Computational Methods: The electronic effects of different functional groups at the 4-position of phenolic lignin monomers on the adsorption energy were investigated via periodic Density Function Theory (DFT) method using the Vienna Ab Initio Simulation Package (VASP). The projector-augmented wave (PAW) method was used to simulate the electron-ion interactions. The generalized gradient approximation (GGA) PBE functional was used to calculate the exchange-correlation energy.

VASP calculation is conducted by using four text files named: INCAR, KPOINTS, POSCAR, and POTCAR. INCAR file stores calculation parameters named "tags", which are shown in parenthesis in the following text. KPOINTS file contains the k-point coordinates

and the mesh size for creating the k-point grid. POSCAR file contains the lattice geometry and the initial geometry coordinates of the molecular complexes. POTCAR file contains the pseudopotential, PAW_PBE pseudopotential in this work, for each atomic element used. A cutoff energy of 400 eV (tag: ENCUT = 400) was selected and employed throughout this study. The Ni (111) and Ni (100) surfaces were built based on a lattice constant of 3.524 Å for a bulk Face-centered Cubic (FCC) Ni crystal. A periodic Ni(111) or Ni (100) slab was constructed with one 25-Ni-atom layer separated by a 10 Å vacuum layer. The Ni layer was fixed (Selective dynamics cartesian) in its optimized configuration during all calculations in this work and all organic substrates were fully relaxed to a force of <0.02 eV/Å on all atoms (tag: EDIFFG = -0.02) without changing the cell shape and volume (tag: ISIF = 2). All self-consistent field calculations were converged to 1×10^{-6} kJ/mol (tags: EDIFF = 0.1E-06, PREC = Normal). Brillouin zone integration was performed using a $1 \times 1 \times 1$ Monkhorst-Pack grid and a Gaussian smearing width of 0.2 eV (tag: ISMEAR = 0; SIGMA = 0.2). Adsorption energies in kcal/mol were calculated according to the following equation where E_{ads} is the adsorption energy, E_{Ni} is the total electronic energy of Ni surface alone, $E_{\mathrm{Sub.}}$ is the total electronic energy of organic substrate in a vacuum, and $E_{\mathrm{Ni+Sub.}}$ is the total electronic energy of the fully optimized structure of a lignin monomer substrate on the Ni surface:

$$E_{ads} = E_{\mathrm{Ni+Sub.}} - E_{\mathrm{Ni}} - E_{\mathrm{Sub.}}$$

Nickel-ammonia plating solution preparation procedure: To a 1 L volumetric flask was added nickel(II) chloride hexahydrate powder 213.02 g and ammonium chloride 30.00 g. 250 mL of DI water was added and the flask was swirled to dissolve the solids. 200

mL of 30% ammonium hydroxide solution was added slowly to the flask over 5 mins. The solution was then diluted with DI water until 1 L.

Cathodic 0.1 M pH 8 borate buffer solution preparation procedure: To a 500 mL volumetric flask was added boric acid 3 g, potassium tetraborate tetrahydrate 1 g, and DI water to dilute the solution till 500 mL.

Anodic 0.1 M pH 7 phosphate buffer solution preparation procedure: To a 1 L volumetric flask was added potassium phosphate dibasic 10.81 and potassium phosphate monobasic 5.3 g.

RaNi cathode preparation standard procedure: Preparation of the RaNi cathode uses a slightly modified version of the method reported by Lessard[19,125] by trapping nickel-aluminum alloy particles in an electro-deposited nickel matrix. The nickel(II) chloride hexahydrate and nickel-aluminum alloy were purchased from Sigma-Aldrich. On the cathodic side, a square of stainless steel 314 screen (50 mesh, 2.5×2.5 cm^2) is submerged in 50 mL of nickel-ammonia plating solution with nickel aluminum alloy powder stirred in suspension; and a nickel bar facing parallel to the stainless mesh is used as the sacrificial anode. The plating current density is maintained at 60 mA cm^{-2} for 6 h. Every 0.5 h, the electrode is turned 180° to get even deposition on both sides. Afterward, the plated electrodes are activated in NaOH solution (30 wt.%) for 6 h at 70 °C.

IPA-RaNi cathode preparation: a RaNi cathode was put into a container with 50 mL of isopropyl alcohol and the container was capped. The cathode was kept in isopropyl alcohol for at least 12 h and rinsed with deionized water before use.

ECH standard procedure: ECH was conducted with a conventional divided cell separated by a Nafion 117 membrane with RaNi cathode and **CoP** anode (stainless steel coated with a water-splitting catalyst cobalt phosphate,[187] rolled up from 12×4 cm^2 stainless steel

314 screens). 30 mL of 0.1 M pH 8 potassium borate buffer was added into the cathodic half-cell and the anodic side was 30 mL of 0.1 M pH 7 potassium phosphate buffer. 10 mg of $Co(NO_3) \cdot 6\,H_2O$ was added into the anodic phosphate buffer to *in situ* deposit a black film of cobalt phosphate water splitting catalyst on the surfaces of the anode along with ECH. The current was set to 50 mA (8 mA cm^{-2}, calculated based on the electrode's single side facing the membrane and anode compartment) and the temperature to 80 °C unless otherwise specified. Before adding organic substrate, the electrode was equilibrated by electrolysis under 50 mA at 90 °C for 30 min, and a layer of a black film is observed forming on the surface of the anode, serving as a protection layer against the corrosion of the stainless steel. Afterward, 20 mM of the substrate is added to the cathode side with 0.1 g NaOH to improve solubilities and subjected to ECH for 6 or 8 h. Then the cathodic aqueous solution was transferred into a 100 mL separation funnel, acidified with HCl until pH below 3, and extracted with 3 × 30 mL aliquots of dichloromethane (DCM). The organic solvent was dried over Mg_2SO_4 and removed by vacuum at room temperature and the product was dissolved in 0.7 mL of $CDCl_3$ for NMR analysis. Afterward, the 0.7 mL $CDCl_3$ solvent was transferred to a 10 mL volumetric flask, and DCM was used to dilute the solution to 10 mL. 1 mL of the resulted DCM solution was transferred into a 2 mL screw top vial for analysis of gas chromatography-mass spectrometry (GC-MS).

Kinetic time course studies were conducted in the same set up described above. A 0.5 mL of sample was withdrawn from the ECH cathodic cell into a 2.0 mL conical vial every 1 h. The sample was acidified by adding 2 drops of concentrated HCl and extracted with 1.0 mL of DCM. 0.5 mL was withdrawn from the DCM layer and sent for GC-MS analysis.

Calibration curves of all starting material and products identified by the GC-MS analysis of the ECH results were prepared by injecting DCM solutions of 16 (in some cases

where a single product was produced as the main product in the final aqueous solution), 8, 4, 2, 1, 0.5, 0.25 mM commercially available or synthetic standards. The peak areas were plotted against concentrations by using OriginPro 9 software. All main products were confirmed by comparing the elution times and EI (Electron Ionization) mass spectra of the identified products with those of the standards.

H/D exchange experiments were conducted by dissolving starting materials in 30 mL of 0.1 M pH 8 borate buffer made up in D_2O to make a 20 mM solution. Since the compound has no phenolic proton, 2 mL of acetone-d*6* was added to make the solution homogeneous. The solution was then heated to 90 °C and the RaNi cathode rinsed with D_2O was added to the solution. An initial sample was withdrawn right after adding the cathode. Then a 0.5 mL sample was withdrawn from the cell every one hour and transferred into an NMR tube. A 10 µL D_2O solution containing the internal standard (dimethylformamide) was added in the NMR tubes to make a total of 4.3 mM concentration, then a proton NMR was obtained.

4.4 Conclusions and outlook

This study theoretically investigated the adsorption energies of 21 lignin monomers on surfaces of Ni (111) and Ni (100) via computational chemistry tools and experimentally analyzed the ECH reactions of 16 lignin monomers with different functional groups on the para-position relative to the phenol OH.

The theoretical work reveal that olefin and carbonyl groups increase the adsorption energy of a lignin monomer compared with the corresponding 4-alkylguaiacols on Ni (111) and Ni (100) surfaces; aryl methoxyl tends to decrease the adsorption energies, while alkyl group and hydroxy on the 4-alkyl chains do not affect adsorption energies in any significant amounts.

The steric effect was generally observed through almost all substrates studied and a longer alkyl chain at the 4-position slows ECH reactions. In contrast, steric-hindrance at the 2-position attached via an ether oxygen, do not affect ECH reactions. Meanwhile, the position of methoxy on arene ring does change the rate of demethoxylation with the highest occurring when hydrogen bonding with the phenolic hydroxy group is possible. However, changes of methoxy positions do not appear to inhibit aromatic ring reduction reactions.

The ECH of non-terminal carbonyl or alcohol compounds lead to no C-C cleavage products, but terminal ones do. The cleavages of C-C bonds under the mild ECH conditions are attributed to deformylation reactions since all α, β, and γ-C sites are able to coordinate with the Ni surface, as shown by H/D exchange experiments. Therefore nickel atoms can coordinate to the terminal aldehyde, insert between the formyl C-H bond, after which CO migration forms an aryl C-Ni bond and cleaves the original C-C bond. Subsequent hydrogenation and desorption lead to the C-C cleavage product released into the bulk solution.

The deformylation reaction is of potential value in reducing the steric hindrance slowing reaction of lignin monomers and can improve ECH efficiency. A practical upgrading of lignin monomers to fuels will require further improvements of deformylation, demethoxylation and aromatic ring reduction reactions. Meanwhile, further deeper understandings of the mechanistic insights on demethoxylation, aromatic ring reduction, and deformylation reactions on the Raney® nickel surface are needed in order to improve the lignin to fuel conversion.

4.5 Acknowledgments

I express my gratitude to Dr. David Tománek who is from Physics and Astronomy Department. Thanks for all of his instructions and kindness to accept me into the group and allow

me to share the research resources.

Chapter 5

Electrocatalytic Hydrogenation of Lignin Dimers and Copper Alkaline Hydrogen Peroxide Lignin

5.1 Introduction

Lignin is the second most abundant renewable biopolymer in the world and is produced as a million-ton level industrial waste from pulping and paper-making processes,[188] Though "You can make anything you want out of lignin – except money" has long been stated till nowadays "Yes, we can make money and useful products out of lignin",[189] appears more appropriate. The values of lignin have proceeded beyond energy applications alone to a wide diversity of exciting products including biofuel, functionalized building block molecules, and specialty/ high-performance materials[189] obtained by depolymerizing lignin to monomers, synthesizing lignin nano-fibers,[190] making lignin nanotube as vehicles for gene delivery,,[191] assembly of lignin into microcapsules for hydrophobic molecule storage/delivery, conversion of lignin to microcapsules,[192] biobased Epoxy resins,,[193] functionalization of lignin to thermo-responsive material,[194] and feedstock for 3D printing[189] applications etc.

Despite these emerging breakthroughs of lignin applications, the structure of natural

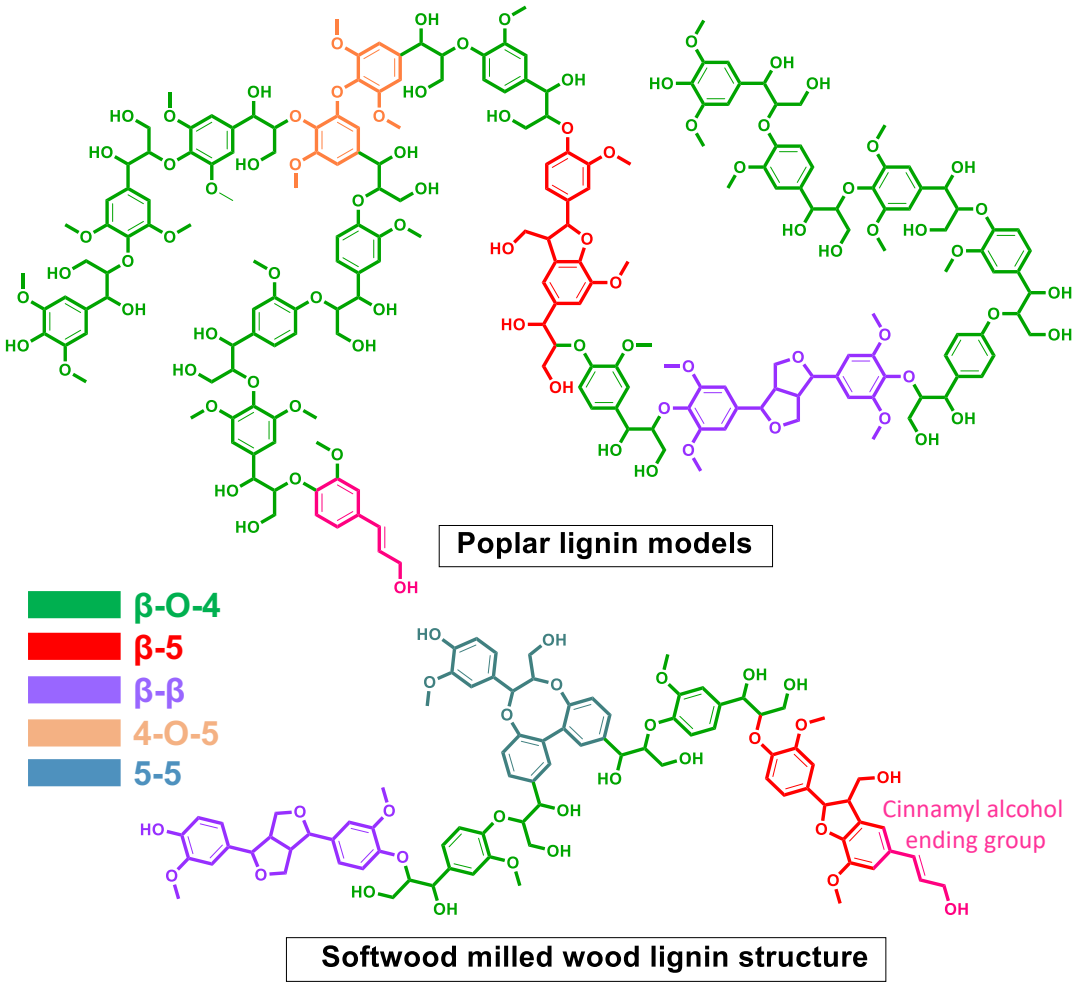

Figure 5.1: The newly proposed lignin structures of hardwood lignin (Poplar) and softwood milled wood lignin.

lignin is still not fully understood. It was long thought that lignin is a 3-dimensional, cross-linked polymer formed from three phenolic monomers: para-Hydroxycinnamyl alcohol (H), Guaiacol (G), and Sinapyl alcohol (S). Recently, Crestini reported that milled wood lignin (MWL) was a linear oligomer with the absence of branching units, which are the etherated 5-5 and 4-O-5 linkages. This was confirmed in both softwood and hardwood MWL samples. Ralph suggested poplar lignin was mainly linear but possibly branched.[195] They proposed a structure of poplar lignin as shown in Figure 5.1.

Widely varying structures and properties are found for lignin obtained from the various

classical separation processes, including ball-milling, Kraft, organic solvent extraction (dioxane lignin), and cellulolytic enzyme lignin processes,[196] and lately developed Ammonium Fiber Explosion(AFEX),[197,198] Copper-Alkaline Hydrogen-peroxide (Cu-AHP),[20] and ionic liquid lignin[199,200] processes. The principal goal in these methods' development was to improve enzymatic digestibility of the cellulose fraction to produce ethanol. Production of relatively clean lignin as a byproduct was a secondary goal. It was well known that the old processes significantly modify or damage lignin structures and most likely these more recent processes influenced lignin structures as well.[17,20,201,202] NMR techniques are very powerful and useful to measure these changes with minimum further alterations to lignin structures, due to handling, particular value are the newly developed quantitative ^{13}C, quantitative ^{31}P,,[203] and quantitative 2D HSQC NMR techniques.[195,196] At the same time, these tools offer new opportunities to conveniently quantify H/G/S ratios, total phenolic hydroxyl contents, normal lignin and condensed lignin linkages (diphenylmethane, diphenyl ethers, and 5-5 biphenyl type coupling structures),[203] and different linkage percentages[195] (β-O-4, β-5, β-β, and, in special cases, 5-5 and 4-O-5[177]). Meanwhile, these tools are also ideal to monitor reactions of lignin, especially depolymerization.

There are many types of lignin depolymerization approaches: thermo-, oxidative, hydroprocessing (hydrogenation/hydrogenolysis), acid-catalyzed, and base-catalyzed depolymerizations, and each method has its own advantages and limitations well reviewed by Zhang etc.[204,205] In general, acid-catalyzed and oxidation depolymerization methods operated at lower temperature (0 - 250 °C), while base-catalyzed and hydroprocessing required high temperatures (100 - 350 °C) and pressures to assist in dissolving solvating and splitting hydrogen gas. Meanwhile, thermo-depolymerization needs the highest temperature (350 - 700 °C) to initiate radical reactions. On the other hand, hydroprocessing products are more

stable and less prone to repolymerizations than those from all other approaches.[205]

Electrocatalytic Hydrogenation (ECH) inherits the advantages of hydroprocessing, and at the same time, not only significantly reduces the operation temperature below 100 °C, but also can run at atmospheric pressure since the reducing agents, surface-bond hydrogens, are generated in-situ on catalysts by the electroreduction of protons.[35,56,97,101,206–208] Phenol has been successfully reduced to cyclohexanol and cyclohexanone by ECH reactions on cathodes of Rh/C,[93–95,100] Rh/G (graphite),[96] Pd/C,[94] Pd/G,[96] Pt-Pt (Platinized Platinum),[36,94,98] Pt/C,[94,95] Pt/G,[96] and RaNi[97,101] with current efficiencies varying from 8-84%, with the top performance by Rh/C cathodes at the room temperature.[94] Guaiacol can be mainly reduced to cyclohexanol at a higher temperature on RaNi cathode,[19,101] and to a mixture of cyclohexanol and 2-methoxycyclohexanol on Ru/ACC cathode[105] with current efficiencies between 3.4 and 31%. Alkyl phenols were even more difficult to reduce by ECH, with no cyclohexanol derivatives reported.[101]

Simple models of lignin dimers haver been studied included α-O-4, β-O-4, and 4-O-5; ECH current efficiencies of these models varied depending on types of linkages, catalysts, temperatures, and solvents. As shown in the last chapter table 1.1, Pd/Al_2O_3 could cleave β-O-4 ether completely but not much hydrogenation of the produced monomers was achieved. On the contrary, Rh/C was a good catalyst for the hydrogenation of aromatic rings while the cleavage of β-O-4 ether was not as great. The effectiveness order of aryl-aryl ether bond (4-O-5) cleavage catalyst was RaNi > Pd/Al_2O_3 > Pd/C > Rh/Al_2O_3 > Pt/C > Ru/C = Pt/Ni > Rh/C.[100,101,107,108] Among all, RaNi was found to be the best cathode for the hydrogenation and cleavages of lignin α-O-4, β-O-4, and 4-O-5 dimer models, and the demethoxylation and hydrogenation of the aromatic rings tended also to proceed well in a basic aqueous solution without alcohols.

As far as we know, there have been no reports on direct depolymerization or hydrogenation of lignin by ECH. Our ECH monomer studies showed that demethoxylation and saturation of aromatic rings proceeded with RaNi efficiently at around 90 °C. Although steric effects were observed as moving from 4-methylguaiacol to 4-propylguaiacol, adding additional carbonyl and alcohol groups on the alkyls improved current efficiencies. Additional aromatic rings in lignin dimers may increase absorption energy, however, the additional steric-hindrance added by alkyl groups to the dimer may cancel out the beneficial effect. Meanwhile, β-5, β-β linkages had never been studied by ECH, while β-O-4 had not been efficiently reduced to cyclohexanol derivatives. In this work, we explored a method to depolymerize Copper Alkaline Hydrogen Peroxide lignin (Cu-AHP Lignin) and to use lignin dimers and computational tools to understand the reaction mechanisms.

5.2 Results and discussion

β-β, β-5, and 5-5 lignin dimers are considered non-cleavable dimers for hydrogenation methodology since all of them contain carbon-carbon bond linkages between monomer subunits. It remained as a question whether the dimer could at least be deoxygenated as occurs in lignin monomers.

5.2.1 β-β

β-β dimer (**1**) is difficult to reduce; the benzyl alkyl ether bond of (**1**) is resistant to ECH at room temperature as shown in entries **1** and **4** of Table 5.1. At room temperature, no products were detected under either acidic or basic conditions with Ru/ACC and RaNi cathodes, respectively.

Table 5.1: The ECH of β-β dimer.

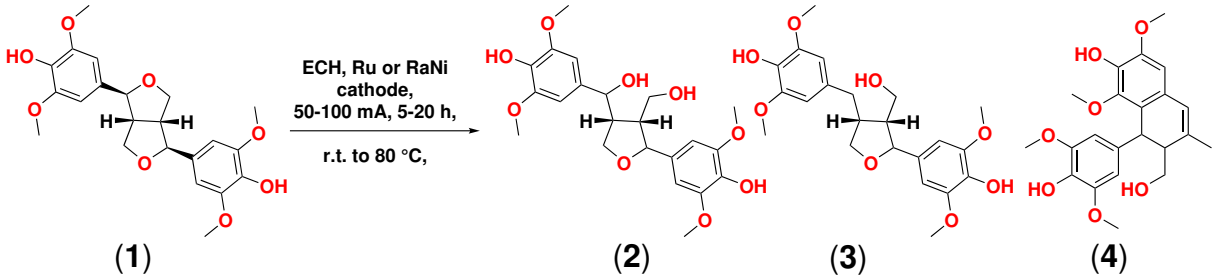

	Cat.	Temp.	Additives in water	T.	I	Product Distribution%				
		°C		h	mA	(1)	(2)	(3)	(4)	C.E.%
1	Ru	r.t.	2 M HCl, EtOH	12	50	100	0	0	0	0
2	Ru	80	2 M HCl, EtOH	12	50	44±5	56±5	0	0	0
3	Ru	80	pH 3.5, 1 M $B(OH)_3$	12	50	-*	-*	-*	-*	-*
4	Ru	80	$Hf(OTf)_4$, EtOH	12	50	-*	-*	0*	7.6*	-*
5	RaNi	r.t.	pH 12, NaOH	20	150	100	0	0	0	0
6	RaNi	80	pH 3 Borate/EtOH	20	50	75±4	25±4	0	0	0
7	w/o	80	pH 12 Borate buffer	20	0	63	37	0	0	0
8	IPA-RaNi	80	pH 9 Borate buffer	20	50	58±2	27±1	15±2	0	0.5

HCl was used to adjust the solution pH below 7. NaOH was used to increase the solution pH.
Cat. is cathode. **T.** is time. **I** is current. **C.E.** is current efficiency. **Ru** is Ru/ACC cathode. **EtOH** is ethanol and it is always mixed with 1/4 of the volume of water (10 mL of ethanol and 40 mL of water).
* All four replicates showed slight brown cathode solutions with a small amount (<10% of mass balance) of brown solid floating on top of the water. After column chromatography separation, NMR showed the presence of (**1**) and (**2**) in significant amounts. However, some degree of polymerization was still evident in the NMR, rendering it impossible to get product distributions from the NMR analysis.
** represents the yield of pure (**4**) that was isolated from ECH of the β-β dimer after flash column chromatography (99:1.5 DCM:MeOH); this yield excluded any (**4**) mixed with other compounds; another isomer of (**4**) was also isolated in such small quantity that the structure could not be confidently assigned due to bad NMR resolution and possible peak overlaps with impurities.
[a] Polymerization was so extensive that dichloromethane insoluble brown solid precipitated at the bottom of the reaction cell during the ECH. No product distribution could be calculated.
[b] 4: 1 ratio of 0.1 M pH 8 borate buffer and ethanol was used as the solution. pH was adjusted by the addition of HCl.
[c] 1 eq of hafnium(IV) triflate compared to substrates (10 mM) was added to pH 1 water solution and ethanol (EtOH/water=1:4).
[d] the product distributions were calculated based on integrals from proton NMR of the final product mixtures.
[e] the end pH was 7.8.

When the temperature was raised up to 80 °C, the first product from (**1**) in both acid (entries 2 and 6) and base (entry 8) conditions is the benzyl ether hydrolysis product (**2**). This reaction happens in the bulk solution and does not require any current or a catalyst, proved by entry **6** where 37% of hydrolysis product (**2**) is produced in the absence of current and cathode. The structure of the hydrolysis compound (**2**) was confirmed only by proton, carbon NMR, and mass spectrometry (see Figure 5.4) data; attempts to obtain pure (**2**) by column chromatography failed since (**2**) and (**1**) behaved similarly on silica and got eluted out together.

Under strong acid conditions (pH below 1) by the additions of HCl (entry **2**), no sign of polymerization was observed during ECH. However, when a concentrated 1 M boric acid solution (pH = 3.5) was used in the cathodic half-cell (entry **3**), extensive polymerization was observed as indicated by the precipitations of DCM non-soluble brown solid, the dark-brown color of the cathodic solution, and continuous and broad proton NMR peaks between 6.3-7.0 ppm (the aromatic area) and 3.0-4.0 ppm (methoxy and geminal-hydroxy CH or CH_2). Boric acid is both a bronsted and a Lewis acid. Since the strong Bronsted acid HCl did not lead to extensive polymerization, it can be concluded that the phenolic β-β dimer (**1**) is prone to be activated and polymerize in a concentrated Lewis acid solution.

Similarly, some degree of polymerization, less extensive than the boric acid case, occurred when a water-resistant Lewis acid $Hf(OTf)_4$ was added in pH 1 HCl solution with the aid of EtOH to make the solution homogeneous. About <10 wt% of the mass balance of brown solid floated on the electrolyte surface after ECH. The product mixtures contained three major compounds: (**1**), (**2**), and (**4**) as shown by NMR. However, the product distribution could not be definitively obtained due to the appearance of some polymers in the proton NMR.

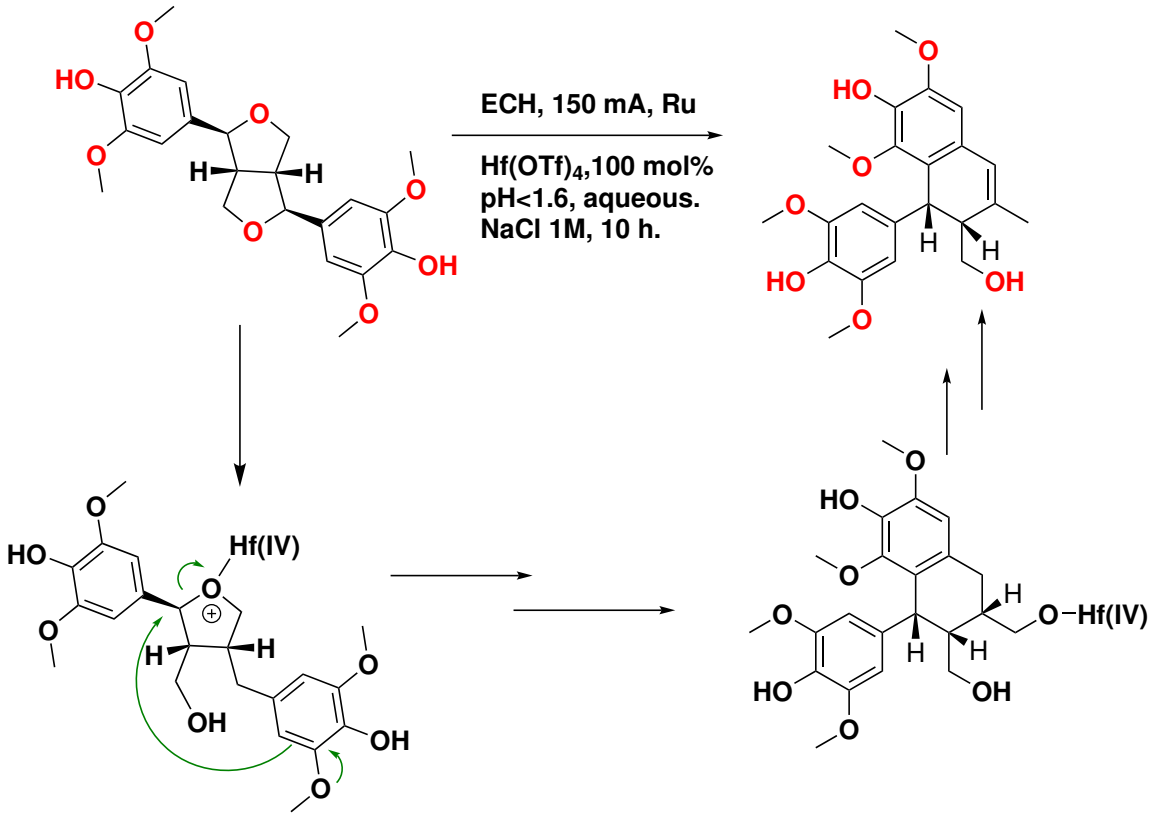

Figure 5.2: The proposed mechanism for the rearrangement reaction during ECH of β-β dimer.

A 7.6% yield of pure (**4**) was obtained by column chromatography with 98:1 DCM/methanol as the mobile phase (ethyl acetate/hexane solutions do not separate the mixture well). The formula of (**4**) was confirmed by mass spectrometry, with structural assignments made based on ^{1}H, ^{13}C, COSY, HSQC, and HMBC NMR. The main H-H and C-C correlations from COSY and HMBC are summarized in Figure 5.3. This remarkable rearrangement reaction product (**4**) was proposed to be formed via the mechanism in Figure 5.2. The hydrogenation of the benzylic ether bond of the THF ring generates the precursor for the rearrangement. Since hafnium triflate is a Lewis acid that can function in water solution,[209, 210] and it is known to coordinate with hydroxyl groups[211] and is able to initiate Friedel-Craft reactions.[212] After Hf(IV) coordinates with the ether oxygen in the remaining THF ring, an intramolecular Friedel-Craft reaction generates the new framework of the product (**4**).

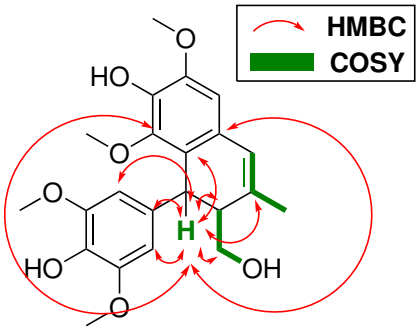

Figure 5.3: The structure elucidation of the rearrangement product by 2D NMR (proton, carbon, COSY, HSQC, HMBC).

Since the new carbon-carbon bonds generated by the Friedel-Craft reaction initiated by a Lewis acid are much stronger than ether bonds a large amount of Lewis acid should be avoided in the ECH.

Under the basic conditions (entry **8** of Table 5.1), the ether hydrogenation product (**3**) was generated in 15% without any signs of polymerization or rearrangement reactions. No demethoxylation product was detected. The hydration product (**2**) was also observed after

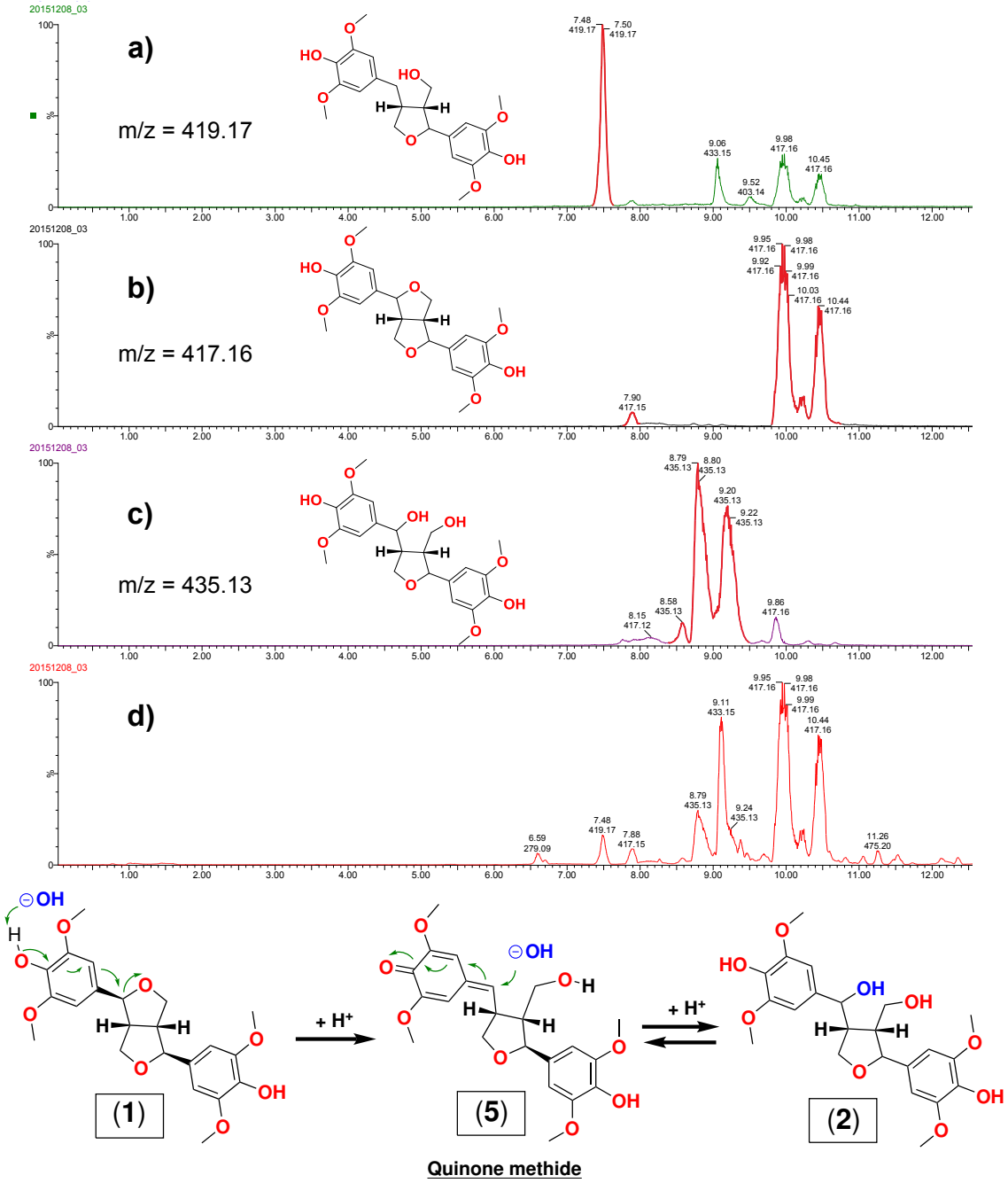

Figure 5.4: The HPLC-MS chromatograph of the ECH product mixture of β-β dimer. d) is the total ion current chromatogram of the product mixture. a), b), and c) are the extracted ion chromatograms for each compound. Only two of the eight hydrolysis intermediate isomers were shown to simplify the figure.

the ECH. Entry **7** of Table 5.1 suggested that this hydration of the benzylic ether bond is not a catalytic surface reaction. Therefore, we proposed the mechanism to form the hydrated product (**2**) as shown in Figure 5.4. Under the basic condition, the phenolic OH can be deprotonated and form a quinone methide intermediate (**5**), followed by a Michael-addition of a hydroxide anion and a protonation to generate (**2**).

In summary, at this stage, the ECH of β-β dimer is limited to hydrogenation of only one of the two benzylic ether bonds, and no demethoxylation or other deoxygenation reactions are observed. A hydration product of the starting material was observed under both acidic and basic conditions with or without the presence of the catalyst, thus it was believed to form via a quinone methide intermediate in the bulk solution. Basic conditions have the advantages over-acid conditions that better solubilities for phenolic substrates enable higher concentrations of substrates and there is much less polymerization during ECH. Lewis acid strategies encourage polymerization of phenolic compounds extensively.

5.2.2 β-5

The β-5 dimer barely dissolved in pure water, as shown in Figure 5.5; the solubility increased with the addition of NaOH up to 50 mM, but then interestingly, the solubility decreased beyond 50 mM NaOH, perhaps the increased ionic strength when adding NaOH decreased the solubility of this relatively nonpolar deprotonated dimer.

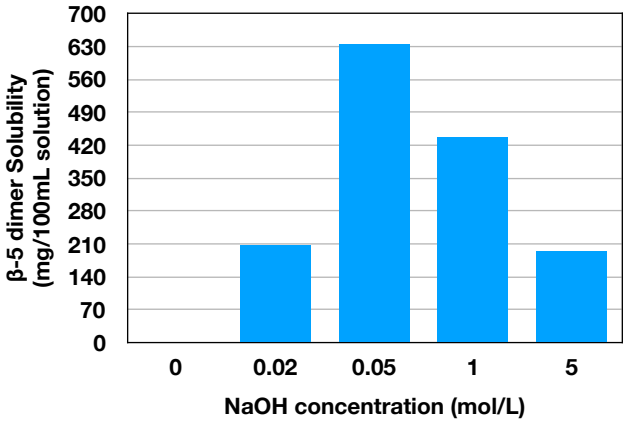

Figure 5.5: The solubility of β-5 dimer in different concentrations of NaOH solution.

β-5 linkage dimer (**6**) has two linkages between two monomers, the benzylic α-O-4, and the strong β-5 C-C bond. Olefin reduction from (**6**) to (**7**) is the first reaction on the surface of RaNi here as shown in Figure 5.7 by the disappear of the peaks of (A), also (**6**), and the appearance of the peaks of (B), also (**7**); within 4.5 h, double bond (d at 6.35 ppm and dq at 6.2 ppm shaded in yellow) disappear almost totally. The benzylic ether bond cleavage product (C), also (**8**), started to appear after 2.5 h and became the only product at the end of the reaction.

Under higher temperature of 80 °C, deoxygenation reactions happened with moderate yield of (**9**) with trace amount of (**10**) and (**11**) detected by HPLC-MS. Consistent with our monomer result, no cleavage of the C-C product was observed with models that are absent of terminal alcohols or carbonyls. The structures of products (**8**) were confirmed by the MS,

Table 5.2: The ECH of β-5 dimer.

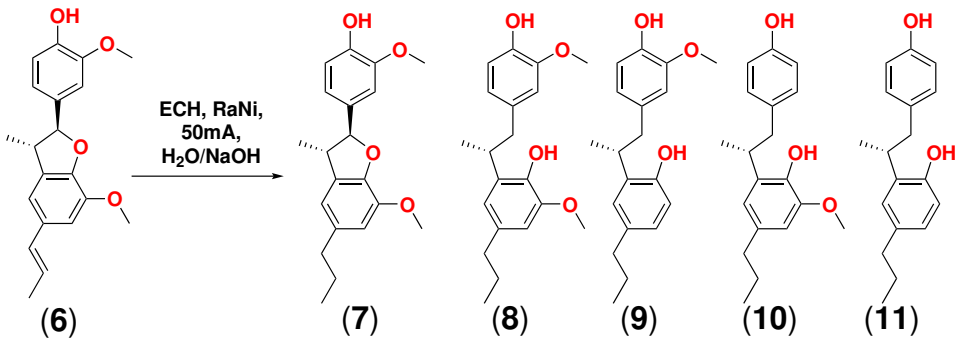

	Temp.	Time	Product Distribution%						
	°C	hour	(6)	(7)	(8)	(9)	(10)	(11)	C.E.%
1	r.t.	1	50	50	0	0	0	0	32
2	r.t.	2.5	0	28	58	0	0	0	37
3	r.t.	4.5	0	25	72	0	0	0	24
4	r.t.	16.5	0	0	100	0	0	0	8
5[a]	80	16	0	0	84	17	trace	trace	9

The product distributions were calculated based on the NMR integrals. Trace amount of the demethoxylation product was not included in the product distribution. [a] This experiment was conducted with a IPA-RaNi cathode in pH 8 borate buffer with 0.1 g NaOH to help the substrate to dissolve.

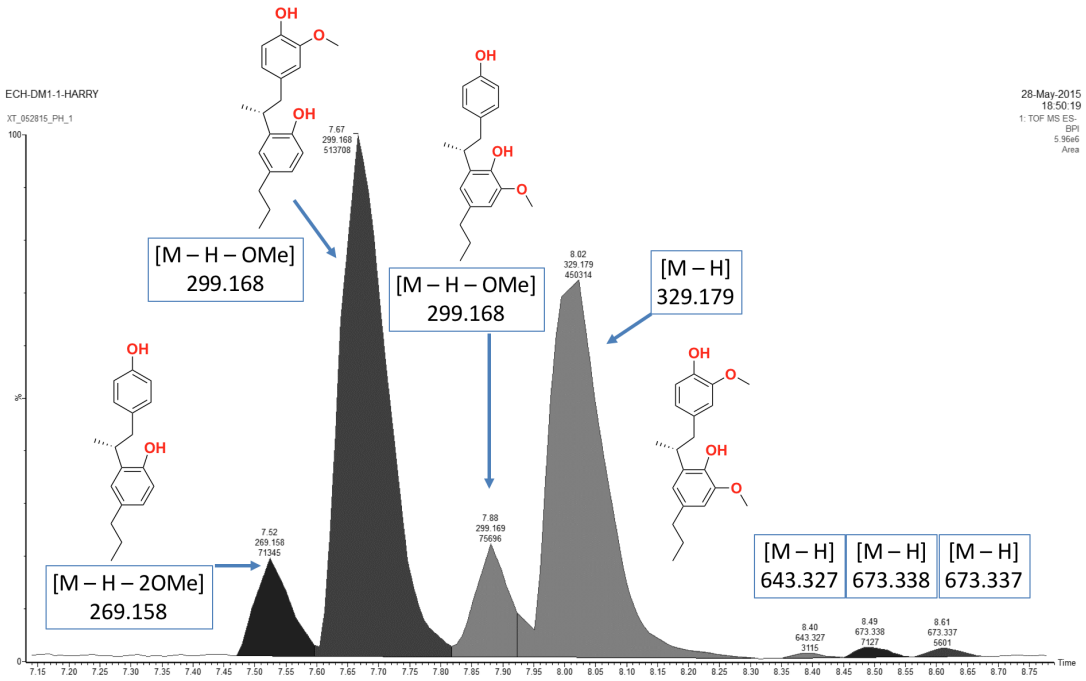

Figure 5.6: The HPLC-MS chromatograph of the ECH product mixture of β-5 dimer.

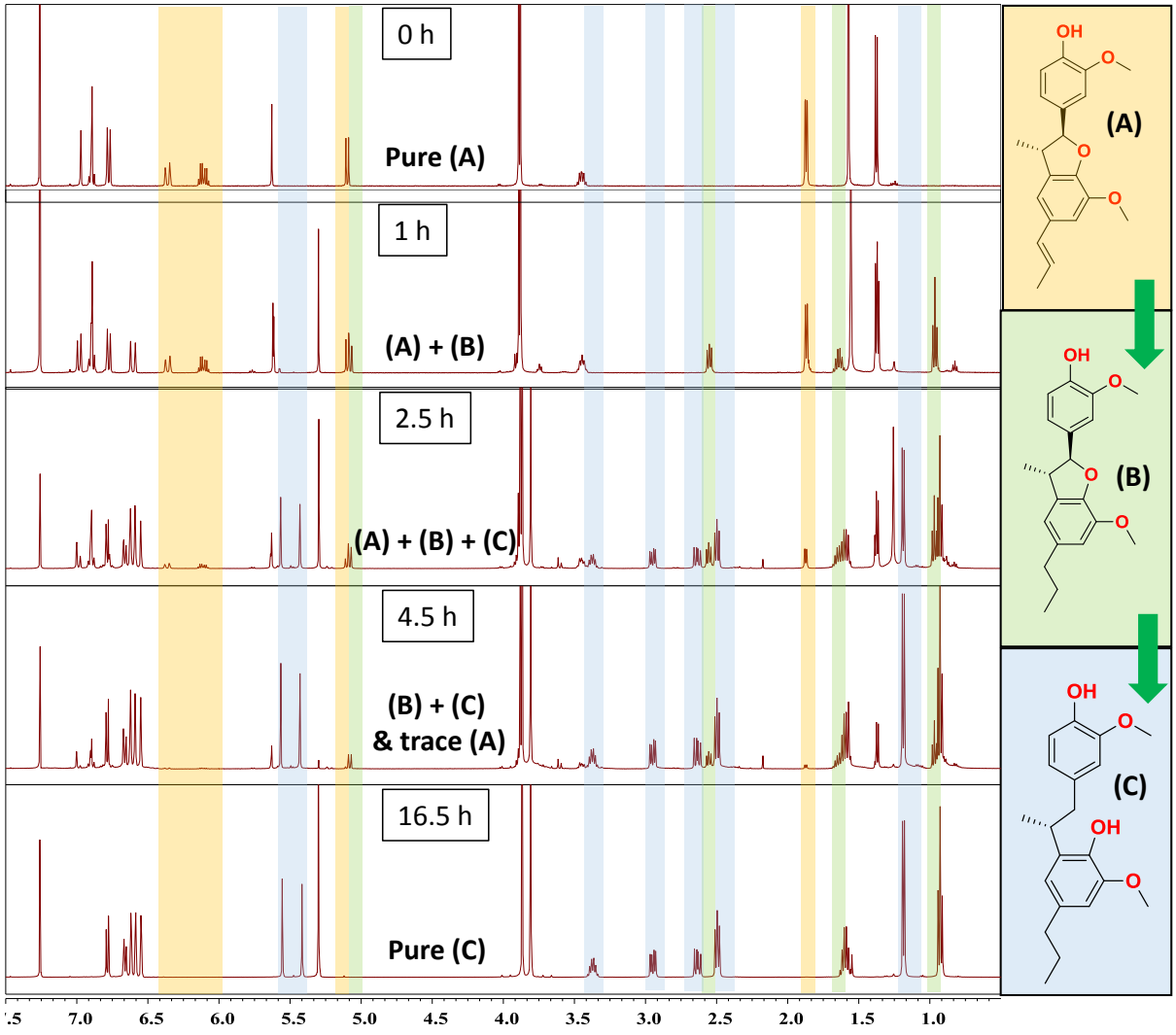

Figure 5.7: The NMR studies of ECH of β-5 dimer with RaNi cathode in 0.05 mM NaOH solution at room temperature. The peaks shaded in yellow are only the characteristic peaks of compound (A). The peaks shaded in green are only the characteristic peaks of compound (B). The peaks shaded in blue are only the characteristic peaks of compound (C).

^{1}H, ^{13}C, COSY, HSQC, and HMBC NMR. Structures of product (**9**) was confirmed by the MS, ^{1}H, and ^{13}C NMR. (**10**) and (**11**) are assigned based on the mass spectrum results.

It is also noticed that the HPLC-MS detected very small amounts of dimerization products (elution time = 8.40, 8.49 and 8.61 min) with M-1 = m/z 643.327, 673.338, and 673.337. We speculate that the two peaks associated with molecule M = 674 are most likely from the hydration product of (**7**) (M = 346) dehydro-dimerizing with (**8**) (M = 330) by removing two protons resulting the product masses as M = 674. However, this does not necessarily represent the actual reaction mechanisms. The other peak with mass M = 644 is most likely from the demethoxylation of one of the compounds with M = 674.

5.2.3 5-5

The 5-5 dimer is another challenging model for ECH reactions at under ECH conditions. The two olefinic groups of bis-eugenol model (**12**) were readily reduced to alkyl groups. However, no demethoxylation products (**13**) were observed under conditions where eugenol can be demethoxylated effectively.

Table 5.3: The ECH of 5-5 dimer.

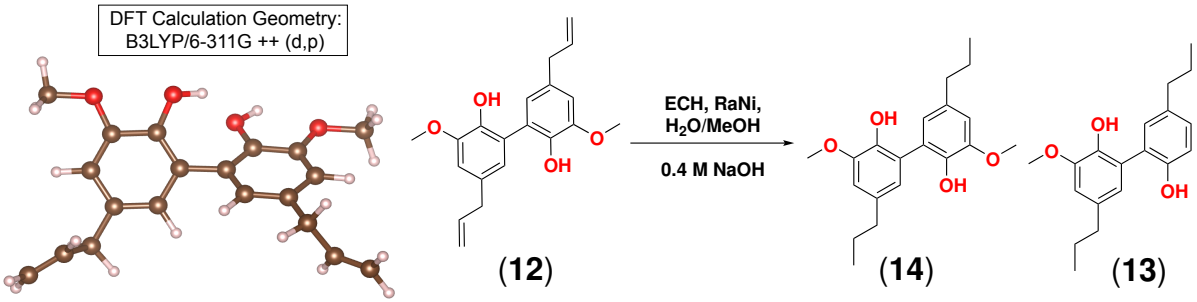

					Product Distribution%		
	Temp.	**Solvent**	**Time**	**Current**	**(14)**	**(13)**	**C.E.%**
1	r.t.	pH 12 H_2O/EtOH	12	50, 200 mA	100	0	5.4, 1.4
2	80	pH 12-13 H_2O/EtOH	20	50 mA	100	0	3.2
3	80	pH 12-13 H_2O	20	50 mA	100	0	3.2
4[a]	90	pH 9 borate	20	50 mA	100	0	3.2

The EtOH is 50 vol % in the solvent. The product distribution was calculated based on proton NMR. The product was also confirmed by GC-MS that no small fragmentation products were produced. [a] This experiment was conducted with a IPA-RaNi cathode.

The optimized geometry of dimer (**12**) showed that there is a dihedral angle of about 52° between the two benzene rings, making it impossible for any of these two aromatic rings to adsorb on the nickel surface in a flat fashion. Meanwhile, the allyl group on the para-position relative to the phenolic hydroxyl groups increased the steric hindrance of the molecule making it even more difficult to adsorb and get demethoxylated.

5.2.4 4-O-5

4-O-5 dimer has a diaryl ether bond, for which the bond dissociation energy is about 20 kcal/mol higher than a benzyl aryl ether bond, and about 6 kcal/mol higher than a phenylethyl-aryl ether bond.[213] Although seemingly the most difficult ether bond to cleave, surprisingly the ECH cleavage of a 4-O-5 bond is almost as easy as the reduction of an olefin on RaNi. All three ortho-, meta-, and para-hydroxyl diaryl ether models (**15**) , (**16**), and (**17**) (see Table 5.4) get cleaved completely within 2 hours (see Figure 5.9). It should be noted that two moles of phenol are released into the solution when every one mole of phenoxyphenol got cleaved, thus the theoretical total concentration of final product phenol should be twice that of starting material phenoxyphenol, if the cleavage product is only phenol.

All three models are reactive on a RaNi cathode while behaving differently in terms of cleavage regio-selectivity. There are two aryl ether C-O bonds, one between the ortho-hydroxyphenyl and oxygen atom (HPO), and the other between the phenyl group and the other oxygen atom (PO). The HPO bond is cleaved in all three cases, producing phenol and cyclohexanol. However, in the case of (**15**), where hydrogen bonding between the phenolic OH and ether oxygen is possible, PO bond cleavage is also observed, as indicated by the product 1,2-dihydroxycyclohexane. The other part of the cleavage product benzene and possibly cyclohexane were too volatile to be captured and observed in this 90 °C reaction.

Only small reactivity differences among the three isomers were found. According to the kinetic studies in Figure 5.9, 3-phenoxyphenol (**16**) is consumed slightly slower than (**15**) and (**17**). Here electronic influences from the resonance of the phenolic hydroxyl group may play a role in accelerating the reactions.

Table 5.4: The ECH of 4-O-5 dimers.

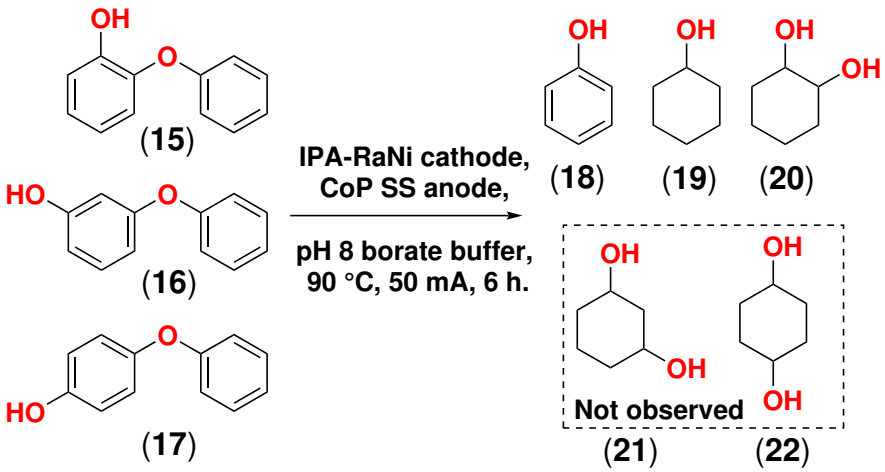

			Observed Product Distribution%			
	S	Conv.	(18)	(19)	(20)	C.E.%
1	(**15**)	99	3	80	15	72
2	(**16**)	100	20	80	-	62
3	(**17**)	98	17	81	-	63

The EtOH is 50 vol % in the solvent. The Product Distributions are calculated based on GC-MS results and calibration curves were obtained for all products except that the amounts of 2-p-tolyloxylphenol and 2-hydroxymethylphenoxylphenol were estimated by using the responds factor of 2-phenoxyethanol.

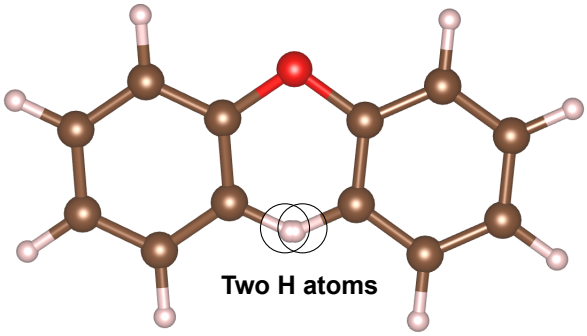

Figure 5.8: The model of a diaryl ether that is forced to be a coplanar geometry.

(a) 2-phenoxyphenol

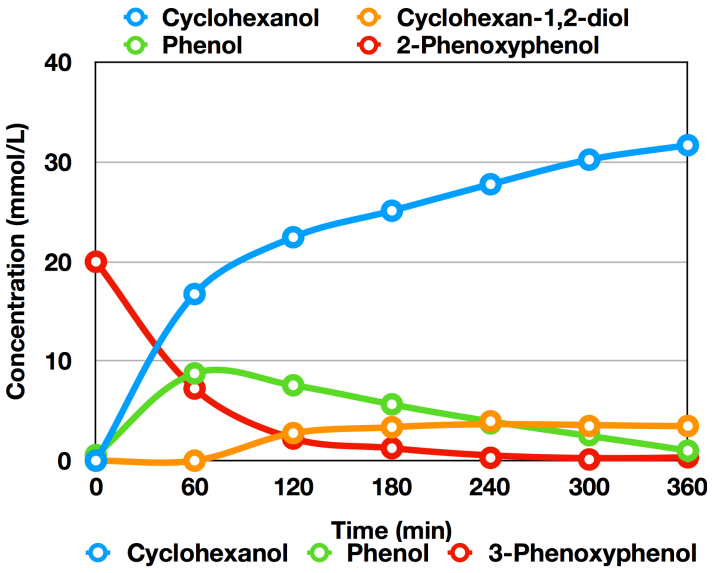

(b) 3-phenoxyphenol

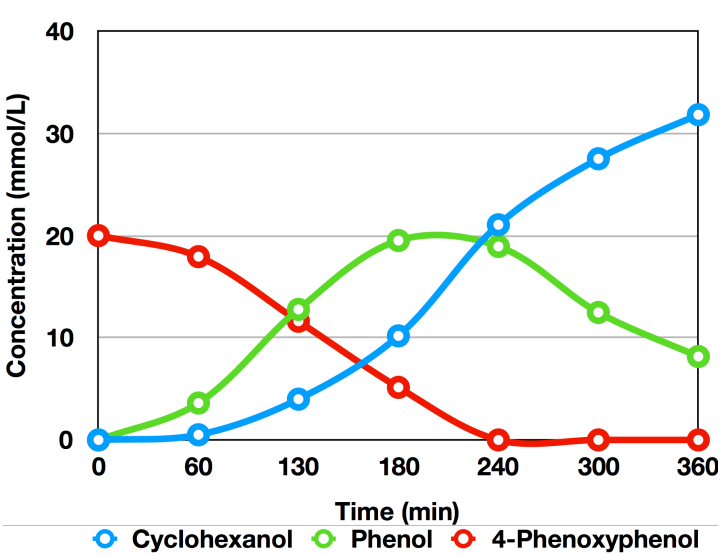

(c) 4-phenoxyphenol

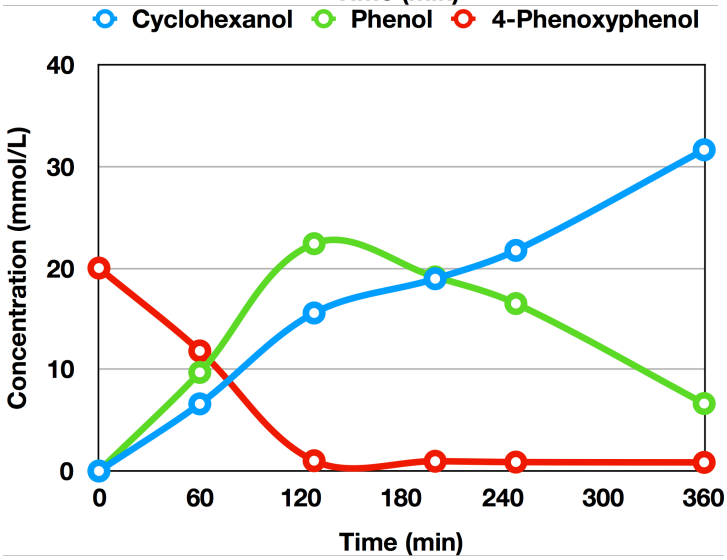

Figure 5.9: The kinetic studies of ECH of 2-, 3-, and 4-phenoxyphenol with RaNi cathode at 90 °C for 6 h.

The 4-O-5 dimer has two aryl rings, however, it is almost impossible for both aromatic rings of diaryl ethers to adsorb on the nickel surface at the same time; when the two aromatic rings are forced to be coplanar, either the two phenyl protons collide as shown in Figure 5.8, or the C-O-C angle becomes much bigger; in either case it would be a high energy geometry.

5.2.5 β-O-4

Table 5.5: The ECH of β-O-4 dimer. The labels in blue color are the compounds represented in the kinetic study figure on the next page.

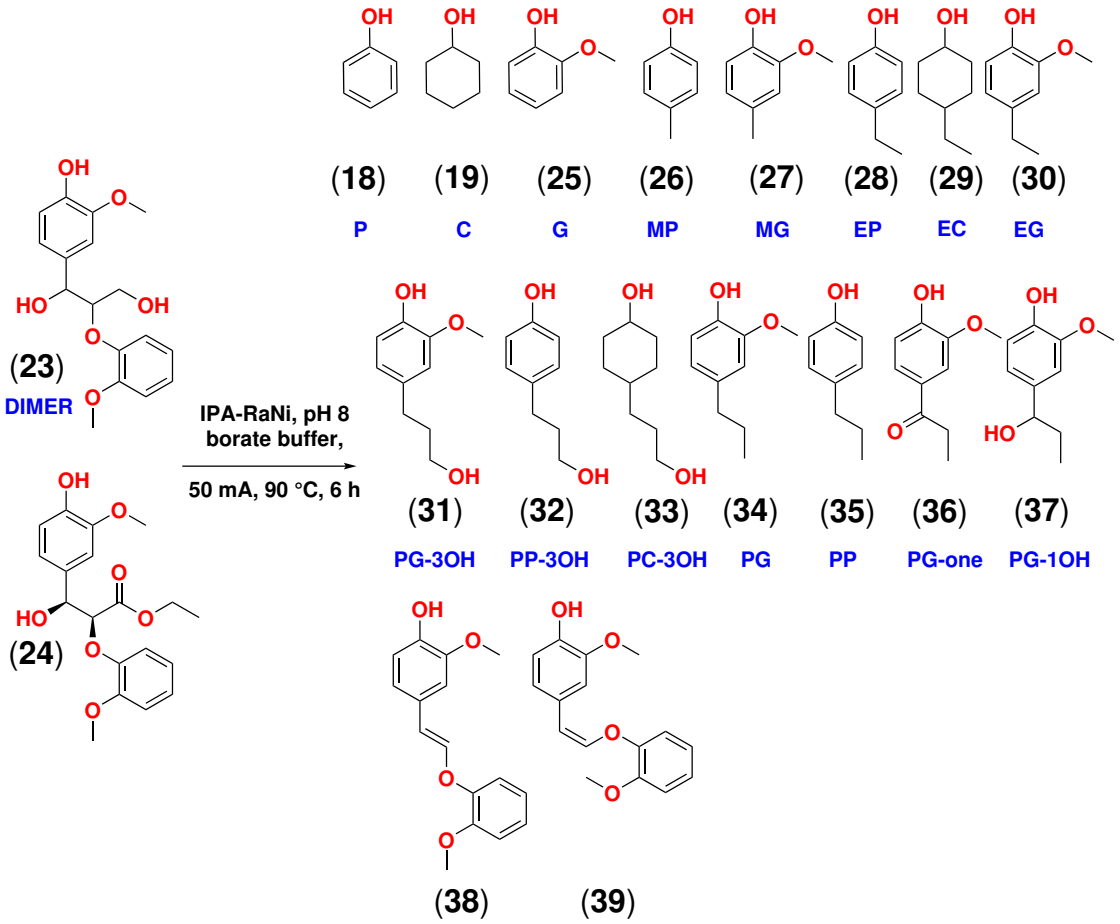

	Product Distributions %[a]																
	(18)	(19)	(25)	(26)	(27)	(28)	(29)	(30)	(31)	(32)	(33)	(34)	(35)	(36)	(37)	(38)	C.E.%
(23)	2±0.1	65±0.5	6±0.4	0	0	7±1.5	3±1.0	1±0.1	3±1.4	1±0.4	5±2.1	0.2±0.0	9±1.1	1±0.1	1±0.1	0	44
(24)	24	11	9	1	1	41	0	5								8	9[b]

The There are several unknown peaks from ECH of (**23**) was not quantified. Mass balance of the reaction is 64% after 6 h. (**39**) appeared in trace amount.
[a] The conversions of the ECH of (**23**) and (**24**) are 99.6% and 100%, respectively.
[b]The ester dimer (**24**) reduction was conducted for 18 h.

β-O-4 dimer (**23**) represents the majority linkage in natural lignin, and the ECH result is very encouraging that an almost 100% cleavage of the β-O-4 ether bond was observed.

The β-O-4 ether bond is cleaved very fast. As indicated in the kinetic study from Figure 5.11, guaiacol, and phenol were released into solution very quickly. About 80% of the total amount of cyclohexanol, phenol, and guaiacol obtained in the 6 h ECH solution

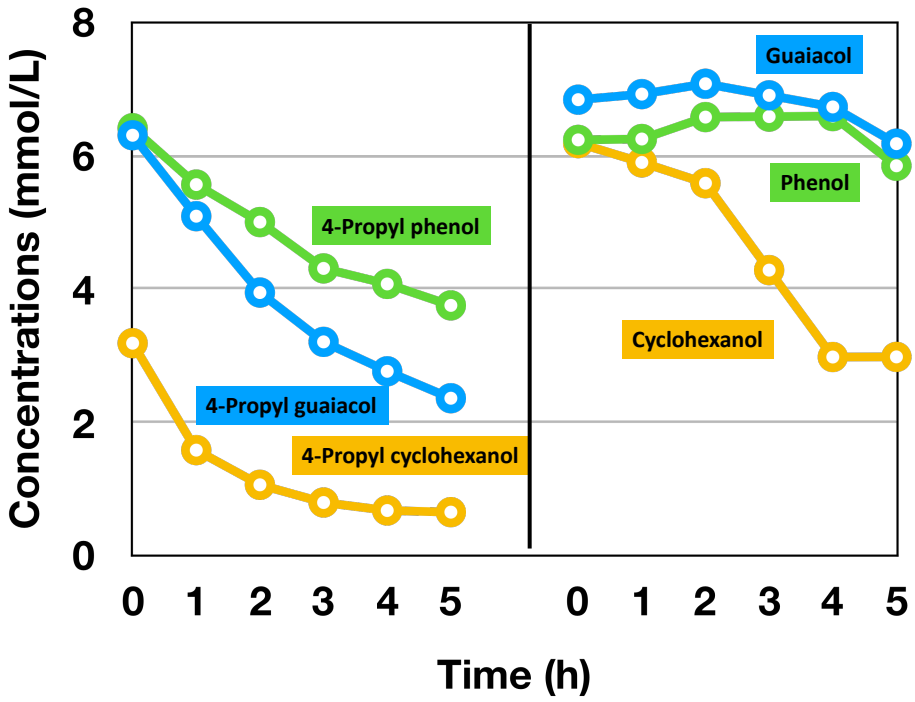

Figure 5.10: The evaporation rates of 4-alkyl guaiacol, 4-alkyl phenol, 4-alkyl cyclohexanol compared with those of guaiacol, phenol, and cyclohexanol. The experiment is done by dissolve the initial concentrations of compounds in 30 mL D_2O with 0.2 g NaOH (pH is 11) in the cathode half-cell at 90 °C without catalysts.

has been released after the first 1 hour of ECH. The amount of cyclohexanol, phenol, and guaiacol in the bulk solution observed over the course of the reaction represented over 70% of the compounds observed, suggesting that cyclohexanol, phenol, and guaiacol desorbed from the RaNi surface quickly while most of the other half of the dimer after ether cleavage were desorbed relatively slower. Since the mass balance of the ECH reactions showed an increasing trend from around 55% to around 65% at the end, it is possible that more products from the guaiacylpropane part of the dimer molecule remained to be desorbed from the catalyst. Another factor that may contribute to the unbalanced ratio could be the result of fast evaporation rates of the more hydrophobic longer 4-alkyl guaiacol, 4-alkyl phenol and 4-alkyl cyclohexanol compounds as shown in Figure 5.10. In contrast, guaiacol and phenol do not evaporate in any significant amounts but cyclohexanol tends to evaporate similarly

as the alkyl compounds.

From our previous ECH of monomer studies with terminal hydroxyl 3-guaicylpropan-1-ol (**31**) and 1-guaiacylpropan-1,3-diol (**40**) in the last chapter, no cyclohexanol, phenol, or guaiacol were observed as products, it is highly unlikely that cyclohexanol, phenol, and guaiacol are produced from (**23**) by the C-C cleavage of the aryl-αC bond. Such C-C cleavage products only appear via deformylation reactions from the ECH of α-terminal alcohol. The α-terminal alcohol that can produce guaiacol comes from reduction of vanillin (4-formyl guaiacol), which maybe produced from the cleavage of the α-β bond of (**23**) via a retro-aldol reaction after the terminal γ-OH is in-situ oxidized to a carbonyl on a nickel surface.

Although theoretically possible, the αC-βC cleavage reaction has not been observed on a RaNi catalyst via ECH from our studies or others. We, therefore, designed an ECH of a γ-carboxylate ester β-O-4 model (**24**) to test if any vanillin (**23**) or vanillin ECH products would be observed. As shown in entry 2 of Table 5.5, though no vanillin was directly observed, 4-methylguaiacol (**27**) and cresol (**26**), familiar ECH products of vanillin, both of which are absent from the ECH of (**23**), were produced in very limited amounts.

Based on all of the monomer studies from the last chapter and the present β-O-4 studies, we mapped the reaction pathways for the ECH of (**23**) to the products as shown in Figure 5.12. The dimer was quickly cleaved into guaiacol (**25**) and 1-guaiacyl-1,3-propanediol (**40**) based on the fast release of guaiacol into the solution. As usual, guaiacol was demethoxylated and hydrogenated to phenol (**18**) and cyclohexanol (**19**). Though (**40**) was not explicitly tested by ECH its benzyl derivative (**41**) was instead, due to the synthetic challenge of debenzylating a benzylic alcohol. Both the benzyl group and α-OH of (**41**) were almost completely hydrogenated within the first 1 hour forming (**31**) and toluene. The direct demethoxylation and hydrogenation of (**31**) generated (**32**) and (**33**). Meanwhile,

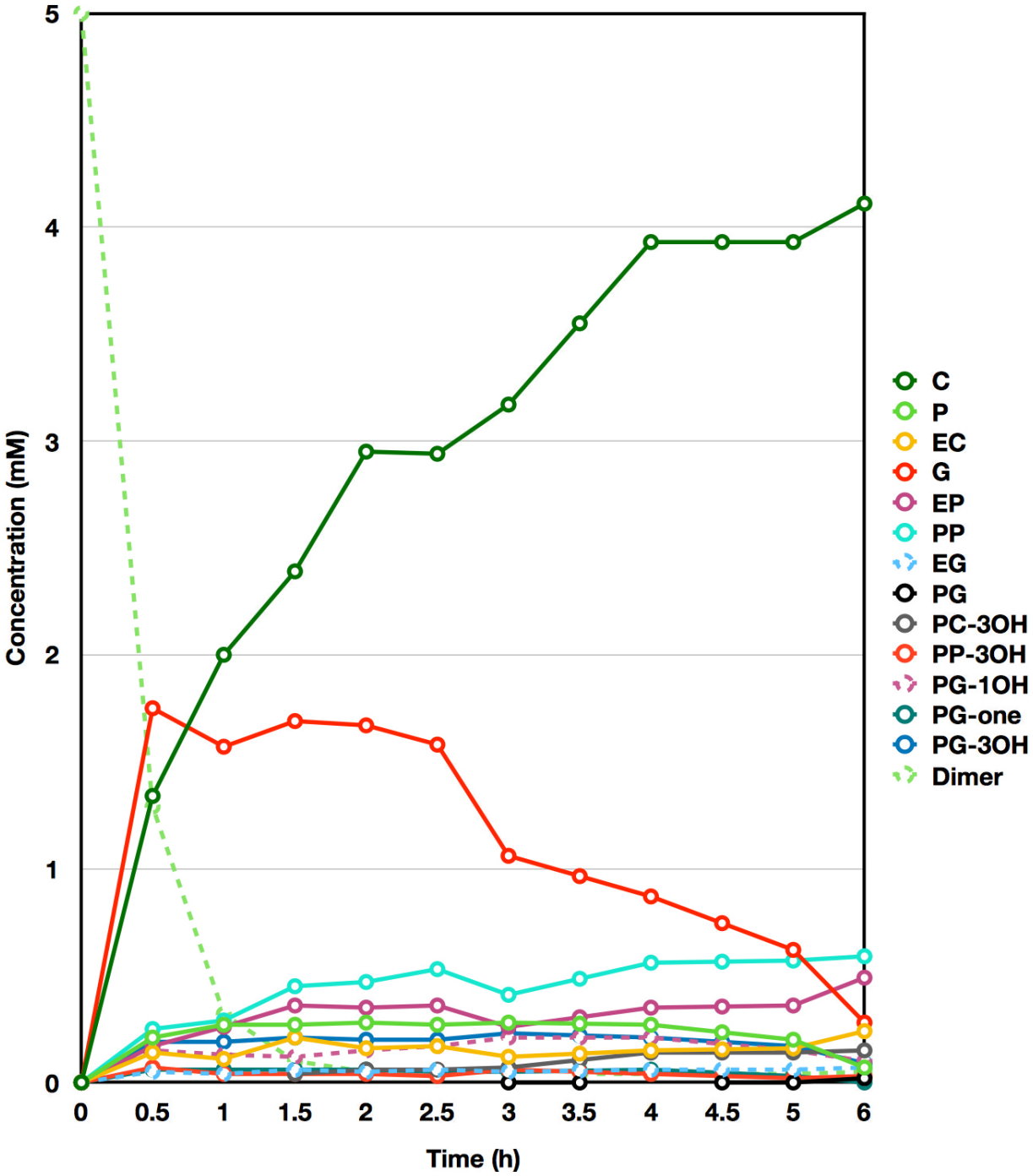

Figure 5.11: The kinetic study of β-O-4 dimer. Concentrations here were normalized so that the mass balance was 100%. The actual mass balance was 65% at the end of the ECH. **C**: cyclohexanol; **P**: phenol; **EC**: 4-ethylcyclohexanol; **G**: guaiacol; **EP**: 4-ethylphenol; **PP**: 4-propylphenol; **EG**: 4-ethylguaiacol; **PG**: 4-propylguaiacol; **PC-3OH**: 4-(3'-hydroxypropyl)cyclohexanol; **PP-3OH**: 4-(3'-hydroxypropyl)phenol; **PG-1OH**: 4-(1'-hydroxypropyl)guaiacol; **PG-one**: propiovanillone; **PG-3OH**: 4-(3'-hydroxypropyl)guaiacol; **Dimer**: the β-O-4 starting material. See Table 5.5 for the structures.

ethylguaiacol (**30**) was generated from the deformylation reaction of (**31**) and the sequential demethoxylation and hydrogenation produced ethylphenol (**28**) and ethylcyclohexanol (**29**). Moreover, (**31**) underwent hydrogenation of the terminal alcohol to form (**34**), and demethoxylation to form (**35**) which was further hydrogenated to (**42**). In addition, very small amounts of (**37**) and (**36**) (see Table 5.5, PG-1OH, and PG-one) were produced; this is most likely the direct hydrogenation of the terminal alcohol of (**40**) and the dehydrogenation reaction on the nickel surface.

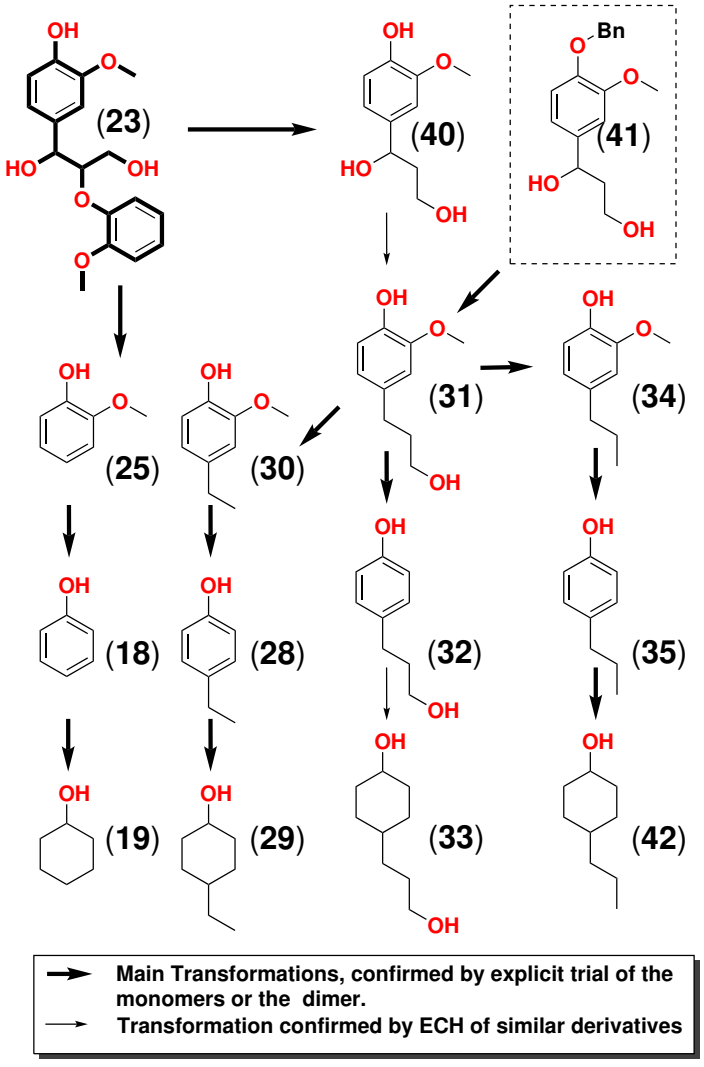

Figure 5.12: The mechanism of β-O-4 dimer ECH.

5.2.6 Lignin

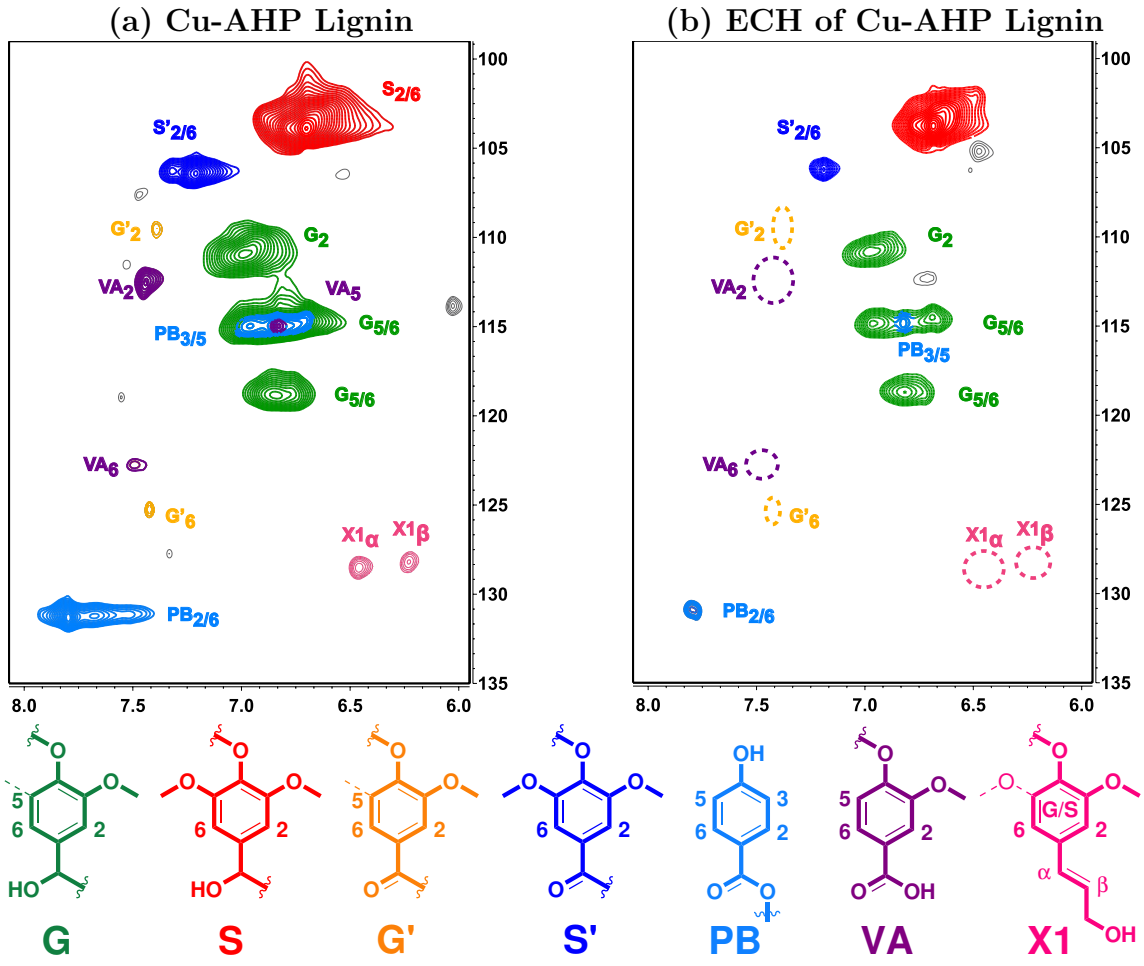

Figure 5.13: The aryl areas of HSQC NMR of (a) the original Cu-AHP lignin sample and (b) that of ECH products of the lignin. The assignments of the HSQC NMR were based on literature assignment of Cu-AHP Lignin.[20]

The success of β-O-4 dimer ECH and the understanding of other lignin linkages including β-5, β-β, 5-5, and 4-O-5 linkages, brings us to the next stage of research, which is to conduct ECH on real lignin polymers. Cupper Alkaline Hydrogen Peroxide Lignin (Cu-AHP Lignin)[20] was kindly offered from Dr. Hegg's group in Department of Biochemistry and Molecular Biology at MSU. Cu-AHP Lignin is collected from the waste stream of an alkaline hydrogen peroxide (AHP) pretreatment of poplar wood in the presence of copper(II) 2,2'-bipyridine, which is an effective method to improve the enzymatic digestibility of poplar and many other

biomass feedstocks.[20] The Cu-AHP pretreatment was performed in a 10% NaOH solution with 1 mM copper and 2 mM 2,2'-bipyridine for 10 h at 30°C, followed by the addition of 100 mg/g biomass loading of H_2O_2 and another 14 h at 30°C.

The Cu-AHP Lignin contains 87 wt% lignin with 2 wt% ash, 3 wt% xylan contents, and residual copper and 2,2'-bipyridine. The HSQC NMR of the original Cu-AHP Lignin (Figure 5.14) shows that the lignin contains many more of the syringyl type aromatic ring subunits than of the guaiacyl type, as, indicated by the S/G ratio of 1.8. It should be pointed out that this analysis does not include 5-5, 4-O-5, and other minor linkages since these linkages have either no or invisible HSQC signals. About 89% of the linkages are β-O-4 linkage. β-5 and β-β linkages only compose only around 10% of all linkages from the HSQC analysis. There are some degree (13%) of α-OH oxidation from the pretreatment with hydrogen peroxide. Cinnamyl alcohol, p-hydroxybenzoate, vanillate end-groups are also observed in the Cu-AHP lignin.

The HSQC (heteronuclear single quantum coherence) NMR was used to monitor lignin structure changes. The assignments of lignin HSQC NMR peaks are according to the database[214] of Dr. John Ralph from University of Wisconsin, Madison and other literature.[21–25,215,216]

The direct ECH of Cu-AHP Lignin does not give a promising result. As shown in Figure 5.14 (b), there is not much different in the linkage areas of the HSQC NMR before and after ECH, except the disappearance of olefin group as indicated by the loss of olefin-protons (see Figure 5.13 and allylic methylene (see Figure 5.14) of allylic alcohol X1. Meanwhile, in the aryl area of the HSQC, as shown in Figure 5.13, the majority of the p-hydroxybenzoate (PB) and all of the vanillate (VA) has been converted to other compounds. From historical data and our previous study of the ECH of a carboxylic acid (ferulic acid), no carboxylic

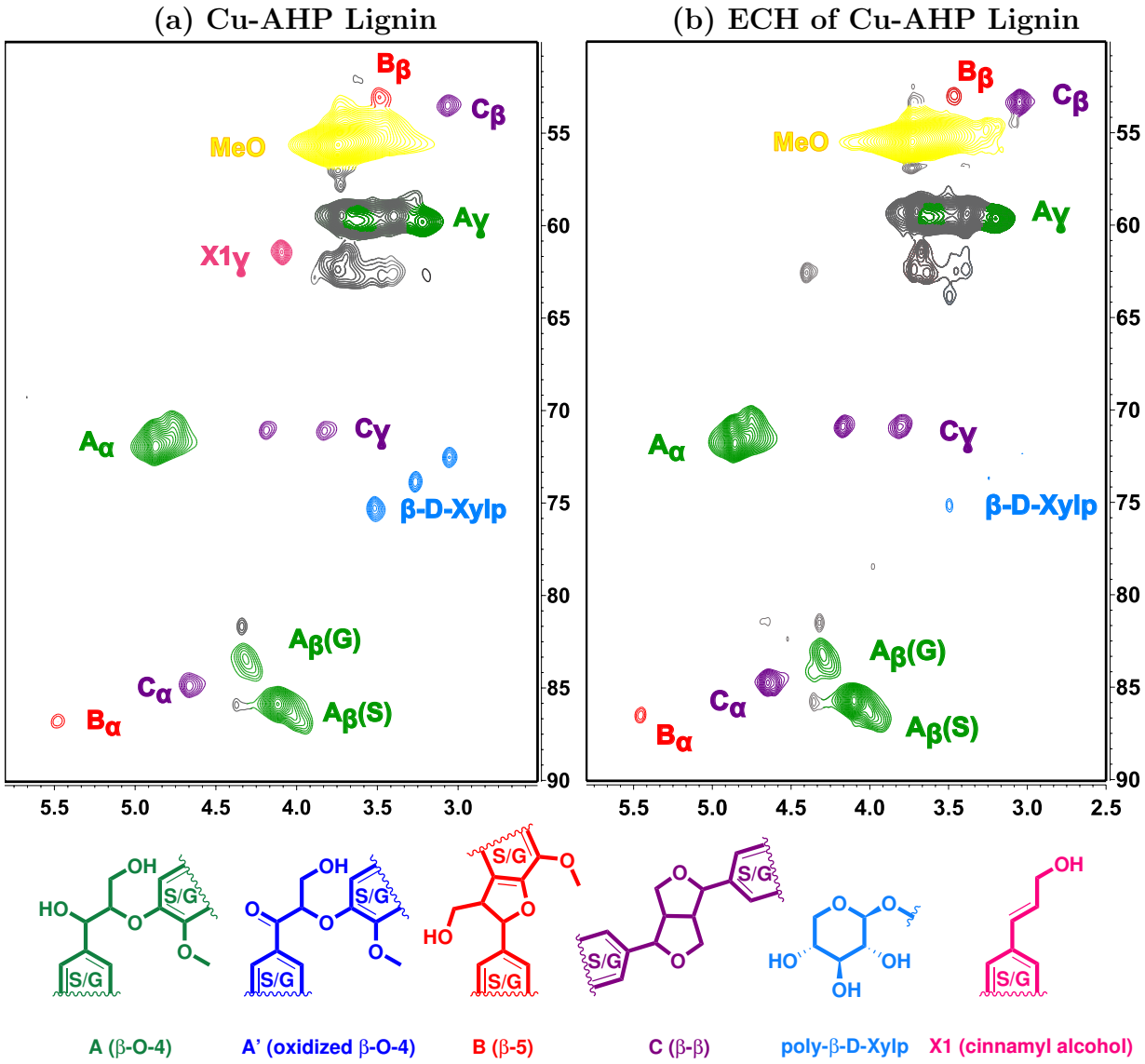

	Link./Ar%				Link. ratio	Ar ratio		
Treatment	A	A'	B	C	(A+A'):B:C	S/G	S'/S	G'/G
No	69	3	5	4	89:6:5	1.8	0.15	0.04
ECH	61	0	3	4	90:4:6	2.3	0.06	0

Link. is linkage. **Ar** is arene. **Link./Ar%** is calculated by using the average HSQC integrals for each linkage, which is normalized to 1 proton per linkage, divided by the average HSQC integral of arene rings, also normalized to 1 proton per aromatic ring. **A**: β-O-4 linkage (green). **A'**:oxidized β-O-4 linkage (blue). **B**: β-5 linkage. **C**: β-β linkage. **S**: syringyl aryl units. **G**: guaiacyl aryl units. **S'**: syringyl unit connected to a α-carbonyl (oxidzed linkage). **G'**: guaiacyl unit connected to a α-carbonyl.

Figure 5.14: The linkage areas of HSQC NMR of (a) the original Cu-AHP lignin sample and (b) that of ECH products of the Cu-AHP lignin. The assignments of the HSQC NMR were based on literature assignments of lignin.[20–24]

acid reduction can be observed under basic condition. The GC-MS analysis does capture some free p-hydroxybenzoic acid in the final product mixtures.

Quantification results from Figure 5.14 were calculated based on the HSQC NMR integrals. Only the non-overlapping peaks of each linkage were selected to calculate the average integrals of each linkage (A, A', B, C), which is then normalized to 1 proton per linkage. Link./Ar% is calculated by using the normalized average integral of each linkage divided by the summation of HSQC integral of arene rings, including S, S', G, G' and also was normalized to 1 proton per type arene ring. Syringyl/Guaaicyl ratio (S/G) was calculated by using the normalized arene ring integrals of syringyl units (S, S') divided by the normalized arene ring integrals of guaiacyl units (G, G').

The HSQC NMR spectra show that after ECH, the Link./Ar%, the Link. ratio did not change significantly. The S/G ratio increased from 1.8 to 2.3 indicated that slight demethoxylation happens, more to guaiacyl than to syringyl units. The drops in S'/S and G'/G ratios indicate that carbonyl reduction did happen.

5.2.7 The oxidation of lignin with DDQ

Based on our monomer studies, we understand that our catalyst is sensitive to steric factors. Since lignin is a big polymer, we suspect that the three-dimensional lignin framework did not get adsorbed on nickel surface easily. We have known that carbonyl groups increased the adsorption energies of lignin monomers from the theoretical calculation results of the previous chapter. Therefore, attempts have been made to oxidize the most oxidation-susceptible α-OH using a DDQ strategy[25] as reported by Westwood's group. Although this strategy is neither economically ideal nor green for the purpose of lignin to fuel conversion, for the starting stage of laboratory demonstration, we apply Westwood's methodology because DDQ oxidation is easy to conduct. It is important to realize that there is a catalytic oxidation of α-hydroxyl of lignin via electrochemistry reported by Shannon Stahl.[202]

The DDQ (2,3-Dichloro-5,6-dicyano-1,4-benzoquinone) oxidation transformed lignin significantly as shown by the dramatic change of the HSQC in Figure 5.15. The majority of α-OH sites from β-O-4 linkages have been oxidized to carbonyl groups as indicated by the A:A' ratio of linkages, which changed from 23:1 to about 0.4:1. The disappearance of linkage B (β-5) and C (β-β) peaks indicated that DDQ not only oxidized α-OH into a carbonyl but also transform linkage B and C into other structures.

As shown in Figure 5.16 a), the β-O-4 dimer (**43**) has been known to be selectively oxidized into a α-keto dimer (**44**) almost completely at room temperature,[25] and this methodology can be also effective to oxidize Cu-AHP lignin, as shown by the increased ratio of A:A'.

β-β linkage peaks (C, colored as purple in Figure 5.15) partially disappeared after the DDQ oxidation, and the linkage per aromatic ring dropped from 4% to 1%. With 1 equivalent

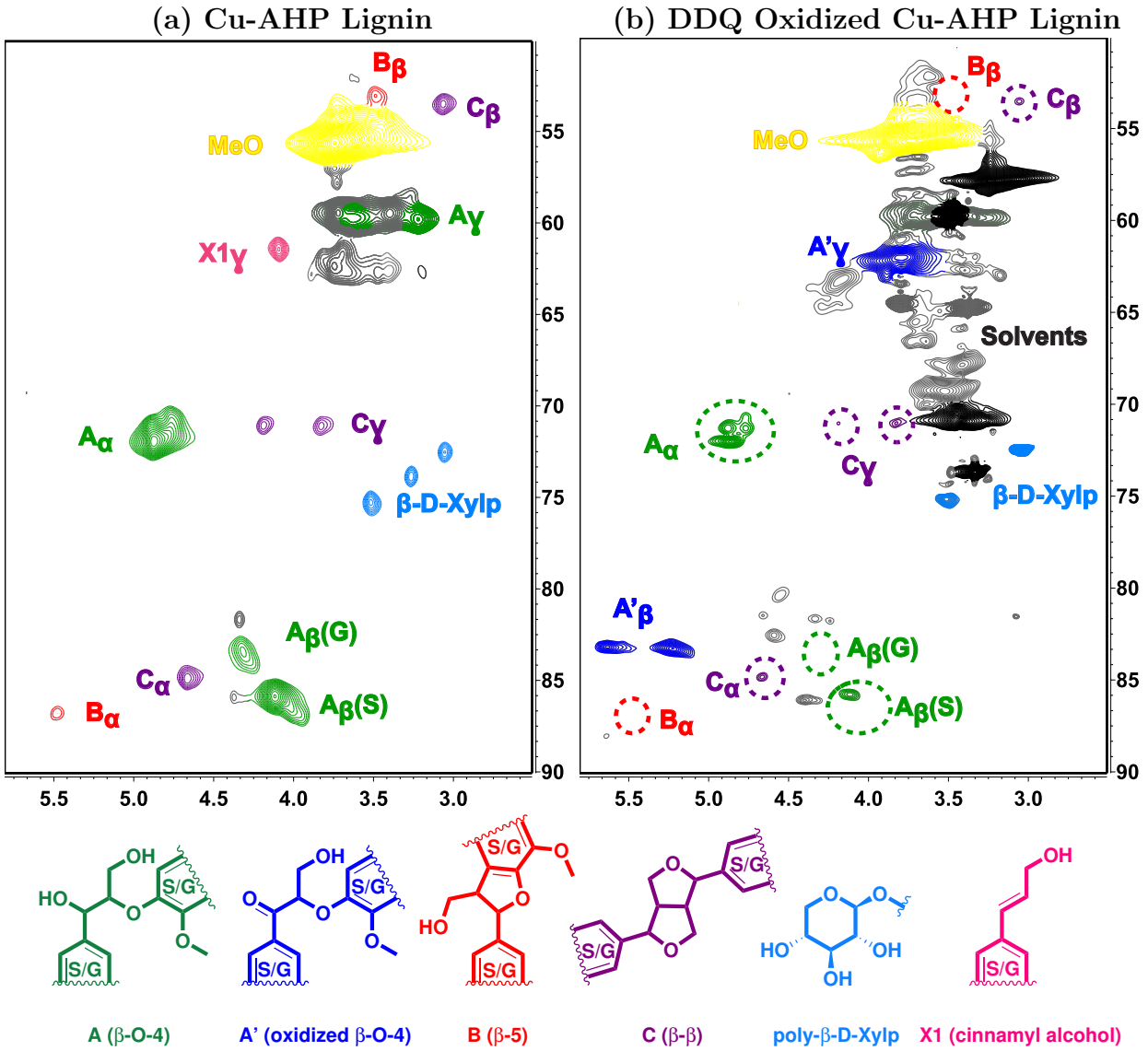

	Link./Ar%				Link. ratio	Ar ratio			GPC MW. (g/mol)		
Treatment	A	A'	B	C	(A+A'):B:C	S/G	S'/S	G'/G	Mn	Mw	DPI
No	69	3	5	4	89:6:5	1.8	0.15	0.04	12396±1408	28680±1567	2.6±0.2
DDQ	20	48	4	1	93:5:2	2.3	0.9	1.9	13341	39777	3.9

The explanations for for abbreviations **A, A', B, C, Link., Ar, S, G, S', G'** see Figure 5.14.

Figure 5.15: The HSQC NMR of (a) the original Cu-AHP lignin sample and (b) that of DDQ oxidation products of the Cu-AHP lignin. The HSQC NMR of the oxidized lignin was assigned according to a similar DDQ oxidation of lignin study reported by Westwood.[25]

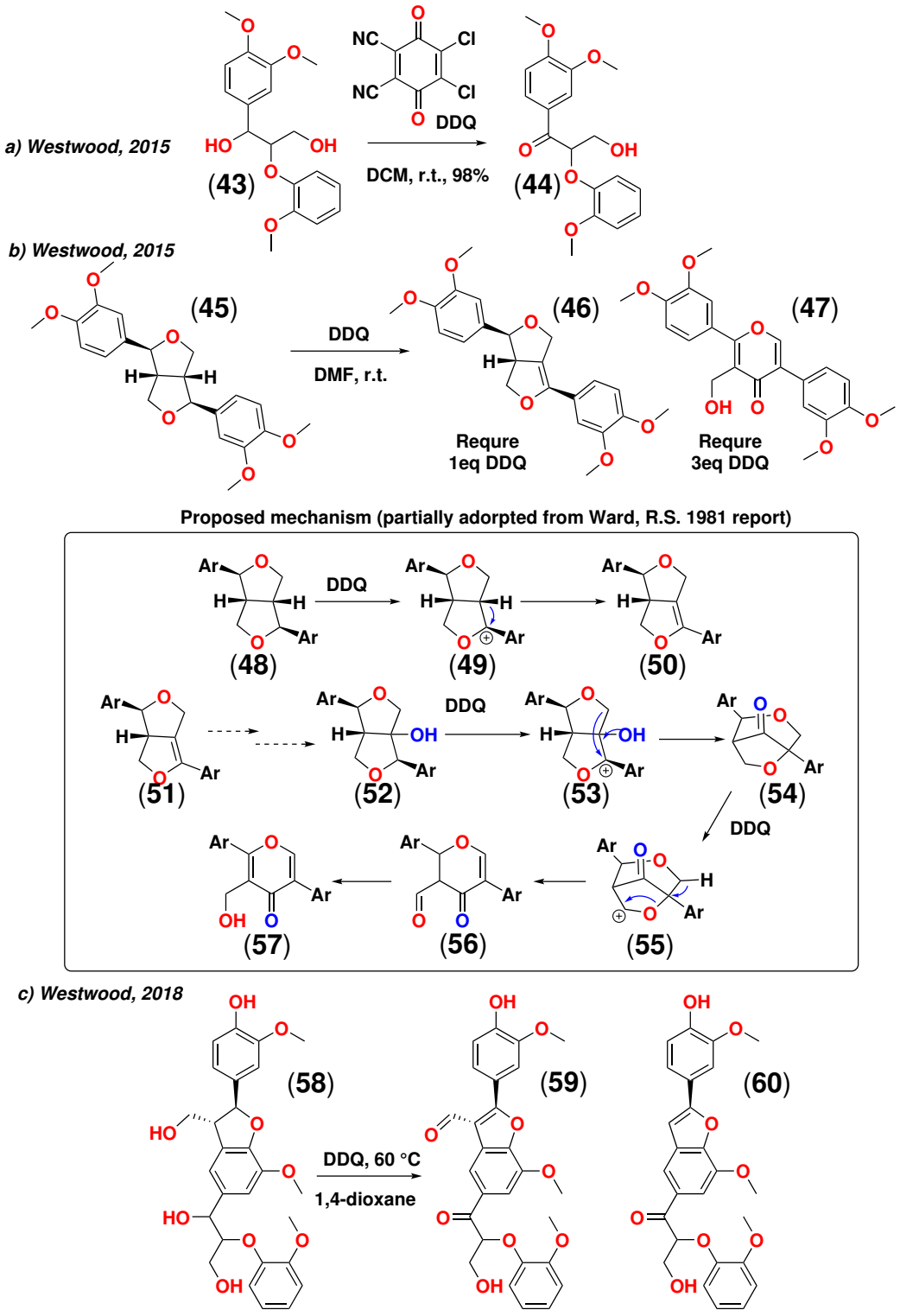

Figure 5.16: The DDQ oxidations of lignin dimers and the proposed mechanism.

of DDQ, β-β dimer (**45**) (C in lignin) was known to become a α-β olefin dimer (**46**) as shown in b). Given 3 equivalent of DDQ, the vinyl dimer (**46**) can be converted into a totally different carbon framework, a pyrone derivative (**47**). It has been long known that the β-hydroxyl derivative of the β-β dimer, (**52**), can be oxidized to a pyrone compound (**57**) through a carbocation intermediate (**53**). The carbocation initiates a rearrangement reaction to generate (**54**) via the mechanism shown in c) of Figure 5.16. Afterwards, the third equivalent of DDQ oxidizes the (**54**) and generates a stabilized carbocation (**55**) next to the ether oxygen, which initiates another rearrangement reaction to the pyrone framwork (**56**). The final product (**57**) is generated after two proton transfer steps from (**56**).[217] Consequently, a hydration reaction bridging (**51**) and (**52**) would explain the generations of a pyrone (**47**) from the DDQ oxidation of (**45**). Westwood's group found that the pyrone formation reaction also occurs to the DDQ oxidation of lignin.[217] However, the pyrone characteristic peaks do not appear in our DDQ oxidized lignin HSQC NMR. The vinyl hydroxyl hydroxymethyl peak (4.7 ppm, 52 ppm) of pyrone (**47**) and the vinyl ether sp^2 C-H peak (8.2 ppm, 147 ppm) are not visible at our NMR resolution. Since Cα, Cβ, and Cγ peaks disappeared partially, the β-β linkage C must be transformed into any of those intermediate structures from the β-β dimer to the pyrone (**47**) type structures in the lignin polymer chain.

Linkage B peaks also partially disappeared after the DDQ oxidation. There is no rearrangement reaction here, like what happens to linkage C. The Westwood group reported[215] that a β-5 dimer (**58**) can be oxidized to an enal (**59**) and a deformylation product (**60**). However, the aldehyde proton from the enal (10.3 ppm, 186.4 ppm) was not visible at our NMR resolution.

5.2.8 The ECH of DDQ oxidized lignin

The ECH of DDQ oxidized lignin not only reduced the α-carbonyl moieties that DDQ had formed from α-OH sites but also led to a lot of other reactions and effectively reduced the molecular size of the lignin. As shown in Figure 5.17, the number average molar mass (Mn) determined by Gel permeation chromatography (GPC) has dropped from the DDQ oxidized lignin of 13341 g/mol to around 2101 g/mol after ECH and the weight average molar mass (Mw) also decreased dramatically from 39777 g/mol to 3077. Meanwhile, the lignin molecules become more uniform as indicated by the DPI decrease from 3.9 to 1.5.

The decrease of molecular size is largely attributed to the cleavage of β-O-4 linkages of A' and A. The Link./AR% has of A' has decreased from 48% (DDQ lignin) to only 0.7% (after ECH) along with the decrease of that of A from 20% to 16%. This indicates that almost all of the β-O-4 linkages of A' and some of A have been cleaved. On the other hand, the Link./Ar% of β-5 (B) decreased presumably via β-ether hydrogenation and that of β-β (C) linkages did not change.

Demethoxylation reaction proceeds much more for guaiacyl units than syringyl units. The S/G ratio increased about 3 times after the ECH of DDQ oxidized lignin. Since the conversion from G to S is considered impossible under our conditions, the S/G ratio increase can only be attributed to the demethoxylation of G units.

The reduction of α-carbonyl from S' units is much less complete than the reduction of G' unit α-carbonyl. The S'/S ratio did not change much after the ECH, while the G'/G decreased dramatically from 1.9 to 0.16.

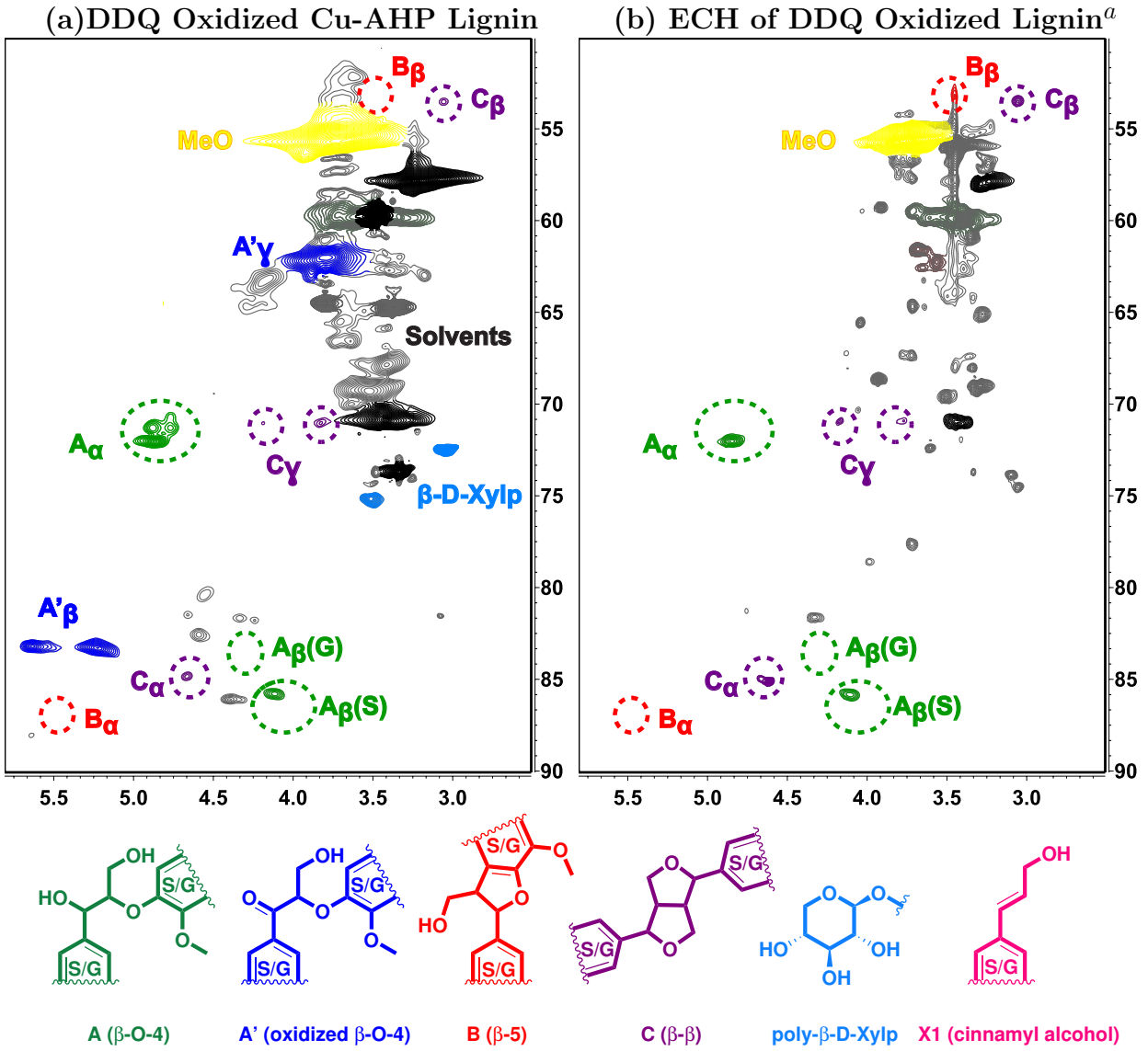

Treatment	Link./Ar%				Link. ratio	Ar ratio			GPC MW. (g/mol)		
	A	A'	B	C	(A+A'):B:C	S/G	S'/S	G'/G	Mn	Mw	DPI
No	69	3	5	4	89:6:5	1.8	0.15	0.04	12396±1408	28680±1567	2.6±0.2
DDQ	20	48	4	1	93:5:2	2.3	0.9	1.9	13341	39777	3.9
DDQ & ECH	16	0.7	0.5	2	87:2:11	5.3	1.1	0.16	2101±321	3077±397	1.5±0.03

The explanations for for abbreviations **A, A', B, C, Link., Ar, S, G, S', G'** see Figure 5.18.
GPC MW: The polymer molecular weights estimated from Gel Permeation Chromatography. **Mn**: Number average molar mass. **Mw**: Mass average molar mass. **PDI**: Polydispersity index. [a] the lignin is Cu-AHP lignin.

Figure 5.17: The HSQC NMR of (a) the DDQ Oxidized Cu-AHP Lignin sample and (b) that of ECH of DDQ oxidized Cu-AHP lignin.

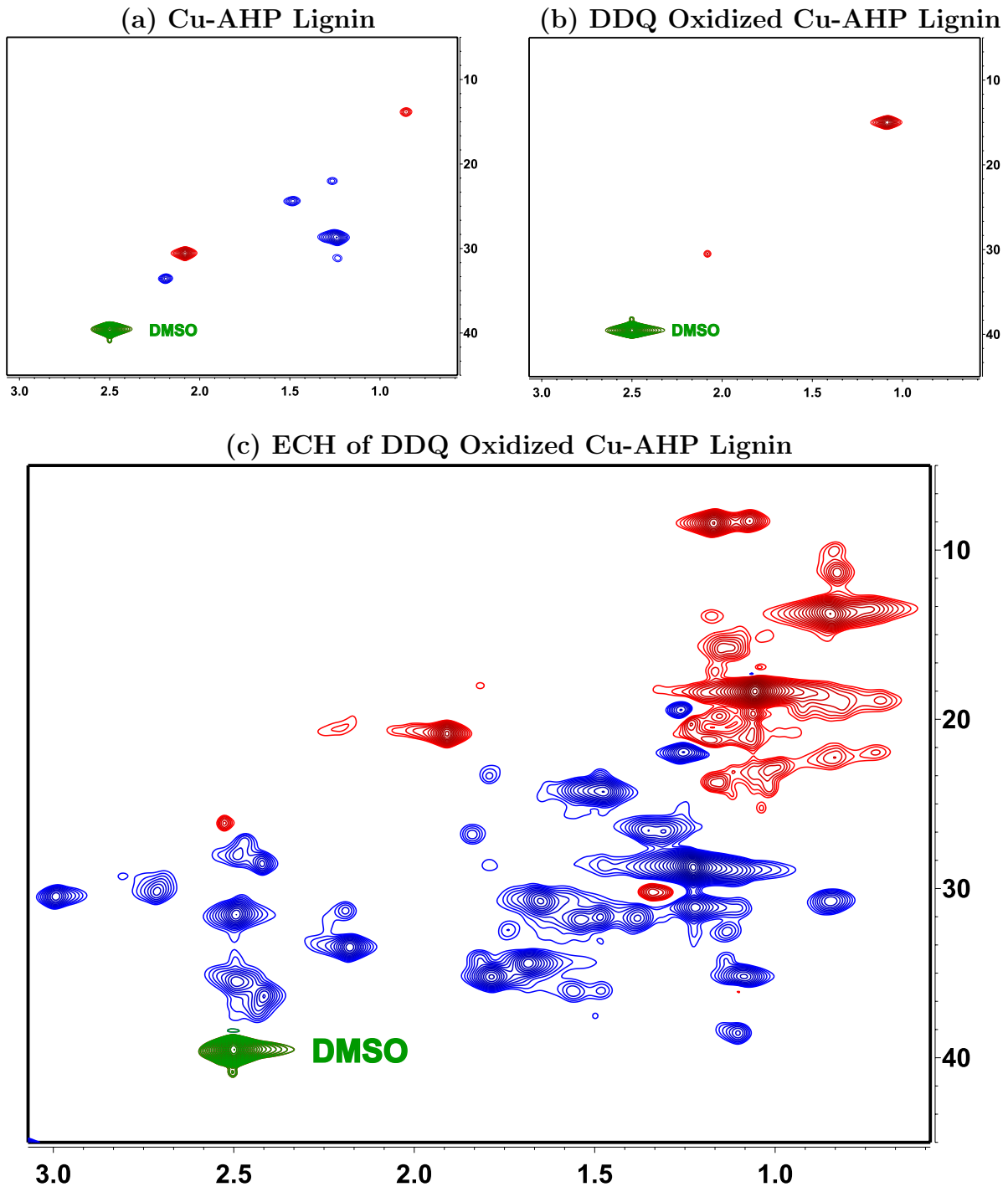

Figure 5.18: The aliphatic area of HSQC NMR of (a) the original Cu-AHP lignin sample, (b) the DDQ oxidized lignin, and (c) that of ECH of DDQ oxidized lignin. Blue color indicates methylene (CH_2) and red color indicates CH or CH_3.

Deoxygenation reactions also proceeded during the ECH of DDQ-lignin. Ether and α-hydroxyl bonds are prone to reduction by ECH as indicated by our dimer studies. In real lignin, similarly, the appearance of a lot of new methylene peaks (blue color indicates methylene) between 2.0 to 3.0 ppm, as shown in Figure 5.18, indicates that these methylene are next to benzene ring, the α-position. The methylene groups from 0.5 to 2.0 ppm are probably partly from the cleavage of β-O-4 bonds resulted in β-methylene, and partly from the hydrogenation of aromatic ring. The red color peaks between 0.5 and 2.0 ppm are mainly β- or γ- methyl groups from the 4-ethyl or 4-propyl substituted aromatic units. The very unique isolated red peak at (1.3 ppm, 30 ppm) is most likely corresponding to the CH at the intersection of alkyl and cyclohexane of 4-alkylcyclohexanol as indicated by the coincidence peak coordinates to the HSQC of 4-methylcyclohexanol (1.3 ppm, 31 ppm).

5.3 Experimental

RaNi cathode preparation standard procedure: Preparation of the RaNi cathode uses a slightly modified method reported by Lessard[19,125] by trapping nickel-aluminum alloy particles in an electro-deposited nickel matrix. The nickel(II) chloride hexahydrate for the plating bath and nickel-aluminum alloy (50:50 by weight) were purchased from Sigma-Aldrich. On the cathodic side, a square of stainless steel 314 screen (50 mesh, 2.5 × 2.5 cm^2) is submerged in 50 mL of nickel-ammonia plating solution with nickel aluminum alloy powder stirred in suspension; and a nickel bar facing parallel to the stainless mesh is used as the sacrificial anode. The plating current density is maintained at 60 mA cm^{-2} for 6 h. Every 0.5 h, the electrode is turned 180° to get even deposition on both sides. Afterward, the plated electrodes are activated in NaOH solution (30 wt.%) for 6 h at 70 °C.

IPA-RaNi cathode preparation: a RaNi cathode was put into a container with 50 mL of isopropyl alcohol and the container was capped. The cathode was kept in isopropyl alcohol for at least 12 h and rinsed with deionized water before use.

ECH standard procedure: ECH was conducted with a conventional divided cell separated by a Nafion 117 membrane with RaNi cathode and **CoP** anode (stainless steel coated in-situ with cobalt phosphate, rolled up from 12 × 4 cm^2 stainless steel 314 screens). 30 mL of 0.1 M pH 8 potassium borate buffer was added into the cathodic half-cell and in the anodic side was 30 mL of 0.1 M pH 7 potassium phosphate buffer. 10 mg of $Co(NO_3) \cdot 6\,H_2O$ was added into the anodic phosphate buffer to *in situ* deposit a black film of cobalt phosphate water splitting catalyst on surfaces of the anode. The current was set to 50 mA (8 mA cm^{-2}, calculated based on the electrode's single side facing the membrane and anode compartment) and the temperature to 80 to 90 °C. Before adding organic substrate, the electrode was equilibrated by electrolysis under 50 mA at 90 °C for 30 min, and the layer of a black CoP film is observed forming on the surface of the anode, serving both as water splitting catalyst and as a protection layer against the corrosion of the stainless steel. Afterward, 20 mM (5 mM for the 5-5 dimer due to its low solubility, and 5 mM for the β-O-4 dimer (**23**)) of the substrate is added to the cathode side and subjected to ECH for 6-20 h, depending on the substrate. Then the cathodic aqueous solution is acidified to pH 3 with HCl and extracted with 3 × 50 mL aliquots of dichloromethane (DCM). The solution was dried over sodium sulfate, and the solvent was removed by vacuum at room temperature, and the product was dissolved in $CDCl_3$ for NMR analysis, dissolved with dichloromethane in a volumetric flask for analysis by gas chromatography-mass spectrometry (GC-MS) analysis, or dissolved in acetonitrile for high-pressure liquid chromatography-mass spectrometry (HPLC-MS) analysis (negative mode).

Kinetic studies were conducted in the same set up described above. A 0.5 mL aliquot of the sample was withdrawn from the ECH cathodic cell into a 2.0 mL conical vial every 1 hour. The sample was acidified by adding 2 drops of concentrated HCl and extracted with 1.0 mL of DCM. 0.5 mL was withdrawn from the DCM layer and sent for GC-MS analysis. Alternatively, 2 mL of the sample was withdrawn from the ECH cathodic cell and extracted with 3 × 2 mL aliquots of DCM. The DCM was removed by vacuum at room temperature and the product was dissolved in 0.8 mL of $CDCl_3$ or d_6-DMSO for NMR analysis.

DDQ oxidation of lignin: The DDQ oxidation of lignin is adapted from Westwood's methodology.[25] To a solution of 400 mg of Cu-AHP lignin[20] in 2.24 mL of 2-methoxyethanol and 3.36 mL of 1,2-dimethoxyethane was added DDQ 40 mg and 36 mg of tert-butyl nitrite. The solution was transferred to a 25 mL pear-shaped flask, which has a septum inlet to connect with the vacuum. A magnetic stir bar was added to the flask. The flask is then equipped with a water condenser with a rubber septum on top of the condenser to seal the apparatus. The solution was cooled down in liquid nitrogen and the vacuum was applied via the side arm adapter. A balloon filled with oxygen gas connected to a syringe and needle was prepared, and the needle was inserted through the rubber septum. The flask was allowed to warm up to room temperature and heated up to 80 °C for 14 h. The dark red solution was cooled down to room temperature and was added 55 mL of diethyl ether. The solution turned orange and light yellow solid precipitated out. The solid was filtered, washed with another 20 mL of diethyl ether, and allowed to dry in a N_2 chamber. The dry product isolated was 366 mg.

ECH of Lignin: 173 mg of Cu-AHP lignin or DDQ oxidized Cu-AHP lignin was dissolved in 2 mL of pH 8 buffer solution, with the addition of 0.1 g KOH only for DDQ oxidized Cu-AHP lignin to improve its solubility. After the lignin dissolved totally, the solution was

added drop-wise into the 28 mL cathodic pH 8 borate buffer solution. The reaction was conducted at 90 °C for 8 h with 50 mA current with a IPA-RaNi cathode and then acidified with concentrated HCl in an ice bath till the pH is less than 5 and extracted with 5 aliquots of ethyl acetate 30 mL. The combined ethyl acetate solution was dried over sodium sulfate, the solvent was removed by evaporation in a N_2 gas flow. There was some insoluble solid after the acidification and extraction. The solid was collected by filtration of the water solution and the filter paper was dried under N_2 gas. The resulted yellow to orange oil from the ethyl acetate portion (130 mg) was combined with the insoluble solid (about 35 mg) from the filtration and dissolved in 5 mL of d_6-DMSO. The d_6-DMSO solution (0.5 mL) was transferred into an NMR tube. The proton and HSQC NMR were collected using the 900 MHz Bruker Avance NMR spectrometer.

5.4 Conclusions

We investigated ECH reaction with 5-types of the main lignin linkages: β-O-4, β-5, β-β, 4-O-5, and 5-5 linkages. ECH cleaved the β-O-4 dimer and 4-O-5 dimers completely and further deoxygenation and hydrogenations of the resulted monomers are similar with the ECH of the individual monomers that we investigated in the last chapter. Deformylation and the reduction of terminal γ-OH sites are also observed. β-5, β-β, and 5-5 dimer molecules are all dimers that are connected by a C-C bond. We do not expect that ECH can cleave any of these three types of linkages. To our delight, however, the hydrogenation of benzylic ether bonds and the demethoxylation of both guaiacyl (β-5 dimer) and syringyl (β-β dimer) units are observed in the more complex biphenyl frameworks.

Basic conditions are considered to be better than acidic conditions for the ECH of lignin

dimers and lignin for at least two reasons. First, the solubility of lignin dimers and lignin itself are much better under basic conditions. Second, extensive polymerizations and formations of new C-C bonds were observed under acidic conditions.

Overall, ECH is proved to be a useful tool for lignin depolymerization, deoxygenation, and hydrogenation. The ECH of the Cu-AHP lignin (containing an average of at least 125 monomeric units) showed very little change in the HSQC spectrum. However, after the oxidization of α-OH sites of β-O-4 dimers to α-carbonyls with DDQ, with additional structural changes of β-5 and β-β dimers as well, the resulting oxidized lignin can be hydrogenated to a much lower molar mass product, containing an average of 13 lignin monomeric units.

The oxidized lignin ECH product showed almost complete cleavage of the α-carbonyl β-O-4 linkages (A') and partially of the β-O-4 linkage (A). As expected, β-5 and β-β dimers are not cleaved. No information about 5-5 and 4-O-5 dimers in lignin was obtained from the HSQC studies.

This work has demonstrated a green ECH method using Raney nickel as an electrocatalyst to depolymerize, deoxygenate, and hydrogenate lignin successfully on lignin at the temperature no more than 90 °C under 1 atmosphere in an aqueous medium. Since we demonstrated that the A' type β-O-4 linkages are preferably hydrogenated to the A type, and about 30% of the β-O-4 linkages were not oxidized by the present DDQ experiments, further improvements on the α-hydroxyl oxidation steps will likely improve the ECH cleavage of lignin.

5.5 Acknowledgment

Thank Dr. Eric Hegg and Dr. Aditya Bhalla from the Department of Biochemistry and Molecular Biology kindly for offering the Cu-AHP lignin samples. Thank Dr. Daniel Holmes from Department of Chemistry at MSU for the 900 Hz NMR training.

5.6 Supplementary material

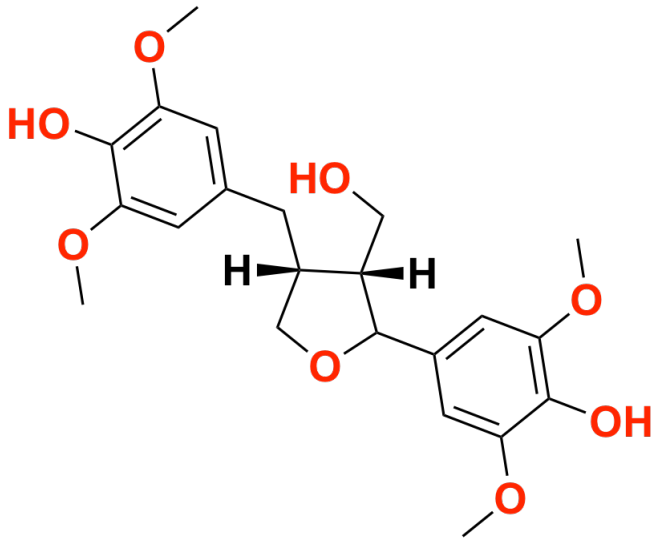

Figure 5.19: The product (3) of ECH of β-β dimer

Yellow solid.

MS (ES^-): 419.17 ($M-H^+$).

^{1}H NMR (500 MHz, Chloroform-*d*) δ 6.58 (s, 2H), 6.42 (s, 2H), 5.45 (d, J = 35.3 Hz, 2H), 4.80 (d, J = 6.5 Hz, 1H), 4.06 (dd, J = 8.6, 6.6 Hz, 1H), 3.99 – 3.92 (m, 1H), 3.90 (s, 7H), 3.88 (s, 6H), 3.85 – 3.80 (m, 1H), 3.78 (dd, J = 8.7, 6.1 Hz, 1H), 2.94 (dd, J = 13.5, 5.0 Hz, 1H), 2.73 (tt, J = 12.2, 5.5 Hz, 1H), 2.54 (dd, J = 13.5, 10.9 Hz, 1H), 2.44 (p, J = 6.9 Hz, 1H).

^{13}C NMR (126 MHz, Chloroform-*d*) δ 147.03, 133.99, 133.92, 133.06, 131.42, 105.18, 102.40, 82.97, 72.86, 60.95, 56.33, 56.31, 52.68, 42.43, 33.87.

The NMR values matches those from the literature.[218]

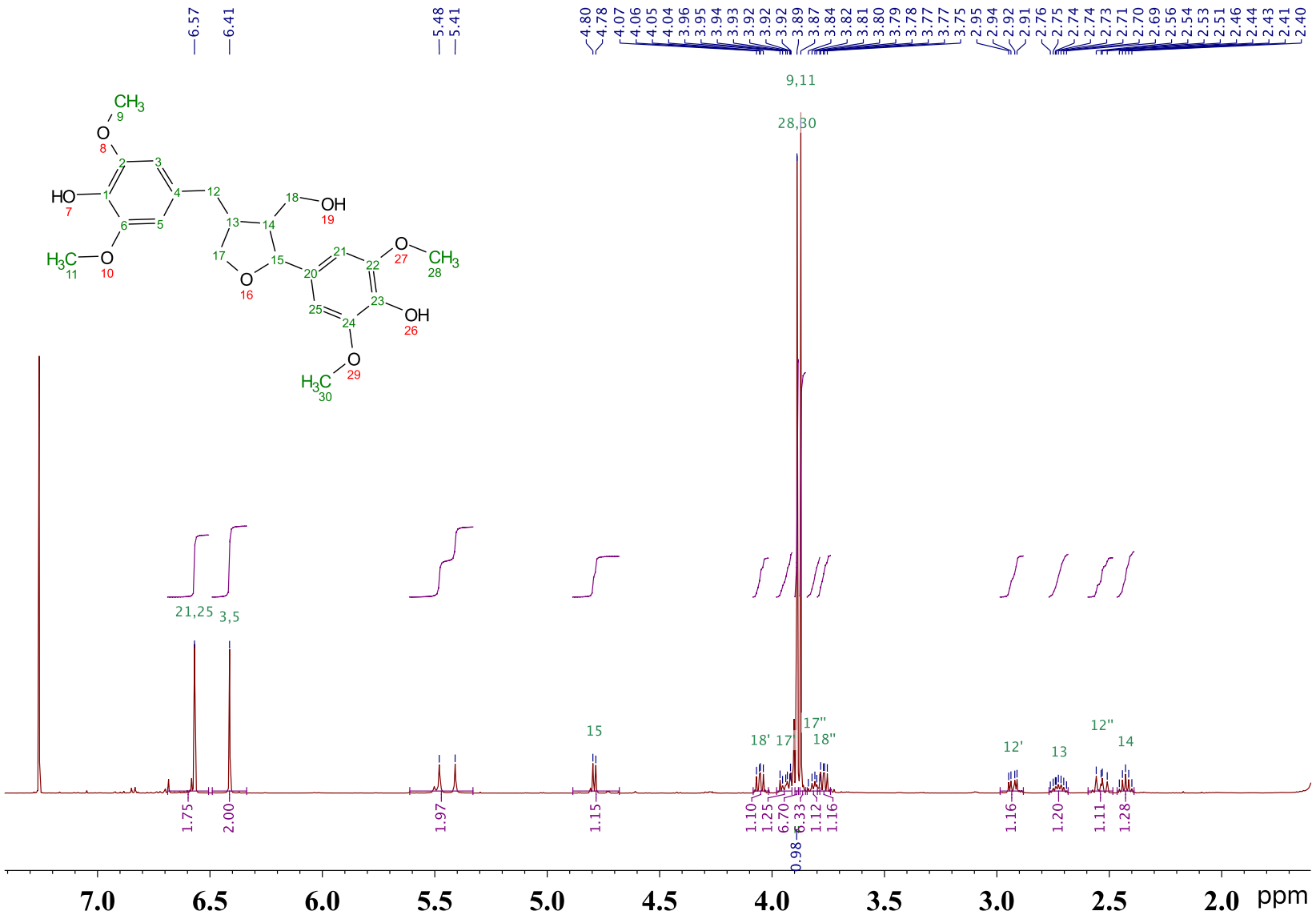

Figure 5.20: The proton NMR of the ECH product (3) of β-β dimer.

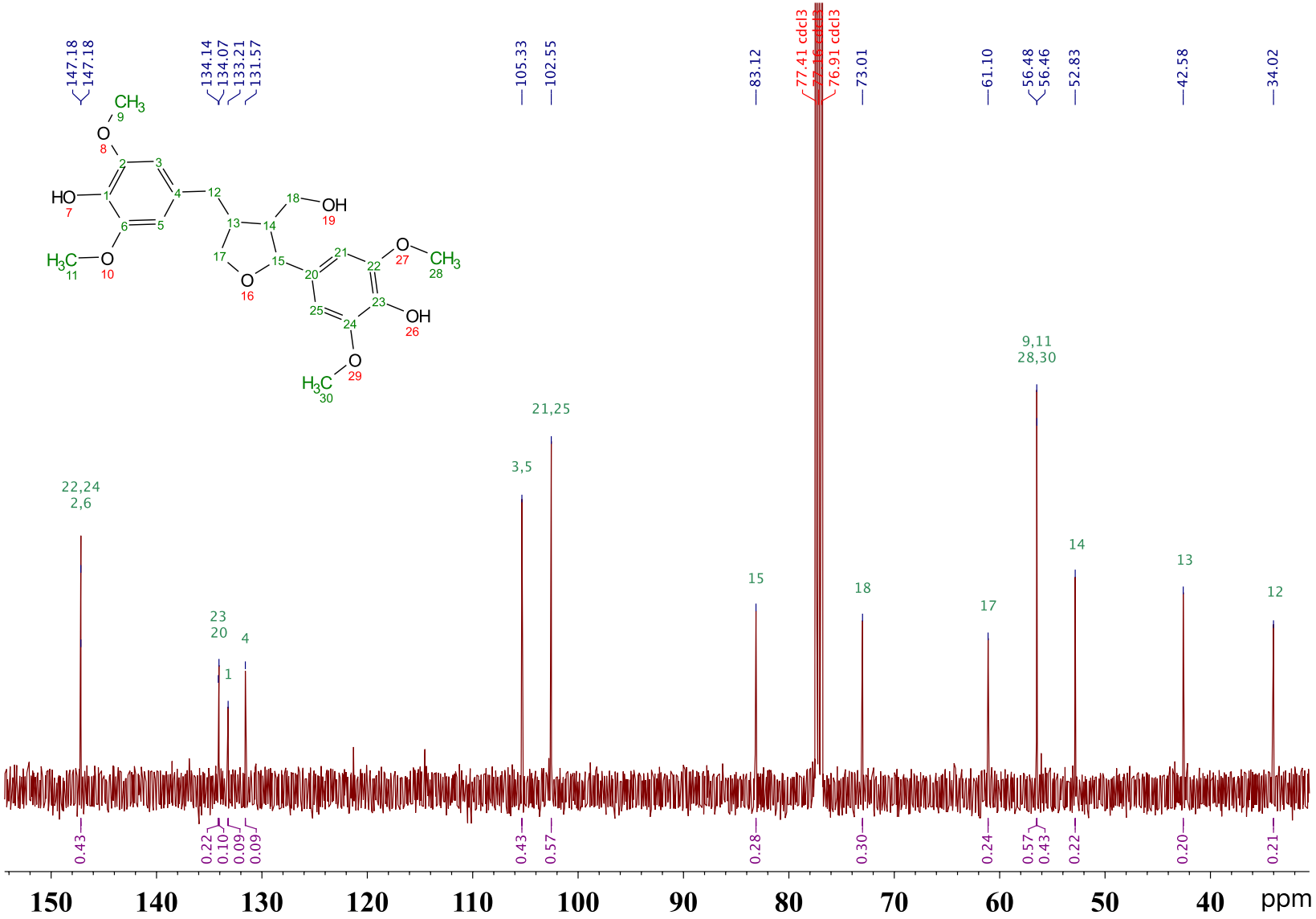

Figure 5.21: The carbon NMR of the ECH product (3) of β-β dimer.

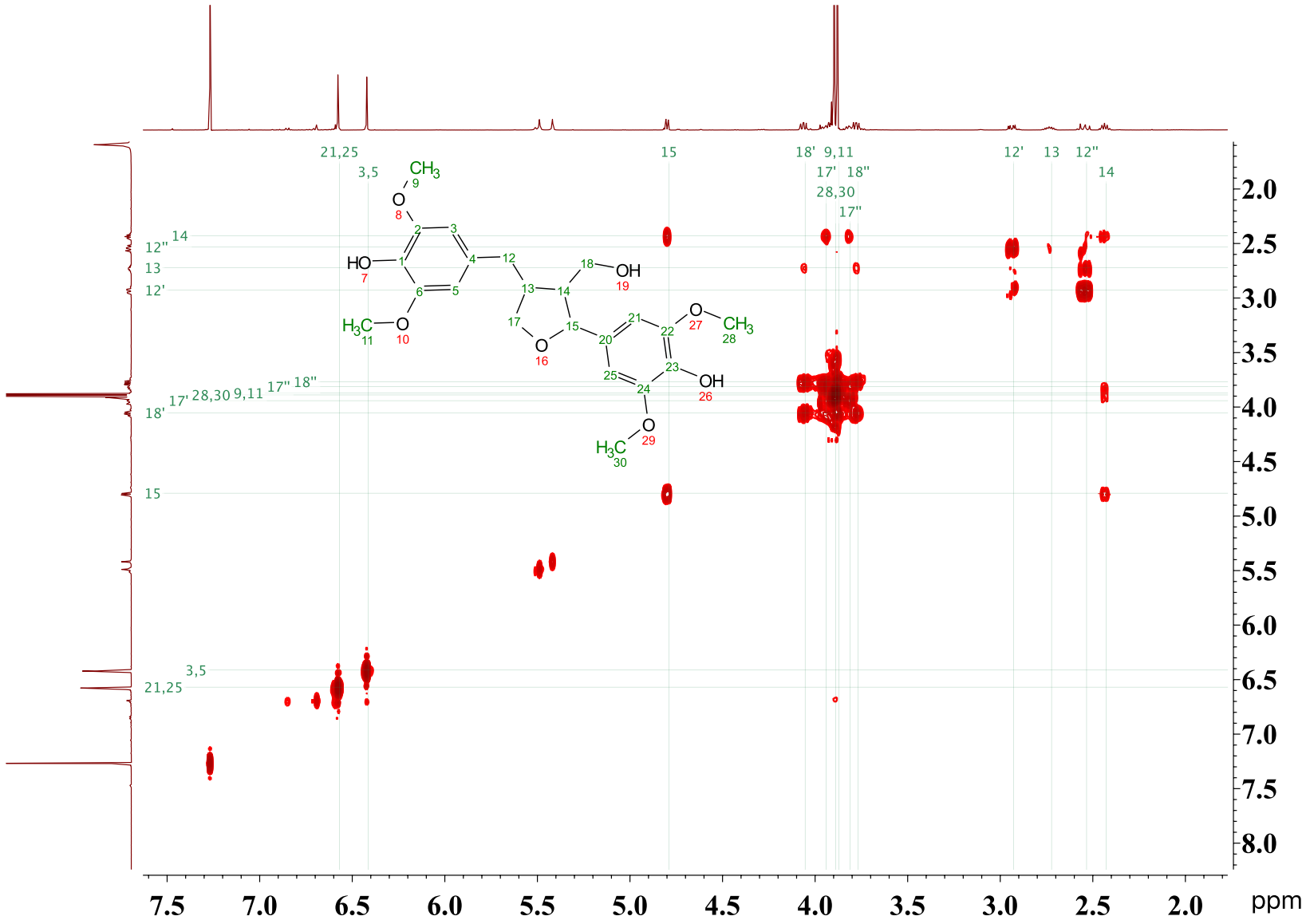

Figure 5.22: The COSY NMR of the ECH product (3) of β-β dimer.

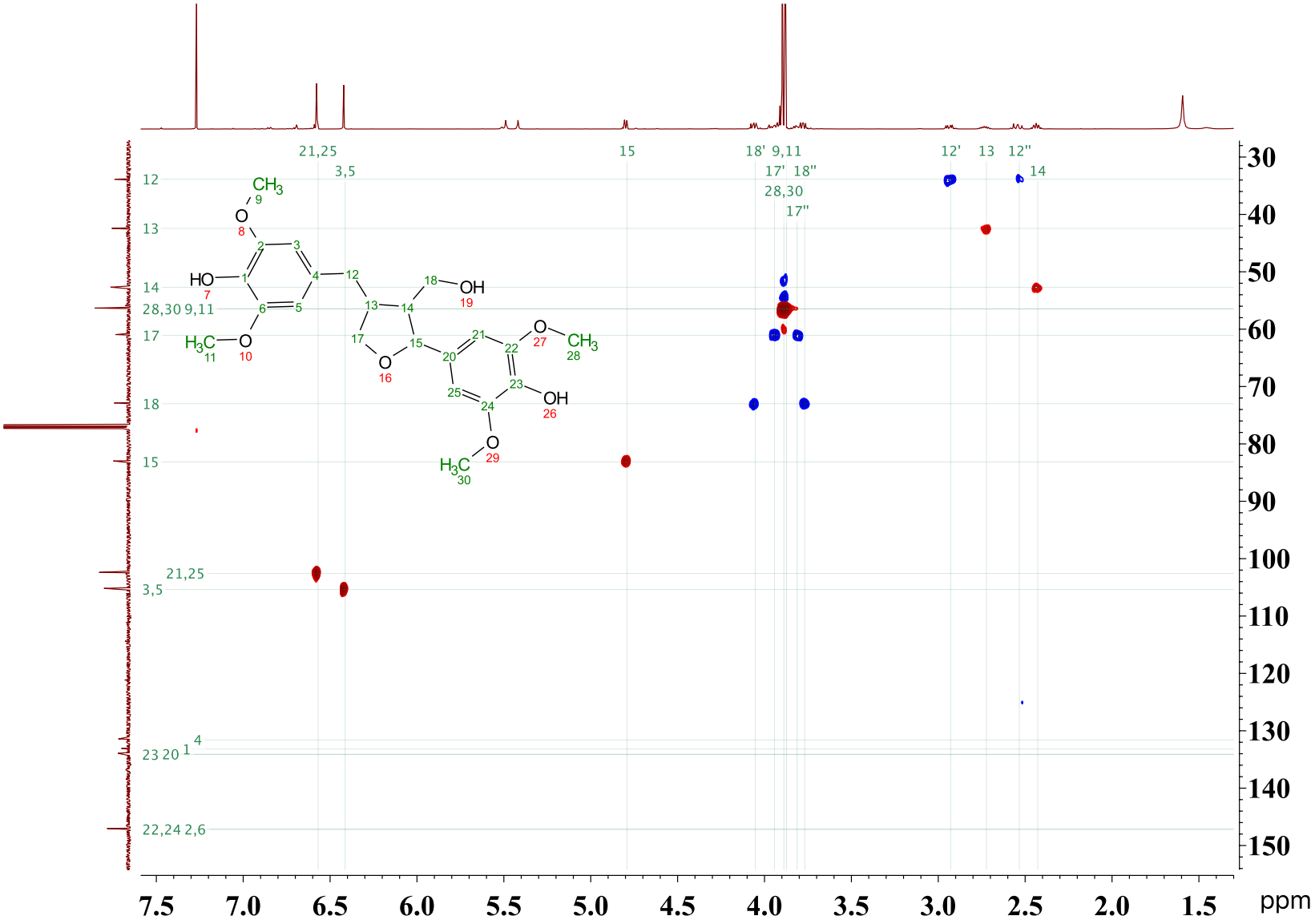

Figure 5.23: The HSQC NMR of the ECH product (3) of β-β dimer.

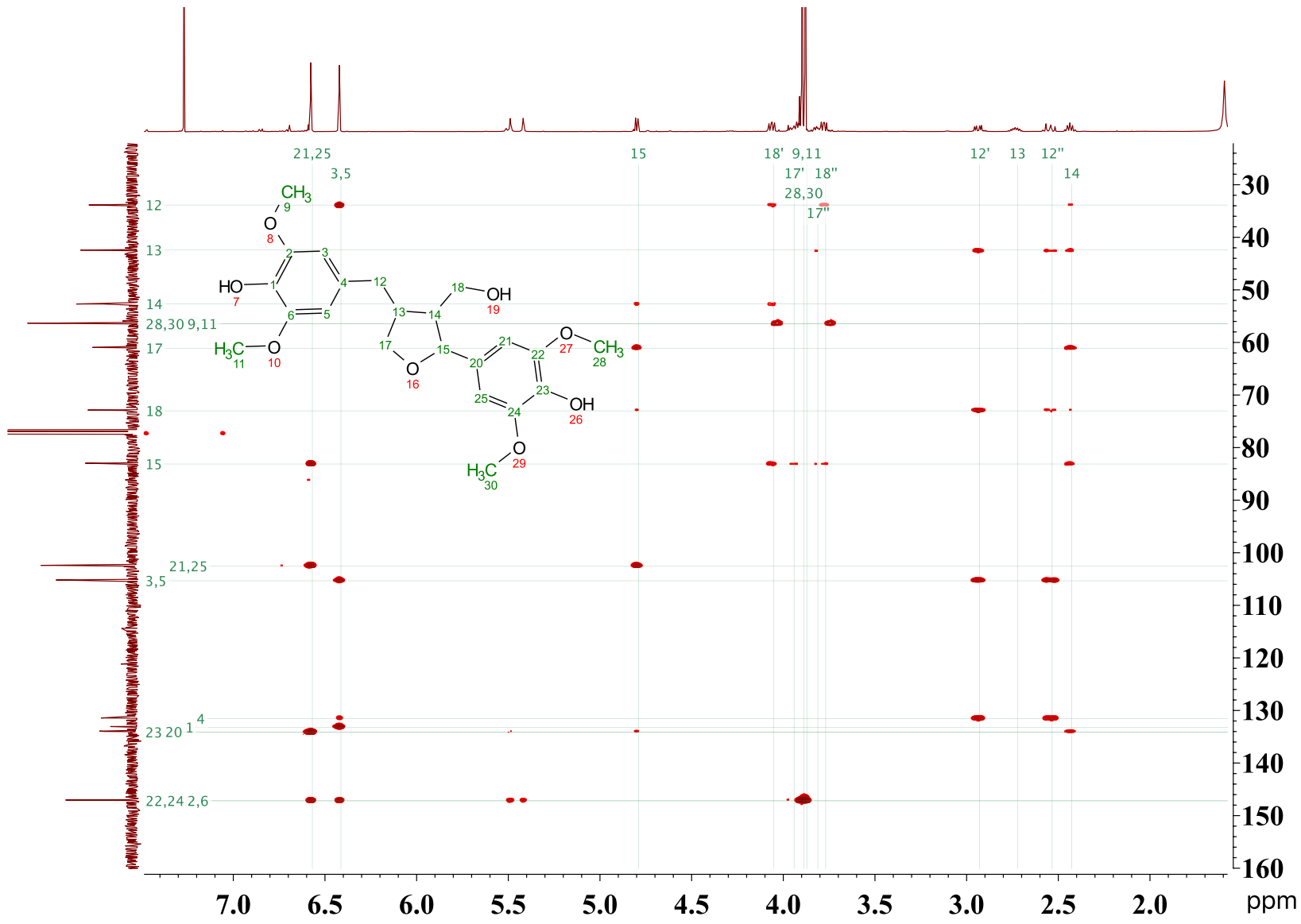

Figure 5.24: The HMBC NMR of the ECH product of (3) β-β dimer.

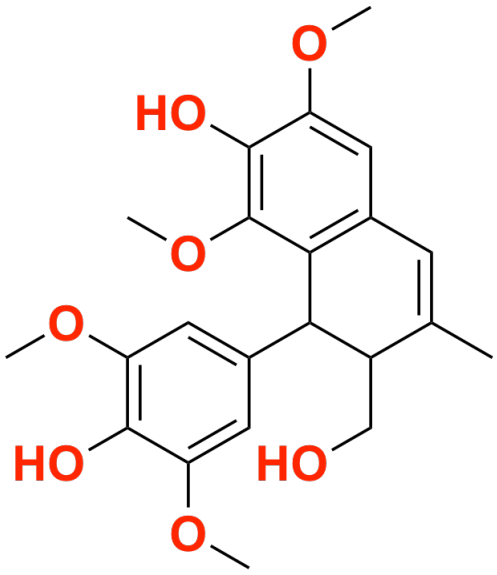

Figure 5.25: The product (4) of ECH of β-β dimer.

Dark yellow oil.

MS (EI): 402.1

^{1}H NMR (500 MHz, Chloroform-*d*) δ 6.44 (s, 1H), 6.37 (s, 2H), 6.22 (d, J = 1.5 Hz, 1H), 5.52 (s, 1H), 5.35 (s, 1H), 4.48 (d, J = 1.2 Hz, 1H), 3.89 (s, 3H), 3.77 (s, 7H), 3.65 (dd, J = 10.7, 4.4 Hz, 1H), 3.55 (s, 3H), 3.34 (dd, J = 10.7, 9.0 Hz, 1H), 2.47 (ddd, J = 9.1, 4.4, 1.2 Hz, 1H), 1.79 (d, J = 1.5 Hz, 3H).

^{13}C NMR (126 MHz, Chloroform-*d*) δ 146.64, 146.32, 145.40, 137.66, 136.13, 133.73, 132.96, 126.04, 123.59, 120.70, 104.53, 104.42, 63.04, 60.58, 56.20, 56.13, 50.68, 38.41, 22.84.

No literature NMR values available.

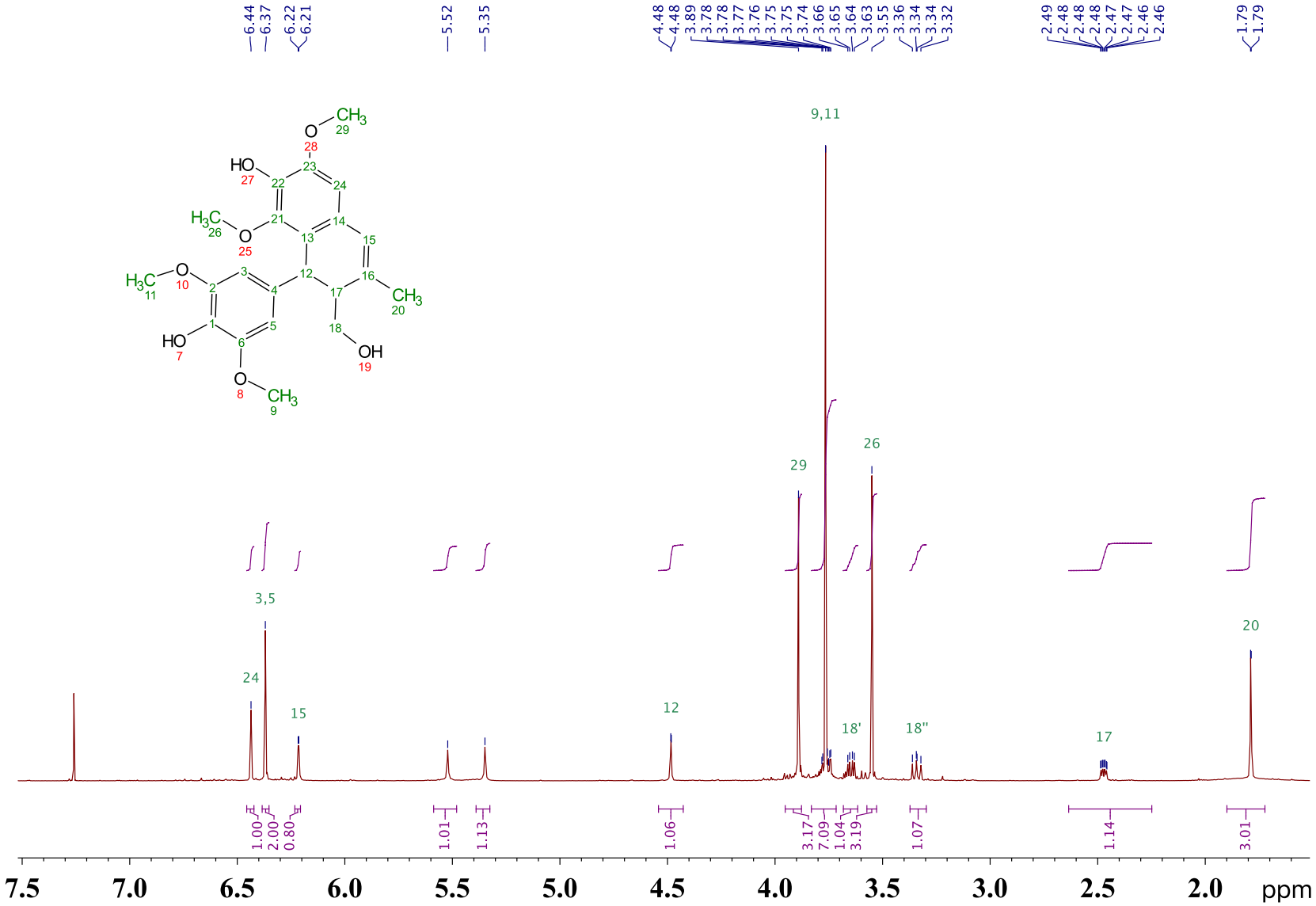

Figure 5.26: The proton NMR of product (4) of ECH of β-β dimer.

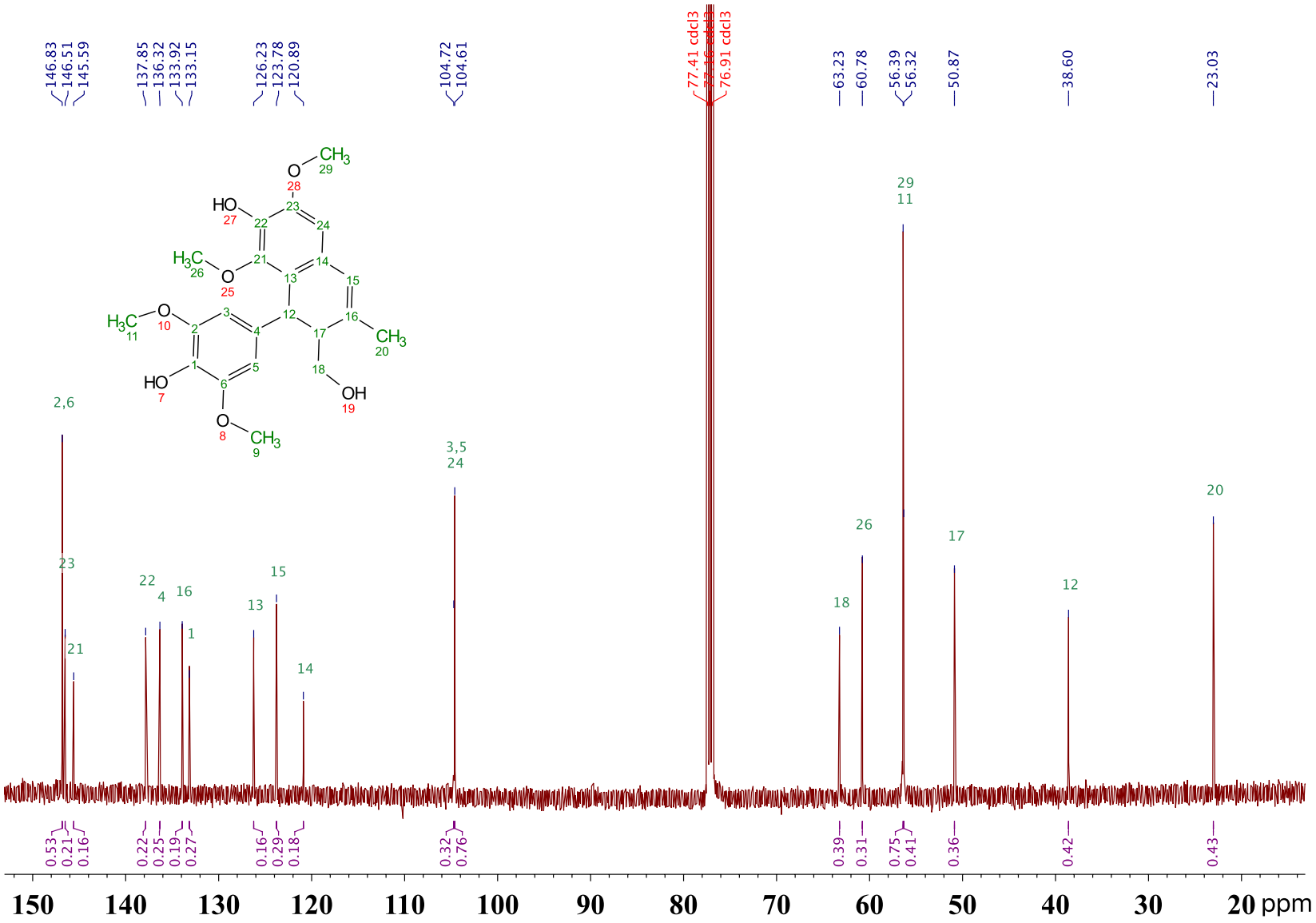

Figure 5.27: The carbon NMR of product (4) of ECH of β-β dimer.

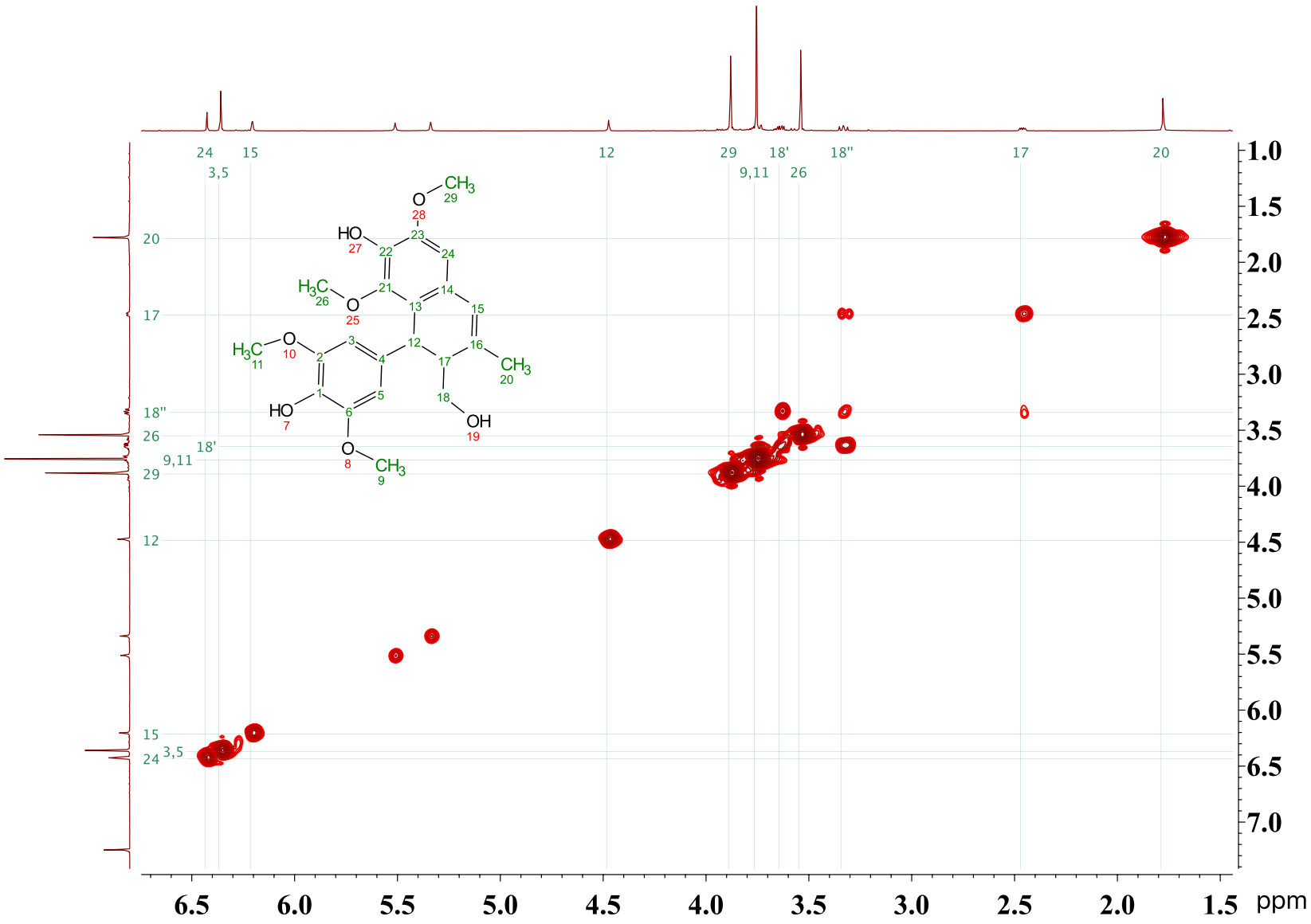

Figure 5.28: The COSY NMR of product (4) of ECH of β-β dimer.

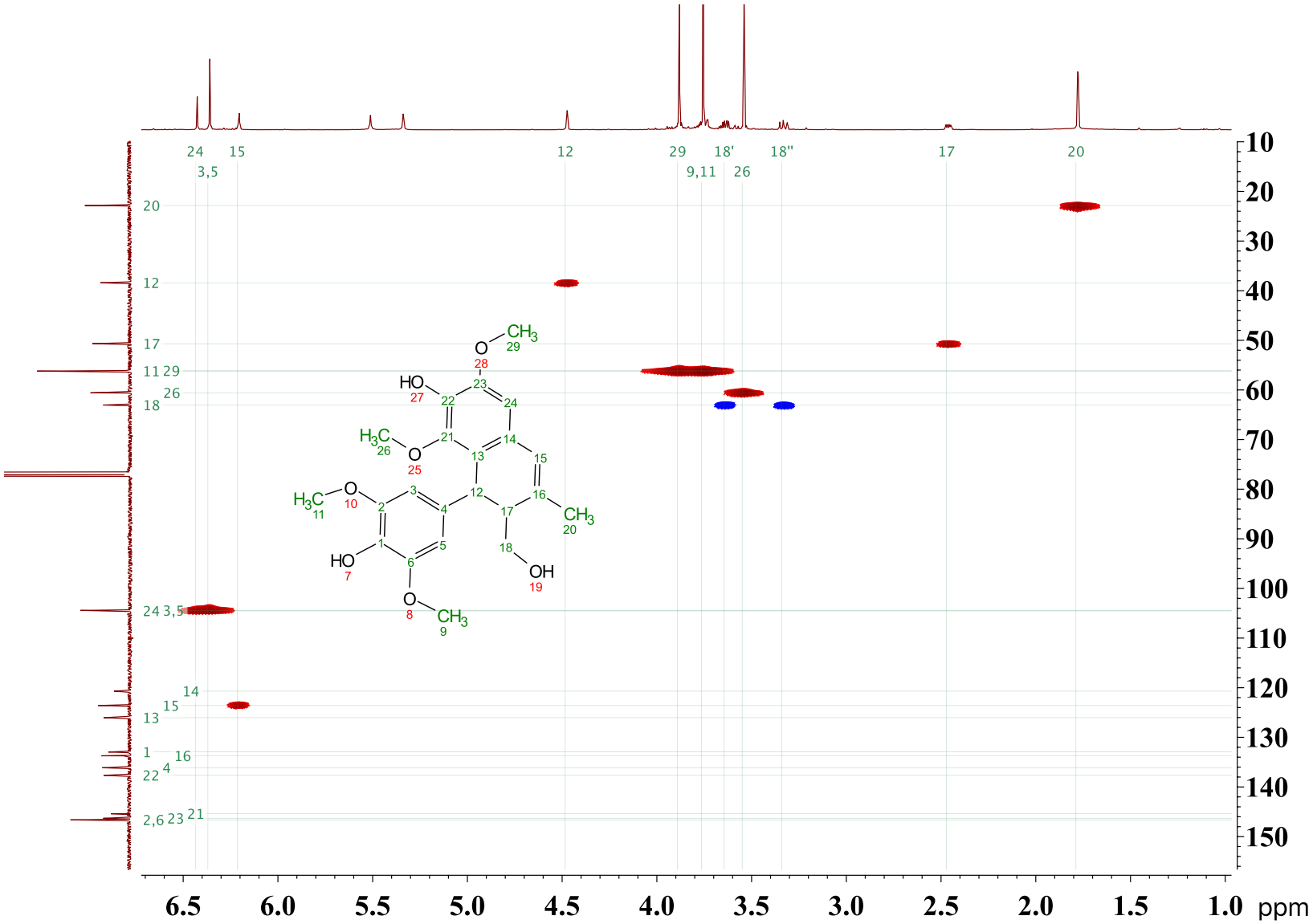

Figure 5.29: The HSQC NMR of product (4) of ECH of β-β dimer.

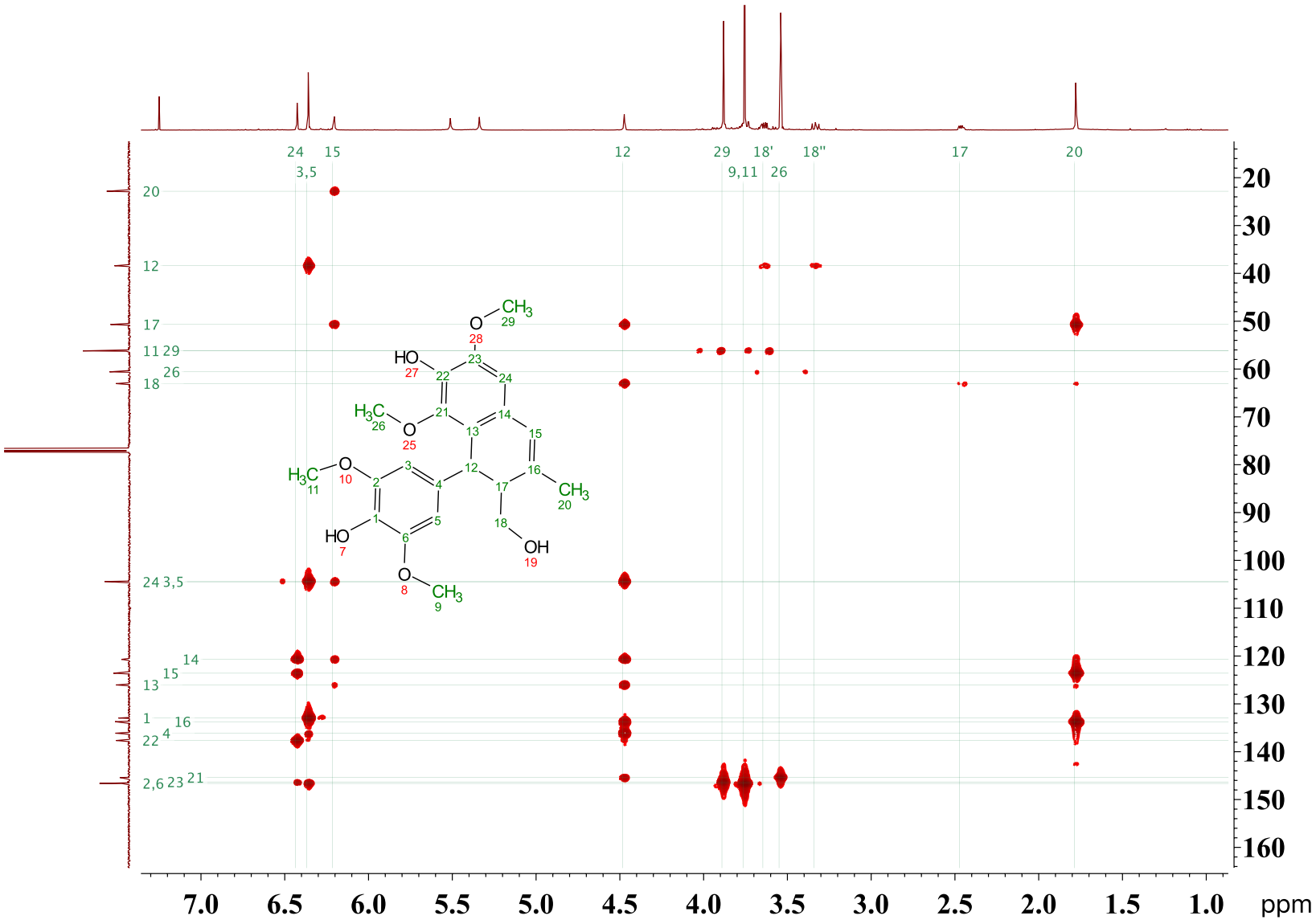

Figure 5.30: The HMBC NMR of product (4) of ECH of β-β dimer.

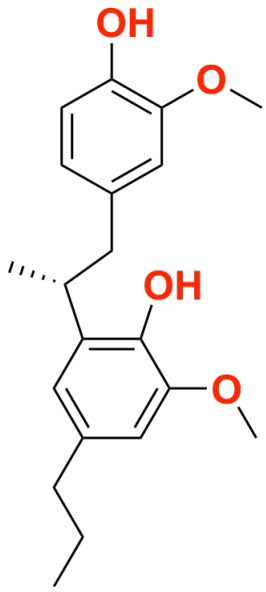

Figure 5.31: The product of ECH of β-5 dimer.

White solid.

MS (ES^-): 329.18 ($M-H^+$).

^{1}H NMR (500 MHz, Chloroform-*d*) δ 6.79 (d, J = 7.9 Hz, 1H), 6.66 (d, J = 8.1 Hz, 1H), 6.62 (s, 1H), 6.59 (s, 1H), 6.55 (d, J = 1.9 Hz, 1H), 5.57 (s, 1H), 5.43 (s, 1H), 3.87 (s, 3H), 3.81 (s, 3H), 3.38 (h, J = 7.0 Hz, 1H), 2.95 (dd, J = 13.5, 5.9 Hz, 1H), 2.64 (dd, J = 13.5, 8.6 Hz, 1H), 2.50 (t, J = 7.7 Hz, 2H), 1.60 (td, J = 14.6, 14.2, 7.1 Hz, 3H), 1.19 (d, J = 6.9 Hz, 3H), 0.93 (t, J = 7.3 Hz, 3H).

^{13}C NMR (126 MHz, Chloroform-*d*) δ 146.02, 145.97, 143.53, 140.82, 133.63, 133.27, 132.06, 121.87, 119.16, 113.76, 111.70, 108.38, 55.95, 55.76, 42.77, 38.03, 34.62, 24.94, 19.35, 13.80.

No literature NMR values available.

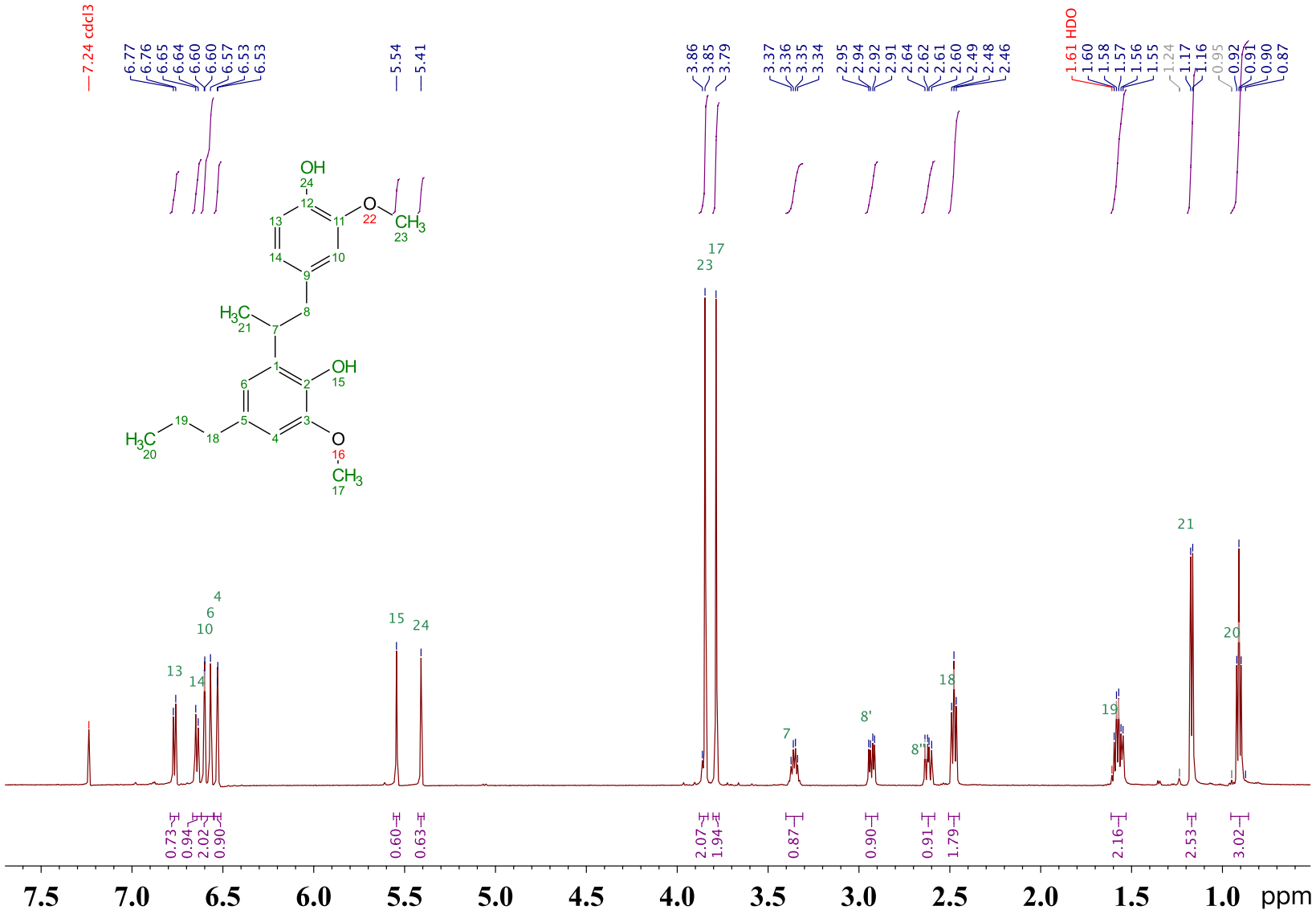

Figure 5.32: The proton NMR of product of ECH of β-5 dimer.

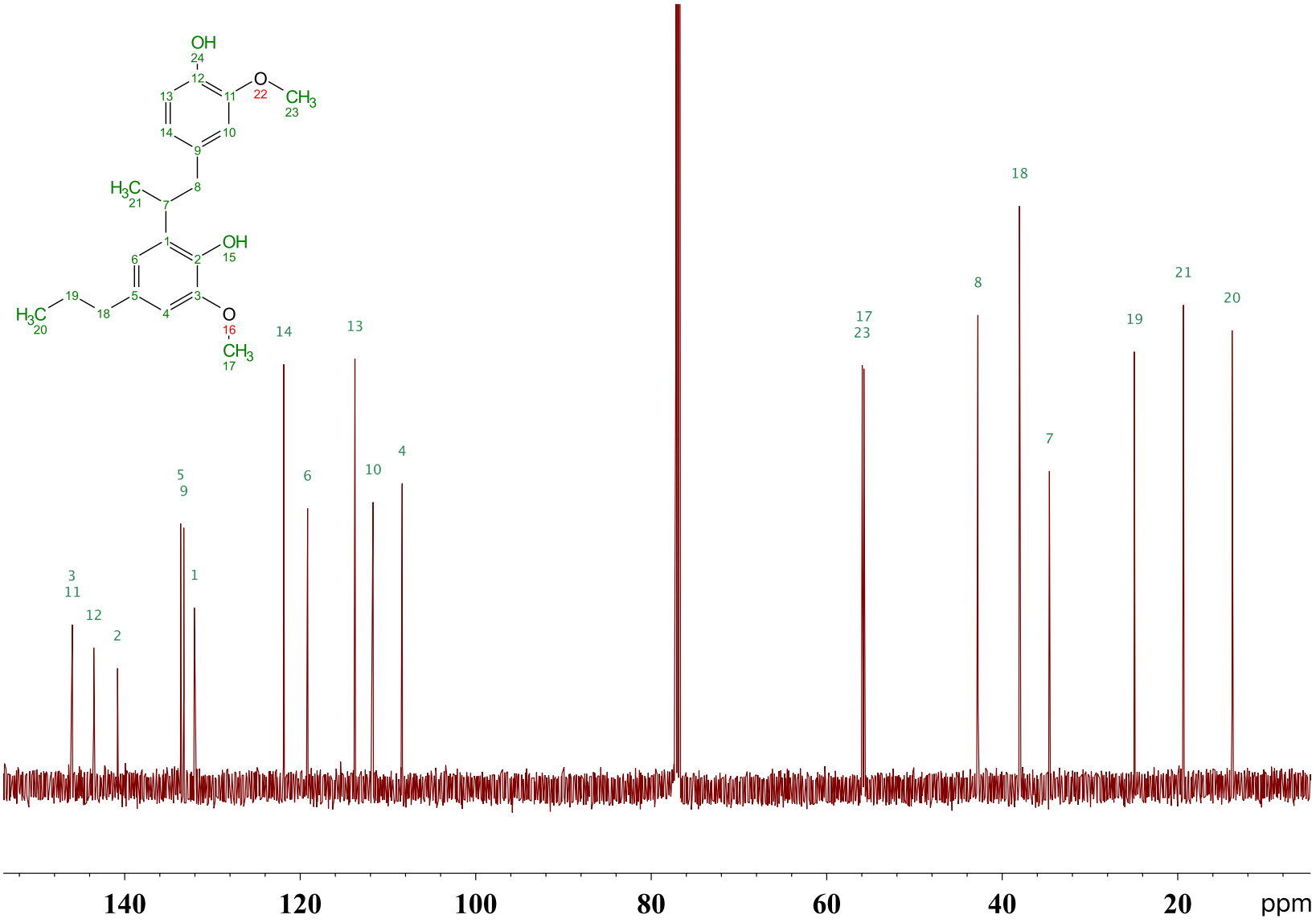

Figure 5.33: The carbon NMR of product of ECH of β-5 dimer.

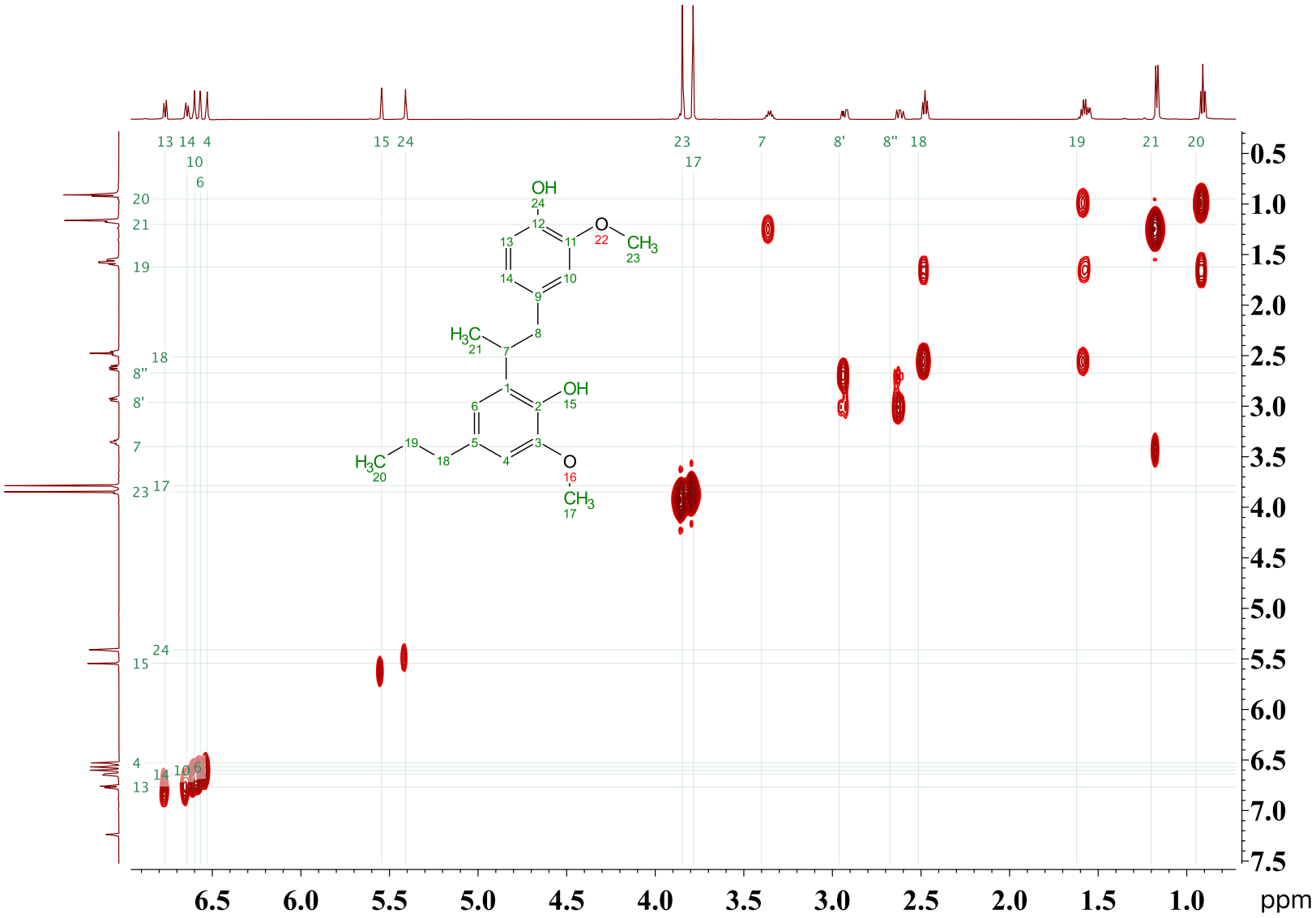

Figure 5.34: The COSY NMR of product of ECH of β-5 dimer.

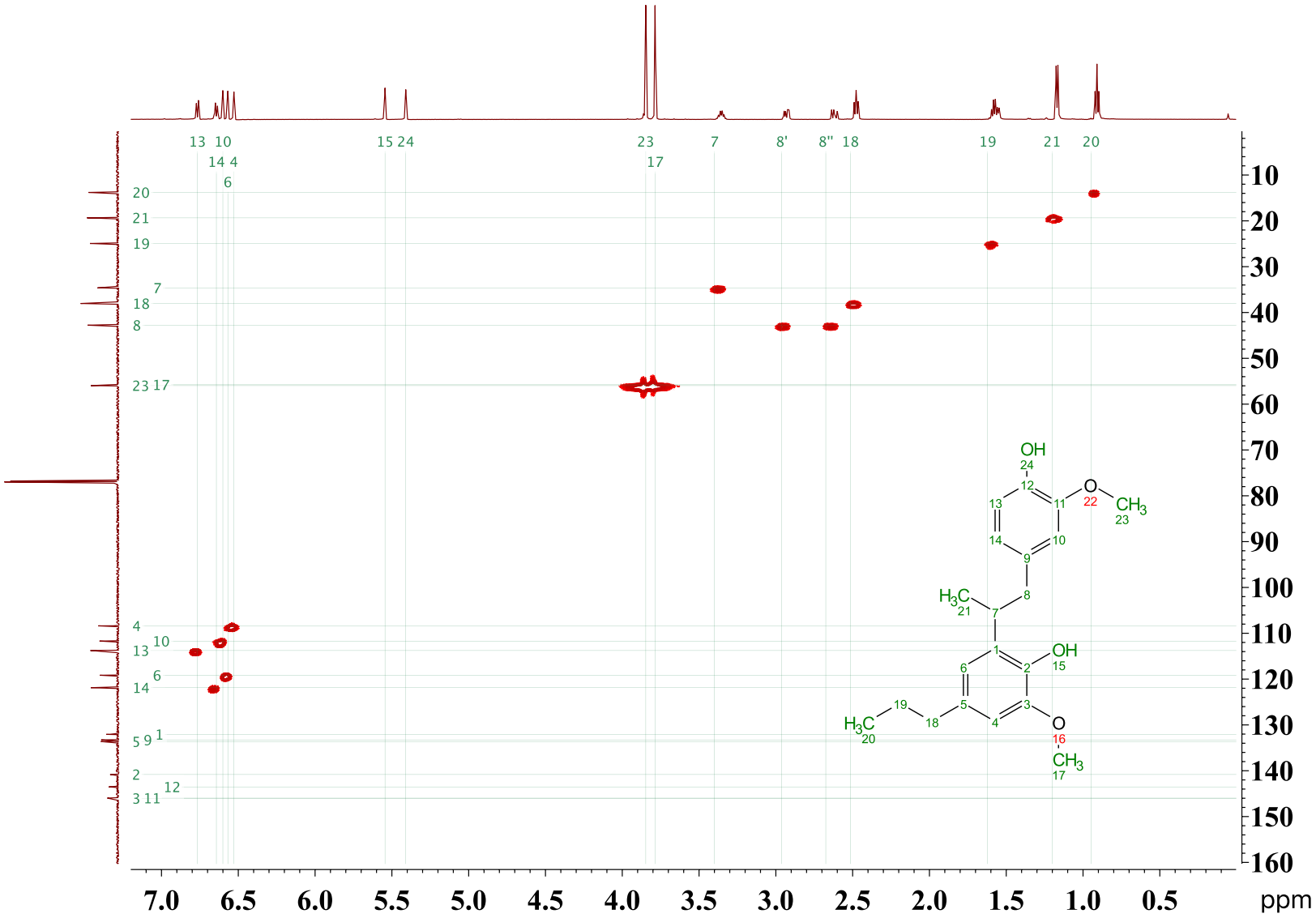

Figure 5.35: The HSQC NMR of product of ECH of β-5 dimer.

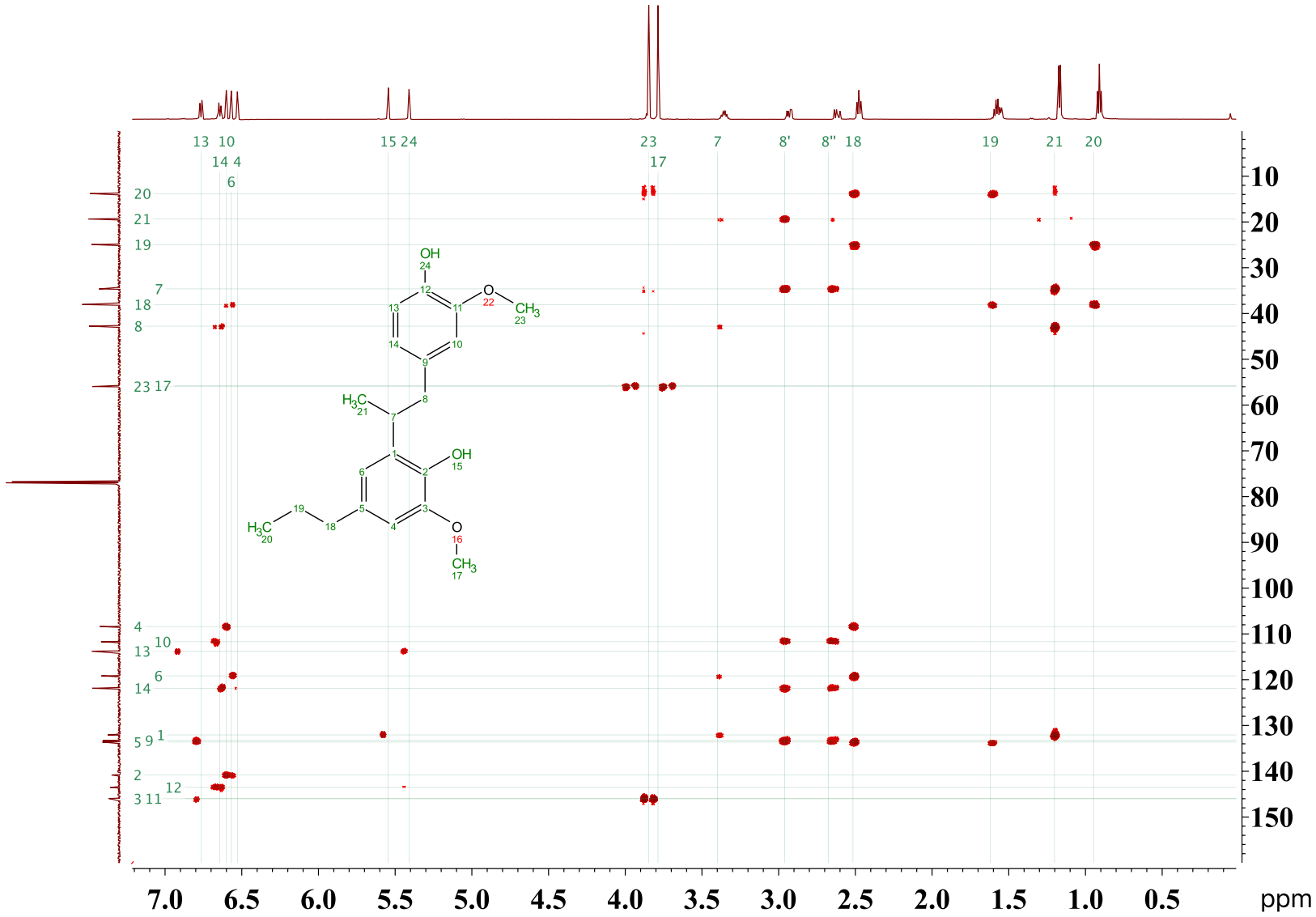

Figure 5.36: The HMBC NMR of product of ECH of β-5 dimer.

Chapter 6

Review of the Reproductive and Neurological Toxicities of Cyclohexanol and Cyclohexane

6.1 Introduction

Development of strategies for biofuel production is important for the replacement of fossil fuel with renewable sources. This priority, on one hand, can reduce net atmosphere CO_2 increases and slow down global warming, and on the other hand, offers an alternative liquid fuel source and addresses the national energy security issue.[219] For the past two decades, the most successful and widely produced biofuel has been ethanol, produced primarily from fermentations of cornstarch and cane sugar. The next most popular biofuel, biodiesel, is manufactured from vegetable oils and animal fats.[220] However, both biofuels face the criticism of the food-energy conflict conundrum, so additional alternatives are still needed to establish economically-competitive food chain independent technologies.[221]

Lignocellulosic biofuel meets the criteria of sustainability by converting biomass feedstock from food crop residues (stalk, leaves) and forestry operations into fuels.[220] Lignin is one of the three major components of lignocellulosic biomass and contributes to its recalcitrance.

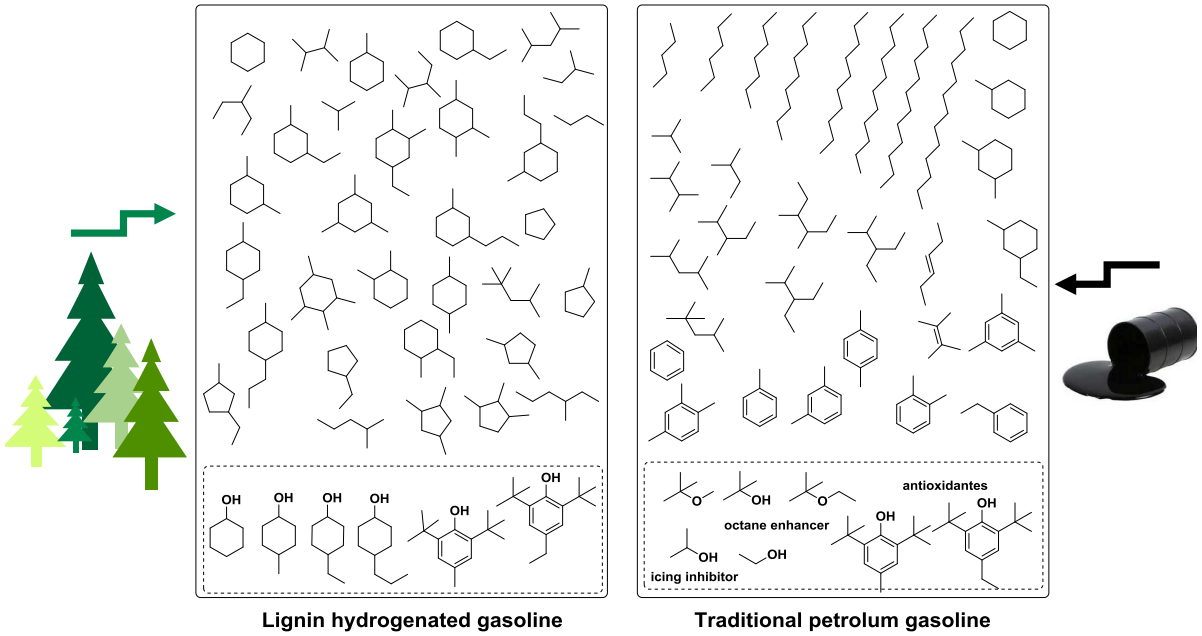

Figure 6.1: The composition change of gasoline produced from lignin biomass and traditional petroleum. The lignin hydrogenated gasoline compositions (outside of the dashed-line box) were from the patent[26] of Shabtai, and the composition of gasoline was based on report[27] of Agency for Toxic Substances and Disease Registry. Chemical from the dash-line boxes are functioning chemicals serving as octane enhancing, antioxidants, and anti-freezing proposes.

Lignin is also the major component of the "black liquor" waste from cellulose extraction in the paper pulping industry. The production of lignocellulosic biofuel can be achieved via pretreatments and depolymerization of biomass, followed by preferably mild hydrogenation to upgrade lignin monomers to liquids with higher fuel value energy content. Under mild conditions, guaiacol and syringol, two of the major monomers from depolymerization of lignin, can be hydrogenated to cyclohexanol,,[19,124,136,222,223] a compound with higher fuel value since the higher heating value of cyclohexanol (35.2 MJ/kg)[224] is higher than that of guaiacol (28.9 MJ/kg)[225] and syringol (26.6MJ/kg).[226] Under more severe conditions, guaiacol and syringol can be further hydrogenated into cyclohexane.[26] Besides guaiacol and syringol, 4-substituted analogues including their C1-, C2-, C3-alkyl and carbonyl derivatives (methyl, ethyl, propyl, formyl, acetyl, propionyl, vinyl, allyl, propenyl, etc.) are also found in the

depolymerization products. These can be reduced to the corresponding 4-alkylcyclohexanols according to our studies in the previous chapters.

If fuel can be produced in large scale from lignin as demonstrated by Shabtai[26,118] or similar hydrogenation methods, the composition of lignin gasoline will be significantly different from that of traditional gasoline distilled from petroleum, as shown in Figure 6.1. A clear composition change is the significant increase of cyclohexane derivatives in lignin hydrogenated gasoline. However, Shabtai's high temperature, high pressure, the highly flammable solvent approach is very energy-consuming, capital-intensive, and dangerous; it has not been commercially realized in industry production since it was patented in 1999. New developments are mainly focusing on making this process greener and milder.[19,86,87,93,100,114,184,227] As outlined in previous chapters, these green reactions use water as solvents and proceed at temperature less than 100 °C, and the main lignin monomer reduction products are cyclohexanol and its derivatives instead of cyclohexane.

Along with the development of new technologies, safety for the personnel and the environment should not be compromized. It is necessary carefully examine the toxicity and potential for exposure to the main products produced from the mild hydrogenation of pretreated lignocellulosic biomass. If a shift of gasoline composition leads to significant health concerns, if cyclohexane, cyclohexanol, and their derivatives lead to high risks of human health issue, these new technologies should be guided in directions where further deoxygenation or even ring-cracking/isomerization reactions are included in the fuel finishing processes.

Cyclohexanol, a potential main component of hydrogenated lignocellulosic biofuel and currently a large scale industrial chemical, has been reviewed and its permitted exposure levels have been determined. Notably, it was added to the Proposition 65 roster of chemicals known to the state of California to cause reproductive toxicity, effective in 1998. However, in

2002, cyclohexanol was delisted from the Proposition 65 list after a public meeting held by the Developmental and Reproductive Toxicant (DART) Committee of the California Office of Environmental Health Hazard Assessment. The reasons for the elimination remain questionable, further review and investigations on the reproductive and developmental toxicity of cyclohexanol should be conducted.

Cyclohexane has been reviewed by U.S. Environmental Protection Agency (EPA) in the Integrated Risk Information System (IRIS), and the concern of its neurotoxicity has been raised.

In this work, we review and compare the toxicity of cyclohexanol and cyclohexane in order to give a guide to chemists and engineers on the direction of the chemistry to be developed in order to transform lignin biomass to safe biofuels. The toxicity of alkylcyclohexanes and alkylcyclohexanols are also important. There is, however, very limited toxicological literature on these alkyl cyclic compounds, and they are not the focus of this work.

6.2 Method

Literature searches were performed on Google, Google scholar, SciFinder, and the web of science by using the keywords: cyclohexanol, cyclohexanone, cyclohexane, toxicity, reproductive toxicity, neurotoxicity, genotoxicity, metabolism, metabolite, human metabolite, risk assessment, exposure, inhalation, occupational, or any combinations of these keywords. Some literature was also obtained with the assistance of U.S. EPA and related personnel.

6.3 Chemical and physical properties of cyclohexanol and cyclohexane

Cyclohexanol ($C_6H_{11}OH$) is a colorless and viscous liquid with a camphor-like odor. The Chemical Abstracts Service (CAS) Registry Number is 108-93-0. Cyclohexane (C_6H_{12}) is a colorless liquid with sweet gasoline-like odor. Its CAS number is 110-82-7.[228,229]

Table 6.1: Physical properties of cyclohexanol and cyclohexane.

Property	**Cyclohexanol**	**Cyclohexane**
Molecular weight (g/mol)	100.16	84.16
Melting Point (°C)	25.2	6.5
Boiling Point (°C)	161.1	80.7
Flash Point (°C)	67.2	-20°C
Density (g/mL)	0.9493	0.7781
$\mathbf{n_D^{25}}$	1.4648	1.4266
Solubility in water (g/100 mL) at 20 °C	3.6	Immiscible
Evaporation rate at 45 °C (mg/min/cm^2)	0.4	9.4
Vapor Pressure (mm Hg) at 25 °C	1.3	97

6.4 Applications and human exposure sources of cyclohexanol and cyclohexane

Most cyclohexanol (> 95% in the U.S.) is consumed on site for the production of adipic acid and caprolactam via the reactions shown in Figure 6.2; only small amounts enter the world's trade markets.[230] Adipic acid and caprolactam are consumed primarily in the production of fibers and resins based on nylon 66 and nylon 6, respectively. As a result, cyclohexanol production and consumption rates follow the nylon fibers and resins industries. The industrial synthesis of caprolactam and adipic acid are shown in Figure 6.2 and Figure 6.3,

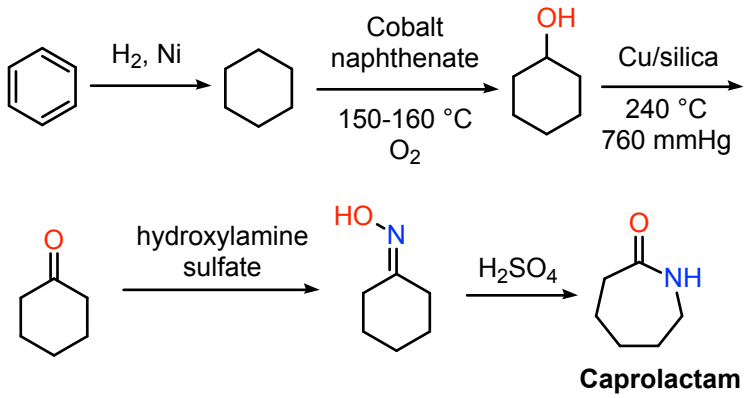

Figure 6.2: The synthesis of caprolactam from cyclohexanol.

respectively.[231]

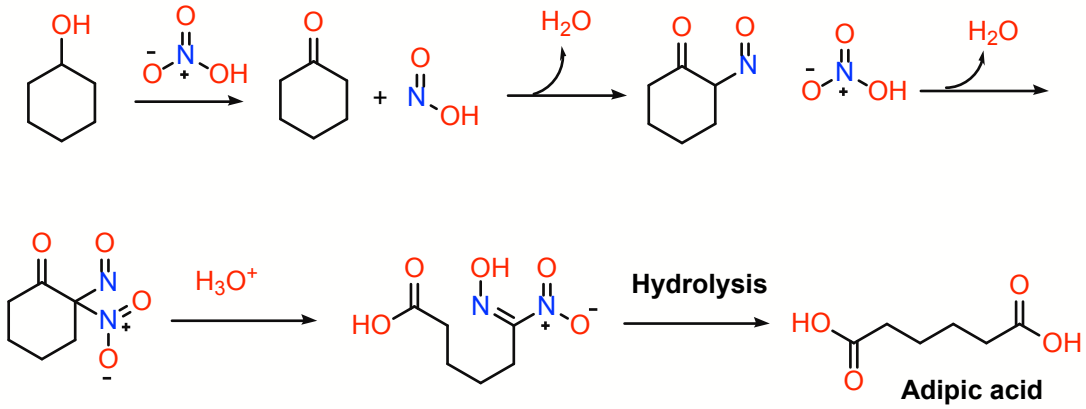

Figure 6.3: The synthesis of adipic acid from cyclohexanol. Reaction conditions: 0.5 °C; solvent: HNO_3; catalysts: ammonium metavanadate, NH_4VO_3, and copper nitrate, $Cu(NO_3)_2$; yield: $> 90\%$.

Less than 4% of cyclohexanol is consumed in markets for products other than nylon. These applications are as solvents for paints and dyes, in pesticides, as intermediates for pharmaceuticals, films, soaps, coatings, corrosion inhibitors, and plasticizers. However, cyclohexanol does not necessarily appear in all these final products. We classify cyclohexanol applications into two categories considering the importance of this aspect of exposure assessment.

6.4.1 Applications that cyclohexanol appears in the final products

In the coating industry, cyclohexanol is used as a solvent that can dissolve many natural resins, cellulose ethers, and phenol formaldehyde resins. Similarly, in the finishes industry, cyclohexanol is used as a solvent for lacquers, shellacs, and varnishes.[232] Lacquer is a clear or colored wood finish that dries by solvent evaporation or a curing process that produces a hard, durable finish. Shellac is a brush-on colorant used for food glaze and wood finish. Cyclohexanol appears in paint or varnish remover.

In the textile industry, cyclohexanol is used as a dye solvent and aid in kier-boiling (kier is a type of container),[232] meaning a scouring process for cotton and linen in which the fibers are treated to remove impurities by boiling with a 1% solution of caustic soda.

Cyclohexanol is used as a stabilizer and homogenizer for soaps and synthetic detergent emulsions.[232]

Cyclohexanol is used to control the surface morphology and the optical properties of the anti-reflective coating films.[232,233]

6.4.2 Applications where cyclohexanol does not appear in the final products

Cyclohexanol is known to be one of the precursors for making pesticide cycloate (S-Ethyl *N*-cyclohexyl-*N*-ethylthiocarbamate).[232] Cyclohexanol is not listed as an active ingredient by the National Pesticide Information Center. We did not find information about cyclohexanol present in pesticides.

Cyclohexanol is used as a precursor for the cyclohexyl groups in some pharmaceutical. We did not find information about cyclohexanol as an ingredient of pharmaceutical formulations.

Cyclohexanol reacting with ammonia in the presence of nickel catalyst can produce cyclohexylamine, which is used as a corrosion inhibitor.[232,234] We did not find information about cyclohexanol as a corrosion inhibitor. Ethynyl cyclohexanol was found to be an active ingredient[235] in an eco-corrosion inhibitor product branded as TITANOS Ethynyl Cyclohexanol.

It is a misunderstanding that cyclohexanol is in plasticizers; it is one of the precursors for the synthesis of plasticizers, monocyclohexyl, and dicyclohexyl phthalates.[232] We did not find information about cyclohexanol as a plasticizer.

In summary, the most likely human exposures to cyclohexanol are either occupational exposure in the nylon, fiber, resin and textile industries, or non-occupational exposures from the coating, varnish, or paint removers, soaps and synthetic detergent containing cyclohexanol. No significant exposures are expected from pesticides, pharmaceuticals, corrosion inhibitors, or plasticizers. It should also be noted that cyclohexanol is naturally occurring in small quantities and it has been qualitatively detected in fried chicken and baked potatoes.[236]

6.4.3 Applications of cyclohexane

Cyclohexane is produced by fractional distillation of naphtha and the hydrogenation of benzene as shown in Figure 6.2. Almost all cyclohexane is used to produce cyclohexanol and cyclohexanone, used as noted above to synthesize caprolactam, adipic acid, and ultimately nylon. Cyclohexane can be used as a non-polar organic solvent.[228] In addition, it is occasionally used as a stabilizer for high-octane gasoline.[237]

6.5 Pharmacokinetics of cyclohexanol

6.5.1 Absorption and distribution of cyclohexanol

Cyclohexanol can be absorbed via oral, inhalation, and dermal routes of exposure.[238] It is absorbed well through oral administrations. In one study, six rabbits received 260 mg/kg each of ^{14}C labeled cyclohexanol and cyclohexane administrated by stomach tube with water. Unlike cyclohexane where 30% of the dose was expired, i.e. breathed out, into the air, no orally administrated ^{14}C cyclohexanol was detected in the air and a total of 75% of the total radioactivity was recovered from the animals' urine, which was collected for 2 days after dosing.[239]

Cyclohexanol can be absorbed through the skin in toxic amounts.[237] Dermal absorption of cyclohexanol 10 mL daily (94400 mg/kg) for 10 days on the abdomen of one rabbit was shown to lead to toxicity signs and eventually death,[240] and it also increases the skin penetration ability of other applied dyes, including Rhodamine B and Evans blue.[241]

6.5.2 Metabolism of cyclohexanol

Cyclohexanol can be oxidized by alcohol dehydrogenase with 67% of the maximal turnover rate of ethanol. It binds to the enzyme more tightly than ethanol and can competitively inhibit the ethanol oxidation process.[237]

The metabolism of cyclohexanol in bacteria, *Nocardia globerula* as shown in Figure 6.4 proceeds via oxidation to cyclohexanone by cyclohexanol dehydrogenase, followed by another oxidation to ε-caprolactone with cyclohexanone oxygenase; this ester was further hydrolyzed to 6-hydroxy caproic acid, which was oxidized to adipic acid enters the fatty acid metabolism (citric acid cycle) to generate acetyl-CoA or succinyl-CoA eventually.[242]

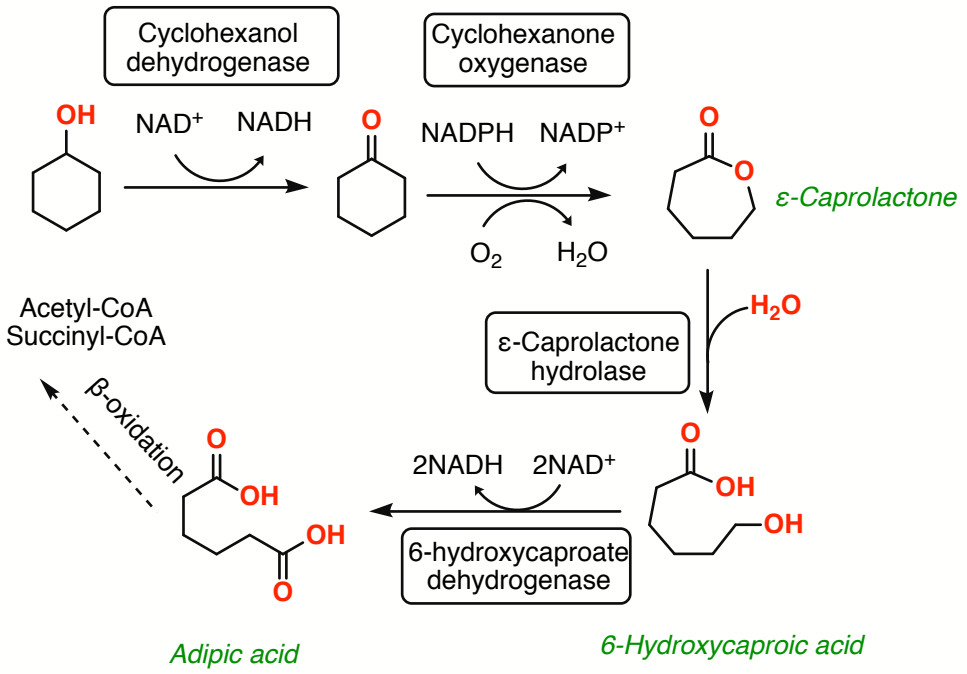

Figure 6.4: Metabolism of cyclohexanol from Bacteria *Nocardia globerula CL1*.

The metabolism of cyclohexanol in rats was reported to form cyclohexanone as well, and an interesting equilibrium between cyclohexanone and cyclohexanol was quickly established indicating a slower elimination rate, which will be discussed in detail in the following sections.[243,244] The major metabolite in urine was glucuronide conjugate of cyclohexanol; minor metabolites from rats included the cysteine conjugate of cyclohexanol, free cyclohexanol, cyclohexanone, and the sulfate conjugate of cyclohexanol.[245] Although cyclohexene was never reported as an urine metabolite in humans or animals, the cysteine conjugate of cyclohexanol indicated that small amount of cyclohexene reactive intermediate may be produced and cytochrome P-450 enzyme oxidizes the cyclohexene to epoxide, which was nucleophilically attacked by the thiol of cysteine and observed as a cysteine conjugate.

Similar metabolism was found in rabbits and dogs as the same that was shown in rats.[245] In rabbits, when ^{14}C labeled cyclohexanol was administrated with water through a stomach tube, 65% of the dose (260 mg/kg) was excreted as the cyclohexyl glucuronide, 6% as the

glucuronide conjugated *trans*-cyclohexane-1,2-diol, and 6% was oxidized to cyclohexanone. When ^{14}C labeled cyclohexanone was administrated in the same way, it was reduced and excreted mainly as the cyclohexyl glucuronide.[239]

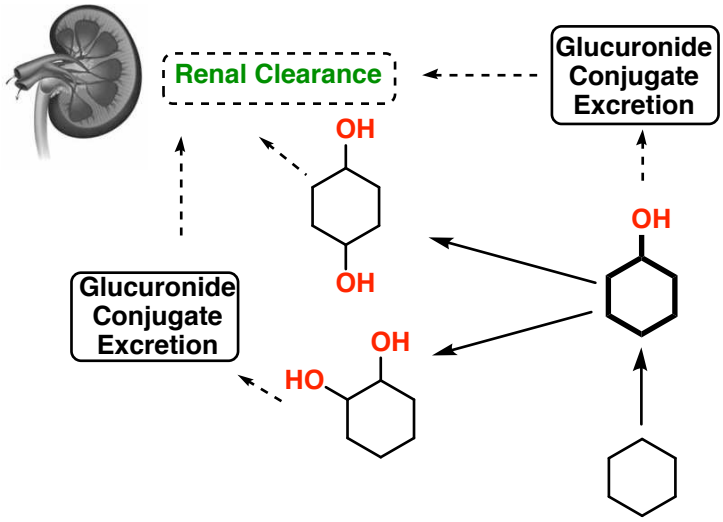

Figure 6.5: Metabolism and excretion of cyclohexanol of humans Kidney picture was adapted from this presentation.[28]

For humans, as shown in Figure 6.5, cyclohexanol is oxidized to cyclohexanone, trans-1,2-cyclohexanediol[239] and 1,4-cyclohexanediol (stereochemistry not specified).[245] Interestingly, the 1,2-cyclohexanediol further gets conjugated with glucuronide, while 1,4-cyclohexanediol glucuronide was not detected in human urine sample.[245]

6.5.3 Metabolism kinetics of cyclohexanol

6.5.3.1 Non-human

The kinetics of cyclohexanol metabolism in non-human have been well studied. Cyclohexanol is a secondary alcohol like isopropyl alcohol, but its metabolism kinetics are distinct from all other secondary and primary alcohols investigated. Primary alcohol elimination in rats occurs with zero-order kinetics at doses of 5-20 mmol/kg, while secondary alcohol

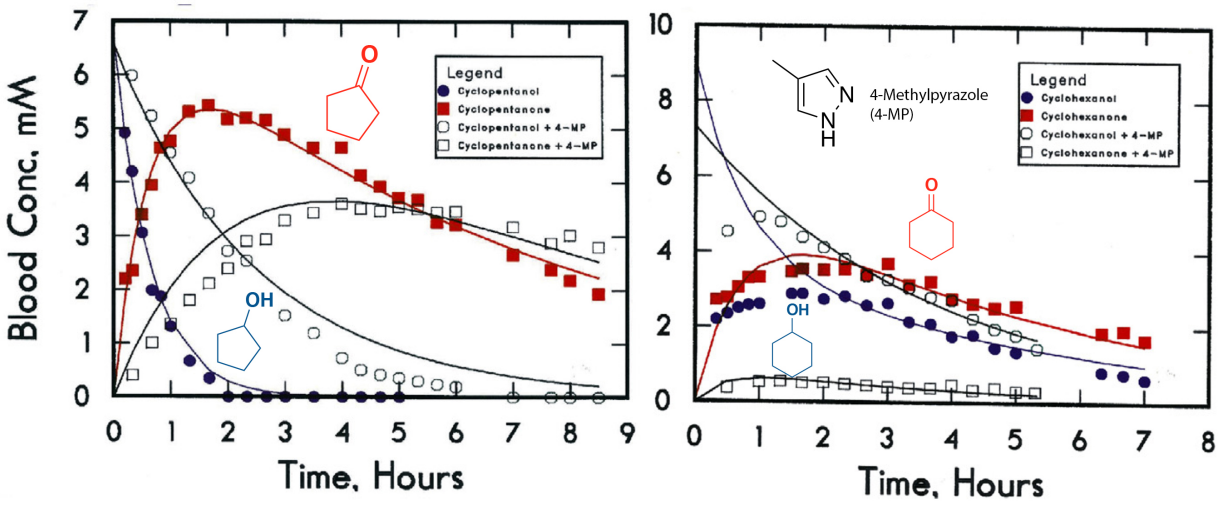

Figure 6.6: The cyclohexanol metabolism kinetics in rats intraperitoneally (injection of a substance into the body cavity) with a dose of 5 mmol/kg. The lines represent the fitted values from simultaneous non-linear least squares fits of data for alcohol and ketone for the uninhibited (or inhibited) state to the differential equations for the first order, sequential reactions. Solid red square: Cyclohexanone; Empty square: Cyclohexanone + inhibitor (1 mmol/kg 4-methylpyrazole); Solid blue circle: Cyclohexanol; Empty circle: Cyclohexanol + inhibitor (1 mmol/kg 4-methylpyrazole). Reprinted with permission from Plapp, B. V. et al. *Chemico-Biological Interactions* **2015**, *234*, 85-95. Copyright {2018} Elsevier.

eliminations, except for cyclohexanol, occur with first-order kinetics at the doses of 5-10 mmol/kg. Compared to the typical secondary alcohol cyclopentanol with a first-order elimination kinetics as shown in Figure 6.6, cyclohexanol follows neither zero-order nor first-order elimination kinetics. Instead, a rapid steady-state equilibrium between cyclohexanone and cyclohexanol is established; this phenomenon has been reported by several different groups with rats in vivo, and with horse liver alcohol dehydrogenase in vitro.[29,243,244]

When cyclohexanol was injected in rats, it was rapidly oxidized to cyclohexanone; similarly, when cyclohexanone was injected, it was rapidly reduced to cyclohexanol, and the kinetic constants for the primary alcohol zero-order reactions are about the same as those determined for cyclohexanol elimination, with cyclohexanol concentration constant slightly larger than that of cyclohexanone.[243]

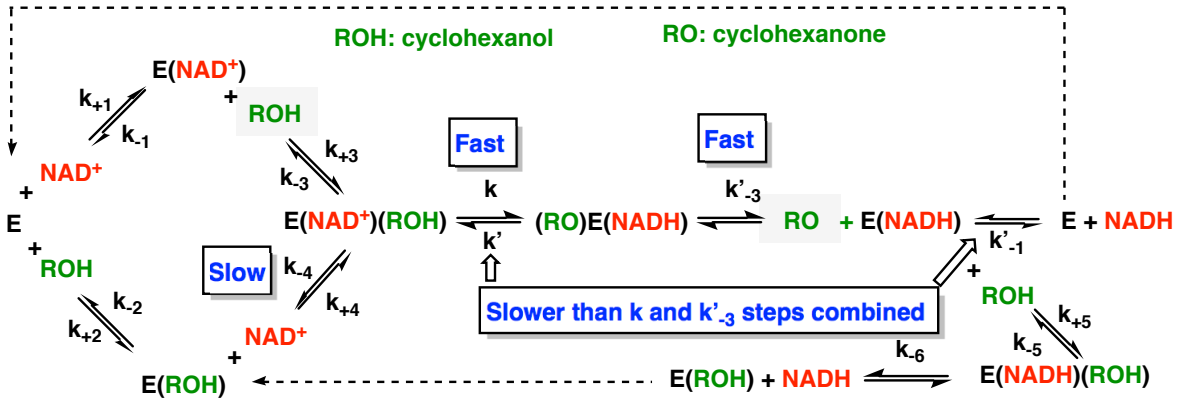

Figure 6.7: The metabolism reaction kinetics graph between the interconversion of cyclohexanol (ROH) and cyclohexanone (RO) with E (horse liver alcohol dehydrogenase).[29]

Dalziel and Dickinson studied the reaction kinetics of cyclohexanol metabolism with horse liver alcohol dehydrogenase. With the rate equation obtained, they found that the rate constant for the elimination of cyclohexanol, a secondary alcohol, resembled that of primary alcohol rather than aliphatic secondary alcohols. Their experimental results validated the proposed mechanism shown in Figure 6.7. ^{14}C labeled isotope experiments indicated that $k'_{-1} << k$, k'_{-3}, $k'_{-1} << kk'_{-3}/k'$, and $k_{-4} << k$ and k_{-3}, which means that compared with steps k and k'_{-3}, step k_{-4} was a slow step, and step k' and steps k'_{-1} combined were slower than k and kk'_{-3} steps combined. These patterns lead to the steady-state equilibrium between cyclohexanol (ROH) and cyclohexanone (RO), where the equilibrium slightly favors RO over ROH, which is consistent with the fact that cyclohexanone is always found in higher concentration than cyclohexanol during the reaction. The following glucuronide conjugation and excretion of ROH lead to the decrease of both ROH and RO in the body.

6.5.3.2 Human

The half-life of cyclohexanol metabolism in humans was estimated in 1990 to be around 12 hours, as estimated by the Dutch Expert Committee.[238] Marz estimated the half-life of

cyclohexanol metabolites eliminations were between 14 and 18 h.[3]

Table 6.2: The half-lives of the eliminations of cyclohexane, cyclohexanol, and 1,2- and 1,4-cyclohexanediol in humans after exposure to the compounds.[3]

Compound	**Route**	**n**	**Half-life of elimination (h)**	
			1,2-cyclohexanediol	1,4-cyclohexanediol
Cyclohexane	Inhalation	8	17.0 ± 5.2	16.1 ± 3.9
Cyclohexanol	Inhalation	8	14.3 ± 1.2	18.0 ± 2.5
1,2-cyclohexanediol	Oral	4	14.9 ± 3.2	-
1,4-cyclohexanediol	Oral	4	-	19.3 ± 4.3

Mraz studied the kinetics of excretion of urine metabolites of 4 men and 4 women exposed via inhalation at 294 ppm cyclohexane and 58 ppm cyclohexanol.[245] He found very similar metabolism patterns for cyclohexane and cyclohexanol. The majority of the cyclohexane and cyclohexanol were converted to 1,2- and 1,4-cyclohexanediol with $\leq 1\%$ of the dose excreted as cyclohexanol in urine within 72 h for both exposures.

According to Table 6.2, the elimination half-lives of 1,2- and 1,4-cyclohexanediol were within the range of 14-20 h, and the cyclohexanediol elimination processes were considered as the rate-limiting steps for three reasons. (1) The conversion rate of cyclohexanol to other metabolites is much faster (half-life 1.5 h). (2) When both 1,2 and 1,4-cyclohexanediol were administered orally, the elimination half-lives were similar to those observed when they were produced as metabolites of cyclohexane and cyclohexanol. (3) 1,2 and 1,4-cyclohexanediol were not significantly absorbed into fat (partition coefficient olive oil/ blood ≤ 0.1) or plasma protein.[245] Therefore, the elimination of 1,2- and 1,4-cyclohexanediol were rate-limiting in both cyclohexane and cyclohexanol metabolisms.

6.5.4 Excretion of cyclohexanol

In the animal studies, specifically rats, rabbits, and dogs, glucuronide of cyclohexanol was the main excretion form in the urine. In contrast, humans produced mainly 1,2-cyclohexanediol glucuronide and free 1,4-cyclohexanediol as major excretion metabolites as shown in Figure 6.5.[238,245–249]

6.6 Pharmacokinetics of cyclohexane

6.6.1 Absorption and distribution of cyclohexane

Cyclohexane is rapidly absorbed into the blood via the lungs, gastrointestinal tract, and skin. At higher doses, some cyclohexane is expired unchanged due to preferential partitioning to alveoli rather than blood, where it has low solubility.[250]

Cyclohexane can cross the blood-brain barrier, as shown by in vivo studies[239,250–253] The concentration of cyclohexane in rat brain is about 10 times higher than that in rat blood when the rats were exposed to 407 ppm to 8135 ppm cyclohexane via inhalations.[252]

The uptake of cyclohexane from the blood into brain and fat tissues (perirenal) has been quantified. In brain and fat of rats, cyclohexane distribution was found to follow a simple linear relationship established in the first week inhalation exposure of 300, 1,000, or 2,000 ppm cyclohexane, $y = 0.05\ x - 9.06$, $r^2 = 0.99$ where y is the brain cyclohexane concentration (nmol/g) and x (nmol/g) is cyclohexane concentration in fat.[251]

As a non-polar, lipophilic molecule, perhaps it is not surprising that cyclohexane partitions preferentially into lipid-rich tissues such as fat, liver, and brain based on studies from human cadaver and rat tissues.[254,255] However, although the fat contents in brain, liver,

and muscle are different, it was shown that there were no significant differences between the partitioning coefficient (concentration in tissue / concentration in air) of cyclohexane in human brain tissue (10.7 ± 1.4), liver tissue (10.8 ± 0.9), and muscle tissues (10.5 ± 0.7), whereas lower values were found for kidney (7.2 ± 1.0), heart (5.8 ± 1.0), lung (2.7 ± 0.1), and blood (1.3 ± 0.1).[254]

6.6.2 Metabolism of cyclohexane

The general scheme of cyclohexane metabolism starts with a cytochrome P-450 oxidation to produce cyclohexanol and then follows the metabolism routes of cyclohexanol as discussed in Figure 6.5.[245]

Cyclohexane metabolism differs between rabbits and rats vs humans. In rabbits, a ^{14}C labeled cyclohexane oral exposure experiment showed that cyclohexane was oxidized to cyclohexanol, and then, to a small extent, was converted to cyclohexanone and *trans*-1,2-cyclohexanediol.[239] The metabolite excreted in urine was mostly the cyclohexanol conjugate with glucuronic acid; only 2.4% of the cyclohexanol content was in free form. The small amount of *trans*-1,2-cyclohexanediol was also mostly converted to its corresponding monoglucuronide, with only 4% remains as a free compound in urine.[239] In humans, the main urine metabolites are 1,2-cyclohexanediol (23.4% of exposure dose) and 1,4-cyclohexanediol (11.3% of exposure dose), with cyclohexanol present in a small amount (0.5% of the dose). The cyclohexanol and more than 95% of the 1,2-cyclohexanediol appeared in urine as the glucuronides; whereas the 1,4-cyclohexanediol was excreted without glucuronide conjugation.[245]

6.6.3 Excretion of cyclohexane

Cyclohexane can be excreted and expired from lung after oral exposure, a process that becomes more efficient at higher dosages. When cyclohexane was administrated to rabbits (adult, doe) with a stomach tube with 35–400 mg/kg in water, about 40% of the ^{14}C (30% as cyclohexane and 10% as CO_2) was expired in air, and 50% was excreted into urine within 2 days. A much smaller dose (0.3 mg/kg) led to only 5% expired in the air and 90% in the urine.[239]

Table 6.3: The concentrations (μmol/kg) of cyclohexane in rat tissues during 3 consecutive 12 h exposure and 12 h recovery. Source: Zahlsen, et al. (1992).[4]

	Concentration of Cyclohexane in Tissues			
Tissue	**Day 1**	**Day 2**	**Day 3**	**Recovery**
Blood	4.0 ± 0.3	4.4 ± 0.1	4.1 ± 0.9	0.1 ± 0.1
Liver	22.6 ± 3.0	22.3 ± 2.9	26.4 ± 1.7	0.5 ± 0.4
Brain	31.7 ± 2.2	33.6 ± 3.2	34.7 ± 1.1	2.0 ± 2.5
Kidney	86.5 ± 2.0	100.1 ± 10.3	99.4 ± 13.0	1.3 ± 0.1
Fat	417 ± 66	475 ± 27	482 ± 3	169 ± 17

Cyclohexane clearance from rat body is fast and does not accumulate in a significant amount. In one study, 15 male Wistar rats per group were exposed to 0, 300, 1000 ppm cyclohexane for 6 h/day, 5 days/week for 2 weeks, after which 5 rats in each group were allowed to recover for 14 days, after which no cyclohexane was observed in brain and perirenal fat tissues.[251] In another study, male Sprague-Dawley rats were exposed to 100 ppm cyclohexane for 12 h for 3 consecutive days and followed by a 12 h recovery period. The cyclohexane concentration in blood, brain, liver, kidney, and perirenal fat tissues of each exposure stages were measured as shown in Table 6.3. It shows that cyclohexane in blood, liver, brain, and kidney almost cleared completely 12 h after exposure, and there was no significant accumulation of cyclohexane shown by the Day 2 and Day 3 exposure measurements.[4]

In humans, a small portion of inhaled cyclohexane can be excreted in the urine, although it is primarily excreted via expiration from the lungs. Ghittori et al. reported a linear relationship between environmental cyclohexane levels (x in ppm) and urinary cyclohexane levels (y in nmol/mL) using the following regression equation: y=0.05x+8.26, r^2=0.79 based on urine measurements from 43 people.[256] In another study, a good correlation between cyclohexane in the air and cyclohexanol in the urine has been found. An equation was found for workers exposed to cyclohexane: y=12x + 39.1, where x (ppm) is the concentration of cyclohexane in the air and y (μg/L) is the concentration of urinal cyclohexanol concentration.[3]

6.7 Toxicities of cyclohexanol

6.7.1 Acute toxicity of cyclohexanol

6.7.1.1 Treon study (1943)

The observed minimum oral lethal dose for rabbits is 2.2-2.6 g/kg.[237,240] The most prominent oral administration toxicities of cyclohexanol are narcosis (see Glossary); other signs of toxicity include ataxia, lethargy, collapse, and loss of reflexes. The effect of narcosis is consistent with the observations reported in mice (Savelova and Brook 1962). Pathological examination revealed kidney damage including subacute and chronic glomerular tubular nephritis (see Glossary).[240]

The observed minimum dermal acute lethal dose for rabbits lies between 12.4-22.7 g/kg/-day.[240] In the study, the dermal exposure was conducted by applying cyclohexanol upon the abdominal skin of the rabbit in two 5 ml portions at 0.5 h intervals until the target

dose. one rabbit received a total of 94.4 g/kg cyclohexanol, which was 9.44 g/kg/day for 10 days, suffered from irritation of the skin, narcosis, tremor, hypothermia, thickening of skins, local ulcers, and eventually death after the 10th treatment. Another three rabbits received dose levels of 12.4, 22.7, and 45.6 g/kg cyclohexanol for only one day, and the two high dose rabbits died. Therefore, it is concluded that the acute lethal dose for rabbit is between 12.4 and 22.7 g/kg.

Cyclohexanol caused moderately severe irritation and reversible corneal injury to eyes of rabbits with cyclohexanol applied directly. No inhalation irritation was observed in dogs with a dose that saturated the air for 10 min/day for 7 days.[237]

6.7.2 Neurotoxicity of cyclohexanol

6.7.2.1 Perbellini study (1981)

Cyclohexanol does not lead to observable neurotoxicity. 19 Sprague-Dawley rats were divided into control (5 rats), cyclohexanol (in peanut oil) (7 rats), and cyclohexanone (in peanut oil) groups (7 rats). After being treated with a total of 400 mg/kg/day dosage of cyclohexanol orally (200 mg/kg, twice a day) for five days per week for three weeks, 2 rats died and thus the administration of cyclohexanol was decreased to 200 mg/kg/day. After another 3 weeks, the 200 mg/kg-day treatment was suspended due to poor growth of rats. Overall, the body weights of cyclohexanol group decreased significantly than control and cyclohexanone groups. After the suspension of the treatment, body weights of cyclohexanol group increased in a similar fashion as the control. Cyclohexanone did not decrease body weights significantly when given by oral administration.[5]

Electrophysiology checks were conducted at the dorsal nerve of the tail at the end of

Table 6.4: Electrophysiological parameters detected after 6 weeks of treatment in the control rats and in those treated with cyclohexanol. MCV: motor conduction velocity, LD: distal motor latency, MSCV: sensory nerve conduction velocity calculated in the initial part of the positive deflection, SCV: sensory conduction velocity at the apex of the peak. Source: Perbellini, et al. (1981).[5]

	Control	Cyclohexanol	Cyclohexanone
MCV (m/s)	33.08±3.92	36.2±6.10	35.8±4.66
LD (ms)	0.49±0.10	0.57±0.12	0.51±0.06
MSCV (m/s)	33.80±1.46	37.2±5.20	36.4±4.78
SCV (m/s)	48.80±2.30	47.8±6.40	47.2±4.50

The table data was analyzed by Dunnet's test and no statistically significant difference was found.

6th and 13th weeks. For all measures, MCV (Motor Conduction Velocity), LD (distal Motor Latency), MSCV (Sensory nerve Conduction Velocity calculated by the initial part of the positive deflection), SCV (Sensory Conduction Velocity calculated at the apex of the peak), there were no statistically significant differences among control, cyclohexanol and cyclohexanone groups as shown in Table 6.4.[5]

Morphological study of tissue samples from sciatic and tibial nerves (see Glossary) was also performed and no significant changes were formed in either the fiber numbers or the fiber section areas; no clinical sign of peripheral neuropathy was observed. Therefore, it was concluded that neither cyclohexanol nor cyclohexanone leads to peripheral neuropathy in rats.[5]

6.7.3 Reproductive and developmental toxicities of cyclohexanol

6.7.3.1 Gondry study (1973)

Gondry's study[257] showed signs of reproductive toxicity of cyclohexanol, indicated by an increase in postnatal mortality rate in mice. 1% cyclohexanol in the feed was applied in two

strains (TB and MNRI) of mice, for a two-generation study. Mice were exposed to the treatment diet during F-0 (meaning parental mice, F is filial) cohabitation and through gestation and lactation. F-1 mice (the offspring of F-0 parental mice) were exposed continuously until the end of the study when F-2 (offspring of F-1 mice) was 21 days of age. Mortality rates were reported for F-1 and F-2 on PND 21 (Postnatal Date 21). In TB mice, the mortality rate was 12.2% (14 death/116 total) for F-1 and 53.5% (52/97) for F-2.[257] The F-1 mortality rate was not different from that of the control mice. In MNRI mice, the mortality rate for F-1 was 43.1% (22/51); F-2 mortality was not studied. The length of maternal premating exposure could be ranging from 1 day to several days; the number of days of exposure before copulation is not reported in the publication. We estimated an average of 42 days exposure of cyclohexanol

One can conclude that, at the 1% dose level in feed, cyclohexanol significantly increases the mortality of the F-1 offspring in MNRI mice and the mortality of the F-2 offspring in TB mice. Based on OECD (the Organisation for Economic Co-operation and Development) approaches, the 1% in feed dosage would be equivalent to 1500 mg/kg body weight per day.[258] Committee for Compounds Toxic to Reproduction, a committee of the Health Council of the Netherlands, estimated 1200 mg/kg by considering extra body weight during gestation period.[259]

Weaknesses of the study include: (1) rates of mating, fertility, and fecundity are not reported, (2) there is only a single test concentration, (3) days of premating parental exposure (cohabitation time) of F-0 are not reported; the premating days varies because the timing of mating is not a controllable factor.

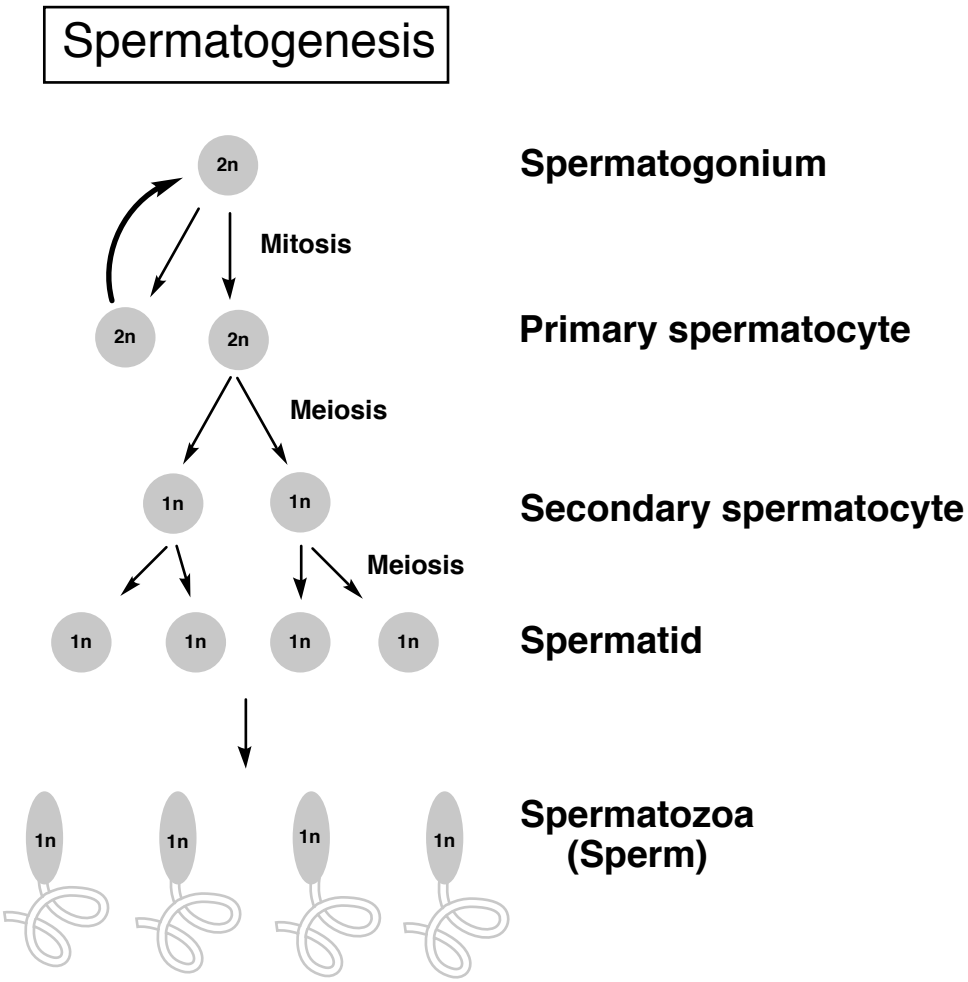

Figure 6.8: Spermatogenesis: the development of sperms.

6.7.3.2 Dixit-Tyagi study (1979)

Subcutaneous exposure to 15 mg/kg-day of cyclohexanol for 21 days in male gerbils (n=20) and for 37 days in male house rats (n=20) resulted in marked inhibitory effects on spermatogenesis and testicular damage. Measurements also included weights of organs (Testes, seminal vesicles, ventral prostate (see Glossary), epididymis (see Glossary), thyroid (see Glossary) and adrenal glands (see Glossary)); total RNA, protein, sialic acid, alkaline phosphatase activity, and cholesterol levels of testis, epididymides, and seminal vesicles; diameters of seminiferous tubules (see Glossary) and Leydig cell (see Glossary) nuclei; serum total

cholesterol, phospholipids, triglycerides, free fatty acids, proteins, and transaminase enzyme activities; and blood sugar and urea.[260]

Seminiferous tubules degenerated in both species and loss of spermatocytes, spermatids, and spermatozoa were also observed (see Glossary Spermatogenesis and Figure 6.8). Sertoli cells displayed varying degrees of vacuolation of the cytoplasm. As shown in Table 6.5, there is a significant decrease in the weights of testes, epididymitis, seminal vesicles, and ventral prostate, and Leydig-cell nuclear dimension without changes in body weights.

In both gerbils and house rats, the spermatogenesis appears to be arrested at the primary spermatocyte level. Histological observations showed the normal appearance of luminal epithelium (see Glossary) and stereocilia (see Glossary), although with patchy areas devoid of spermatozoa. The evident decrease in the size of Leydig-cell nucleus and marked elevation of cholesterol concentration suggest interruption of steroidogenesis in Leydig cells. Serum cholesterol concentration remains in the normal range.[260]

Concentrations of measured biochemical components significantly decreased in the reproductive tissues as seen in Table 6.5, including over 50% of reduction of glycogen concentration in testes. The exceptions are elevated cholesterol concentration and alkaline phosphatase (ALP) activity in the testes; testicular cholesterol concentration increased 72% in gerbils and 244% in-house rats, while testicular ALP activities increase more than 100% in both species. The increasing levels of testicular cholesterol indicated the low functioning of the system. The decrease of protein, RNA, sialic acid (see Glossary) concentrations in testes are consistent with the inhibition of spermatogenesis and Leydic cell suppression.[260]

Hematological studies (red cells, hemoglobin, and packed cell volume, and leucocytes) and biochemical parameters measured in serum and blood, including blood sugar, urea, ALP, and serum transaminases were all in the normal ranges.[260]

In summary, the above observations indicated that, at the tested dosage, testicular tissues and spermatogenesis are targets of reproductive toxicity of cyclohexanol in gerbils and house rats.

6.7.3.3 Dixit study (1980)

In a 40-day study of 25 mg/kg/day of oral treatment of cyclohexanol (dissolved in olive oil) in 15 male rabbits, Dixit et al. (1980) examined the testes with similar parameters as those described in the study by Tyagi, Dixit et al. (1979) in gerbils and house rats. Additional parameters were measured to examine potential effects on glycolysis and liver metabolic function. These included liver histology, adrenal ascorbic acid, blood sugar, blood urea, serum triglycerides, and bilirubin. The study also included a recovery group on which observations were performed 70 days after cessation of the 40-day treatment.[261]

Similar to the results in gerbils and house rats,[260] treated rabbits lose type A spermatogonia, spermatocytes, spermatids, and spermatozoa in the testes. There were also shrunken Leydig cells with scant cytoplasm and small nuclei in diameter. As shown in Table 6.5, Cyclohexanol significantly decreased the weights of testes (66% decrease), epididymis (31% decrease), seminal vesicles (22%), and ventral prostate (30% decrease). Similarly to those observed by Tyagi et al., testicular glycogen decreased about 50%. Cholesterol concentrations increased in both testes and serum in the rabbits. The concentrations of serum triglycerides and blood sugar, urea, and bilirubin were also elevated in rabbits. Adrenal ascorbic acid concentrations were diminished. Hematological parameters of cyclohexanol treated rabbits were in the normal range. Seventy days after the cessation of the exposure, spermatogenesis, organ weights, and histological observations of the testes recovered significantly toward the normal range. Serum, blood, and tissue parameters also recovered partially to subnormal

values, except that concentrations of serum phosphatase activity, blood sugar, blood urea, and serum bilirubin, which remained elevated.[261]

In summary, an oral dosage of 25 mg/kg per day for 40 days diminished spermatozoa in epididymis and ductus deferens in rabbits (b.w. 1.5 – 2 kg, five per treatment group). Spermatogenesis was interrupted at the spermatocyte and spermatid level. The 25 mg/kg per day subacute exposure is an apparent effective dose in reducing spermatogenesis, Leydig cell function, most likely the steroidogenesis, and testicular glycogen metabolism and hepatic carbohydrate metabolism.

The effects observed in testis, epididymis, and steroidogenesis are partially reversed 70 days after cessation of treatment, with a tendency to return toward normal concentrations of testicular protein, RNA, sialic acid, cholesterol, and glycogen. Serum protein, SGPT (Serum Glutamic Pyruvic Transaminase), triglycerides, serum glucose, and blood urea concentrations also recovered. Testicular acid phosphatase and adrenal ascorbic acid concentrations partially recovered. Nonetheless, there is little evidence for recovery of the elevated concentration of serum cholesterol, phospholipids, phosphatase activity, and bilirubin concentration. Histological examination revealed no hepatic changes and the liver weight was not reported.

6.7.3.4 Lake study (1982)

Gastric intubation of 455 mg/kg/day cyclohexanol (in corn oil) for 7 days in 30-day old male Sprague-Dawley rats (n = 12) did not produce observable testicular atrophy (Lake et al. 1982). Relative liver weight increased about 12%, without significant changes in relative kidney and testes weights. The treatment also increased hepatic microsomal cytochrome P-450 and stimulated the hepatic activity of biphenyl 4-hydroxylase, 7-ethoxycoumarin O-deethylase, and aniline-4-hydroxylase (CYP2E1).[262]

Table 6.5: Summary of cyclohexanol toxicity on body/organ weight and clinical chemistry studies.

Study	**Dixit-Tyagi (1979)**		**Dixit (1980)**	
	House Rats	**Gerbils**	**Rabbits**	
			Treatment	**Recovery**
Dosage mg/kg/day (Days)	15(37)	15(21)	25 (40)	0 (70)
Administration Route	Injection	Injection	Oral	-
Body Weight Change	Not signi.	Not signi.	Not signi.	Not signi.
Organ Weight/Diameter Changes % [a]				
Testes	− 39%**	− 36%*	− 66%*	− 30%
Epididymides	− 58%**	− 46%**	− 31%*	− 10%
Seminal Vesicles	− 27%*	− 37%	-	-
Ventral Prostate	− 48%*	− 44%*	-	-
Seminiferous Tubule diam. (μm)	− 26%*	− 34%*	− 27%*	+ 15%
Leydig Cell Nuclear diam. (μm)	− 17%*	− 28%*	− 30%*	− 6%
Composition Concentration Changes in Testis% [b]				
Protein	− 52%*	− 49%*	− 42%*	− 18%
RNA	− 51%*	− 46%*	− 34%*	− 11%
Sialic acid	− 45%*	− 43%*	− 42%*	− 9%
Glycogen	− 58%*	− 56%*	− 48%*	+ 13%
Cholesterol	+ 244%*	+ 68%*	+ 51%*	+ 16%
Composition Concentration Changes in Epididymides% [b]				
Protein	− 42%*	− 58%*	− 39%*	+ 24%
RNA	− 51%*	− 37%*	− 41%*	− 14%
Sialic acid	− 50%*	− 61%*	− 39%*	− 29%

Student's 't' test was applied for statistic analysis. * indicates the original treated group was statistically significantly different ($p < 0.01$) from control, and ** indicates $p < 0.001$.

[a] = (organ weight /100 g body weight of control – that of treated group)/(organ weight/100 g body weight of control); organ weights were mean values for 20 house rats, 20 gerbils, and 5 rabbits.

[b] = (concentration (mg/g tissue) in the control – that of treated group)/(concentration in the control); concentrations were mean values for 6 determinations.

The study used pre-pubertal rats with 7-day cyclohexanol exposure without observing any testicular toxicity; one can argue that 7-day may be too short to observe apparent reproductive toxicity of cyclohexanol. It should be noted that 7-day exposure is possible for observing reproductive toxicities for other chemicals, for example, a complete loss of germinal cells from seminiferous tubules were observed with 7-day oral exposure of dicyclohexyl phthalate.[262]

6.7.3.5 A comprehensive cyclohexanol reproductive, developmental and neurotoxicity study - MPI study (2006)

MPI Research, Inc. examined the effects of whole-body inhalation exposure of cyclohexanol in the aspects of reproductive, F-1 developmental, and neurological toxicities, applying the guidelines for Repeat Dose Toxicity and Reproduction/Toxicity Screening Study (OECD 422).[30] Despite extensive effort, we were unable to obtain the original study report from EPA and MPI Research, Inc. To our thrill and luck, Dr. Henry J. Trochimowicz, the sponsor representative of the report, kindly shared the full report with us.

As shown in Figure 6.9, 15 males Sprague-Dawley rats per treatment (0, 50, 150, and 450 ppm) were randomly assigned to Repeat Dose group (or RD group, meaning exposed to cyclohexanol repeatedly), and 30 females Sprague-Dawley rats (7-week age) per treatment (0, 50, 150, and 450 ppm) were assigned into two sub-groups, 15 for Reproductive Group and 15 for Repeat Dose group (RD group). For 10 weeks, both male and female rats were exposed to 0, 50, 150 and 450 ppm cyclohexanol for 6 h/day, 5 days/week. After the 10-week pretreatment, male and female rats were cohabitated for mating. During and after mating (gestation and lactation), for the 11th to 16th weeks, female rats were exposed to the same corresponding concentrations for 6 h/day, 7 days/week, except the highest dose. The highest

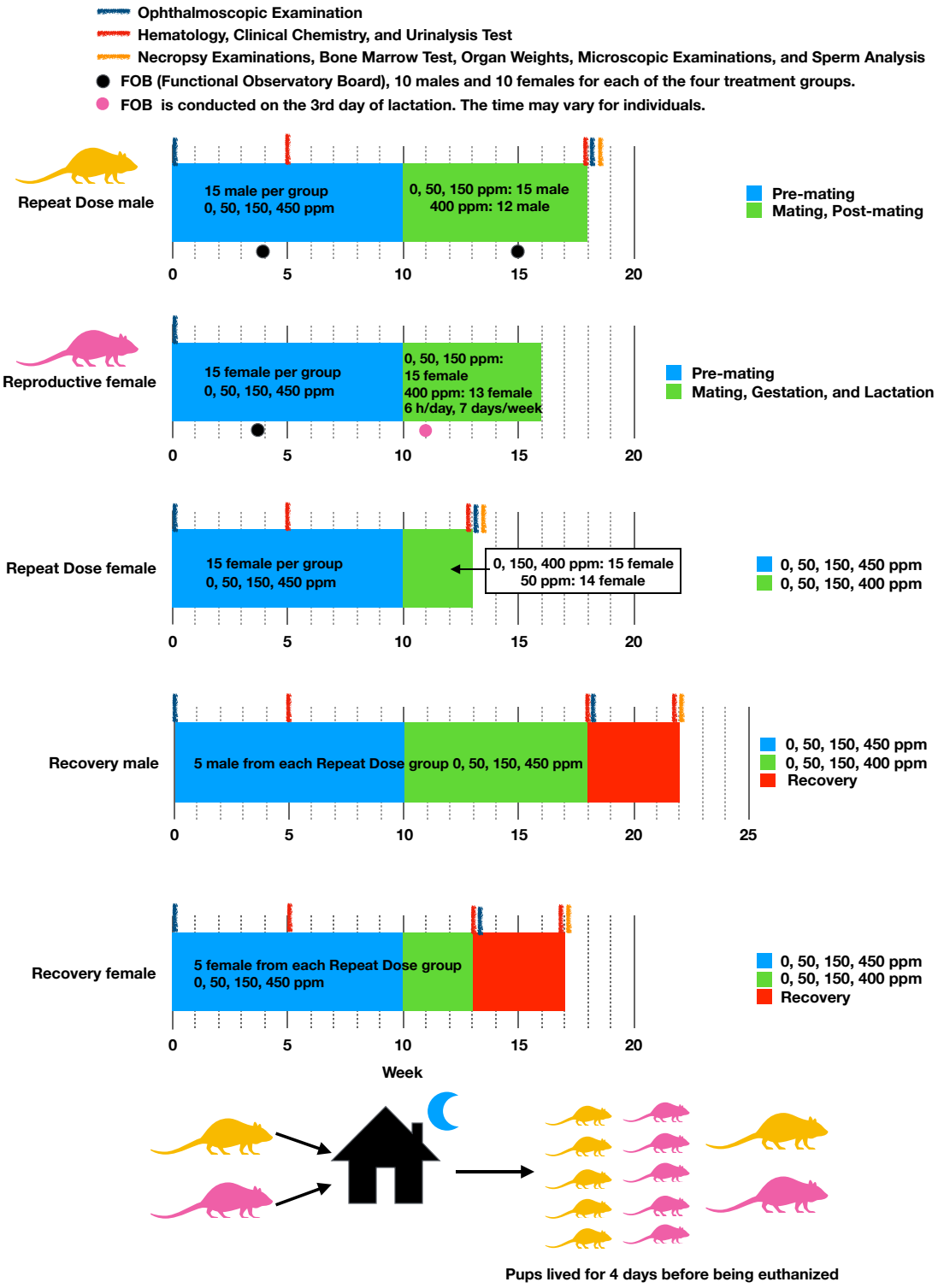

Figure 6.9: The study design of MPI study. Blue represents 0, 50, 150, 450 ppm treatment, green indicates 0, 50, 150, 400 ppm treatments. All exposures was conducted 6 h/day, 5 days/week except the reproductive female during mating, gestation and lactation as shown in the graph. Source: Newton, et al. (2006).[30]

dose was decreased from 450 ppm to 400 ppm on the first day of breeding because 3 female and 1 males died during the premating period in this group. For male rats, during the 11th to 18th weeks, the highest dose was also lowered to 400 ppm. During mating period, one male and one female of the same dosage group were paired nightly, therefore when females were exposed 7 days/week, males could and were continuously exposed 5 days/week. The mating period was described as up to 2 weeks. Pups were examined and euthanized on postnatal day 4 (PND 4).

In the second part of the study, after a total of 13 and 18 weeks of exposure described above, five female and five male rats, respectively, from each Repeat Dose groups were selected for a 4-week recovery study. At the end of the 22nd week, sperm motility and concentration were measured. Four weeks after the cessation of the exposure, sperm counts in the 450/400 ppm group had sperm counts similar to the concurrent controls.

Body weight measurement and neurobehavioral examinations were conducted weekly prior to and during the exposure of cyclohexanol, and body weight was also recorded at the termination. FOB (Functional Observatory Board), ophthalmoscopic examination, hematology, clinical chemistry, urinalysis tests, necropsy examinations, bone marrow test, organ weights, microscopic examinations, and sperm analysis were conducted in various periods, which are shown in Figure 6.9 as indicated by different colored bars. Motor activity was measured during the same interval as the FOB observation.

Body Weight:

Exposure to cyclohexanol did not significantly affect body weight in both the repeat dose male and female rats through the study. Nonetheless, during gestation, the maternal body weight gain (gestation date 0-20) is significantly less in the 450/400 ppm group (mean 112.9 g, SD 30.25), compared with the controls (135.6 g, SD 14.69). The low body weight gain

in the 450/400 ppm treatment group, at least in part, is caused by smaller litter size (see results on litter size below.) Differences in food consumption among treatment groups did not result in any discernible significance.

Mortality:

Results indicate that 450 ppm inhalation exposure is a lethal dose. Among the 6 rats (3 males and 3 females) that died before mating, 5 rats (3 males died on day 37, 38 and 60; 2 female died on day 31 and 32) were from the 450 ppm treatment group and the other female was from 50 ppm group. One of the female rat died from the 450 ppm group was euthanized in extremis on day 17. There were no remarkable pathological findings among these 6 rats. In addition to these 6 rats, another male rat in the 50 ppm group died on day 126 due to blood collection.

Clinical and neurobehavioral observations:

Table 6.6: Incidences of rat prostration and decreased activity observed in 450 ppm due to cyclohexanol exposures.

	Prostration/Total	**Decreased Activity/Total**
Male	3/15	4/15
Female	4/30	8/30

Data were extracted from the original full report. Source: Newton, et al. (2006)[30]

Among the 45 rats treated with 450 ppm cyclohexanol during premating, 27% of rats (see Table 6.6) showed decreased activity, among them 3 males and 4 females presented in the form of prostration (see Glossary). No remarkable clinical signs or neurobehavioral changes were observed in other treatment groups, or any of the treatment groups after the initiation of mating, which is when 450 ppm treatment was switched to 400 ppm.

Ophthalmoscopic Examination:

One case of superficial keratitis in the left eye in one 150 ppm treated male rat, one case of chorioretinal hypoplasia in the right eye in 450/400 ppm treated male and one case red conjunctivitis in the left eye in 450/400 ppm treated a female.

Only one incidence of lacrimation during premating Day 10-11 was observed in one female in the 450 ppm group; the same rat also displayed decreased activity and prostration. Brown material around eyes was observed during the first 10 week exposure: 3 in control, 1 in 50 ppm, 1 in 150 ppm, and 3 in 450 ppm treated rats.

Locomotor Activity and Functional Observational Battery:

Motor activity and functional observational battery were conducted after 4 weeks of initiation of treatment in males and females, as well as males after 15 weeks and females on day 3 of lactation. The total distance of the locomotor activity, in 30 minutes, was significantly increased in male rats at week 15 in the 150 ppm treatment. No other measurements (horizontal activity, stereotypy activity, and vertical activity counts) from the locomotor activity achieved any statistically significant observations. The increase in activity was not observed in the 450/400 ppm treatment group because of the apparent effects of decreases in activity and prostration described in the previous paragraph. Results from the functional observational battery (FOB) did not demonstrate any treatment-related effects.

Hematology and Clinical Chemistry:

Mean blood cholesterol levels in week 18 in male rats, as shown in Table 6.7, were elevated in all treatment groups when compared with the control, but only the 450/400 ppm group achieved statistical significance ($p < 0.01$). In the female rats, elevated cholesterol levels in week 13 showed the same dose-related trend, which is consistent with the testes cholesterol increase observations from the Dixit and Dixit-Tyagi studies in Table 6.5. Other changes in blood analysis include decreases in alkaline phosphatase, increases in Aspartate

Table 6.7: Mean values of blood cholesterol concentrations.

	Mean (Cholesterol mg/dL)			
	0 ppm	**50 ppm**	**150 ppm**	**450/400 ppm**
Male (Week 5)	54.2±8.07	56.6±9.24	49.8±7.73	59.2±7.16
Male (Week 18)	56.9±12.17	64.8±10.29	63.3±15.06	74.7±11.35**
Female (Week 5)	66.4±16.07	73.0±11.36	75.6±12.82	72.8±20.64
Female (Week 13)	66.0±13.63	74.6±15.04	80.2±9.30	87.4±23.83*

** $p < 0.01$ * $p < 0.05$

On week 5, only 5 rats each sex and each treatment group were tested, and 10 rats were tested on week 18 or 13. Source: Newton, et al. (2006)[30]

transaminase, and an increase in serum globulin in the 450/400 ppm treatment group.

Microscopic Observations:

The numbers of rats having chronic progressive nephropathy in kidney increased in both 150 ppm and 450/400 ppm male rats compared to control. Mineralization in tubular or renal pelvis appeared in both control and treated groups. Meanwhile, one female rat in the highest dose had inflammation in the renal pelvis (pyelitis). No other test article-related microscopic changes were observed.

Sperm Analysis:

To evaluate spermatogenesis, at the end of 18-week exposure and at the end of the additional non-exposure recovery period, the following parameters were examined in male rats: sperm motility, total cauda epididymal (see Glossary) sperm cells, sperm concentration per gram of cauda epididymis, number of homogenization resistant sperm head in testis, daily sperm production (DSP) per testis, and spermatogenic efficiency (DSP per gram testis). Some important findings are summarized in Table 6.9. Male rats (F-0, Filial-0 is the parental rats) in the 450/400 ppm group showed a decrease in daily sperm production per gram testis at the completion of the exposure period (18 weeks). No other observations were different from the controls. At the end of the recovery period, no remarkable changes in

Table 6.8: Summary of abnormal microscopic observations.

	Numbers of rats that have abnormal kidney microscopic observations			
	0 ppm	**50 ppm**	**150 ppm**	**450/400 ppm**
			Male	
Infiltration, lymphocytic	3	3	0	1
nephropathy, chronic progressive	1	0	7	3
mineralization, tubular	0	0	1	0
			Female-Repeat Dose Group	
Infiltration, lymphocytic	2	1	2	2
mineralization, tubular	2	0	0	1
pyelitis	0	0	0	1
			Female-Reproductive Group	
Infiltration, lymphocytic	4	-	-	3
nephropathy, chronic progressive	1	-	-	3
mineralization, pelvic	4	-	-	2
mineralization, tubular	1	-	-	2

10 male and female rats were tested in the repeat dose group, and 15 for female reproductive group 0 and 450/400 ppm group.

Data was extracted from MPI full report Table 34, 35, and 36. "-" means data was not measured. Source: Newton, et al. (2006)[30]

Table 6.9: Summary of sperm evaluation results.

	Summary of sperm evaluation			
	0 ppm	**50 ppm**	**150 ppm**	**450/400 ppm**
	Repeat Dose male			
SC (10^8/g of cauda eipididymis)	6.827±1.5048	6.954±0.6941	6.479±1.7397	7.478±2.1969
HRSHC (10^8/testis)	1.973±0.2385	1.537±0.1743	1.581±0.1156	1.764±0.2453
DSP (10^8)/testis)	0.323±0.0390	0.252±0.0284	0.259±0.0191	0.289±0.0401
SE (10^8/g of testis)	0.175±0.0194	0.132±0.0163	0.134±0.0156	0.149±0.0117**
	Recovery male			
SC (10^8/g of cauda eipididymis)	8.986±1.0352	8.019±0.7664	8.623±1.5633	8.453±1.4727
HRSHC (10^8/testis)	1.375±0.1581	-	-	1.715±0.0912**
DSP (10^8)/testis)	0.225±0.0258	-	-	0.281±0.0150**
SE (10^8/g of testis)	0.119±0.0139	-	-	0.147±0.0065**

Numbers shown here are verbatim from the Table 24 of the MPI original report. Source: Newton, et al. (2006)[30]
SC: Sperm Conc. per gram cauda epididymis
HRSHC: Homogenization Resistant Sperm Head Count
DSP: Daily Sperm Production, it is the numbers of sperm heads per testis.
SE: Spermatogenic Efficiency (DSP/g of testis)
**: Significantly different from control; ($p < 0.01$)
The statistics of repeat dose SC, HRSHC, DSP was not reported.

these parameters could be made in relation to reproductive function or any effects under the influence of either cyclohexanol treatment or recovery.

Reproductive and Developmental Study:

In the reproductive study, although all pairs in all treatment groups mated, as shown in Table 6.10, 14 of the 15 control pairs mated within 4 days (one estrus cycle),[263] and one pair (one out of 15 pairs) mated on day 9, during second or third estrus cycle. All pairs (15 pairs each treatment) in the 50 ppm and 150 ppm groups mated within the first estrus cycle. Of the 13 pairs in the 450/400 ppm group (2 reproductive females died before pairing), 10 pairs mated during the first estrus cycle. For one pair mating was not detected, although pregnancy resulted. One pair mated on day 12, another pair on day 13. Overall, three pairs resulted in no pregnancy or no live birth.

Two of the 11 pregnant rats in the 450/400 ppm treatment group produced no viable

Table 6.10: Summary of reproductive parameters in MPI study.

	0 ppm	**50 ppm**	**150 ppm**	**450/400 ppm**
	Reproductive Female			
Total number	15	15	15	15
Mortality	0	0	0	2
Numbers of mated rats	15	15	15	13
Numbers of pregnant rats	14	15	15	11
Fertility %	93	100	100	85
Mating during 1st estrus cycle	14	15	15	10
Mating delayed	1(d9)	0	0	2(d12, d13)
Rats have vital offspring	14	15	15	9
Numbers of litter	14	15	15	10
Litter size (mean±SD)	13.9±2.2	12.9±3.0	13.8±2.9	12.1±4.5
Pup died / Litter (mean±SD)	0.57±0.82	0.73±1.73	0.13±0.50	0.60±0.66
Sex ratio (mean±SD, male/total)	0.49±0.13	0.47±0.14	0.48±0.10	0.57±0.19

(d9) means mating delayed till day 9; (d12, d13) means one rat's mating delayed till day 12, and the other day 13. Data were extracted from all individual data tables in Appendix Q, S, and U of the MPI full report. Source: Newton, et al. (2006)[30]

pups at parturition (meaning giving birth). F-0 Female rats sacrificed on PND (Postnatal Date) 4, had no remarkable histology finding in organs and tissues in any of the F-0 female rats in all treatment groups.

There was no statistical significance in litter size at birth or pups died from PND 0 to PND 4. Mean sex ratio (0.57 male/total pups) appears to be higher in the 450/400 ppm group, but it was in part driven by one litter with only a single stillborn male. After eliminating the stillborn male, the ratio drops to 0.52. In either of the calculation, the differences in sex ratio among the treatment groups could not achieve statistical significance with the number of observations in this study, 10 to 15 litters per treatment. The sex ratio calculated from total male/total pups is 0.54. Lower pup body weights were observed on PND 0 and PND 4, in the 450/400 ppm dose group; only PND 0 achieved statistical significance, $p < 0.05$.

Based on the results of the MPI inhalation study, 450/400 ppm is an effective dose for

reproductive toxicity. Using the conservative approach, the NOAEL(no observed adverse effect level) for reproductive toxicity is determined to be at 150 ppm for 6 hours/day, 5 days/week, for 10 weeks.

6.7.4 Carcinogenicity and mutagenicity

No information was found to suggest carcinogenicity of cyclohexanol.

No mutagenic effect of cyclohexanol was found at the dose levels tested. One sub-chronic inhalation study reported that 50 three-month-old healthy male ICR (strain name of the mice, from Institute of Cancer Research in the USA) mice were exposed to 1.73 ppm cyclohexanol for 6 continuous weeks and neither chromosomal aberration, nor micronucleus induction were observed. In the sister chromatic exchange (SCE) study, a significant elevation of the SCE frequency was observed in the cyclohexanol mice group. SCE is the exchange of genetic material between two identical sister chromatids and a more frequent SCE may be related to formation of tumors.[264] However, a positive SCE response does not necessarily mean that the compound is mutagenic.[265]

Cyclohexanol has been observed to be an antimutagen towards the nitrosoamine NNK (see Figure 6.10) and NDEA in *Salmonella typhimurium* (one type of pathogenic bacteria) strain TA100. ^{14}C labeled NNK experiments indicated that cyclohexanol altered the kinetics of metabolism. The inhibition of NNK and NDEA metabolism contributed to cyclohexanol's antimutagenicity effect.[266] Notably, the author also mentioned that at higher concentrations, cyclohexanol toxicity started to appear, although the details of the toxicity effects were not mentioned.

On the other hand, Villa-Trevino showed that cyclohexanol can help other two carcinogens, AAF and NDEA, in the development of liver tumors by increasing CYP2E1 enzyme

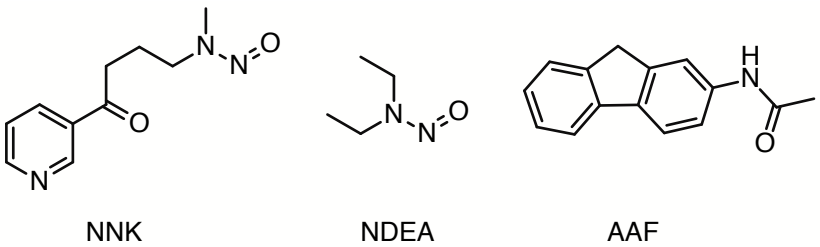

Figure 6.10: The chemical structures of NNK, NDEA, and AAF.

and reactive oxygen species (ROS).[267] Their well designed 6 group parallel Fisher rat experiments with different combinations of NDEA (injection), cyclohexanol, and tumor promoter 2-acetylaminofluorene (AAF, oral) administrations showed that tumor developed severely in the presence of NDEA, repeated doses of AAF and repeated doses of cyclohexanol; tumor appeared much less with NDEA and repeated AAF, or with NDEA, repeated AAF, and single dose of cyclohexanol; tumor disappeared except a small dot of stain positive area was observed with NDEA and repeated cyclohexanol without AAF. Although the author claimed cyclohexanol was a co-carcinogenic effect chemical, the evidence was too weak to support this effect, but cyclohexanol was a true inducer in the presence of both NDEA and repeated doses of AAF.

6.7.5 Cyclohexanol toxicities in humans

There have been no study found on human reproductive toxicity or neurotoxicity of cyclohexanol.

Acute dermal exposures of cyclohexanol with 4% of cyclohexanol in petrolatum patched on human skin for 48 h led to edema.[268]

The toxicity of cyclohexanol inhalation is inconclusive. A group of 174 women and 279 men exposed daily to less than the permitted concentrations of cyclohexanol, benzene, cyclohexane, cyclohexanone, cyclohexanone oxime and caprolactam during the caprolactam

production, 114 individuals showed non-specific disturbances of the autonomic nervous system for two years.[269] The concentrations of solvents in the air were not specified and there was no evidence that the symptoms were solely due to the exposures of cyclohexanol.

Cyclohexanol at 100 ppm leads to irritations to the eyes, nose, and throat of humans.[268]

6.7.6 Summary of cyclohexanol toxicities

Cyclohexanol has acute toxicity on rabbits, rats, and mice, but no human acute toxicity study was found. As summarized in Table 6.11, the lethal oral dose for rabbits is 2200–2600 mg/kg, lethal dermal dose is 12400–22700 mg/kg, intravenous LD_{50} is 1420 mg/kg and intravenous LD_{50} for mice is 270 mg/kg.[237,240] The main acute toxicity symptoms include narcosis, ataxia, lethargy, collapse, loss of reflexes, loss of body weight, and death for oral administration; narcosis, tremor, hypothermia, thickening of skins, local ulcers, loss of body weight, and death occurred for dermal administration.[240] Most of the toxicity symptoms are recoverable within hours after both oral and dermal acute exposures except the skin symptoms. The body weight loss can be regained during a period ranging from one week to a month.[240]

Cyclohexanol has minimal neurotoxicity found for rats at the dose tested orally (400/200 mg/kg). After treatment of 400 mg/kg oral dose of cyclohexanol for 3 weeks, 2 rats (7 rats totally) died and the dose was decreased to 200 mg/kg for another 3 weeks. The electrophysiological tests on the dorsal nerve of tail did not show any difference from the control group. Morphologically, no nerve fiber abnormality was observed.[5] Although some central nerve irritation in the form of tremor and athetoid movement on rabbits were shown with dermal administration dose of 3500 mg/kg/day cyclohexanol after several exposures, these symptoms for oral administrations with 800–2600 mg/kg/day were not observed on rabbits.[240]

Moreover, the subchronic MPI study did not observe any neurobehavioral, locomotor activity, and FOB parameter changes with dose up to 450 ppm via inhalation of cyclohexanol on rats.

Cyclohexanol may have male reproductive toxicities via oral ingestion shown by Gondry, Dixit-Tyagi, and Dixit subacute studies, however, no similar toxicity was observed by acute Lake oral study and subchronic MPI inhalation study. Gondry[257] showed 1200 mg/kg cyclohexanol oral exposure increased the postnatal mortality rates of TB mice second generation (F-2) and that of F-1 MNRI mice, with no apparent increase of mortality rate for TB mice F-1. Dixit-Tyagi[260] and Dixit[261] studies showed degenerations of multiple male reproductive organs or its substructures in gerbils, house rats, and rabbits. Symptoms include dramatic weight decreases of testes, epididymis, seminal vesicles, and ventral prostate, the disappearances of several stages of germinal cells, increases in the concentrations of testicular cholesterol, and decreases in testicular glycogen concentrations. Lake study[262] did not see testis atrophy or germinal cell loss for 7-day cyclohexanol oral administration to rats, which may be due to the short period of exposure. MPI study[30] showed cyclohexanol has no effect on spermatogenesis, testes weight, although statistically non-significant decreases were observed on numbers of rats having vital offspring, numbers of mated rats, fertility, numbers of litter, and mean litter size.

This contradiction may be understandable considering that the dosage, route of administration, and schedule of administration are different. Gondry, Dixit-Tyagi, and Dixit experiments are oral or subcutaneous administrations, while that of MPI study is inhalation. As discussed in the later part of the chapter in Table 6.19, after adjustments of the inhalation dosage in MPI study into mg/kg/day including the corrections from 6 h/day, 5 days/week schedule in MPI study compared with 7 days/week schedule in all other studies,

the dosage in MPI study is the same as the Dixit study, both of which are 25 mg/kg/day. Since the short half lifetime of cyclohexanol (less than 20 min in rat with the intraperitoneal administration, injection directly into the peritoneum, the body cavity), 2 day recovery time each week in MPI study may enable the development of germinal cells.

It is not clear about the systematic toxicity mechanism of cyclohexanol. It was suggested by the Villa-Trevino study[267] that cyclohexanol assisted liver tumor development by increasing CYP2E1 enzyme and reactive oxygen species, and by Lake study[262] that cyclohexanol led to inductions of hepatic xenobiotic metabolism. Several liver enzyme activities were elevated significantly including cytochrome P-450, biphenyl 4-hydroxylase, 7-ethoxycoumarin O-deethylase, and aniline-4-hydroxylase. Since no hepatic toxicity was observed in any cases, the correlations between local oxidative stress and cyclohexanol exposure should be studied in order to prove this oxidative stress toxicity mechanism hypothesis.

Table 6.11: Summary of cyclohexanol toxicity studies.

Study	Animal	Dose	Days	NOAEL	LOAEL	Death[b]	Toxicity Findings
Human							
Dermal exposures of cyclohexanol lead to skin edema.							
Animal							
Dermal (mg/kg-day)							
Treon	Rabbit	3500	10	-	3500	1(1)	First dose no response, second and succeeding dose caused narcosis for several hours, tremor, athetoid movement, hypothemia, local ulcers, thickening of skin, death after the 10th dose
		12400	1			0(1)	Slightly anesthetized for 1.5 h, body temperature decreased and recovered 2 h after treatment
		22700	1			1(1)	Deeply anesthetized, hypothermia, death
		45600	1			1(1)	Deeply anesthetized, hypothermia, death
Oral (mg/kg-day)							
Treon	Rabbit	800 to 2200	1	-	-	0(0)	Weight loss
		2200 to 2600	1	-	-	3(4)	Narcosis, death

Continued on the next page

Table 6.11 (cont'd)

Study	Animal	Dose	Day	NOAEL	LOAEL	Death[b]	Toxicity Findings
Perbellini	Rat (SD)	400	21	-	200	2(7)	Body weight decrease (reversible), no neuropathy, no neuron fiber number/thickness change, no electrophysiological abnormality, death.
		200	21	-		0	
Gondry	Mice (TB)[g]	1200	42	-	1200	14(116)[c] 52(97)[d]	Growth inhibition slightly for male and considerably for female; increase of F-2 postnatal mortality rate.
	Mice (MNRI)[g]	1200	42	-	1200	22(51)[c]	Growth inhibition slightly for male and considerably for female; increase of F-1 postnatal mortality rate.
Dixit	Rabbit[f]	25	40	-	25	0(15)	Disappear of type A spermatogonia, spermatocytes, spermatids, and spermatozoa in the testes; Leydig cells shrunken. The decrease in weights of testes, epididymitis, seminal vesicles, and ventral prostate, and concentration of testicular glycogen, an increase of testicular cholesterol concentration.
Lake	Rat (SD)[a]	455	7	-	455	0(7)	Increase in liver weight and hepatic enzyme activities include P-450, CYP2E1 etc. No testicular atrophy observed.
Subcutaneous (mg/kg-day)							

Continued on the next page

Table 6.11 (cont'd)

Study	Animal	Dose	Day	NOAEL	LOAEL	Death[b]	Toxicity Findings
Dixit-Tyagi	Gerbil[f]	15	21	-	15	0(20)	Seminiferous tubule degeneration; loss of Type A spermatogonia, spermatocytes, spermatids and spermatozoa; vacuolation of sertoli cells; decreases in weights of teste, epididymis, seminal vesicles, and ventral prostate; decrease in Leydig-cell nuclear dimension. Decrease in the concentration of testicular glycogen. These changes described above are partially recoverable. The increases of testicular cholesterol, phopholipids, bilirubin concentration, and the elevated phosphatase activity are not recoverable.
	House Rat[f]	15	37	-	15	0(20)	Same as above
Inhalation (ppm)							

Continued on the next page

Table 6.11 (cont'd)

Study	Animal	Dose	Day	NOAEL	LOAEL	Death[b]	Toxicity Findings
MPI	Rat (SD)[g]	50, 150, 450[e] ppm	91-126	150	450[e]	6(180)	Death at high dose, prostration, decreased activity, elevation in blood cholesterol level, increase incidences of chronic progressive nephropathy. Numbers of rats having vital offspring, numbers of mated rats, fertility, numbers of litter, mean litter size decreased in 450/400 ppm group, although not statistically significant. No compound-related effects on body weight, mortality, ophthalmoscopic, locomotor activity, FOB, other hematology parameters, organ pathology examination, and sperm analysis.

LOAEL: lowest observed adverse effect level; **NOAEL**: no observed adverse effect level. **SD**: Sprague-Dawley strain of rats. [a] pre-puberty rat [b] number in ( ) means total number of treatment animals. [c] the mortality of F-1 parent generation. [d] the mortality of F-2 generation. [e] the 450 ppm was changed to 400 ppm. [f] female. [g] male. [h] both male and female.

6.8 Toxicities of cyclohexane

6.8.1 Acute toxicity of cyclohexane

6.8.1.1 Treon-2 study (1943)

In a study by Treon et al.,[270] 4 rabbits were exposed to cyclohexane via inhalation for 6 h/day, 5 days/week for 2 weeks at cyclohexane concentration ranging from 435 ppm – 26,572 ppm. The minimum lethal inhalation dose is 7444 ppm in rabbits (Treon et al. 1943). At sublethal doses, 434 ppm – 3330 ppm, the toxicity signs include elevated respiration rate, cyanosis, severe diarrhea, weight loss, and conjunctival congestion.

The oral lethal dose of cyclohexane for rabbits was 5500 – 6000 mg/kg and the effect was mainly diarrhea.[240]

The dermal lethal dose of cyclohexane for rabbits was more than 180,000 mg/kg, much higher than that of cyclohexanol 12,000 – 22,700 mg/kg. The huge amount of dose perhaps is not surprising considering cyclohexane evaporates quickly on the skin.[240] The author did not quantify how much cyclohexane evaporated, thus the actual dermal lethal dose should be much smaller than the 180,000 mg/kg.

6.8.2 Neurotoxicity of cyclohexane

n-Hexane was known to have human neurotoxicity. In the 1960s and early 1970s, several outbreaks of nerve disorders occurred among shoe workers in Japan and Italy. The cause of the disease was determined to be a high concentration of n-hexane in the air. The symptoms varied from numbness, muscle weakness in the feet and lower legs, to paralysis of the arms and legs, caused by peripheral neuropathy.[271] The neurotoxicity origin of n-hexane is mainly

through its metabolite 2,5-hexandione reacting with lysine forming dimethylpyrrole and radical oxidation of dimethylpyrole followed by coupling leading to cross-linking of proteins.[272] Although this mechanism does not apply to cyclohexane, sedation effects of cyclohexane were well documented for cyclohexane and may indicate neurotoxicity.[273–276]

6.8.2.1 Lammers study (2009)

Lammars, et al. (2009) studied the neurobehavioral effects of 0, 407, 2324, and 8135 ppm cyclohexane in adult male Wistar-derived WAG/RijCR/BR rats (159 in total) through inhalation for 8 h/day for 3 consecutive days.[252]

The FOB (Functional Observational Battery) observations of 8 rats per exposure group showed altered gait and tremoring (only one rat) of rats in the 8135 ppm group. Approach-response showed a dose-response relationship in the 3 consecutive day experiment, from which, in the 8135 ppm exposure group, approach-response were significantly ($p < 0.05$) increased compared with control, indicating more exaggerated reactions in the high-dose group.

No significant effects were observed in the forelimb grab strength, hindlimb grip strength, mean foot splay, touch response, click response, tail-pinch response, arousal, and motor activity by cyclohexane exposure in any exposure groups.

One important conclusion from this study is that cyclohexane can cross the brain-blood barrier. The concentrations of cyclohexane in brain tissue were approximately 10-fold higher than that in the blood of rats (n=95). No difference between concentrations of cyclohexane in brain or blood after the first day 8 h-exposure and that after 3 consecutive day exposure was observed, indicating that cyclohexane does not accumulate in brain and blood in any significant amounts.

The author also conducted a human study (n=12 males) with inhalation of 25 ppm and 249 ppm cyclohexane for 4 hours in 2 sessions (7 days interval). 7 out of 12 people after exposure to the high concentration experienced headache and 5 out of 12 experienced dry throat. After the low dose exposure, only 1 person experienced headache and 2 experienced dry throat. The author described this as minimal effect on the central nervous system (CNS).

6.8.2.2 Campos study (2015)

20 male Balb/C mice were exposed to 0 and 9000 ppm cyclohexane for 30 min/day for 30 consecutive days.[253] FOB (Functional Observational Battery) tests were conducted daily during the 30 exposure days. Spatial learning and memory tests were performed during a 9-day period after the exposure. Brain sections were obtained 9 days or longer after the end of the 30-day exposure.

The FOB test showed that cyclohexane inhalation led to reversible functional deficits with signs of naso-oral hyper-secretion and motor hyperactivity followed by lethargy and sedation.[253] There were statistically significant (p-value 0.009 – 0.014) differences in gait, activity function, sensory auditory function, two-hand handling, forelimb/hindlimb grip strength, salivation, and lacrimation. It was also mentioned that all of these behaviors and signs were transient and lasted less than 10 min after the end of cyclohexane exposure.[253]

Results of the spatial learning and memory study indicate that cyclohexane did not impair memory acquisition and retention.

In the CA1 (see Glossary) region of the hippocampus, cyclohexane significantly increased the number and intersections of microglial cells.[253] The number of microglial cells also increased in the CA3 (see Glossary) region. Acting as sensors for pathological events in the brain, numbers, and intersections of microglial cells are sensitive indicators for a variety

of alternations in the brain. The number and intersections of astrocytes, another glial cell whose numbers increased in response to CNS injuries, also increased in both the CA1 and CA3 regions following inhalation exposure to cyclohexane.

Elevated concentrations of AP endonuclease 1 (APE1) in the CA1 and CA3 regions suggested that cyclohexane promotes an oxidative stress response in the hippocampus. APE1 is a DNA repairing enzyme for which the expression increases in response to oxidative stress.

6.8.2.3 DP1996a study (1996)

DuPont (abbreviated as DP here) had conducted a series of studies, labeled as DuPont HLP 1996a-d and 1997a-c, that systematically evaluated acute and subchronic effects of cyclohexane by examining various species, mice, rats, and rabbits, in the aspects of neurological behavior, clinical pathology, ophthalmological, hematological, urinalysis evaluations, and two-generation reproductive study with inhalation exposure of cyclohexane at doses of 0, 500, 2000, and 7000 ppm.

DP1996a, was a 90-day cyclohexane inhalation toxicity study with 20, 10, 10, and 20 Crl:CD-1 BR (Crl: Charles River Laboratories, this is the mice's strain name) mice per 0, 500, 2000, and 7000 ppm inhalation groups, respectively, for a total of 67 exposures over a 14-week period.[277] It was designed to evaluate the subchronic toxicity of cyclohexane by examinations of body weight, mortality, ophthalmology, hematologic parameters, gross and microscopic organ evaluations, and behavior towards alerting stimulus observations.

A NOAEL (no observed adverse effect level) of 500 ppm was decided based on the diminished or no response to an alerting stimulus a dosages under 2000 ppm while hyperactive sign of toxicity appeared under the 7000 ppm exposure. The clinical sign of toxicity included hyperactivity, circling, jumping, hopping, excessive grooming, kicking and spasms of rear

Table 6.12: Summary of the significant changes of hematological parameters in mice which were exposed with 0, 500, 2000, and 7000 ppm cyclohexane for 90 days and recovered for 1 month in the study of DuPont HLR 1996a.

	Day 59 Sampling				**Day 91 Sampling**				**After Recovery**	
ppm	0	500	2000	7000	0	500	2000	7000	0	7000
RBC						+ (m)	+ (m)	+ (f,m)		+ (f)[a]
PLAT		– (m)		– (m)		– (m)	– (m)	– (m)		– (f,m)
Hb				+ (f,m)				+ (f)		+ (m)[a]
Ht				+ (f)		+ (m)	+ (m)	+ (f,m)		+ (m)[a]
PPC				+ (m)[a]						
MCV										– (f)[a]
MCH										– (f)[a]
Neut						– (m)				– (f)
Mono						– (m)				– (f)
Eosin						– (f,m)	– (f)			

Parameters lack of statistical significance are not shown.
[a] the magnitude of the changes were minuscule and biologically inconsequential.
+ indicates the number is significantly larger than control; – indicates the number is significantly smaller than control;
(f) indicates the change is only for female mice; (m) indicate the change is only for male mice; (f,m) indicates that the change is for both male and female mice.

legs, standing on front legs, and occasional flipping behavior.

Hematology and pathology studies concluded a NOAEL (no observed adverse effect level) of 7000 ppm. However, in both male and female mice, significant changes occurred during different periods, as shown in Table 6.12, including erythrocyte numbers (RBC), leukocytes (WBC), platelets (PLAT), plasma protein concentration (PPC), hematocrit (Ht), hemoglobin (Hb), mean corpuscular volume (MCV), mean corpuscular hemoglobin (MCH), relative numbers of neutrophils (Neut), monocytes (Mono), and eosinophils (Eosin) concentrations. Most of the changes were not considered important because no dose-response relationships were observed.

Only the changes of RBC, Hb, Ht, and PPC for all 7000 ppm groups were attributed to the exposure of cyclohexane since they were evident for both sexes at both 59- and 91-day

sampling times, which usually indicated mice were in dehydration state. However, the author stated that it was highly unlikely that dehydration was a manifestation of compound-related toxicity due to the lack of weight decrease, clinical and pathologic evidence. Thus the clinical meaning of these changes was not conclusive.

Organ weight data showed liver weight (absolute or relative to the body) increased in the 7000 ppm male and female group; kidney weight (absolute or relative to the body) increase happened in the 500 ppm male group. However, no compound-related microscopic changes were observed. Cartilage degeneration was diagnosed in several of the control and treated groups of both sexes, which was interpreted as likely resulting from injury when animals were handled during the study.

Limitations of this experiment include two aspects. (1) Body weights occasionally dropped during the three-month exposures for both male and female mice, and after one-month recovery, a 20-26% body weight loss was observed right before clinical and pathological examination due to a period of fasting. No comments on the reasons that led to the body weight change were mentioned in the report. It is unknown if cyclohexane led to the poor health of the mice. (2) 500 ppm could be an adverse dose if exposure time was extended, indicated by the death of one female mouse in the 500 ppm group. In this case, an error occurred; the mouse was not removed from the exposure case after the 18th exposure (over-exposure time was not mentioned); there were no further efforts studying long time exposures at 500 ppm.

6.8.2.4 DP1996b study (1996)

20 adult Crl:CD BR rats/gender for 0 and 7000 ppm, and 10 rats for 500 and 2000 ppm cyclohexane inhalation were exposed for 6 h/day, 5 days/week, over a 90 day period, followed

by one-month recovery.[273] This study was designed to evaluate the subchronic neurotoxicity of cyclohexane in rats.

No hyperactive response was observed as reported by DP1996c[278] when rats were given an alerting stimulus, but rather sedation effect in all 2000 and 7000 ppm groups of both sexes. A NOAEL (no observed adverse effect level) of 500 ppm was determined based on sedation behavior towards alerting stimulus observations, and other parameters: body weight, mortality, hematologic, ophthalmological, clinical chemical, gross or microscopic evaluations of organs, and urinalysis evaluation.

No apparent decrease of body weights in this experiment was found. The body weights of rats steadily increased through the 3-month exposure and 1 month recovery times for both sexes. Along with occasionally significant body weight changes compared with control, the corresponding food consumption and food efficiency changed in the same trends as well.

Hematology, clinical chemical, urine analysis, gross and microscopic observations concluded a NOAEL of 7000 ppm. Many parameters changed significantly, as summarized in Table 6.13, but these changes were either biologically inconsequential or could not establish dose-response relationships. Significant hematological changes included lymphocyte count (Lymph), monocyte count (Mono), leukocyte count (WBC). Significant clinical chemical changes included alanine aminotransferase (ALT), aspartate aminotransferase (AST), sorbitol dehydrogenase (SDH), gamma-glutamyl transpeptidase (GGT), creatine phosphokinase (CPK), glucose (Glu), calcium (Ca), bilirubin (BlLRN), cholesterol (CHOL), creatinine (CREAT), triglycerides (TRIG), total protein (TPROT), albumin (ALBMN), globulin (GLOBN). Urine composition significant changes included osmolality (OSMOL), and pH.

The following parameters were also measured but no significant differences were found: numbers of erythrocytes (RBC), leukocytes (WBC), platelets (PLAT), hemoglobin con-

Table 6.13: Statistically significant changes of hematological and urine parameters in the study of DuPont HLR 1996b.

	Day 46 Sampling				**Day 92 Sampling**			
ppm	0	500	2000	7000	0	500	2000	7000
Lymph (blood)		– (m)	– (m)	– (m)		– (m)		
Mono (blood)		– (f)	– (f)	– (f,m)		– (f)		– (f)
WBC (blood)		– (m)	– (m)	– (m)		– (m)		
ALP, serum								+ (f)[a]
AST, serum			– (m)					
SDH, serum			– (f)	– (f,m)			– (f)	– (f,m)
GGT, serum							+ (f)	
CPK, serum			– (f,m)	– (f)			+ (f)	
Glu, serum		+ (f)		+ (f)				
LDH, serum			– (f,m)	–(f)			– (f)	– (f)
Ca, serum		–m		– (f,m)[a]				
BILRN, serum			– (m)	– (m)			– (f)	– (f)
CHOL, serum						– (m)		
CREAT, serum				– (f)				
TRIG, serum						– (m)	– (m)	– (m)
TPROT*, serum		– (m)	–(f)	– (f,m)		– (m)	– (m)	– (f,m)
ALBMN*, serum				– (f)			– (m)	– (f,m)
GLOBN, serum							–(m)	–(m)
OSMOL, urine				+ (m)[a]				
pH,urine				– (m)[a]				

This table shows only for the changes that are significantly different from the control at 5% level by Dunnett criteria.

The data was extracted from table 18, 19, 20, 21, 22, and 23 in DuPont HLP 1996b full report. Parameters lack statistical significance are not shown.

[a] the magnitude of the changes were minuscule and, therefore, biologically inconsequential.

+ indicates the number is significantly larger than control; – indicates the number is significantly smaller than control.

(f) indicates the change is only for female mice; (m) indicate the change is only for male mice; (f,m) indicates that the change is for both male and female mice.

centrations (Hb), hematocrit (Ht), mean corpuscular volume (MCV), mean corpuscular hemoglobin (MCH), mean corpuscular hemoglobin concentration (MCHC), band neutrophils (Band), atypical lymphocytes (Alym), eosinophils (Eosin), and basophils (Baso).

In contrast with the increase in plasma protein concentration in mice in the DP1996a study,[277] in this study shown in Table 6.13, total serum protein decreased in male rats of all groups on Day 92. On day 46, the decrease in total serum protein in females demonstrated a dose-response relationship on both Day 46 and 92, although only the decreases among higher treatment groups achieved statistical significance. Besides, albumin and globulin decreased in all rats.[273]

There was a statistically non-significant trend of decreases in urine volume in rats of all treatment groups on day 45 and 90. There was also a trend of increases in urine osmolality and only the increase in the 7000 ppm treated rats on day 45 was statistically significant (1996b). There was a transient decrease in urine pH in rats from the 7000 ppm group, from 6.5 to 5.3, on Day 45.

Organ examination showed that higher liver weight at 90 days correlated with the microscopic observation of centrilobular hepatocellular hypertrophy (see Glossary). The adrenal weights of Male in the 7000 ppm group were found to be significantly larger in the recovery group, but this was considered not important since no dose-response relationship was observed.

In 2000 and 7000 ppm dose groups, the clinical toxicity signs included sedation, larger livers, higher adrenal weights of male, centrilobular hepatocellular hypertrophy for both sexes; transient colored discharge from the mouth (clear or brown), stained chin, and wet chin for males; transient stained perineum and wet perineum for female. These observations, except sedation, liver weight, and centrilobular hepatocellular hypertrophy, were not considered

as toxicologically important since no adverse functional or morphological changes could be correlated with them.

6.8.2.5 DP1996c study (1996)

This is a feed-restricted (10% below ad libitum feeding weight) study. 10 male Crl:CD BR rats per 0, 500, 2000, 7000 ppm groups were exposed to cyclohexane through inhalation 6 h/day, 5 days/week for 6-7 weeks with neurological schedule-controlled operant behavior tests for 30 mins right after the termination of exposure to examine acute neurotoxicity of cyclohexane inhalation.[278] The NOAEL for behavior neurotoxicity was determined to be 2000 ppm. Parallel with the cyclohexane experiment, two positive controls with the same methodology were studied except, instead of the inhaling cyclohexane, these groups received, respectively, injections of amphetamine, a potent central nervous system stimulant, and chlorpromazine, a low-potency typical antipsychotic, which induces sedation effect. With the potent stimulant and low-potency chlorpromazine as two different scales for testing the sensitivity of this methodology, the study evaluated the neurobehavioral effect of cyclohexane relative to that of chlorpromazine and amphetamine.

The amphetamine and chlorpromazine experiments were preformed with 40 rats divided equally into 4 groups (group I, II, III, and IV). Group I recieved the lowest concentrations in injection sets, Group IV recieved the highest dose of the injection sets, and Group II and III recieved the corresponding 2nd and 3rd highest dosages. There were 4 injection sets that were applied to the 4 groups according to this order: Amphetamine A (0, 0.5, 1.0, 2.0 mg/kg), Chlorpromazine A (0, 1.0, 2.0, 4.0 mg/kg), Chlorpromazine B (0, 2.0, 2.5, 3.0 mg/kg), and then Amphetamine B (0, 1.5, 2.0, 2.5 mg/kg), which were conducted at the 4th, 10th, 19th, and 31th test day, respectively.

The rats were trained to press levers and get reinforcement under two reinforcement schedules: fixed-ratio (FR) schedule, and fixed-interval (FI) schedule. A FR schedule is a schedule of reinforcement where a response is reinforced only after a specified number of responses, for instance 20. A FI schedule is a schedule of reinforcement where the first response is rewarded only after a specified amount of time has elapsed.[279]

Amphetamine at 2.0 and 2.5 mg/kg single intraperitoneal injection (IP) injection significantly decreased in the FR schedule performance (about 20-40% decrease in response/minute). Mean FR pause duration decreased from 5.7 seconds to 3.1 seconds, a 46% decrease, at 1.5 mg/kg dose. At higher doses (2.0 and 2.5 mg/kg) the magnitude of the decrease is in a similar range (40-42%). FI rate of response increased 52% at 1.0 mg/kg, 78% at 1.5 mg/kg, 68-73% at 2.0 mg/kg. At the highest tested dose, 2.5 mg/kg, the increase (31%) was not statistically significant. The index of curvature decreased after the treatment from about 0.50 to close to zero, indicating that the rate of response is more evenly distributed between the beginning and the ending of the 120-second interval.

The FI index of curvature was defined as the equation as following:

$$Index\ of\ curvature = (9R_{10} - 2(R_1 + R_2 + ... + R_9))/(10R_{10})$$

where R_n is the cumulative numbers of responses from the beginning of the experiment till the nth intervals. An positive FI index of curvature indicates that the rate was lower at the beginning than at the end.[278]

Chlorpromazine significantly decreased FR rate of response, with a dose-response relationship; decreases of 39%, 33%, 49%, and 53% comparing with the baselines, at 2.0, 2.5, 3.0 and 4.0 mg/kg doses, respectively. FR pause duration also increased in a dose-response

manner: 76%, 106%, and 114% after treatments of 2.5, 3.0 and 4.0 mg/kg doses, respectively. A trend of increases in the FR pause duration observed after 1.0 mg/kg and 2.0 mg/kg treatments were not statistically significant. The rate of response decreased significantly at doses of 2.5 mg/kg and above, ranging from 29% to 60%, without a clear dose-response trend. FI index of curvature decreased after the treatment from about 0.50 to 0.23 and 0.16, at 3.0 mg/kg and 4.0 m/kg, respectively, indicating that the rate of response is more evenly distributed between the beginning and the ending of the 120-second interval. The decreases in the index of curvature were not as apparent as that seen after amphetamine treatments.

From above positive controls, we can see that, for response rate and duration between responses, dose-response relationships were only observed for the chlorpromazine case; amphetamine decreased the duration while chlorpromazine increased it, which is understandable since amphetamine is a stimulant and chlorpromazine has sedative effect. However, both amphetamine and chlorpromazine decreased the FI index of curvature, which gave difficulty to interpret the physiological meaning, if any, of the trends.

The responses from cyclohexane exposure were much weaker compared with amphetamine and chlorpromazine cases. No significant body weight changes were observed. Mean FR rate of response (responses/minute) remain about the same through the 12 sessions of cyclohexane test, except in that the 7000 ppm group a slight decrease from 242 responses/minute on Day -1 (the day before initiation of the exposure) to 211 responses/minute on Day 1 (first session, i.e. Day 1 exposure of the 12 exposure days). No effects on mean FR pause duration, mean FI rate of response and mean FI index of curvature were observed.

Compared with DP1996b, where sedation effect was observed from day 1 till the rest of exposures in 7000 ppm group of both sexes, here during 5 days per week for 6 to 7 week exposure, no sedation effect was observed except that the decreased fixed ratio rate response

may suggest a mild sedative effect.

No effect was observed on body weights, clinical observation except that 2 rats had alopecia in the 500 and 1 rat in the 2000 ppm group, and 1 rat had teeth missing in the 7000 ppm group.

6.8.2.6 DP1996d study (1996)

Young adult male and female Crl:CD BR rats, 12/gender/concentration, were exposed to 0, 500, 2000, and 7000 ppm cyclohexane inhalation for 6 h/day, 5 days/week over approximately 90 days.[274] This study was designed to evaluate the potential neurotoxicity of cyclohexane when administered by inhalation to groups of male and female rats sub-chronically by conducting functional observational battery (FOB) assessments, motor activity (MA), and histopathology. The NOAEL was determined as 500 ppm based on the sedative effect observed above 500 ppm.

The 2000 ppm and 7000 ppm groups had an increase of incidences of transient stained chin immediately after removal from the exposure chambers. The 7000 ppm group also had increased transient wet-chin and stained face incidences.

Significantly lower incidences of defecation were observed in the 7000 ppm group male and female. No food consumption weight data was available to examine if it is due to the decrease of food intake.

Significant lower motor activity parameters were observed in the 2000 ppm group, including duration and number of movements.

No mortality was observed. Body weight gain of the rats increased steadily and no change was found except that the 500 and 7000 ppm male group significantly increased during day 92-99, whose corresponding food consumption efficiency increased significantly

as well compared with the control group.

The sedative effects were observed in both 2000 and 7000 ppm groups, with diminished or no responses towards an alerting stimulus noted as the main toxicity-related symptoms, indicating cyclohexane-exposure related sedative effect. The sedative response was only observed during exposure; once rats were removed from the exposure chambers, the sedative effect ceased to be detectable.[274]

Six male and six female rats from the control and 7000 ppm groups were examined for the microscopic lesions in neuropathology and the results are summarized in Table 6.14. In the control, 5 male and 5 female rats showed minimal dilation of axon or myelin sheath in the cervical dorsal root fiber and ganglion (DRF&G); 4 male and 3 female in the lumbar area, 1 male and 2 female in the cervical area. 1 male and 2 female rats in the control group also showed minimal degeneration of the axon/myelin sheath in tibial nerve. Among the 7000 ppm treated rats, 4 male and 2 female rats showed minimal dilation of the myelin sheath in the DRF&G (dorsal root fibers and ganglia) in the lumbar area, while 2 male showed lumbar ventral root fiber (VRF) degeneration of axon/myelin sheath and 2 female show cervical DRF&G dialation. Only 1 female control rat had sciatic nerve degeneration of axon or myelin.

These axon/myelin degeneration and myelin dilation in nerve fibers for both 0 and 7000 ppm groups may not be compound related. The Dow Chemical Company had reported that the swollen axons and degenerations of single nerve fibers in the nervous system of 30-week-old Fischer 344 rats from subchronic 13-week inhalation exposures had occurred spontaneously in both control and treated groups.[280] This may be encountered in rats from this cyclohexane subchronic neurotoxicology studies and should be differentiated from treatment-related toxicity.

Table 6.14: Summary of neuropathology incidences and lesion grades in DuPont 1996d Study.

	Male		Female	
	0	7000	0	7000
Total numbers of rats examined	6	6	6	6
Total numbers of rats having $\geq$ 1 conditions	5	4	5	4
Number of rats having each condition				
Tibial nerve degeneration, axon/myelin	1	-	2	-
Cervical DRF&G dilation, myelin sheath	1	-	2	2
Lumber DRF&G dilation, myelin sheath	4	4	3	2
Lumber VRF degeneration, axon/myelin	-	2	-	-
Sciatic nerve degeneration, axon/myelin	-	-	1	-

DRF&G: the dorsal root fiber and ganglion.
VRF: the ventral root fiber.
Lesion grades for all of the incidences are minimal. The lesion grading system has 5 levels: presence, minimal, mild, moderate, and severe.

6.8.3 Reproductive and developmental toxicities

6.8.3.1 DP1997a study (1997)

DuPont HLR 1997a was a two-generation reproduction study with inhalation exposure of 0, 500, 2000, and 7000 ppm cyclohexane for both male and female Crl:CD BR rats (30/gender/concentration, exposure of 6 h/day, 5 days/week over 65 exposures in a 90-day period except weekends and holidays. Young 43-day old female and 45-day old male Crl:CD BR rats (F-0), exposed to cyclohexane for at least 10 weeks of pre-mating, were bred and allowed to deliver and rear the offspring until the postpartum day (PND) 25. The F-1 male and females were exposed continuously from birth, through breeding and reproduction of F-2.[275] The systemic-toxicity NOAEL level was 500 ppm and the reproductive NOAEL was 2000 ppm. The systemic-toxicity NOAEL was based on the compound-related sedative effect observed during exposure at 2000 ppm. The reproductive NOAEL was based solely on the decrease in pup weights in both the F-1 and F-2 generations observed at 7000 ppm.

Similar to the wet-chin clinical findings in DP1996b and DP1996d, salivation, brown-stained perioral area, stained-chin, and wet-chin were observed in both 2000 and 7000 ppm groups of both F-0 and F-1 generations of both sexes. This compound related response was regarded as toxicologically not important because no adverse functional or morphological changes could be correlated with this phenomenon.

The gross and microscopic examination of reproductive organs of both sexes showed that prostate inflammation incidence slightly increased in the 7000 ppm male rats of both F-0 and F-1 generations. However, it was known that the spontaneous inflammation in prostate was a common age-related background finding in rats,[281] and considering the severity of the lesions was mild, the prostate inflammation was not judged to be a compound-related response.

6.8.3.2 DP1997b study (1997)

DuPont HLR 1997b[276] was a one generation developmental study with only female rats exposed to cyclohexane via inhalation at concentrations of 0, 500, 2000, 7000 ppm on gestation days 7-16. The dams were euthanized on gestation day 22 and gross examinations of organs and fetus were conducted. There were two control groups, one normal control where feeding was ab libitum, and another pair-feed control, where feeding was limited to the same amount as in the 7000 ppm group.

This experiment not only confirmed some of the findings in 1997a, for example, sedation, stained-chin, salivation, no effect on mating, and pregnancy rate, but also showed that cyclohexane has no effect on early delivery rate, total resorption rate (defined as (numbers of corpora lutea – numbers of viable pups)/(numbers of corpora lutea)), the mean number of live fetuses per litter, sex ratio of pups. fetus weight.

There was a significant decrease in the mean number of implantations for females in the 7000 ppm group. The mean number of corpora lutea (see Glossary) for that group were comparable to those of the control group suggesting pre-implantation loss. Although the report claimed that the decrease in the mean number of implantations for females in the 7000 ppm group was not considered to be compound-related developmental toxicity, it is clear that cyclohexanol led to the preimplantation loss, which should be considered as a compound-related adverse effect. Therefore, the NOAEL should be 2000 ppm for reproductive toxicity. Since there were sedative effects observed in both 2000 and 7000 group, the systemic-toxicity NOAEL was 500 ppm; the reproductive and systematic toxicity LOAEL (lowest observed adverse effect level) should be 2000 ppm.

6.8.3.3 DP1997c study (1997)

Pregnant rabbits (Hra:(NZW)SPF, 20/concentration) were exposed to 0, 500, 2000, and 7000 ppm cyclohexane by inhalation on day 6-18 of gestation. On day 29, the does were euthanized and subjected to organs and uterus examinations.[282]

Clinical observation showed more rabbits (4 rabbits in the 7000 ppm and 2 for other groups) with alopecia and stained tails (brown or yellow) for the high exposure group, but it was not statistically significant.

There were several statistically significant differences in a number of parameters:

Offspring sex ratio (male/total) increased significantly ($p < 0.05$) from 0.48 in the control group to 0.59 in the 2000 ppm and 0.54 in the 7000 ppm treatment groups. The numbers of female and male pups were not reported, therefore, we cannot examine the total male/female pup ratio.

Mean number of corpora lutea decreased from 10.2 in the controls to 8.9 and 8.8 in the

2000 ppm and 7000 ppm treated groups, respectively ($p < 0.05$). Litter size was slightly smaller in all three treated groups but without statistical significance.

The maternal body weight gain showed decreases between gestation day (GD) 16 and 29 that are associated with the treatments. Nonetheless, the individual rabbits' body weight changes were extremely irregular through gestation in all treatment groups. For example, in the control group, rabbit 31322 gained 853.8 g between GD 19-24, while rabbit 31332 lost 648.1 g during the same period. Both carried 10 fetuses (31332 had alopecia left side on GD 28-29). The body weights appeared to be self-correct in the next body weight measurement, suggesting data recording errors. These same types of errors occurred in all groups when examining individual body weight records.

In summary, no effects were found between control and treatment in pregnancy rate, abortion rate, total resorption rate, the mean number of implantations per litter, or the mean number of live fetuses per litter. Unlike rat studies where sedations was observed consistently from several studies, no effects on the alerting response during exposure were observed. Although the corpora lutea decreased significantly, thus was not considered to be a compound related effect since corpora lutea are produced prior to ovulation, and the ovulation and implantation had occurred prior to the exposure to cyclohexanol. The NOAEL for maternal and developmental toxicity was therefore determined to be 7000 ppm.

6.8.4 Carcinogenicity and mutagenicity

There is no available information on cyclohexane regarding carcinogenic effects. The genotoxicity studies that were performed using cyclohexane were generally negative. No increased numbers of sister chromatid exchanges either in the presence or the absence of exogenous metabolic activation in cultured hamster ovary cells were observed; rates of DNA synthesis

in cultured human lymphocytes was not affected by cyclohexane either in the presence or the absence of exogenous metabolic activation; no significant increases in chromosome structural aberration frequency was observed in bone marrow cells of male or female rats.[250]

6.8.5 Summary of cyclohexane toxicities

Cyclohexane acute toxicity in rats, mice, and rabbits, and very limited research on humans has been investigated. As summarized in Table 6.15, at 26,572 ppm, all 4 rabbits died within one hour of cyclohexane inhalation, and the lowest lethal concentration reported was 7444 ppm;[270] on the other hand, in DP1997c, at 7000 ppm, no mortality of rabbit was reported.[282] For rats and mice, a concentration above 7444 ppm (8135, 9000 ppm, respectively) did not lead to lethargy, however, psychomotor speed slowing down, altered gait were apparent on rats, and toxicity-signs, for instance, transient salivation, lacrimation, gait change were shown on mice.

Cyclohexane subacute toxicity studies conducted by DuPont consistently showed transient sedation effect on mice and rats, and hyperactivity on mice at 7000 ppm. This biphasic effect, sedation at low dose and hyperactivity at high dose, could be because the lower body weight of mice lead to a higher dosage for mice than rats at the same concentration of cyclohexane in the air.

The neurotoxicity of cyclohexane is evident. Cyclohexane is a highly lipophilic compound and readily penetrates the blood-brain barrier to establish a 10 fold higher concentration in the brain than in the blood of mice.[253] Six reports (Campos, DP1996a, DP1996b, DP1996d, DP1997a, DP1997b) shown that the sedation effect was transient, reversible, with rapid recovery within hours after cessation of daily exposure. However, microscopically, the cyclohexane effects on astrogliosis, microglia, APE1 enzyme activities, measured 9 days or longer

after the end of the 30 days exposure,[253] and hematological parameters such as RBC, PLAT, Hb, Ht, MCV, MCH, Neut, and Mono (Table 6.12), measured after one month recovery period, were not completely recoverable.[277]

Cyclohexane seems to affect the tear/saliva secretion and grooming activity of rats, mice, and rabbits. Alopecia, stained-tail/chin/perineum had been observed repeatedly in DP1996b, DP1996d, DP1997a, DP1997b and somewhat in DP1997c. These abnormal phenomena cannot easily be related to pathological observations or organ functionality of these animals. The stain could be the result of Naso-oral hypersecretion[253] or the lack of grooming caused by the sedative effects. It may, however, be an important indicator of the poor health state of the animals.

One cyclohexane toxicity mechanism may be oxidative stress, as suggested by Campos's enzyme composition analysis in mouse brains that revealed elevation of AP endonuclease (APE1), an oxidative stress response enzyme.

Another cyclohexane toxicity mechanism may be membrane function disruption. It was suggested that cyclohexane produced effects related to many membrane functions similar to the case of another lipophilic solvent 1,1,2-trichloro-1,2,2-trifluoroethane, where it interrupted mitochondrial production of energy, however, there is no direct evidence given for cyclohexane.[251,283]

Reproductive and developmental toxicity of cyclohexane was found to be minimal at the doses tested. A 7000 ppm reproductive or developmental NOAEL (DP1997a, DP1997b, DP1997c) were decided by all three reproductive and developmental studies from DuPont.[275,276,282] However, it should be noted that decreases in body weight, sedation, stain, and wet-chin in both P1 and F-1 were observed in DP1997a.[275]

Table 6.15: Summary of cyclohexane toxicity studies.

Study	Animal	Dose	Days	NOAEL	LOAEL	Death	Toxicity Findings[b]
Human, Inhalation							
Lammars	human	25, 249	2	-	-	0(12)	Headache, dry throat, limited CNS effect.
Animal							
Dermal, mg/kg-day							
Treon	Rabbits	2597	12	2597[d]	15580[d]	0(1)	No effect.
		15580	14			0(1)	Irritation, thickening of skin, no narcosis, weight loss during exposure, and regained the lost weight within a month.
Oral, mg/kg-day							
Treon	Rabbits	1000–5500	11	1000	-	0(6)	Weight loss, regained lost weight within a week after treatments above 1000 mg/kg.
		6000–10000	11	-	-	4(4)	Weight loss, death, severe diarrhea, conjunctival congestion, lethargic, no narcosis, no convulsions.
Inhalation ppm							

Continued on the next page

Table 6.15 (cont'd)

Study	Animal	Dose	Days	NOAEL	LOAEL	Death	Toxicity Findings[b]
Treon-2	Rabbits	435, 786, 1243, 3330, 7444, 9220, 12574, 18565, 26572	130, 10, 10, 10, 10, 25, 10, 10, 1	3339	7444	0(4), 0(4), 0(4), 0(4), 1(4), 3(4), 1(4), 3(4), 4(4)	No effect observed below 7444 ppm. Lethargy, narcosis, increased respiration, diarrhea at 7444 ppm; tremors, lethargy, temporary paresis of legs, salivation at 9220 ppm; spasmodic convulsions/jerking, lethargy, tremors, rhythmic "running-like" movements of feet, narcosis, labored respiration at higher than 9220 ppm. Death at the highest dose.
Lammars	Rats[a]	0, 407, 2324, 8135	3	2324	8135	0(8), 0(8), 0(8), 0(8)	Altered gait, one rat tremoring. No significant effects on forelimb grab, hind limb grip strength, mean foot splay, touch, click, tail-pinch responses, arousal, and motor activity
Campos	Mice[a]	0, 9000	30	-	9000	0(10), 0(10)	Reversible functional deficits from FOB test (only last for less than 10 mins), Transient salivation, lacrimation, sedation, change of gait, increase of numbers and intersections of microglial cells, astrocytes, elevation of APE1 level. No effect on memory acquisition and retention.
DP1996a	Mice[b]	0, 500, 2000, 7000	90	500	2000	0(20), 1(10), 0(10), 0(20)	Hyperactivity, circling, jumping, hopping, excessive grooming, kicking and spasms of rear legs, standing on front legs, and occasional flipping behavior. Liver and kidney weights increased in the 500 ppm. No effects on hematology and pathology parameters with a few exceptions (see Table 6.12.)

Continued on the next page

Table 6.15 (cont'd)

Study	Animal	Dose	Days	NOAEL	LOAEL	Death	Toxicity Findings[b]
DP1996b	Rats[b]	0, 500, 2000, 7000	90	500	2000	0(20), 0(20), 0(20), 0(20)	Sedation, larger livers, higher adrenal weights of male, centrilobular hepatocellular hypertrophy for both sexes; transient colored discharge from the mouth, stained chin, and wet chin for male; transient stained perineum and wet perineum for female. No body weight change. Several hematological, clinical chemical, and urine parameters changed significantly (see Table 6.13).
DP1996c	Rats[a]	0, 500, 2000, 7000	90	2000	7000	0(10), 0(10), 0(10), 0(10)	Slight decreased of fixed ratio rate of response in the 7000 group. No effect observed on body weights, clinical observation except that 2 rats have alopecia in the 500 ppm group and 1 rat in the 2000, 1 rat has tooth missing in the 7000 ppm group.
DP1996d	Rats[b]	0, 500, 2000, 7000	99	500	2000	0(24), 0(24), 0(24), 0(24)	Reversible and transient sedative effect, microscopic neuron lesion and axon/myelin minimal degeneration (see Table 6.14). Stain-chin, wet-chin, and stained face incidences increased in the 7000 group. Motor activity in the 2000 group decreased significantly. No mortality, FOB, histopathology changes.

Continued on the next page

Table 6.15 (cont'd)

Study	Animal	Dose	Days	NOAEL	LOAEL	Death	Toxicity Findings[b]
DP1997a	Rats[b]	0, 500, 2000, 7000	90	500	2000	0(60), 0(60), 0(60), 0(60)	Reduced pup weight, sedation, salivation, brown-stained perioral area, stain and wet-chin in both 2000 and 7000 ppm of both P1 and F-1 generations of both sexes. Prostate slight inflammation in the 7000 ppm. No effects on mating, fertility, gestation indices, implantation efficiency, gestation length in F-0 and F-1 generations.
DP1997b	Rats[c]	0, 500, 2000, 7000	10	500	2000	0(50), 0(25), 0(25), 0(25)	Sedation, stained-chin, salivation. No mating, pregnancy rate, early delivery rate, total resorption rate, mean number of live fetuses per litter, sex-ratio changes.
DP1997c	Rabbits[c]	0, 500, 2000, 7000	13	7000	-	0(20), 0(20), 0(20), 0(20)	Alopecia and stained tail (brown or yellow). Offspring sex ratio increased and mean number of corpora lutea decreased in the 2000 and 7000 ppm.

DP is short for DuPont

[a] male

[b] male and female

[c] female

[d] calculated under the assumption that the rabbit has a body weight of 3 kg.

6.9 Exposure

The general human population may be exposed to cyclohexanol and cyclohexane via inhalation of air, ingestion of food and drinking water, and dermal contact with this compound or other consumer products containing leachable cyclohexanol and cyclohexane, but these issues are not considered or explored in this exposure assessment. This report, focuses on inhalation exposures in occupational settings or at gas stations, since this assessment is motivated by the future potential settings of lignin derived biofuels where the presences of cyclohexane and cyclohexanol are expected. There is no actual exposure of cyclohexane or cyclohexanol in biofuels so far employed until this point.

6.9.1 Occupational exposure

Table 6.16: Occupational exposure limits of cyclohexanol and cyclohexane.

Organization	Cyclohexanol	Cyclohexane
ACGIH TLV	50 ppm	100 ppm
OSHA PEL	50 ppm	300 ppm
NIOSH REL	50 ppm	300 ppm
NIOSH IDLH	400 ppm	1300 ppm

ACGIH TLV: American Conference of Governmental Industrial Hygienists, Threshold Limit Value.
OSHA PEL: Occupational Safety and Health Administration, Permissible Exposure Limit.
OSHA REL: Occupational Safety and Health Administration, Recommended Exposure Limits.
NIOSH IDLH: National Institute for Occupational Safety and Health, Immediately Dangerous To Life or Health.

Occupational exposure to cyclohexanol and cyclohexane is the most probable exposure pathway through fumes in the air or dermal contact with biofuel.

NIOSH conducted the surveys during 1981–1983 and statistically estimated that 68,715 workers were potentially exposed to cyclohexanol in the USA, and the number was 898,132

during 1972-1974. The range of exposure dose was not mentioned.

The regulatory limits of cyclohexanol and cyclohexane air concentrations are shown in Table 6.16. Cyclohexane has higher limit levels than cyclohexanol.

6.9.2 Non-occupational exposure

If biofuel contains a significant amount of cyclohexane or cyclohexanol and their derivatives, inhalation exposure to them may raise to health concerns. However, since there are no quantitative data available about concentrations of cyclohexane or cyclohexanol in hydrogenated biofuel produced from lignin, we cannot estimate the exposure in the non-occupational cases. In this work, the potential non-occupational exposure times to cyclohexane or cyclohexanol in lignin biofuel are assumed to be the same as those of gasoline.

An estimation of gasoline exposure time in a year shows that people owning a car may have about 23 days in a year when they expose to gasoline according to Table 6.17. The benzene exposure of gasoline suggested that only during refueling are people exposed to significant amounts of gasoline than in garage and in transit settings. In this analysis, only the refueling time is considered as gasoline exposure time.

Table 6.17: Estimation of probable non-occupational exposure activity and quantification.

	Garage	**In Transit**	**Refueling**
Daily Time (min)	5	80	5
Total time/year (h)	30.4	486.7	30.4
Benzene Exposure from gasoline (ppb)			
Average	16.0	13	630
Maximum	48	80	1000

The data is extracted from *Environmental Health Perspectives Supplements* **1993**, *101*, 27.

6.10 Conclusions

6.10.1 Reproductive and developmental toxicities

Cyclohexanol may lead to reproductive toxicity by ingestion according to the Dixit group, while no reproductive toxicity was observed through inhalation from the MPI study. "Dixit" and "Dixit-Tyagi" studies showed loses of germinal cells along with significant weight decreases in male reproductive organs of rabbits with a total of 1000 mg/kg (25 mg/kg $\times$ 40) oral dose and of gerbils and house rats at a total of 315 mg/kg and 555 mg/kg subcutaneous doses, respectively. In contrast, MPI inhalation rat study showed no testes weigh changes and no sperm production changes during cyclohexanol exposure. No developmental toxicity was observed in MPI study.

Cyclohexane does not have reproductive or developmental toxicity at an inhalation dose of 2000 ppm, whereas reduced pup weight was observed at dose 7000 ppm. DP1997a and DP1997b found that cyclohexane had no effects on mating, fertility, gestation indices, implantation efficiency or gestation length in both F-0 and F-1 generation rats, and no effect on early delivery rate, total resorption rate, and mean number of live fetus per litter. DP1997a showed significantly reduced pup weight, while in DP1997b, no significant change was found in fetus weight of F-0 generation rats. DP1997c showed no effect of cyclohexane inhalation on rabbits' pregnancy rate, abortion rate, total resorption rate, the mean number of implantation per litter, mean number of live fetuses per litter. Only offspring sex ratio increased significantly and litter size slightly decreased in the 7000 ppm group.

6.10.2 Neurotoxicity

Cyclohexanol does not show significant neurotoxicity. In Perbellini's study, after rats were treated with 400/200 mg/kg cyclohexanol orally for 6 weeks, no significant changes were found in any of the electrophysiological parameters (MCV, LD, MSCV, and SCV) or in any neuron tissue morphological parameters (fiber numbers and fiber section areas). No clinical sign of peripheral neuropathy was noticed.

Cyclohexane leads to transient and reversible signs of neurotoxicity including sedation, narcosis, lethargy, and hyperactively at a higher dose. Treon-2, Campos, DP1996a, DP1996b, DP1996d, DP1997a, and DP1997b all showed the sedative or hyperactive effects of cyclohexane.

6.10.3 Carcinogenicity and mutagenicity

Cyclohexanol and cyclohexane are not significantly mutagenic and no information was found relevant to their potential carcinogenicity.

6.10.4 Ophthalmology

Cyclohexanol causes moderately severe irritation to rabbit eyes when it is applied directly. Incidences of superficial keratitis, chorioretinal hypoplasia, red conjunctivitis, and lacrimation occurred randomly for only 1 rat each in the MPI inhalation study.

Cyclohexane can also cause eye irritation. During the 90-day studies DP1996a and DP1996b, generalized retinal degeneration, shrunken globe, and eye corneal opacity were observed randomly in one or two rats only. The Campos study showed lacrimation in mice exposed to 9000 ppm cyclohexane.

6.10.5 Hematology, clinical chemistry, and urinalysis

Cyclohexanol raised blood cholesterol concentration in almost all treated groups in the MPI study. It decreased alkaline phosphatase, increased aspartate transaminase and serum globulin in the 450/400 ppm group only. No pathologically meaningful changes were observed.

Cyclohexane caused significant changes of hematological parameters include RBC, PLAT, Hb, Ht, PPC, MCV, Mono, and Eosin in the DP1996a study. The DP1996b also showed significant hematological changes in Mono, Lymph, WBC, ALP, AST, SDH, GGT, CPK, Glu, LDH, Ca, BILRN, CHOL, CREAT, TRIG, TPROT, ALBMN, and GLOBN. Urinalysis conducted by DP1996b showed osmolarity increase and pH decrease for male rats only. None of these findings can be related to pathological importance.

6.10.6 Dose-response assessment

Cyclohexanol has different inhibition effect on different sexes of rats at the same dose, the growth rates of males was inhibited slightly and females were affected significantly as shown by Gondry's study.[257] The same trends were also observed in the MPI study on rats.[30]

The minimal lethal dose of cyclohexanol to rabbits orally lies between 2.2-2.6 g/kg, and that of cyclohexane lies between 5.5-6.0 g/kg orally and 7444 ppm by inhalation reported by Treon-2.

Table 6.18 is summarized from Table 6.11 and Table 6.15, and the methods to extrapolate inhalation dose in ppm to oral dose in mg/kg/day or the reverse processes are all described in detail in the subsequent sections. From the table, the lowest LOAEL from oral studies of cyclohexanol is 25 mg/kg for rabbits; the inhalation LOAEL is 450 ppm and the NOAEL is 150 ppm for rats. Since subcutaneous exposures of cyclohexanol and cyclohexane are much

Table 6.18: Summary of the lowest LOAEL and NOAEL regardless of animal species for each route of exposure of cyclohexanol and cyclohexane based on all studies reviewed.

	ppm		mg/kg/day			
Route	**LOAEL**	**NOAEL**	**LOAEL**	**NOAEL**	**Animal**	**Study**
			Cyclohexanol			
Inhalation	**450**	**150**	140	47	Rat	MPI
Oral	48	-	**25**	-	Rabbit	Dixit
Subcut.	-	-	**15**	-	Gerbil&Rat	Dixit-Tyagi
Dermal	-	-	**3500**	-	Rabbit	Treon
			Cyclohexane			
Inhalation	**2000**	**500**	150	38	Rat	[a]
Oral	8026	-	**1000**	-	Rabbit	Treon
Dermal	-	-	**15580**	**2597**	Rabbit	Treon

[a] The studies are DP1996b, DP1996d, DP1997a, and 1997b.

Numbers in bold are original data without extrapolation estimations.

more unlikely than other routes, they are excluded from dose-response discussions.

6.10.6.1 Estimation of oral exposure dose (mg/kg/day) of cyclohexanol from the extrapolation of inhalation data (ppm) in MPI study

MPI male rats mean weights from week 1 to week 18 change from 200 g to 560 g, RD female rat mean weights from week 1 to week 13 increase from 160 g to 300 g. We choose an average weight of 0.3 kg as the typical body weight of all rats for purposes of the calculation. This approach is also consistent with the recommended rat weight in the standardized method reported by the National Research Council.[284]

Conversion of cyclohexanol concentration from ppm to mg/m^3 (P: pressure, V: volume, n: number of moles of cyclohexanol, R: gas constant, T: temperature, m: mass of cyclohexanol, M: molar mass of cyclohexanol, ρ: density):

$$1 \text{ ppm} = 1 \text{ mL}/\text{m}^3$$

$$PV = nRT$$

$$PV = mRT/M$$

$$\rho = m/V$$

Since P = 101.325 kPa, T = 298 K, R = 8.314 kPa L mol^{-1} K^{-1}, and M = 100.16 g/mol,

$$\rho = PM/RT = 4.094 \text{ g/L}$$

Thus at 1 atm pressure and room temperature 25 °C,

$$1 \text{ ppm cyclohexanol} = 4.094 \text{ mg/m}^3 \text{ cyclohexanol}$$

For rats: According to the U.S. EPA,[285] the relationship of respiratory rate V_E (L/min) and body weight (W in kg) of rats:

$$log(V_E) = -0.578 + 0.821 logW$$

Volume of air that a rat inhales (V_{Rat}) over 6 h/day (since all EPA experiments were conducted on a 6 h/day schedule):

$$V_{Rat} = V_E \text{ L/min} \times 60 \text{ min/h} \times 6 \text{ h/day} = 360 V_E \text{ L}$$

Concentrations of n ppm cyclohexanol ($C_{cyclohexanol}$) in air is:

$$C_{cyclohexanol} = 4.094 \text{ mg/m}^3\text{/ppm} \times n \text{ ppm} \times 1 \text{ m}^3\text{/1000 L}$$

$$= 4.094n \times 10^{-3} \text{ mg/L}$$

According to human cyclohexanol inhalation experiments, the retention ratio of cyclohexanol in the respiratory tract is 64.2%.[245] Assuming that the retention of cyclohexanol is the same for a rat as that for a human, the dose (DR, R is rat) of cyclohexanol absorbed by rat pulmonary tract per day for rats on a 6 h/day dosing schedule per body weight (W):

$$DR_{cyclohexanol} = 64.2\ \% \times (V_{Rat}) \times (C_{cyclohexanol}) \div W$$

$$DR_{cyclohexanol} = 0.945n/W \times 10^{(-0.578+0.821logW)} \text{ mg/kg/day}$$

Thus for a rat with body weight of 0.3 kg with an exposure of n ppm cyclohexanol,:

$$DR_{cyclohexanol} = 0.310n \text{ mg/kg/day}$$

If a human was exposed to the same amount of n ppm cyclohexanol, since the human respiratory rate is 11.7 L/min,[245] the volume of air that a human inhales (V_{Human}) for 6 h/day :

$$V_{Human} = 11.7 \text{ L/min} \times 60 \text{ min/h} \times 6 \text{ h/day} = 4212 \text{ L}$$

Concentrations of n ppm cyclohexanol ($C_{cyclohexanol}$) in air is:

$$C_{cyclohexanol} = 4.094n \times 10^{-3} \text{ mg/L}$$

Dose of cyclohexanol absorbed by human pulmonary tract (DH) per body weight (BW = 70

kg) per day, the default value for humans according to U.S. EPA[285]):

$$DH_{cyclohexanol} = 64.2\ \% \times (V_{Human}) \times (C_{cyclohexanol}) \div BW$$

$$= 0.158n \text{ mg/kg/day}$$

Therefore, 0, 50, 150, 450/400 ppm cyclohexanol inhalation can be equivalent to absorptions of 0, 16, 47, and 140/124 mg/kg/day dose of cyclohexanol for rats, and that is 0, 8, 24, and 71/63 mg/kg/day for a human. Since the cyclohexanol enters the pulmonary bloodstream without the effects of first-pass metabolism by the liver, the blood concentration of cyclohexanol may be higher than if the gastrointestinal tract absorbed the same amount of cyclohexanol.

6.10.6.2 Estimation of inhalation dose (ppm) from the oral data of cyclohexanol exposure in Dixit study

For Rabbits: According to the U.S. EPA,[285] the average body weight of New Zealand rabbits for subchronic study are 3 kg and the relationship of respiratory rate V_E (L/min) and body weight (W in kg) of rabbits:

$$log(V_E) = -0.783 + 0.831 logW$$

$$V_E = 0.411 \text{ L/min}$$

Volume of air that a rabbit inhales (V_{Rabbit}) for 24 h/day:

$$V_{Rabbit} = V_E \text{ L/min} \times 60 \text{ min/h} \times 24 \text{ h/day} = 591.3 \text{ L}$$

Concentrations of n ppm cyclohexanol ($C_{cyclohexanol}$) in air is:

$$C_{cyclohexanol} = 4.094 \text{ mg/m}^3\text{/ppm} \times n \text{ ppm} \times 1 \text{ m}^3\text{/1000 L}$$

$$= 4.094n \times 10^{-3} \text{ mg/L}$$

According to human cyclohexanol inhalation experiments, retention ratio of cyclohexanol in respiratory tract is 64.2%.[245] Assuming that the retention of cyclohexanol in respiratory tract of rabbit is the same as that for humans, the dose of cyclohexanol absorbed by rat pulmonary tract (DRb) per body weight (W = 3 kg) per day:

$$DRb_{cyclohexanol} = 64.2\ \% \times (V_{Rabbit}) \times (C_{cyclohexanol}) \div W$$

$$DRb_{cyclohexanol} = 0.518n \text{ mg/kg/day}$$

Thus $\text{DRb}_{cyclohexanol}$ = 25 mg/kg/day oral dose of cyclohexanol exposure is equivalent to 48 ppm of cyclohexanol exposure via inhalation for 24 h/day under a subchronic setting for rabbits.

6.10.6.3 Estimation of oral exposure dose (mg/kg/day) of cyclohexane by extrapolation from the inhalation data (ppm) in DuPont study

In DuPont 1996b, male rats mean weights from day 1 to day 90 are increased from 175 g to 540 g, RD female rat mean weights are increased from 150 g to 320 g. In DuPont 1996d, male rats weight 225 g to 550 g and females weigh 160 to 285 g. In DuPont 1997a, weights of male rats are 267 g to 520 g and those of females are 320 to 315 g. In DuPont 1997b, female rats weight from 250 to 318 g during the exposure period. We choose an average weight of

0.3 kg as the typical body weight of all rats for purposes of the calculation. This approach is also consistent with the recommended rat weight in the standardized method reported by the National Research Council.[284]

Conversion of cyclohexane concentration ppm to mg/m^3 (P: pressure, V: volume, n: number of moles of cyclohexane, R: gas constant, T: temperature, m: mass of cyclohexane, M: molar mass of cyclohexane, ρ: density):

$$1 \text{ ppm} = 1 \text{ mL/m}^3$$

$$PV = nRT$$

$$PV = mRT/M$$

$$\rho = m/V$$

Since P = 101.325 kPa, T = 298 K, R = 8.314 kPa L mol^{-1} K^{-1}, and M = 84.16 g/mol,

$$\rho = PM/RT = 3.442 \text{ g/L}$$

Thus at 1 atm pressure and room temperature 25 °C,

$$1 \text{ ppm cyclohexane} = 3.442 \text{ mg/m}^3 \text{ cyclohexane}$$

For rats: According to the U.S. EPA,[285] the relationship of respiratory rate V_E (L/min) and body weight (W in kg) of rats:

$$log(V_E) = -0.578 + 0.821 logW$$

Volume of air that a rat inhales (V_{Rat}) for 6 h/day :

$$V_{Rat} = V_E \text{ L/min} \times 60 \text{ min/h} \times 6 \text{ h/day} = 360V_E \text{ L}$$

Concentrations of n ppm cyclohexane ($C_{cyclohexane}$) in air is:

$$C_{cyclohexane} = 3.442 \text{ mg/m}^3\text{/ppm} \times n \text{ ppm} \times 1 \text{ m}^3\text{/1000 L}$$

$$= 3.442n \times 10^{-3} \text{ mg/L}$$

According to human cyclohexane inhalation experiment, retention ratio of cyclohexane in respiratory tract is 18.4%.[245] Assuming that the retention of cyclohexane in respiratory tract of rat is the same as that for humans, the dose of cyclohexane absorbed by rat pulmonary tract (DR) per body weight (W) per day:

$$DR_{cyclohexane} = 18.4 \text{ \%} \times (V_{Rat}) \times (C_{cyclohexane}) \div W$$

$$DR_{cyclohexane} = 0.228n/W \times 10^{(-0.578+0.821logW)} \text{ mg/kg/day}$$

Thus for a rat with body weight of 0.3 kg with an exposure of n ppm cyclohexane,:

$$DR_{cyclohexane} = 0.075n \text{ mg/kg/day}$$

If a human was exposed to the same amount of n ppm cyclohexane, since the human respiratory rate is 11.7 L/min,[245] the volume of air that a human inhales (V_{Human}) for 6

h/day :

$$V_{Human} = 11.7 \text{ L/min} \times 60 \text{ min/h} \times 6 \text{ h/day} = 4212 \text{ L/day}$$

Concentrations of n ppm cyclohexane ($C_{cyclohexane}$) in air is:

$$C_{cyclohexane} = 3.442n \times 10^{-3} \text{ mg/L}$$

Dose of cyclohexane absorbed by the human pulmonary tract (DH) per body weight (BW = 70 kg) per day :

$$DH_{cyclohexane} = 18.4 \text{ \%} \times (V_{Human}) \times (C_{cyclohexane}) \div BW$$

$$= 0.0381n \text{ mg/kg/day}$$

Therefore, 0, 500, 2000, 7000 ppm cyclohexane inhalation can be equivalent to absorptions of 0, 38, 150, and 525 mg/kg/day dose of cyclohexane for rats, and that is 0, 19, 76, and 266 mg/kg/day for humans.

6.10.6.4 Estimation of inhalation dose (ppm) of cyclohexane exposure by extrapolation from the oral dose in Treon study

For Rabbits: According to the U.S. EPA,[285] the average body weight of New Zealand rabbits for subchronic study are 3 kg and the relationship of respiratory rate V_E (L/min) and body weight (W in kg) of rabbits:

$$log(V_E) = -0.783 + 0.831 logW$$

$$V_E = 0.41 \text{ L/min}$$

Volume of air that a rabbit inhales (V_{Rabbit}) for 24 h/day:

$$V_{Rabbit} = V_E \text{ L/min} \times 60 \text{ min/h} \times 24 \text{ h/day} = 590.4 \text{ L}$$

Concentrations of n ppm cyclohexane ($C_{cyclohexane}$) in air is:

$$C_{cyclohexane} = 3.442 \text{ mg/m}^3\text{/ppm} \times n \text{ ppm} \times 1 \text{ m}^3\text{/1000 L}$$

$$= 3.442n \times 10^{-3} \text{ mg/L}$$

According to human cyclohexane inhalation experiment, retention ratio of cyclohexane in respiratory tract is 18.4%.[245] Assuming that the retention of cyclohexane in respiratory tract of rabbits is the same as that for humans, the dose of cyclohexane absorbed by the rabbit pulmonary tract (DRb) per body weight (W = 3 kg) per day :

$$DRb_{cyclohexane} = 18.4 \text{ \%} \times (V_{Rabbit}) \times (C_{cyclohexane}) \div W$$

$$DRb_{cyclohexane} = 0.1246n \text{ mg/kg/day}$$

Thus $\text{DRb}_{cyclohexane}$ = 1000 mg/kg/day oral dose of cyclohexane exposure is equivalent to 8026 ppm of cyclohexane exposure via inhalation for 24 h/day under a subchronic setting for rabbits.

6.10.6.5 Adjustments of inhalation doses for reference concentration (RfC)

Inhalation exposures conducted by MPI for cyclohexanol and DuPont for cyclohexane are limited to 5 days/week and 6 h/day. While oral administration studies conducted by Dixit and Treon are 7 days/week (oral exposure, the assumption is 24 h/day). To fairly compare these data, we adjusted the Inhalation MPI study and DuPont study according to this equation:

$$Dose_{adjusted} = Dose \times (5/7) \times (6/24)$$

Meanwhile, to calculate reference concentration (RfC), which is defined as under 24 h/day continuous inhalation exposure and in unit of mg/m^3 (the standard unit for reference concentration according to the U.S. EPA) and the MPI inhalation exposure time was 6 h/day, we calculate the adjusted dose in mg/m^3 according to the following equations:

$$Dose_{adjusted} = Dose \times (5/7) \times (6/24)$$

$$1 \text{ ppm cyclohexanol} = 4.094 \text{ mg/m}^3$$

$$1 \text{ ppm cyclohexane} = 3.442 \text{ mg/m}^3$$

The table below (Table 6.19) summarizes the adjusted values of Table 6.18.

6.10.6.6 Calculations of adjusted concentrations for cyclohexanol and cyclohexane

For cyclohexanol, the lowest LOAEL observed from all studies reviewed as summarized in Table 6.19 is 196 mg/m^3 by the Dixit Study, a 40-day oral study on the rabbit, and the lowest NOAEL is 109.7 mg/m^3 reported by the MPI study. The NOAEL 109.7 mg/m^3 from

Table 6.19: Summary of the lowest adjusted LOAEL and NOAEL for each route of exposure of cyclohexanol and cyclohexane based on all studies reviewed.

	$\textbf{Dose}_{adjusted}$					
	$\textbf{mg/m}^3$		**mg/kg/day**			
Route	**LOAEL**	**NOAEL**	**LOAEL**	**NOAEL**	**Animal**	**Study**
			Cyclohexanol			
Inhalation	328.6	109.5	25	8.4	Rat	MPI
Oral	196.5	-	25	-	Rabbit	Dixit
Subcut.	-	-	15	-	Gerbil&Rat	Dixit-Tyagi
Dermal	-	-	3500	-	Rabbit	Treon
			Cyclohexane			
Inhalation	1226.8	306.8	26.8	6.8	Rat	[a]
Oral	27760	-	1000	-	Rabbit	Treon
Dermal	-	-	15580	2597	Rabbit	Treon

[a] The studies are DP1996b, DP1996d, DP1997a, and 1997b.

MPI study was selected to calculate reference concentration RfC, because it is lower than the LOAEL of Dixit study, and the MPI study is a comprehensive study with 4 different doses investigated having a much larger sample size (120 female rats and 60 male rats) and longer study period (91-126 days) than Dixit study, where only a single dose was used on 15 male rabbits for 40 days.

For cyclohexane, the lowest LOAEL observed as shown in Table 6.19 is 1229.3 mg/m^3 and the lowest NOAEL is 307.3 mg/m^3, which were both reported by DuPont subchronic inhalation studies on rats.

The interspecies (rats to human) uncertainty factor (UF) is 10 considering that there are major metabolism differences between human and rats. Intraspecies UF (sensitive human population) is 10. Subchronic to chronic extrapolation UF is 3 (rodent, 3 months). Since inhalation experiments observed NOAEL, the NOAEL data was preferably used to determine inhalation reference dose values of cyclohexanol and cyclohexane for humans chronic

exposures.

$$RfC_{Cyclohexanol} = NOAEL_{lowest}/UFs = 109.7 \text{ mg/m}^3/(10 \times 10 \times 3) = 0.37 \text{ mg/m}^3$$

$$RfC_{Cyclohexane} = NOAEL_{lowest}/UFs = 307.3 \text{ mg/m}^3/(10 \times 10 \times 3) = 1.0 \text{ mg/m}^3$$

6.10.7 Considerations for biofuel applications

Cyclohexanol does not leads to reproductive toxicity under the dosage tested by inhalation but may cause spermatogenesis disruption via oral exposure. Meanwhile, its neurotoxicity is minimal. Cyclohexane inhalation leads to evident neurotoxicity predominately displaying as sedation or hyperactivity in rats and mice, but less evident in rabbits, while no reproductive toxicity can be correlated to it. Considering the RfC value of cyclohexanol is 64% lower than that of cyclohexane via inhalation exposure, nevertheless cyclohexane is much more volatile than cyclohexanol, with an evaporation rate 24 times higher than that of cyclohexanol at 45 °C and a vapor pressure 75 times higher than that of cyclohexanol at room temperature, there are no apparent benefit from the conversion of cyclohexanol to cyclohexane from the considerations of both hazards and exposures.

From fuel energy density point of view, there is a need to drive chemists and engineers to reduce cyclohexanol further to cyclohexane, and there is no immediate need to develop ring-cracking/isomerization reactions based on all of the information available. However, appropriate caution that the toxicity evaluations of lignin biofuel or each of the component of the lignin biofuel should be conducted, especially for neurotoxicity and reproductive toxicity. There is a major data gap on the reproductive and neurological toxicities of alkyl cyclohexanols and alkyl cyclohexanes. As the development and commercialization of lignin

biofuels proceeds, the corresponding in vitro and in vivo animal studies should be conducted.

From our non-occupational exposure analysis, an estimated exposure time to liquid fuel vapors for a human is 30.4 h/year. The RfC of cyclohexanol 0.37 mg/m^3 and RfC of cyclohexane 1.0 mg/m^3 are calculated based on 24 h/day continuous exposure scenario. Therefore, to protect the public health, the headspace concentration ($C_{Headspace}$ analysis of a lignin biofuel product should meet the following requirements at 25 °C under 101.325 kPa:

$$C_{Headspace} = RfC \div (30.4\ h/365\ day \div 24\ h/day)$$

For cyclohexanol:

$$C_{Headspace} \leq 106.6\ \text{mg/m}^3$$

For cyclohexane:

$$C_{Headspace} \leq 288.2\ \text{mg/m}^3$$

For occupational exposure, the concentrations of cyclohexanol and cyclohexane in the air should meet the following standards:

$$C_{Air} = RfC \div (8\ h/day \div 24\ h/day)$$

For cyclohexanol:

$$C_{Air} \leq 1.1\ \text{mg/m}^3$$

For cyclohexane:

$$C_{Air} \leq 3.0\ \text{mg/m}^3$$

It should also be noted that the purpose of this work is to give a concept to chemists and

engineers as to how much cyclohexanol and cyclohexane should be limited in the final biofuel products, not to attempt regulation standard setting, which should consider much more factors than those mentioned in this work. Concentrations of fuel exposure in different settings, wind, pressure, temperature affecting the evaporation of lignin biofuel. Furthermore, compositions of biofuels, synergistic or antagonistic effects of different biofuel composition on their toxicities, etc may require further considerations.

6.11 Acknowledgments

This analysis has been instructed mainly by Dr. Karen Chou from the Department of Animal Science and Institute for Integrated Toxicology at Michigan State University. Gemini Bhalsod who has graduated from the Department of Plant, Soil, and Microbial Sciences at Michigan State University also made major contributions to the literature searching, data collecting, and contacts with governmental agency and business company for the MPI study original report and the whole series of DuPont HLP studies (1996a-d and 1997a-c). Meanwhile, she has also spent tremendous amount of time discussing and reviewing the toxicities of cyclohexanol with Dr. Karen Chou and me. Moreover, special thanks to Dr. Henry J. Trochimowicz (Sc.D., D.A.B.T.) who kindly shared the original report with us. In addition, Feng Gao from the Department of Plant, Soil, and Microbial Sciences also contributed to the literature searching and discussions on the cyclohexanol toxicities.

6.12 Glossary of toxicology

- **Adrenal glands**: The adrenal glands (also known as suprarenal glands) are endocrine glands that produce a variety of hormones including adrenaline and the steroids aldos-

terone and cortisol. They are found above the kidneys. (Wikipedia)

- **Ataxia**: Ataxia is a neurological sign consisting of lack of voluntary coordination of muscle movements that includes gait abnormality. Ataxia is a non-specific clinical manifestation implying dysfunction of the parts of the nervous system that coordinate movement, such as the cerebellum. (Wikipedia)

- **Athetoid movement**: Also called athetosis. It is a symptom characterized by slow, involuntary, convoluted, writhing movements of the fingers, hands, toes, and feet and in some cases, arms, legs, neck, and tongue. (Wikipedia)

- **Bilirubin**: Bilirubin is a yellow compound that occurs in the normal catabolic pathway that breaks down heme in vertebrates. This catabolism is a necessary process in the body's clearance of waste products that arise from the destruction of aged red blood cells. (Wikipedia)

- **CA1** Field CA1 in the ventral hippocampus sends axons to the main olfactory bulb, the anterior olfactory nucleus, and to the primary olfactory cortex. There continues to be some interest in hippocampal olfactory responses, in particular, the role of the hippocampus in memory for odors, but few specialists today believe that olfaction is its primary function. (Wikipedia-Hippocampus)

- **CA3** Field CA3 in the hippocampus receives excitatory input from the pyramidal cells and then give an inhibitory feedback to the pyramidal cells. This recurrent inhibition is a simple feedback circuit that can dampen excitatory responses in the hippocampus. The pyramidal cells gives a recurrent excitation which is an important mechanism found in some memory processing microcircuits. (Wikipedia-Hippocampus)

- **Cauda epididymal:** The epididymis can be divided into 3 main regions: the head (Caput), the body (Corpus), and the tail (Cauda). The tail has the thinnest epithelium of the three regions and the greatest quantity of smooth muscle. (Wikipedia-Epididymis)

- **Centrilobular hepatocellular hypertrophy:** Centrilobular is the area closest to the central vein of the hepatic lobule. Hepatocellular is the liver cell. Hypertrophy is the increase in the volume of an organ or tissue due to the enlargement of its component cells. (Wikipedia-Hypertrophy)

- **Chorioretinal hypoplasia**: hypoplasia affecting the choroid and the retina of the eye. (Merriam Webster dictionary)

- **Collapse**: Collapse is a sudden and often unannounced loss of postural tone (going weak), often but not necessarily accompanied by loss of consciousness. (Wikipedia)

- **Copulation**: In zoology, copulation is animal sexual behavior in which a male introduces sperm into the female's body, especially directly into her reproductive tract. (Wikipedia)

- **Corpora lutea**: The plural form of Corpus luteum. It is the remains of the ovarian follicle that has released a mature ovum during a previous ovulation. The corpus luteum (Latin for "yellow body"; plural corpora lutea) is a temporary endocrine structure in female ovaries and is involved in the production of relatively high levels of progesterone, moderate levels of estradiol, inhibin A and small amounts of estrogen. (Wikipedia)

- **Cyanosis**: is defined as the bluish or purplish discoloration of the skin or mucous

membranes due to the tissues near the skin surface having low oxygen saturation. (Wikipedia)

- **Eosinophils:** Eosinophils sometimes called eosinophiles or, less commonly, acidophils, are a variety of white blood cells and one of the immune system components responsible for combating multicellular parasites and certain infections in vertebrates.

- **Epididymitis**: Epididymitis is a medical condition characterized by inflammation of the epididymis, a curved structure at the back of the testicle. (Wikipedia)

- **Functional Observational Battery:** The Functional Observational Battery (FOB) is a neurobehavioral assessment tool describing various behaviourlogical and activity related parameters of a rat strain. (www.mds-usa.com)

- **Glomerular tubular nephritis:** Nephritis is inflammation of the kidneys and may involve the glomeruli, tubules, or interstitial tissue surrounding the glomeruli and tubules. Glomerular tubular nephritis is the inflammation of the nephron tubules. (Wikipedia)

- **Hemoglobin**: Abbreviated Hb or Hgb, is the iron-containing oxygen-transport metalloprotein in the red blood cells. (Wikipedia)

- **Hypoplasia**: A condition of arrested development in which an organ or part remains below the normal size or in an immature state. (Merriam Webster dictionary)

- **Keratitis**: Keratitis is a condition in which the eye's cornea, the clear dome on the front surface of the eye, becomes inflamed. (Wikipedia)

- **Lacrimation**: the secretion of tears especially when abnormal or excessive. (Merriam Webster dictionary)
- **Lethargy**: Lethargy is a state of tiredness, weariness, fatigue, or lack of energy. It can be accompanied by depression, decreased motivation, or apathy. (Wikipedia)
- **Leucocytes**: White blood cell. (Wikipedia)
- **Leydig Cell**: Leydig cells, also known as interstitial cells of Leydig, are found adjacent to the seminiferous tubules in the testicle. They produce testosterone in the presence of luteinizing hormone (LH). (Wikipedia)
- **Luminal epithelium:** A lumen (plural lumina) is the inside space of a tubular structure. Epithelial tissues line the outer surfaces of organs and blood vessels throughout the body, as well as the inner surfaces of cavities in many internal organs. (Wikipedia)
- **Mineralization, pelvic:** The renal pelvis or pelvis of the kidney is the basin-like or funnel-like dilated proximal part of the ureter in the kidney. Mineralization is the phenomenon that calcium salts precipitate in tissue. (Wikipedia-Renal pelvis)
- **Narcosis**: Unconsciousness induced by a narcotic drug or through anesthesia. (Wikipedia)
- **Parturition:** The action of giving birth to young; childbirth.(Google Dictionary)
- **Peripheral neuropathy**: Peripheral neuropathy (PN) is damage to or disease affecting nerves, which may impair sensation, movement, gland or organ function, or other aspects of health, depending on the type of nerve affected. (Wikipedia)
- **Prostration**: the action of lying stretched out on the ground. (Google dictionary)

- **Reflexes**: A reflex, or reflex action, is an involuntary and nearly instantaneous movement in response to a stimulus. A reflex is made possible by neural pathways called reflex arcs which can act on an impulse before that impulse reaches the brain. The reflex is then an automatic response to a stimulus that does not receive or need conscious thought. (Wikipedia)

- **Sciatic and tibial nerves:** The sciatic nerve is a large nerve in humans and animals. It begins in the lower back and runs through the buttock and down the lower limb. The tibial nerve is a branch of the sciatic nerve. (Wikipedia)

- **Seminiferous tubules**: Seminiferous tubules are located within the testes, and are the specific location of meiosis, and the subsequent creation of male gametes, namely spermatozoa. (Wikipedia)

- **Sialic acid**: Administration of estrogen to castrated mice leads to a dose-dependent reduction of the sialic acid content of the vagina. Conversely, the sialic acid content of mouse vagina is a measure of the potency of the estrogen. (Wikipedia)

- **Spermatogenesis**: Spermatogenesis is the process in which an animal produces spermatozoa from spermatogonial stem cells by way of mitosis and meiosis. The initial cells in this pathway are called spermatogonia (spermatogonium), which yield primary spermatocytes by mitosis. The primary spermatocyte divides meiotically (Meiosis I) into two secondary spermatocytes; each secondary spermatocyte divides into two spermatids by Meiosis II. These develop into mature spermatozoa, also known as sperm cells. Type A spermatogonia have two types: dark cells and pale cells. Type A (dark) cells are reserve spermatogonial stem cells which do not usually undergo active mitosis. Type A (pale) cells are the spermatogonial stem cells that undergo active mitosis.

These cells divide to produce Type B cells. Type B cells, which divide to give rise to primary spermatocytes.(Wikipedia)

- **Stereocilia:** The stereocilia of the epididymis are long cytoplasmic projections that have no motility and which aid in absorption. These numerous apical modifications are often referred to as "stereocilia", as under the light microscope they look like cilia. (Wikipedia)

- **Steroidogenesis**: Steroidogenesis in the adrenal, gonads, and placenta is a directional process designed to synthesize one or a few final steroid products unique to each cell type. (Handbook of Neuroendocrinology, 2012)

- **Thyroid**: The thyroid gland, or simply the thyroid, is an endocrine gland in the neck, consisting of two lobes connected by an isthmus. It is found at the front of the neck, below the Adam's apple. The thyroid gland secretes thyroid hormones, which primarily influence the metabolic rate and protein synthesis. (Wikipedia)

- **Vas deferens**: (Latin: "carrying-away vessel") is part of the male reproductive system of many vertebrates; these vasa transport sperm from the epididymis to the ejaculatory ducts in anticipation of ejaculation. (Wikipedia)

- **Ventral prostate**: The prostate of rodents, unlike that of man, contains separate lobes: ventral, dorsal, lateral (the dorsal and lateral lobes are frequently combined as dorsolateral), and anterior (coagulating gland). (Atlas of Laboratory Mouse Histology)

BIBLIOGRAPHY

BIBLIOGRAPHY

[1] Gallezot, P.; Cerino, P. J.; Blanc, B.; Flèche, G.; Fuertes, P. *Journal of Catalysis*, **1994**, *146*(1), 93–102.

[2] Delle Site, L.; Alavi, A.; Abrams, C. F. *Physical Review B*, **2003**, *67*(19), 193406.

[3] Mráz, J.; Gálová, E.; Nohová, H.; Vítková, D. *International Archives of Occupational and Environmental Health*, **1994**, *66*(3), 203–208.

[4] Zahlsen, K.; Eide, I.; Nilsen, A. M.; Nilsen, O. G. *Pharmacology & Toxicology*, **1992**, *71*(2), 144–149.

[5] Perbellini, L.; Grandis, D. D.; Semenzato, F.; Bongiovanni, L. *La Medicina del Lavoro*, **1981**, *72*(2), 102–106.

[6] Petersen, J. *Zeitschrift für Elektrochemie und Angewandte Physikalische Chemie*, **1905**, *11*(34), 549–553.

[7] Wolfrom, M. L.; Konigsberg, M.; Moody, F. B.; Goepp, R. M. *Journal of the American Chemical Society*, **1946**, *68*(1), 122–126.

[8] Wolfrom, M. L.; Moody, F. B.; Konigsberg, M.; Goepp, R. M. *Journal of the American Chemical Society*, **1946**, *68*(4), 578–580.

[9] Wolfrom, M. L.; Lew, B. W.; Goepp, R. M. *Journal of the American Chemical Society*, **1946**, *68*(8), 1443–1448.

[10] Wolfrom, M. L.; Lew, B. W.; Hales, R. A.; Goepp, R. M. *Journal of the American Chemical Society*, **1946**, *68*(11), 2342–2343.

[11] Wolfrom, M. L.; Binkley, W. W.; Spencer, C. C.; Lew, B. W. *Journal of the American Chemical Society*, **1951**, *73*(7), 3357–3358.

[12] Ghiringhelli, L. M.; Caputo, R.; Site, L. D. *Physical Review B*, **2007**, *75*(11), 113403.

[13] Yoon, Y.; Rousseau, R.; Weber, R. S.; Mei, D.; Lercher, J. A. *Journal of the American Chemical Society*, **2014**, *136*(29), 10287–10298.

[14] Lu, J.; Behtash, S.; Mamun, O.; Heyden, A. *ACS Catalysis*, **2015**, *5*(4), 2423–2435.

[15] Nimz, H. *Angewandte Chemie International Edition in English*, **1974**, *13*(5), 313–321.

[16] Wong, D. W. S. *Appl Biochem Biotechnol*, **2009**, *157*, 174–209.

[17] Sarkanen, K.; Ludwig, C. *Lignins: occurrence, formation, structure and reactions*. Wiley-Interscience, 1971.

[18] Hoffmann, J.; Pedersen, T. H.; Rosendahl, L. A. *Hydrothermal Conversion in Near-Critical Water – A Sustainable Way of Producing Renewable Fuels*. Near-critical and Supercritical Water and Their Applications for Biorefineries. Springer Netherlands, Dordrecht, 2014.

[19] Lam, C. H.; Lowe, C. B.; Li, Z.; Longe, K. N.; Rayburn, J. T.; Caldwell, M. A.; Houdek, C. E.; Maguire, J. B.; Saffron, C. M.; Miller, D. J.; Jackson, J. E. *Green Chemistry*, **2015**, *17*(1), 601–609.

[20] Li, Z.; Bansal, N.; Azarpira, A.; Bhalla, A.; Chen, C. H.; Ralph, J.; Hegg, E. L.; Hodge, D. B. *Biotechnology for Biofuels*, **2015**, *8*(1), 123.

[21] Bonawitz, N. D.; Kim, J. I.; Tobimatsu, Y.; Ciesielski, P. N.; Anderson, N. A.; Ximenes, E.; Maeda, J.; Ralph, J.; Donohoe, B. S.; Ladisch, M.; Chapple, C. *Nature*, **2014**, *509*, 376.

[22] Mansfield, S. D.; Kim, H.; Lu, F.; Ralph, J. *Nature Protocols*, **2012**, *7*, 1579.

[23] Wen, J.-L.; Sun, S.-L.; Yuan, T.-Q.; Xu, F.; Sun, R.-C. *Journal of Agricultural and Food Chemistry*, **2013**, *61*(46), 11067–11075.

[24] Shen, X.-J.; Wang, B.; Pan-li, H.; Wen, J.-L.; Sun, R.-C. *RSC Advances*, **2016**, *6*(51), 45315–45325.

[25] Lancefield, C. S.; Ojo, O. S.; Tran, F.; Westwood, N. J. *Angewandte Chemie*, **2015**, *127*(1), 260–264.

[26] Shabtai, J. S. Process for conversion of lignin to reformulated hydrocarbon gasoline. The University of Utah Research Foundation, US5959167, 1999.

[27] Toxicological profile for gasoline. Technical report, Agency for Toxic Substances and Disease Registry, Jun. 1995. Report Number: PB/95/264206/AS.

[28] Antibiotic dosing during renal failure. https://www.slideshare.net/nels1937/antibiotic-dosing-during-renal-failure, (accessed Mar 18, 2018).

[29] Dalziel, K.; Dickinson, F. M. *Biochemical Journal*, **1966**, *100*(2), 491–500.

[30] Newton, P. E.; Schroeder, R. E.; Nelson, D. T.; VanSteenhouse, J. L. An inhalation combined repeat dose toxicity study and reproduction/developmental toxicity screen-

ing (oecd 422) study in rats with cyclohexanol. Technical report, MPI Research, Inc., May 10, 2006 2006. Report No. 683-004.2005.

[31] Thermoelectric generator. https://en.wikipedia.org/wiki/Thermoelectric_generator, (accessed Oct. 18, 2016).

[32] Rechargeable battery. https://en.wikipedia.org/wiki/Rechargeable_battery#Price_history, (accessed Oct. 18, 2016).

[33] Electrolysis of water. https://en.wikipedia.org/wiki/Electrolysis_of_water, (accessed Oct. 18, 2016).

[34] Polar ice cap. https://en.wikipedia.org/wiki/Polar_ice_cap, (accessed Mar 18, 2018).

[35] Lessard, J. *Electrocatalytic hydrogenation*. Organic Electrochemistry. Taylor & Francis, fifth edition edition, 2015.

[36] Bancroft, W. D.; George, A. B. *Transactions of the American Electrochemical Society*, **1930**, *57*(1), 399–406.

[37] Marie, C. *Zeitschrift für Elektrochemie*, **1903**, *9*(32), 633–633.

[38] Marie, C. *Abstracts of Chemical Papers Published in British and Foreign Journals*, volume 84 of *Journal of the Chemical Society*. The Chemical Society., London, Great Britain, 1903.

[39] Fokin, S. *Zeitschrift für Elektrochemie und Angewandte Physikalische Chemie*, **1906**, *12*(41), 749–762.

[40] Ellis, C.; Mcelroy, K. P. Process of reducing formic acid. U.S. Patent, US867575, 1907.

[41] Allen, M. J. *Organic Electrode Processes*. Reinhold Publishing Corporation, New Jersey, 1958.

[42] Mettler, C. *Berichte der Deutschen Chemischen Gesellschaft*, **1905**, *38*(2), 1745–1753.

[43] Mettler, C. *Berichte der Deutschen Chemischen Gesellschaft*, **1906**, *39*(3), 2933–2942.

[44] Dalavoy, T. S.; Jackson, J. E.; Swain, G. M.; Miller, D. J.; Li, J.; Lipkowski, J. *Journal of Catalysis*, **2007**, *246*(1), 15–28.

[45] Dalavoy, T. S. *Electrocatalytic hydrogenation of α-functionalized carboxylic acids*. Michigan State University, 2006.

[46] Elbs, K.; Wohlfahrt, T. *Zeitschrift für Elektrochemie*, **1902**, *8*(41), 789–791.

[47] Elbs, K.; Brand, K. *Zeitschrift für Elektrochemie*, **1902**, *8*(41), 783–788.

[48] Lofrano, R. C. Z.; Madurro, J. M.; Abrantes, L. M.; Romero, J. R. *Journal of Molecular Catalysis A: Chemical*, **2004**, *218*(1), 73–79.

[49] Vilar, M.; Oliveira, J. L.; Navarro, M. *Applied Catalysis A: General*, **2010**, *372*(1), 1–7.

[50] Yamada, T.; Osa, T.; Matsue, T. *Chemistry Letters*, **1987**, *16*(8), 1611–1612.

[51] Deronzier, A.; Moutet, J. C.; Saint-Aman, E. *Journal of Electroanalytical Chemistry*, **1992**, *327*(1), 147–158.

[52] Santana, D. S.; Melo, G. O.; Lima, M. V. F.; Daniel, J. R. R.; Areias, M. C. C.; Navarro, M. *Journal of Electroanalytical Chemistry*, **2004**, *569*(1), 71–78.

[53] Cirtiu, C. M.; Brisach-Wittmeyer, A.; Menard, H. *Catalysis Communications*, **2007**, *8*(5), 751–754.

[54] Coche, L.; Moutet, J. C. *Journal of the American Chemical Society*, **1987**, *109*(22), 6887–6889.

[55] Coche, L.; Ehui, B.; Limosin, D.; Moutet, J. C. *The Journal of Organic Chemistry*, **1990**, *55*(23), 5905–5910.

[56] Chambrion, P.; Roger, L.; Lessard, J.; Béraud, V.; Mailhot, J.; Thomalla, M. *Canadian Journal of Chemistry*, **1995**, *73*(6), 804–815.

[57] Chardon-Noblat, S.; de Oliveira, I. M. F.; Moutet, J.-C.; Tingry, S. *Journal of Molecular Catalysis A: Chemical*, **1995**, *99*(1), 13–21.

[58] Tafel, J.; Hahl, H. *Berichte der Deutschen Chemischen Gesellschaft*, **1907**, *40*(3), 3312–3318.

[59] Tafel, J.; Jürgens, W. *Berichte der Deutschen Chemischen Gesellschaft*, **1909**, *42*(2), 2548–2556.

[60] Tafel, J. *Berichte der Deutschen Chemischen Gesellschaft*, **1912**, *45*(1), 437–452.

[61] Tafel, J.; Friedrichs, G. *Berichte der Deutschen Chemischen Gesellschaft*, **1904**, *37*(3), 3187–3191.

[62] Stenzl, H.; Fichter, F. *Helvetica Chimica Acta*, **1934**, *17*(1), 669–681.

[63] Wawzonek, S.; Durham, J. E. *Journal of The Electrochemical Society*, **1976**, *123*(4), 500–503.

[64] Ono, S. J. *Journal of the Electrochemical Society of Japan*, **1955**, *23*, 117.

[65] Leipzig, B. *Zeitschrift für Elektrochemie*, **1898**, *4*(22), 506–514.

[66] Shine, H. J.; Zmuda, H.; Park, K. H.; Kwart, H.; Horgan, A. G.; Collins, C.; Maxwell, B. E. *Journal of the American Chemical Society*, **1981**, *103*(4), 955–956.

[67] Shine, H. J.; Zmuda, H.; Park, K. H.; Kwart, H.; Horgan, A. G.; Brechbiel, M. *Journal of the American Chemical Society*, **1982**, *104*(9), 2501–2509.

[68] Ahrens, F. B. *Zeitschrift für Elektrochemie*, **1896**, *3*(5), 99–100.

[69] Baillie, T. B.; Tafel, J. *Berichte der Deutschen Chemischen Gesellschaft*, **1899**, *32*(1), 68–77.

[70] Ahrens, F. B. *Zeitschrift für Elektrochemie*, **1896**, *2*(26), 577–581.

[71] Nasri, N. S.; Jones, J. M.; Dupont, V. A.; Williams, A. *Energy & Fuels*, **1998**, *12*(6), 1130–1134.

[72] Pieters, W.; Freel, J.; Anderson, R. Regeneration of sulfur-poisoned raney nickel catalyst. U.S. Patent, US3674707, 1972.

[73] Allen, M. J.; Steinman, H. G. *Journal of the American Chemical Society*, **1952**, *74*(15), 3932–3933.

[74] Schwarzenbach, G.; Rudin, E. *Helvetica Chimica Acta*, **1939**, *22*(1), 360–376.

[75] Verfahren zur darstellung von sulfosäuren der benzol- und naphtalinreihe. Deutsches Reichspatentamt (D.R.P.), DE255724, 1911.

[76] Hailwood, A. J. Electrolytic desulphonation of anthraquinone sulphonic acids. British Patent, GB273043, 1926.

[77] Pezzatini, G.; Wei, H.; Innocenti, M.; Guidelli, R. *Electroanalysis*, **1995**, *7*(5), 454–460.

[78] Parker, E. A.; Swann, S. *Transactions of The Electrochemical Society*, **1947**, *92*(1), 343–368.

[79] Hales, R. A. Reducing sugars. U.S. Patent, US2289190, 1942.

[80] Brown, K. R. Process for electrolytic reduction. U.S. Patent, US2280887, 1942.

[81] A, H. R. Electrolysis of sugars. U.S. Patent, US2303210, 1942.

[82] Cantor, S. M.; Peniston, Q. P. *Journal of the American Chemical Society*, **1940**, *62*(8), 2113–2121.

[83] Jung, S.; Biddinger, E. J. *ACS Sustainable Chemistry & Engineering*, **2016**, *4*(12), 6500–6508.

[84] Nilges, P.; Schroder, U. *Energy & Environmental Science*, **2013**, *6*(10), 2925–2931.

[85] Green, S. K.; Lee, J.; Kim, H. J.; Tompsett, G. A.; Kim, W. B.; Huber, G. W. *Green Chemistry*, **2013**, *15*(7), 1869–1879.

[86] Roylance, J. J.; Choi, K.-S. *Green Chemistry*, **2016**, *18*(10), 2956–2960.

[87] Roylance, J. J.; Kim, T. W.; Choi, K.-S. *ACS Catalysis*, **2016**, *6*(3), 1840–1847.

[88] Li, Z.; Kelkar, S.; Lam, C. H.; Luczek, K.; Jackson, J. E.; Miller, D. J.; Saffron, C. M. *Electrochimica Acta*, **2012**, *64*, 87–93.

[89] Sutton, A. D.; Waldie, F. D.; Wu, R.; Schlaf, M.; Iii, L. A. P. S.; Gordon, J. C. *Nature Chemistry*, **2013**, *5*, 428–432.

[90] Fichter, F.; Suter, R. *Helvetica Chimica Acta*, **1922**, *5*(2), 246–255.

[91] Fichter, F.; Stocker, R. *Berichte der Deutschen Chemischen Gesellschaft*, **1914**, *47*(2), 2003–2019.

[92] Drechsel, E. *Journal für Praktische Chemie*, **1884**, *29*(1), 229–252.

[93] Singh, N.; Song, Y.; Gutierrez, O. Y.; Camaioni, D. M.; Campbell, C. T.; Lercher, J. A. *ACS Catalysis*, **2016**, *6*(11), 7466–7470.

[94] Miller, L. L.; Christensen, L. *The Journal of Organic Chemistry*, **1978**, *43*(10), 2059–2061.

[95] Song, Y.; Gutierrez, O. Y.; Herranz, J.; Lercher, J. A. *Applied Catalysis B: Environmental*, **2016**, *182*(Supplement C), 236–246.

[96] Zhao, B.; Guo, Q.; Fu, Y. *Electrochemistry*, **2014**, *82*(11), 954–959.

[97] Ilikti, H.; Rekik, N.; Thomalla, M. *Journal of Applied Electrochemistry*, **2002**, *32*(6), 603–609.

[98] Sasaki, K.; Kunai, A.; Harada, J.; Nakabori, S. *Electrochimica Acta*, **1983**, *28*(5), 671–674.

[99] Willstätter, R.; Hatt, D. *Berichte der Deutschen Chemischen Gesellschaft*, **1912**, *45*(2), 1471–1481.

[100] Song, Y.; Chia, S. H.; Sanyal, U.; Gutiérrez, O. Y.; Lercher, J. A. *Journal of Catalysis*, **2016**, *344*, 263–272.

[101] Cyr, A.; Lessard, J. *Canadian Journal of Chemistry/Revue Canadienne de Chimie*, **2000**, *78*, 307–315.

[102] Schmiemann, U.; Baltruschat, H. *Journal of Electroanalytical Chemistry*, **1993**, *347*(1), 93–109.

[103] Pintauro, P. N.; Bontha, J. R. *Journal of Applied Electrochemistry*, **1991**, *21*(9), 799–804.

[104] Sitaraman, M. V.; Raman, V. V. *Current Science*, **1947**, *16*, 23.

[105] Li, Z.; Garedew, M.; Lam, C. H.; Jackson, J. E.; Miller, D. J.; Saffron, C. M. *Green Chemistry*, **2012**, *14*(9), 2540–2549.

[106] Pearl, I. A. *Journal of the American Chemical Society*, **1952**, *74*(17), 4260–4262.

[107] Mahdavi, B.; Lessard, J. *Journal of Applied Electrochemistry*, **1997**, *27*, 605–611.

[108] Dabo, P.; Cyr, A.; Lessard, J.; Brossard, L.; Menard, H. *Canadian Journal of Chemistry/Revue Canadienne de Chimie*, **1999**, *77*, 1225–1229.

[109] Benzyl ethers. http://www.organic-chemistry.org/protectivegroups/hydroxyl/benzyl-ethers.htm, (accessed Mar 18, 2018).

[110] McCormick, R. L. Liquid fuels from biomass. Technical report, National Renewable Energy Laboratory, Aug 23 2006.

[111] Bridgwater, T. Biomass pyrolysis. Technical report, IEA Bioenergy, Jan 2007. IEA Bioenergy: T34: 2007: 01.

[112] Jahirul, M.; Rasul, M.; Chowdhury, A.; Ashwath, N. *Energies*, **2012**, *5*(12), 4952.

[113] Patwardhan, P. R. *Understanding the product distribution from biomass fast pyrolysis*. 2010.

[114] Lam, C. H.; Das, S.; Erickson, N. C.; Hyzer, C. D.; Garedew, M.; Anderson, J. E.; Wallington, T. J.; Tamor, M. A.; Jackson, J. E.; Saffron, C. M. *Sustainable Energy & Fuels*, **2017**, *1*(2), 258–266.

[115] Li, Z.; Kelkar, S.; Raycraft, L.; Garedew, M.; Jackson, J. E.; Miller, D. J.; Saffron, C. M. *Green Chemistry*, **2014**, *16*(2), 844–852.

[116] Dalavoy, T. S.; Jackson, J. E.; Swain, G. M.; Miller, D. J.; Li, J.; Lipkowski, J. *Journal of Catalysis*, **2007**, *246*(1), 15–28.

[117] White, R. H. *Wood and Fiber Science*, **1987**, *19*(4), 446–452.

[118] Zmierczak, W.; Miller, J. Processes for catalytic conversion of lignin to liquid bio-fuels and novel bio-fuels. U.S. Patent, US7964761, 2011.

[119] Future use of lignin in value added products. Technical report, LigniMatch, 2009.

[120] Fichter, F. *Zeitschrift für Elektrochemie und Angewandte Physikalische Chemie*, **1910**, *16*(15), 610–613.

[121] Drechsel, E. *Journal für Praktische Chemie*, **1884**, *29*(1), 229–252.

[122] Martel, A.; Lessard, J. *Canadian Journal of Chemistry*, **1997**, *75*, 1862–1867.

[123] Ilikti, H.; Thomalla, M. *Journal of Applied Electrochemistry*, **2004**, *34*, 127–136.

[124] Cyr, A.; Lessard, J. *Canadian Journal of Chemistry/Revue Canadienne de Chimie*, **2000**, *78*, 307–315.

[125] Robin, D.; Lessard, J. *Canadian Journal of Chemistry*, **1990**, *68*, 1218–1227.

[126] Al-Mawlali, D.; Saleh, J. M. *Journal of the Chemical Society, Faraday Transactions 1: Physical Chemistry in Condensed Phases*, **1981**, *77*(12), 2977–2988.

[127] Alonso, F.; Riente, P.; Yus, M. *Tetrahedron*, **2008**, *64*(8), 1847–1852.

[128] Alonso, F.; Riente, P.; Yus, M. *Tetrahedron*, **2009**, *65*(51), 10637–10643.

[129] Alonso, F.; Riente, P.; Yus, M. *Accounts of Chemical Research*, **2011**, *44*(5), 379–391.

[130] Barta, K.; Matson, T. D.; Fettig, M. L.; Scott, S. L.; Iretskii, A. V.; Ford, P. C. *Green Chemistry*, **2010**, *12*(9), 1640–1647.

[131] Fouilloux, P. *Applied Catalysis*, **1983**, *8*(1), 1–42.

[132] Mebane, R. C.; Holte, K. L.; Gross, B. H. *Synthetic Communications*, **2007**, *37*(16), 2787–2791.

[133] Shorthouse, L. J.; Roberts, A. J.; Raval, R. *Surface Science*, **2001**, *480*(1–2), 37–46.

[134] Song, Q.; Wang, F.; Cai, J.; Wang, Y.; Zhang, J.; Yu, W.; Xu, J. *Energy & Environmental Science*, **2013**, *6*(3), 994–1007.

[135] Wang, X.; Rinaldi, R. *Energy & Environmental Science*, **2012**, *5*(8), 8244–8260.

[136] Wang, X.; Rinaldi, R. *ChemSusChem*, **2012**, *5*(8), 1455–1466.

[137] Fidalgo, B.; Zubizarreta, L.; Bermúdez, J. M.; Arenillas, A.; Menéndez, J. A. *Fuel Processing Technology*, **2010**, *91*(7), 765–769.

[138] Shunsuke, M.; Hideaki, M.; Sadami, S.; Makoto, S.; Kenji, T. Method of reactivation of raney nickel. Google Patents, 1975.

[139] Pattison, J. N.; Degering, E. F. *Journal of the American Chemical Society*, **1951**, *73*(1), 486–487.

[140] Pattison, J. N.; Degering, E. F. *Journal of the American Chemical Society*, **1951**, *73*(2), 611–613.

[141] Choudhary, V. R.; Chaudhari, S. K. *Reaction Kinetics and Catalysis Letters*, **1985**, *29*(1), 153–158.

[142] Boerjan, W.; Ralph, J. *Annual Review of Plant Biology*, **2003**, *54*, 519–546.

[143] Zakzeski, J.; Bruijnincx, P. C. A.; Jongerius, A. L.; Weckhuysen, B. M. *Chemical Reviews*, **2010**, *110*, 3552–3599.

[144] Adler, E. *Wood Science Technology*, **1977**, *11*, 169–218.

[145] Rencoret, J.; Marques, G.; Gutiérrez, A.; Nieto, L.; Martínez, A. T.; del Río, J. C. *Industrial Crops and Products*, **2009**, *30*, 137–143.

[146] Capanema, E. A.; Balakshin, M. Y.; Kadla, J. F. *Journal of Agricultural and Food Chemistry*, **2005**, *53*, 9639–9649.

[147] Ralph, J.; Lundquist, K.; Brunow, G.; Lu, F.; Kim, H.; Schatz, P. F.; Marita, J. M.; Hatfield, R. D.; Ralph, S. A.; Christensen, J. H.; Boerjan, W. *Phytochemistry Reviews*, **2004**, *3*, 29–60.

[148] Davin, L. B.; Wang, H.-B.; Crowell, A. L.; Bedgar, D. L.; Martin, D. M.; Sarkanen, S.; Lewis, N. G. *Science*, **1997**, *275*, 362–367.

[149] Gellerstedt, G.; Henriksson, G. *Lignins: Major Sources, Structure and Properties*. Monomers, Polymers and Composites from Renewable Resources. Elsevier, Amsterdam, 2008.

[150] Ralph, J.; Helm, R. F.; Quideau, S.; Hatfield, R. D. *Journal of the Chemical Society, Perkin Transactions 1*, **1992**, (21), 2961–2969.

[151] Wang, H.; Wei, Q.-Y.; Jiang, H.; Jiang, Z.-H. *Research on Chemical Intermediates*, **2012**, *38*(1), 207–213.

[152] Zeng, Q. One synthesis methode for ethyl cinnamate derivatives. Faming Zhuanli Shenqing, CN101121664 B, 2008.

[153] Chappellet, S.; J.F., E.; Palika, S.; Tang, Q. Photoaligning materials. World Intellectual Property Organization, WO2013050122A1, 2013.

[154] Quideau, S.; Ralph, J. *Journal of Agricultural and Food Chemistry*, **1992**, *40*(7), 1108–1110.

[155] Wang, X.; Li, X.; Xue, J.; Zhao, Y.; Zhang, Y. *Tetrahedron Letters*, **2009**, *50*(4), 413–415.

[156] Njiojob, C. N.; Rhinehart, J. L.; Bozell, J. J.; Long, B. K. *The Journal of Organic Chemistry*, **2015**, *80*(3), 1771–1780.

[157] Chouhan, M.; Sharma, R.; Nair, V. A. *Organic Letters*, **2012**, *14*(22), 5672–5675.

[158] Buendia, J.; Mottweiler, J.; Bolm, C. *Chemistry – A European Journal*, **2011**, *17*(49), 13877–13882.

[159] Maeda, S.; Masuda, H.; Tokoroyama, T. *Chemical & Pharmaceutical Bulletin*, **1994**, *42*(12), 2500–2505.

[160] Janssen, D. E.; Wilson, C. V. *Organic Syntheses*, **1956**, *36*, 46.

[161] Xu, R.; Zeng, Q. Preparation method of cinnamate derivates. Faming Zhuanli Shenqing, CN101774918 (A), 2010.

[162] Vafiadi, C.; Topakas, E.; Wong, K. K. Y.; Suckling, I. D.; Christakopoulos, P. *Tetrahedron: Asymmetry*, **2005**, *16*(2), 373–379.

[163] Salum, M. L.; Robles, C. J.; Erra-Balsells, R. *Organic Letters*, **2010**, *12*(21), 4808–4811.

[164] Putt Karson, S.; Nesterenko, V.; Dothager Robin, S.; Hergenrother Paul, J. *ChemBioChem*, **2006**, *7*(12), 1916–1922.

[165] Sakakibara, N.; Nakatsubo, T.; Suzuki, S.; Shibata, D.; Shimada, M.; Umezawa, T. *Organic & Biomolecular Chemistry*, **2007**, *5*(5), 802–815.

[166] Lu, Z.; Hu, C.; Guo, J.; Li, J.; Cui, Y.; Jia, Y. *Organic Letters*, **2010**, *12*(3), 480–483.

[167] Zhou, Y.; Gao, G.; Li, H.; Qu, J. *Tetrahedron Letters*, **2008**, *49*(20), 3260–3263.

[168] Grond, S.; Papastavrou, I.; Zeeck, A. *European Journal of Organic Chemistry*, **2002**, *2002*(19), 3237–3242.

[169] Lancefield, C. S.; Ojo, O. S.; Tran, F.; Westwood, N. J. *Angewandte Chemie International Edition*, **2015**, *54*(1), 258–262.

[170] Buendia, J.; Mottweiler, J.; Bolm, C. *Chemistry – A European Journal*, **2011**, *17*(49), 13877–13882.

[171] Snyder, S. A.; Kontes, F. *Journal of the American Chemical Society*, **2009**, *131*(5), 1745–1752.

[172] Reale, S.; Attanasio, F.; Spreti, N.; De Angelis, F. *Chemistry - A European Journal*, **2010**, *16*(20), 6077–87.

[173] Forsythe, W. G.; Garrett, M. D.; Hardacre, C.; Nieuwenhuyzen, M.; Sheldrake, G. N. *Green Chemistry*, **2013**, *15*(11), 3031–3038.

[174] Vermes, B.; Seligmann, O.; Wagner, H. *Phytochemistry*, **1991**, *30*(9), 3087–3089.

[175] de Farias Dias, A. *Phytochemistry*, **1988**, *27*(9), 3008–3009.

[176] Ralph, J.; Quideau, S.; Grabber, J. H.; Hatfield, R. D. *Journal of the Chemical Society, Perkin Transactions 1*, **1994**, (23), 3485–3498.

[177] Li, Y.; Akiyama, T.; Yokoyama, T.; Matsumoto, Y. *Biomacromolecules*, **2016**, *17*(6), 1921–1929.

[178] Biofuels and the environment: First triennial report to congress. Technical report, U.S. Environmental Protection Agency, Dec 2011 2011. Report Number: EPA/600/R-10/183F.

[179] Bruijnincx, P.; Weckhuysen, B.; Gruter, G.-J.; Westenbroek, A.; Engelen-Smeets, E. Lignin valorisation: the importance of a full value chain approach. Technical report, Utrecht University, Jun 2016 2016.

[180] 2016 billion-ton report. Technical report, U.S. Department of Energy, Jul 2016. Report Number: ORNL/TM-2016/160.

[181] Pasquariello, D.; Foise, J.; Kershaw, R.; Zoski, G.; Dwight, K.; Wold, A. *The Journal of Physical Chemistry*, **1985**, *89*(7), 1243–1245.

[182] Langer, S. H.; Yurchak, S. *Journal of The Electrochemical Society*, **1969**, *116*(9), 1228–1229.

[183] Quiroz, M. A.; Córdova, F.; Lamy-Pitara, E.; Barbier, J. *Electrochimica Acta*, **2000**, *45*(25), 4291–4298.

[184] Takano, K.; Tateno, H.; Matsumura, Y.; Fukazawa, A.; Kashiwagi, T.; Nakabayashi, K.; Nagasawa, K.; Mitsushima, S.; Atobe, M. *Bulletin of the Chemical Society of Japan*, **2016**, *89*(10), 1178–1183.

[185] Ding, K.; Xu, S.; Alotaibi, R.; Paudel, K.; Reinheimer, E. W.; Weatherly, J. *The Journal of Organic Chemistry*, **2017**, *82*(9), 4924–4929.

[186] Fristrup, P.; Kreis, M.; Palmelund, A.; Norrby, P.-O.; Madsen, R. *Journal of the American Chemical Society*, **2008**, *130*(15), 5206–5215.

[187] Kanan, M. W.; Yano, J.; Surendranath, Y.; Dincă, M.; Yachandra, V. K.; Nocera, D. G. *Journal of the American Chemical Society*, **2010**, *132*(39), 13692–13701.

[188] Abdelkafi, F.; Ammar, H.; Rousseau, B.; Tessier, M.; El Gharbi, R.; Fradet, A. *Biomacromolecules*, **2011**, *12*(11), 3895–3902.

[189] Graichen, F. H. M.; Grigsby, W. J.; Hill, S. J.; Raymond, L. G.; Sanglard, M.; Smith, D. A.; Thorlby, G. J.; Torr, K. M.; Warnes, J. M. *Industrial Crops and Products*, **2017**, *106*(Supplement C), 74–85.

[190] Gao, G.; Dallmeyer, J. I.; Kadla, J. F. *Biomacromolecules*, **2012**, *13*(11), 3602–3610.

[191] Ten, E.; Ling, C.; Wang, Y.; Srivastava, A.; Dempere, L. A.; Vermerris, W. *Biomacromolecules*, **2014**, *15*(1), 327–338.

[192] Tortora, M.; Cavalieri, F.; Mosesso, P.; Ciaffardini, F.; Melone, F.; Crestini, C. *Biomacromolecules*, **2014**, *15*(5), 1634–1643.

[193] van de Pas, D. J.; Torr, K. M. *Biomacromolecules*, **2017**, *18*(8), 2640–2648.

[194] Kim, Y. S.; Kadla, J. F. *Biomacromolecules*, **2010**, *11*(4), 981–988.

[195] Crestini, C.; Melone, F.; Sette, M.; Saladino, R. *Biomacromolecules*, **2011**, *12*(11), 3928–3935.

[196] Lin, S.; Dence, C. *Methods in Lignin Chemistry*. Springer Berlin Heidelberg, 2012.

[197] Alizadeh, H.; Teymouri, F.; Gilbert, T. I.; Dale, B. E. *Applied Biochemistry and Biotechnology*, **2005**, *124*(1), 1133–1141.

[198] Chundawat, S. P. S.; Venkatesh, B.; Dale, B. E. *Biotechnology and Bioengineering*, **2007**, *96*(2), 219–231.

[199] Swatloski, R. P.; Spear, S. K.; Holbrey, J. D.; Rogers, R. D. *Journal of the American Chemical Society*, **2002**, *124*(18), 4974–4975.

[200] Singh, S.; Simmons, B. A.; Vogel, K. P. *Biotechnology and Bioengineering*, **2009**, *104*(1), 68–75.

[201] Ralph, J.; Lundquist, K.; Brunow, G.; Lu, F.; Kim, H.; Schatz, P. F.; Marita, J. M.; Hatfield, R. D.; Ralph, S. A.; Christensen, J. H.; Boerjan, W. *Phytochemistry Reviews*, **2004**, *3*, 29–60.

[202] Rahimi, A.; Ulbrich, A.; Coon, J. J.; Stahl, S. S. *Nature*, **2014**, *515*(7526), 249–252.

[203] Granata, A.; Argyropoulos, D. S. *Journal of Agricultural and Food Chemistry*, **1995**, *43*(6), 1538–1544.

[204] Zakzeski, J.; Bruijnincx, P. C. A.; Jongerius, A. L.; Weckhuysen, B. M. *Chemical Reviews*, **2010**, *110*(6), 3552–3599.

[205] Li, C.; Zhao, X.; Wang, A.; Huber, G. W.; Zhang, T. *Chemical Reviews*, **2015**, *115*(21), 11559–11624.

[206] Bridgwater, A. V.; Meier, D.; Radlein, D. *Organic Geochemistry*, **1999**, *30*(12), 1479–1493.

[207] Kersten, S.; Garcia-Perez, M. *Current Opinion in Biotechnology*, **2013**, *24*(3), 414–420.

[208] Dabo, P.; Mahdavi, B.; Ménard, H.; Lessard, J. *Electrochimica Acta*, **1997**, *42*(9), 1457–1459.

[209] Lawton, M. *Metal triflate catalysed organic transformations*. University of Johannesburg, 2009.

[210] Kobayashi, S.; Sugiura, M.; Kitagawa, H.; Lam, W. W. L. *Chemical Reviews*, **2002**, *102*(6), 2227–2302.

[211] Li, Z.; Assary, R. S.; Atesin, A. C.; Curtiss, L. A.; Marks, T. J. *Journal of the American Chemical Society*, **2013**, *136*(1), 104–107.

[212] Noji, M.; Ishii, K. *The Journal of Organic Chemistry*, **2003**, *68*(24), 9340–9347.

[213] He, J.; Zhao, C.; Lercher, J. A. *Journal of the American Chemical Society*, **2012**, *134*(51), 20768–20775.

[214] Ralph, J.; Ralph, S.; Landucci, L. Nmr database of lignin and cell wall model compounds. Technical report, US Forest Products Laboratory & US Dairy Forage Research Center, 2015.

[215] Lahive, C. W.; Lancefield, C. S.; Codina, A.; Kamer, P. C. J.; Westwood, N. J. *Organic & Biomolecular Chemistry*, **2018**.

[216] Tran, F.; Lancefield, C. S.; Kamer, P. C. J.; Lebl, T.; Westwood, N. J. *Green Chemistry*, **2015**, *17*(1), 244–249.

[217] Ward, R. S.; Pelter, A.; Jack, I. R.; Satyanarayana, P.; Rao, B. V. G.; Subrahmanyam, P. *Tetrahedron Letters*, **1981**, *22*(41), 4111–4114.

[218] Achenbach, H.; Stöcker, M.; A. Constenla, M. *Phytochemistry*, **1988**, *27*(6), 1835–1841.

[219] McKone, T. E.; Nazaroff, W. W.; Berck, P.; Auffhammer, M.; Lipman, T.; Torn, M. S.; Masanet, E.; Lobscheid, A.; Santero, N.; Mishra, U.; Barrett, A.; Bomberg, M.; Fingerman, K.; Scown, C.; Strogen, B.; Horvath, A. *Environmental Science & Technology*, **2011**, *45*, 1751–1756.

[220] Hood, E. *F1000 Research*, **2016**, *5*(185), 1–9.

[221] Mussatto, S. I. *Biofuel Research Journal*, **2016**, *3*(1), 331–331.

[222] Bykova, M. V.; Zavarukhin, S. G.; Trusov, L. I.; Yakovlev, V. A. *Kinetics and Catalysis*, **2013**, *54*(1), 40–48.

[223] Chang, J.; Danuthai, T.; Dewiyanti, S.; Wang, C.; Borgna, A. *ChemCatChem*, **2013**, *5*(10), 3041–3049.

[224] Cyclohexanol. http://webbook.nist.gov/chemistry/, (accessed Apr 9, 2018).

[225] Doolittle, A. K. *Industrial & Engineering Chemistry*, **1935**, *27*(10), 1169–1179.

[226] Matos, M. A. R.; Miranda, M. S.; Morais, V. M. F. *Journal of Chemical & Engineering Data*, **2003**, *48*(3), 669–679.

[227] Alonso, D. M.; Wettstein, S. G.; Dumesic, J. A. *Chemical Society Reviews*, **2012**, *41*(24), 8075–8098.

[228] Cyclohexane. https://en.wikipedia.org/wiki/Cyclohexane, (accessed Mar 18, 2018).

[229] Cyclohexanol. https://en.wikipedia.org/wiki/Cyclohexanol, (accessed Mar 18, 2018).

[230] Cyclohexanol and cyclohexanone. https://ihsmarkit.com/products/cyclohexanol-chemical-economics-handbook.html, (accessed Mar 18, 2018).

[231] van Asselt, W. J.; van Krevelen, D. W. *Recueil des Travaux Chimiques des Pays-Bas*, **1963**, *82*(1), 51–67.

[232] Fisher, W. B.; VanPeppen, J. F. *Cyclohexanol and Cyclohexanone*. Kirk-Othmer Encyclopedia of Chemical Technology. John Wiley & Sons, Inc., 2000.

[233] Fujihara, S.; Kadota, Y.; Kimura, T. *Journal of Sol-Gel Science and Technology*, **2002**, *24*(2), 147–154.

[234] Qi, Y.; Yu, H.; Cao, Q.; Dong, B.; Mu, X.; Mao, A. *Catalysts*, **2016**, *6*(5), 63.

[235] Duwell, E. J.; Todd, J. W.; Butzke, H. C. *Corrosion Science*, **1964**, *4*(1), 435–441.

[236] *Handbook of environmental fate and exposure data for organic chemical*, **1989**, *4*, 102–109.

[237] Patty, F.; Clayton, G.; Clayton, F. *Patty's Industrial hygiene and toxicology*. Wiley, 1982.

[238] Agency, C. E. P. Evidence on the developmental and reproductive toxicity of cyclohexanol. Technical report, 2001.

[239] Elliott, T. H.; Parke, D. V.; Williams, R. T. *Biochemical Journal*, **1959**, *72*(2), 193–200.

[240] Treon, J. F.; William E. Crutchfield, J.; Kitzmiller, K. V. *The Journal of Industrial Hygiene and Toxicology*, **1943**, *25*, 199–214.

[241] Opdyke, D. *Cyclohexanol A2*. Monographs on Fragrance Raw Materials. Pergamon, 1979.

[242] Norris, D. B.; Trudgill, P. W. *Biochemical Journal*, **1971**, *121*(3), 363–370.

[243] Plapp, B. V.; Leidal, K. G.; Murch, B. P.; Green, D. W. *Chemico-Biological Interactions*, **2015**, *234*, 85–95.

[244] Jansson, B.; Jörnvall, H.; Rydberg, U.; Terenius, L.; Vallee, B. L. *Toward a Molecular Basis of Alcohol Use and Abuse*. Birkhäuser Basel, 1989.

[245] Mráz, J.; Gálová, E.; Nohová, H.; Vítková, D. *International Archives of Occupational and Environmental Health*, **1998**, *71*(8), 560–5065.

[246] *Cyclohexanol [MAK Value Documentation in German language, 2010].* The MAK-Collection for Occupational Health and Safety. Wiley-VCH Verlag GmbH & Co. KGaA, 2002.

[247] Mills, G. A.; Walker, V. *Clinical Chemistry*, **1990**, *36*(6), 870.

[248] Mráz, J.; Gálová, E.; Nohová, H.; Vítková, D.; Tichý, M. *Scandinavian Journal of Work, Environment & Health*, **1999**, (3), 233–237.

[249] Takeuchi, A.; Ogawa, Y.; Endo, Y.; Kawai, T.; Namera, A.; Yamamuro, K.; Sumino, K.; Endo, G. *Journal of Occupational Health*, **2015**, *57*(4), 365–370.

[250] Toxicological review of cyclohexane - in support of summary information on the integrated risk information system (iris). Technical report, U.S. Environmental Protection Agency, Aug 2003. Report Number: EPA 635/R-03/008.

[251] Savolainen, H.; Pfäffli, P. *Toxicology Letters*, **1980**, *7*(1), 17–22.

[252] Lammers, J. H. C. M.; Emmen, H. H.; Muijser, H.; Hoogendijk, E. M. G.; McKee, R. H.; Owen, D. E.; Kulig, B. M. *International Journal of Toxicology*, **2009**, *28*(6), 488–497.

[253] Campos-Ordonez, T.; Zarate-Lopez, D.; Galvez-Contreras, A. Y.; Moy-Lopez, N.; Guzman-Muniz, J.; Gonzalez-Perez, O. *Cellular and Molecular Neurobiology*, **2015**, *35*(4), 503–512.

[254] Perbellini, L.; Brugnone, F.; Caretta, D.; Maranelli, G. *British Journal of Industrial Medicine*, **1985**, *42*(3), 162–167.

[255] Gargas, M. L.; Burgess, R. J.; Voisard, D. E.; Cason, G. H.; Andersen, M. E. *Toxicology and Applied Pharmacology*, **1989**, *98*(1), 87–99.

[256] Ghittori, S.; Imbriani, M.; Pezzagno, G.; Capodaglio, E. *American Industrial Hygiene Association Journal*, **1987**, *48*(9), 786–790.

[257] Gondry, E. *Journal européen de toxicologie*, **1973**, *5*(4), 227–238.

[258] Environment directorate joint meeting of the chemicals committee and the working party on chemicals, pesticides and biotechnology. Technical report, Environment, Health and Safety Publications, Organisation for Economic Co-operation and Development, Sep. 4 2002. Report Number: ENV/JM/MONO(2002)19.

[259] Cyclohexanol - evaluation of the effects on reproduction, recommendation for classification. Technical report, Committee for Compounds Toxic to Reproduction, Health

Council of the Netherlands, Netherlands, 2004. Report Number: DGV/MBO/U-932542.

[260] Tyagi, A.; Joshi, B.; Kumar, S.; Dixit, V. *Indian journal of experimental biology*, **1979**, *17*(12), 1305–130.

[261] Dixit, V.; Gupta, R.; Kumar, S.; Joshi, B. *Indian J Physiol Pharmacol*, **1980**, *24*(4), 278–286.

[262] Lake, B. G.; Foster, J. R.; Collins, M. A.; Stubberfield, C. R.; Gangolli, S. D.; Srivastava, S. P. *Acta Pharmacologica et Toxicologica*, **1982**, *51*(3), 217–226.

[263] Eldridgea, J. C.; Wetzel, L. T.; Tyrey, L. *Reproductive Toxicology*, **1999**, *13*(6), 491–499.

[264] Sister chromatid exchange. https://en.wikipedia.org/wiki/Sister_chromatid_exchange, (accessed Mar 18, 2018).

[265] Sivikova, K.; Dianovsky, J.; Piesova, E.; Holeckova, B. *Acta Biologica Hungarica*, **2007**, *58*(4), 389–396.

[266] Espinosa-Aguirre, J.; Vilchis, C.; Ostrosky-Wegman; L. Benitez b, I. L.; Rubio, J. *Mutation Research*, **1993**, *300*, 151–154.

[267] Márquez-Rosado, L.; Trejo-Solís, C.; del Pilar Cabrales-Romero, M.; Arce-Popoca, E.; Sierra-Santoyo, A.; Alemán-Lazarini, L.; Fatel-Fazenda, S.; Carrasco-Legleu, C. E.; Villa-Treviño, S. *Molecular Carcinogenesis*, **2007**, *46*(7), 524–533.

[268] National library of medicine hsdb database - cyclohexanol. https://toxnet.nlm.nih.gov, (accessed Mar 18, 2018).

[269] Opdyke, D. *Monographs on Fragrance Raw Materials: A Collection of Monographs Originally Appearing in Food and Cosmetics Toxicology*. Elsevier Science, 2013.

[270] Treon, J. F.; William E. Crutchfield, J.; Kitzmiller, K. V. *The Journal of Industrial hygiene and Toxicology*, **1943**, *25*(8), 323–347.

[271] Toxicological profile for n-hexane. Technical report, U.S. Department of Health and Human Services, Jul. 1999.

[272] Dekant, W.; Vamvakas, S. *Toxicology, 1. Fundamentals*. Ullmann's Encyclopedia of Industrial Chemistry. Wiley-VCH Verlag GmbH & Co. KGaA, 2000.

[273] Malley, L. A. 90-day inhalation toxicity study with cyclohexane in rats. Technical report, Haskell Laboratory for Toxicology and Industrial Medicine, 1996. Haskell Laboratory Report DuPont HLR number 298-96.

[274] Malley, L. A. 90-day inhalation neurotoxicity study with cyclohexane in rats. Technical report, Haskell Laboratory for Toxicology and Industrial Medicine, 1996. Haskell Laboratory Report DuPont HLR number 752-95.

[275] Kreckmann, K. H. Reproductive and fertility effects with cyclohexane inhalation multigeneration reproduction study in rats. Technical report, Haskell Laboratory for Toxicology and Industrial Medicine, 1997. Haskell Laboratory Report DuPont HLR number 409-96.

[276] Kreckmann, K. H. Inhalation developmental toxicity study of cyclohexane in rats. Technical report, Haskell Laboratory for Toxicology and Industrial Medicine, 1997. Haskell Laboratory Report DuPont HLR number 881-96.

[277] Bamberger, J. R. 90-day inhalation toxicity study with cyclohexane in mice. Technical report, Haskell Laboratory for Toxicology and Industrial Medicine, 1996. Haskell Laboratory Report Number: 17-96.

[278] Christoph, G. R. Acute operant behavior study of cyclohexane by inhalation in rats. Technical report, Haskell Laboratory for Toxicology and Industrial Medicine, Haskell Laboratory for Toxicology and Industrial Medicine, 1996. Haskell Laboratory Report DuPont HLR number 732-95.

[279] Verywellmind. Fixed-interval schedule and operant conditioning. https://www.verywellmind.com/what-is-a-fixed-interval-schedule-2795189, (accessed Mar 18, 2018).

[280] Eisenbrandt, D. L.; Mattsson, J. L.; Albee, R. R.; Spencer, P. J.; Johnson, K. A. *Toxicology Pathology*, **1990**, *18*, 154–164.

[281] Creasy, D.; Bube, A.; Rijk, E. d.; Kandori, H.; Kuwahara, M.; Masson, R.; Nolte, T.; Reams, R.; Regan, K.; Rehm, S.; Rogerson, P.; Whitney, K. *Toxicologic Pathology*, **2012**, *40*(6), 40S–121S.

[282] Kreckmann, K. H. Inhalation developmental toddty study of cydobeune in rabbits. Technical report, Haskell Laboratory for Toxicology and Industrial Medicine, 1997. Haskell Laboratory Report DuPont HLR number 883-96.

[283] Savolainen, H.; Pfäffli, P. *Toxicology Letters*, **1980**, *6*(1), 43–49.

[284] National Research, C. *Drinking Water and Health,: Volume 6*. The National Academies Press, Washington, DC, 1986.

[285] Methods for derivation of inhalation reference concentrations and application of inhalation dosimetry. Technical report, U.S. Environmental Protection Agency, North Carolina, Oct. 1994. EPA/600/8-90/066F.